

AD-A265 527



LMF-138
DECEMBER 1992
CATEGORY: UC-48

(1)

INHALATION TOXICOLOGY RESEARCH INSTITUTE ANNUAL REPORT

1991 - 1992

by the Staff of the
Inhalation Toxicology Research Institute

ITRI

DTIC
ELECTED
JUN 07 1993
S E D

INHALATION TOXICOLOGY RESEARCH INSTITUTE
LOVELACE BIOMEDICAL & ENVIRONMENTAL RESEARCH INSTITUTE
P.O. Box 5890

Albuquerque, NM 87185

93-12603



DISTRIBUTION STATEMENT
Approved for public release
Distribution Unlimited

PREPARED FOR THE OFFICE OF HEALTH
AND ENVIRONMENTAL RESEARCH
OF THE U.S. DEPARTMENT OF ENERGY
UNDER CONTRACT NUMBER DE-AC04-76EV01013

93 6 04 029

This report was prepared as an account of work sponsored by the United States Government. Neither the United States nor the United States Department of Energy, nor any of their employees, nor any of their contractors, subcontractors, or their employees, makes any warranty, expressed or implied, or assumes any legal liability or responsibility for the accuracy, completeness or usefulness of any information, apparatus, product or process disclosed, or represents that its use would not infringe privately owned rights.

The research described in this report involved animals maintained in animal care facilities fully accredited by the American Association for Accreditation of Laboratory Animal Care. The research described in this report that involved humans was conducted in compliance with government regulations protecting human subjects.

Printed in the United States of America

Available to DOE and DOE contractors from the Office of Scientific and Technical Information, P. O. Box 62, Oak Ridge, TN 37831: prices available from (615) 576-8401, FTS 626-8401.

Available to the public from the National Technical Information Service, U. S. Department of Commerce, 5285 Port Royal Rd., Springfield, VA 22161.

LMF-138
December 1992
Category: UC-48

**Annual Report of the
Inhalation Toxicology Research Institute
Operated for the
United States Department of Energy
by the
Lovelace Biomedical and Environmental Research Institute**

October 1, 1991 through September 30, 1992

DTIC QUALITY INSPECTED 2

**by the Staff of the
Inhalation Toxicology Research Institute**

J. L. Mauderly, Director

**G. L. Finch, Senior Editor
K. J. Nikula, Associate Editor
P. L. Bradley, Technical Editor**

December 1992

Accesion For	
NTIS	CRA&I <input checked="" type="checkbox"/>
DTIC	TAB <input type="checkbox"/>
Unannounced <input type="checkbox"/>	
Justification	
By	
Distribution /	
Availability Codes	
Dist	Avail and / or Special
A-1	

**Prepared for the Office of Health and Environmental Research of the
U. S. Department of Energy Under Contract Number DE-AC04-76EV01013**

TABLE OF CONTENTS

INTRODUCTION	viii
PREVIOUS ANNUAL REPORTS	x
I. CHARACTERIZATION OF AIRBORNE MATERIALS AND GENERATION OF EXPERIMENTAL EXPOSURE ATMOSPHERES	
Statistical Limitations in the Sensitivity of Continuous Air Monitors for Alpha-Emitting Radionuclides <i>M. D. Hoover and G. J. Newton</i>	1
Update on Selection and Use of Filter Media in Continuous Air Monitors for Alpha-Emitting Radionuclides <i>M. D. Hoover and G. J. Newton</i>	5
Studies of the Homogeneity of Particle Collection in Alpha Continuous Air Monitors <i>G. J. Newton, M. D. Hoover, and W. C. Griffith</i>	8
Influence of Salt Dust on Alpha Energy Spectra and Detection Efficiency in Continuous Air Monitors for Alpha-Emitting Radionuclides <i>M. D. Hoover and G. J. Newton</i>	11
A Radon Progeny Generation System for Performance Evaluations of Alpha Continuous Air Monitors <i>G. J. Newton, M. D. Hoover, and Y. S. Cheng</i>	14
Design, Construction, and Testing of a 54" Aerosol Chamber for Instrument Evaluation <i>E. B. Barr and Y. S. Cheng</i>	18
Calibration and Performance of an API Aerosizer <i>Y. S. Cheng, E. B. Barr, I. A. Marshall, and J. P. Mitchell</i>	21
Reconfiguration and Calibration of the ITRI Whole-Body Counter <i>M. B. Snipes, S. B. Ebara, B. B. Boecker, J. E. Johnson, and R. A. Guilmette</i>	24
A Human Aerosol Exposure System <i>Y. S. Cheng, H. C. Yeh, and S. Q. Simpson</i>	28
Air Ventilation and Aerosol Concentration in a Rectangular Room <i>Y. S. Cheng, C. C. Yu, and W. E. Bechtold</i>	31
A Case Study on Determining Air Monitoring Requirements in a Radioactive Materials Handling Area <i>G. J. Newton, M. D. Hoover, and F. Ghanbari</i>	34
Characterization of Enriched Uranium Dioxide Particles from a Uranium Handling Facility <i>M. D. Hoover, G. J. Newton, R. J. Howard, and S. M. Trotter</i>	37
Size Distribution Measurements of Vector Aerosols Used for Animal Inhalation Studies with Radon Progeny <i>G. J. Newton, Y. S. Cheng, H. C. Yeh, and N. F. Johnson</i>	40

Comparison of Activity Size Distributions of Thoron Progeny by Alpha- and Gamma-Counting Methods <i>Y. S. Cheng, C. C. Yu, and K. W. Tu</i>	43
Classification of Carbon Fibers by Length Based on Their Electrical Properties <i>B. T. Chen, H. C. Yeh, and C. H. Hobbs</i>	45
Characterization of Aerosols Produced During Surgical Procedures in Hospitals <i>H. C. Yeh, R. S. Turner, R. K. Jones, B. A. Muggenburg, J. Smith, L. S. Martin, and P. W. Strine</i>	48
Thermal Oxidation of Cigarette Smoke Exhaust <i>B. T. Chen, W. E. Bechtold, G. L. Finch, J. A. Lopez, and J. J. Thompson</i>	51
An Efficient Method for Synthesizing [d_6]-Butadiene Monoepoxide <i>K. R. Maples, J. L. Lane, and A. R. Dahl</i>	54

II. DEPOSITION AND CLEARANCE OF INHALED TOXICANTS

Flow Measurement and Theoretical Calculation of Aerosol Deposition in a Human Tracheobronchial Tree Model <i>Y. S. Cheng, S. M. Smith, and H. C. Yeh</i>	57
<i>In Vivo</i> Deposition of Inhaled Ultrafine Particles in Airways of Rhesus Monkeys <i>H. C. Yeh, B. A. Muggenburg, and J. R. Harkema</i>	60
Factors Influencing the Deposition of Inhaled Particles in F344 Rats with Pre-Existing Pulmonary Emphysema <i>D. L. Lundgren, M. D. Hoover, F. F. Hahn and J. L. Mauderly</i>	63
Deposition of Monodisperse Liquid Droplet Aerosols in an MRI-Based Nasal Airway Replica <i>R. A. Guilmette</i>	66
A System to Measure Vapor Uptake in F344 Rat Lungs and Noses with Set Respiratory Parameters for Cyclic Breathing <i>A. R. Dahl and L. K. Brookins</i>	69
Effects of Cigarette Smoke Exposure on F344 Rat Lung Clearance of Insoluble Particles <i>G. L. Finch, B. T. Chen, E. B. Barr, and I. Y. Chang</i>	71
Effects of Repeated Inhalation Exposure of F344 Rats and B6C3F ₁ Mice to Nickel Oxide and Nickel Sulfate Hexahydrate on Lung Clearance <i>J. M. Benson, I. Y. Chang, Y. S. Cheng, F. F. Hahn, and M. B. Snipes</i>	74
Clearance of Particles Deposited in the Conducting Airways of Beagle Dogs <i>M. B. Snipes, W. C. Griffith, K. J. Nikula, B. A. Muggenburg, and R. A. Guilmette</i>	77
Systemic Absorption of Plutonium from the Nasal Airways and GI Tract When Administered as Nitrate or Oxide Aerosols <i>R. A. Guilmette and B. A. Muggenburg</i>	79
Toxicokinetics of Inhaled Nickel Oxide in F344 Rats <i>J. M. Benson, Y. S. Cheng, and K. R. Maples</i>	83

Stability and Cellular Toxicity of Hoechst 33342 Nuclear Labeling of Canine Alveolar Macrophages <i>In Vitro</i>	86
<i>J. A. Hotchkiss and R. A. Guilmette</i>	

III. METABOLISM AND MARKERS OF INHALED TOXICANTS

Effect of Dose on the Disposition of 2-Ethoxyethanol after Inhalation by F344 Rats	89
<i>C. H. Kennedy, W. E. Bechtold, and R. F. Henderson</i>	
Human Metabolism of 1,3-Butadiene	92
<i>W. E. Bechtold, M. R. Strunk, I. Y. Chang, and R. F. Henderson</i>	
Metabolism of 3,9-Dinitrofluoranthene and 3-Nitrofluoranthene by F344 Rat Lung Subcellular Fractions	94
<i>C. E. Mitchell, W. E. Bechtold, and S. A. Belinsky</i>	
Alkaline Phosphatase in Lavage Fluid: An Indicator of Type II Cell Secretions?	97
<i>R. F. Henderson, G. C. Scott, and J. J. Waide</i>	
Multidimensional HPLC Analysis of Butadiene Monoepoxide/Guanosine Adducts with Electrochemical Detection	99
<i>W. E. Bechtold and M. R. Strunk</i>	
Nonanedioic Acid: A Biomarker of Exposure to Ozone	101
<i>C. H. Kennedy, A. A. Hunt, W. E. Bechtold, W. A. Evans, and J. R. Harkema</i>	

IV. CARCINOGENIC RESPONSES TO TOXICANTS IN THE RESPIRATORY TRACT

Influence of Particle-Associated Organic Compounds on the Carcinogenicity of Diesel Exhaust	105
<i>K. J. Nikula, M. B. Snipes, E. B. Barr, W. C. Griffith, R. F. Henderson, and J. L. Mauderly</i>	
Two-Year Inhalation Studies of Nickel Sulfate Hexahydrate, Nickel Oxide, and Nickel Subsulfide in F344 Rats and B6C3F ₁ Mice	108
<i>J. M. Benson, Y. S. Cheng, F. F. Hahn, K. R. Maples, K. J. Nikula, C. H. Hobbs, and W. Eastin</i>	
Effects of Inhaled ²³⁹ PuO ₂ and Cigarette Smoke in F344 Rats	110
<i>G. L. Finch, E. B. Barr, W. E. Bechtold, B. T. Chen, W. C. Griffith, M. D. Hoover, J. L. Mauderly, C. E. Mitchell, and K. J. Nikula</i>	
Combined Exposure of F344 Rats to Beryllium Metal and ²³⁹ PuO ₂ Aerosols	112
<i>G. L. Finch, F. F. Hahn, W. W. Carlton, A. H. Rebar, M. D. Hoover, W. C. Griffith, J. A. Mewhinney, and R. G. Cuddihy</i>	
Effects of Combined Exposure of F344 Rats to ²³⁹ PuO ₂ and Whole-Body X-Radiation	115
<i>D. L. Lundgren, F. F. Hahn, W. C. Griffith, W. W. Carlton, M. D. Hoover, and B. B. Boecker</i>	
Effects of Combined Exposure of F344 Rats to Inhaled ²³⁹ PuO ₂ and a Chemical Carcinogen (NNK)	118
<i>D. L. Lundgren, S. A. Belinsky, K. J. Nikula, W. C. Griffith, and M. D. Hoover</i>	
Effects of Thoracic and Whole-Body Exposure of F344 Rats to X Rays	121
<i>D. L. Lundgren, F. F. Hahn, W. C. Griffith, and B. B. Boecker</i>	

Carcinogenic Effects of Inhaled $^{244}\text{Cm}_2\text{O}_3$ in F344 Rats <i>D. L. Lundgren, R. A. Guilmette, F. F. Hahn, and W. W. Carlton</i>	123
Biological Effects of $^{91}\text{YCl}_3$ Inhaled by Beagle Dogs <i>A. F. Hubbs, B. A. Muggenburg, F. F. Hahn, W. C. Griffith, and B. B. Boecker</i>	127
Life-Span Health Effects of Relatively Soluble Forms of Internally Deposited Beta-Emitting Radionuclides <i>B. B. Boecker, B. A. Muggenburg, F. F. Hahn, K. J. Nikula, and W. C. Griffith</i>	130
Primary Lung Cancer in the Longevity Study/Control Population of the ITRI Beagle Dog Colony <i>F. F. Hahn, B. A. Muggenburg, and W. C. Griffith</i>	133

V. MECHANISMS OF CARCINOGENIC RESPONSES TO TOXICANTS

Development of Techniques to Detect Gene Dysfunctions in α -Radiation-Induced Lung Cancer <i>J. F. Lechner, L. A. Tierney, S. A. Belinsky, C. E. Mitchell, J. M. Samet, and G. Saccomanno</i>	137
Arbitrarily Primed-Polymerase Chain Reaction Amplification as a Means to Discern Gene Alterations in Lung Cancer <i>C. H. Kennedy, P. Economou, and J. F. Lechner</i>	139
Development of a DNA Methyltransferase Assay <i>C. Nickell and S. A. Belinsky</i>	141
Flow Cytometric Analysis of Micronucleus Induction Following X Irradiation <i>A. W. Hickman and N. F. Johnson</i>	143
Characterization of Intron Sequences Flanking the Conserved Regions of the p53 Tumor Suppressor Gene in the F344 Rat Lung <i>S. A. Belinsky and S. Wachocki</i>	145
Examination of the K-ras Proto-oncogene in Lung Tumors Induced in the F344 Rat by X Rays <i>S. A. Belinsky, C. E. Mitchell, and F. F. Hahn</i>	147
Comparative Pulmonary Tumorigenicity of NNK and Beryllium in Strain A and C3H Mice <i>S. A. Belinsky, K. J. Nikula, and G. L. Finch</i>	149
Role of MCM3 in Regulating the Cell Cycle <i>G. Kelly and T. R. Carpenter</i>	151
Identification of Yeast Analogues of p53 by Association with the SV40 Large T Antigen <i>G. Kelly, T. R. Carpenter, and N. F. Johnson</i>	153

VI. NONCARCINOGENIC RESPONSES TO INHALED TOXICANTS

Response of the Lung to Instilled Versus Inhaled Particles <i>R. F. Henderson, K. E. Driscoll, R. C. Lindenschmidt, J. R. Harkema, E. B. Barr and I. Y. Chang</i>	157
--	-----

Inflammatory and Proliferative Responses of Pulmonary Airway Epithelium in F344 Rats After Exposure to Bacterial Endotoxin	160
<i>J. A. Hotchkiss, N. F. Johnson, S. A. Belinsky, D. G. Thomassen, J. F. Lechner, and J. R. Harkema</i>	
Rat Strain and Substrain Differences in Response to Ozone	163
<i>R. F. Henderson, J. A. Hotchkiss, D. G. Burt, C. H. Hobbs, and J. R. Harkema</i>	
Strain-Related Differences in Ozone-Induced Secretory Metaplasia in the Nasal Epithelium of F344 Rats	166
<i>J. R. Harkema, C. M. Wierenga, L. K. Herrera, J. A. Hotchkiss, W. A. Evans, D. G. Burt, and C. H. Hobbs</i>	
Effects of Inhaled Beryllium Metal on C3H Mouse Lung Clearance and Toxicity	169
<i>G. L. Finch, M. D. Hoover, and K. J. Nikula</i>	
Characterization of Beryllium-Induced Granulomatous Lung Disease in Strain A and C3H Mice	171
<i>K. J. Nikula, M. D. Tohulka, D. S. Swafford, M. D. Hoover, and G. L. Finch</i>	
Immune Memory Response in Lung	173
<i>D. E. Bice and B. A. Muggenburg</i>	
Effect of Cigarette Smoke Exposure on the Immunologic Status of F344 Rats	176
<i>S. M. Savage, G. L. Finch, B. T. Chen, and M. L. Sopori</i>	
Bone and Blood Measurement from F344 Rats Exposed to Cigarette Smoke	178
<i>M. Bhattacharyya, C. Wang, S. Abrikosova, S. Brown, B. T. Chen, and G. L. Finch</i>	

VII. MECHANISMS OF NONCARCINOGENIC RESPONSES TO INHALED TOXICANTS

Ultrastructural Evaluation of a Lung Epithelial Cell Strain as an Alveolar Type II Cell Model	181
<i>N. F. Johnson, A. W. Goldrath and E. K. Perryman</i>	
Differentiation Pattern of F344 Rat Alveolar Type II Cells	184
<i>N. F. Johnson, E. K. Perryman, and A. W. Goldrath</i>	
<i>In Vitro Expression of F344 Rat Olfactory-Specific Cytochrome P4502G1</i>	187
<i>J. A. Hotchkiss, J. L. Francis, L. K. Brookins, and A. R. Dahl</i>	
Comparative Localization of Carboxylesterase in F344 Rat, Beagle Dog, and Human Nasal Tissue	190
<i>K. J. Nikula, J. L. Lewis, R. Novak, and A. R. Dahl</i>	
Role of Neutrophils in the Development and Resolution of Cigarette Smoke-Induced Lesions in F344 Rat Nasal Epithelium	192
<i>J. A. Hotchkiss, G. L. Finch, and J. R. Harkema</i>	
Continued Antibody Production in Pulmonary Allografts in Nonimmune Recipients	195
<i>D. E. Bice, A. J. Williams, and B. A. Muggenburg</i>	
Lymphocyte Characteristics and Mitogen-Specific <i>In Vitro</i> Proliferation in Unexposed Rhesus Monkeys	198
<i>G. L. Finch, D. E. Bice, K. F. Pavia, and P. J. Haley</i>	

VIII. UNIVERSITY OF UTAH STUDIES OF INJECTED ACTINIDES

Static and Dynamic Bone Histomorphometry of ^{239}Pu -Treated Dogs <i>W. S. S. Jee, R. B. Setterberg, Y. F. Ma, M. Li, X. G. Liang, F. Johnson, and H. Z. Ke</i>	201
Statistics of Hits to Bone Cell Nuclei <i>I. L. Kruglikov, E. Polig, and W. S. S. Jee</i>	203
Skeletal Malignancies Among Beagle Dogs Injected with ^{241}Am <i>R. D. Lloyd, G. N. Taylor, W. Angus, S. C. Miller, and B. B. Boecker</i>	206
Occurrence of Metastases in Beagle Dogs with Skeletal Malignancies Induced by Internal Irradiation <i>R. D. Lloyd, W. Angus, G. N. Taylor, G. B. Thurman, and S. C. Miller</i>	208
Thyroid Lesions Induced by ^{241}Am in the Beagle Dog <i>G. N. Taylor, R. D. Lloyd, F. W. Bruenger, and S. C. Miller</i>	210

IX. THE APPLICATION OF MATHEMATICAL MODELING TO HEALTH ISSUES

Age-Specific Lung Cancer Risk Estimates for Exponentially Decaying Patterns of Irradiation <i>B. R. Scott and B. B. Boecker</i>	213
Prediction of Survival Times After Repeated Exposures Based on Survival Times Following a Single Exposure of Beagle Dogs by Inhalation to $^{239}\text{PuO}_2$ <i>J. H. Diel</i>	215
Analysis of Software of the Proposed NCRP Respiratory Tract Dosimetry Model <i>I. Y. Chang, R. H. Mooty, W. C. Griffith, and H. C. Yeh</i>	217
Recommendations for Limiting Risk of Stochastic Effects of Exposure of the Respiratory Tract to β/γ -Emitting Hot Particles <i>B. R. Scott, Y. S. Cheng, and B. B. Boecker</i>	221
Evidence of Errors in DS86 Neutron Kerma Based on Biological Dosimetry <i>B. R. Scott</i>	224

X. APPENDICES

A. Status of Longevity and Sacrifice Experiments in Beagle Dogs	227
B. Organization of Personnel as of December 31, 1992	228
C. Organization of Research Programs. October 31, 1991 - December 31, 1992	237
D. Publication of Technical Reports. October 1, 1991 - September 30, 1992	240
E-1. ITRI Publications in the Open Literature. October 1, 1991 - September 30, 1992	241
E-2. University of Utah Publications in the Open Literature. October 1, 1991 - September 30, 1992	251

F.	Presentations Before Regional or National Scientific Meetings and Educational and Scientific Seminars. October 1, 1991 - September 30, 1992	253
G.	Seminars Presented by Visiting Scientists. October 1, 1991 - September 30, 1992	262
H.	Adjunct Scientists as of December 31, 1992	264
I.	Educational Activities at the Inhalation Toxicology Research Institute	265
J.	Author Index	267

INTRODUCTION

The Institute

The Inhalation Toxicology Research Institute (ITRI) is a federally funded research and development center operated for the U. S. Department of Energy (DOE) by the Lovelace Biomedical and Environmental Research Institute, a nonprofit subsidiary of the Lovelace Medical Foundation. ITRI is designated as a "Special Purpose Laboratory" within the DOE Office of Health and Environmental Research, Office of Energy Research. Approximately 75% of the Institute's research is funded by DOE; the remainder is funded by a variety of governmental, trade association, and private sources.

The mission of ITRI is to conduct basic and applied research to improve our understanding of the nature and magnitude of the human health impacts of inhaling airborne materials in the home, workplace, and general environment. Institute research programs have a strong basic science orientation with emphasis on the nature and behavior of airborne materials, the fundamental biology of the respiratory tract, the fate of inhaled materials and the mechanisms by which they cause disease, and the means by which data produced in the laboratory can be used to estimate risks to human health. Disorders of the respiratory tract continue to be a major health concern, and inhaled toxicants are thought to contribute substantially to respiratory morbidity. As the largest laboratory dedicated to the study of basic inhalation toxicology, ITRI provides a national resource of specialized facilities, personnel, and educational activities serving the needs of government, academia, and industry.

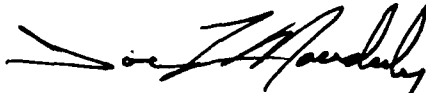
The Institute's multidisciplinary staff works in specialized facilities and takes a collaborative research approach to resolving scientific issues. ITRI is located on Kirtland Air Force Base East, approximately 10 miles southeast of Albuquerque, New Mexico. The more than 280,000 square feet of laboratory and support facilities include unique facilities and equipment for basic biological research and exposures of animals to all types of airborne toxicants. The staff of approximately 200 includes doctoral-level scientists in physical, chemical, biological, medical, and mathematical disciplines. Working with the scientists are highly trained scientific technicians, laboratory animal technicians, and a full range of support staff. The entire range of biological systems is employed, including macromolecules, cells, tissues, laboratory animals, and humans. The research includes both field and laboratory studies. Strong emphasis is placed on the quality of research and resulting data; the Institute has a Quality Assurance Unit and is fully capable of research in adherence to Good Laboratory Practices guidelines.

The Institute's scientific and support staffs are organized into disciplinary and functional scientific groups and support units (see Appendix B). The research is organized into programs which are administered by the Assistant Directors (see Appendix C). The programs are composed of projects having common research themes, but which typically cut across research disciplines. For example, the Pathogenesis Program contains projects oriented largely toward the development of non-cancerous respiratory tract disease, but the projects involve molecular biology, biochemistry, pathology, physiology, and inhalation exposure technology.

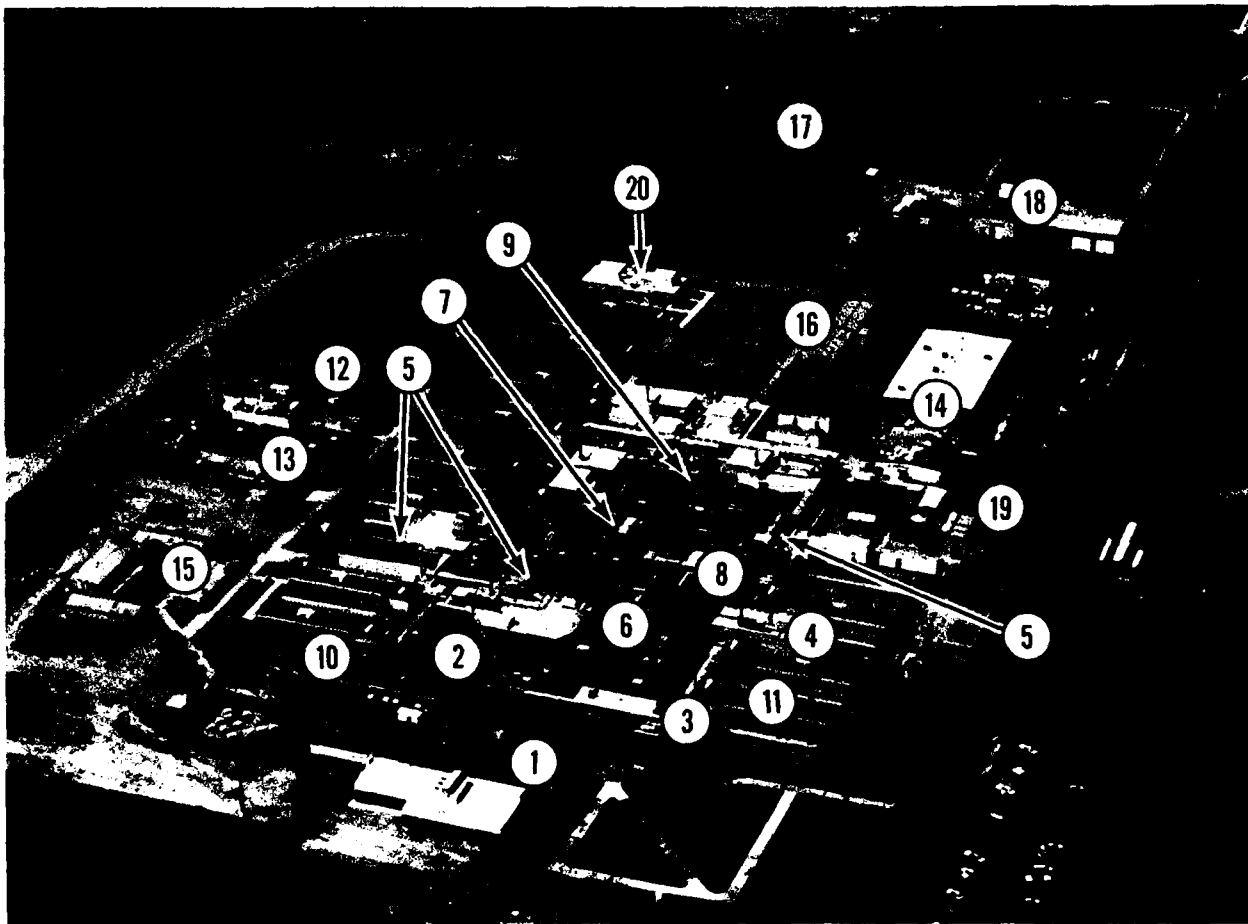
The Report

The papers in this report are organized along topical lines, rather than by research program, so that research within specific disciplines is more readily identified. The papers include summaries of research funded by both DOE and non-DOE sources, to represent the full scope of Institute activities. The source of funding is acknowledged for each paper. One section consists of summaries of research on the effects of injected actinides, conducted for DOE at the University of Utah. This effort is currently administered through ITRI's DOE contract. The appendices summarize the organization of the Institute's staff and research programs, publications and presentations by ITRI and University of Utah Scientists, seminars by visiting scientists, collaborations with scientists in other institutions, and a description of ITRI's educational activities.

A separate series of reports entitled, Annual Report on Long-Term Dose-Response Studies of Inhaled or Injected Radionuclides, summarize the design and status of the long-term studies of the health effects of radionuclides in dogs, conducted at ITRI and the University of Utah. This separate report also contains the status of each dog, the detailed tables which were previously included as appendices in the ITRI Annual Report. The dog report can be obtained from NTIS, and by request from the Institute.



Joe L. Mauderly, D.V.M.
Director



An aerial view of the Inhalation Toxicology Research Institute was constructed in several increments, starting in June 1962. The Institute's facilities consist of (1) an administrative area, including housing for the directorate, personnel, business and purchasing offices, editorial offices, a cafeteria, conference rooms, and health protection operations; (2) a central laboratory and office area, including aerosol science, radiobiology, pathology, chemistry and toxicology laboratories; (3) cell toxicology laboratories; (4) pathophysiology laboratories; (5) a specially designed and equipped chronic inhalation exposure complex with some laboratories suitable for use with carcinogenic materials; (6) an exposure facility for acute inhalation exposures to chemical toxicants and beta- and gamma-radiation; (7) exposure facilities for acute inhalation exposures to alpha-emitting radionuclides; (8) a veterinary hospital and facilities for detailed clinical observations; (9) small-animal barrier-type housing facilities; (10) a modern library and quality assurance facilities; (11) 13 kennel buildings, nine capable of housing 100 dogs each and four for housing 120 dogs each; (12) an analytical chemistry building; (13) an engineering and shop support building; (14) a receiving, property management, and storage building; (15) a health protection building; (16) several temporary laboratories; (17) sewage lagoons; (18) a hazardous waste storage and treatment facility; (19) standby power facility; and (20) animal quarantine facility.

PREVIOUS ANNUAL REPORTS

Selective Summary of Studies on the Fission Product Inhalation Program from July 1964 through June 1966;

LF-28, 1965

LF-33, 1966

Fission Product Inhalation Program Annual Report 1966-1972;

LF-38, 1967

LF-41, 1969

LF-44, 1971

LF-39, 1968

LF-43, 1970

LF-45, 1972

Inhalation Toxicology Research Institute Annual Report 1972-1990;

LF-46, 1973

LMF-84, 1980

LMF-115, 1986

LF-49, 1974

LMF-91, 1981

LMF-120, 1987

LF-52, 1975

LMF-102, 1982

LMF-121, 1988

LF-56, 1976

LMF-107, 1983

LMF-126, 1989

LF-58, 1977

LMF-113, 1984

LMF-129, 1990

LF-60, 1978

LMF-114, 1985

LMF-134, 1991

LF-69, 1979

Long-Term Dose-Response Studies of Inhaled or Injected Radionuclides 1988-1990;

LMF-128, 1989

LMF-130, 1990

LMF-135, 1991

**I. CHARACTERIZATION OF AIRBORNE MATERIALS
AND GENERATION OF
EXPERIMENTAL EXPOSURE ATMOSPHERES**

STATISTICAL LIMITATIONS IN THE SENSITIVITY OF CONTINUOUS AIR MONITORS FOR ALPHA-EMITTING RADIONUCLIDES

M. D. Hoover and G. J. Newton

Design and implementation of a technically defensible air monitoring program for alpha-emitting radionuclides require an understanding of the inherent statistical limitations of alpha continuous air monitors (CAMs). The basic limitations arise because radioactive decay is a statistical process in which the fundamental unit is the rate of decay. This rate can be described by a Poisson distribution in which (1) the number of possible decays in any unit of time (the rate) is not limited to a fixed number, (2) the decays are independent (the number of decays in one unit does not affect the number in other units), and (3) the average number of decays per unit of time remains the same from unit to unit.

In a simple example, assume that a CAM operates under the following conditions: the plutonium air concentration is 4.44 dpm/m³ (1 derived air concentration, or DAC, for soluble forms of plutonium-239), the flowrate is 0.0283 m³/min (1 cfm), and the detection efficiency is 0.20 cpm/dpm (typical for a 2.5-cm diameter filter with a 2.5-cm diameter solid state detector). During an 8-h period with a concentration of 1 DAC, workers would receive an integrated exposure of 8-DAC-h. The U.S. Department of Energy's Radiological Control Manual requires that alpha CAMs used in DOE facilities be capable of triggering an alarm when presented with an 8-DAC-h exposure under laboratory conditions (low radon progeny concentration and low airborne dust concentration). The average plutonium count rate seen by the CAM under these conditions would be:

$$(4.44 \text{ dpm/m}^3) * (0.0283 \text{ m}^3/\text{min}) * (480 \text{ min}) * (0.2 \text{ cpm/dpm}) = 12 \text{ cpm} . \quad (1)$$

By the nature of Poisson statistics, the square root of the average count rate is a good approximation of the standard deviation of the count rate. That is, 68% of the time, the observed plutonium count rate, n_i , will be in the range $[n - n^{0.5}]$ to $[n + n^{0.5}]$, and 95% of the time, n_i will be in the range of $[n - 2n^{0.5}]$ to $[n + 2n^{0.5}]$. Thus, we can expect to detect an average of 12 cpm, with a 68% confidence range of 12 ± 3.5 , and a 95% confidence range of 12 ± 7 . Note also that the relative uncertainty can be reduced by extending the counting period to take advantage of the fact that the ratio $n^{0.5}/n$ decreases as n increases. The major improvement in uncertainty occurs if we extend the counting period from 1 min (12 ± 7 cpm) to 5 min (60 ± 15 counts per 5 min, which is 12 ± 3 cpm). Longer counting periods reduce the response time of the CAM without providing substantially lower uncertainty.

The limitations of statistical uncertainties become more restrictive when we attempt to quantify concentration (DAC), rather than integrated concentration (DAC-h). Measuring concentration is useful when a CAM is expected to operate for more than an 8-h period. In such cases, the accumulation of plutonium from earlier in the sampling period must be subtracted from the more recent accumulation of plutonium. For example, the counts accumulated in sequential 20-min periods can be compared to estimate the air concentration in the most recent period. In 20 min, a 1-DAC concentration will provide an average of 10 new counts more than in the previous period (an accumulation of 0.5 cpm which is 1/24 of the 12 cpm which would result from sampling 1 DAC for 8 h). If there were no plutonium present in the previous interval, then the CAM should report 10 ± 6 new counts. The estimate of the concentration during the previous 20-min period would therefore be expected to range from 0.4 DAC to 1.6 DAC (assuming that the actual concentration is 1 DAC). If 8-DAC-h of plutonium had accumulated up to the start of the new interval, then the new counts would be in addition to 240 ± 31 counts from the previously collected material ($12 \text{ cpm} * 20 \text{ min} = 240 \text{ counts}$ with a 95% confidence interval of ± 31).

Because the statistical variation of the background is three times larger than the value of interest in this example, it would not be possible to detect the presence of the new plutonium. In fact, even with no addition of new plutonium, the statistical variation in the background would produce a fluctuating positive/negative report of the concentration. For example, if $240 - 31 = 209$ counts were reported in one interval and $240 + 31 = 271$ counts were reported in the next interval, then the apparent net counts in the new interval would be 62, or 6.2 DAC. During the next interval, it is likely that fewer than 271 counts would be reported, resulting in

a negative concentration value. Under these conditions, only an addition of counts equal to several times the variation in background (perhaps 100 new counts, or 10 DAC) would provide a reliable estimate of concentration.

The statistical situation becomes even more difficult when the calculations are adjusted for the natural radon progeny background aerosol. The most troublesome radionuclide is ^{218}Po , which has an alpha energy of 6.0 MeV. The thoron progeny radionuclide ^{212}Bi has the same energy, but is less prevalent. The lower energy tail of the ^{218}Po alpha energy distribution extends into the region of the 5.48-MeV alpha from ^{238}Pu and the 5.15-MeV alpha from ^{239}Pu . The ^{214}Po radon progeny (alpha energy 7.68 MeV) is also present. If ^{222}Rn is present at an ambient concentration of 1 pCi/L (2220 dpm/m³), and is in 50% equilibrium with its daughter radionuclide ^{218}Po (typical for indoor conditions), then the ^{218}Po concentration will be 0.5 pCi/L (1110 dpm/m³). Since those concentrations are substantially greater than the 4.44 dpm/m³ DAC for ^{239}Pu , gross alpha counting cannot be used to reliably detect plutonium in the presence of ambient radon progeny. Some sort of correction algorithm must be used to subtract the lower energy tail of the ^{218}Po peak (about 1/5 of the ^{218}Po activity) from the plutonium region of interest (ROI).

The most widely used algorithm for radon progeny background subtraction counts the decays in each of four energy ROIs and relates them by the following equation:

$$\text{Pu counts} = \text{ROI}_1 - k * \text{ROI}_2 * \text{ROI}_3 / \text{ROI}_4 , \quad (2)$$

where ROI_1 covers the energy range for the plutonium isotopes, ROI_2 covers the upper tail of the ^{218}Po peak, ROIs-3 and 4 cover the lower and upper tails of the ^{214}Po peak, and k is an empirically determined factor based on the ratio of counts in the four ROIs when no plutonium is present.

In the absence of plutonium, the four-region algorithm nominally reports a plutonium accumulation of 0 ± 5 cpm (0 ± 3 DAC-h), when a 1-min averaging period is used, and when the ambient radon concentration is around 1 pCi/L. The uncertainty becomes greater at higher radon progeny concentrations.

To more fully estimate the statistical limitations of all the factors described above, we used a PC-based Monte Carlo forecasting program called Crystal Ball (Decisioneering, Inc., Boulder, CO). Crystal Ball runs within the Microsoft Excel spreadsheet in the Microsoft Windows environment. Assuming Poisson statistics, we selected a number of plutonium and radon progeny concentration conditions that might be encountered in the workplace, and used Crystal Ball to simulate how the CAM might handle them. We provided the mean decay rate for each of the plutonium and radon concentrations. Crystal Ball then selected a random value from each Poisson distribution in the calculation, and calculated the plutonium cpm result for that trial. This Monte Carlo approach produced minute-by-minute reports typical of those expected from a CAM sampling under the given conditions. Long simulations (an accumulation of 1000 trials, for example) provided the average statistical uncertainty for the reported plutonium concentration under the selected conditions.

Table 1 summarizes the statistical uncertainties for various radon and plutonium concentrations of interest in the workplace. Figures 1A and 1B illustrate the individual forecasts produced by Crystal Ball. This approach should be useful for understanding the limitations of CAMs and planning for their appropriate use. Note that other uncertainties related to sampling flowrate, sample collection efficiency, uniformity of collection on the filter, and detection efficiency will further contribute to the overall uncertainty in CAM performance.

Table 1
 Statistical Limitations (Expected reporting values in cpm and 95% confidence intervals)
 for Alpha Continuous Air Monitors
 at Different Plutonium and Radon Progeny Concentrations*

	No Plutonium Present	0.3 DAC-h Plutonium	1 DAC-h Plutonium	8 DAC-h Plutonium	24 DAC-h Plutonium
No Radon Progeny	0 ± 0 cpm	0.5 ± 1.3	1.5 ± 2.3	12 ± 6	36 ± 12
0.1 pCi/L Radon Progeny	0 ± 2	0.5 ± 2	1.5 ± 3	12 ± 6	36 ± 12
1 pCi/L Radon Progeny	0 ± 5	0.5 ± 5	1.5 ± 6	12 ± 8	36 ± 13
2 pCi/L Radon Progeny	0 ± 7	0.5 ± 7	1.5 ± 7	12 ± 9	36 ± 14
5 pCi/L Radon Progeny	0 ± 12	0.5 ± 12	1.5 ± 12	12 ± 13	36 ± 16
10 pCi/L Radon Progeny	0 ± 16	0.5 ± 16	1.5 ± 16	12 ± 17	36 ± 19

*12 cpm corresponds to a plutonium accumulation of 8 DAC-h.

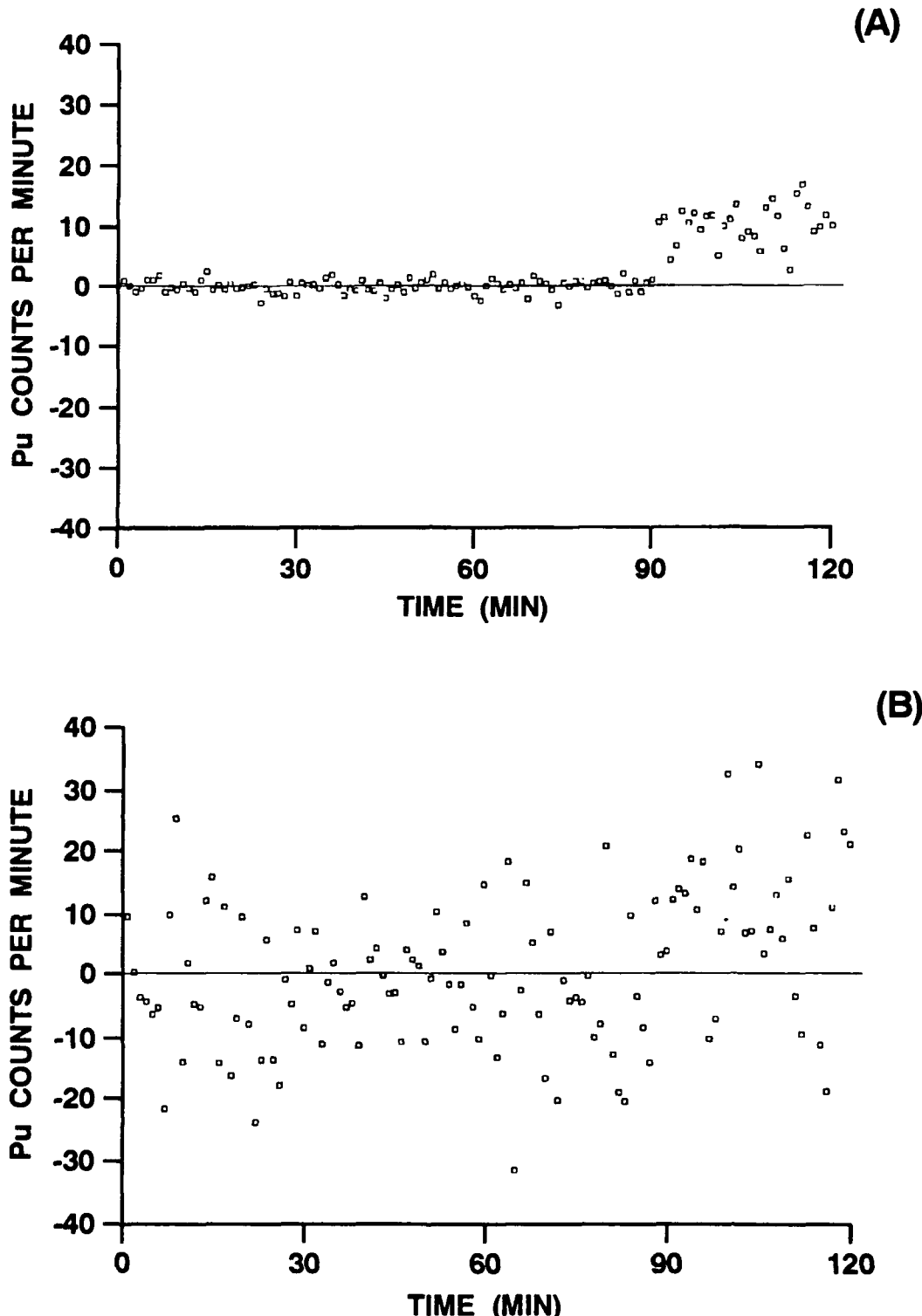


Figure 1. Monte Carlo simulations of minute-by-minute reports for an alpha continuous air monitor. In panel (A) radon progeny are sampled at 0.1 pCi/L for 90 min, followed by an instantaneous release of 8-DAC-h of plutonium. The 8-DAC-h release is easily distinguished. In panel (B) radon progeny are sampled at 10 pCi/L for 90 min, followed by an instantaneous release of 8-DAC-h of plutonium. The 8-DAC-h release is difficult to distinguish because of the statistical variation in the background.

(This research was conducted under DOE Contract No. DE-AC04-76EV01013 with funding from DOE's Assistant Secretary for Environment, Safety and Health, and Martin Marietta Energy Systems Y-12 Plant.)

UPDATE ON SELECTION AND USE OF FILTER MEDIA IN CONTINUOUS AIR MONITORS FOR ALPHA-EMITTING RADIONUCLIDES

M. D. Hoover and G. J. Newton

In our 1990-91 Annual Report (p. 16), we described acceptable performance criteria for filters to be used in continuous air monitors (CAMs) for alpha-emitting radionuclides, and we evaluated candidate filters. We concluded that a fiber-supported, teflon membrane filter (such as the Fluoropore filter from Millipore Corporation, Bedford, MA) would be the best choice for use in alpha CAMs if a distinctive colored backing could be developed for the support side. A clearly visible difference between the smooth collection side and the fibrous support side is needed because collection of alpha-emitting particles on the fiber side leads to loss of resolution due to unacceptably broad energy spectra. We also noted that it would be useful to have an acceptable alternative filter that could be dissolved for chemical analyses. This year, we report that a suitable black-fiber backing has been developed for the Fluoropore filter and that the Millipore AW-19 membrane filter has been identified as an acceptable alternative when a dissolvable filter is needed. Some of the tradeoffs in making these selections are described.

Table 1 summarizes our evaluations of filters for use in solid-state detector/multichannel analyzer CAMs to determine the alpha energy spectrum from particles collected on a filter. Tradeoffs can be seen in three areas: (1) sharpness of the alpha energy spectrum so that alpha disintegrations of plutonium or uranium can be distinguished from the higher-energy disintegrations of naturally occurring radon progeny such as ^{218}Po , (2) high efficiency for particle collection so that the results are not biased by sample losses, and (3) low pressure drop so that samples can be collected at reasonably high flowrates of 25 to 60 L/min (1 to 2 cfm). Radon progeny collection results are normalized to those of the Millipore SMWP, 5- μm pore size, mixed cellulose ester filter, because the good front-surface collection characteristics of the SMWP made it the early filter of choice for use in alpha CAMs. Collection efficiency for the SMWP over the size range 0.035 μm to 1.0 μm aerodynamic diameter is 98.1% to greater than 99.99% (Liu, B. Y. H. *et al.* In *Aerosols in the Mining and Industrial Work Environments*, Ann Arbor Science, Ann Arbor, MI, p. 989, 1983). In light of the demonstrated equivalence or superiority of the more rugged alternatives, the fragile SMWP is no longer recommended for use in alpha CAMs. Particle collection efficiency and gravimetric confirmation of particle mass collected with the SMWP filter are unreliable because of breakage of the SMWP filter under field conditions.

CAM users are free to select from a number of suitable filters, as long as they calibrate their instruments with the selected filter. Filters other than those we evaluated may also be selected if they are shown to provide suitable ruggedness, spectral quality, efficiency, and pressure drop. The Versapor-3000 (an acrylic copolymer on a non-woven nylon fiber support, Gelman Sciences, Ann Arbor, MI) provides a lower pressure drop and has a performance similar to that of the Millipore SMWP. The Durapore 5- μm pore size polyvinylidene fluoride membrane filter from Millipore can also be considered, although it provides a poorer spectral quality. All types of fiber filters are unacceptable due to poor spectral quality from burial of particles in the fiber bed. Small-pore filters are unacceptable because of their high pressure drop.

The best overall performance is from the teflon membrane filters such as the Fluoropore filter (polytetrafluoroethylene membrane with a polypropylene fiber backing). Spectral performance of the 3- μm pore size Fluoropore filter is slightly better than that of the 5- μm pore size Fluoropore filter, but the larger pore size version was selected for use with the high contrast backing because it provides a significantly lower pressure drop (less than half) with only a third less spectral quality. It is important to note that filters are not sieves, and that particles much smaller than the pore size are collected by diffusion and impaction mechanisms. Investigators such as Lindeken *et al.* (*Health Phys.* 10: 495, 1964) have demonstrated that, compared to filters with submicrometer pore size, large-pore membrane filters show no serious sacrifice in collection efficiency until the pore diameters exceed 5 μm . Thus, larger pore filters are preferred in many applications because they retain good particle collection efficiency with a lower pressure drop, which allows longer sampling times before the sampling rate is degraded by pressure buildup across the filter (Liu *et al.*, 1983).

Table 1
Characteristics of Filters Evaluated for Use in Alpha Continuous Air Monitors

Filter Type	Filter Composition and Durability	Typical Flow Rate (L/min per cm ²) ^a	FWHM of the Po-218 PEAK (keV) ^b	Relative Radon Progeny Counts in the Pu ROI ^c	Relative Radon Progeny Collection Efficiency ^d
MILLIPORE SMWP 5.0 µm pore size Millipore Corporation, Bedford, MA (\$ 72.60/100)	mixed esters of cellulose acetate and cellulose nitrate (fragile; electrostatic; both sides similar)	16	670	1	1
MILLIPORE AW19 5.0 µm pore size - Prefilter Millipore Corporation (\$ 33.20/100)	homogeneous microporous polymers of cellulose esters formed around a cellulose web (rugged; both sides similar)	16	470	0.57	0.99±0.01
DURAPORE 5.0 µm pore size Millipore Corporation (\$ 78.20/100)	polyvinylidene fluoride (rugged; both sides similar)	14	790	1.55	0.67±0.01
FLUOROPORE 3.0 µm pore size Millipore Corporation (\$ 231.00/100)	polytetrafluoroethylene bonded to polypropylene high-density fibers (rugged; front is membrane; back is fibers; sides barely distinguishable by naked eye)	23	350	0.47	1.04±0.02
FLUOROPORE 5.0 µm pore size Millipore Corporation (\$ 89.00/100)	polytetrafluoroethylene bonded to polypropylene high-density fibers (rugged; front is membrane; back is fibers; sides distinguishable by naked eye - high contrast backing)	59	460	0.67	0.96±0.04
VERSAPOR 3000 3.0 µm pore size Gelman Sciences, Ann Arbor, MI (\$ 59.00/100)	acrylic copolymer on a nylon fiber support (rugged; both sides similar)	25	590	0.94	0.75±0.02
GELMAN A/E GLASS 1.0 µm pore size Gelman Sciences (\$ 24.00/100)	borosilicate glass fiber without binder (breakable during handling; both sides similar)	25	≥ 1000	1.31	0.92±0.01
WHATMAN EPM 2000 0.6 µm particle retention Whatman LabSales, Hillsboro, OR (\$ 20.00/100)	borosilicate glass microfiber without binder (breakable during handling; both sides similar)	20	≥ 1000	1.48	1.00±0.03
WHATMAN 41 20-25 µm particle retention Whatman LabSales (\$ 10.25/100)	cotton cellulose filter paper (rugged; currently used primarily for liquid filtration; both sides similar)	25	≥ 1500	1.65	0.42±0.01
NUCLEPORE 0.6 µm pore size VWR Scientific, Pleasanton, CA (\$ 75.00/100)	polycarbonate membrane (rugged; thin; very electrostatic; currently used primarily for liquid filtration; collection side recommended by mfr. is the shiny side)	4	500	0.89	0.85±0.02
MILLIPORE (Black) 0.8 µm pore size Millipore Corporation (\$ 110.00/100)	mixed esters of cellulose (fragile; electrostatic; collection side is darker)	7	520	0.91	1.05±0.01

^aFlow rate determined under vacuum at 5 psig.

^bFWHM is the typical full width at half maximum of the Po-218 peak obtained during sampling of room air at ITRI.

^cRadon progeny background counts in the Pu region of interest for the filter of interest, divided by similar counts obtained simultaneously on a Millipore SMWP filter.

^dTotal radon progeny background counts on the filter of interest, divided by similar counts obtained simultaneously on a Millipore SMWP filter. Mean and standard error for five replicate tests.

To confirm the particle collection efficiency of the new, high-contrast backed Fluoropore filter, we arranged with Dr. B.Y.H. Liu (University of Minnesota, Minneapolis, MN) for penetration tests to be conducted using the method in Liu *et al.* (1983). He reported collection efficiency for the 5- μm pore-size filter to be 98.3% to greater than 99.99% over the size range 0.03 μm to 1.0 μm diameter. He also confirmed the collection efficiency for the standard 3- μm pore-size Fluoropore filter to be 99.90% to greater than 99.99% over that same size range. In addition, we used a plutonium dioxide aerosol at ITRI to conduct five aerosol penetration tests of 2.5-cm diameter Fluoropore filters operated at 28.3 L/min. The radioactivity of plutonium dioxide aerosol (physical diameter 0.3 μm , aerodynamic diameter 1.0 μm , geometric standard deviation 1.6) collected on each filter was compared to the radioactivity that penetrated to a backup filter. Efficiency was $99.94\% \pm 0.03\%$, which confirms the excellent performance of the new filter.

In addition to completing our evaluation of the high contrast Fluoropore filter, we continued to evaluate other filters for use in CAMs. In some applications, it is useful to be able to dissolve the filter and its collected particles in order to do elemental or radiochemical analyses. The Millipore AW-19 has a spectral quality similar to the Fluoropore filters and is an excellent choice in such cases. It is an inexpensive, rugged filter which consists of homogeneous microporous cellulose ester polymers formed around a cellulose web. It readily dissolves in nitric acid. Its drawback is that its pressure drop is approximately four times higher than that of the 5- μm pore size Fluoropore filter. The high-contrast backed Fluoropore filter remains the best overall choice for general use.

(This research was conducted under DOE Contract No. DE-AC04-76EV01013 with funding from DOE's Rocky Flats Plant under Purchase Order No. 67-517DD.)

STUDIES OF THE HOMOGENEITY OF PARTICLE COLLECTION IN ALPHA CONTINUOUS AIR MONITORS

G. J. Newton, M. D. Hoover, and W. C. Griffith

Calibration of monitoring instruments for airborne radioactivity is fundamental to a defendable health protection quality assurance program. Use of alpha spectroscopy-based instruments for real-time plutonium monitoring in the workplace requires a thorough understanding of the spatial deposition of collected alpha-emitting particles on the filters and the resultant alpha spectrum. The net alpha-counting efficiency is determined using an electroplated alpha source of the same size (diameter of the active area should correspond to the collection area of the filter in the continuous air monitor [CAM]) and have verified homogeneity of the alpha radioactivity per unit area of the source. Because deposition of airborne, alpha-emitting radioactive particles is also assumed to be uniform across the filter, it is essential that the homogeneity of the collected particles on the surface of the CAM filter be determined.

Previously, we developed an experimental, automated, particle-imaging system for locating (X,Y or R, θ coordinates) monodisperse, fluorescent, polystyrene latex (PSL) microspheres on filters (1990-91 Annual Report, p. 10). The imaging system includes an 80486-based personal computer (PC) which controls the motor-driven stage (X and Y coordinates) of an optical microscope, a charge-coupled-device attached to the microscope that serves as a detector for the fluorescent particles, and an epi-fluorescent, tunable ultraviolet light source. Filters containing collected PSL particles are mounted between glass plates and loaded onto the motor-driven stage; a program on the PC determines the location of all particles on the filter. The system automatically (a) moves the stage to a position, (b) records the coordinates of each particle in a pre-defined field of view, and (c) moves to the next position.

Monodisperse "Fluoresbrite" PSL microspheres (Polysciences, Inc., Warrington, PA) have been available with fluorescent dyes in bright-blue (excitation max. 365 nm, emission max. 468 nm), yellow-orange (excitation max. 554 nm, emission max. 580 nm), and yellow-green (excitation max. 458 nm, emission max. 540 nm). Most of our studies used the yellow-green dye and nominal particle diameters of 10, 6, 3, and 1 μm . The standard deviation of the geometric diameter was approximately 3%. However, Polysciences, Inc. can no longer supply monodisperse 10 μm diameter yellow-green particles. Therefore, midway through the studies, bright-blue 10 μm particles were used in place of the yellow-green labeled PSL particles.

The imaging software, OPTIMAS (BioScan Corporation, Edmonds, WA), is user-friendly and was designed for a Windows environment. OPTIMAS extracts data from the images and saves it as ASCII files. The software provides a flexible sampling scheme to include: (a) scanning of the entire filter surface; (b) scanning of a selected area; or (c) sampling of preselected fields. Ordinary spreadsheets cannot store all the positions of a typical scan which normally requires from 50,000 to 250,000 positions. Therefore, the ASCII files are moved to a UNIX workstation capable of handling the large (2-8 MB) files.

Preliminary studies indicated that the reproducibility of the particle count was questionable. Repeat scans of individual filters and single fields on filters indicated decreased detection of particles even though the particles were still visible to the eye. Early efforts focused on depth-of-field relationships. Depth-of-field for the charge-coupled detector is more restrictive than for the human eye and becomes increasingly important at higher magnifications of the optical microscope where downward drift in the Z direction affects focus. Efforts to determine the cause of the lack of reproducibility finally focused on the alignment of the mercury vapor lamp. Once all of the optical alignment problems were addressed, the scanning system yielded very reproducible results, and there were no losses of particles for repeat scans.

We also investigated the possibility of using nonlabeled plain PSL microspheres. By using a filter having a dark substrate and modifying the threshold and contrast controls in the OPTIMUS software, enough contrast was obtained to count plain PSL particles. This capability will extend the useful range of the scanning system.

Candidate CAMs have been tested to quantify the level of homogeneity of collected PSL particles across the surface of the CAM filters. Our results suggest that it may be necessary to modify the alpha-counting efficiency of candidate CAMs because of nonhomogeneous particle collection. This is a multi-step process that includes: (1) determining the net alpha-counting efficiency using a homogeneous electroplated alpha source of the same size; (2) determining the homogeneity of the collected particles on the CAM filter using monodisperse PSL fluorescent microspheres; and (3) calculating a net counting efficiency based on the particle deposition patterns on the filter and the relationship of alpha-counting efficiency vs. radius of the active area of the CAM filter.

Figure 1 shows results for the Eberline Alpha 6 CAM (Eberline Instruments, Santa Fe, NM) with an inline sampling head. Panels A and B show results for the CAM collecting 10 μm diameter particles onto (A) 25 mm and (B) 42 mm diameter collection areas of a 47 mm diameter membrane filter at a sampling flow rate of 56.6 L/min. Both of the sets of tests with the Eberline Alpha 6 used a 25 mm diameter detector. Homogeneity of particle deposition was quite uniform. Panel C shows results for collecting 6 μm diameter particles in a prototype sampling head that introduced the particle-laden air through a narrow slit which caused the particles to initially flow parallel to the plane of the filter. Apparently, inertial forces carried the particles toward the far side of the collection area, resulting in a significantly nonhomogeneous particle collection pattern. Results of correcting the gross alpha-counting efficiencies for nonideal particle collection change the net alpha-counting efficiency from: (1) 23% to 21% for the Eberline CAM collecting particles onto a 25 mm diameter collection area; (2) 10% to 9.5% for the Eberline CAM collecting particles onto a 42 mm diameter collection area; and (3) 30% to 9.3% for the prototype slit inlet CAM head onto a 42 mm diameter collection area. The Eberline tests used 10 μm diameter particles, whereas the other CAM was tested with 6 μm diameter particles. All CAMs will be tested with 10, 6, 3, and 1 μm diameter particles before a modified net alpha-counting efficiency can be calculated.

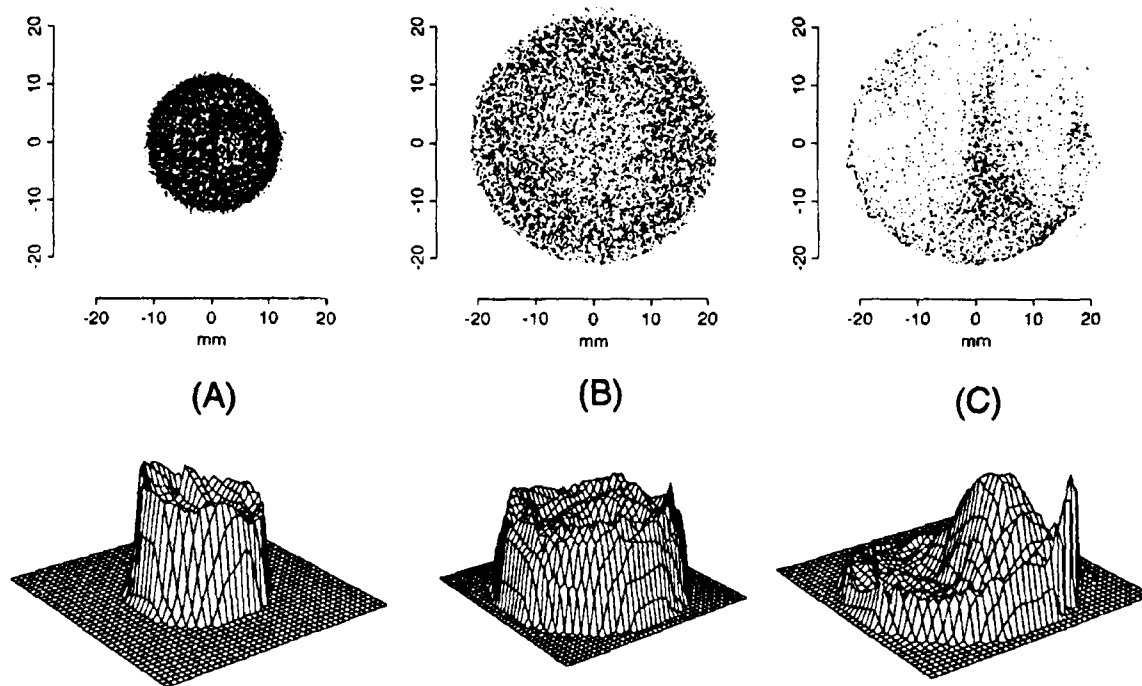


Figure 1. Results of particle collection homogeneity studies in two CAMs with an inline sampling head after sampling monodisperse fluorescent PSL microspheres. The figure is divided into three panels, A, B, and C. Each panel consists of a scatter plot of the collected monodisperse microspheres and a contour plot of the collected particles. The contour plots of the collected particles show the number of particles per mm^2 . Panels A and B show results for 10 μm diameter particles collected with an Eberline Alpha 6 with an inline sampling head. Filter collection areas are for (A) a 25 mm diameter area and (B) a 42 mm diameter area. Panel C shows results for 6 μm diameter particles collected onto a 42 mm diameter collection area with the prototype slit inlet CAM sampling head.

Using the automatic particle imaging system, the potential effect of nonhomogeneous collection of particles vs. net alpha-counting efficiency can be determined, and suitable CAM systems can be selected on a sound technical basis. We consider the current generation of CAMs to be prototypes, and we have shared the results of our homogeneity tests with the CAM manufacturers. We anticipate that the final versions will have corrected these nonideal collection characteristics. When completed, these results will provide a data base so that candidate CAMs can be ranked according to their adjusted net alpha-counting efficiencies. The scanning system for fluorescent PSL particles can be adapted to study other aerosol distribution patterns that can be determined by collection on filters.

(Research sponsored by the Assistant Secretary for Defense Programs and Field Office, Albuquerque, U. S. Department of Energy, under Contract No. DE-AC04-76EV01013.)

INFLUENCE OF SALT DUST ON ALPHA ENERGY SPECTRA AND DETECTION EFFICIENCY IN CONTINUOUS AIR MONITORS FOR ALPHA-EMITTING RADIONUCLIDES

M. D. Hoover and G. J. Newton

Accumulation of dust on the collection filter of an alpha continuous air monitor (CAM) reduces the energy of alpha radiation reaching the detector and may result in underestimation of the amount of plutonium on the filter. Interference from dust is not a concern for detection of sudden, large releases of plutonium because an alarm will occur before burial becomes significant. Concern is for the slow release of plutonium over a long period of time in a dusty environment. In previous work (1990-91 Annual Report, p. 20), we demonstrated that the Eberline Alpha-6 CAM (Eberline Instrument Corporation, Santa Fe, NM) can measure one Derived Air Concentration (DAC) of plutonium under laboratory conditions (low radon, thoron, and dust conditions) when integrated over 8 h (8 DAC-h). Here, we evaluated whether performance could be improved by decreasing the lower energy boundary of the plutonium region of interest (ROI); measured the detection efficiency of the Alpha-6 as a function of ROI setting for a range of salt and mylar burial conditions; and tested the ability of the Alpha-6 to provide a predictable alarm response to slow releases of plutonium in the presence of salt dust. This work was done to provide an improved technical basis for the use of CAMs at the DOE Waste Isolation Pilot Plant (WIPP) near Carlsbad, NM.

The Alpha-6 consists of a collection filter, a solid-state detector that faces the filter, and a 256-channel analyzer that records the energy of alpha particles that reach the detector. The lower energy discriminator of the multichannel analyzer is normally set to accept alpha emissions with energy greater than 2.7 MeV (emissions in channel 50 and above). Decreasing the lower energy discriminator below 2.7 MeV is possible, but interference from detector noise can become a problem at lower energies. The design of the Alpha-6 CAM allows the user to select an appropriate energy ROI for detecting alpha-emitting radionuclides of interest. The ROI originally recommended by the manufacturer for ^{239}Pu (5.16 and 5.11 MeV alpha energy) covered 4.2 to 5.3 MeV (channels 90 to 117). The ROI presently used at WIPP for monitoring ^{239}Pu and ^{238}Pu (5.50 and 5.46 MeV alpha energy) covers 4.3 to 5.6 MeV (channels 92 to 126). That window was selected because calibration tests with National Institute of Standards and Technology (NIST)-traceable plutonium sources (*Hoover, M. D. et al. Evaluation of the Eberline Alpha-6 Continuous Air Monitor for Use in the Waste Isolation Pilot Plant: Report for Phase II*, ITRI, Albuquerque, NM, 1990) showed that those channels captured 95% of the alpha emissions of ^{239}Pu and ^{238}Pu . Recognizing that channels 92 to 126 were selected for conditions without salt attenuation, the current study has evaluated the advantages of decreasing the lower energy boundary of the plutonium ROI so that alpha emissions attenuated by salt can still be detected.

We compared the standard plutonium ROI (channels of 92 to 126) to windows covering either channels 50 to 126 (2.7 to 5.6 MeV), or channels 65 to 126 (3.3 to 5.6 MeV). We determined the detection performance of the alternate ROIs by placing plutonium-239-laden filters (either 2.5-cm or 4.2-cm diameter collection area) in a standard Alpha-6 with a 2.5-cm diameter detector. Initial counting efficiencies were determined, and the changes in efficiencies were measured as known amounts of salt aerosol were collected on the filters. In addition, NIST-traceable ^{239}Pu sources (2.5-cm and 4.2-cm diameter active areas) were layered with Mylar film (E.I. du Pont de Nemours & Co., Wilmington, DL, 0.22 mg/cm² per layer) to confirm the general influence of mass loading on the detection efficiency for the alternate windows. Detection efficiency by the ZnS(Ag) counting method was also determined as a function of salt or Mylar loading.

Figures 1A and 1B illustrate how detection efficiency is reduced by the successive addition of energy-absorbing layers to 2.5-cm or 4.2-cm diameter plutonium samples. Taking into account density effects for alpha attenuation, one layer of Mylar corresponds to 0.36 mg/cm² salt. ZnS(Ag) counting had the highest overall detection efficiency because the scintillating material directly contacts the filter. Efficiency began at approximately 50% (nearly 100% of 2 Pi geometry) for unattenuated plutonium and decreased to a few percent for plutonium that had been covered by about 5.5 mg/cm² salt. Channels 50 to 126 provided the best performance of the Alpha-6 options. Channels 65 to 126 perform nearly as well, but was less efficient at higher mass loadings. Channels 92 to 126

were substantially poorer performers, especially at high mass loadings. For channels 50 to 126, plutonium detection remained significant until salt accumulation was greater than 3.6 mg/cm^2 (more than 10 Mylar layers), a factor of two improvement over detection in channels 92 to 126, which dropped to zero after accumulation of only 1.8 mg/cm^2 salt (five layers of Mylar). Note that a salt loading of 1.8 mg/cm^2 will accumulate on a 2.5-cm diameter filter which samples an airborne salt concentration of 0.7 mg/m^3 at 28.3 L/min for 8 h. It was for that reason that WIPP established an operational limit of 0.2 mg/m^3 salt for CAM operation (Steinbruegge, K. B. *Waste Isolation Pilot Plant Alpha Continuous Air Monitoring System*, 1991) to ensure that plutonium attenuation would be negligible due to burial.

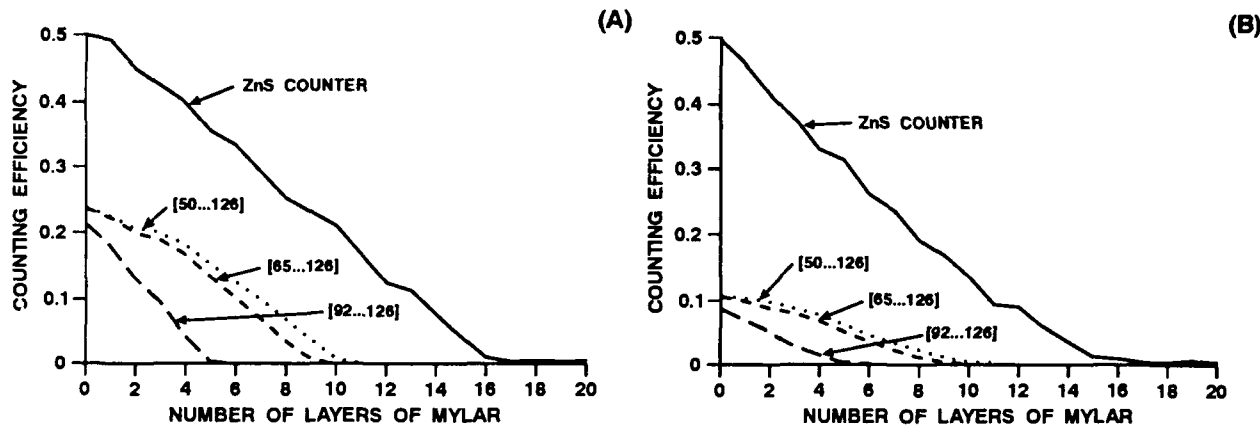


Figure 1. Detection efficiency as a function of mass attenuation for the ZnS(Ag) counting method and for different plutonium ROIs in an alpha CAM with a 2.5-cm diameter detector for (A) 2.5-cm diameter samples and (B) 4.2-cm diameter samples. Each Mylar layer (0.22 mg/cm^2) is equivalent to 0.36 mg/cm^2 salt.

Knowing the general influence of salt loading and ROI selection on plutonium detection, we challenged the Alpha-6 with a series of low-level plutonium and salt aerosols to confirm the adequacy of the WIPP operating requirement that salt concentrations be maintained below 0.2 mg/m^3 during plutonium handling operations. Homogeneous mixtures of known plutonium and salt concentration were nebulized and dried to provide the Alpha-6 with challenge aerosols simulating the accumulation of 8 DAC-h of plutonium in the presence of salt concentrations ranging from 0.1 to 0.6 mg/m^3 . The mass of salt collected was determined gravimetrically. The amount of plutonium collected during the test was confirmed by the ZnS(Ag) method. Expected and actual plutonium reports were compared for the alternate ROIs. Salt concentrations equivalent to 0.2 mg/m^3 for an 8-h period resulted in negligible attenuation of the collected plutonium alpha radiation. Some variation in the estimated and reported plutonium counts was noted due to Poisson counting statistics. Underreporting of the collected plutonium increased with increasing salt concentration, and could be predicted based on the accumulation of salt on the filter. As shown in Figure 2A for a test that simulated 14 DAC-h of plutonium in the presence of 0.6 mg/m^3 salt, the plutonium count per minute (cpm) reported in the original plutonium ROI was 60% low and would not have triggered the alarm setpoint of 8 DAC-h (five sequential reports above 12 cpm), even when the plutonium accumulation was more than twice the 8-DAC-h limit. Reporting in the ROI covering channels 50 to 126 (Fig. 2B) was accurate and would have triggered an alarm.

We recommend that the expanded plutonium ROI be implemented at WIPP. This will require a recalculation and minor adjustment to the CAM's calculation algorithm (k-factor), but the adjustment should be small because radon progeny interference is at higher energy and there is negligible radon progeny interference in the expanded ROI. We also recommend a combination of filter weighing and ZnS(Ag) counting as a simple method to retrospectively confirm the plutonium content of filter samples collected in the CAMs. We further recommend that the expanded ROI be used as a prudent measure even in areas where dust interference is not expected. It will provide an added safety factor at a negligible cost.

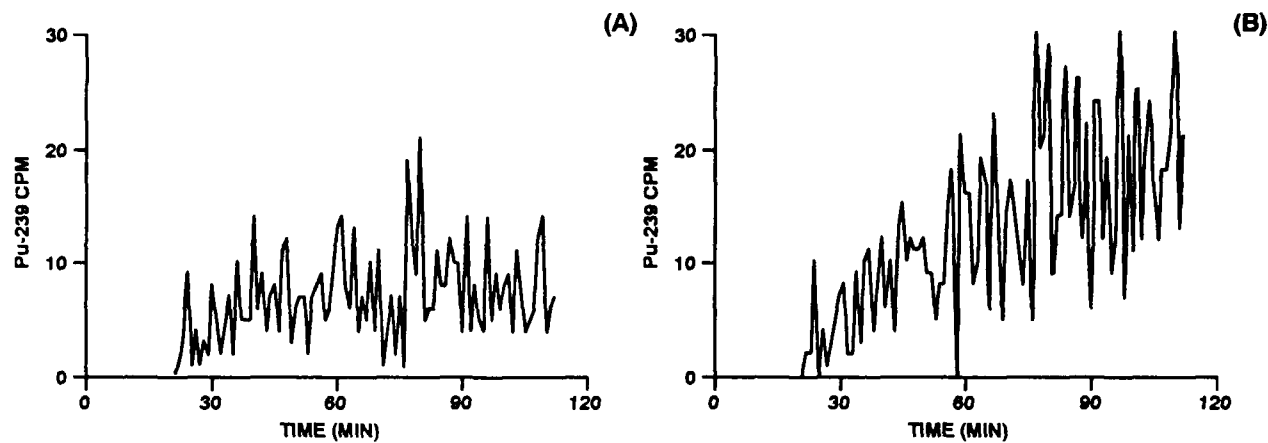


Figure 2. Plutonium cpm reported in (A) the standard plutonium ROI of channels 92 to 126, and (B) in the modified plutonium ROI of channels 50 to 126 by an Alpha-6 CAM with a 2.5-cm diameter detector and 2.5-cm diameter filter operating at 28.3 L/min during a slow release of ^{239}Pu and salt at a concentration equivalent to 0.6 mg/m³ salt and an accumulation of 14 DAC-h (19 cpm) of plutonium. At this salt concentration, the plutonium cpm was underreported in the standard ROI, but correctly reported in the modified ROI.

(This research was sponsored by the U.S. Department of Energy Waste Isolation Pilot Plant Office under DOE Contract No. DE-AC04-76EV01013.)

A RADON PROGENY GENERATION SYSTEM FOR PERFORMANCE EVALUATIONS OF ALPHA CONTINUOUS AIR MONITORS

G. J. Newton, M. D. Hoover, and Y. S. Cheng

Use of alpha spectroscopy-based instruments for real-time monitoring of airborne plutonium in the workplace requires knowledge of the interferences caused by radon progeny. The DOE Order 5480.11 along with DOE/EH-0256T (DOE's Radiation Control Manual) and 10 CFR 835 (draft 12/9/92) are the operative orders for ES&H in DOE facilities. In 5480.11, a target sensitivity for plutonium alpha continuous air monitors (CAMs) is listed as 8 DAC-h. A derived air concentration (DAC) is obtained by dividing the annual limit of intake by the amount of air assumed to be inhaled (2,500 m³) by a reference man during an assumed 2,000 hour working year. A DAC-h is an exposure at a concentration of 1 DAC for 1 h. For Class W forms of ²³⁸Pu and ²³⁹Pu, the DAC is equal to 3×10^{-12} and 2×10^{-12} $\mu\text{Ci}/\text{mL}$, respectively. Thus, 8 DAC-h for Class W forms of ²³⁹Pu is equivalent to 35.52 dpm/m³. This required sensitivity must be achieved in the presence of naturally occurring, alpha-emitting radon progeny, ²¹⁸Po and ²¹⁴Po, that can range from about 400 to 130,000 dpm/m³ (0.1 to 30 pCi/L). Because of the new sensitivity requirements for alpha CAMs, DOE operating contractors are faced with the selection and purchase of several thousand new generation CAMs that sample workplace atmospheres for airborne plutonium and other transuranic alpha emitters. Thus, tests at elevated radon progeny concentrations are needed to exercise radon progeny correction algorithms.

Challenge tests should be run with particulate radon progeny rather than with ²²²Rn gas. Furthermore, the relative equilibrium between ²¹⁸Po and ²¹⁴Po should be within ratios seen in actual workplace situations. Therefore, the radon progeny challenge aerosol system must include a vector aerosol to which the progeny can attach and provide holdup times adequate for ingrowth of the longer lived ²¹⁴Po. Without a vector aerosol, the unattached fraction would have very high diffusion coefficients and would "plate out" on the walls of the aerosol generation/delivery system.

For this project, we needed to conduct laboratory studies using a variable source of radon progeny in order to test the ability of alpha (CAMs) to correct the resultant spectrum of naturally occurring radon progeny alpha background for interference in a plutonium region-of-interest (ROI). These tests are required to: (1) demonstrate the CAM's ability to provide an adequate alarm for airborne plutonium in simulated environments of the nuclear weapons production facilities, (2) limit false alarms due to radon progeny, (3) verify the ability of the radon progeny correction algorithms to maintain "0" Pu counts in the Pu ROI when no Pu is present and when radon progeny concentrations range over levels encountered in the DOE production complex, and (4) determine the effects of dusty environments and elevated radon progeny concentrations that result in alpha peak width broadening and false plutonium counts. This type of information is needed to guide in the evaluation of candidate CAM systems.

A 55-gal barrel has been fitted to generate a low level radon progeny aerosol (Fig. 1). The barrel contains 12.2 kg of uranium mill tailings from the Church Rock Mine in New Mexico. The stated ²²⁶Ra concentration is 27.6 Bq/g or a total of 3.4×10^5 Bq of ²²⁶Ra. At equilibrium, the assumed 200 L headspace could contain 1.7×10^3 Bq/L if the emanation rate was 100%. However, a measurement of the ²²²Rn by an Eberline RGM-3 (Eberline Instruments, Santa Fe, NM) radon monitor indicated that the equilibrium radon concentration was about 4.8×10^2 Bq/L, suggesting that the true emanation rate is about 28%. This emanation rate could be expected for this mineral form. This particular setup enables us to reliably operate the radon progeny generator in the range of about 3.7×10^{-3} to 1.1 Bq/L (0.1 to 30 pCi/L). The system injects a vector aerosol into the headspace of the barrel and allows sufficient time for attachment of the radon progeny onto the vector particles to take place. We found 10-15 min to be adequate for a fan-stirred 200 L volume.

The vector aerosol generator is a small methyl-methacrylate chamber containing a burning oriental incense stick (this report, p. 40). Ventilation of the incense smoke generator is 500 mL/min by a peristaltic pump that pushes the smoke particles into the 55-gal drum. The challenge aerosol consisting of vector incense smoke particles onto which radon progeny are attached is pushed out of the 55-gal drum by the peristaltic pump to the line connected to the CAM being tested. Operation of the valve systems requires a checklist for proper sequence and valve positioning.

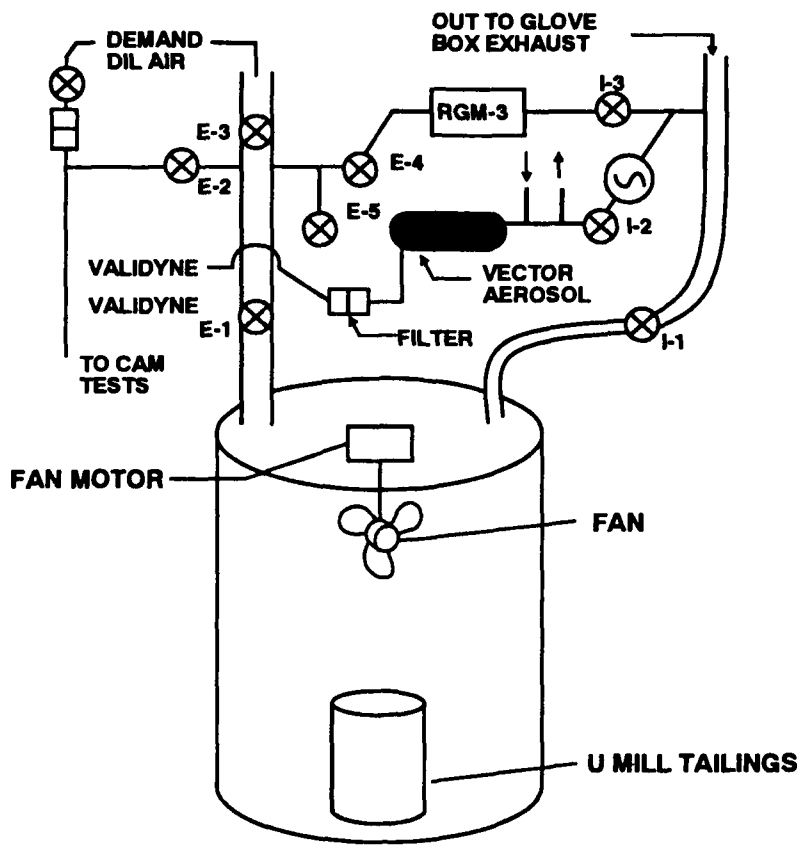


Figure 1. Schematic diagram of the aerosol control system on the 55-gal radon progeny drum fitted with the gas-tight top, stirring fan, and an open container of uranium mill tailings. The schematic shows the inlet and exhaust valves and the vector aerosol generator.

For operational considerations, we wanted to operate the system at a flow rate Q , through the vector aerosol generator of 0.5 L/min. This is also the flow rate through the radon barrel and also corresponds to the washout flow rate. By keeping Q as small as possible, effects on the concentration of ^{222}Rn in the barrel due to washout will be minimized. The radioactivity concentration for ^{222}Rn in the barrel after equilibrium obtained for ^{226}Ra and ^{222}Rn is 13,000 pCi/L. If the radon is washed out of the barrel by continuously flushing at a flow rate of 60 L/min for 5.0 min, then washout is stopped, ^{222}Rn will begin ingrowth indicated by

$$C_t = C_\infty (1 - e^{-\lambda t}), \quad (1)$$

where C_t = the concentration of radioactivity at time t , λ = the decay constant of ^{222}Rn , and C_∞ = concentration of radioactivity at time t_∞ . Rate of ingrowth is 5.92×10^{-2} Bq/min. Washout dilutes the concentration as seen by

$$C_{tw} = C_t e^{-\frac{Qt}{V}}, \quad (2)$$

where C_{tw} = the concentration of radioactivity at time t , corrected for washout, Q = the washout volumetric flow rate, and V = the volume of system = ~200 L.

Ideally, we would solve for t by assuming a desired concentration of ^{222}Rn . However, the equation does not have an explicit solution. Therefore, we used a spread sheet (PlanPerfect, WordPerfect Corp., Orem, UT)

to calculate the buildup of ^{222}Rn in 1-min increments. By looking up the closest time, t , to yield the required ^{222}Rn concentration, we can obtain the starting conditions for a ^{222}Rn challenge to a CAM. The actual equation used in the calculations was

$$C(t) = \frac{G}{V\lambda_{dw}} (1 - e^{-\lambda_{dw}t}), \quad (3)$$

where C is the radon concentration in the drum, G is the effective radon generation rate from the mill tailings, V is the volume of the drum (L), and λ_{dw} is a new combined rate constant for radioactive decay and washout, given by

$$\lambda_{dw} = (\lambda_d + Q/V), \quad (4)$$

where λ_d is the radioactive decay constant for ^{222}Rn . If there is no radioactive decay, then λ_{dw} reduces to washout only. If there is no washout, then λ_{dw} reduces to radioactive decay only. If there is neither decay nor washout, then λ_{dw} is 0, and the equation reduces to $C(t) = Gt/V$. (Note that this occurs because the limit as λ_{dw} goes to 0 of $[(1 - \exp(-\lambda_{dw}t))]/\lambda_{dw}$ is t . The expansion used for $(1 - \exp(-\lambda_{dw}t))$ to calculate this limit is $(\lambda_{dw}t - \lambda_{dw}^2t^2 + \dots)$). Because Q/V is usually much greater than λ_d (1.26×10^{-4} L/m), $\lambda_{dw} \approx Q/V$.

To operate the system for a challenge concentration expressed as $^{222}\text{Rn}/\text{L}$, we: (1) selected the closest ingrowth time from the spreadsheet that yields the required concentration, (2) purged the barrel at 60 L/min for 35 min (10 air changes), (3) closed all valves and allowed ingrowth of radon progeny to begin, (4) started vector aerosol generation and began injecting particles into the drum, and (5) initiated CAM challenge tests. Because the flow rate from the drum is only 0.5 L/min, dilution is negligible, and the concentration of radon progeny remains relatively stable. The ratio of ^{214}Po to ^{218}Po observed at the Waste Isolation Pilot Plant and at the ITRI has been about 0.23:1, whereas that produced by the experimental test system has been about 0.25:1, a reasonable approximation of values seen in actual working environments. The system can produce a range of concentration, expressed as $^{222}\text{Rn}/\text{L}$ ranging from 5.9×10^{-2} to 4.8×10^2 Bq/L (1.6 to 1.3×10^4 pCi/L), depending on the time allowed for ingrowth since purge. This range of radon progeny concentration is more than adequate for the challenge tests for the CAMs, and the maximum concentrations achievable will make the system useful for basic studies on the dynamics of radon progeny aerosol behavior. Figure 2 shows excellent agreement between two alpha energy spectra from room air at the ITRI and from the radon progeny aerosol generation system.

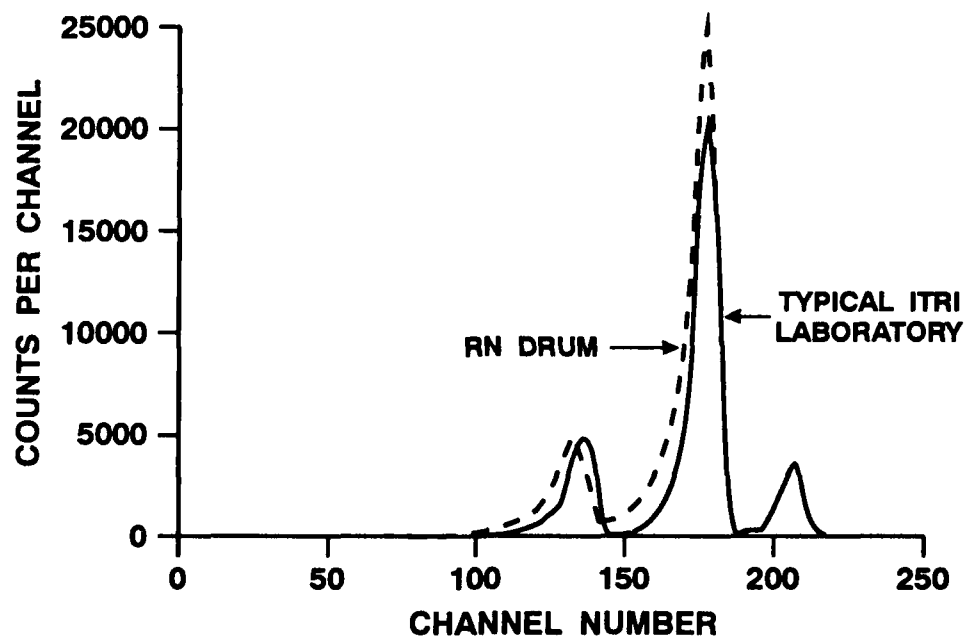


Figure 2. Comparison of radon progeny alpha pulse height spectra from room air (Room 301A) and from the radon progeny challenge system.

Alpha CAMs are important but are only part of a comprehensive health protection program in the DOE nuclear weapons fabrication facilities. The CAM tests with varying radon progeny concentrations are part of ongoing studies of the responses of candidate CAMs that will become part of the technical basis for selection and use of CAM systems in the DOE's plutonium and uranium handling facilities.

(Research sponsored by the Assistant Secretary for Environmental Restoration/Waste Management, U.S. Department of Energy, under Contract No. DE-AC04-76EV01013.)

DESIGN, CONSTRUCTION, AND TESTING OF A 54" AEROSOL CHAMBER FOR INSTRUMENT EVALUATION

E. B. Barr and Y. S. Cheng

Evaluation of sampling instruments is important in determining their efficiency and suitability for a specific use. It is particularly important that area or environmental samplers be evaluated in a manner which simulates the actual operating conditions. In order to best simulate environmental conditions, it is desirable to expose an entire instrument to a homogeneous aerosol with no sampling lines or probes on the inlet. We describe an aerosol chamber that provides an atmosphere for whole instrument evaluation and which is large enough to accommodate several instruments at a time. Due to the relatively large test section volume in the chamber (1.8 m^3), several features have been incorporated into the design to ensure that the aerosol concentration was uniform and stable.

We used a modified 54" exposure chamber. A schematic diagram of the chamber system is shown in Figure 1. The chamber's overall dimensions are 3 m H x 1.36 m W x 1.36 m L, with a mixing chamber and honeycomb flow straightener mounted above the effective sampling area (1.34 m W x 1.34 m L x 1 m H = 1.8 m^3 volume). The aerosol generation system is mounted directly on top of the mixing plenum; this provides a minimum distance from the generator to the chamber, thus minimizing line losses, particularly for large aerosols ($>5 \mu\text{m}$). Dilution air enters through opposing jets to ensure thorough mixing of the aerosol. A 10-inch boxer fan mounted beneath the aerosol entrance provides additional mixing. The aerosol flows through a 10 cm thick honeycomb structure to reduce turbulent flow and to present the sampling area with a well-defined downward air flow. To minimize spatial variation of concentration and size distribution, samplers are set up on a 76 cm diameter rotating platform. Rotational speed was set at 0.5 rpm to ensure that rotation did not affect sampler efficiencies.

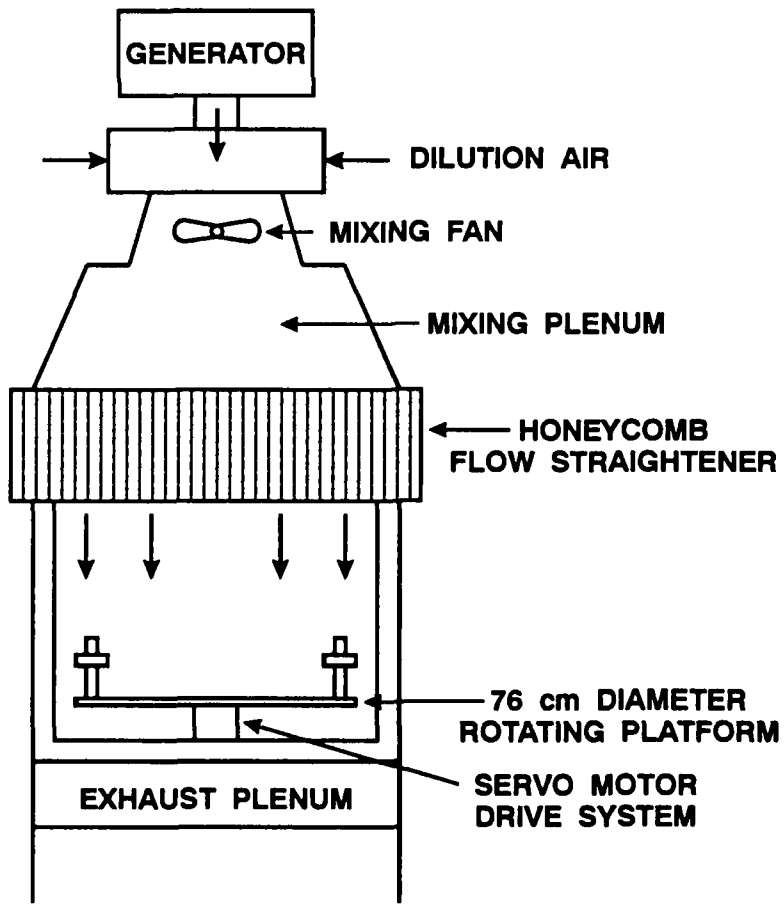


Figure 1. Modified 54" aerosol chamber.

The homogeneity and stability of a large test aerosol ($>10 \mu\text{m}$) has been evaluated. Eight 25 mm Zefluor filter samplers were placed in the test chamber, with the inlets in the vertical position, parallel to chamber inlet flow. Six samplers were placed on each arm of the turntable at the outside rim, and two were placed in the center of the turntable (see Fig. 2). Four test conditions were studied to investigate the effects of the two design components in the chamber for providing uniform aerosol concentration: (1) fan off and the turntable off (NF/NT); (2) fan on and the turntable off (F/NT); (3) fan off and the turntable on (NF/T); (4) fan and turntable on (F/T). A Lovelace multi-jet cascade impactor (LMJI) was set up in the chamber to measure the aerosol size distribution. The chamber flow was $1.4 \text{ m}^3/\text{min}$; this provided a face velocity of 1.3 cm/sec . Filter samplers were operated at 2 lpm for 2-h sample periods.

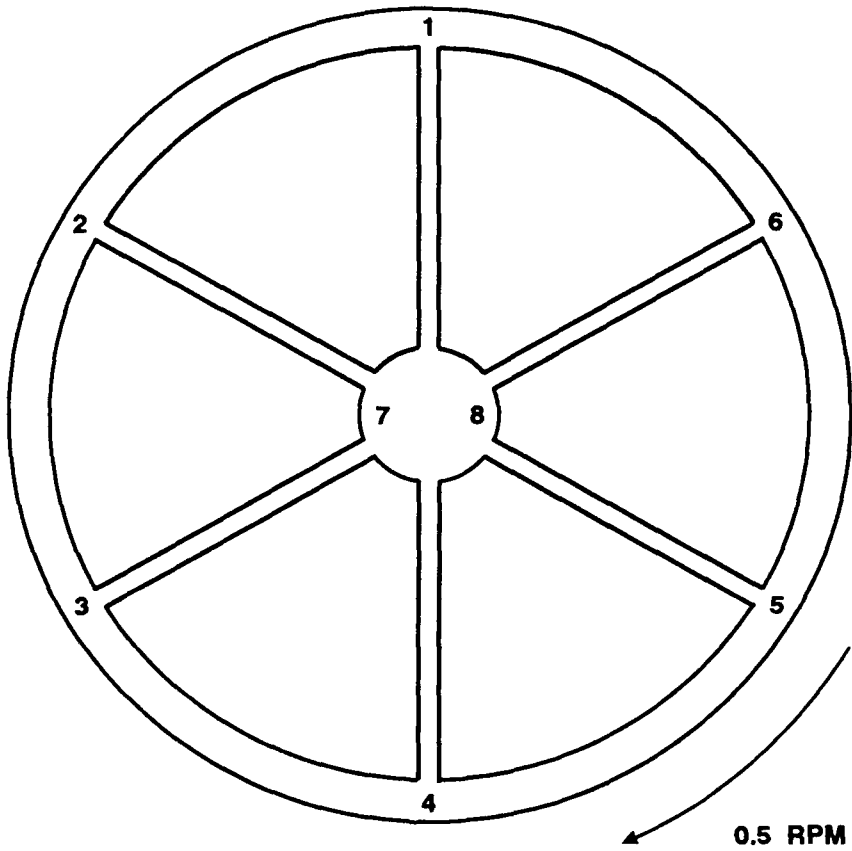


Figure 2. Rotating turntable and test sample positions.

Table 1 shows the results of test runs for the four test conditions. The concentration for NF/NT was 3.08 mg/m^3 compared to 1.86 mg/m^3 for F/NT, and the concentration was 3.62 mg/m^3 for NF/T compared to 1.87 mg/m^3 for F/T. When the fan was used, concentrations dropped by 40% and 48%, respectively. Also, the size distribution dropped from $9.9 \mu\text{m}$ to $6.8 \mu\text{m}$ for NF/NT compared to F/NT, and from $12.3 \mu\text{m}$ to $9.0 \mu\text{m}$ for NF/T compared to F/T. The %CV was reduced significantly when the fan was used without the turntable, but was not affected when the turntable was used.

The results indicate that although the fan helps to ensure a more homogeneous aerosol, a significant amount of aerosol is lost and mass median size is reduced. This suggests that the turbulent mixing of the fan affects the larger particles on the walls of the mixing plenum. Use of the rotating turntable with the fan did not affect concentration or size distribution, but did reduce the %CV, indicating that homogeneity of the test aerosol was improved with the turntable.

Table 1

Chamber Homogeneity and MMAD as a Function of Fan and Turntable Conditions

Sampling Position	Filter Concentration, mg/m ³			
	Fan off, Turntable off [NF/NT]	Fan on, Turntable off [F/NT]	Fan off, Turntable on [NF/T]	Fan on, Turntable on [F/T]
1	2.967	1.841	3.542	2.020
2	2.908	1.891	3.806	1.874
3	3.056	1.849	3.676	1.939
4	3.501	1.921	3.691	1.928
5	3.028	1.917	3.453	1.910
6	3.513	1.842	3.581	1.906
7	2.473	1.796	3.303	1.628
8	3.185	1.828	3.920	1.743
Mean	3.08	1.86	3.62	1.87
%CV ^a	10.9	2.4	5.4	6.7
LMJ MMAD, μm	9.9	6.8	12.3	9.0

^a%CV is defined as $\frac{\text{standard deviation}}{\text{mean}} \times 100$.

In summary, a test chamber was designed, constructed, and tested for generating homogeneous aerosols for use in evaluation of sampling instruments. The large testing volume allows several sampling devices to be tested simultaneously, and the rotating turntable ensures that the instruments are sampling a homogeneous atmosphere. The mixing fan which was intended to ensure greater mixing did improve aerosol homogeneity, but high wall losses for larger particles makes the fan inappropriate for aerosols in the 10 μm or larger size range. When the turntable is used without the fan, there is minimal reduction in the median size, and chamber homogeneity is improved.

(Research sponsored by the Office of Health and Environmental Research, U. S. Department of Energy, under Contract No. DE-AC04-76EV01013.)

CALIBRATION AND PERFORMANCE OF AN API AEROSIZER

Y. S. Cheng, E. B. Barr, I. A. Marshall, and J. P. Mitchell**

In studies of the behavior of airborne particulates in ambient and occupational environments, researchers have an increasing need to monitor the aerosol size distribution in real time. Recently, several instruments have been developed commercially based on the time-of-flight (TOF) principle. These instruments include the Aerodynamic Particle Sizer (APS33B; TSI, St Paul, MN) and the Aerosizer (API Mach II, manufactured by Amherst Process Instruments, Inc., Amherst, MA). They are near real-time instruments capable of high resolution. The nominal operating range of the Aerosizer is broader (from 0.5 to 200 μm aerodynamic diameter), and it is designed to sample particles in both aerosol and powder forms. A specially designed powder disperser can be attached to the Aerosizer inlet, enabling particles larger than 15 μm in aerodynamic diameter to be measured apparently without high losses in the inlet section, although such losses have yet to be quantified. Particles are accelerated in the Aerosizer by passing through a critical orifice at sonic flow. The Aerosizer is a relatively new instrument; therefore, little information is available concerning its performance. Hence, this study is important because it describes the first evaluation of two API units using spherical and nonspherical particles of well-defined shapes, enabling the effects of particle density, shape, and ambient pressure on the instrument response to be examined.

The experimental validation of the calibration curves is provided by the manufacturer using a few sizes of monodisperse spherical particles of polystyrene latex (PSL) (density = 1.05 g/cm³) and glass microspheres (density = 2.45 g/cm³). However, the calibration curves used in the data analysis have not been validated. Two API instruments located at our laboratory (ITRI; unit A) and at Winfrith Technology Centre (WTC; Unit B) were used in this study, and the experimental procedures are described below.

At ITRI, monodisperse PSL particles whose diameters varied from 0.5 to 136 μm together with glass beads whose sizes varied from 1.6 to 146 μm (Duke Scientific, Palo Alto, CA) were used as calibrants. Aerosols of the PSL particles smaller than 7 μm were produced using a Lovelace nebulizer, whereas larger particles were dried and placed in the powder disperser of the API before aerosolization. Size distribution and TOF measurements for each calibrant were recorded at the reduced ambient pressure in Albuquerque (625 mm Hg [83 kPa] and 20°C). The density of 1.05 g/cm³ was assumed for all sizes of PSL particles, whereas the pycnometer-measured density was used for each size of glass beads. The measured densities of glass beads ranged from 2.40 to 2.56 g/cm³ with mean and standard deviation of 2.46 \pm 0.05 g/cm³.

At WTC, monodisperse PSL particles ranging from 2.60 to 10 μm in geometric diameter were used to calibrate the Aerosizer under the normal ambient pressure and temperature (750 mm Hg [100 kPa] and 20°C). Each particle size of PSL was first generated using a small-scale powder disperser (SSPD; TSI Inc., St Paul, MN) and aerodynamically classified in a specially-designed Timbrell spectrometer (Marshall, I. A. *et al.* *J. Aerosol Sci.* 21: 969, 1990). The Aerosizer responses for nonspherical natrojarosite particles ($\text{Na Fe}_3(\text{SO}_4)_2(\text{OH})_6$) were determined using Unit B. The preparation and characterization of the uniform-sized particles formed as single, symmetrical truncated cubes were described previously (Marshall, I. A. *et al.*, *J. Aerosol Sci.* 22: 73, 1991). The particle density of 3.11 g/cm³ was determined using a helium pycnometer (Marshall *et al.*, 1991). Particles of different size ranges from 7.3 to 18.8 μm aerodynamic diameter were prepared and aerodynamically size-classified in a Timbrell spectrometer.

TOF data from API unit A for PSL particles and glass microspheres are presented as a function of particle size in Figure 1. These data were obtained at ITRI, where API Unit A was operated at a reduced ambient pressure of 625 mm Hg (83.3 kPa). The TOFs obtained for PSL and glass particles were higher than predicted by the manufacturer's calibration curves for the size range from 0.4 to 150 μm geometric diameter. However, the calibration tables have been developed for normal ambient conditions. The magnitude of the overestimation of particle size by the Aerosizer is expressed in terms of the ratio of the geometric diameter measured by the

*AEA Environment and Technology, Winfrith, United Kingdom

Aerosizer to the true geometric diameter from microscopy (D_{API}/D_g). This ratio has values between 1.08 and 1.27 for the PSL particles and glass beads. The TOF values for TOF obtained from Aerosizer Unit B at WTC under normal ambient conditions (750 mm Hg and 20 °C) agreed with the factory calibration data in the size range from 2 to 10 μm (Fig. 1).

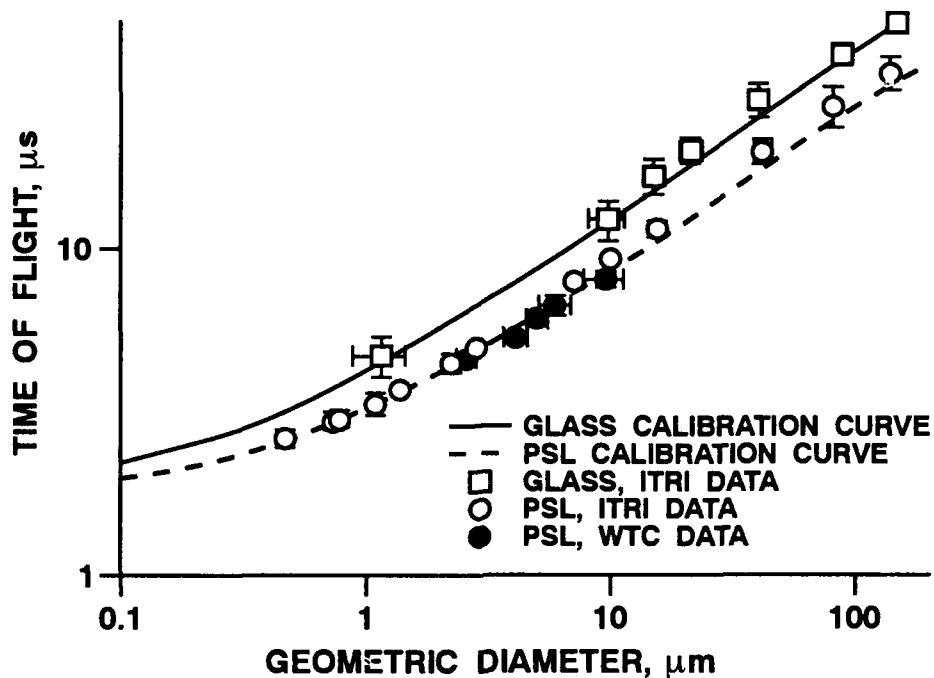


Figure 1. Calibration data of PSL particles (circles (density = 1.05 g/cm³)) and glass beads (squares (density = 2.46 g/cm³)). The curves are derived from manufacturers' data. Solid circles are experimental data at WTC (ambient pressure = 750 mm Hg), and hollow circles and squares are experimental data at ITRI (ambient pressure = 625 mm Hg). The error bars are standard deviation of the measurement.

The count mean aerodynamic diameters measured by the Timbrell spectrometer and the Aerosizer are compared in Figure 2 as a function of true aerodynamic diameter. In all cases, the Aerosizer undersized the natrojarosite particles significantly, and the degree of size reduction was size-dependent. Thus, the largest particles with true aerodynamic diameters close to 18.8 μm were undersized by as much as 51%, whereas the smallest particles analyzed with true aerodynamic diameters of 7.3 μm were undersized by only 21%.

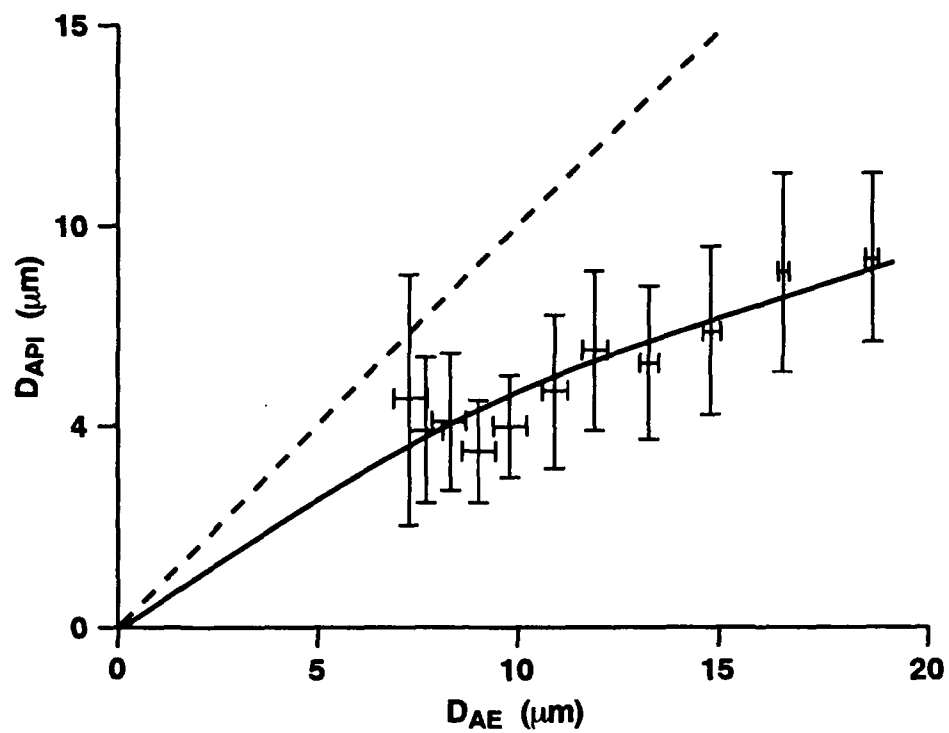


Figure 2. Comparison between the Timbrell spectrometer and the API-measured aerodynamic diameters of PSL natrojarosite at normal ambient pressure (750 mm Hg). The error bars are standard deviation of the measurement.

(Research sponsored by the Office of Health and Environmental Research, U. S. Department of Energy, under Contract No. DE-AC04-76EV01013.)

RECONFIGURATION AND CALIBRATION OF THE ITRI WHOLE-BODY COUNTER

S. B. Ebara*, J. E. Johnson**, M. B. Snipes, R. A. Guilmette, and B. B. Boecker

Bioassay is an important aspect of assessing exposure to internally deposited radionuclides. One method for quantifying internally deposited, photon-emitting radionuclides is to conduct whole-body counts. The type of counting system is an important consideration. If the radionuclide emits photons having energies less than 0.1 MeV, Phoswich crystals can be used as radiation detectors; another option is to use an array of one or more germanium detectors. Photons having energies greater than 0.1 MeV can be quantified using a NaI(Tl) detector, the type of detector described in this report.

The ITRI whole-body counting room consists of a 15.2-cm thick steel shield having internal dimensions of 4.72 m long, 2.44 m wide, and 2.44 m high. Prior to 1992, ITRI used a whole-body scanning system. The scanning system used a pair of 20.3 cm diameter, 10.2 cm thick NaI(Tl) detectors. The detectors were positioned on the same centerline, with one detector located above and one below a scanning table. A whole-body scan was made by positioning the subject on the scanning table and moving the table and subject horizontally between the detectors. The table was motor-driven, and each scan required about 7 min. The system was useful for screening purposes, the scan time was relatively short, and the results were not used to quantify suspected body burdens of photon-emitting radionuclides. Individuals suspected of having body burdens of these radionuclides needed to be further evaluated at another facility having more sophisticated whole-body counting capabilities. The purpose for modifying the system was to allow ITRI to quantify suspected internally deposited photon emitters in humans.

The ideal geometry for whole-body counting is considered to be a 1-meter arc (International Atomic Energy Agency, *Directory of Whole-Body Radioactivity Monitors*, Vienna, Austria, 1964). This configuration places essentially every part of the human body equidistant from the detector, minimizing counting variation due to individual shape and size. Unfortunately, the arc is not a comfortable position, and a compromise was made. This compromise is known as the Argonne standard chair (International Atomic Energy Agency, 1964). The chair geometry approximates the arc, but all parts of the body are not equidistant from the detector. However, the Argonne chair geometry has been adopted and used successfully worldwide, and considerable data have been produced using these systems. Adoption of the Argonne chair for human whole-body counters represented a significant step toward standardizing geometries of these counting systems. The chair configuration has proven to be effective and provides excellent and repeatable whole-body counting results using a single large NaI(Tl) detector.

The counting system was configured to incorporate the Argonne chair. This required removing the scanning table and one of the NaI(Tl) detectors. Three photomultiplier (PM) tubes are coupled to the single NaI(Tl) detector, which is positioned above the chair. The detector/PM tube assembly is mounted on an adjustable support that allows the assembly to be raised and lowered to adjust its vertical height relative to the chair. The PM tubes are operated at 1030 volts. Signals from the PM tubes are summed into a preamplifier, then sent to a linear amplifier, and count data are collected in a PC-based multichannel analyzer (MCA).

A linear conversion of channel number to energy was used to define the pulse height distribution to be 2 keV/channel. The software package provides a nonlinear (higher-order) fit if more than two energies are used for calibration, so only two sources are used for reference energies: ^{133}Ba (356.01 keV) and ^{60}Co (1173.2 keV). ^{133}Ba was chosen rather than ^{137}Cs (661.65 keV) because the ^{137}Cs photopeak energy was inadequate to provide a suitable conversion for the lower portion of the photon energy spectrum. However, ^{137}Cs is routinely used as a source to confirm the linear conversion of channel number to energy, and as a check source to determine if gain shifts have occurred within the system. The check source distance (center of detector face to reference

*University of New Mexico Graduate Student supported by Office of Aerospace Studies, U. S. Department of Defense, and currently at Sandia National Laboratories, Albuquerque, New Mexico

**University of New Mexico, Albuquerque, New Mexico

point of chair) is 69.9 cm, which is the collective average of the reviewed counting systems having the Argonne chair configuration (International Atomic Energy Agency, 1964).

Variation in background count rate was initially checked over a period of about 1 mo for the energy range 0.1-2.0 MeV. Four time intervals were checked: (1) morning (0800-1200); (2) afternoon (1200-1630); (3) evening (1700-2000), and (4) weekend (1700 Friday-0800 Monday). This resulted in nine morning counts, 11 afternoon counts, 10 evening counts, and five weekend counts. Means ranged from 2460-2480 counts per minute (C/min), with coefficients of variation of 1.3-2.1%. An example background spectrum is shown in Figure 1. The Student's *t* test was used to compare the mean integral background count rates for the four time intervals. Confidence of equivalence values of 80 to 100% resulted, indicating that background count rates for these four time intervals were not significantly different.

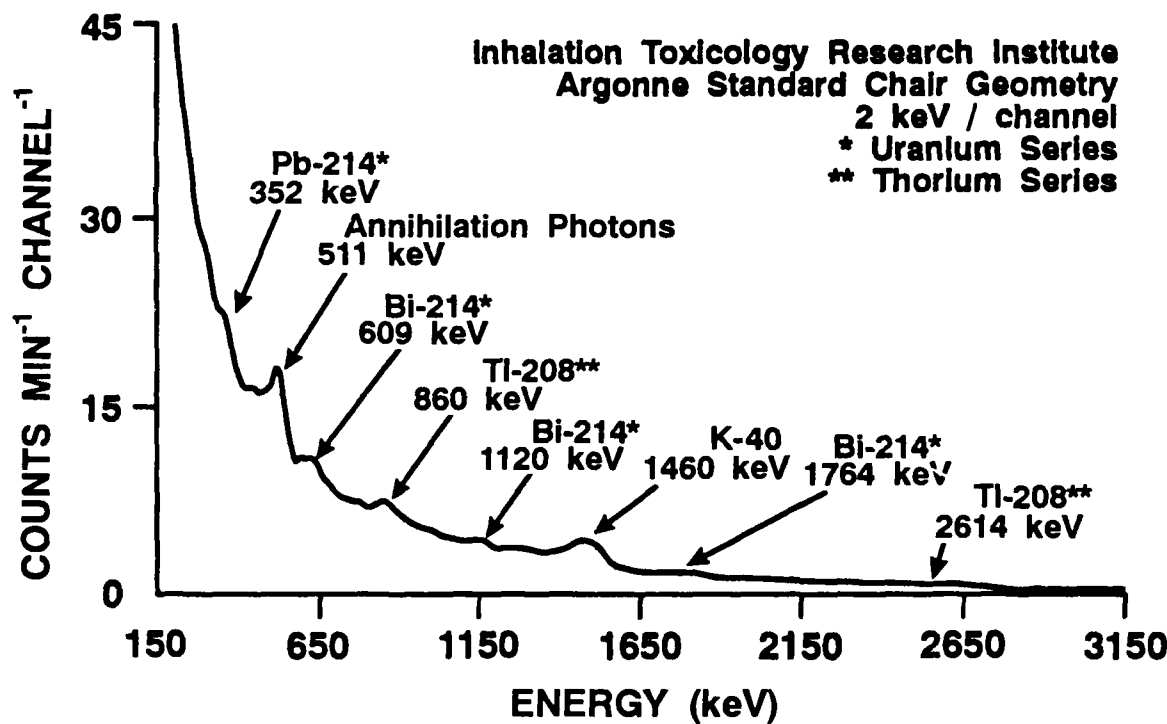


Figure 1. Background spectrum for ITRI human whole-body counter.

Because of the availability of a substantial database for single-crystal NaI(Tl) counting systems having the Argonne chair configuration, calibration of the ITRI system was simplified. We needed only two uniformly distributed radionuclides (^{137}Cs and ^{40}K) for actual counting, along with calibration curves from other counting systems that are similar to the ITRI system, to produce our calibration curve. Two Bottle Mannequin Absorption Phantoms (BOMAB) described by Kramer *et al.* (*Health Phys.* 61: 895, 1991) were borrowed from Battelle Pacific Northwest Laboratories (Richland, WA). One phantom contained homogeneously distributed ^{137}Cs (10,800 Bq); the other phantom contained ^{40}K (35,400 Bq; specific activity 31.5 Bq/g naturally occurring K). The morning and afternoon background count rates were combined to determine the mean background count rate for energy regions of interest (ROI) established for ^{137}Cs and ^{40}K . The ROI were chosen as the centroid channel \pm 27 channels (610-719 keV) for ^{137}Cs and the centroid channel \pm 40 channels (1380-1540 keV) for ^{40}K .

The ^{137}Cs and ^{40}K phantoms were counted seven and 13 times, respectively, using a standardized count time of 40 min. Multiple counts were taken to assure that the true mean for the gross count rate in the ROI were known within 1%. Table 1 contains the results of these counts.

Table 1

Calibration Results for ^{137}Cs and ^{40}K in BOMAB Phantoms

Region of Interest	Resolution ^a	Counts per Minute (C/min) ^b			Calibration Constant ^c
		Gross	Background	Net	
^{137}Cs	8.1%	3010 ± 8.9	126.0 ± 3.1	2736 ± 11	0.00497
^{40}K	5.5%	924 ± 4.9	78.7 ± 1.6	845 ± 5	0.00361

^a (Photopeak count rate at half maximum width) / (Photopeak count rate at maximum width) x 100.

^bValues for counts per minute and calibration constants are mean \pm standard deviation.

^c(Net C/min)/(Bq*60*yield), where yield = photons/disintegration = 0.85 for ^{137}Cs and 0.11 for ^{40}K .

Calibration constants are available for numerous whole-body counters. ITRI generated only two calibration points and compared them with points for the same radionuclides on the calibration curve from another facility. The Oak Ridge National Laboratories (ORNL) whole-body counter calibration constants were chosen because their system is technically the same as the ITRI system in the following ways: (1) the same size NaI(Tl) detector; (2) the counting room shield is low background steel; and (3) the Argonne chair configuration with the same detector positioning relative to the chair. Importantly, their whole-body counter has calibration constants for a variety of photon emitters. Figure 2 was produced after converting calibration results to counts/photon. The similarity in the ORNL and ITRI results for ^{137}Cs and ^{40}K allows us to conclude that Figure 2 represents a reasonable calibration curve for the ITRI human whole-body counter. However, further calibrations with nonuniformly distributed radionuclides should be performed to confirm this calibration curve.

With a 40-min count time, the ITRI human whole-body counter can be used to accurately quantify relatively small body burdens of photon-emitting radionuclides having energies greater than 250 keV. The system can also be used for quantifying photon-emitters with energies as low as about 100 keV, but with less certainty, due to higher background counts/channel and the need to extrapolate the calibration curve from 250 keV to the lower energies. The lower limit of detection (LLD) for a given photon-emitting radionuclide depends on the background count rate for the defined energy ROI. The LLD is the net count rate (C/min) at which the probability is 95% that the activity in the subject is above background. The LLD is equal to 4.65 times the standard deviation of the mean background rate for the ROI divided by the efficiency and multiplied by the photon yield (Currie, L. A. *Anal. Chem.* 40: 586, 1968). As an example, the LLD for a distributed body burden of ^{137}Cs is $3.1 * 4.65 = 14.4$ C/min or 0.24 C/sec. The calibration curve (Fig. 2) indicates 0.005 counts/photon for the photon energy associated with ^{137}Cs , so the LLD for ^{137}Cs converts to 48.1 photons/sec. However, the photon yield for ^{137}Cs is 0.85 photons/dis, so the LLD becomes 56.5 dis/sec = 56.5 Bq. The calculated LLD for ^{40}K is 393 Bq. The LLD for other photon-emitting radionuclides can also be determined by defining the energy ROI and determining the standard deviation of the background C/min for the region.

The ITRI human whole-body counter has been successfully reconfigured and calibrated to quantify uniformly distributed radionuclides in humans. It is being used in a steel shield that has a relatively low background, and the system can be used to quantify relatively small body burdens of photon-emitting radionuclides with energies higher than about 100 keV.

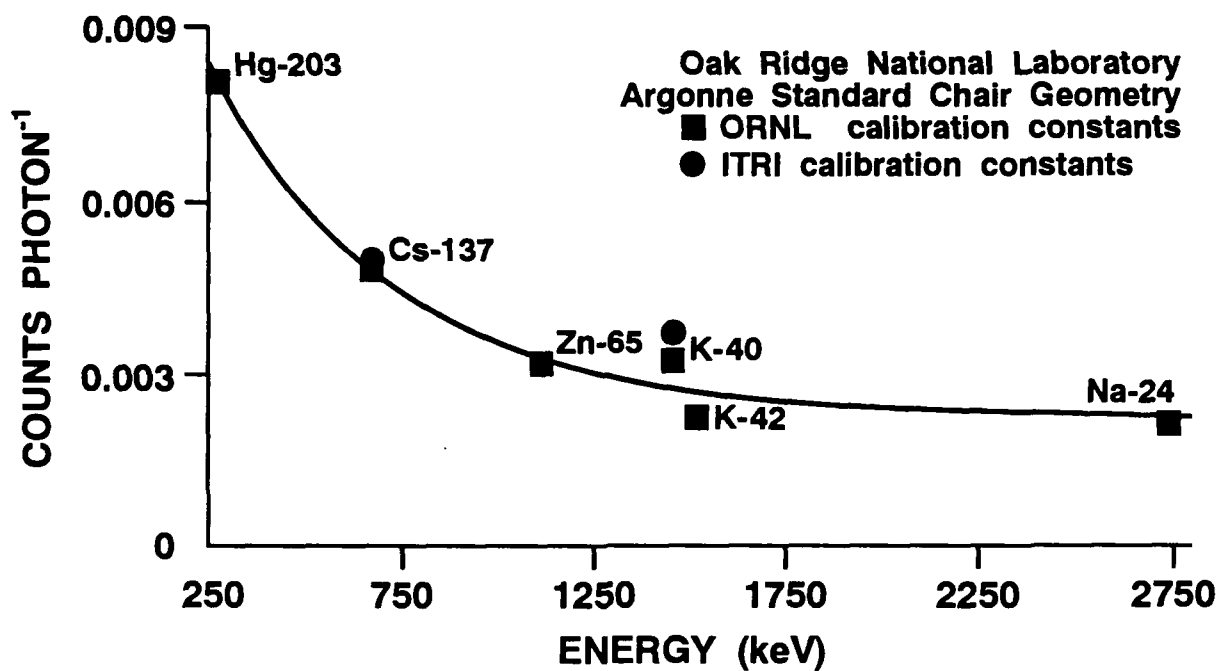


Figure 2. Calibration curve for ITRI human whole-body counter. The equation for the curve is: counts gamma⁻¹ = 0.0111 exp(0.0021X) + 0.0024, where X = centroid energy in keV of the full-energy absorption peak.

(Research sponsored by the Office of Health and Environmental Research, U. S. Department of Energy, under Contract No. DE-AC04-76EV01013.)

A HUMAN AEROSOL EXPOSURE SYSTEM

Y. S. Cheng, H. C. Yeh, and S. Q. Simpson*

Very large and small particles most often deposit in the nasal airways (Cheng, Y. S. et al. *Radiat. Prot. Dosim.* 38: 41, 1991). Human volunteers are most often used in studies with particles larger than 1 μm , whereas recent data on ultrafine particle deposition came from physical airway models (Cheng, Y. S. et al. *J. Aerosol Sci.* 19: 741, 1988; Yamada, Y. et al. *Inhal. Toxicol. Premier Issue 1*: 1, 1988). Studies in airway models provide large data sets with which to evaluate the deposition mechanism. However, verification with data obtained in human subjects is needed to validate the results obtained with nasal models because of possible artifacts in the models. The only published study of *in vivo* deposition for ultrafine particles in people (George A. and A. J. Breslin. *Health Phys.* 17: 115, 1969) examined both total respiratory deposition of radon-progeny-bearing particles in mining and laboratory environments, and nasal deposition in laboratory experiments on three subjects. The nasal deposition for "unattached ^{218}Po " was found to range from 80% for a 3 L/min $^{-1}$ flow rate to 60% for flow rates in excess of 30 L/min $^{-1}$. Unfortunately, the particle size of the radon progeny was not determined; therefore, it was not possible to relate the deposition to the particle size and flow rate without making certain assumptions for the particle size. Thus, there is a need to conduct human studies of nasal deposition of ultrafine particles in the size range of 1 to 200 nm. To accomplish this goal, we have developed a human exposure system.

This study is being conducted in compliance with government regulations protecting human subjects in research. Four adult male, non-smoking, healthy human volunteers (ages 20 to 55 yr) will be invited to participate in this study. Each person will undergo the nasal deposition experiments at constant flow rates of 4, 10, and 20 L/min. The exposure will be conducted in the Human Exposure Laboratory at ITRI. The room layout is shown in Figure 1. Monodisperse aerosols of silver particles (5, 8, 20, and 50 nm) will be used. The maximum particle size and aerosol concentration will be 50 nm and 1×10^3 particles/mL, and the calculated mass concentration is 0.0008 mg/m 3 , below the TLV of 0.1 mg/m 3 . The exposure system including the aerosol generator, charge neutralizer, diluting air, nasal mask, mouth tube, and two condensation particle counters (CPC) is shown in Figure 2.

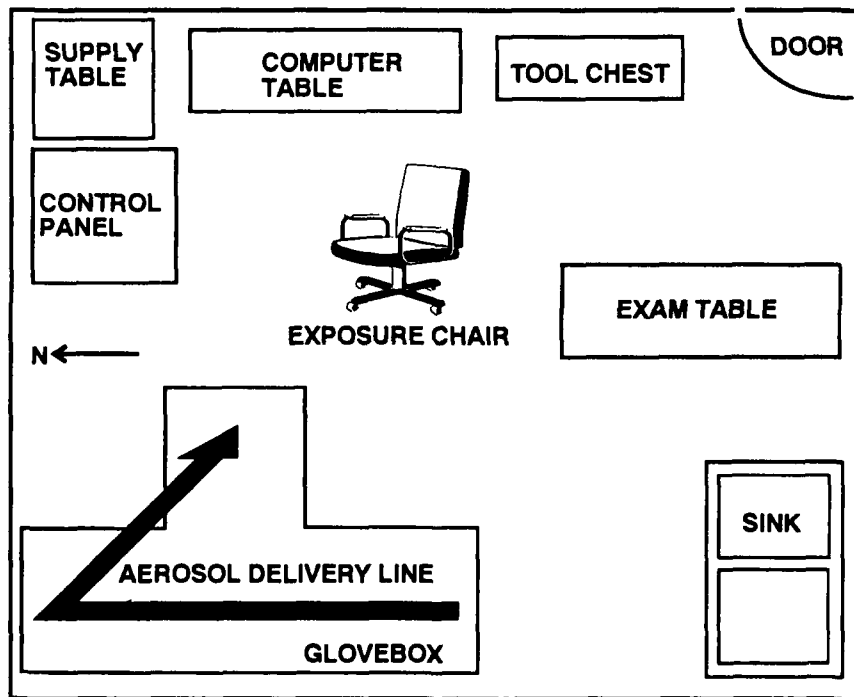


Figure 1. Human exposure lab layout

*University of New Mexico, Albuquerque, New Mexico

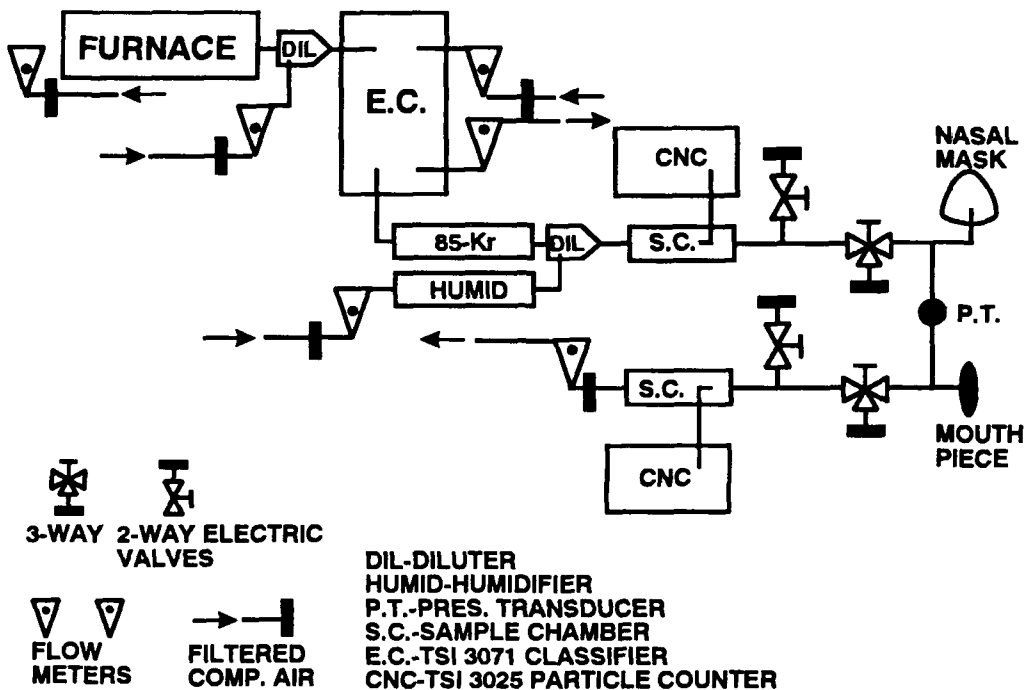


Figure 2. Human exposure system diagram

A human volunteer will sit comfortably in a chair in front of the exposure apparatus. He will be fitted with a nasal mask and mouth tube. He will breathe filtered air normally through the nasal mask and mouth tube for several minutes. The volunteer will then practice holding his breath for at least 30 to 40 sec. During that time, the air is drawn from the nose and exited through the mouth tube at a constant flow. After the subject is comfortable in wearing the mask and tube, and in holding his breath, he will participate in the aerosol deposition study. He will breathe the filtered air normally for several minutes. The aerosol flow will then be switched on. Two-way and three-way solenoid ball valves (Quality Control Inc., Tilton, NH) will be used to control the flow direction. The subject will hold his breath for at least 30 sec but not over 1 min. During that time, an aerosol will be drawn through the nasal airway and exited through the mouth tube. Aerosol concentrations in the supply and exhaust air will be measured. After the maneuver, the aerosol flow will be switched off. The volunteer will be able to relax. The same maneuver will be repeated. The volunteer can stop the experiment if he does not feel comfortable in any stage.

Aerosol number concentrations (particles/cc) will be determined by one TSI CPC (Model 3025, St. Paul MN). The inlet and outlet concentrations will be determined by sampling the aerosol through a three-way Delta solenoid valve (Fluororcarbon, Anaheim, CA). The signals from the CPC, the temperature probe, and the flow sensors are electronically connected to a data acquisition and control system (Analogue Connection, Strawberry Tree, Inc., Sunnyvale, CA) and an IBM 386-based PC. Labtech Note software (Wilmington, MA) will be used to control and manage the system.

The deposition efficiency in the nasal airway will be calculated as follows:

$$D_e = 1 - \frac{P_{\text{measured}}}{P_1 P_2} , \quad (1)$$

where P_{measured} is the measured penetration estimated from the aerosol concentrations of inhaled and exhaled air ($P_{\text{measured}} = C_{\text{ex}}/C_{\text{in}}$); P_1 is the aerosol penetration from the sampling point of the inhaled air to the nasal mask; and P_2 is the aerosol penetration from the mouth tube to the sampling point for the exhaled air.

Our system uses a single CPC, minimizing potential measurement errors. The data recording system is automated for improved data quality and better system control. The volunteers have been recruited and examined. The system has been built and tested. We have obtained some preliminary data from the first volunteer, and are determining the aerosol losses in the system (P_1 and P_2).

(Research sponsored by the Office of Health and Environmental Research, U. S. Department of Energy under Contract No. DE-AC04-76EV01013)

AIR VENTILATION AND AEROSOL CONCENTRATION IN A RECTANGULAR ROOM

Y. S. Cheng, C. C. Yu, and W. E. Bechtold*

Exposures to hazardous airborne material in indoor environments are of increasing concern because they occur over long exposure times. Sources of indoor pollutants include radon and thoron gases, biological organisms, environmental tobacco smoke, combustion products, and volatile organic vapors from many consumer products. Concentrations of airborne materials depend on the source, removal processes in homes, and ventilation. We describe here methods for determining the ventilation and aerosol concentration profile in a room.

Combustion aerosols from burning incense sticks were used in this study (Jinsing Incense Company, Hsinchu, Taiwan). The incense material was attached to a bamboo stick approximately 27 to 29 cm long. Aerosol concentrations were determined by using a real-time aerosol sampler. A RAM-1 aerosol mass monitor (MIE, Bedford, MA), operated at 2 L/min, was used to determine the aerosol mass concentration in $\mu\text{g}/\text{m}^3$ as a function of time. This monitor is operated on light scattering principles; therefore, the instrument response depended on particle size and the refractive index (Cheng, Y. S. *et al. Fundam. Appl. Toxicol.* 10: 321, 1988). The RAM-1 response to the incense smoke was calibrated using a QCM cascade impactor (Model PC-2, California Measurements, Inc., Sierra Madre, CA), operated at 240 mL/min. This unit provides information of mass concentration and aerodynamic particle size distribution in a short period of time, usually within a few minutes.

The study was conducted in a rectangular office having three doors and no window. The volume of the room was calculated to be about 34 m^3 . The room had a separate air supply and exhaust vents. The air could also move through the door seals. During measurements, the doors were closed. The time-dependent change of incense aerosol concentration, C_i , can be described by the following equation:

$$\frac{dC_i}{dt} = G - (\lambda_v + \lambda_w) C_i , \quad (1)$$

where G is the aerosol production rate, λ_v and λ_w are the wall deposition rate of the incense particles and the air ventilation rate in min^{-1} , respectively.

During the experiment, the ventilation rate was first determined by using the SF_6 tracer gas method, described below. Then, the incense smoke was produced and monitored in real-time by using the RAM-1 monitor. The output from the RAM-1 unit was recorded in a chart recorder. The incense aerosol concentration as a function of time was then analyzed with the aid of a mathematical model (Eq. (1)) to estimate the incense aerosol generation rate and wall deposition rate.

Trace amounts of the inert gas SF_6 were released to the room, and the decay of SF_6 concentration with time was determined. A similar equation for the concentration change of SF_6 was written to follow the concentration decay:

$$\frac{dC_g}{dt} = -\lambda_v C_g . \quad (2)$$

This equation assumed that SF_6 was mixed thoroughly upon release, that it did not react with the wall and other surfaces in the room, and that it was absorbed into the surfaces. With initial conditions of $t = 0$, $C_g = C_{go}$, Eq. (2) can be solved:

$$C_g = C_{go} \exp(-\lambda_v t) . \quad (3)$$

By fitting the equation to data, we derived the ventilation rate in terms of air exchange per unit time.

*National Tsing Hua University, Taiwan

SF_6 concentrations were measured using the gas chromatography/electron capture detection (GC/ECD) method. A Varian model 3700 GC was fitted with a ^{63}Ni ECD. Five mL aliquots of gas were injected onto a Valco six-port valve using a 250 μL fixed loop. The GC column was a Chrompak Al_2O_3 porous layer open tubular column, 10 m long with an i.d. of 0.32 mm. The carrier gas was ultra-pure nitrogen maintained at a head pressure of 25 psig. The injector and detector temperatures were 200 and 290°C, respectively. A 507 mL bulb was filled with 1.01% SF_6 stock (24.7 mg) and released in front of the GC. Within 1 to 2 min after release, a 5 mL aliquot of room air was acquired and immediately injected onto the GC/ECD. Five mL aliquots were subsequently taken and injected every 1.5 min thereafter. Samples were acquired until the SF_6 concentrations approached the limits of quantitation or until sufficient points (>20) had been taken to define the ventilation. The incense aerosol generation rate, G ($\mu\text{g}/\text{m}^3/\text{min}$), was determined experimentally by modeling the aerosol concentration profile with time. In this model, a polynomial function was used for the time-dependent generation rate ($G = a + bt + ct^2 + dt^3$), and Eq. (1) can be solved with the initial condition that $t = 0$, $C_i = 0$:

$$C(t) = \frac{a}{\lambda}(1-e^{-\lambda t}) + b\left(\frac{t}{\lambda} - \frac{1}{\lambda^2}(1-e^{-\lambda t})\right) + c\left(\frac{t^2}{\lambda} - \frac{2t}{\lambda^2} + \frac{2}{\lambda^3}(1-e^{-\lambda t})\right) + d\left(\frac{t^3}{\lambda} - \frac{3t^2}{\lambda^2} + \frac{6t}{\lambda^3} + \frac{6}{\lambda^4}(1-e^{-\lambda t})\right), \quad (4)$$

where $\lambda = \lambda_v + \lambda_w$.

Figure 1 shows the measured concentration decay of SF_6 in the room on three different days under different ventilation conditions. Equation (3) fitted to the data quite well. The estimated ventilation rates, λ_v , were 0.0338, 0.0429, 0.119 room volume/min, respectively. Figure 2 shows the incense aerosol concentration by burning one incense stick in the same room, when the ventilation rate was 0.0338 min^{-1} . The incense aerosol concentration continued to increase during the 90-min burning period. Equation (5) fitted to the data quite well. When the combustion process was completed, the aerosol concentration decreased, following the same decay function (Eq. (2)). The aerosol removal rate, λ , is the sum of removal by air ventilation and deposition to the wall surfaces. By subtracting λ_v from λ , the wall deposition rate, λ_w , can also be estimated. The aerosol deposition rate in this case was 0.0042 min^{-1} . The incense aerosol size as determined by the QCM impactor was 0.23 μm MMAD with σ_g of 1.5.

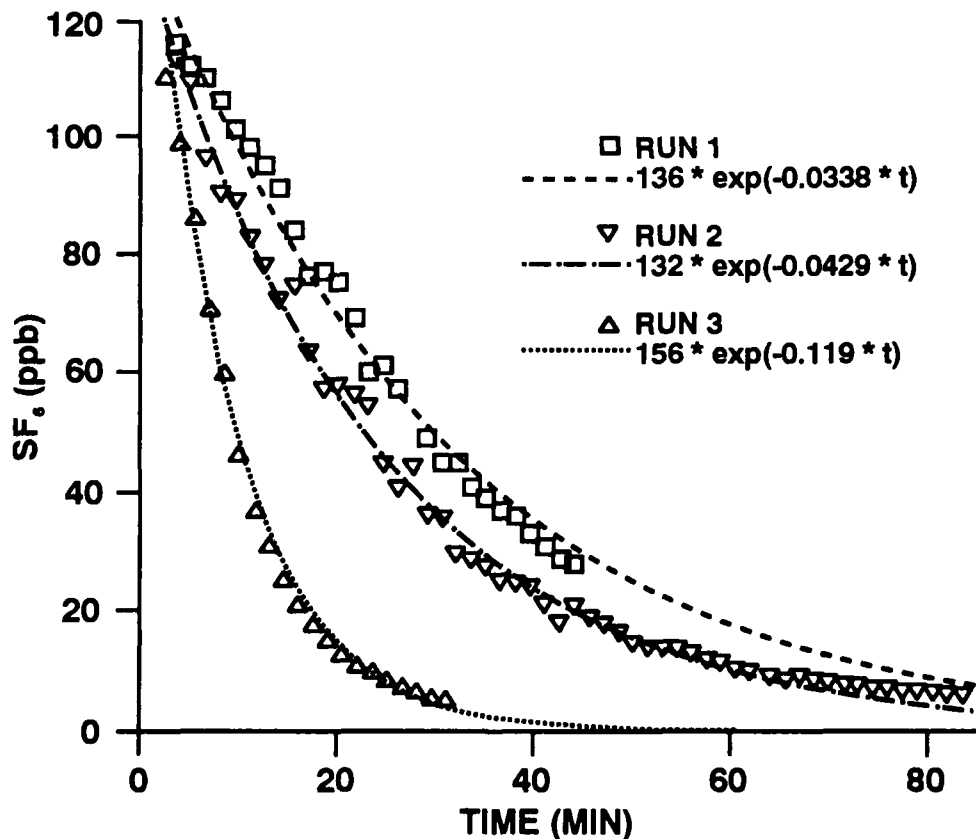


Figure 1. Clearance of SF_6 gas from the room.

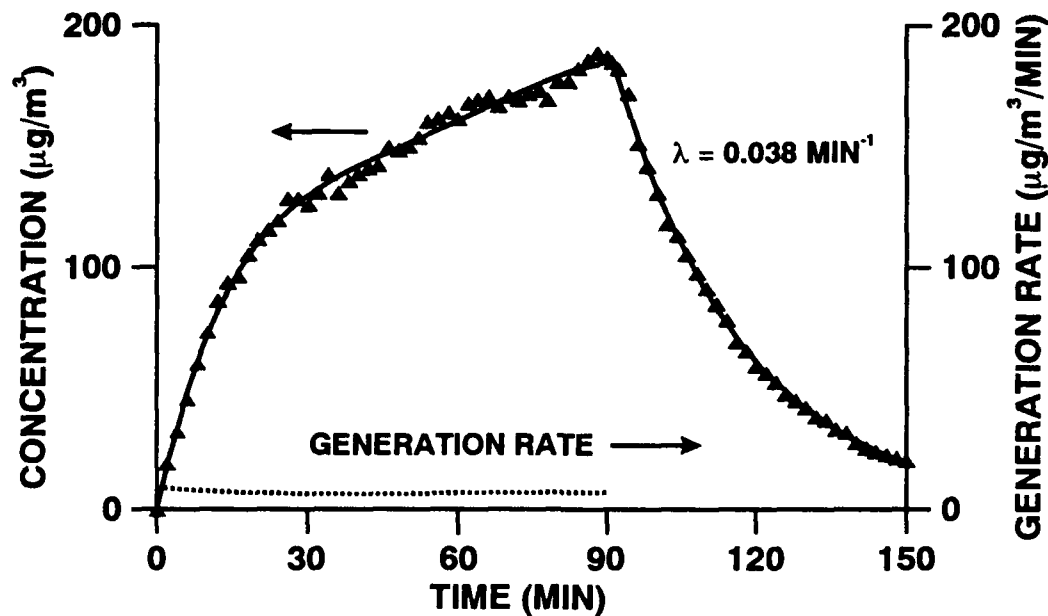


Figure 2. Generation and clearance of incense aerosol in the room.

In summary, we have described here methods to determine the air ventilation rate and aerosol concentration profile in a room. A mathematical model was used to simulate the decay of trace gases and aerosol generation and removal with time. These models are also useful for estimating ventilation rate, aerosol production rate and wall deposition rate.

(Research sponsored by the Office of Health and Environmental Research, U. S. Department of Energy, under Contract No. DE-AC04-76EV01013.)

A CASE STUDY ON DETERMINING AIR MONITORING REQUIREMENTS IN A RADIOACTIVE MATERIALS HANDLING AREA

G. J. Newton, M. D. Hoover, and F. Ghanbari*

Criteria for determining air monitoring requirements in a radioactive materials handling area are listed in several sources including DOE Order 5480.11, 10 CFR 835 (draft 12/9/91), and DOE's RadCon Manual (DOE/EH-0256T) which are the operative orders for Environmental Safety and Health (ES&H) in DOE facilities. The Rad Con Manual has precedence over other regulatory guidelines for DOE facilities. In 5480.11, a target sensitivity for alpha continuous air monitors (CAMs) is listed as 8 DAC-h under laboratory conditions. A derived air concentration (DAC) is obtained by dividing the annual limit of intake (ALI) for a radionuclide by the amount of air assumed to be inhaled ($2,500 \text{ m}^3$) by a reference man during an assumed 2000-h working year. A DAC-h is an exposure at a concentration of 1 DAC for 1 h. The RadCon Manual defines requirements for CAMs. Figure 1 summarizes these requirements for different approaches to air sampling. If a facility never exceeds 0.1 DAC-h and it is unlikely to exceed 0.02 of the ALI, no air sampling is required. If a facility never exceeds 0.1 DAC-h but exposures are likely > 0.02 of an ALI, retrospective air sampling is required. If a facility periodically exceeds 1.0 DAC-h, CAMs are required. Finally, if a facility routinely exceeds 1 DAC-h, special air sampling and monitoring are required. An example is monitoring to verify that respiratory protection limits are not exceeded during normal operations.

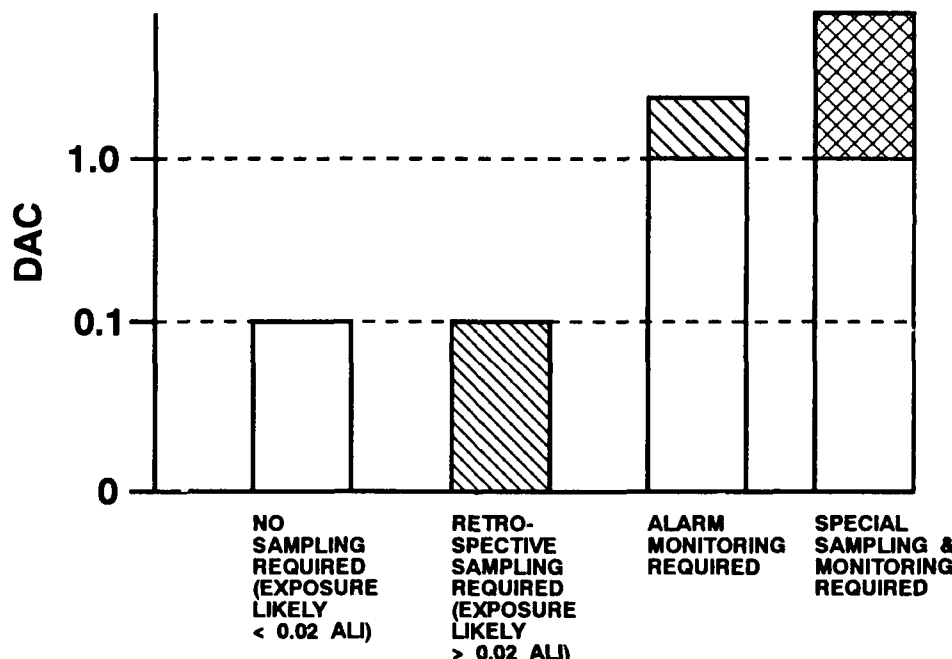


Figure 1. Requirements for air monitoring as a function of derived air concentration (DAC) versus action levels defined in the DOE RadCon Manual based on historical air sampling data ranging from no air sampling required, retrospective air sampling, alarming or continuous air monitors (CAMs), and specialized air sampling.

Sandia National Laboratory's (SNL) underground Hot Cell Facility in Area V (Fig. 2) handles short-term irradiated nuclear fuel (enriched ^{235}U) where the alpha-emitting radionuclide of concern is ^{234}U . If the enrichment of ^{235}U is above 93%, even though the mass fraction of ^{234}U is about 1%, more than 99% of the alpha-emitting radioactivity is from ^{234}U . The Hot Cell Facility has had a CAM program for many years. However, the technical bases for many of the operational decisions (calibration procedures, number and location of CAMs, counting systems for retrospective analyses of CAM filters, and CAM sampling flow rates) have not been documented. There are several approaches to develop the technical basis for air monitoring requirements in a radioactive materials

*Sandia National Laboratories, Albuquerque, New Mexico

handling area. The easiest method is to use historical air sampling data. Along with process and physicochemical knowledge, engineered controls, and an informed hazard analysis, a defendable air sampling program can be developed. The analyses and conclusions in this report are part of a case study for an air sampling program for the SNL Hot Cell Facility.

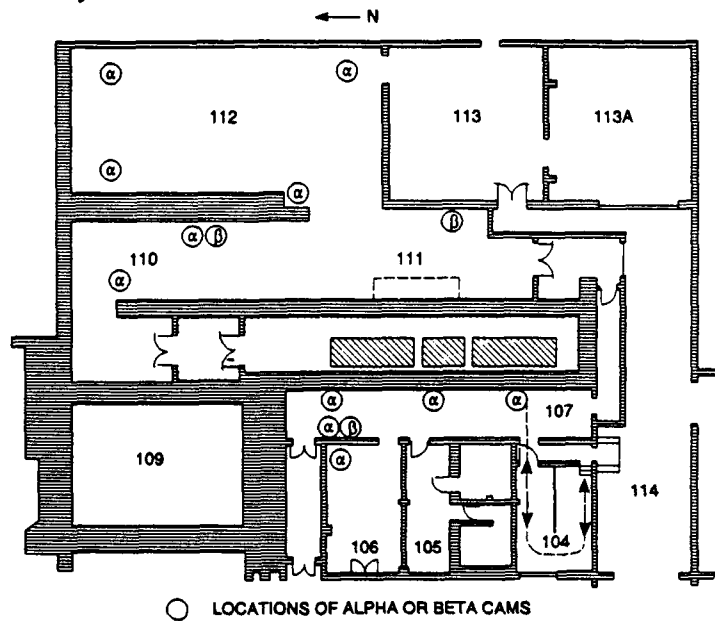


Figure 2. Floor plan of the underground Hot Cell Facility in Sandia National Laboratories Area V showing the manipulator cells, glovebox laboratory, specialized laboratories, and locations of alpha and beta CAMs.

Table 1 lists the DACs for several radionuclides of concern within the Hot Cell Facility. The Class Y form of enriched ^{234}U is the most restrictive chemical form, and its DAC is $2 \times 10^{-11} \mu\text{Ci/mL}$. Thus, 1 DAC for the Class Y form of ^{234}U is equivalent to $44.4 \text{ dpm}/\text{m}^3$, an order of magnitude higher than that required for plutonium. This required sensitivity must be achieved in the presence of naturally occurring, alpha-emitting radon progeny, ^{218}Po and ^{214}Po , that can range from about 400 to 130,000 dpm/m^3 , (0.1 to 30 pCi/L). Although the required sensitivity is not easy to demonstrate, there are no technical reasons that this sensitivity cannot be achieved with the new generation of alpha CAMs.

Table 1
DAC Values Listed in 10 CFR 835, Draft 12/9/91 ($\mu\text{Ci/mL}$)

Radionuclide	Solubility Class		
	D (days)	W (weeks)	Y (years)
^{137}Cs	7.0×10^{-8}	—	—
^{134}Cs	4.0×10^{-8}	—	—
^{90}Sr	8.0×10^{-9}	—	2.0×10^{-9}
^{234}U	5.0×10^{-10}	3.0×10^{-10}	2.0×10^{-11}

Because there is also concern for beta-emitting radionuclides in the Hot Cell Facility, beta CAMs are also used. For health protection concerns for beta emitters, the limiting radionuclide is Class Y $^{90}\text{Sr}-^{90}\text{Y}$ and has a DAC of $2.0 \times 10^{-9} \mu\text{Ci/mL}$. The ^{90}Sr DAC is 8.75 times more restrictive than the DAC for $^{137}\text{Cs}-^{137}\text{Ba}$. Beta CAMs are calibrated with pure beta emitters, ^{36}Cl , $^{90}\text{Sr-Y}$, ^{14}C , and ^{99}Tc . During calibration the response to $^{137}\text{Cs-Ba}$ can be determined. Thus, electroplated sources of either ^{137}Cs or ^{90}Sr are typically used for field functional tests.

Air sampling data, collected from alpha and beta CAMs in the underground Hot Cell Facility dated April 1983 through December 1990, were entered into a spread sheet (Plan Perfect, WordPerfect Corp., Orem, UT), and the DAC values were calculated for ^{234}U and ^{90}Sr . Results of calculating the DACs for ^{234}U and ^{90}Sr suggested that at no time during the periods considered, did the concentration exceed 0.02 DAC for either ^{234}U or ^{90}Sr . A strict interpretation of the results of these calculations suggests that only retrospective air sampling is required. However, we did not advise SNL to remove CAMs from the Hot Cell Facility because (1) we believe that conservative health physics practices would require a combination of retrospective air samples and alpha and beta CAMs because of process knowledge and inventories of radionuclides; and (2) the existence of technically defensible, conservative, health physics approaches reassures SNL staff about their protection and serves to demonstrate to oversight and regulatory groups that SNL has more than adequate health protection programs.

To determine appropriate numbers and placement for CAMs, visible smoke release tests (Fig. 3) with video recording were conducted with smoke released at potential release sites in the Hot Cell Facility. Smoke was rapidly cleared from all areas, no evidence of stagnation or air recirculation was found. These results provided a basis for removing redundant CAMs and optimizing the placement of the remaining CAMs. For example, on the west side of the manipulator cell, six sets of remote manipulators penetrate the shielded Hot Cell. Three alpha CAMs are mounted between each set of paired manipulators, and each CAM is connected to an extractive sampling probe made of stainless steel tubing with an inlet nozzle near a manipulator penetration. Thus, each alpha CAM receives air extracted from four different manipulator penetrations. These alpha CAM sampling lines have multiple bends and several feet of horizontal runs. Thus, large transport line losses of micrometer-sized particles would be expected. Results of smoke dispersion tests showed that any release from the manipulator penetrations would be sampled by a CAM located in the general area; therefore, we can eliminate the questionable transport line arrangement and reduce the number of CAMs. These three CAMs and multiple sample nozzles will be replaced by one Eberline Alpha 6 CAM equipped with a remotely locatable, radial-entry sampler placed near the wall facing the manipulators.

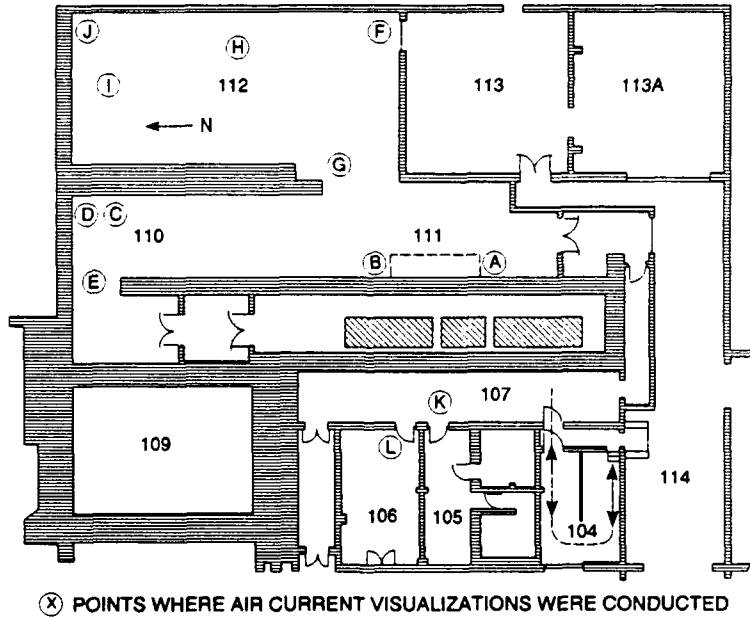


Figure 3. Floor plan of the underground Hot Cell Facility in Sandia National Laboratories Area V showing the manipulator cells, glovebox laboratory, specialized laboratories, and locations of the points where smoke was released for the ventilation flow visualization studies.

In conclusion, we have described an approach to optimize CAM usage and document the technical basis for an air sampling program in a specific laboratory at SNL. Similar analyses are recommended for any facility that must establish a defendable air sampling program for health protection purposes.

(Research sponsored by SNL under PO #AB-2791 to the U. S. Department of Energy under Contract No. DE-AC04-76EV01013.)

CHARACTERIZATION OF ENRICHED URANIUM DIOXIDE PARTICLES FROM A URANIUM HANDLING FACILITY

M. D. Hoover, G. J. Newton, R. J. Howard, and S. M. Trotter**

Information about the amount and characteristics of radioactive particles that might be released in the workplace is needed to set appropriate aerosol control levels and to assess the effective dose to workers from inhalation exposures. A cooperative ITRI/Y-12 Plant study is underway to characterize the concentration, aerodynamic size, and biological solubility of uranium aerosols to which Y-12 workers might be exposed.

A survey of work at the Y-12 Plant was conducted to determine which of the uranium handling processes might pose the most significant inhalation risks to workers. Typical work operations include handling of uranium ingots, melting and casting of uranium metal, cleanup of the melting crucibles and casts, cleaning and finishing of cast parts, inspection and analyses of parts and materials, and solution chemistry. Cleanup of the melting and casting process was chosen as the operation of greatest concern. During melting and casting, uranium metal is melted under vacuum in a carbon crucible and allowed to flow into specially shaped carbon molds. When the crucible and molds are opened to room air, residue (skull) in the crucible is oxidized, along with material on the surfaces of the molded parts. Cleaning of the uranium oxide from crucibles and molded parts forms dusts which might be released from the glovebox enclosures.

The fraction of the total uranium mass in the melt that remains as residual oxide in the crucible ranges from 0.05 to 0.15, depending on the amount of oxide or other contaminants present in the uranium feed stock. Typically, 0.08 of the uranium metal mass involved in the melt remains as an oxide residue in the crucible. A 150-g sample of the residue from the crucible cleaning operation was removed for analysis in this study. The sample had a volume of 75 cm³, indicating that the bulk density of the loose powder was approximately 2 g/cm³. Gas pycnometry will be done to determine the actual density of the particles, which is expected to be approximately 8 g/cm³. Chemical analysis at the Y-12 Plant Laboratory showed that the sample is 0.846 uranium by mass. This corresponds to the theoretical uranium mass fraction for the U₃O₈ form of enriched uranium:

$$(235*3)/(235*3 + 16*8) = 0.846.$$

The isotopic concentration of the uranium is given in Table 1, along with the fraction of total alpha radioactivity contributed by each of the uranium isotopes. Note that ²³⁴U contributes 0.96 of the radioactivity content of the uranium, even though it contributes less than 0.01 of the mass.

Table 1

Isotopic Composition and Specific Activity of Residual Uranium from the Melting and Casting Operation

Isotope	Specific Activity (μ Ci/g)	Fraction of the U Mass	Contribution to Specific Activity (μ Ci/g)	Fraction of the U Activity
²³³ U	9479.2	< 0.00001	0.09	0.0014
²³⁴ U	6251.3	0.00995	62.20	0.9627
²³⁵ U	2.2	0.93164	2.02	0.0313
²³⁶ U	64.7	0.00430	0.28	0.0043
²³⁸ U	0.3	0.05410	0.02	0.0003
Total:		1.00000	64.61	1.0000

*Martin Marietta Energy Systems Y-12 Plant, Oak Ridge, Tennessee

The uranium oxide sample was aerosolized using a dry powder blower (Model 175, DeVilbis, Somerset, PA) and was separated by aerodynamic diameter using a five-stage aerosol cyclone train (Smith, W. B. *et al.* *Environ. Sci. Tech.* 13: 1387, 1979). Material too large to be entrained in the air stream of the powder blower was estimated to have an aerodynamic diameter greater than 50 μm . Material entrained by the airstream, but collected by gravitational settling in the horizontal drift tube between the generator and the cyclone was estimated to have an aerodynamic diameter less than 50 μm , but greater than 20 μm . Total flowrate through the cyclone train was set at 10 L/min so that the cutoff diameter for stage 1 would be 10 μm , which corresponds to the largest aerodynamic particle size expected to penetrate to the pulmonary region of the lung. Cutoff diameters for the other cyclone stages were 4.3, 2.9, 2.0, and 1.2 μm . Particles small enough to pass through the cyclone were collected on a filter. Table 2 shows the mass fraction of the residual uranium oxide material found in each size range. Approximately 0.01 of the residual uranium oxide mass is smaller than the 10 μm aerodynamic diameter associated with a concern for pulmonary deposition.

Table 2 also shows the mass in each particle size range as a fraction of the total uranium mass processed in the melt. Noting that approximately 0.08 of the total mass processed was retained as residual oxide, and that approximately 0.01 of that mass was less than 10 μm aerodynamic diameter gives an estimate that 1×10^{-3} of the material processed might be respirable. That provides a useful way to predict the respirable aerosol hazard as a function of the total mass of material processed. Assumptions about the fraction of the powders that might be released from containment can provide guidance for improving engineered controls, designing air monitoring programs, and selecting respiratory protection for workers.

Table 2

Aerodynamic Size Distribution of Residual Uranium Oxide Particles
from the Melting and Casting Operation

Collection Location	Aerodynamic Size (μm)	Fraction of the Residual Oxide Mass	Fraction of the Total Mass in the Melt	Fraction of the Mass < 10 μm Aerodynamic Size
Retained in the powder blower	d > 50	0.64	5.1×10^{-2}	NA
Collected in the drift tube	$20 < d < 50$	0.22	1.8×10^{-2}	NA
Cyclone				
Stage I	$10 < d < 20$	0.12	1.0×10^{-2}	NA
Stage II	$4.3 < d < 10$	0.0051	4.1×10^{-4}	0.44
Stage III	$2.9 < d < 4.3$	0.0043	3.4×10^{-4}	0.37
Stage IV	$2.0 < d < 2.9$	0.0018	1.4×10^{-4}	0.16
Stage V	$1.2 < d < 2.0$	0.0002	1.6×10^{-5}	0.02
Backup Filter	d < 1.2	< 0.0001	< 1×10^{-5}	< 0.01

Knowledge of the particle size distribution of the respirable material also provides a more realistic basis for setting limits on acceptable air concentrations in the workplace. The allowed Annual Limits on Intake (ALIs) for worker exposures to radionuclides are determined by methods from Report 30 of the International Commission on Radiological Protection (ICRP 30, *Limits on Intakes of Radionuclides by Workers*, Pergamon Press, Oxford, 1979 and addendums). In the absence of particle size information, the ICRP method assumes that all particles have an aerodynamic diameter of 1 μm and calculates a Derived Air Concentration (DAC) to which a worker could be exposed 8 h per day, 5 days per wk, for 50 wk (an entire work yr of 2000 h), without exceeding the ALI for the radionuclide. The worker is assumed to breathe at the rate of 20 L/min as given for the ICRP Reference Man (ICRP 23, *Reference Man: Anatomical, Physiological and Metabolic Characteristics*, Pergamon Press, Oxford, 1975). If particle size information is known, the ICRP method allows the DAC to be adjusted

accordingly. The DAC for particles larger than 1 μm is generally higher because larger particles are less of an inhalation hazard since they tend to deposit more in the upper respiratory tract and less in the pulmonary region.

Table 3 shows how the DAC for ^{234}U (the major concern for exposures to enriched uranium) is increased for the particle size distribution measured in this study. For the more insoluble forms of ^{234}U (dissolution half-times on the order of weeks or years), the pulmonary region of the lung is the target organ because particles deposited in the naso-pharyngeal and tracheo-bronchial region are quickly cleared to the gastrointestinal tract by mucociliary action or swallowing. Because the pulmonary deposition efficiency for the aerosol size distribution in Table 2 is only 0.41 of the pulmonary deposition for 1- μm diameter particles, the ALI and the DAC are a factor of 2.4 higher. For the more soluble forms of ^{234}U (dissolution half-time on the order of days), material deposited in all three regions of the respiratory tract can dissolve and be translocated to the bone surface, kidneys, and red bone marrow. Some radiation dose to the pulmonary lung can also occur. For the soluble material, the larger particle size distribution results in only 0.81 of the radiation dose from 1- μm particles, and the ALI and DAC are therefore 1.24 higher.

Table 3

Derived Air Concentrations for Uranium-234
as a function of Solubility Class and Particle Size Distribution

	DAC based on an Assumed Particle Aerodynamic Size of 1 μm ($\mu\text{Ci/mL}$)	DAC based on the Measured Particle Size Distribution from this Study ^a ($\mu\text{Ci/mL}$)
DAC for Solubility Class D (half-time on the order of days)	5.0×10^{-10}	6.2×10^{-10}
DAC for Solubility Class W (half-time on the order of weeks)	3.0×10^{-10}	7.3×10^{-10}
DAC for Solubility Class Y (half-time on the order of years)	2.0×10^{-11}	4.9×10^{-11}

^aAll material detected by air sampling and monitoring is assumed to be respirable (< 10 μm aerodynamic diameter), and the particle size distribution of the respirable particles shown in Table 2 is used to calculate the DAC.

Samples of the size-separated materials are now scheduled for shipment from the Y-12 Plant to ITRI for evaluation of *in vitro* solubility. This will help in selecting the appropriate ICRP 30 solubility class, ALI, and DAC for the material. The Y-12 Plant currently makes the conservative assumption that material to which workers are exposed has solubility class Y (dissolution half-time of years). If the material is more soluble than class Y, then the DAC can be adjusted upwards, as shown in Table 3, by as much as a factor of 25. Use of the measured particle size distribution could also be used in the workplace to either further adjust the DAC upward, or to demonstrate that the assumed DAC is conservative.

(This research was conducted under U. S. Department of Energy Contract No. DE-AC04-76EV01013 with funding from Martin Marietta Energy Systems Y-12 Plant.)

SIZE DISTRIBUTION MEASUREMENTS OF VECTOR AEROSOLS USED FOR ANIMAL INHALATION STUDIES WITH RADON PROGENY

G. J. Newton, Y. S. Cheng, H. C. Yeh, and N. F. Johnson

Measurement of the size distributions of aerosols is fundamental to understanding the deposition sites within the respiratory tract after inhalation exposures to radon progeny. Radon progeny are clusters of single atoms, neutralized by charged species, range in size from about 0.5 to 5 nm diameter, and are typically attached to atmospheric aerosols encountered in the environment. Addition of a vector aerosol is necessary in a laboratory animal inhalation exposure system because unattached radon progeny have high diffusion coefficients and therefore rapidly deposit in tubing and pipes in the exposure system. Because the radioactivity size distribution depends on the vector aerosol size distribution, measurements were made for size and number concentration for: (1) the background aerosol, presumed to be from animal dander and other particles from the rats, (2) cigarette smoke at number concentrations ranging from 0 to 10^4 particles per mL in the presence of radon progeny that would result in about 1000 working level months (WLM) per 3 h of exposure, (3) and for 0.23 μm diameter polystyrene latex (PSL) microspheres. Measurements of number concentration and size distribution of radon progeny without any vector aerosol will help predict the potential for inhalation exposures of rats to relatively high unattached fractions of radon progeny.

Planned laboratory animal inhalation exposures require high levels of radon progeny attached to different vector aerosols and relatively high fractions of the unattached fraction. Previous inhalation exposures at ITRI used cigarette smoke particles at concentrations ranging from 10^3 to 5×10^4 particles/mL, while the radon progeny exposures have ranged from 300 to 1500 WLM (Newton, G. J. et al. In *Indoor Radon and Lung Cancer: Myth or Reality?* Twenty-Ninth Hanford on Health and the Environment [F. T. Cross, ed.], p. 709, Battelle Press, 1992.) Our next experiments used radon progeny attached to monodisperse PSL particles. The first particle size used was 0.23 μm diameter PSL.

Polystyrene latex particles, 0.23 μm diameter, were aerosolized by a modified Retec nebulizer with two generators and a 200 mL reservoir. The mathematics of the required dilutions were summarized by O. Raabe (*Am. Ind. Hyg. Assoc. J.* 29: 439, 1968). A number concentration of 3.5×10^8 particles/mL was required. The actual procedure involved transferring by pipette 0.089 mL of the stock suspension into about 50 mL of deionized filtered water in a polycarbonate centrifuge tube, centrifuging the suspension and decanting the supernatant, thereby removing the surfactant. This was repeated three times. Following these procedures, the particles were resuspended in 100 mL of deionized filtered water. Previous studies determined that the charge on PSL particles suspended in water can be neutralized by maintaining a pH of about 10. This pH adjustment is achieved by blowing NH_3 gas over the suspension while stirring with a teflon-coated stirring bar. It is essential that solutions containing $[\text{OH}]^-$ are not used to adjust the pH because this procedure would compromise the particle size distribution and the number concentration.

The estimated number concentration was calculated by assuming a Retec generator output of 0.36 mL/min. This system would add about $0.36 \text{ mL/min} \times 3.5 \times 10^8 \text{ particles/mL} = 1.3 \times 10^8 \text{ particles/min}$. A 200 mL separatory flask was used to transfer, by gravity feed, the PSL suspension into the 10 mL generator reservoirs. At a consumption of 0.36 mL/min plus evaporative losses, the generator could operate for about 5 h. To eliminate increasing the volume of the exposure atmosphere, compressed air to aspirate the Retec nebulizer was obtained downstream of the compressor. The output of the Retec nebulizer was diluted with about 30 L/min of air, and the aerosol-laden stream, at a flow rate of about 50 L/min, was piped via 5/8-in diameter stainless steel tubing into the aging chamber of the radon progeny exposure system.

To generate a cigarette smoke vector aerosol, a research cigarette was placed into a hole in a rubber stopper that was inserted into the bulkhead of a 2.5 L plexiglass chamber. The chamber was placed in a sealed plexiglass box. Air from the aging chamber was pulled through the burning cigarette by a peristaltic pump and then piped back into the aging chamber. A cigarette was burned every 10 min during the radon progeny exposures. For cigarette smoke, about 10^9 to 10^{10} particles/mL were added at a flow rate of 200 mL/min. Inline filters on

the exit side of the animal exposure chamber were bypassed, and the atmosphere was recirculated without filtration. A minimum of 10^3 particles/mL was needed in the exposure atmosphere.

The unattached fraction of radon progeny is a function of the number of available vector particles and the residence time in the animal inhalation exposure chamber. Because of their high diffusion coefficients, unattached radon progeny cannot be transported through the transport lines in the exposure system. Therefore, the only way to increase the concentration of the unattached fraction is to increase the residence time of radon in the exposure chambers to permit more ingrowth while maintaining the number concentration of vector particles as low as possible. This was accomplished by reducing the ventilation flow rate through the 27-in chambers from 40 L/min to 5 L/min. Cross *et al.* at Battelle Pacific Northwest Laboratory (personal communication, June 16, 1992) exposed rats to elevated concentrations of unattached radon progeny. They characterized the aerosol with a filter preceded by a single 80 mesh screen having 100 μm wire diameter and 200 x 200 μm openings. Face velocity through the screen was 2.6 cm/s (765.8 mL/min). Their criterion for the "unattached" fraction was < 3.0 nm diameter. They achieved an unattached fraction of about 10%. The criterion for "unattached" fraction is not a fixed number; therefore, our criterion for the "unattached" is < 5 nm diameter, a number that is accepted by aerosol scientists investigating radon progeny aerosols.

With 16 F344/N rats from the Institute's colony in a 27-in exposure chamber, a flow rate of 5 L/min through the chamber and a radon progeny concentration of about 80,000 WL, rats were maintained for 0.5 h to establish a steady-state vector aerosol concentration. This vector aerosol was the animal dander, food particles, and other particles that the rats stir up in the chambers. After an equilibrium period, three sets of filter samples were obtained under both (1) standard conditions (no screen type diffusion battery used) and (2) through a single-screen diffusion battery with a 50% cutoff at about 5 nm. Filters were counted using the standard low efficiency counter for a maximum of 30 min. Analyses were by the Tsivoglou-Thomas 3-interval method.

Two types of aerosol measurements were made. First, aerosol samples were obtained with a quartz crystal microbalance 10-stage cascade impactor (California Measurement Systems, Sierra Madre, CA) that produced size measurements from 35.50 to 0.173 μm aerodynamic diameter. Number concentrations of vector aerosols were determined by a Model 3020 condensation nucleus counter (TSI, Inc., St Paul, MN). The unattached fraction was measured by obtaining two separate membrane filter samples, (1) an open face filter sample containing all particle sizes, and (2) a filter sample preceded by a single screen diffusion battery. A study was also conducted beginning with low number concentrations of cigarette smoke vector aerosol and slowly increasing the number concentrations. These data were required to assure that previous studies where the number concentration has been as low as 10^3 /mL have similar size distributions as did aerosols with a higher number concentration. The same sampling strategy was used. This sequence was followed for 1.0×10^4 and 5.0×10^4 particles/mL. Previous measurements of the unattached fraction, using cigarette smoke vector aerosols, indicated that the unattached fraction was 3-5%. Here, our measured unattached fraction was about 6%, somewhat less than our goal of > 10%.

Table 1 shows the results of the number concentration and size distribution measurements. Generation of monodisperse 0.23 μm diameter PSL was adequate for the experimental goal. Concentrations > 10^4 particles/mL were achieved at 5 L/min in the unfiltered mode. At 40 L/min through the chamber, particle number concentrations of 10^5 /mL were achieved for both the filtered mode (1.7×10^5) and the unfiltered mode (2.3×10^5). Thus, the number concentration only increased about 35% when the exposure atmosphere was unfiltered. For the cigarette smoke studies, three exposures demonstrated number concentrations of about 10^4 particles/mL. Additional runs with lower number concentrations of cigarette smoke are needed to determine the effect on the MMAD.

The number concentration seen with no animals and no radon progeny was 10^3 particles/mL. When radon progeny at 60,000 WL were introduced and no animals were present, the number concentration ranged from 10^2 to 10^3 per mL. Additional measurements need to be made to better define the number concentration contributed by the animal dander and animal-generated particles. Exposures to high levels of unattached radon progeny are dependent on low number concentrations and long residence times of aerosols in the exposure chambers. It may be necessary to place the animals in nose-only exposure tubes to reduce animal-generated particles, thus potentially enabling the generation of higher unattached fractions of radon progeny.

Table 1

Size Distribution Measurements of Vector Aerosols Used in Radon Progeny Inhalation Studies^a

Replicate Runs	Conditions	Number Conc., CNC (No./mL) ± SD	QCM Mean Conc. (mg/m ³) ± SD	Size, QCM (MMAD) (μm) ± SD
3	Background, pre-exposure mode, no animals, 40 L/min, atmosphere filtered	N/A	(2.66 ± 0.39) × 10 ⁻³	N/A
4	Background, pre-exposure mode, radon progeny present, no animals, 40 L/min	(2.15 ± 0.49) × 10 ³	(6.07 ± 2.18) × 10 ⁻³	0.114
3	Exposure conditions, radon progeny present, animals present, 40 L/min, atmosphere filtered	(3.00 ± 0.71) × 10 ²	(2.28 ± 0.70) × 10 ⁻²	8.15 ± 6.36
3	Exposure conditions, radon progeny present, with animals, 5 L/min, atmosphere not filtered	(1.99 ± 1.90) × 10 ²	(1.66 ± 0.49) × 10 ⁻²	1.34 ± 0.39
4	PSL particles, radon progeny present, with animals, 40 L/min, atmosphere not filtered	(2.31 ± 0.14) × 10 ⁵	(6.41 ± 2.32) × 10 ⁻²	0.167 ± 0.046
3	PSL particles, radon progeny present, with animals, 5 L/min, atmosphere not filtered	(8.56 ± 0.91) × 10 ⁴	(6.11 ± 7.06) × 10 ⁻²	0.123 ± 0.002
3	PSL particles, radon progeny present, with animals, 40 L/min, atmosphere filtered	(1.73 ± 0.06) × 10 ⁵	(8.20 ± 7.06) × 10 ⁻²	0.116 ± 0.004
3	Cigarette smoke, radon progeny present, with animals, 40 L/min, atmosphere not filtered	(4.03 ± 0.02) × 10 ⁴	(4.71 ± 2.02) × 10 ⁻¹	0.163 ± 0.006
3	Cigarette smoke, radon progeny present, with animals, 5 L/min, atmosphere not filtered	(3.23 ± 0.13) × 10 ⁴	(4.83 ± 0.62) × 10 ⁻¹	0.156 ± 0.002
3	Cigarette smoke, radon progeny present, with animals, 40 L/min, atmosphere filtered	(4.01 ± 0.10) × 10 ⁴	(7.72 ± 0.61) × 10 ⁻¹	0.175 ± 0.012

^aCNC = Condensation nucleus counter. QCM = Quartz crystal microbalance. MMAD = Mass median aerodynamic diameter.

(Research sponsored by the Assistant Secretary for Environmental Restoration/Waste Management, U. S. Department of Energy, under Contract No. DE-AC04-76EV01013).

COMPARISON OF ACTIVITY SIZE DISTRIBUTIONS OF THORON PROGENY BY ALPHA- AND GAMMA-COUNTING METHODS

Y. S. Cheng, C. C. Yu*, and K. W. Tu**

Concerns over the potential health effects of inhaled radon progeny in mining and indoor environments prompted the development of measurement techniques and research on the properties of radon progeny. Radon progeny are small particles primarily in the size range of 1 to 200 nm, produced by the decay of radon gases (^{220}Rn and ^{222}Rn). Transport, attachment, and deposition of radon progeny both in the environment and in the human respiratory tract depend on the physical size of the progeny particles. Graded diffusion batteries (GDB) of various designs have been used to determine the progeny activity size distributions. For ^{220}Rn progeny, both alpha- and gamma-counting methods (Cheng, Y. S. et al. *J. Aerosol Sci.* 23: 361, 1992) can be used to determine the activities, because one of the decay products, ^{212}Pb , is a beta and gamma emitter with a 10.6-h half-life.

Activity size distributions of radon progeny using alpha- and gamma-counting methods have not been previously compared. Here, we report results of an interlaboratory comparison of ^{220}Rn progeny activity size distributions between our laboratory and the Environmental Measurement Laboratory (EML). An ITRI GDB was used, and gamma activities collected on screens, and the backup filter counted. Results were compared to those obtained from an EML four-stage, GDB by alpha-counting methods.

Thoron progeny were generated in a chamber at ITRI and sampled by the two devices described above. The experiment was designed to produce ^{212}Pb in the size range of 0.8 to 3 nm so that we could test and compare these instruments for a wide, unattached size fraction. Radon-220 gas was generated from a 1.11×10^7 Bq (0.3 mCi) dry ^{228}Th source (Su, Y. F. et al. *Health Phys.* 56: 309, 1989). Air (0.5 L/min) passed through the source thus entraining ^{220}Rn gas. Radon-220 gas was filtered to remove any decay products before entering the chamber. The following conditions were chosen for this study. Three different gases were used: pure N_2 , pure O_2 , and 1 ppm of NO in O_2 . The flow rates through the chamber were set at either 6 or 3 L/min corresponding to a mean residence time of 14 and 28 min, respectively. The particle concentration in the chamber was monitored continuously by a TSI ultrafine condensation particle counter (UCPC) (Model 3025, TSI Inc., St. Paul, MN).

Experimental conditions during the study are listed in Table 1. The measured aerosol concentration indicated that higher aerosol concentrations were produced at a chamber flow of 3 L/min than at 6 L/min. Also, low aerosol concentrations were detected in the chamber with trace amounts of NO. A shift to lower particle concentration may be an indication of smaller progeny size. The UCPC was primarily used in this study to ensure that the chamber condition was stable during the sampling period for the two GDBs.

Table 1
Experimental Conditions During the Study

Gases	Chamber Flow Rate (L/min)	UCPC Concentration (lb/cm ³)
O_2	6	$2.0-2.1 \times 10^4$
O_2	3	$3.5-3.6 \times 10^4$
N_2	6	$2.6-3.2 \times 10^3$
N_2	3	$2.5-2.6 \times 10^4$
1 ppm NO in O_2	6	5.5-6.2
1 ppm NO in O_2	3	$4.0-4.5 \times 10^2$

*National Tsing Hua University, Taiwan

**Environmental Measurement Laboratory, New York, New York

Activity particle size distributions of ^{212}Pb under the described experimental conditions are plotted in Figure 1. In general, the size distributions obtained from the two different methods agreed; however, the detailed spectra of size distributions showed some differences. Figure 1 shows the particle size distribution in oxygen. At 6 L/min chamber flow, bimodal size distributions were obtained in both measurements: one size mode at 1 nm and another mode at about 4 to 6 nm. At 3 L/min chamber flow, the measured size distribution was also bimodal with a 1-nm mode and a larger size mode around 8 nm. Data for other experimental condition were also obtained but not shown here.

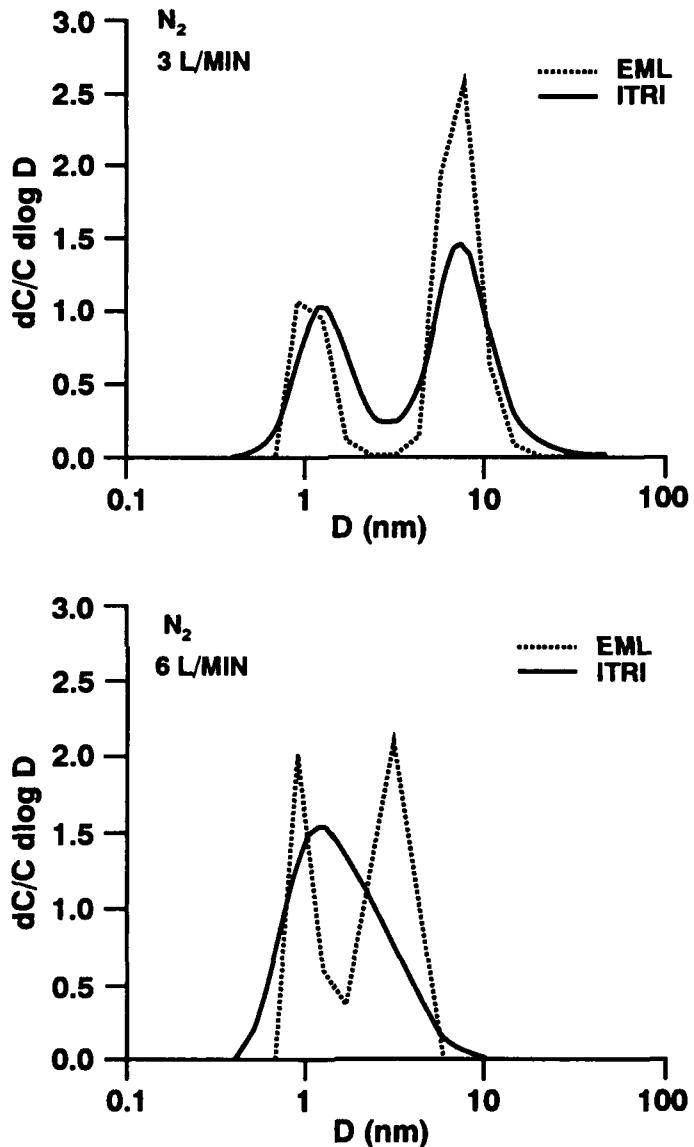


Figure 1. Activity-weighted size distribution of ^{212}Pb in an oxygen environment.

Our results indicated that the alpha- and gamma-counting methods for analyzing the activity size distribution of thoron progeny produced similar results. The agreement between the two data set was much closer than the results obtained in previous interlaboratory comparisons (Chu, K. D. *et al.* In *Radon and Its Decay Product* [P. K. Hopke, ed.], American Chemical Society, Washington, DC, p. 365, 1987; Hopke, P. K. *et al.* *Health Phys.* (in press), 1992). The better agreement was attributed to a more stable test environment in the small chamber, and to improved techniques for determining radon progeny size distributions.

(Research sponsored by the Office of Health and Environmental Research, U. S. Department of Energy, under Contract No. DE-AC04-76EV01013.)

CLASSIFICATION OF CARBON FIBERS BY LENGTH BASED ON THEIR ELECTRICAL PROPERTIES

B. T. Chen, H. C. Yeh, and C. H. Hobbs

Fundamental studies of physical behavior, lung deposition and clearance, and toxicity of fibrous aerosols require the use of fiber-like particles with well-defined diameters and lengths. Classifying these fiber-like particles by size is difficult because both the fiber diameter and the fiber length must be considered during the classification process. No single mechanism can separate fiber particles simultaneously based on these two parameters. Because the aerodynamic diameter of fibers depends strongly on the fiber diameter ($5/6$ power) and only weakly depends on fiber length ($1/6$ power) (Stöber, W. In *Assessment of Aerosol Particles* [T. T. Mercer, ed.] C. C. Thomas, Springfield, IL, p. 249, 1972), devices such as sedimentation elutriators and spiral centrifuges classify fiber particles primarily according to diameter (Spurny, K. R. et al. *Am. Ind. Hyg. Assoc. J.* 40: 20, 1979). There are few data available in the literature to demonstrate the feasibility of classifying fibers based on their lengths (Timbrell, V. *Ann. Occup. Hyg.* 18: 299, 1975; Zebel, G. et al. *J. Aerosol Sci.* 8: 205, 1977). We hypothesize that, in a unipolar charger, the fibers are charged based on their lengths, and, consequently, they can be classified by length based on their electrical mobilities. Thus, the objective of this study is to test the validity of this hypothesis by classifying carbon fibers in an electrical aerosol analyzer (EAA).

Carbon fibers provided by Hercules, Inc. (Wilmington, DE) were used in this study. The fiber-like particles were monodisperse in diameter (count median diameter = $3.74 \mu\text{m}$, geometric standard deviation (GSD) = 1.06) and polydisperse in length (count median length = $35.8 \mu\text{m}$, GSD = 2.08). Fiber-like particles were dispersed and delivered into the EAA for length classification (Fig. 1). In the EAA, the aerosol particles were positively charged and then electrically precipitated onto a central rod of a cylindrical condenser according to their electrical mobilities. Thin-layer, Mylar® segments were placed on the rod for particle collection. After each experiment, the particles collected on each segment were sized using an image analyzer.

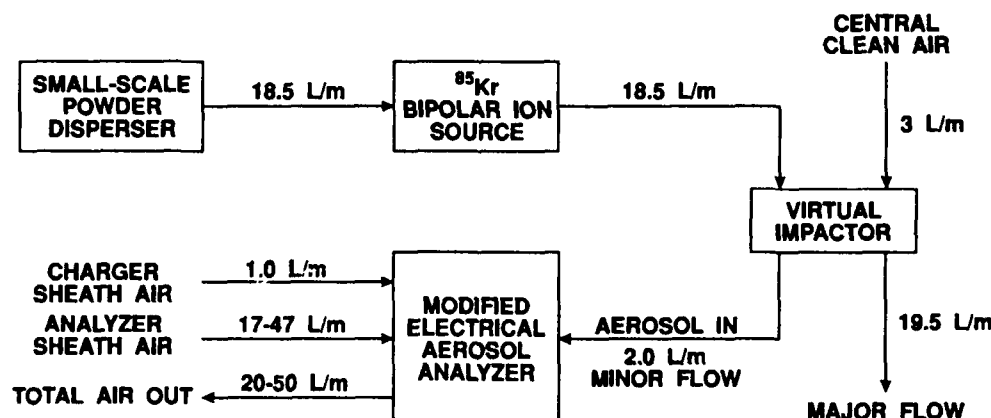


Figure 1. Schematic diagram of the experimental setup for carbon fiber classification.

Several operating conditions were used to study the effects of charging time, flow rate, and analyzer voltage on the classification efficiency of fibers. The results indicated that the higher the flow rate, the longer the fiber collected on a given precipitating distance, and the better the resolution in fiber classification. Similarly, at a lower analyzer voltage, longer fibers were deposited on a given distance with a better resolution. In addition, the results suggested that the number of charges on each fiber would reach a state of near-charge equilibrium as long as the charging time in the EAA was ≥ 0.22 sec. Further analysis illustrated that all data obtained from the various operating conditions could be consolidated by a linear equation relating electrical mobility to fiber

length (Fig. 2). Besides using this equation to predict the length of fibers collected on a given distance of the rod under given operating conditions, we used it to estimate the mean charge on carbon fibers in a unipolar charging mechanism (Fig. 3). Based on our results, the number of charges on a carbon fiber increases monotonically with the aspect ratio of the fiber.

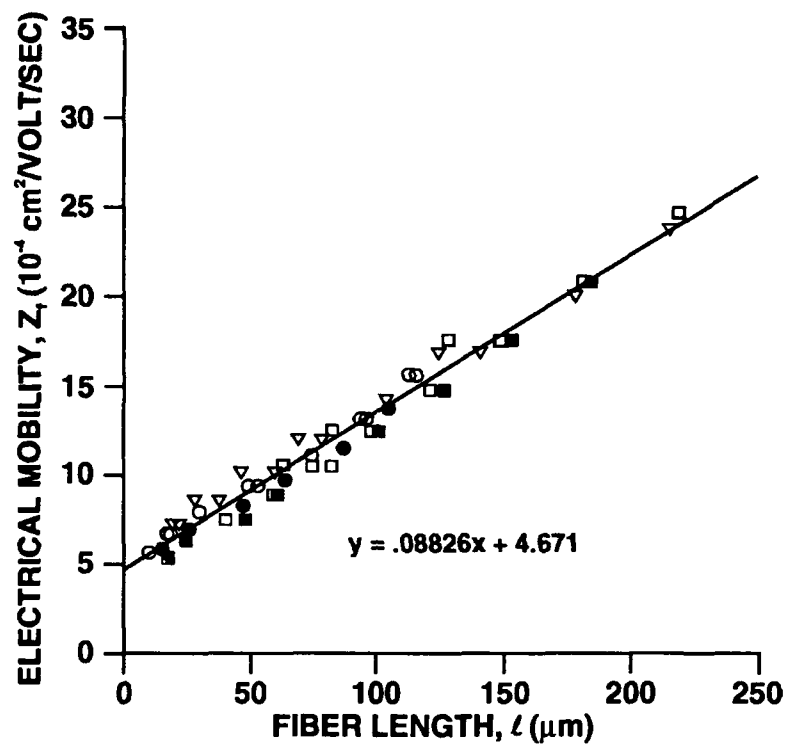


Figure 2. The relationship between the mean length (l) of the fibers collected and their mean electrical mobility (Z_f). Different symbols represent the data obtained from different operating conditions.

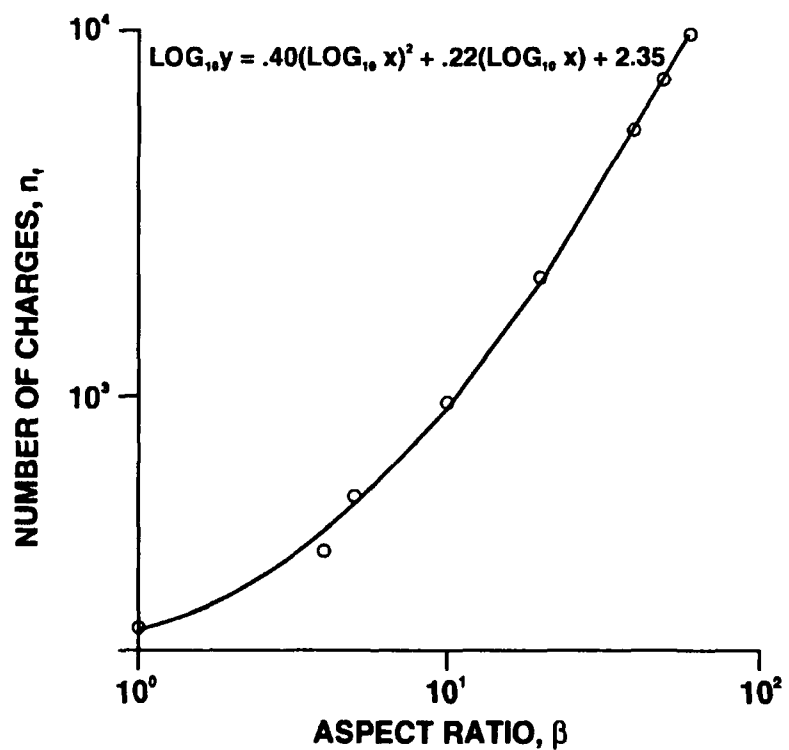


Figure 3. The relationship between the mean number of charges (n_f) on carbon fibers and the aspect ratio (β).

Preliminary results from this study demonstrated that fiber length can be classified using an electrical method. Polydisperse glass fibers with smaller diameters will be classified using a two-stage virtual impactor and the electrical classifier. Results from these studies will provide information on the optimal operating conditions in fiber classification and on the design criteria of a monodisperse fibrous aerosol generator.

(Research sponsored by the Office of Health and Environmental Research, U. S. Department of Energy, under Contract No. DE-AC04-76EV01013.)

CHARACTERIZATION OF AEROSOLS PRODUCED DURING SURGICAL PROCEDURES IN HOSPITALS

H. C. Yeh, R. S. Turner*, R. K. Jones, B. A. Muggenburg,
J. Smith**, L. S. Martin**, and P. W. Strine**

The potential for transmitting HIV from infected patients to health care workers via blood aerosol inhalation, particularly during orthopedic surgery, has added to the concerns about the hazards of working with HIV-positive patients in the medical profession (Day, L. *Can. Med. Assoc. J.* 139: 1935, 1988; Goldman, B. *Can. Med. Assoc. J.* 138: 736, 1988). In orthopedic surgical procedures, several types of surgical tools are used, including thermal energy tools such as surgical lasers and electrocautery, and mechanical power tools such as bone saws, reamers, and drills. It has been demonstrated, during simulated surgery in the laboratory, that respirable aerosols can be produced by these surgical instruments commonly used in orthopedic surgery (Heinsohn, P. *et al. Appl. Occup. Environ. Hyg.* 6: 773, 1991; Jewett, D. L. *et al. Am. Ind. Hyg. Assoc. J.* 53: 228, 1992). It has also been demonstrated that if HIV is present in the blood, the virus may be recovered from the aerosols produced (Johnson, G. K. and W. S. Robinson. *J. Med. Virol.* 33: 47, 1991). The aims of this study are (1) to characterize the aerosol produced during some orthopedic surgical procedures, and (2) to quantify the potential for aerosolization of blood-associated aerosols during various surgical procedures in hospital laminar flow operating rooms.

The primary surgical procedure chosen for the study was total hip replacement, although other procedures, such as knee and back surgeries were also studied. For the purpose of aerosol collection, the surgical procedure was divided into four segments related to the surgical instruments used. Table 1 lists the four main segments involved in a hip replacement surgery and the associated primary surgical tools used in each segment. Segment one involves a skin incision, separation of the muscles, and opening of the joint capsule. The primary surgical instruments used in this part of the surgery are a scalpel, an electrocautery, and occasional irrigation and suction. In segment two, the head of the femur is cut off, the femoral marrow cavity is reamed for the prosthesis, and the acetabulum is enlarged and fitted with the acetabular prosthesis. The primary tools used are power saws, drills, and an acetabular reamer with occasional irrigation and suction. Segment three involves cleaning the surgical site and final installation of the prosthesis. Some hammering is involved, in addition to pulse irrigation/suction, and finally closing the operative site. Segment four involves cleaning the room after the surgery. This step is included in aerosol measurement because considerable blood and tissue fragments are present on the surgical drapes and equipment, and a substantial increase in movement may resuspend the particles in the room.

A number of different aerosol instruments were chosen to collect and measure the aerosol produced during orthopedic surgery in the hospital. The purposes for these aerosol instruments are listed in Table 2. Marple personal impactors (Andersen Instruments Inc., Atlanta, GA) were worn by three surgeons, a nurse, and an aerosol

Table 1

The Surgical Segments of a Total Hip Replacement and the Tools Used During Each Segment

Surgical Segment	Tools Used
Skin incision and exposure of hip joint	Scalpel, electrocautery, irrigation/suction
Femur cutting, acetabulum forming	Bone drill, saw, acetabular reamer, irrigation/suction
Cleaning and installation of prosthesis, closure of site	Rreamers, hammer, pulse irrigation/suction
Room cleanup	Spray, vacuum

*Lovelace Medical Center, Albuquerque, New Mexico

**Centers for Disease Control, NIOSH, Atlanta, Georgia

sampling technician to collect breathing zone samples in order to determine size distribution and concentration of the aerosol during surgery. To avoid interfering with the movement of the surgeons, a fixed aerosol probe was placed above the patient, about 15-30 inches from the surgical site, to provide sample flow to a chamber from which the aerosols were analyzed using a Quartz Crystal Microbalance Cascade Impactor System (QCM) (model PC-2 Air Particle Analyzer, California Measurements, Inc., Sierra Madre, CA). In addition, filter samples and electrostatic precipitator (ESP) samples were obtained. The QCM is used to measure the size distribution of the aerosol produced in real-time in order to obtain size information during the use of the different surgical tools. The filter samples were taken to estimate the aerosol mass concentration or rate of aerosol production. The ESP was used mainly for obtaining samples for electron microscopic evaluation of particles. In addition, three area filter samples were taken to evaluate the spread of aerosols throughout the surgical room. A Chemstrip 9 (hemastix) analysis to measure hemoglobin (an indicator of red-blood-cell associated aerosols) was applied to samples collected at each stage of the Marple personal impactors as well as QCM and filter samples. The Marple personal impactors and the aerosol probe were cleaned and sterilized for each experimental run.

Table 2

Purpose of the Aerosol Sampling and Measurement Instruments Used

Instrument Type	Purpose
Marple personal impactors	Personal exposure and size distribution
Quartz crystal microbalance cascade impactor system	Real-time assessment of aerosol produced from different tools/processes-size distribution
Filters	Aerosol mass concentration
Electrostatic precipitator	Samples for electron microscopy

Ten surgical procedures were sampled as follows: five total hip replacements, one back vertebral fusion, three total knee replacements, and one hip reconstruction. Although the dynamics of aerosol mass concentration and size distribution varied widely from procedure to procedure and from time to time during the same procedure, some general observations can be made as follows: (1) the respirable aerosol concentration (mass) was higher during the total hip replacement procedures than during the total knee replacement procedures; (2) among the people wearing the Marple personal impactors, the impactors from the three surgeons had measurable amounts of aerosol, although the amounts were very low (on the order of 10 µg or less). Analysis by Chemstrip 9 (hemastix) consistently indicated positive results (3+, 2+ and 1+) for the first four to five Marple impactor stages which correspond to an aerodynamic particle size of 1.45 µm to over 14.2 µm (Fig. 1); (3) during the knee surgery, a tourniquet was applied, and no blood was observed during most of the procedure. Filter samples obtained during this time period were negative for hemoglobin by Chemstrip 9 analyses, while the filter sample obtained after the release of the tourniquet, followed by irrigation/suction to clean the site for suturing, showed a 1+ response, similar to observations during the total hip replacement procedure. From these observations, we hypothesize that most of the blood-associated aerosols might be produced during the irrigation/suction procedure; (4) QCM data indicated that aerosol mass concentration was highest (although the absolute values were very low) during the earliest stage of surgery, i.e., opening the surgical site when a scalpel, an electrocautery, and occasional irrigation and suction were applied. The other procedures produced a much lower mass concentration of aerosols; (5) occasionally, area filter samples and one or two stages of Marple impactor samples from personnel other than surgeons showed positive responses from Chemstrip 9 (either trace or 1+). This was probably due to splashing during the irrigation/suction procedure; and (6) room clean-up did not re-suspend any blood associated aerosols (negative results from Chemstrip 9 analysis).

The preliminary results from this study strongly suggested that blood-associated, respirable aerosols were produced during the orthopedic surgical procedures. However, Chemstrip 9 can also react to myoglobin from muscle, although with lesser degree of sensitivity. To identify the blood-associated aerosols, we are doing a similar total hip replacement experiment on dogs, with ⁵¹Cr labeled blood, so that red-blood-cell-associated iron can be positively identified. Preliminary results from this latter study do support the current results.

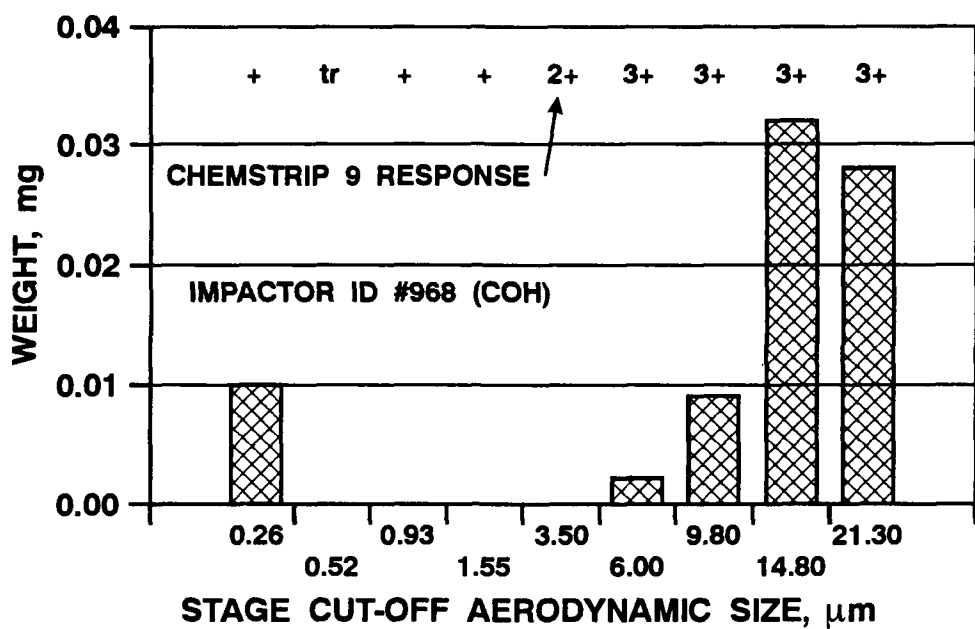


Figure 1. Size distribution determined by a Marple personal impactor worn by the chief surgeon. (The amount of hemoglobin detected on each stage by Chemstrip 9: negative = 0 erythrocytes/ μL , trace = 5 ery/ μL , 1+ = 10 ery/ μL , 2+ = 50 ery/ μL , 3+ = 250 ery/ μL . Sample size = 20 μL .)

(Research sponsored by the National Institute of Occupational Safety and Health under Interagency Agreement No. 92-05 with the U. S. Department of Energy, Contract No. DE-AC04-76EV01013.)

THERMAL OXIDATION OF CIGARETTE SMOKE EXHAUST

B. T. Chen, W. E. Bechtold, G. L. Finch, J. A. Lopez, and J. J. Thompson

Incineration of hazardous waste can be useful prior to disposal. The goal of incineration is to convert the objectionable, combustible compounds in the wastes by thermal oxidation to H_2O and CO_2 , thereby reducing the mass and the toxicity of the material for ultimate disposal. In our study of life-span evaluations of laboratory animals exposed to mainstream cigarette smoke, more than 6,000 research cigarettes are burned during a 6-h exposure each day. By combining the exhaust from the mainstream smoke in the animal exposure chambers and from the sidestream smoke in the smoke generator, more than 350 g of smoke particles, 500 g of carbon monoxide, and 150 g of hydrocarbons are produced in the emission exhaust per day. Conventional methods of using high-efficiency particulate air (HEPA) filters, vapor-adsorbing charcoal, or water scrubbers have been used to remove the various smoke components from the emission stream. However, each method has its own disadvantages. For example, when HEPA filters are used to remove smoke particles, frequent flow adjustments and filter changes are needed to compensate for the pressure drop increase caused by particle buildup on the filters; furthermore, such filters do not remove gases and vapors. Similarly, liquid waste containing tar presents a difficult waste disposal problem when a water scrubber is used. Thus, thermal oxidation is the only practical way to reduce the mass and the toxicity of the smoke exhaust during chronic smoke generation.

The goal of this study was to evaluate the feasibility of destroying total particulate matter (TPM) and toxic gases/vapors in cigarette smoke exhaust by thermal oxidation. This report describes the experimental testing of a bench-scale thermal oxidizer by examining the effects on oxidation efficiency of temperature, residence time and turbulence in the oxidizer, and mass concentration and particle size distribution in the cigarette smoke exhaust. The information obtained was then used to provide specifications for a full-scale thermal oxidizer having operating characteristics designed to minimize emissions of the smoke exhaust.

Figure 1 shows the experimental setup of the bench-scale thermal oxidizer. A quartz-tube heating furnace was used as a combustion chamber and a propane flame as a burner. The burner was used to initiate pre-combustion of smoke and to enhance turbulent mixing for oxygen and smoke. Cigarette smoke was generated by puffing 1R3 research cigarettes in a modified Walton smoke machine (Chen, B. T. et al. *Fundam. Appl. Toxicol.* 13: 429, 1989). Particle size distribution and mass concentration of cigarette smoke aerosol were determined by collecting impactor and filter samples, respectively. A gas chromatograph (GC) with a flame ionization detector was used to determine the concentration of total hydrocarbons in the smoke stream. Petroleum ether with an average molecular weight of 60 g/mole was used for the GC calibration standard. The oxidation efficiency was calculated from the concentrations of total hydrocarbon vapor observed before and after the heating furnace. The mass of TPM in the filter samples was also measured. The tube furnace was operated at various temperatures to study the effect of temperature on the oxidation efficiency.

Figure 2 shows the percentage of hydrocarbons oxidized at different furnace temperatures either with or without the use of the burner. For this test, the smoke mass concentration ranged between 450 and 600 mg/ m^3 with a furnace residence time of 0.75 sec. Oxidation efficiency increased with furnace temperature, reaching 100% at approximately 760°C without the burner, and 740°C with the burner. This result indicated that the use of the propane flame enhanced turbulent mixing for oxygen and smoke and, consequently, lowered the furnace temperature required for complete oxidation. Filter samples collected downstream from the furnace did not show any measurable quantity of TPM except for a few filters collected at temperatures less than 550°C (without the burner). At a constant flow rate of 5 L/min and temperature of 760°C, quartz tubes having different inner diameters were used to study the effects of residence time on the oxidation efficiency. As the residence times were varied between 0.25 and 0.5 sec, the efficiency increased from 6 to 73% and reached 100% when the residence time was 0.75 sec or longer. This result was expected because longer residence times in the furnace allowed more complete destruction of the substances in the smoke. Different smoke concentrations (250-950 mg/ m^3) and particle sizes (0.45-0.53 μm mass median aerodynamic diameter) were used to study their effects on oxidation efficiency. No conclusive effects of the sizes or concentrations examined on combustion efficiency were observed, indicating that these properties of the smoke aerosol may not be sensitive parameters compared to oxidation temperature, residence time, and flame turbulence.

This study demonstrated the feasibility of using thermal oxidation to reduce smoke exhaust and identified the important parameters in the oxidation process. The results obtained from this study were used as a guideline for designing a full-scale thermal oxidizer used to minimize smoke exhaust.

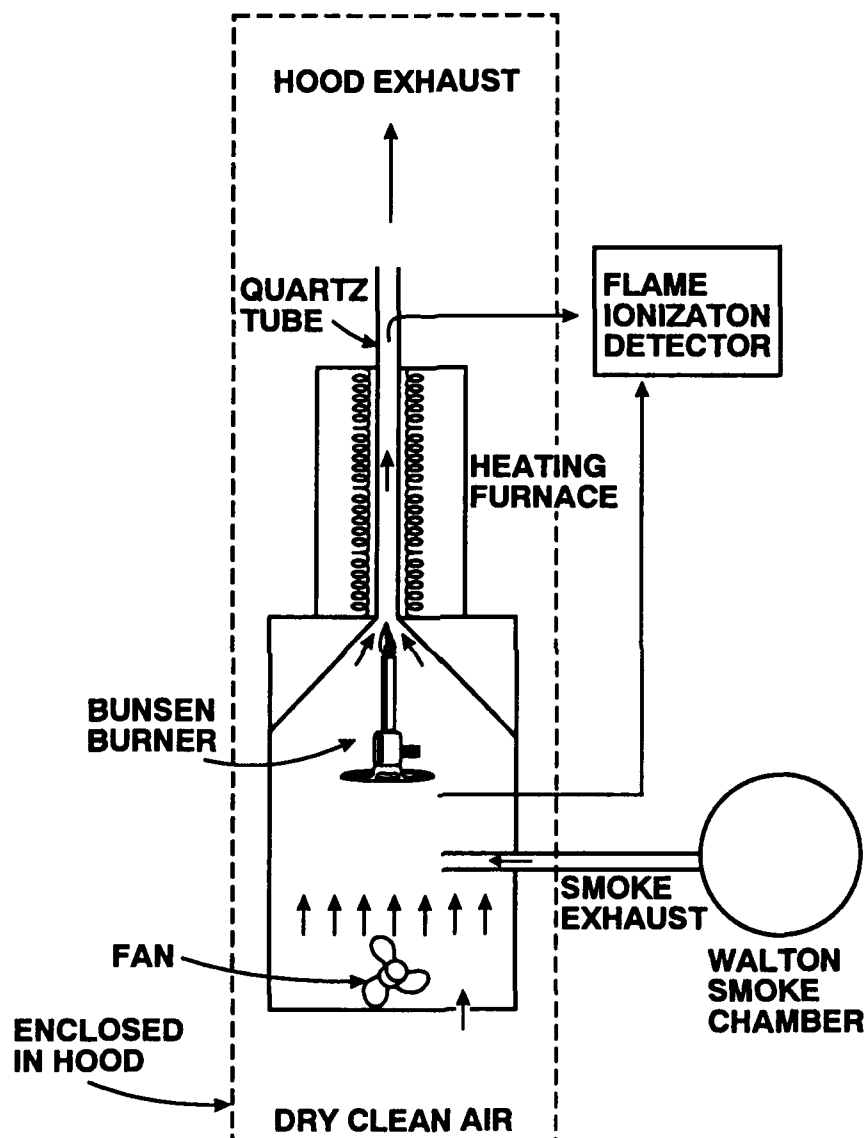


Figure 1. Schematic diagram of a bench-scale setup for thermal oxidation of cigarette smoke exhaust.

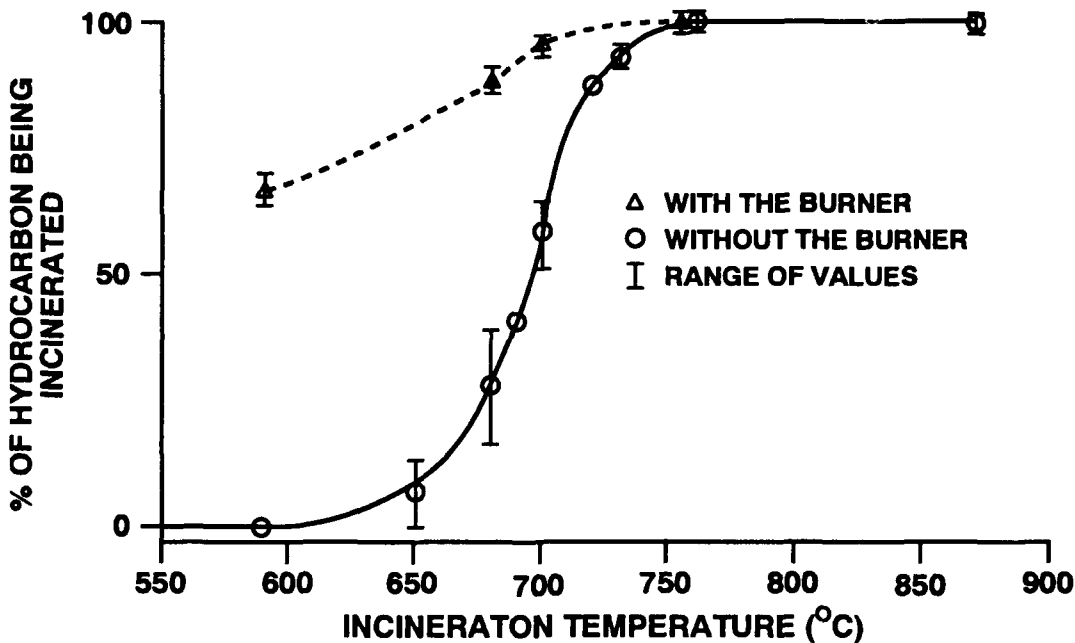


Figure 2. The oxidation efficiencies of the hydrocarbon concentration in the smoke exhaust at different temperatures in the furnace.

(Research sponsored by the Assistant Secretary for Defense Programs, U. S. Department of Energy, under Contract No. DE-AC04-76EV01013.)

AN EFFICIENT METHOD FOR SYNTHESIZING [d_6]-BUTADIENE MONOEPOXIDE

K. R. Maples, J. L. Lane, and A. R. Dahl

1,3-Butadiene is a high-volume chemical used in industry. The standards for occupational exposure to 1,3-butadiene are currently under review by the Occupational Safety and Health Administration due to the reported carcinogenicity of butadiene in rodents. Carcinogenicity of 1,3-butadiene is believed to be due to epoxide metabolites, but few studies have quantitated the *in vivo* concentration of butadiene monoepoxide and diepoxide following inhalation exposure to butadiene (Bond, J. A. *et al.* *Toxicol. Appl. Pharmacol.* 84: 617, 1986; Dahl, A. R. *et al.* *Toxicol. Appl. Pharmacol.* 110: 9, 1991).

We have shown the utility of using gas chromatography/mass spectroscopy (GC/MS) isotope dilution assays to monitor *in vivo* blood epoxide levels following inhalation exposure to alkenes (Maples, K. R. and A. R. Dahl. *Inhal. Toxicol.*, in press). An analogous investigation of 1,3-butadiene required synthesis of [d_6]-butadiene monoepoxide, a compound that is not commercially available. We have modified the method of Brougham *et al.* (*Synthesis* 11: 1015, 1987) using monoperoxyphthalic acid (MMPP) to synthesize [d_6]-butadiene monoepoxide from [d_6]-1,3-butadiene.

MMPP (0.5 g, 0.81 mmoles) was stirred into 5 mL water (pH 5.5) contained in a 25-mL, three-neck flask at room temperature. Attachments for gas introduction were fitted on two necks, and a 14/20 rubber septum was attached to the third neck as a sampling port. The internal volume of this assembly was *ca.* 100 mL. The reaction flask was evacuated, and the reaction was started by adding 1 atmosphere of 1,3-butadiene (\approx 3.4 mmoles at 620 Torr in Albuquerque) into the flask. During the 50-min synthesis, 1- μ L aliquots of the aqueous mixture were tested using a GC/MS (Hewlett-Packard, GC mode: 5890 series II, 5970 series Mass Selective Detector) equipped with a 40-m, 180- μ m, DB-Wax capillary column (J & W Scientific, Folsom, CA) at various times for butadiene monoepoxide formation. The GC/MS was operated under the following conditions: isothermal column temperature, 100°C; injector temperature, 220°C; and head pressure, 200 kPa. We used selective ion monitoring for the GC/MS detection (ions 39, 42, and 69 for [H_6]-butadiene monoepoxide; ions 42, 48, and 74 for [d_6]-butadiene monoepoxide; ions 29, 55, and 85 for [H_6]-butadiene diepoxide; and ions 30, 58, and 90 for [d_6]-butadiene diepoxide). The elution time for the butadiene monoepoxide was 4.2 min and for the butadiene diepoxide, 9.4 min. The concentration of butadiene monoepoxide was determined from a calibration curve of known concentrations of pure butadiene monoepoxide. This synthesis was repeated seven times, five using 1,3-butadiene and twice using [d_6]-1,3-butadiene.

The reaction flask was attached to a high vacuum line and cryogenically distilled using four removable U-tubes. The first U-tube after the reaction flask was immersed in an *o*-xylene slush (-23°C) to collect water as well as side products, such as butadiene diepoxide and 1-butene-3,4-diol. The second U-tube was immersed in a *m*-xylene slush (-45°C) to trap any unanticipated volatile materials passing the first trap (there were none). The third U-tube was immersed in a toluene slush (-95°C) to collect butadiene monoepoxide. The fourth U-tube was immersed in liquid nitrogen (-196°C) and trapped unreacted 1,3-butadiene. Following distillation, air was introduced into the collection tubes, and a sample from each U-tube was analyzed by GC/MS.

The concentration of butadiene monoepoxide in the aqueous solution increased over the first 40-50 min and then leveled off. The results from the five trials using 1,3-butadiene are shown in Figure 1. Analogous results were obtained using [d_6]-1,3-butadiene as the substrate. We obtained a $94 \pm 20\%$ ($X \pm SE$, $n = 5$) yield of the butadiene monoepoxide by the end of a 50-min reaction period. This yield is based on the MMPP used in our synthesis. Under the conditions used, little (< 1%) butadiene diepoxide was formed as determined by GC/MS.

To our knowledge, this is the first example of an epoxide synthesized from a gaseous alkene using MMPP. Preliminary work in our laboratory with other gaseous alkenes, such as isobutylene, has produced good epoxide yields in a short time, suggesting wide applicability of this method. Thus, this method of synthesis provides a simple and inexpensive means for the microsynthesis of epoxides from gaseous substrates.

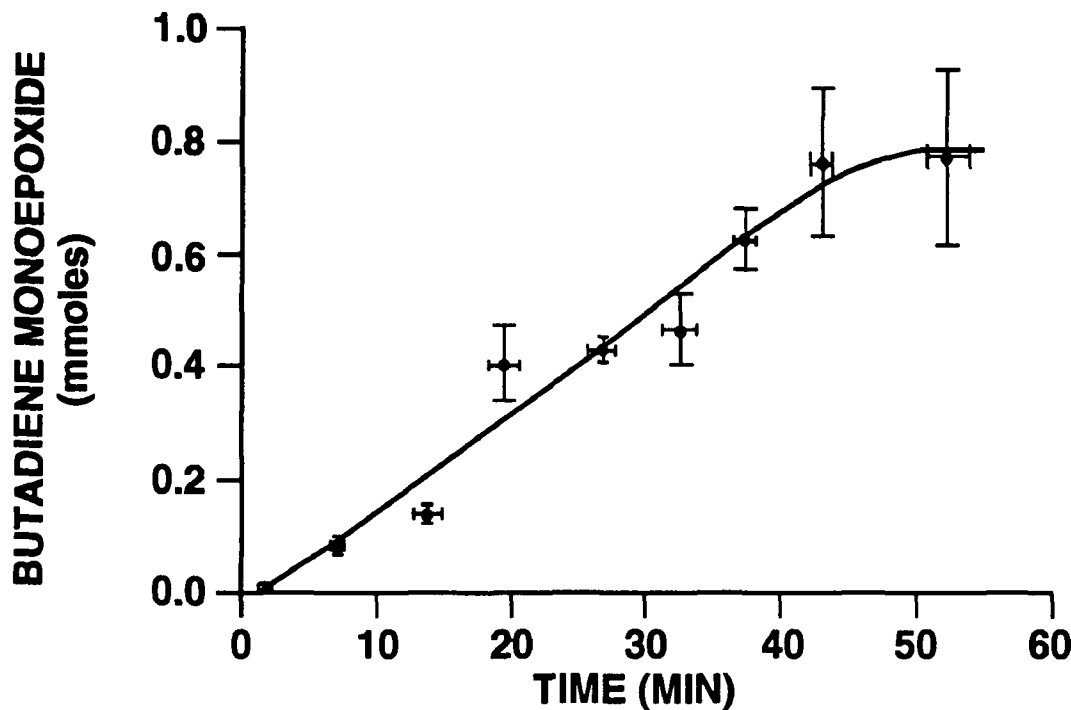


Figure 1. Butadiene monoepoxide formation during synthesis from 1,3-butadiene. Points represent the mean butadiene monoepoxide formed \pm SE for five determinations within the specified time range (mean \pm SE).

(Research supported by NIH Grant 04422 from the National Institute of Environmental Health Sciences with contributing support from the Chemical Manufacturers' Association under Funds-In-Agreement No. DE-FI04-91AL66351 in facilities provided by the U. S. Department of Energy under Contract No. DE-AC04-76EV01013.)

II. DEPOSITION AND CLEARANCE OF INHALED TOXICANTS

FLOW MEASUREMENT AND THEORETICAL CALCULATION OF AEROSOL DEPOSITION IN A HUMAN TRACHEOBRONCHIAL TREE MODEL

Y. S. Cheng, S. M. Smith*, and H. C. Yeh

The deposition efficiency and distribution pattern of inhaled aerosols are important for determining the dose of an aerosol to the human respiratory tract. The pattern of deposition is particularly important for aerosols that exert most of their toxic effects upon contact with lung tissue, such as α -emitting radionuclides. Studies in models of the human tracheobronchial tree are useful in providing data to evaluate the deposition of aerosols. The calculation of dose from ultrafine aerosols, $< 0.2 \mu\text{m}$, to the human tracheobronchial tree is important. Particles with potential health effects in this size range are generated by gasoline and diesel engines, kerosene heaters, cigarette smoke, and also include the ^{222}Rn decay products. Casts prepared from specimens of the human tracheobronchial tree were used by R. B. Schlesinger *et al.* (*Am. Ind. Hyg. Assoc. J.* 33: 237, 1972) to study particle deposition. Initial studies all used particles with diameters $> 0.04 \mu\text{m}$ in diameter (Gurman, J. L. *et al.* *Aerosol Sci. Technol.* 3: 245, 1984). No data are available for the deposition of smaller particles in the human tracheobronchial tree. The purpose of our initial study was to determine the theoretical deposition of ultrafine aerosols in a human tracheobronchial tree model.

A hollow silicone rubber model of the upper airways of the tracheobronchial tree of a 23-yr-old male was used in the study. The tracheobronchial model has up to 10 generations. Airway diameters vary, from 1.6-11.0 mm excluding the trachea (20 mm) and main bronchi (9.5-16.0 mm). The cast was not symmetrical in terms of generation number or airway diameter. Production method was similar to that used by E. L. Patra *et al.* (EPA 600/D-84-038 c.2, p. 1, 1984). A detailed examination of airflow in the cast was performed at flow rates of 10, 20, and 30 LPM. A hot wire anemometer probe (TSI Model 8470) was used to measure the velocity of air flowing from each terminal opening of the cast. Velocity measurements from each open end were used to determine the total flow rate through each airway path. The velocity at each end airway was measured at several different positions. Readings were taken at the center line as well as at the point of maximum velocity. A mean velocity was calculated for each end airway. The airflow rate through each end airway was then calculated from its area and measured mean velocity. Extensive morphometric measurements had been performed on the original master cast. Flow through proximal airways was calculated by summing the branched flow of daughter airways.

Several empirical equations are available for predicting the deposition of ultrafine particles in cylindrical tubes. The deposition efficiencies measured in casts can be compared with values predicted for deposition by diffusion and impaction. This information is useful in verifying predicted deposition efficiencies and in helping to develop detailed knowledge of deposition efficiency useful in evaluating risk from exposure to hazardous aerosols. From the detailed examination of flow rates through the cast, it is possible to compare the deposition fraction calculated from several different equations.

Two equations were used to calculate the deposition fraction in this study. The Ingham equation (Ingham, D. B. *Aerosol Sci.* 6: 124, 1975) governs the diffusion of aerosols through a cylindrical tube. The Ingham equation is based upon the plug flow assumption, i.e., the velocity at the walls of the pipe is equal to the velocity through the center of the pipe. The second equation predicts aerosol deposition based upon fully developed parabolic airflow. When airflow is fully developed, the velocity along the pipe walls is at a minimum and the velocity is maximal through the center of the pipe. These equations can be used to predict both inspiratory and expiratory deposition in a tracheobronchial tree cast. The total aerosol deposition in the cast can be calculated by:

$$D_{I+E} = 1 - P_I \cdot P_E ,$$

where, P_I = inspiratory penetration
 P_E = expiratory penetration.

*UNM/ITRI Inhalation Toxicology Graduate Student

Deposition was predicted for aerosols between 0.00475-0.10 μm in diameter. Figure 1 shows the predicted inspiratory aerosol deposition at 20 LPM (near normal breathing rate for a human adult at rest). Particle size dependence of deposition efficiency was observed. Deposition efficiency increased with decreasing flow rate (Fig. 2). The Ingham equation consistently predicts a higher deposition fraction than does the equation for fully developed flow. Both equations also predict higher deposition efficiencies for expiratory flow than for inspiratory flow (Fig. 3). The deposition fraction from each equation will be compared with the deposition fraction measured experimentally to determine a best fit equation.

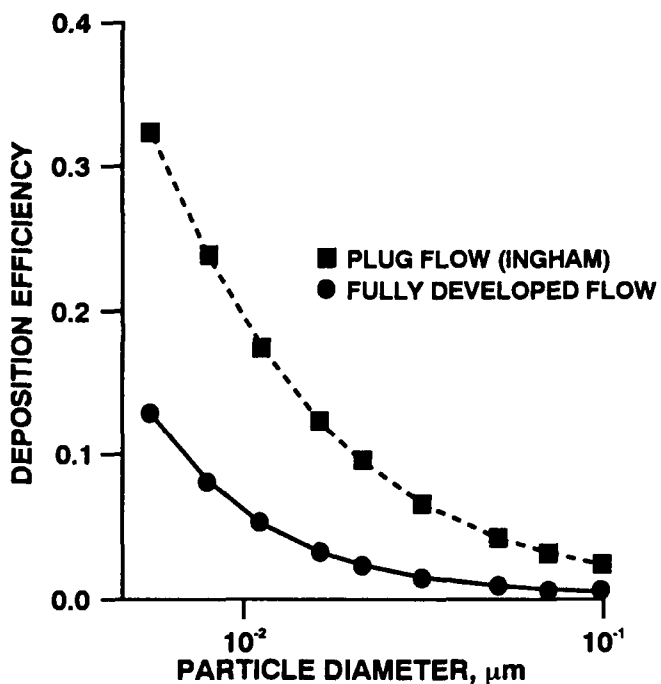


Figure 1. Predicted deposition efficiency of ultrafine aerosols in the ITRI tracheobronchial tree model for 20 LPM inspiratory flow.

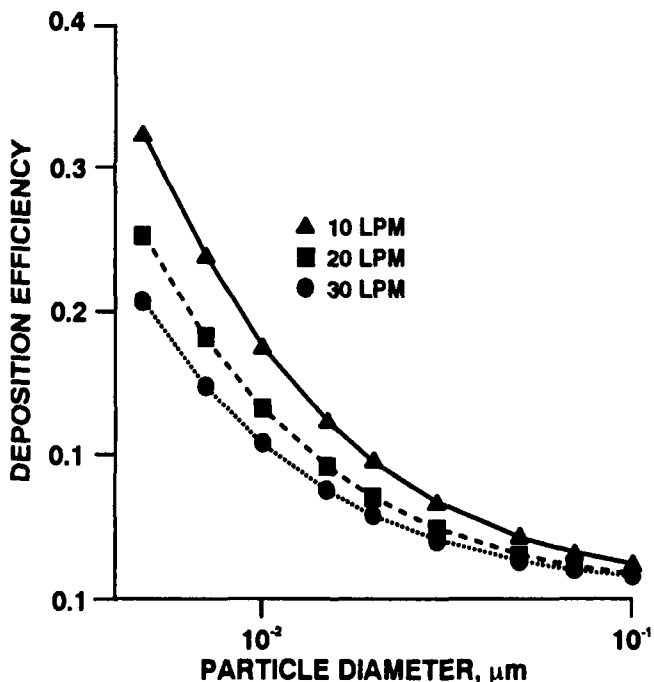


Figure 2. Air flow rate dependence of predicted ultrafine deposition efficiency in the ITRI tracheobronchial tree model for inspiratory plug flow.

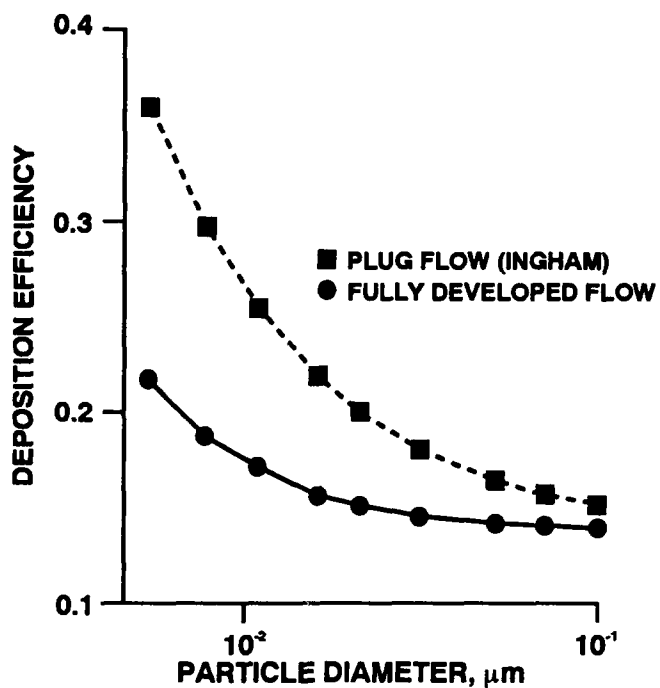


Figure 3. Predicted inspiratory and expiratory aerosol deposition for plug flow in the ITRI tracheobronchial tree model at 20 LPM.

(Research sponsored by the Office of Health and Environmental Research, U. S. Department of Energy, under Contract No. DE-AC04-76EV01013.)

IN VIVO DEPOSITION OF INHALED ULTRAFINE PARTICLES IN AIRWAYS OF RHESUS MONKEYS

H. C. Yeh, B. A. Muggenburg, and J. R. Harkema

The nasal airways represent the first line of defense from inhaled particles. The particles that deposit in the nasal airways cannot reach either the tracheobronchial or the pulmonary regions. Thus, information on the deposition of inhaled particles in the nasal airways is important for a better understanding of the potential risk to the respiratory tract from inhaled particles. For inhaled radon progeny, the particle sizes of interest are those between 0.001 to 0.005 μm , the effective size of unattached progeny, and 0.005 to 0.5 μm , the most common sizes reported for attached radon progeny in mines and homes (NCRP Report No. 78, 1984; James, A. C. *et al.* In *Radiation Hazards in Mining: Control, Measurement, and Medical Aspects* [M. Gomez, ed.], Kingsport Press, Kingsport, TN, 1981).

The results of recent morphologic and morphometric studies indicate that, of the commonly used laboratory animals, nonhuman primates have nasal structures that most closely resemble those of humans (1988-89 Annual Report, p. 27; Harkema, J. R. *et al.* *Am. J. Anat.* 180: 266, 1987). In a previous report (1990-91 Annual Report, p. 44), we presented results of an *in vivo* deposition of unattached ^{220}Rn progeny in the rhesus monkey. As a continuation of that work, we present here the results of an *in vivo* deposition study in the rhesus monkey, using monodisperse, 0.1 μm $^{59}\text{Fe}_2\text{O}_3$ particles to simulate the attached fraction of the radon progeny. These data, along with the previous results, will be used to validate nasal cast studies (1989-90 Annual Report, p. 29) and also provide a data base for the rhesus monkeys.

Four adult rhesus monkeys, between 7 and 8 yr old and ranging in body weight between 7.3 and 10.4 kg, were used in this study. Figure 1 shows the experimental apparatus. The aerosol was produced by nebulizing a ^{59}Fe -labeled iron nitrate solution, using a Lovelace nebulizer. The aerosol was then heat treated by two furnaces set at 200° and 1150°C to become $^{59}\text{Fe}_2\text{O}_3$ particles. The monodisperse 0.1 μm $^{59}\text{Fe}_2\text{O}_3$ aerosol was obtained by using an electrostatic classifier (Model 3071, TSI Inc., St. Paul, MN). The activity concentration of the ^{59}Fe -labeled iron nitrate solution was 5 mCi/mL. For the inhalation exposure, the monkey was anesthetized using ketamine and xylagaine.

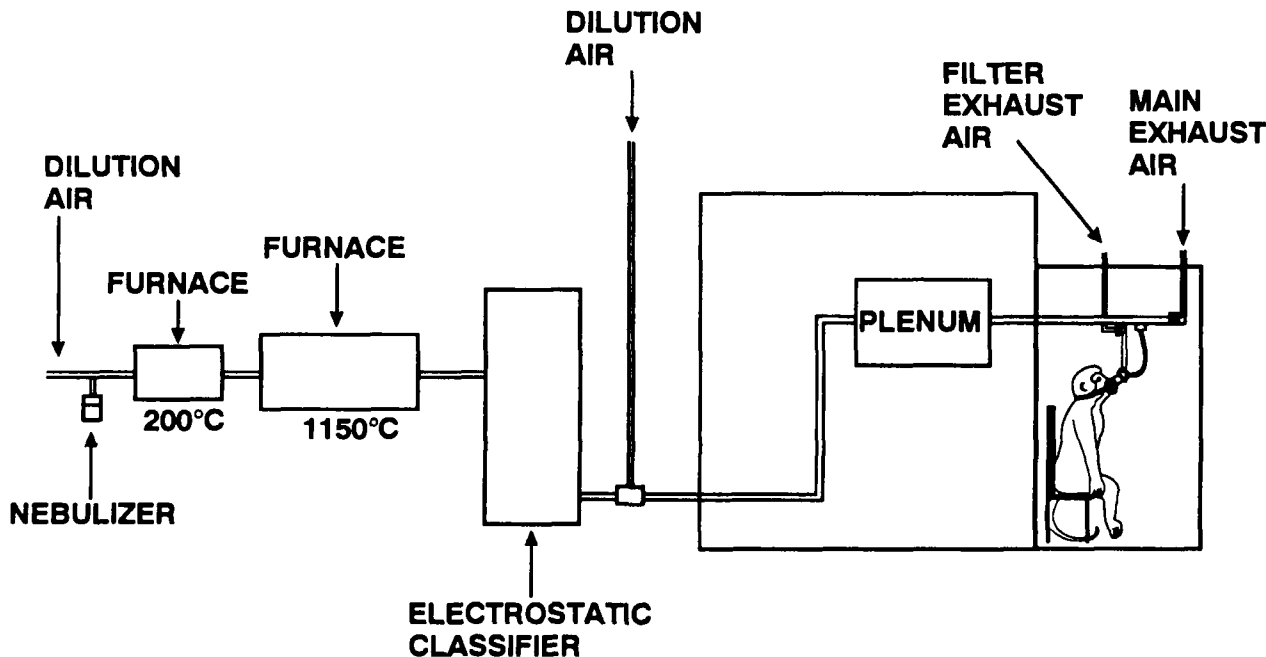


Figure 1. Schematic diagram of the $^{59}\text{Fe}_2\text{O}_3$ monkey exposure system.

During the experiment, the monkey's mouth was taped closed to ensure nasal breathing. A specially made face mask with a pneumotach and a Rudolf valve was used. The breathing pattern was recorded from the pneumotach, and the Rudolf valve was used to avoid mixing the inhaled and exhaled air. To minimize the effect of respiratory clearance on the determination of the amount of particles deposited, a short, 8-min inhalation exposure was used. Immediately after the exposure, the monkey was sacrificed (within about 5 min) by exsanguination under deep anesthesia and a necropsy performed. Respiratory tract tissues, such as various nasal tissues, larynx, trachea, individual lung lobes, and the GI tract were collected. The regional deposition was estimated from the amounts of radioactivity measured in these tissues, the face mask, various parts of the connecting tubing, and the backup filter for exhaled air using a 3" x 5" NaI(Tl) crystal spectrometer. The particle size of the $^{59}\text{Fe}_2\text{O}_3$ particles was verified by a screen-type diffusion battery.

Table 1 lists the results from this study. Also included are those from the previous study with ^{220}Rn progeny. For the current study, the measured nasal deposition efficiency was 6.8%, as compared to 11% and 56% for ^{220}Rn progeny of 0.014 μm and 0.005 μm , respectively, indicating that the smaller particle size had the higher deposition fraction. On the other hand, 38% of the 0.1 μm Fe_2O_3 particles deposited in the lung, as compared to 68% and 34% for 0.014 μm and 0.005 μm ^{220}Rn progeny, respectively, indicating that there is a peak deposition efficiency between 0.005 μm and 0.1 μm .

Table 1

Regional Deposition of Ultrafine Particles of $^{59}\text{Fe}_2\text{O}_3$
and ^{220}Rn Progeny in Rhesus Monkeys (mean \pm SD)

Particle Diameter, μm	0.005 \pm 0.001	0.014 \pm 0.001	0.10 \pm 0.005
Body Weight, kg	6.4 \pm 1.2	5.8 \pm 0.4	8.7 \pm 1.3
Number of Monkeys	2	2	4
Nasal Deposition, %	56 \pm 8.5	11 \pm 2.1	6.8 \pm 1.3
Lung Deposition, %	34 \pm 9.1	68 \pm 9.63	38 \pm 14.6

Figure 2 shows the nasal deposition from the current *in vivo* study, as well as those from previous ^{220}Rn progeny studies, as compared with a previous nasal deposition study using rhesus monkey nasal casts made at ITRI and CIIT (1989-90 Annual Report, p. 27). Good agreement between the results of the *in vivo* studies and those from the nasal cast study indicates that, for detailed studies of the deposition of radon and radon progeny in nasal airways, the approach of using nasal casts seems to be justified. As indicated in the previous study, substantial nasal deposition occurs for ultrafine particles, and the effect of the air flow rate is minimal. Within this size range, the deposition mechanism is dominated by diffusion. For particle sizes larger than 0.5 μm where inertia is the dominant deposition mechanism, the use of nasal casts for deposition studies may not apply, and further study is required to verify this possibility.

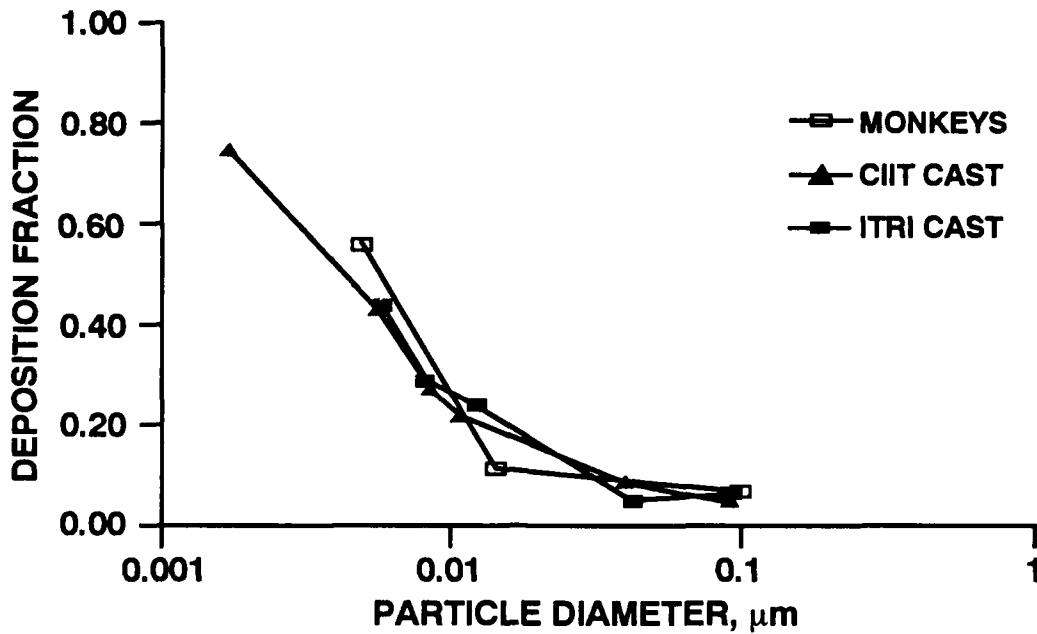


Figure 2. Comparison of *in vivo* and nasal cast deposition of the rhesus monkey.

(Research sponsored by the Office of Health and Environmental Research, U. S. Department of Energy, under Contract No. DE-AC04-76EV01013.)

FACTORS INFLUENCING THE DEPOSITION OF INHALED PARTICLES IN F344 RATS WITH PRE-EXISTING PULMONARY EMPHYSEMA

D. L. Lundgren, M. D. Hoover, F. F. Hahn, and J. L. Mauderly

The possible consequences of the exposure of sensitive subpopulations, including individuals with pre-existing pulmonary disease, to toxic substances by inhalation are of concern. However, experimental work has only recently been undertaken in toxicant-exposed laboratory animals to determine the modifying effects of well-characterized, pre-existing pulmonary diseases. One pre-existing pulmonary disease, emphysema, has been associated with increased susceptibility to the effects of inhaled pollutants in humans and has been studied in laboratory animals exposed by inhalation to various toxic substances. Although rats with pre-existing pulmonary emphysema do not appear to be uniquely sensitive when exposed by inhalation to toxic substances, they do appear to have a lower fractional rate of deposition of inhaled particles when compared with control animals (Lundgren, D. L. et al. *Human Toxicol.* 9: 295, 1990; Mauderly, J. L. et al. *Am. Rev. Respir. Dis.* 141: 1333, 1990). Similar observations have been reported in emphysematous rats or Syrian hamsters during brief (minute to hour) or longer exposures to aerosols. Differences in the quantities of inhaled particles that deposit in the lung of emphysematous rodents compared with control rodents may result in differences in their responses when exposed to the same concentrations of toxic particles.

The present study was initiated to gain a better understanding as to why the deposition of aerosols is lower in animals with pre-existing pulmonary emphysema than in control animals. Such information would be valuable in planning and interpreting results from future studies of the effects of inhaled toxic substances in animals with pre-existing pulmonary diseases. The particle sizes of the exposure aerosols used (Table 1) were selected so that the rats would receive either (1) a physically small aerosol that would be deposited primarily by diffusion or (2) a larger aerosol that would be deposited primarily by inertial and sedimentation mechanisms.

Table 1

Particle Size Distributions for the Small and Large Iron Oxide Aerosols
Used in the Study of Aerosol Deposition and Clearance in Emphysematous Male Rats

Aerosol	Physical Size ^a				Aerodynamic Size ^b	
	Count Median Diameter (μm)	Geometric Standard Deviation (σ_g)	Mass Median Diameter (μm)	Geometric Standard Deviation (σ_g)	Activity Median Aerodynamic Diameter (μm)	Geometric Standard Deviation (σ_g)
Small	0.02	3.1	0.2	1.7	0.8	1.7
Large	0.04	3.7	0.9	1.5	2.4	1.7

^aCount distributions were determined based on projected area diameters measured by electron microscopy. Mass distributions were determined from volume transformations of the count distributions, assuming that particle density was constant for all particle sizes. Nominal particle density for the iron oxide aerosol is 5 g/cm³.

^bAerodynamic size distributions were determined by cascade impactors.

A total of 92 male F344/N rats approximately 12 wk of age and reared at this Institute were used. About 70 days before exposure to aerosols of $^{59}\text{Fe}_2\text{O}_3$, pulmonary emphysema was induced in the rats by the intratracheal instillation of elastase (Calbiochem-Behring, La Jolla, CA), 0.5 IU g⁻¹ of body mass, in approximately 1 mL of saline, while the rats were under halothane-induced anesthesia, as previously described (Harkema, J. R. et

al. Am. Rev. Respir. Dis. 126: 1058, 1982). Other rats received 1 mL of normal saline intratracheally on the same day that the rats were treated with elastase. Thirty-two to 34 days after the instillation of elastase and 14 to 19 days before exposure to $^{59}\text{Fe}_2\text{O}_3$, 15 rats treated with elastase and 15 treated with saline were selected at random and screened for respiratory function parameters (Harkema *et al.*, 1982) that could be indicative of pulmonary emphysema.

Mild pulmonary emphysema in the rats prior to their exposure to $^{59}\text{Fe}_2\text{O}_3$ was indicated by respiratory function measurements and confirmed by morphological measurements at the end of the study. Histologic examination of the lungs of the elastase-treated rats indicated the presence of panacinar emphysema, consisting of enlarged air spaces with ruptured alveolar septa without inflammation, which was distributed in a patchy manner in all lung lobes. There were no significant lesions in the lungs of the control rats.

Up to six rats at a time were exposed by nose-only inhalation of $^{59}\text{Fe}_2\text{O}_3$ aerosols while in plethysmographic exposure units described in detail elsewhere (Medinsky, M. A. *et al.* *Toxicol. Appl. Pharmacol.* 78: 215, 1985). The rats were exposed to the $^{59}\text{Fe}_2\text{O}_3$ while connected to a rodent inhalation exposure chamber (Raabe, O. G. *et al.* *Toxicol. Appl. Pharmacol.* 26: 264, 1973). The respiratory rate and volume of each rat were recorded during the exposures. During eight exposures of 43 rats (21 emphysematous and 22 controls) to the relatively small particles, the aerosol concentrations of ^{59}Fe ranged from 41 to 64 kBq/L (49 ± 8 ; mean \pm SD), and exposure durations ranged from 20 to 30 min (25 ± 5). During eight exposures of 48 rats (23 emphysematous and 25 controls) to the relatively larger particles, the aerosol concentrations of ^{59}Fe ranged from 18 to 41 kBq/L (29 ± 8), and exposure durations ranged from 30 to 40 min (35 ± 5).

The ^{59}Fe lung burdens in all rats were determined by whole-body counting using large-volume, well-type liquid scintillation detectors on days 7, 10, 14, 17, 24, and 28 after exposure to the radiolabeled Fe_2O_3 aerosols. The initial lung burden of each rat was determined from the whole-body counting data by fitting single-component, negative exponential functions to these data (corrected for physical decay) and then extrapolating to the time of exposure. The slopes of these curve fits were converted to clearance half-times, which are good approximations of clearance half-times from the pulmonary region. The clearance half-times of the ^{59}Fe from the emphysematous rats exposed to the small (50 ± 16 days; mean \pm SD) and the large (38 ± 9 days) particles were not significantly different (F test; $p > 0.05$) from the clearance half-times in the respective control groups that were 53 ± 9 for the small particles and 40 ± 13 for the large particles. It is evident that both the control and the emphysematous rats cleared the smaller particles from the lungs significantly more rapidly (Student's *t* test; $p < 0.05$) than the larger particles. The correlation coefficients for all groups were similar, indicating similar variability in the data from each group of rats.

All rats were sacrificed by the intraperitoneal injection of a lethal dose of sodium pentobarbital 28 days after inhalation exposure to $^{59}\text{Fe}_2\text{O}_3$ and necropsied. The lungs were fixed by intratracheal perfusion with 10% neutral buffered formalin for 12 h, at constant pressure of 20 cm. The volumes of the fixed lungs were determined by the displacement of normal saline. Fixed lungs were trimmed, embedded in paraffin, sectioned at 5 μm , stained with hematoxylin and eosin, and examined microscopically.

Because the emphysematous rats had higher minute volumes (Student's *t* test; $p < 0.05$), they inhaled more of the labeled aerosol of both particle sizes than the control rats (Table 2). However, smaller fractions of the inhaled aerosols (large and small) were deposited in the lungs of the emphysematous rats (Table 2) than in the lungs of the control rats (Student's *t* test; $p < 0.05$). Also, less of the inhaled larger particles than smaller particles was deposited in the lungs of both the emphysematous and control rats (Table 2) (Student's *t* test; $p < 0.05$). These differences in the inhalation and deposition of aerosols should be considered in planning studies of inhaled particles in rats with pre-existing pulmonary emphysema. Modeling efforts, such as those described by G. M. Schum *et al.* (*Bull. Math. Biol.* 42: 1, 1980), are underway to examine the mechanisms of deposition, biological differences, and physical properties of the aerosols that may have resulted in the decreased deposition in the emphysematous rats.

Table 2

Respiratory Parameters, Activity Inhaled, and Activity Deposited in the Lungs of Unsedated Control and Emphysematous Male Rats Exposed by Inhalation to Aerosols of $^{59}\text{Fe}_2\text{O}_3$

Particle Sizes	Treatment Groups	Respiratory Rate (breaths/min)	Minute Vol. (mL) ^a	kBq Inhaled	kBq Deposited in Lungs	Inhaled Aerosol Deposited (%)
Small	Control	146 ± 19 ^b	173 ± 35	180 ± 54	19 ± 9.1	10.6 ± 5.1
	Emphysema	150 ± 21	244 ± 43 ^c	264 ± 65 ^c	22 ± 8.2	8.2 ± 2.6 ^d
Large	Control	146 ± 13	201 ± 37	204 ± 62	15 ± 6.7	8.0 ± 4.5
	Emphysema	157 ± 20 ^c	252 ± 45 ^c	242 ± 68	12 ± 6.8	4.9 ± 2.5 ^d

^aMinute volume corrected for the barometric pressure, temperature, and relative humidity at exposure (Dahl, A. R. *et al. Am. Ind. Hyg. Assoc. J.* 48: 505, 1987).

^bMean ± SD.

^cSignificantly greater (Student's *t* test; $p < 0.05$) than controls.

^dSignificantly less (Student's *t* test; $p < 0.05$) than controls.

(Research sponsored by the Office of Health and Environmental Research, U. S. Department of Energy, under Contract No. DE-AC04-76EV01013.)

DEPOSITION OF MONODISPERSE LIQUID DROPLET AEROSOLS IN AN MRI-BASED NASAL AIRWAY REPLICA

R. A. Guilmette

The nasal airways are the first tissue sites available for deposition of inhaled aerosols in normally nose-breathing people. These airways are also known sites for the development of cancer from inhaled particles and vapors in humans and experimental animals. The complex anatomy of the nasal airways has made the prediction of particle deposition difficult. However, sparse data indicate that the deposition patterns will be heterogeneous within the airways, and will likely depend strongly on particle size, flow rate, and anatomy.

To better understand the patterns of particle deposition in nasal airways, we have developed a method for constructing anatomically accurate replica models that use *in vivo* morphometric data obtained from magnetic resonance imaging (MRI) (1989-90 Annual Report, p. 33; Guilmette, R. A. and T. J. Gagliano. In *Proceedings of Inhaled Particles VII Symposium 1991*, in press). The replica model used in this study was derived from MRI of a nonsmoking Caucasian male, 53 yr of age, 73 kg body mass, and 173 cm in height; he had no obvious nasal airway deformity or disease.

We have reported the deposition of monodisperse ultrafine particles of NaCl or Ag (1990-91 Annual Report, p. 35). This study used larger-sized particles that deposit primarily by inertial impaction, i.e., from 1.0 to 9.0 μm MMAD. The aerosols consisted of monodisperse liquid droplets of uranine-labeled di-(2-ethylhexyl) sebacate (DES) produced by a vibrating orifice generator (TSI Model 3050, St. Paul, MN). After passing through a ^{85}Kr discharger, the aerosols were drawn through a split-flow system whereby half of the aerosols were collected on a membrane filter (inlet concentration, C_{in}) and the other half through the nasal airway model. A similar membrane filter was placed on the exit end of the model to collect the aerosols that did not deposit in the nasal airway replica (outlet concentration, C_{out}). Following each exposure, the filters were removed, the fluorescent DES dissolved from the filter in isopropyl alcohol, and the fluorescence intensity measured in a standard fluorometer (Hitachi Model F-1200, somewhere in CA). Both inspiratory and expiratory flow depositions were measured at constant flow rates. Deposition efficiencies (D_e) were calculated according to the relationship

$$D_e = 1 - (C_{\text{out}}/C_{\text{in}}) . \quad (1)$$

Figure 1 shows the deposition results for inspiratory air flow, and Figure 2 for expiratory air flow. In both cases, the data are plotted in terms of the impaction parameter, d^2Q , where d is the particle diameter in μm and Q is the flow rate in L min^{-1} . The curves plotted with the flow-rate-specific data sets were obtained by a Marquardt-based nonlinear regression fitting procedure (NLIN, SAS Statistical Software, Cary, NC). A single model formulation based on the earlier work of Cheng *et al.* (*Radiat. Prot. Dosim.* 38: 41, 1991) was used to fit the data:

$$D_e = 1 - e^{-ad^b Q^c} , \quad (2)$$

where a , b , and c were fit parameters. Several iterations were done, including fitting all three parameters simultaneously, fixing $b = 2$ and $c = 1$, and fixing $c = 1$. The optimal fits, based on both the magnitude and the random patterning of the residuals resulted from fixing $c = 1$. Because the fitted parameters were found to be highly correlated, the model fit was further restricted as follows. All four flow-specific data sets were fit simultaneously, allowing four different coefficients, a_i , but only allowing a single common exponent for particle size, b . Thus, the fitted curves illustrated in Figures 1 and 2 were derived from the following model:

$$D_e = 1 - e^{-(a_1 v_1 + a_2 v_2 + a_3 v_3 + a_4 v_4) d^b Q} , \quad (3)$$

where a_i is the flow-rate-specific coefficient, and v_i equal 1 for the i th flow rate, 0 otherwise, and $c = 1$.

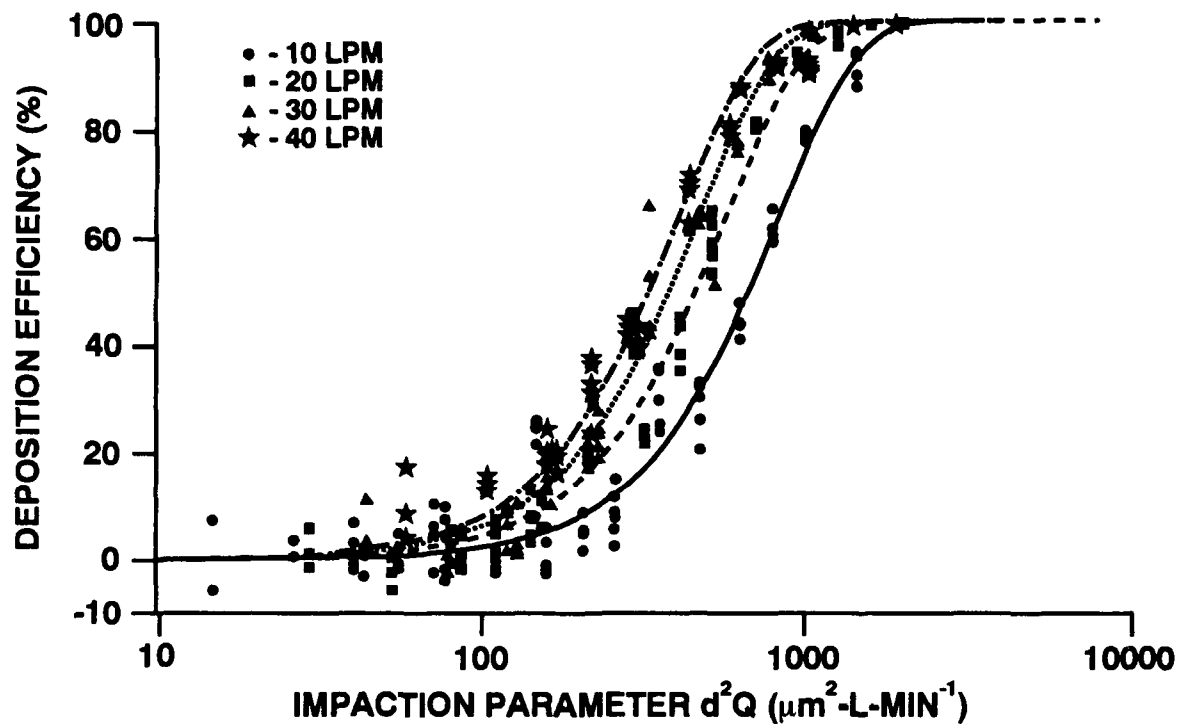


Figure 1. Inspiratory deposition efficiency vs. the impaction parameter d^2Q for four flow rates. Curves are the fits obtained using Eq. (3).

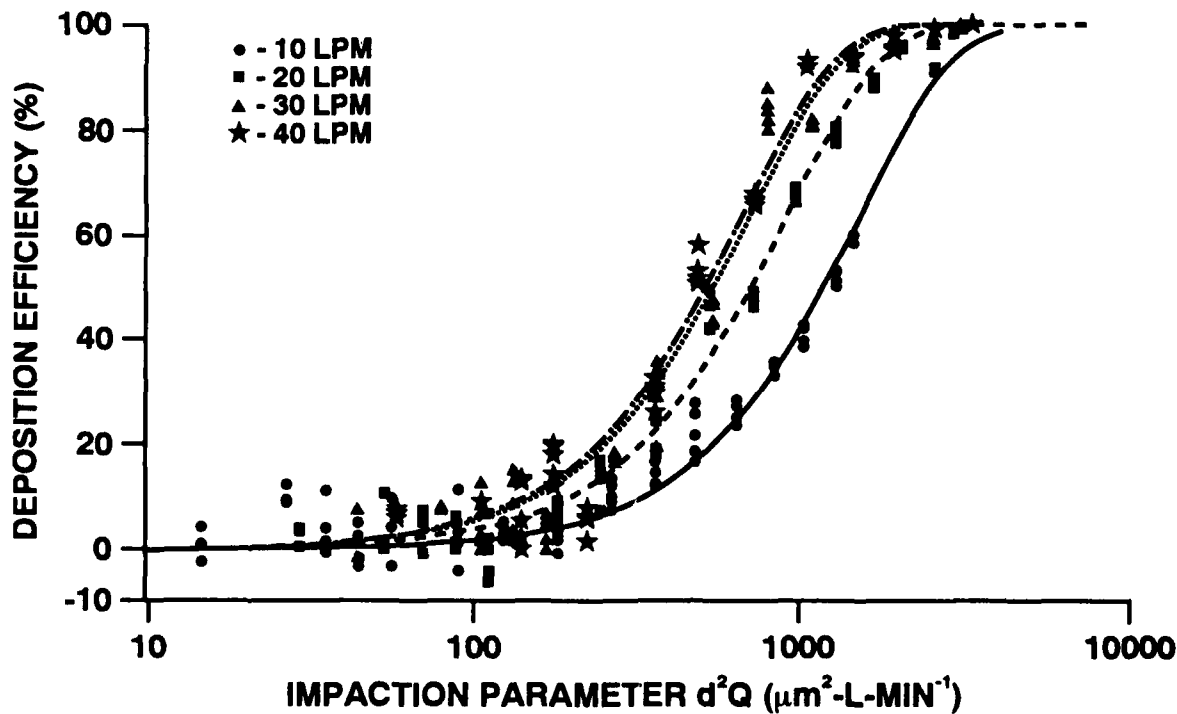


Figure 2. Expiratory deposition efficiency vs. the impaction parameter of d^2Q for four flow rates. Curves are the fits obtained using Eq. (3).

The results of this study have shown similarities and differences from other studies. The sigmoidal shapes of the deposition efficiency curves appear to be a common feature when the deposition data are plotted against the impaction parameter, d^2Q . However, the exponent for the particle size was not quadratic; for inspiratory airflow, $b = 3.6$, for expiratory, $b = 3.0$. These slopes were statistically different. Additionally, expressing the data in terms of d^2Q did not result in a convergence of the data, i.e. there was still a marked dependence of particle-size-specific deposition efficiency on flow rate for both inspiratory and expiratory airflow. According to the model fits, the coefficient, a , was shown to increase nearly linearly with flow rate, and with similar values for both inspiratory and expiratory flow (Fig. 3). These deposition data show flow-specific patterns similar to those observed *in vivo* by Heyder and Rudolf (*In Inhaled Particles IV*, p. 107, 1977) and suggest several possible explanations: (1) The model formulation used for fitting is inappropriate. For example, Martonen and Zhang (*J. Aerosol Sci.* 23: 667, 1992) have used a logistic model to fit similar data. (2) Constraining the model fits as was done here may not be optimal. Since the three original parameters were so highly correlated, constraining the variables was considered appropriate, but there does not appear to be a good theoretical basis for a d^3 or a $d^{3.6}$ relationship. (3) Assuming that the flow characteristics within the nasal airways are similar in terms of velocity profiles and turbulence for different flow rates may not be valid. Integration of parameters relating to Reynolds number, for example, may require consideration. Other models such as the logistical model are being investigated.

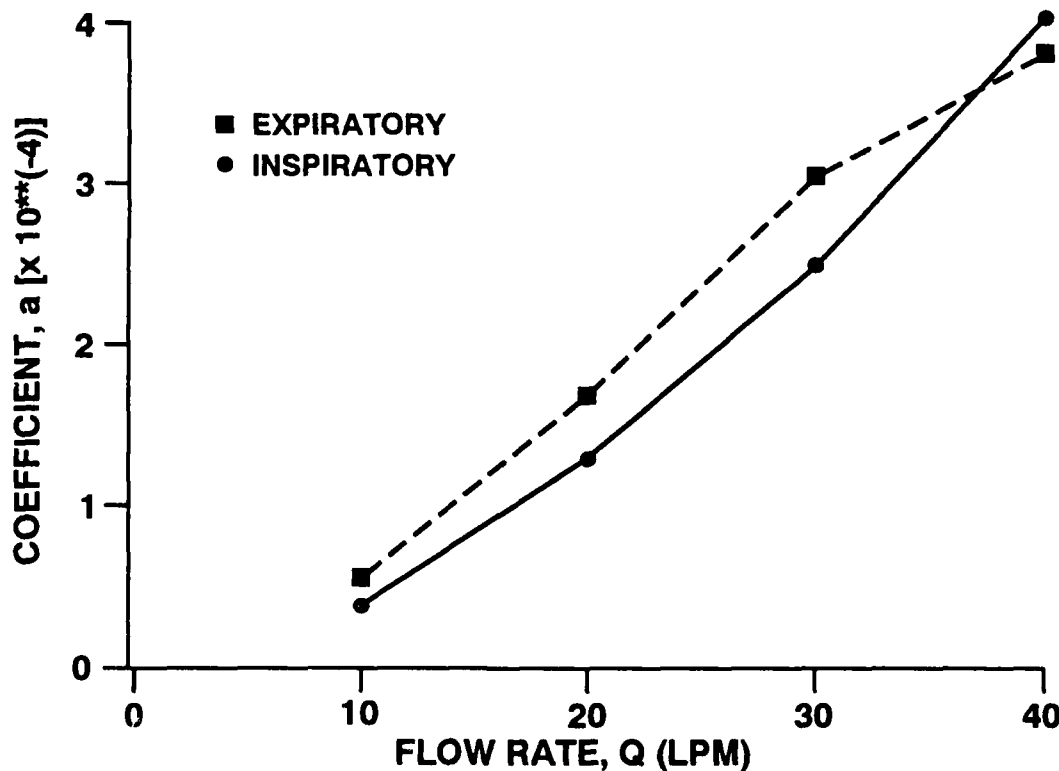


Figure 3. Relation of the fit parameter a_i from Eq. (3) to the flow rate for inspiratory and expiratory steady-state flow.

It is interesting to note that for a given particle size and flow rate the deposition was greater for inspiratory than expiratory flow. The differences were on the order of a factor of two. Nevertheless, these data confirm earlier views that the effect of deposition of particles in nasal airways on expiration will contribute to the total deposited amount in those airways.

(Research sponsored by the Office of Health and Environmental Research, U. S. Department of Energy, under Contract No. DE-AC04-76EV01013.)

A SYSTEM TO MEASURE VAPOR UPTAKE IN F344 RAT LUNGS AND NOSES WITH SET RESPIRATORY PARAMETERS FOR CYCLIC BREATHING

A. R. Dahl and L. K. Brookins

Our previous determinations of inhaled vapor uptake in dogs indicated that inclusion of the lungs in a cyclic breathing paradigm was essential for quantitatively understanding vapor uptake. After investigating the phenomenon of vapor desorption in the dog (Dahl, A. R. et al. *Toxicol. Appl. Pharmacol.* 10: 263, 1991; Gerde, P. and Dahl, A. R. *Toxicol. Appl. Pharmacol.* 109: 276, 1991), we developed a system for recording similar data in the F344/N rat (Fig. 1). This system will allow us to further validate the model derived using dogs and also will provide for an accurate description of vapor uptake in this important experimental animal. In addition, if vapor uptake in rats turns out to be accurately predicted by our existing model, confidence that we can accurately predict vapor uptake in humans will be increased.

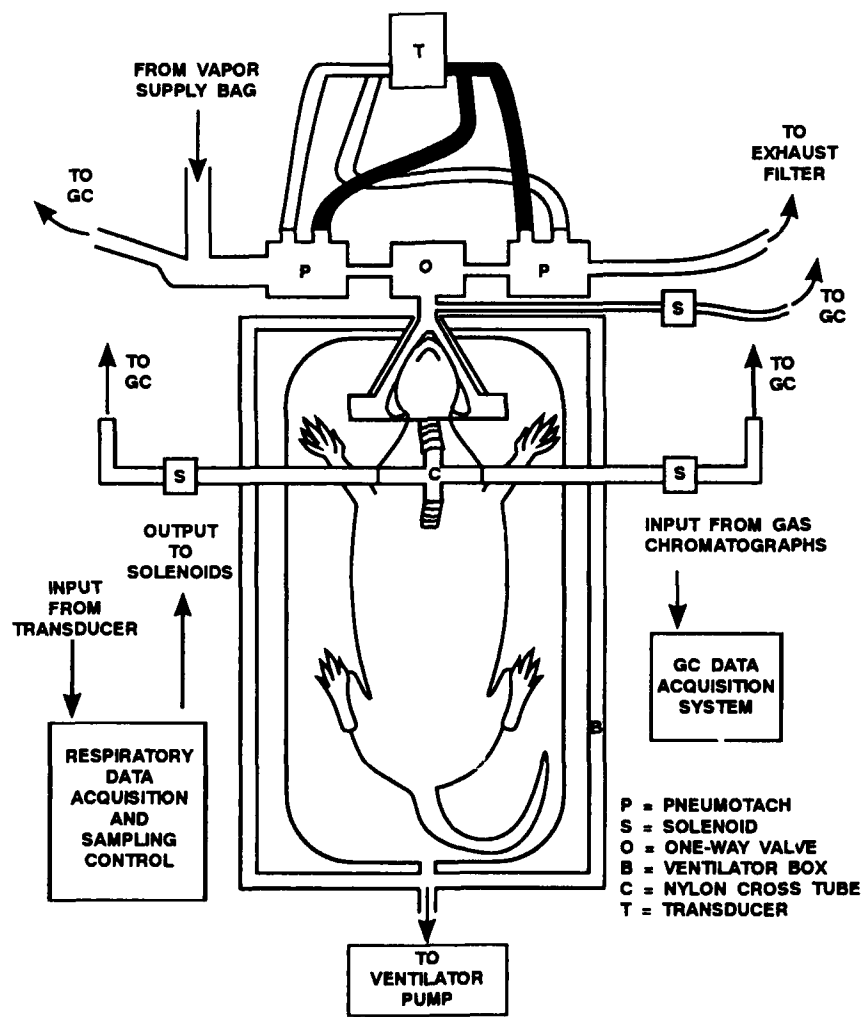


Figure 1. Schematic diagram of the rat exposure system.

To experimentally validate our model in rats, we must measure vapor concentrations in the trachea and at the nose during inhalation and exhalation with both lung and nose in the circuit. These requirements presented a challenge that was met for the dog (Snipes, M. B. et al. *Fundam. Appl. Toxicol.* 16: 81, 1991), but, because the rat is smaller and breathes more rapidly, a modified approach was needed. Rats are anesthetized by urethane injection, and the trachea is surgically invaded via a tracheotomy. A cross-shaped tube, through which we can

sample post-nasal air during inhalation and post-pulmonary air during exhalation, is glued to the ends of the severed trachea (Fig. 1). Air volumes approximating 10% of the rat minute volume are drawn from the trachea and through a GC sampling loop. Breathing parameters for the rat, as was the case for the dog, are controlled by a respiratory pump. For measuring vapor uptake, tracheal air will be sampled using rapidly switching solenoids activated by output from the respiratory monitor so that one is activated during inhalation, the other during exhalation.

Sampling from the rat's nose presents fewer difficulties than sampling from the trachea since we have a one-way valve (Fig. 1) that was successfully used to introduce vapors into isolated perfused rat lungs. Dead space in the breathing zone is minimized by use of two pneumotachographs, connected to a single transducer, placed before and after the non-rebreathing valve rather than between the rat's nose and the non-rebreathing valve (Fig. 1).

Initial experiments will determine the nasal absorption, desorption, and lung uptake of 2,4-dimethylpentane, 1,3-dioxolane, 2-butanone, di-n-propyl ether, and ethanol vapors at both 10 and 600 ppm. These vapors were used in previous experiments. In addition to determining uptake under "normal" respiration, we will vary breathing frequency, tidal volume, or minute volume by factors of at least two to determine the effects of these parameters on vapor uptake. In pilot studies we could easily vary the breathing frequency of urethane-anesthetized rats by a factor of 4 and the tidal volume by a factor of 2 (Fig. 2). The solenoids controlling air sampling from the trachea and at the nose kept pace with the imposed respiration parameters.

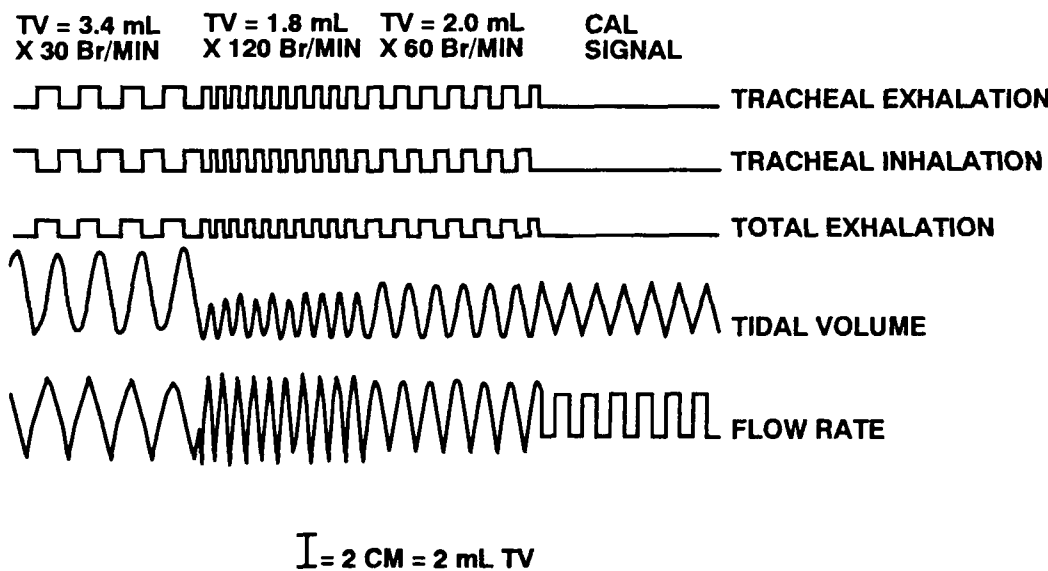


Figure 2. Respiratory monitor output from a rat in the apparatus shown in Figure 1. Breathing frequency ranged from 30 to 120 breaths per minute, and the tidal volume ranged from 1.8 to 3.4 mL. Square waves (except for the calibration signal) indicate the opened or closed status of the sampling solenoids.

The successful development of a system to measure rat nasal and lung uptake of vapors in a cyclic breathing paradigm will be useful to inhalation toxicologists, physiologists, and pharmacologists who need accurate dosimetric data for inhaled vapors. The validation of a mathematical model describing vapor uptake in the rat will increase confidence in the extrapolation of the model results to prediction of dose in humans. Finally, both the experimental system and mathematical model can be used to test further hypotheses regarding uptake and disposition of vapors.

(Research sponsored by the NIH under Grant ES04422 from the National Institute for Environmental Health Sciences in facilities provided by the Office of Health and Environmental Research, U. S. Department of Energy, under Contract DE-AC04-76EV01013.)

EFFECTS OF CIGARETTE SMOKE EXPOSURE ON F344 RAT LUNG CLEARANCE OF INSOLUBLE PARTICLES

G. L. Finch, B. T. Chen, E. B. Barr, and I. Y. Chang

It is widely recognized that cigarette smoking can induce a variety of carcinogenic and noncarcinogenic effects in people who smoke. Less certain are the type and magnitude of the influence that smoking might have on responses to other inhaled toxic materials. This influence can take the form of a direct physical effect, in which smoking influences the disposition of another inhaled agent. For example, it is generally accepted that cigarette smoking can delay the mucociliary clearance of inhaled, insoluble particles in humans (Bohning, D. E. et al. *Ann. Occup. Hyg.* 26: 259, 1982) and experimental animals (Mauderly, J. L. et al. In *Biological Interaction of Inhaled Mineral Fibers and Cigarette Smoke* [A. P. Wehner and D. L. Felton, eds.], Battelle Press, p. 223, 1989).

We are conducting a chronic study in rats to determine how smoking and the inhalation of $^{239}\text{PuO}_2$ might interact to produce lung cancer (this report, p. 110). As a part of this study, we are investigating how either subchronic or chronic exposure to smoke might influence the clearance of inhaled relatively insoluble particles. To this end, we selected 72 rats from Block B of our chronic study for acute exposure to ^{85}Sr -labeled fused aluminosilicate particles (^{85}Sr -FAP). The rats were scheduled to receive their ^{85}Sr -FAP exposure at 90 and at 540 days after initiation of cigarette smoke exposure. Equal numbers of males and females were chosen from each of three groups receiving either filtered air or mainstream cigarette smoke administered at levels of 100 or 250 mg/m³ total particulate matter (TPM). This clearance study does not include any of the rats that received $^{239}\text{PuO}_2$ during the chronic smoke inhalation study.

Details of the receipt, housing, and exposure of the strain CDF®(F344)/CrlBR rats are given elsewhere in this report (p. 110). The rats were exposed to filtered air or cigarette smoke from the ages of 6 to 12 wk, at which time they were removed from their cages and housed in polycarbonate shoebox cages, with food and water available *ad libitum*, for a period of 1 wk. During this time, the rats were sham exposed to the aerosol vehicle (distilled water) while other animals in the chronic study were exposed by acute nose-only inhalation of $^{239}\text{PuO}_2$. After being returned to their chambers, smoke exposures were resumed until the rats were 20 wk old. During this week, the designated 72 rats were conditioned to exposure tubes twice, for 30-60 min, before that day's smoke exposure began. Then on the Friday of their 20th week, the rats were exposed to the ^{85}Sr -FAP aerosol. We nebulized a suspension of ^{85}Sr -labeled clay, passed the aerosol through a tube furnace held at 1150°C, then delivered the aerosol to a 96-port, nose-only rodent exposure chamber, using techniques detailed by Newton et al. (In *Generation of Aerosols* [K. Willeke, ed.], Ann Arbor Press, p. 399, 1980). The ^{85}Sr -FAP had an AMAD of 1.5 µm, a σ_g of 1.7, and an air concentration of 10 kBq/L. The exposure was conducted for 90 min, after which the rats were whole-body counted in well-type, liquid scintillation counting units for ^{85}Sr activity. The rats were housed in polycarbonate shoebox cages for 3 days, then returned to their respective H2000 chamber for continued exposure to cigarette smoke or filtered air. Periodic whole-body counting for ^{85}Sr continues; as of September 30, 1992, counting data up through 122 days post exposure (dpe) are available.

Data describing the retention of ^{85}Sr were corrected for radioactive decay. To determine initial lung burdens (ILBs) for each rat, a single-component exponential function was fitted to all counting data between 7 and 60 dpe, and the function was then evaluated at zero time. To normalize differences in body weight, ILBs were also expressed on the basis of activity per 100 g body weight. The mean ILBs achieved were as desired and are shown in Table 1. When normalized for differences in body weights, female rats deposited more ^{85}Sr -FAP than males. In addition, the males exposed to cigarette smoke deposited significantly more ^{85}Sr -FAP compared with controls, as determined by a Student's *t*-test corrected for multiple comparisons (BMDP 7D, BMDP Statistical Software, Los Angeles, CA).

To model clearance, all data were converted to the \log_{10} -transformed percentage of ILB. For both sexes and each exposure group, one- and two-component, negative exponential functions were fitted to the data. A likelihood ratio test (Gallant, A. R. *Amer. Statistician* 29(2): 73, 1975) indicated that two-component functions were required for all groups. In cases where the second components of the function were positive, the slopes

were set to zero (no clearance), and the functional fit was repeated. More whole-body retention data are being collected, and we anticipate that the second components of clearance will then be better defined.

Table 1

Initial Lung Burdens (ILBs) of
 ^{85}Sr -FAP Achieved in Groups of Rats^a

Cigarette Smoke Exposure Level	Sex	^{85}Sr ILB (kBq)	^{85}Sr ILB (kBq)/100 g Body Weight
0 mg/m ³	M	15.6 (1.9)	5.4 (0.6)
	F	15.0 (1.7)	8.4 (0.8)
100 mg/m ³	M	16.9 (1.7) ^b	6.6 (0.8) ^b
	F	14.4 (1.3)	9.0 (0.9) ^b
250 mg/m ³	M	15.6 (1.7)	6.5 (0.6) ^b
	F	12.2 (1.7) ^c	7.9 (0.9)

^aValues in parentheses are standard deviations; 12 rats per group.

^bValue is significantly ($p < 0.05$) greater than the corresponding control.

^cValue is significantly ($p < 0.05$) less than the corresponding control.

Parameters of the fitted functions and evaluation of the fits at 122 dpe are shown in Table 2. An unbalanced repeated measures analysis of variance model (BMDP 5V) was used to investigate the influence of smoke exposure level on clearance, and the influence of sex for each smoke exposure level. The analysis demonstrated a highly significant ($p < 0.001$) influence of smoke exposure concentration on clearance, with increasingly retarded clearance with increasing smoke exposure concentration.

Table 2

Parameters of Functions Fitted to Clearance Data from Rats Exposed to ^{85}Sr -FAP^a

Cigarette Smoke Exposure Level	Sex	First Component of Clearance		Second Component of Clearance		Calculated Amount of ^{85}Sr Present at 122 dpe (Percent of ILB) ^b
		A ₁ (%)	t _{1/21} (d)	100-A ₁ (%)	t _{1/22} (d)	
Controls	M	80	30	20	410	20
	F	86	28	14	870	17 ^c
100 mg/m ³	M	83	43	17	→ ∞	29
	F	82	38	18	→ ∞	27
250 mg/m ³	M	73	58	27	→ ∞	44
	F	61	51	39	→ ∞	50 ^d

^aFunctions were fitted to log₁₀-transformed retention data. The forms used were $y = \log_{10}[(A_1 \exp(-\lambda_1 x)) + ((100 - A_1) \exp(-\lambda_2 x))]$; thus, all functions were constrained to equal 100% of the ILB. Clearance half-times were calculated by $t_{1/2i} = -0.69315/\lambda_i$. In cases where λ_2 was positive (a positive-exponential component), λ was set to zero, and the clearance half-time was said to approach infinity ($\rightarrow \infty$).

^bPercentage of ILB at 122 days after exposure calculated by evaluation of the appropriate clearance function.

^cFemale control rats cleared significantly ($p < 0.001$) more ^{85}Sr than male controls.

^dFemale rats exposed to 250 mg/m³ of smoke cleared significantly ($p < 0.01$) less ^{85}Sr than males.

This portion of our study continues. Our results to date indicate that smoke exposure significantly retards particle clearance from the lungs of rats. These data will assist us in interpreting results describing the interaction between smoking and $^{239}\text{PuO}_2$ in our chronic study. Moreover, because this effect is similar to that observed in humans, these results suggest that the rat constitutes a useful model for examining the relationships between cigarette smoking and disposition of inhaled particles.

(Research supported by the Assistant Secretary for Defense Programs, U. S. Department of Energy, under Contract No. DE-AC04-76EV01013.)

EFFECTS OF REPEATED INHALATION EXPOSURE OF F344 RATS AND B6C3F₁ MICE TO NICKEL OXIDE AND NICKEL SULFATE HEXAHYDRATE ON LUNG CLEARANCE

J. M. Benson, I. Y. Chang, Y. S. Cheng, F. F. Hahn, and M. B. Snipes

Nickel oxide (NiO) and nickel sulfate ($\text{NiSO}_4 \cdot 6\text{H}_2\text{O}$) are two compounds encountered in the nickel refining, smelting, and electroplating industries. The compounds are of toxicological interest because of epidemiological data indicating an increased incidence of lung and nasal cancers among workers in certain nickel refining operations. Further, results of rodent inhalation studies indicate the compounds to be potent inflammogens in lung. The purpose of the studies described in this paper was to determine whether repeated inhalation of NiO or $\text{NiSO}_4 \cdot 6\text{H}_2\text{O}$ impairs the ability of lungs to clear a subsequently inhaled "dose" of either ^{63}NiO or $^{63}\text{NiSO}_4 \cdot 6\text{H}_2\text{O}$.

Male F344/N rats and B6C3F₁ mice were whole-body exposed to NiO or $\text{NiSO}_4 \cdot 6\text{H}_2\text{O}$ 6 h/day, 5 days/wk for up to 6 mo. NiO exposure concentrations were 0, 0.62, and 2.5 mg NiO/m³ for rats and 0, 1.25, and 5.0 mg NiO/m³ for mice. $\text{NiSO}_4 \cdot 6\text{H}_2\text{O}$ exposure concentrations were 0, 0.12, or 0.5 mg $\text{NiSO}_4 \cdot 6\text{H}_2\text{O}/\text{m}^3$ for rats and 0, 0.25 or 1.0 mg $\text{NiSO}_4 \cdot 6\text{H}_2\text{O}/\text{m}^3$ for mice. After 2 mo and 6 mo of whole-body exposure, groups of rats and mice were exposed "nose-only" to aerosols of ^{63}NiO (NiO-exposed animals) or $^{63}\text{NiSO}_4 \cdot 6\text{H}_2\text{O}$ ($\text{NiSO}_4 \cdot 6\text{H}_2\text{O}$ -exposed animals). Following exposure to the radiolabeled aerosols, animals were sacrificed at selected time points ranging from 0 h to 200 days post exposure to ^{63}NiO or from 0 h to 32 days post exposure to $^{63}\text{NiSO}_4 \cdot 6\text{H}_2\text{O}$. At sacrifice the following tissues were taken for quantitation of ^{63}Ni activity: skull, nasal turbinates, larynx/trachea, lungs, liver, kidney, blood, GI tract, and carcass. Tissues were processed and analyzed for ^{63}Ni activity according to previously described procedures (1990-91 Annual Report, p. 42). In addition, groups of four or five rats and mice per exposure level per compound were sacrificed after 2 and 6 mo of whole-body exposure and at 2 and 4 mo following the end of the 6 mo of exposure for evaluation of histopathological changes in left lung and for quantitation of Ni in right lung.

Nickel accumulated in lungs of rats (Fig. 1A) and mice (Fig. 1B) inhaling NiO for up to 6 mo, with some clearance of the accumulated lung burden occurring during the 4-mo hold period. Concentrations of Ni in lungs of rats and mice exposed to $\text{NiSO}_4 \cdot 6\text{H}_2\text{O}$ remained below the limit of detection of the analytical method (2 µg Ni/lung). Histopathological changes in lungs of NiO and $\text{NiSO}_4 \cdot 6\text{H}_2\text{O}$ -exposed rats included alveolar macrophage hyperplasia and chronic alveolitis. The severity of the lesions was greater among NiO-exposed than $\text{NiSO}_4 \cdot 6\text{H}_2\text{O}$ -exposed rats due to the higher NiO aerosol concentrations. The lesions persisted throughout the 4-mo post-exposure hold period. Histopathological changes in lungs of mice exposed to NiO and $\text{NiSO}_4 \cdot 6\text{H}_2\text{O}$ included alveolar macrophage hyperplasia and interstitial pneumonia, with the $\text{NiSO}_4 \cdot 6\text{H}_2\text{O}$ -exposed mice being only minimally affected. The lung lesions among the NiO-exposed mice persisted throughout the 4-mo hold period after termination of whole-body exposures.

Appropriate functions (generally one or two-component, negative-exponential equations) were fit to the ^{63}Ni lung burden data. Half-times for clearance of ^{63}NiO and $^{63}\text{NiSO}_4 \cdot 6\text{H}_2\text{O}$ from lungs of air control rats and mice and from rats and mice previously exposed to NiO are given in Table 1. Statistical analyses of the clearance curves indicate that previous exposure to NiO for 2 or 6 mo impairs the ability of lungs to clear a subsequently inhaled dose of ^{63}NiO . Further, the extent of impairment increased with NiO exposure concentration and duration of exposure. Repeated exposure of rats and mice to $\text{NiSO}_4 \cdot 6\text{H}_2\text{O}$ for 2 or 6 mo did not statistically impair the ability of lungs to clear subsequently inhaled $^{63}\text{NiSO}_4 \cdot 6\text{H}_2\text{O}$ (data not shown).

Results of this study confirm that nickel oxide is an insoluble particle that accumulates in lung upon continued inhalation exposure and indicate that chronically inhaled NiO impairs its own clearance after only a few months of exposure. The impaired clearance most likely arises from a high particle burden of cytotoxic particles within alveolar macrophages. The clearance half-time of the accumulated NiO lung burden (from the repeated NiO exposures) is estimated to be at least 120 days, based on the findings that lung burdens of NiO at 4 mo post exposure are 50% or more of those present in animals sacrificed after 6 mo of exposure (Fig. 1). By comparison, clearance half-times of ^{63}NiO from lungs of rats and mice previously exposed to NiO are > 116 days.

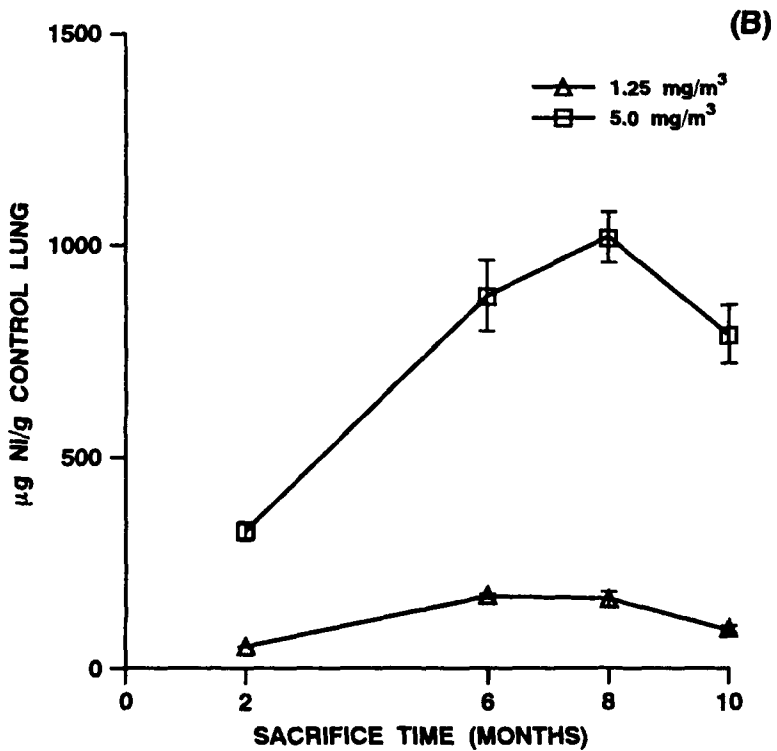
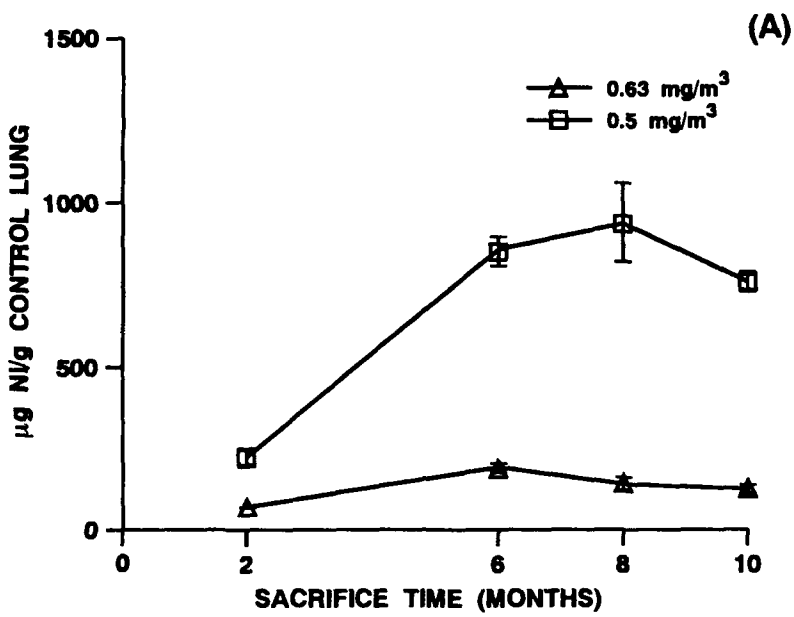


Figure 1. Concentrations of Ni in lungs of (A) rats and (B) mice inhaling NiO.

On the other hand, $\text{NiSO}_4 \cdot 6\text{H}_2\text{O}$ is a soluble compound whose clearance from lung depends on dissolution rather than mechanical clearance mediated by alveolar macrophages. Therefore, although $\text{NiSO}_4 \cdot 6\text{H}_2\text{O}$ is cytotoxic and produces an inflammatory response in lung *in vivo*, the pathway for clearance of this material was not affected by repeated inhalation. This does not preclude the possibility that repeated inhalation of $\text{NiSO}_4 \cdot 6\text{H}_2\text{O}$ may not affect the ability of lungs to clear inhaled insoluble particles.

These results suggest that repeated inhalation of NiO may potentiate its own inherent toxicity by impairing particle clearance from lung, but also may compromise the ability of lungs to clear other inhaled pollutant particles.

Table 1
Effect of NiO Inhalation on the Clearance of ^{63}NiO from Lungs of Rats and Mice

Months of NiO Exposure	mg NiO/m ³	Rats						Mice								
		$\mu\text{g Ni/g}$ Control Lung	A_1^a	A_2	$T_{1/2}^b$	B_1^c	B_2	$T_{1/2}$	mg NiO/m^3	$\mu\text{g Ni/g}$ Control Lung	A_1^a	A_2	$T_{1/2}^b$	B_1^c	B_2	$T_{1/2}$
2	0	—	92	0.021	33	8.5	0	—	0	—	80	0.068	10	20	0.009	77
2	0.62	69	43	0.110	6.2	56	0.003	231	1.25	49	70	0.063	11	30	0.004	173
2	2.5	221	30	0.162	4.3	70	0.001	693	5.0	327	55	0.021	33	45	0	—
6	0	—	84	0.021	33	16	0	—	0	—	95	0.033	21	5	0	—
6	0.62	188	100	0.006	116	0	NA	—	1.25	170	79	0.043	16	21	0	—
6	2.5	1652	100	0.002	346	0	NA	—	5.0	1283	100	0.002	346	0	NA	—

^a A_1 = Percent of initial lung burden clearing with the rate constant A_2 .

^b $T_{1/2}$ = Clearance half-time = $\frac{0.693}{A_2}$ or $\frac{0.693}{B_2}$

^c B_1 = Percent of initial lung burden clearing with the rate constant B_2 .
 $A_1 + B_1 = 100$

(Research sponsored by the Nickel Producers Environmental Research Association under Funds in Agreement No. DE-FI04-87AL44742 with the U. S. Department of Energy under Contract No. DE-AC04-76EV01013.)

CLEARANCE OF PARTICLES DEPOSITED IN THE CONDUCTING AIRWAYS OF BEAGLE DOGS

M. B. Snipes, W. C. Griffith, K. J. Nikula, B. A. Muggenburg, and R. A. Guilmette

The proposed new respiratory tract dosimetry model of the International Commission on Radiological Protection (ICRP) incorporates long-term retention of radioactive particles in conducting airways in its radiation dosimetry calculations. This represents a significant change from the current ICRP model (ICRP Publication 30, Part 1; Ann. ICRP 2:3/4, 1979). Some portion of inhaled particles that deposit on the conducting airways may be retained for an indefinite time. In addition, it is also possible that some of the particles being cleared via the mucociliary escalator are incorporated into epithelium of the conducting airways and contribute to the long-term dose to airway epithelium. The challenge facing proponents of the new model is to determine the extent to which particles are retained in association with the conducting airways, as well as their location relative to target cells.

We are evaluating a new procedure to study airway retention and clearance of particles to provide information useful for accurately applying the new ICRP model for respiratory tract dosimetry. The procedure involves instillation of particles at specific locations in the airways of an animal model, followed by an evaluation of the retention and clearance patterns of the instilled particles. The Beagle dog is the animal model, chosen because its long-term retention pattern for inhaled particles is similar to humans, and the dog is large enough to allow the use of a fiberoptic bronchoscope to locate specific sites in its lung airways. All dogs used in these studies came from the Institute's dog colony.

In our procedure, a dog was anesthetized with isoflurane in oxygen and placed on its back on an operating table. A fiberoptic bronchoscope was inserted into the tracheobronchial airways and the tip of the bronchoscope positioned at the location of interest, either a 4-, 8-, or 15-mm airway site. After positioning the tip of the bronchoscope, a polyethylene tube with an ITRI multiport microspray nozzle on the end was inserted through the biopsy channel of the bronchoscope (1989-90 Annual Report, p. 21). The anesthetized dog was temporarily rendered apneic by hyperventilation so that it will not be breathing when the test particles are sprayed onto the surface of the airway. Then, a suspension of radiolabeled test particles in 20 μL of saline solution was expelled through the microspray nozzle using 1 mL of air from a syringe attached to the external end of the polyethylene tube. The bronchoscope and dosing tube were carefully withdrawn from the dog, and it was allowed to recover from anesthesia. After recovery, the dog was counted for radioactivity using a NaI(Tl) counting system positioned to measure radioactivity within the thorax region. Thoracic burdens of the radionuclides were quantified until amounts of radionuclide retained in the thorax were below the detection limit (about 1% if the instilled dose), or for as long as 42 days.

To date, we have evaluated clearance of two types of radioactive particles that were sprayed onto airways of two groups of dogs, 1 to 4 yr old. The suspension volume (20 μL) was kept constant for both studies. In the first study, 3-4 μm polystyrene latex (PSL) microspheres radiolabeled with ^{59}Fe or ^{46}Sc (1.5×10^7 microspheres instilled; 0.3 mg total mass of microspheres) were used in four male and four female dogs. Internal airway diameters at the instillation sites were 15, 8, and 4 mm. The microspheres cleared to less than detectable amounts during the first 3 days in three dogs, but 7 to 54% of the microspheres were retained longer than 3 days in the 15-mm airways of five dogs. Six to 69% and 2 to 84% of the microspheres were retained longer than 3 days in 8- and 4-mm airways, respectively, of all eight dogs.

In the second study, four male and four female dogs were instilled only in the 4-mm and 15-mm airways with a 20 μL suspension of about 10^5 polydisperse fused aluminosilicate particles (FAP) radiolabeled with ^{169}Yb or ^{46}Sc , having a mass median diameter of 1.5 μm . Results in the study with PSL were essentially identical for the 4-mm and 8-mm airways, so clearance from the 8-mm airways was not evaluated in the second study. The FAP allowed the use of fewer particles (about 10^5) and a significantly smaller mass (about 2 μg) per instillation. The deposited FAP cleared from the 4-mm deposition sites within 2 days in two dogs, but 40-50% of the particles were retained for longer than 3 days in the six other dogs. Only one dog retained a detectable amount of particles at the 15-mm deposition site for more than 3 days. In both studies, retention and clearance patterns varied considerably, but the particles retained longer than 3 days cleared with half-times on the order of several months.

The next phase of these studies was to determine the anatomic locations of the particles that did not clear within 3 days. Three of the dogs in the studies described above were sacrificed 6 days after instilling 4- and 15-mm airway sites with a mixture of radiolabeled and fluorescent PSL microspheres ($3-4 \mu\text{m}$; 1.5×10^7 microspheres). The lungs were fixed by intravascular perfusion to reduce the possibility of the PSL microspheres being displaced from their retention sites by the liquid fixative. On historical examination it was determined that some microspheres were retained on the surface of airways, and a small number of microspheres appeared to be trapped within the epithelium of the airways. Unexpectedly, examination of the samples of lung tissue taken proximal and distal to the instillation sites showed that significant portions of the instilled microspheres were in the alveoli. We decided not to pursue quantifying the retention patterns of microspheres near the instillation sites until after we determined the reason for the alveolar deposition and retention of significant portions of the instilled particles.

We are now attempting to determine why particles deposited on airway surfaces using our instillation procedure moved into the alveoli. The numbers of particles and/or volume of the particle suspension may have influenced the retrograde movement. Several studies were conducted with dogs in the late 1960s and early 1970s to evaluate powdered tantalum metal as a radiographic contrast medium. Large amounts of tantalum were insufflated into the conducting airways of the dogs. The results of these studies were discussed by Morrow (*Radiology* 121: 415, 1976). Retrograde movement of some of the tantalum *in vivo* was apparently responsible for the observations that significant alveolar burdens of tantalum were present in essentially all of the dogs after about 1 day. A similar phenomenon may have occurred with the test suspensions that we used. Even though the instilled volume was $20 \mu\text{L}$, the numbers and mass of particles per unit area of airway epithelium were relatively high, especially with the PSL. We estimate that the 1.5×10^7 microspheres were delivered to about 50 mm^2 of airway surface at the 4-mm diameter sites and to about 200 mm^2 at the 15-mm diameter airway sites. The mass of PSL was about $6 \mu\text{g}/\text{mm}^2$ at the 4-mm sites and about $1.5 \mu\text{g}/\text{mm}^2$ at the 15-mm sites. Numbers of PSL microspheres were about $3 \times 10^5/\text{mm}^2$ at the 4-mm sites and about $7.5 \times 10^4/\text{mm}^2$ at the 15-mm sites. The 8-mm diameter dosing sites had values between the values for the 4-mm and 15-mm sites.

The volume of instilled suspension for the FAP was also $20 \mu\text{L}$, but the numbers and mass of particles deposited per unit area of airway epithelium were both substantially less than for the PSL microspheres. The fact that long-term clearance patterns were relatively similar for both studies suggests that numbers of particles or mass of particles may have been less important than the volume of material that was sprayed onto the airway surfaces. These results suggest that instillations with a smaller volume of particle suspensions may be necessary to avoid retrograde movement of a portion of instilled particles into alveoli.

Our current emphasis in this study is to determine the mechanism(s) by which particles reach the alveoli after being sprayed onto the surface of conducting airways of dog lungs using our procedure, and smaller volumes of particle suspensions are being used to determine if volume is an important factor. Gravitational effects are being minimized by careful orientation of the lungs during the instillation procedure.

(Research sponsored by the Office of Health and Environmental Research, U. S. Department of Energy, under Contract No. DE-AC04-76EV01013.)

SYSTEMIC ABSORPTION OF PLUTONIUM FROM THE NASAL AIRWAYS AND GI TRACT WHEN ADMINISTERED AS NITRATE OR OXIDE AEROSOLS

R. A. Guilmette and B. A. Muggenburg

Current respiratory tract dosimetry models predict varying amounts of transnasal absorption, depending on solubility class. For example, 10% of materials designated as class W that deposit on nasal-pharyngeal airways are said to be absorbed to blood, 1% for class Y (ICRP Report 30, 1979). Depending on the fraction of inhaled aerosol depositing on these airways, which in turn depends on particle size and breathing pattern, these absorbed fractions can contribute significantly to the committed effective dose equivalent on which radiation protection guidance is based.

Unfortunately little information is known about how much of an actinide aerosol deposited on nasal airway surfaces is available for uptake to blood and subsequent systemic deposition. This study was designed specifically to address the question of nasal absorption of Pu aerosols. It features the use of an aerosol exposure technique that limits deposition to airways proximal to the larynx of Beagle dogs, and two chemical forms of Pu, nitrate and oxide, which were designed to bracket the range of solubilities expected in cases of accidental occupational inhalation.

Six male and six female adult dogs, 10-11 yr at exposure and in good health were used in this study. The dogs were assigned randomly in groups of two males and two females to the three experimental groups in this study. The two different aerosols used were: (1) $\text{Pu}(\text{NO}_3)_4$ produced by nebulizing solutions of either $^{238}\text{Pu}^{+4}$ (7.4 MBq mL⁻¹) or $^{239}\text{Pu}^{+4}$ (0.74 MBq mL⁻¹) in 0.27M HNO_3 , and (2) PuO_2 produced by nebulizing a colloidal suspension of both isotopic forms of $\text{Pu}(\text{OH})_4$ (2.5 mg mL⁻¹) and heat treating the droplets at 1150°C. The average particle size for all aerosols was 1.3 ± 0.3 (sd) AMAD and 2.3 ± 0.4 σ_g .

Because it was highly likely that most of the aerosol deposited in the nasal airways of the dog would be cleared rapidly and swallowed, provision was made to measure both systemic absorption occurring in the nasal airways and that occurring in the gastrointestinal (GI) tract after the nasally deposited material had been swallowed. To accomplish this, each dog was exposed to two different isotopes of Pu, ^{238}Pu , and ^{239}Pu , in the same chemical form; one isotopic form was aerosolized for exposure of the nasal airways as described above. The second isotope was placed directly into the stomach by gavage using a fiberoptic gastroscope.

For the nitrate-exposed animals, consideration was also given to the possible differences in biochemical behavior of relatively soluble ^{238}Pu and ^{239}Pu due to the known mass-dependent hydrolysis-polymerization reactions likely to occur after deposition (the specific activity of ^{238}Pu is 280 times that of ^{239}Pu). To provide for this possibility, two groups of dogs were exposed to $\text{Pu}(\text{NO}_3)_4$ aerosols; the first group was given ^{238}Pu in the nasal airways, and ^{239}Pu by gavage, the second group vice versa. In the oxide study, $^{238}\text{PuO}_2$ was deposited on the nasal airways and $^{239}\text{PuO}_2$ was gavaged. All nasal airway exposures were done using the technique of S. L. Whaley *et al.* (*J. Toxicol. Environ. Health* 23: 519, 1988). Each dog was killed 24 h after exposure by exsanguination under pentobarbital anesthesia, and a necropsy was done. Careful attention was paid to possible cross-contamination of samples recognizing that most of the activity was likely to be present in the GI tract. All tissue and collected excreta samples were analyzed by α -spectrometric methods.

To account for the differential systemic absorption that occurs both in the nasal airways and in the GI tract, we used the following calculational scheme. The GI absorption factor for each dog was determined from the data from the gavaged ^{239}Pu isotope:

$$A_{gi} = f_{gi} D_{gi},$$

where A_{gi} = the systemically absorbed quantity of Pu, defined here as the amounts measured in liver, bone, and soft tissue (the large amount of cross-contamination between urine and feces samples prevented an accurate assay of urinary Pu content); D_{gi} = the total quantity of Pu gavaged; and f_{gi} = the fractional absorption of Pu from GI tract to blood.

Similarly the nasal absorption of Pu into blood was defined by the relationship:

$$A_{np} = f_{np}D_{np} + f_{gi}(D_{np} - f_{np}D_{np} - B_{np}) ,$$

where A_{np} = the systemically absorbed quantity of Pu originally deposited in the nasopharyngeal airways (defined as Pu measured in liver, bone, and soft tissue); D_{np} = the quantity of Pu deposited in the nasopharyngeal region (defined as the sum of all activities measured in tissues and excreta for the Pu isotope to which the nasal airways were exposed); f_{np} = the fractional absorption of NP-deposited Pu to blood; and B_{np} = the amount of Pu retained in the nasal airways and pharynx at death.

The above equations can then be solved algebraically for f_{np} using only measured quantities:

$$f_{np} = \frac{\frac{A_{np}}{D_{np}} - \frac{A_{gi}}{D_{gi}}[1 - \frac{B_{np}}{D_{np}}]}{1 - \frac{A_{gi}}{D_{gi}}} .$$

Current preliminary results of the radiochemical analysis of tissue and excreta samples are summarized for intranasal deposition (Table 1) and intragastric instillation (Table 2). Several general points can be made. (1) The individual GI uptake fractions (f_{gi}) were less than the respective nasopharyngeal airway uptake fractions (f_{np}), usually by approximately an order of magnitude. (2) There appears to be an inverse relationship between measured fractional absorption and the quantity of Pu deposited (data not shown), i.e., dogs having the smallest depositions had the largest fractional absorption values. This may be due to mass-dependent biochemical mechanisms, or to statistical biases in analyzing samples whose Pu amounts are very near background levels (this latter bias will tend to increase the systemic burden).

For the dogs exposed to the Pu oxide particles, the average nasal absorption fraction was 1.8×10^{-3} , and the average GI absorption factor was 1.6×10^{-4} . The value for nasal absorption measured here is about 20% the value assumed by ICRP 30 for a class Y material (0.01). In terms of GI absorption factor, the value measured in this study is somewhat larger than those obtained in other studies (summarized in ICRP Report 48, 1986). However, the diversity of experimental designs used in GI uptake studies makes direct comparison of data difficult.

For the dogs exposed to the nitrate form of Pu, the average fractional absorption values for the combined ^{238}Pu - and ^{239}Pu -nitrate-exposed groups was 0.044. Although more analyses are being done on these data, it appears that the f_{np} for Pu is about one half the value assumed by ICRP 30 for a class W compound (0.10). The measured GI absorption factor was 2.1×10^{-3} , about 10 times higher than those measured in other studies (ICRP 48, 1986).

Of potential significance is the amount of Pu nitrate measured in nasal tissues at 1 day after exposure, averaging about 5% of the deposited Pu. This retained Pu was significantly more than that measured in other dogs exposed intranasally to Am nitrate aerosols, in which the average 1-day retained value was 0.8%. If the Pu is retained for a long time in nasal tissues, then the dose to nasal epithelial cells could be significant (provided the site of retention of the Pu is within α -particle range of the epithelial cells). Further studies would be required to address this issue.

Table 1
Pu Distribution in Dogs^a Intranasally Exposed to Oxide or Nitrate Aerosols

Chemical Form	Isotope	Dog #	Fraction Deposited Pu (%)					f_{na}
			GI + Excreta	Liver	Bone	Soft Tissue	NP Region	
Oxide	²³⁸ Pu	1208T	99.70	0.0025	0.057	0.17	0.059	2.2x10 ⁻³
		1196A	99.58	0.0014	0.038	0.25	0.12	2.8x10 ⁻³
		1194A	99.89	0.0036	0.010	0.040	0.040	3.6x10 ⁻⁴
Nitrate	²³⁸ Pu	1198A	88.0	0.46	1.48	0.45	9.41	5.4x10 ⁻²
		1210S	92.1	0.031	1.18	1.01	5.54	3.8x10 ⁻²
		1213T	95.3	0.32	0.26	0.44	3.58	1.9x10 ⁻²
Nitrate	²³⁹ Pu	1201A	91.0	0.11	0.20	5.61	1.74	1.2x10 ⁻¹
		1212T	98.4	0.0087	0.74	0.33	0.46	1.1x10 ⁻²
		1213U	88.9	0.070	0.14	0.26	10.6	2.2x10 ⁻²

^aOne dog from each experimental group was omitted because of incomplete data analysis; their data will be incorporated later.

Table 2
Pu Distribution in Dogs^a Intragastrically Exposed to Oxide or Nitrate Aerosols

Chemical Form	Isotope	Dog #	Fraction Deposited Pu (%)				
			GI + Excreta	Liver	Bone	Soft Tissue	f_{na}
Oxide	²³⁹ Pu	1208T	99.86	0.0016	0.0051	0.0063	1.3×10^{-4}
		1196A	99.98	0.00067	0.0017	0.0074	9.8×10^{-5}
		1194A	99.97	0.00071	0.0012	0.024	2.6×10^{-4}
Nitrate	²³⁹ Pu	1198A	99.46	0.014	0.15	0.055	2.2×10^{-3}
		1210S	99.61	0.011	0.11	0.068	1.9×10^{-3}
		1213T	99.78	0.011	0.013	0.063	1.9×10^{-3}
Nitrate	²³⁸ Pu	1201A	99.39	0.013	0.054	0.40	4.7×10^{-3}
		1212T	99.90	0.0039	0.035	0.022	6.1×10^{-4}
		1213U	99.62	0.039	0.040	0.074	1.5×10^{-3}

^aOne dog from each experimental group was omitted because of incomplete data analysis; their data will be incorporated later.

(Research sponsored by the Office of Health and Environmental Research, U. S. Department of Energy, under Contract No. DE-AC04-76EV01013.)

TOXICOKINETICS OF INHALED NICKEL OXIDE IN F344 RATS

J. M. Benson, Y. S. Cheng, and K. R. Maples

Toxicological interest in nickel oxide (NiO) exists because of the increased incidences of lung and nasal cancers that occur among workers in certain nickel refining operations. As part of our Institute's effort to study the inhalation toxicity of selected nickel compounds, a toxicokinetic study was conducted on NiO to help establish a relationship between the deposition and clearance of an acutely inhaled "dose" of the material and the nickel lung burdens and the toxicological effects occurring from repeated inhalation exposure to NiO.

The radiolabeled NiO used in this study was prepared by reacting $^{63}\text{nickel chloride}$ with ammonium bicarbonate to form $^{63}\text{nickel carbonate}$ which was subsequently calcined at 1200°C for 1 h to form ^{63}NiO (specific activity 1.01 mBq/mg Ni). Thirty-nine male F344/N rats (Taconic Farms, Germantown, NY) were exposed nose-only to ^{63}NiO (9.9 mg $^{63}\text{NiO}/\text{m}^3$; MMAD = 1.39 μm ; $\sigma_g = 2.74$) for 70 min. Pulmonary functions were measured on four rats during the exposure in order to estimate the total and regional deposition of the aerosol within the respiratory tract. Following the exposure, three of the exposed rats were placed in metabolism cages for collection of urine and feces. The remainder of the rats were sacrificed, in groups of three, at selected time points up to 200 days post exposure. Tissues were processed for ^{63}Ni analysis according to previously described procedures (1990-91 Annual Report, p. 42).

Approximately 11% of the inhaled ^{63}NiO was deposited in the rats, with 4.3% of the inhaled ^{63}NiO deposited in the lungs and bronchi (lower respiratory tract). Clearance of ^{63}NiO from the upper respiratory tract was rapid, with little or no activity detected in skull, turbinates, or trachea/larynx by 4 days post exposure (Table 1). Clearance of ^{63}NiO from the lung was modeled using a single component negative exponential function (Fig. 1). The calculated half-time for clearance of ^{63}NiO from the lung was 120 days. No detectable ^{63}Ni activity distributed through the blood to extra-respiratory tract tissue (Table 1). No ^{63}Ni activity was detected in liver, kidney, or bladder at any time post exposure (data not shown).

No ^{63}Ni activity was detected in urine from animals housed in metabolism cages for 14 days post exposure. Fecal excretion of the inhaled material occurred chiefly during the first 4 days post exposure, suggesting clearance of material deposited in the upper respiratory tract.

Results of this toxicokinetic study indicate that ^{63}NiO calcined at 1200°C behaves as expected for an insoluble particulate aerosol. The pulmonary deposition of the particles is similar to the value reported for 1 μm particles by Raabe *et al.* (In *Inhaled Particles VI* [Dodgson, J. *et al.*, eds.], Pergamon Press, Oxford, UK, p. 53, 1988). The clearance half-time of 120 days falls within the range of values (50-390 days) reported for the long-term clearance of other insoluble aerosols of similar aerodynamic diameter from rat lung (Wolff, R. K. *et al.* *Health Phys. (Suppl 1)*, 57: 61, 1989; Snipes, M. B. In *Concepts in Inhalation Toxicology*, Hemisphere Publishing Co., New York, p. 193, 1989.) The lack of distribution of ^{63}Ni activity to extra-respiratory tract tissues indicates that the inhaled ^{63}NiO is not dissolving appreciably within the lung and that clearance is most likely occurring through "mechanical," macrophage-mediated processes. The results of this study are consistent with the findings of our subchronic studies in which inhaled NiO accumulated in lung and resulted in a granulomatous inflammatory response in lung characteristic of both nickel and insoluble particle exposure (Dunnick, J. K. *Fundam. Appl. Toxicol.* 12: 584, 1989).

Table 1

Percentage of Deposited ^{63}Ni Present in Tissues after Exposure of Rats to $^{63}\text{NiO}^{\text{a}}$
Toxicokinetics of ^{63}Ni After Inhalation of Nickel Oxide

Days Post Exposure	% Ni Deposited (mean \pm SEM)						Carcasses
	Lungs	Skull	Turbinates	Trachea/Larynx	GI Tract	Blood	
0	37.7 \pm 5.73	0.0 \pm 0.0	0.05 \pm 0.05	0.94 \pm 0.37	61.2 \pm 30.8	0.04 \pm 0.02	0.00 \pm 0.00 (3)
0.08	46.1 \pm 5.18	0.02 \pm 0.01	0.47 \pm 0.18	0.84 \pm 0.53	225 \pm 99.9 ^b	0.00 \pm 0.00	0.32 \pm 0.32
0.25	38.3 \pm 0.84	1.32 \pm 1.32	0.0 \pm 0.0	0.00 \pm 0.00	324 \pm 84 ^b	0.00 \pm 0.00	0.00 \pm 0.00
1.0	35.8 \pm 3.69	0.24 \pm 0.24	0.21 \pm 0.21	0.00 \pm 0.00	26.9 \pm 18.9	0.00 \pm 0.00	ND
4.0	35.6 \pm 2.80	0.0 \pm 0.0	0.0 \pm 0.0	0.05 \pm 0.01	0.0 \pm 0.0	0.00 \pm 0.00	ND
8.0	31.2 \pm 8.07	ND ^c	0.0 \pm 0.0	0.06 \pm 0.02	ND	0.00 \pm 0.00	ND
16	43.3 \pm 5.93	ND	0.0 \pm 0.0	0.11 \pm 0.04	ND	0.00 \pm 0.00	ND
30	26.6 \pm 4.17	ND	ND	0.03 \pm 0.03 (n = 2)	ND	0.00 \pm 0.00	ND
60	34.9 \pm 2.79	ND	ND	0.01 \pm 0.01	ND	ND	ND
90	23.8 \pm 1.89	ND	ND	0.00 \pm 0.00	ND	ND	ND
120	14.4 \pm 3.14	ND	ND	ND	ND	ND	ND
180	14.2 \pm 0.96	ND	ND	ND	ND	ND	ND

^aResults represent the mean \pm SEM of 3 values except in the cases of rats sacrificed immediately after exposure, where n = 4 and rats sacrificed after 180 days, where n = 9.

^bData are suspect.

^cSamples not analyzed because no activity was detected in samples analyzed during the previous sacrifice or sacrifices.

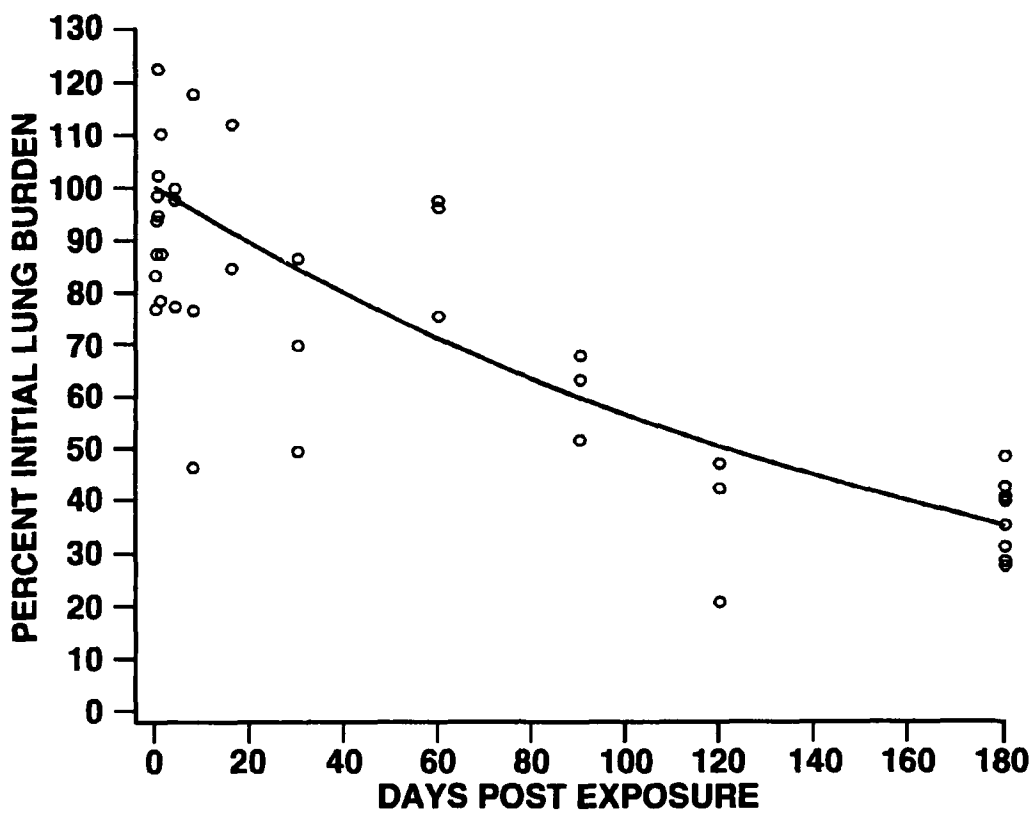


Figure 1. Lung clearance of $^{63}\text{nickel}$ oxide from rats.

(Research sponsored by the National Institute of Environmental Health Sciences National Toxicology Program under Interagency Agreement No. Y01-ES-30108 with the U. S. Department of Energy under Contract No. DE-AC04-76EV01013.)

STABILITY AND CELLULAR TOXICITY OF HOECHST 33342 NUCLEAR LABELING OF CANINE ALVEOLAR MACROPHAGES *IN VITRO*

J. A. Hotchkiss and R. A. Guilmette

Inhalation of relatively insoluble particles present in the environment can lead to significant accumulations of material in the respiratory tract. This can result in the development of such lung diseases as pneumoconiosis or hypersensitivity pneumonitis, and bacterially induced pneumonias. The primary defense mechanisms limiting particle accumulation is the translocation of particles out of the respiratory tract by mucociliary clearance and the transport of particles from the lung to the regional tracheobronchial lymph nodes. Pulmonary macrophages play a role in both processes by engulfing particles and retaining them in phagolysosomes. In mucociliary clearance, many particles are carried up the airways within alveolar macrophages (AM) and are eventually swallowed (Brain, J. D. *Arch. Intern. Med.* 131: 477, 1970). Alveolar macrophages may also play a major role in the clearance of particles to the tracheobronchial lymph nodes (Harmsen, A. G. *et al. Science* 230: 1277, 1985).

The potential biological consequences resulting from particle inhalation are related to the toxicity of the particles, the length of time the particles are retained in the lung as well as the anatomic location of the retained particles. Therefore, it is important to understand retention and clearance processes for inhaled materials to allow accurate projections for the consequences of inhalation exposures. However, there are significant species differences in the long-term pulmonary retention of inhaled particles (Snipes, M. B. In *Concepts in Inhalation Toxicology*, p. 193, 1989). Monkeys, dogs, guinea pigs and humans have significantly longer pulmonary retention times than rats, mice, and hamsters. The biological basis for the differences is unknown. However, it may be due to differences in primary clearance pathways within lungs of different species.

In order to better understand how inhaled particles are cleared from the lungs of different species, a generalized technique is needed to uniquely label and follow inhaled particles and the AM that phagocytize them. Fluorescently labeled particles are commercially available in a range of respirable sizes; however, no techniques are available to specifically label alveolar macrophages.

Hoechst 33342 is one of a series of UV-excited, blue fluorescent bisbenzimidazol dyes originally synthesized for Hoechst as antiprotozoal drugs. The dyes act as DNA-specific fluorochromes as a consequence of their affinity for strings of three or more A-T base pairs in DNA. Hoechst 33342 has been used to stain live cells, which are then sorted based on DNA content by fluorescence activated cell-sorting and subsequently grown in culture. The purpose of the present study was to evaluate the use of using Hoechst 33342 to label alveolar macrophages *in vitro*.

Bronchoalveolar lavage was performed on one Beagle dog from the ITRI colony. The entire lung and airways were lavaged with 1 L of sterile, pyrogen-free, saline. The lavaged fluids were collected in centrifuge tubes and stored on ice. Cells were recovered by centrifugation. The total number of cells was determined manually using a hemocytometer. Cell viability was inferred from the ability of live cells to exclude the dye trypan blue. The total number of viable alveolar macrophages was estimated by multiplying the total number of viable cells by the fraction of alveolar macrophages present in the lavaged sample. The cells were washed twice with ice cold Hank's balanced salt solution.

A stock solution of Hoechst 33342 in water (10 mg/mL) was filter-sterilized (0.22 µm filter) and diluted to 0.0, 0.1, 0.5, 1.0, 5.0, and 10.0 µg/mL (0.0, 0.2, 0.9, 1.8, 9.0, and 18 µM, respectively) in culture media (RPMI-1640 with 20% heat-inactivated fetal bovine serum) and warmed to 37°C. Stoichiometric vital staining of DNA by Hoechst 33342 generally requires exposure of cells to 5-10 µM dye for at least 30 min. Vital staining of AM was performed by resuspending 1×10^8 AM in each concentration of Hoechst 33342 and incubating them at 37°C, on a rotating platform, for either 30 min (0.0, 0.1, 0.5, and 1.0 µg/mL) or 15 min (5.0 and 10.0 µg/mL). After staining, the cells were washed twice with culture media and aliquoted into 6-well tissue culture plates (3×10^6 AM/well). Fluorescent latex particles (FLP; 1.7 µm diameter) were added to half of the cultures (2×10^7 FLP/well; 7 FLP/cell). All cultures were placed in an incubator maintained at 37°C and 5% CO₂.

III. METABOLISM AND MARKERS OF INHALED TOXICANTS

Immediately following staining, as well as after 1, 8, and 15 days in culture, all AM were analyzed by flow cytometry (FACSTAR PLUS, Becton Dickinson) for cell size (small angle light scatter) and nuclear (blue) fluorescence intensity. Cells that were incubated with FLP were also analyzed for the number of phagocytized FLP at each time point.

There was no significant effect of dye concentration or staining time on AM viability. However, there was a significant decrease in cell viability associated with time in culture (95-98% viable on day 1 vs. 75-80% viable on day 15). Increasing the concentration of Hoechst 33342 over the range of 0.1 to 5.0 µg/mL resulted in an increase in the mean nuclear fluorescent intensity of vitally stained AM (Table 1). There was no further increase in nuclear staining observed at the highest concentration of 10.0 µg/mL compared to 5 µg/mL. There was no apparent decrease in mean nuclear fluorescence intensity during the 2 wk in culture except in AM labeled with 10.0 µg/mL Hoechst 33342. Vital labeling of AM did not affect the ability of AM to phagocytize FLP. On each day that AM were analyzed for FLP content, there were no significant differences in the number of FLP per AM between cells stained with the various Hoechst dye concentrations. In addition, over the 2 wk in culture, there was no significant change in the number of FLP per AM (5-10% of AM contained 1-4 FLP, 6-9% contained 5-8 FLP, and 80-90% contained greater than 8 FLP).

Table 1
Mean Nuclear Fluorescence Intensity^a
of Alveolar Macrophage Stained with Hoechst 33342

	Hoechst 33342 Concentration (µg/mL)				
	0.1	0.5	1.0	5.0	10.0
Day 1	601.2 (5.3)	668.7 (5.1)	692.0 (4.7)	725.8 (4.5)	722.5 (8.1)
Day 8	552.3 (4.4)	699.7 (6.3)	737.9 (6.1)	754.0 (6.9)	743.7 (8.2)
Day 15	608.6 (9.0)	660.1 (7.9)	669.2 (9.2)	ND ^b	661.9 (10.0)

^aMean channel number of 50,000 cells (coefficient of variance).

^bND = Not determined.

The results of this study suggest that vital staining with Hoechst 33342 may be a useful technique to label AM. The staining with the dye had no observed effect on cell viability or their abilities to phagocytize particles over the range of dye concentrations used in the present study. In addition, there was no detectable loss of nuclear fluorescence over the course of the experiment. This suggests that the dye is stably incorporated into the genome of the AM without affecting the functional capabilities of the cell. Further studies are being done to assess the effect of Hoechst labeling on other cellular functions such as motility and oxidative metabolism. If the Hoechst label proves to be stable *in vivo* and does not alter the metabolic activity of AM, then studies will be done to evaluate the role of particle-containing AM in the clearance of particles from the lung in different species.

(Research sponsored by the Office of Health and Environmental Research, U. S. Department of Energy, under Contract No. DE-AC04-76EV01013.)

EFFECT OF DOSE ON THE DISPOSITION OF 2-ETHOXYETHANOL AFTER INHALATION BY F344 RATS

C. H. Kennedy, W. E. Bechtold, and R. F. Henderson

2-Ethoxyethanol (EE) is used as a solvent in the manufacture of protective coatings (e.g., lacquers, enamels, and varnishes), and in varnish removers, thinners, cleaning products, soaps, pesticides, aviation fuels, automotive brake fluids, and anti-stalling products (NIOSH/OSHA *Occupational Health Guideline for 2-Ethoxyethanol*, 1978). Inhalation and dermal absorption are the most likely routes of human exposure to EE. When administered repeatedly (either chronic or subchronic exposure) to rats, EE causes testicular atrophy and is fetotoxic, hematotoxic, and teratogenic (Barbee, S. J. et al. *Environ. Health Perspect.* 57: 157, 1984; Doe, J. E. et al. *Environ. Health Perspect.* 57: 33, 1984; Foster, P. M. D. et al. *Environ. Health Perspect.* 57: 207, 1984; Nelson B. K. et al. *Environ. Health Perspect.* 57: 255, 1984).

The purpose of this study was to determine the effect of dose on the absorption, metabolism, and excretion of ^{14}C -radiolabeled EE by F344/N rats after inhalation exposure. We also compared the disposition of EE after inhalation to the disposition of EE after dermal application (Sabourin, P. J. et al. *Fundam. Appl. Toxicol.* 19: 124, 1992) and oral (drinking water) administration (Medinsky, M. A. et al. *Toxicol. Appl. Pharmacol.* 102: 443, 1990).

Male F344/N rats (11-13 wk old) purchased from Taconic (Germantown, NY) were exposed for 5 h 40 min to a target concentration of 5 ppm EE or 6 h to a target concentration of 50 ppm EE. One group of four rats was used to determine the fractional uptake of EE and the amount of ^{14}C present in the body at the end of the exposure (body burden). These rats were exposed to $[^{14}\text{C}]$ EE in plethysmograph tubes to measure respiratory parameters (minute volume, tidal volume, and breathing frequency). The rats were euthanized; the entire carcass was digested to determine the body burden and the fraction of inhaled EE retained.

A second group of four rats was used to determine the pathways of excretion of $[^{14}\text{C}]$ EE equivalents and to identify the major metabolites excreted. These rats were transferred to glass metabolism cages after exposure, and excreta (urine, feces, and exhaled breath) were collected for 66 h. The rats were then euthanized; the carcasses were digested and analyzed for ^{14}C . To check for mass balance, the sum of the ^{14}C in the carcasses and excreta was compared to the total ^{14}C in the animals at the end of the exposure.

The actual exposure concentrations were 5.03 ± 0.23 ppm and 46.0 ± 2.2 ppm (mean \pm SD, n = 65 and 35, respectively) as determined by infrared spectroscopy. Minute volume values obtained from the plethysmograph data were not significantly different between the two exposure groups.

The body burden of EE was 1.23 ± 0.08 $\mu\text{moles}/\text{ppm}$ for the 5.0 ppm exposure and 1.46 ± 0.02 $\mu\text{moles}/\text{ppm}$ for the 46 ppm exposure (mean \pm SE, n = 4). The percent of inhaled EE retained was $28 \pm 1\%$ for the 5.0 ppm exposure and $29 \pm 2\%$ for the 46 ppm exposure (mean \pm SE, n = 4).

The excretion of $[^{14}\text{C}]$ EE equivalents was similar for the two exposure concentrations (Table 1). Significant percentages of the retained dose were exhaled as $^{14}\text{CO}_2$ during (22%) and after exposure (16%). Forty-six percent of the retained dose was excreted in the urine.

The urinary metabolites were analyzed by reverse-phase, high pressure liquid chromatography and were similar for both exposure concentrations. The major urinary metabolite was ethoxyacetic acid (EAA; ~65% of recovered urinary metabolites), the putative toxic metabolite of EE. N-Ethoxyacetyl glycinate, the glycine conjugate of EAA, was present at ~14% and ethylene glycol at ~16%.

The effect of route of administration on EE metabolite profiles is shown in Figure 1. The amount of retained EE excreted as EAA followed the order dermal > oral (drinking water) > inhalation and was inversely related to the amount exhaled as $^{14}\text{CO}_2$.

Table 1
Excretion of [¹⁴C]Ethoxyethanol Equivalents

Route of Excretion	μmoles [¹⁴ C]EE Equivalents ^a			
	5 ppm	(%) ^b	46 ppm	(%) ^b
¹⁴ CO ₂ during exposure ^c	1.4	(21)	14	(22)
¹⁴ CO ₂ post exposure	1.1 ± 0.1	(16)	10 ± 1	(16)
Urine	3.1 ± 0.1	(46)	29 ± 1	(46)
Feces	0.04 ± 0.01	(0.6)	1.0 ± 0.2	(1.6)
Exhaled EE post exposure	0.29 ± 0.09	(4.2)	2.4 ± 0.3	(3.7)
Carcass	0.74 ± 0.06	(11)	6.6 ± 0.2	(10)
Total ^d	6.6 ± 0.3	(100)	64 ± 2	(100)

^aValues are mean for four rats ± SE.

^bValues in parentheses are the percent of total ¹⁴C excreted and remaining in the carcass after 72 h.

^c¹⁴CO₂ exhaled during exposure was determined as total ¹⁴CO₂ in chamber exhaust divided by the number of rats in the chamber.

^dThe body burden, as measured by digestion of rats at the end of the exposure, was 6.2 ± 0.4 μmoles for the 5.0 ppm exposure and 67 ± 1 μmoles for the 46 ppm exposure (mean ± SE, n = 4).

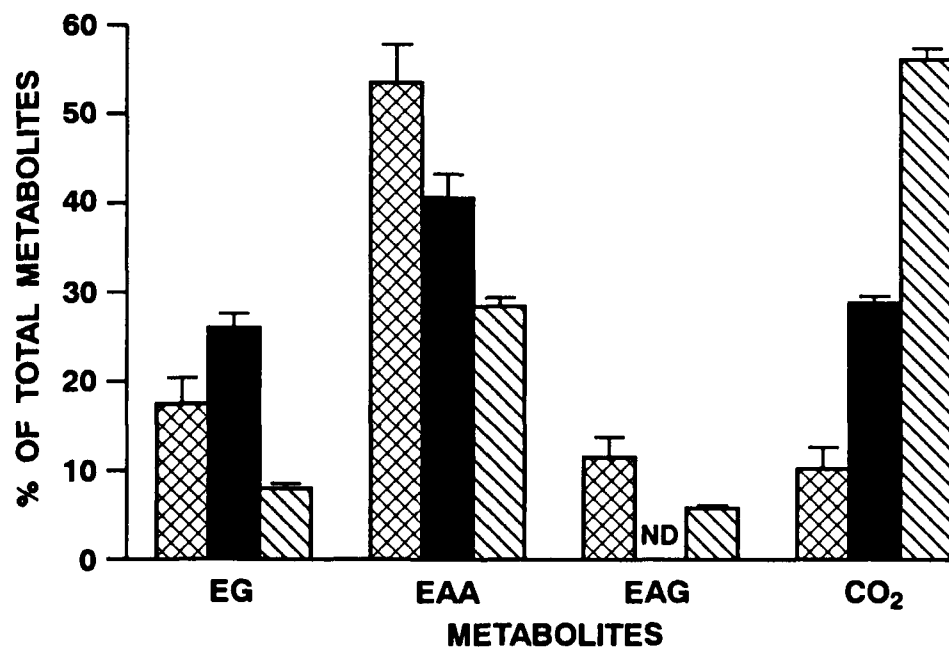


Figure 1. Effect of exposure route on the profile of metabolites of [¹⁴C]EE. Values are the mean for four rats ± SE. Cross-hatched bars, dermal exposure; solid bars, oral (drinking water) exposure; hatched bars, inhalation exposure. Abbreviations: EG, ethylene glycol; EAA, ethoxyacetic acid; EAG, N-ethoxyacetyl glycinate; ND, not detected. Internal doses of EE (μmoles/kg): dermal, 278 ± 40; oral (drinking water), 210 ± 16; inhalation, 219 ± 5 (mean ± SE, n = 4).

The results of this study suggest that the toxicity of inhaled EE should be directly proportional to the exposure concentration up to 46 ppm if the toxicity of EE is due to EAA. The results of metabolite comparison after administration of EE by different routes suggest that absorption of EE by dermal exposure should result in greater toxicity than absorption of an equivalent amount by inhalation exposure.

(Research sponsored by the National Institute of Environmental Health Sciences/National Toxicology Program under Interagency Agreement No. Y01-ES-20092 with the U.S. Department of Energy under Contract No. DE-AC04-76EV01013.)

HUMAN METABOLISM OF 1,3-BUTADIENE

W. E. Bechtold, M. R. Strunk, I. Y. Chang, and R. F. Henderson

1,3-Butadiene (BD) is a reactive gas used as a monomer in the production of styrene-butadiene and polybutadiene rubber. Lifetime inhalation carcinogenicity studies of BD have been carried out in both B6C3F₁ mice (Huff, J. E. et al. *Science* 227: 548, 1985) and Sprague-Dawley rats (Owen, P. E. et al. *Am. Ind. Hyg. Assoc. J.* 48: 407, 1987). The primary tumor incidences for rats exposed by inhalation to a given dose of BD were considerably less than those observed in mice. Recent studies at the ITRI have shown that mice, rats, hamsters, and monkeys (Sabourin, P. J. et al. *Carcinogenesis* 13: 1633, 1992) produce two urinary metabolites of BD, 1,2-dihydroxy-4-(N-acetylcysteinyl-S)-butane (M1) and 1-hydroxy-2-(N-acetylcysteinyl-S)-3-butene (M2). M2 is formed by the conjugation of the toxic monoepoxide of BD (BDO), while M1 is the conjugate of the detoxicated hydrolysis product of the BDO. When all four species were compared, the ratio of M1 to the total M1 + M2 was linearly related to hepatic epoxide hydrolase levels, the enzyme responsible for hydrolyzing BDO. These results suggested that the insensitivity of rats in the bioassay relative to mice may be due in part to the relatively high rate of detoxication (hydrolysis) of the mutagenic epoxides. Humans are known to have epoxide hydrolase levels similar to monkeys, and higher than rats (Schmidt, U. and E. Loeser. *Arch. Toxicol.* 57: 222, 1985). Taken together, we postulated that humans would produce more M1, which would reflect the rapid hydrolytic detoxication of BDO. We describe here a method, based on isotope dilution gas chromatography/mass spectroscopy (GC/MS), capable of selectively and sensitively measuring M1 and M2 in the urine of humans occupationally exposed to BD. We used this method to measure production of these metabolites in the urine of workers exposed to BD.

M1, M2, and their deuterated analogues were previously synthesized and characterized at ITRI. For analysis of M1 and M2, aliquots of their deuterated analogues were added to 5 mL of urine. The urine was partially purified by passing it through C18 extraction columns. After evaporation the residue was reconstituted in methanol and selectively precipitated by the addition of acetone. The precipitate was removed by centrifugation and the supernatant dried. M1 and M2 were derivatized using N,O-bis(trimethylsilyl)trifluoracetamide and were analyzed by GC/MS as previously described (1990-91 Annual Report, p. 85).

All urine samples from human exposures were analyzed blind. The study subjects consisted of four sets of workers at the Texaco Chemical Co. Plant in Port Neches, TX, a plant that manufactures BD. Exposed workers performed in two areas with historical 8-h, time weighted average concentrations of 2-3 ppm BD. Workers exposed to an intermediate level of BD were rovers who spent variable amounts of time in low and high exposure areas. Nonexposed workers performed in areas with historical time weighted average concentrations of less than 0.1 ppm BD. Outside controls from the same region had no known exposures to BD. Urine samples from seven, three, ten, and nine workers from the above four groups were analyzed, respectively. Urine was collected at the end of an 8-h shift. BD was monitored in the work areas using GC.

M1 and M2 in urine were identified by coelution of peaks with deuterated internal standards, and by comparisons of the appropriate peak ion area ratios between standards and samples. Urine samples from workers exposed to BD at the plant were analyzed for M1 and M2. When injected onto the GC/MS, peaks were found to coelute with the M1 deuterated internal standard. The difference in retention time of M1 analyte and the deuterated analogue was 0.87 ± 0.05 sec (SEM, n = 7) for the analysis of urine samples from exposed workers. Further, the peaks coeluting with M1 possessed ion ratios identical to the standard (Table 1).

In contrast, no peaks were detected with retention times within 3 sec of the internal standard peak for M2. All analyte peaks eluting within several seconds of the internal standard were analyzed and found to have ion ratios inconsistent with those of M2 (Table 1).

The average values of M1 for exposed, intermediately exposed, nonexposed, and outside control workers performing in areas with historical average BD levels of 2-3 ppm were 3200 ± 1600 , 1390 ± 550 , 630 ± 189 ,

and 320 ± 70 ng/mL, respectively (SEM, n = 7, 3, 10, and 9). A nonparametric method, Kruskal-Wallace one-way analysis of variance, was used to test the group differences. Exposed individuals were tested to be statistically different from the outside control group at an overall p value of 0.05. None of the rest of the comparisons were different. Based on spikes of analytes into the pooled control urine samples, the limits of detection for the metabolites were estimated to be 100 ng/mL (signal to noise greater than 3 to 1).

Table 1

Ion Ratios for Metabolite Standards M1 and M2,
and Peaks Coeluting with M1 in the Urine of Workers Exposed to BD

	129/452 ^a	228/452	244/362	318/362
M1 (n = 4)	36 ± 2	6.2 ± 0.4	NA ^b	NA
M2 (n = 3)	NA	NA	30 ± 21	6.0 ± 3.0
Urine (n = 7)	36 ± 3	7.5 ± 0.6	ND ^c	ND

^aRatio of areas of peaks from ion chromatograph with retention times at analyte peaks; unitless.

^bNot applicable.

^cNot detected.

Results from the analysis of urine from workers exposed to BD in a processing plant support our hypothesis that higher levels of epoxide hydrolase in humans would result in preferential formation of M1 over M2. The limits of sensitivity for our assay are 100 ng/mL for either metabolite. Generally, individuals who worked in areas of the processing plant with historical averages of 2-3 ppm BD had values of 3200 ± 1600 ng/mL M1 and no measurable values of M2. This yields a percentage of M1 of at least 97% relative to the sum of the two. Although the implications for toxicity are not definitive, these results suggest that from the perspective of detoxication of the epoxide, humans are more efficient at hydrolysis of the monoepoxide than either mice and rats and thus may be even less sensitive than rats to BD toxicity.

M1 may be a suitable metabolite for biological monitoring of BD. While a statistically significant difference was found between exposed and control groups, the exact dosimetry of the individuals was unknown. Further, the implications of M1 in control urine samples are unknown. This background could result from endogenous or exogenous BD, or some alternate metabolic pathway. We are acquiring urine from workers in the same BD production plant who have been monitored for exposure with personal dosimeters. Urine samples from the workers will be measured for M1. These results should allow discrimination of the sensitivity of M1 as a biological exposure index.

In summary, we have measured two metabolites of BD in the urine of production workers. Consistent with our hypothesis, the metabolite representing the hydrolysis of the initial epoxide of BD, but not the glutathione conjugate of the epoxide, was detected.

(Research sponsored by the Office of Health and Environmental Research, U. S. Department of Energy, under Contract No. DE-AC04-76EV01013.)

METABOLISM OF 3,9-DINITROFLUORANTHENE AND 3-NITROFLUORANTHENE BY F344 RAT LUNG SUBCELLULAR FRACTIONS

C. E. Mitchell, W. E. Bechtold, and S. A. Belinsky

Nitrofluoranthenes (NFs) are ubiquitous environmental contaminants produced by combustion of fossil fuels, tobacco, and coal tar (Tokiwa, H. and Y. Ohnishi. *CRC Crit. Rev. Toxicol.* 17: 23, 1986). They are also formed in the atmosphere from the reaction of polycyclic aromatic hydrocarbons (PAHs) with nitrogen oxides, and from HNO_3 nitration of PAH in engine or burner exhausts (Tokiwa and Ohnishi, 1986). Dinitrofluoranthene (3,9-DNF) is the most carcinogenic form of NFs in rats (Horikawa, K. et al. *Carcinogenesis* 12: 1003, 1991). This NF has been detected in the atmosphere at levels of 9-102 ng/g particles (Tokiwa, H. et al. *Genetic Toxicology of Complex Mixtures*, Plenum Publishing Corp., New York, p. 165, 1990). Intrapulmonary implantation of 3,9-DNF (0.2 mg) into the lungs of the F344 rats produces a 90% incidence of lung tumors, while only a 5% tumor incidence is observed following exposure to 1 mg of 3-NF (Horikawa, K. et al., 1991). At present, the molecular mechanisms involved in the difference in sensitivity for the induction of lung tumors in rats by 3-NF and 3,9-DNF remain to be defined. These compounds most likely induce carcinogenesis by metabolic activation to electrophilic metabolites that bind to DNA as promutagenic adducts. Previous studies (1990-91 Annual Report, p. 137) have demonstrated that both oxidative and reductive pathways are involved in the metabolism of 3-NF by the rat liver. However, the activation pathways involved in the metabolism of the mononitroisomers and dinitroisomers of NF by the rat lung, a target organ for these compounds, have not been identified. The purpose of these investigations was to determine the activation pathways in the rat lung for the metabolism of the mono- and dinitroisomers of NF.

The results of these investigations indicate that the major pathway for the metabolism of 3,9-DNF by lung cytosolic and microsomal enzymes was nitroreduction. In contrast, both nitroreduction and aerobic oxidative metabolism were involved in the activation of 3-NF. These results were obtained following the anaerobic and aerobic metabolism of 3-NF and 3,9-DNF. One major metabolite of 3,9-DNF and one of 3-NF were detected following anaerobic incubation with lung cytosol (the supernatant fraction obtained after centrifugation of lung homogenates at 100,000 g). The metabolites of 3-NF and 3,9-DNF were tentatively identified as 3-aminofluoranthene (3-AF) by HPLC with an authentic standard, and aminonitrofluoranthene (ANF) by gas chromatography/mass spectroscopy, respectively (Fig. 1). Rates of reduction of 3-NF and 3,9-DNF, mediated by rat lung cytosol fractions from uninduced and 3-methylcholanthrene (3-MC)- and phenobarbital (PB)-induced rats, are shown in Table 1. The rate of ANF formation from 3,9-DNF was approximately two times the rate of 3-AF. The induction of cytochrome P-450 isozymes by PB and 3-MC did not affect the rate of cytosolic metabolism of 3-NF or 3,9-DNF.

Rates of microsomal anaerobic metabolism were also two times greater with 3,9-DNF compared to 3-NF. No differences were observed when comparing rates of cytosolic versus microsomal metabolism for the 3-NF and 3,9-DNF. Treatment with 3-MC increased the formation of both 3-NF and ANF by 2.5 and 2.0 times, respectively, when compared to untreated controls. An increase in the formation of 3-AF but not ANF was also observed in microsomes from PB-induced rats.

One major and three minor metabolites were observed during the aerobic metabolism of 3-NF (data not shown). Two of the metabolites were identified by coelution with standards as 3-NF-8-ol and 3-NF-7-ol or 3-NF-10-ol. The HPLC profiles of the organic extracts of 3,9-DNF incubated aerobically with microsomes showed no significant peaks either with microsomes from control rats or from 3-MC- or PB-treated rats.

These studies show that 3,9-DNF was anaerobically metabolized at a rate two times that of 3-NF and suggest that the nitro group at the three position is a good substrate for the nitroreductases even in the presence of a second nitro group at the nine position. This conclusion is supported by a lower k_m for the cytosolic metabolism of 3,9-DNF than for 3-NF. In Figure 1, suggested reductive and oxidative pathways for the metabolism of 3-NF and 3,9-DNF are shown. As can be seen, 3-AF is most likely formed from 3-NF by the sequential reduction of the nitro group to the nitroso, then to the hydroxylamine derivative (Belisario, M. A. et al. *Carcinogenesis* 11: 213, 1990), or oxidized to phenols. 3,9-DNF may be activated by nitroreduction followed by O-acetylation.

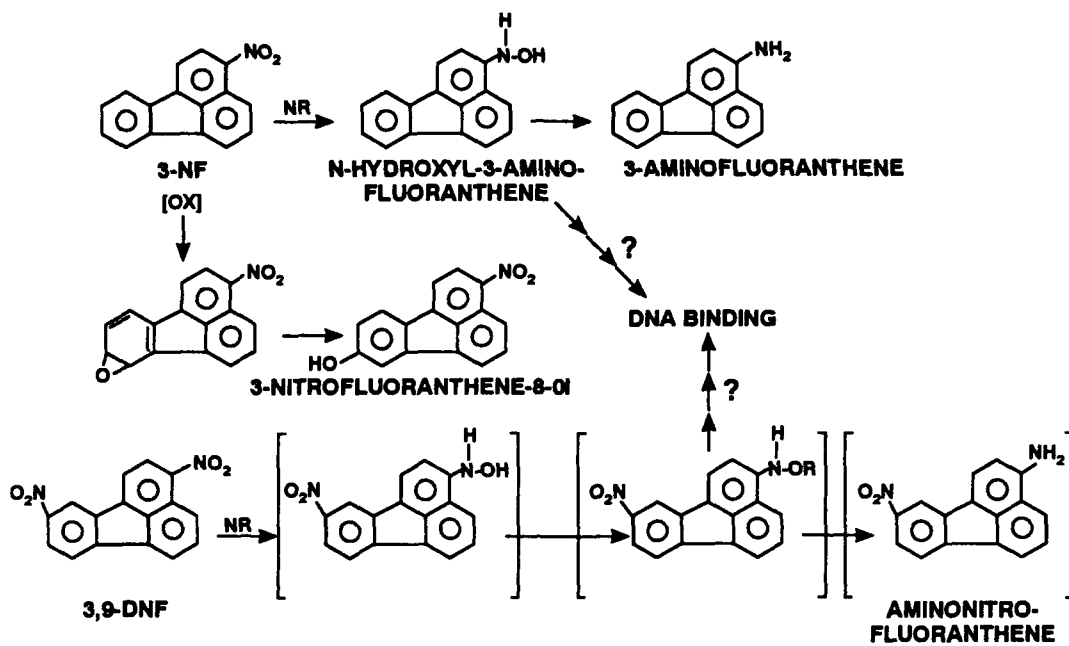


Figure 1. Proposed oxidation and reduction pathways for the metabolic activation of 3-nitrofluoranthene and 3,9-dinitrofluoranthene. 3-NF is metabolized by nitroreduction (NR) to N-hydroxyl-3-amino-nitrofluoranthene that is rearranged to form a reactive intermediate which binds to DNA. Alternatively, 3-NF is metabolized by oxidation to phenolic compounds. 3,9-DNF is metabolized to N-hydroxy-3-amino-9-nitrofluoranthene, then to N-acetoxyaminofluoranthene that is rearranged to form a reactive intermediate which binds to DNA. The formations of potential reactive intermediates of the proximate metabolites are indicated by (>>?>>).

Table 1

Nitroreduction Rates of 3-NF and 3,9-DNF by Rat Lung Microsomal and Cytosolic Fraction from Uninduced and Induced Rats

Substrate	NF Amino-derivative Formed (nmol/mg protein/min)		
	Uninduced	PB	3-MC
Cytosol Fraction			
3-NF	1.13 ± 0.17 ^{a,b}	0.82 ± 0.10 ^b	0.85 ± 0.02 ^b
3,9-DNF	2.06 ± 0.20	2.04 ± 0.18	2.18 ± 0.28
Microsomal Fraction			
3-NF	0.70 ± 0.11	1.02 ± 0.20 ^{b,c}	1.76 ± 0.40 ^{b,c}
3,9-DNF	1.58 ± 0.23	1.73 ± 0.30	3.22 ± 0.39 ^c

^aMean ± SD of duplicate or triplicate determination.

^bp < 0.05 vs. 3,9-DNF substrate.

^cp < 0.05 vs. uninduced.

However, 3,9-DNF is not metabolized extensively to phenols. The lack of formation of a major metabolite of 3,9-DNF aerobically suggests that ring hydroxylation of this compound is inhibited due to the presence of an additional nitro group at the nine position. Several cytosolic enzymes responsible for the nitroreduction of NF have been identified using purified enzymes in reconstituted *in vitro* systems (Beland, F. A. *et al.* In *Polycyclic Hydrocarbons and Carcinogenesis*, American Chemical Society, Washington, DC, p. 371, 1985). The metabolism of 3-NF to 3-aminonitrofluoranthene (3-ANF) by xanthine oxidase and aldehyde oxidase has been demonstrated (Beland, F. A. *et al.*, 1985). However, the enzymes present in rat lung cytosol, which are responsible for the nitroreduction of 3-NF and 3,9-DNF have not been identified. Microsomal rates of metabolism of both NFs were increased by lung microsomes from rats induced with 3-MC. Thus, cytochrome P-450 isozyme 1A1 that is induced by 3-MC (Gonzalez, F. J. *Pharmacol. Ther.* 45: 1, 1990) is possibly involved in the metabolism of 3-NF and 3,9-DNF. Cytochrome P-450 reductase, which is also induced by 3-MC, has been implicated in the metabolism of 1-NP to 1-aminopyrene (Saito, K. *et al.* *Cancer Res.* 44: 3169, 1984). Thus, increased rates of 3-NF and 3,9-DNF metabolism may, in part, involve both cytochrome P-450 1A1 and cytochrome P-450 reductase.

The scheme (Fig. 1) suggests that the generation of a reactive intermediate such as a N-acetoxy-derivative during the O-acetylation of the arylhydroxylamine may be responsible for the carcinogenicity observed in rats after treatment with 3,9-DNF. The addition of a strong electron withdrawing group such as a nitro group has been proposed to lower the redox potential of the NO₂ group (Bock, H. and U. Lechner-Knoblauch. *Z. Naturforsch.* 40B: 1463, 1985) which would, in turn, increase the mutagenic and carcinogenic potency of this metabolite. Although the formation of a specific adduct of 3,9-DNF has not been identified *in vivo*, the fact that 3-ANF is formed from 3,9-DNF by cytosol and microsomes suggests that the generation of a N-acetoxy-derivative intermediate could lead to DNA damage.

In conclusion, these studies suggest that 3-NF can be metabolized in the lung by both nitro-reductive and oxidative pathways. The absence of any significant oxidative metabolism of 3,9-DNF suggests that this carcinogen is metabolized by nitroreduction. The higher rate of metabolism of 3,9-DNF over 3-NF, the reactivity of the proximate metabolite, and/or the repair of the metabolite may be responsible for the differential potency of the two carcinogens to cause lung cancer in rats following treatment. Knowledge of the pathway(s) for the activation of 3,9-DNF and other NFs will contribute to defining the molecular mechanisms by which NFs induce carcinogenicity in rats.

(Research sponsored by the Office of Health and Environmental Research, U. S. Department of Energy, under Contract No. DE-AC04-76EV01013.)

ALKALINE PHOSPHATASE IN LAVAGE FLUID: AN INDICATOR OF TYPE II CELL SECRETIONS?

R. F. Henderson, G. C. Scott*, and J. J. Waide

In the alveolar portion of the lung, the only site of alkaline phosphatase (AP) activity observed by histochemical staining is the apical portion of the alveolar type II cell (Kuhn, *C. Am. J. Pathol.* 53: 809, 1968). Investigators have suggested that the enzyme may have some role in the secretion of surfactant from the type II cell but that role has never been defined. Analysis of bronchoalveolar lavage fluid from laboratory animals indicates that there are measurable levels of AP in the lavage fluid, and those levels appear to increase or decrease in response to specific inhaled toxins. We hypothesized that the AP in lavage fluid comes from the type II cell and can be used as a marker for type II cell secretions.

To test this hypothesis, we examined the isoelectric focusing (IEF) patterns of AP from various tissues, cells, and fluids from the body of the rat. The samples included serum, lavage fluid, type II cells, lung, heart, aorta, kidney, liver, intestine, bone, and neutrophils. IEF is a form of electrophoresis that uses ampholytes in the gel to cause the proteins to migrate to their isoelectric point on the gel.

Adult female F344/N rats (Taconic, Germantown, PA) were used in this study. Animals were anesthetized with 5% halothane anesthesia and the heart/lung block removed. The lung was lavaged two times with 0.15 M saline and the cells removed by centrifugation. The supernatant fluid was concentrated using Centricell 30K Ultrafilters (Polysciences, Inc., Warrington, PA), and this concentrate was further concentrated using the Centricon 10K Microconcentrators (Amicon, Danvers, MA). The concentrates were stored at -70°C until analysis. Soft tissues (heart, aorta, kidney, liver, intestine, lung) were rinsed in physiological saline and then homogenized in a volume of saline equal to three times the mass of the samples. The homogenates were centrifuged to remove debris and the supernatants frozen at -70°C until analysis. Bone was prepared according to the method of Skillen and Rahbani-Nobar (*Calcif. Tissue Int.* 30: 67, 1980). PMN were isolated from blood by Ficoll gradient techniques (Bentwood, B. J. and P. M. Henson. *J. Immunol.* 124: 855, 1980) and type II cells were isolated by standard ITRI techniques (ITRI SOP No. 0884).

All samples were analyzed for AP activity using the Monarch Automated Enzyme Analyzer (Instrumentation Laboratory, Lexington, MA) before IEF analysis. The AP activity was used to determine how much sample to use in the IEF analyses. The IEF method (Isolab, Inc., Akron, OH) required that 15 µL of sample containing 30-40 International Units/L be used in order to visualize the activity on the gel. Samples (100 µL) were treated with 0.5 milliunits of phospholipase C, phosphatidylinoitol specific, at 37°C for 60 min to release the AP activity from membranes.

The results of the IEF analyses are shown in Figures 1 and 2. The lavage fluid was very dilute in AP and hard to visualize. However, two bands running toward the anode could be seen, and these bands were clearly visible in the type II cells and the whole lung sample. Serum AP ran toward the cathode suggesting that the lavage fluid AP was not derived from the serum. The IEF pattern for bone (not shown) was distinguishable from the type II cell pattern. Unfortunately, the AP from PMN corresponds closely with that of the type II cells. Because most toxins that induce type II cell hyperplasia and hypersecretion also induce an influx of PMN into the alveoli, it would not be possible to conclude that lavage fluid AP activity was derived solely from type II cells based on the IEF pattern alone. Further work is required to determine if the AP from type II cells can be distinguished from the AP from PMN. Further work is also required to concentrate the lavage fluid AP enough to fully characterize it.

*New Mexico Teacher Research Associate Program Participant

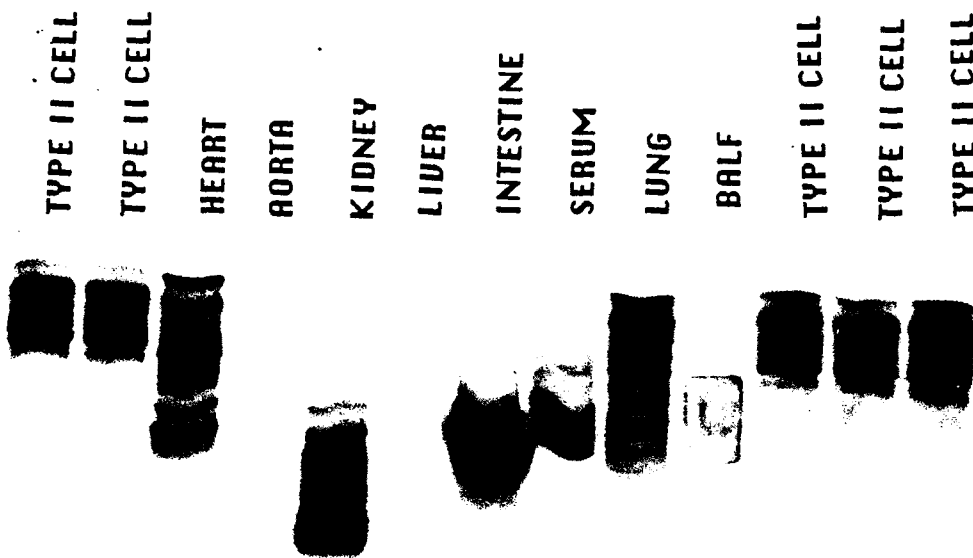


Figure 1. IEF patterns for AP from rat tissue samples. The liver sample used in this analysis was inadvertently too dilute. Other liver samples also contained several lighter bands running toward the cathode. The rectangle associated with the bronchoalveolar lavage fluid (BALF) samples is an artifact.

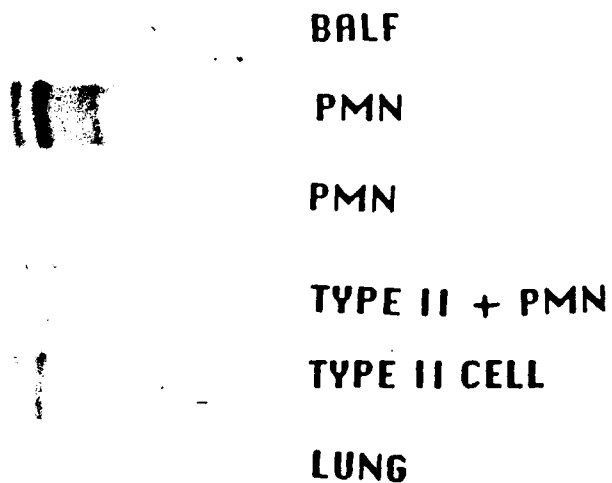


Figure 2. IEF patterns of AP in PMN and type II cells.

(Research sponsored by the Office of Health and Environmental Research, U. S. Department of Energy, under Contract No. DE-AC04-76EV01013.)

MULTIDIMENSIONAL HPLC ANALYSIS OF BUTADIENE MONOEOXIDE/GUANOSINE ADDUCTS WITH ELECTROCHEMICAL DETECTION

W. E. Bechtold and M. R. Strunk

1,3-Butadiene (BD) is widely used in the manufacture of plastics and rubber and is also present in cigarette smoke, urban air, and gasoline vapor. A remarkable species difference in the carcinogenic response of B6C3F₁ mice, Sprague-Dawley rats, and humans to BD is well known. Metabolism of BD by B6C3F₁ mice *in vivo* leads to the formation of 1,2-butadiene monoepoxide (BDO) in lung and bone marrow tissues (this report, p. 92). BDO in turn can react with guanosine bases in DNA (Citti, L. *et al.* *Carcinogenesis* 5: 1, 1984). Species differences in the toxic effects of BD may be due in part to differences in the formation of alkyl-DNA adducts, because DNA adduct formation has been implicated as a primary event in multistage chemical carcinogenesis.

Our goal is to determine the formation, removal, and urinary excretion of DNA adducts to BDO in rats and mice. DNA adduct formation and persistence will be compared as a function of species and exposure concentration. If species differences in the formation and removal of BDO/DNA adducts in target tissues are reflected in their urinary excretion, the relative susceptibility of humans can be implied by measuring the same adducts in urine after well-characterized occupational exposures. Furthermore, determination of urinary excretion of BDO/DNA adducts promises to be an effective integrative biological marker of butadiene exposure in humans that is available in a matrix more easily acquired than blood.

To meet these goals, we developed a method for analyzing thermal hydrolysates of DNA for the two major BDO guanosine adducts, 7-(2-hydroxy-3-buten-1-yl)guanine and 7-(1-hydroxy-3-buten-2-yl)guanine. The two DNA adducts were synthesized by reacting BDO with 2'-deoxyguanosine at 37°C and pH 7.4. The synthetic mixture was hydrolyzed, analyzed, and purified by high pressure liquid chromatography (HPLC), and yielded three components that accounted for more than 90% of the total mass. The components were collected, dried under nitrogen, and derivitized by trimethylsilylation. Analysis by gas chromatography/mass spectroscopy indicated that the components were unreacted guanine and the expected isomeric N-7 adducts. Isomeric discrimination and standard solution concentrations were determined by UV spectroscopy, as previously described (Citti, 1984).

The two DNA adducts were separated by multidimensional HPLC, using three buffers. Buffer A, used for separation on a Partisil 10 SCX 250 x 4.6 mm (10 µm) column, was 100 mM ammonium formate (pH = 2.8). Buffer B, used for separation on a OD-MP Spheri-5 RP-18 100 mm x 4.6 mm (5 µm) column, was 100 mM potassium phosphate (pH = 5.5). Buffer C was a 1:1 solution of acetonitrile:buffer B. Samples were injected onto the SCX Partisil column. At the appropriate elution time, the adducts were collected and re-focused by diverting flow through a Brownlee OD-GU Spheri-5 monofunctional RP-18 30 mm x 4.6 mm (5 µm) guard column. Once the elution of adducts was complete, the guard column was rinsed with buffer B for 2 min. The pre-column was backflushed onto the RP-18 column and washed with buffer B for 5 min. A 5-min linear gradient from 100% buffer B to a 9:1 mixture of buffer B:buffer C was used to elute the adducts from the RP-18 column. Injection and flow control were managed by the switching of two Rheodyne 6-port valves actuated in tandem, and by a third, 6-port Rheodyne valve used for the final injection.

Column eluant for the adducts was monitored by HPLC/electrochemical detection (ECD). The optimum potentials for the screening and analytical coulometric cells were determined to be 500 mV and 750 mV, respectively. Response from the electrochemical cell was linear between 43.8 fmol and 21.9 pmol total adduct. The absolute detection limit was approximately 20 fmol for each adduct with a signal-to-noise ratio of better than 3 to 1.

Salmon sperm DNA (1.9 mg) was incubated with graded concentrations of BDO for 1 h at 37°C. The two adducts were cleaved from the DNA by neutral thermal hydrolysis for 30 min at 100°C, followed by precipitation of the DNA in ice cold ethanol. When the supernatant was lyophilized and analyzed by two-dimensional HPLC/ECD, two peaks were observed with retention times matching the synthetic standards. Formation of the DNA adducts was dose dependent (Fig. 1).

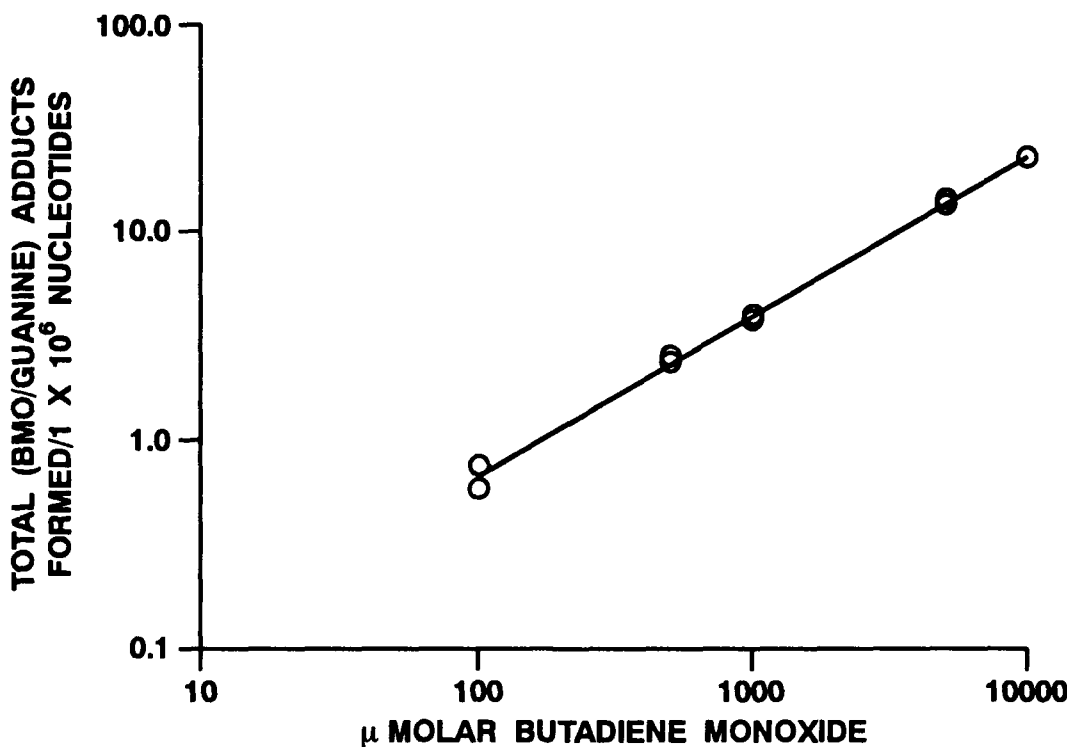


Figure 1. Adducts/1 $\times 10^6$ nucleotides formed in salmon sperm DNA. Circles represent duplicate treatments of DNA at each of the concentrations.

The retention times of several modified guanine bases, including 7-methylguanine, 9-ethylguanine, and guanine itself, were run in comparison with the 2 BDO adducts. None was found to coelute with the BDO adducts either on the cation exchange column or the two-dimensional system. Our assay thus appears to be valid for determining guanine adducts for BDO.

Recently, male B6C3F₁ mice were exposed to 625 ppm butadiene for 2 days, as part of a larger experiment designed to address the formation of lymphocyte *hprt* mutations. DNA will be isolated from liver, lung, kidney, heart, and bone marrow from these mice, and the equivalent number of control mice, and analyzed for the formation of the two adducts. Results from these analyses should indicate if our method is sufficiently sensitive to observe adduct formation under a broader range of exposure times and concentrations.

(Research sponsored by the Office of Health and Environmental Research, U. S. Department of Energy, under Contract No. DE-AC04-76EV01013.)

NONANEDIOIC ACID: A BIOMARKER OF EXPOSURE TO OZONE

C. H. Kennedy, A. A. Hunt*, W. E. Bechtold, W. A. Evans**, and J. R. Harkema

Because ozone (O_3) is the major oxidant in photochemical smog and acute exposure to ambient concentrations of this chemical has been implicated in the development of increased airway reactivity (Golden, J. A. et al. *Am. Rev. Respir. Dis.* 118: 287, 1978), development of a biomarker for exposure to O_3 would greatly facilitate determining if clinical symptoms (e.g., asthma attacks) in humans can be related to dose of O_3 (Schoettlin, C. E. and E. Landau. *Public Health Rep.* 76: 545, 1961).

Unsaturated fatty acids (UFA) in both mucus and lung surfactant are proposed to be primary targets for O_3 (Pryor, W. A. and D. F. Church. *Free Rad. Biol. Med.* 11: 41, 1991). Aldehydes resulting from the interaction of O_3 with UFA may be detected as volatile derivatives of their corresponding acids by gas chromatography (Rabinowitz, J. L. and D. J. Bassett. *Exp. Lung Res.* 14: 477, 1988). Nonanedioic acid (NDA) is produced by ozonizing either oleic, linoleic, or linolenic acid, and oxidizing and saponifying the sample. If NDA can be detected in bronchoalveolar lavage fluid (BALF) and/or nasal lavage fluid (NLF) after O_3 exposure in a rodent model, these biomarkers may be used to determine O_3 concentrations to which humans have been exposed.

The purposes of this preliminary study were to: (1) prepare a dose-response curve for the formation of NDA after exposure of dioleoyl phosphatidylcholine (DOPC, a phospholipid that has two oleic acid side chains) to a range of concentrations of O_3 and (2) determine the amount of NDA present in BALF and NLF after exposure of rats to either air or 2 ppm O_3 for 4 h.

A dose-response curve was prepared to relate the amount of pentafluorobenzyl derivative of NDA detected by gas chromatography/mass spectrometry (GC/MS) to the amount of ozone bubbled through DOPC. Liposomal solutions of DOPC were prepared by sonication and bubbled with various amounts of ozone. The ozonized solutions were spiked with decanedioic acid (internal standard), oxidized with silver (I) oxide, saponified with potassium hydroxide, extracted with dichloromethane, and derivatized with pentafluorobenzyl bromide. Aliquots of the derivatized samples were analyzed by GC/MS.

Sixteen week-old male CD rats (Charles River, Raleigh, NC) were exposed for 4 h to either air or 2 ppm O_3 . Ozone was generated from O_2 using a silent-arc-discharge O_3 generator (OREC, Phoenix, AZ). The concentration of O_3 was monitored continuously using a chemiluminescent O_3 analyzer (Bendix, Lewisburg, WV). After exposure, the animals were euthanized, and nasal and tracheobronchial airways were lavaged with saline solution. The resulting BALF and NLF samples were stored at -70°C prior to chemical workup. Aliquots of the samples were spiked with the internal standard, oxidized, saponified, derivatized as described above, and analyzed by GC/MS.

A dose-response curve for the formation of NDA *in vitro* is shown in Figure 1. A linear relationship was observed when the ratio of the peak area of the NDA to the peak area of the internal standard (determined by GC/MS analysis) was plotted against the amount of ozone bubbled through the DOPC solution.

The amount of NDA detected in BALF and NLF after exposure of rats to either air or ozone is shown in Figure 2. In the BALF, no significant difference was found between the O_3 -exposed and air-exposed groups. The amount of NDA detected in the NLF was significantly greater in the O_3 -exposed group than in the air-exposed group. The levels of NDA in both fluids from the air-exposed animals were high. This may be due to peroxidation of the samples during chemical workup, as 9-oxononanoic acid, the aldehyde precursor of NDA, is a minor product of lipid peroxidation (Kaneko, T. *Chem.-Biol. Interactions* 63: 127, 1987).

*Department of Energy/Associated Western Universities Summer Student Research Participant

**Postdoctoral Participant

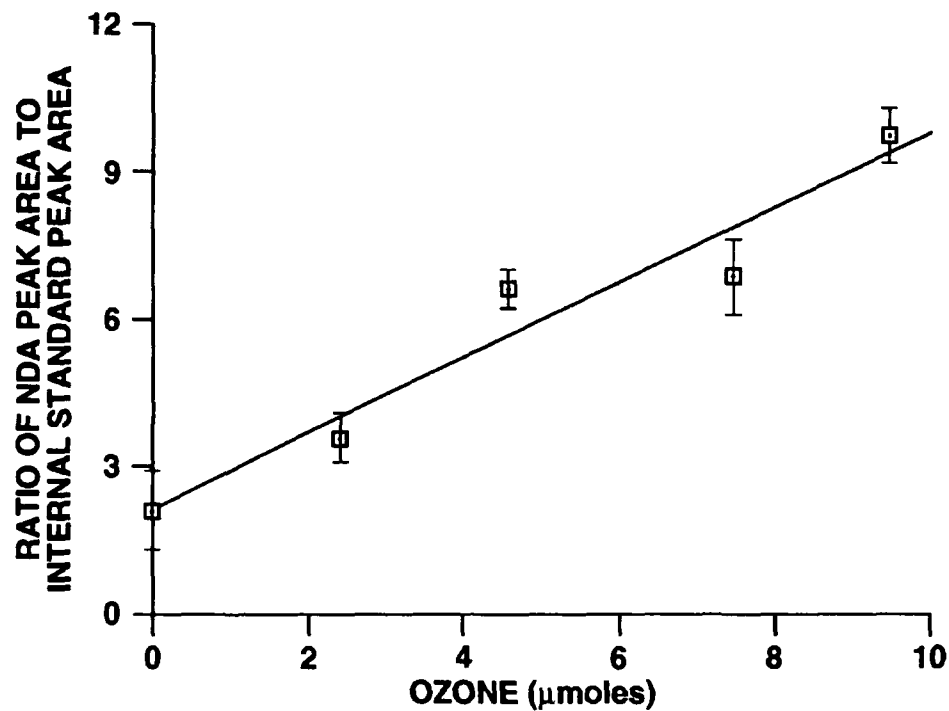


Figure 1. Dose-response curve for the formation of NDA following ozonolysis of DOPC liposomes. Values are the mean of three measurements \pm SE.

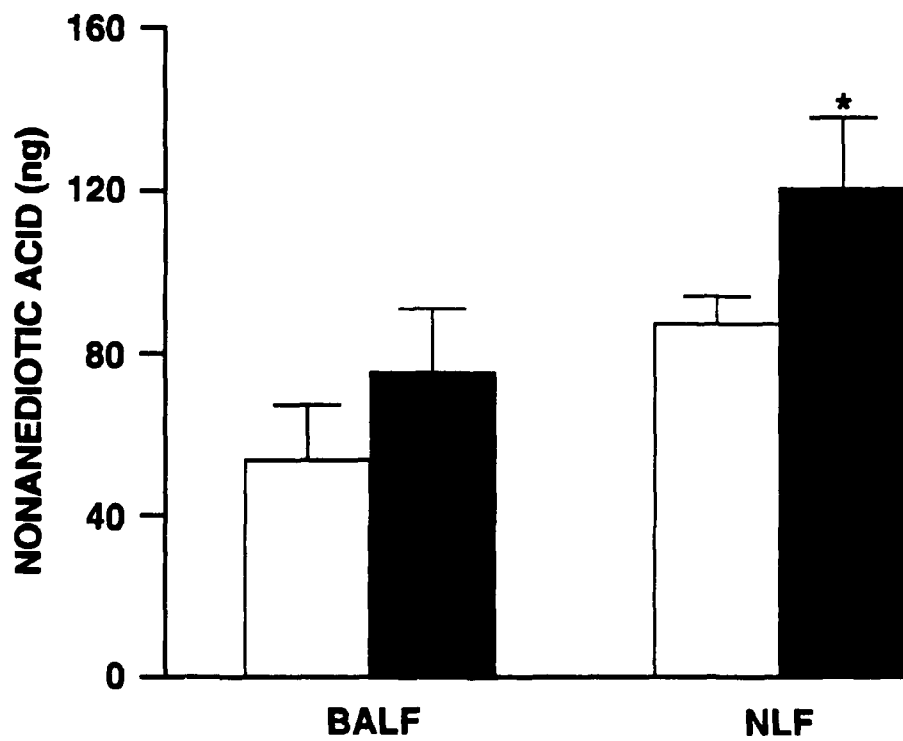


Figure 2. Biomarker levels in lavage fluids after exposure of rats to either air or 2.0 ppm ozone for 4 h. Values are the mean for six rats \pm SE. Open bars, air-exposed group; solid bars, ozone-exposed group. Abbreviations: BALF, bronchoalveolar lavage fluid; NLF, nasal lavage fluid. The symbol * indicates that the ozone-exposed group was statistically different from the air-exposed group with $p < 0.05$.

The results of the *in vitro* part of this study indicate that the amount of biomarker formed is directly proportional to ozone dosage. The *in vivo* results suggest that NDA may be a useful biomarker for O₃ exposure if the amount of NDA in BALF and NLF from air-exposed rats can be reduced by inhibiting lipid peroxidation during sample preparation.

We would like to express our gratitude to Gary E. Hatch and Joel Norwood (Health Effects Research Laboratory, U.S. Environmental Protection Agency, Research Triangle Park, NC) for performing the animal exposures and collecting lavage samples.

(Research sponsored by the Office of Health and Environmental Research, U. S. Department of Energy, under Contract No. DE-AC04-76EV01013.)

**IV. CARCINOGENIC RESPONSES TO TOXICANTS
IN THE RESPIRATORY TRACT**

INFLUENCE OF PARTICLE-ASSOCIATED ORGANIC COMPOUNDS ON THE CARCINOGENICITY OF DIESEL EXHAUST

K. J. Nikula, M. B. Snipes, E. B. Barr, W. C. Griffith, R. F. Henderson, and J. L. Mauderly

This study examined the importance of diesel-soot-associated organic compounds in the pulmonary carcinogenicity of inhaled diesel exhaust (DE) in rats. Lung neoplastic responses were compared following chronic exposures to high concentrations of DE and to carbon black (CB), a particle that simulates the carbonaceous matrix of exhaust soot, but is essentially devoid of organic compounds. F344/N rats raised at the Institute were exposed 16 h/day, 5 days/wk for up to 24 mo to DE or CB at target particle concentrations of 2.5 or 6.5 mg/m³ or to air as controls. See Table 1 for the actual exposure concentrations, sacrifice schedule, and numbers of rats. Whole DE was generated by 1988 model General Motors 6.2 L engines burning D-2 control fuel meeting EPA certification standards and operated by a computer-dynamometer system on the U.S. Federal Test Procedure urban cycle. Fresh DE was diluted with clean air and routed to exposure chambers without delay or exposure to light. Cabot Elftex-12 CB was aerosolized by an air-jet method (Jet-O-Mizer) and diluted to final concentrations with clean air.

Table 1
Experimental Design

Exposure Group	Actual Mean Particle Concentration (mg/m ³)	No. Male	No. Female
Control	0	118	114
Low DE	2.4	114	114
High DE	6.4	115	115
Low CB	2.5	115	116
High CB	6.6	115	114

Interim sacrifices, three males/three females per group, after 3, 6, 12, 18, 23 mo.
Final sacrifice 6 wk after last exposure.

The particle size distributions of both DE soot and CB were bimodal around mean aerodynamic diameters of 0.1 and 2.0 µm, with a greater fraction of CB than DE in the larger mode. Because of this size difference, the rate of pulmonary deposition was expected to be higher for DE than CB. As expected, the lung burdens of particles, which increased progressively during exposure, were greater for DE than for CB (Fig. 1). During the later portion of the study, the lung burdens were similar for the low DE and the high CB rats. Similarly, the lung weights and inflammatory and cytotoxic responses detected by bronchoalveolar lavage were slightly greater for DE than for CB (data not presented). Exposure affected life span, particularly for male rats exposed to CB (Table 2). Lung pathology was evaluated for unscheduled deaths, interim sacrifices, and the final sacrifice. Non-neoplastic histologic lung lesions were similar in DE- and CB-exposed rats, although the incidence and severity of several lesions were slightly greater in the DE-exposed rats. The neoplastic response occurred late in life (Fig. 2). Multiple neoplasm phenotypes (adenomas, adenocarcinomas, and squamous cell carcinomas) were induced by both CB and DE exposure. For both exposure levels, there was no difference as determined by logistic regression in the prevalence of lung neoplasms between DE- and CB-exposed rats (Fig. 2). If exposure concentration is used as the dose term, CB and DE are equally carcinogenic under these exposure conditions. However, per unit of lung burden, CB was more carcinogenic than DE.

These results suggest that the high lung burden of carbonaceous particles is the principal cause for the increased prevalence of lung neoplasms in rats exposed to high concentrations of DE. The soot-associated, organic compounds do not appear to contribute significantly to the prevalence of neoplasms in this bioassay. Therefore, the results

of this study do not support the estimation of human lung cancer risk from rat data on the basis of the carcinogenicity of the particle-associated organic compounds. To the extent that this bioassay model might be predictive of a carcinogenic hazard for humans, the results raise the question of the need to consider fine carbonaceous particles as a special subclass of urban or occupational airborne particulate material.

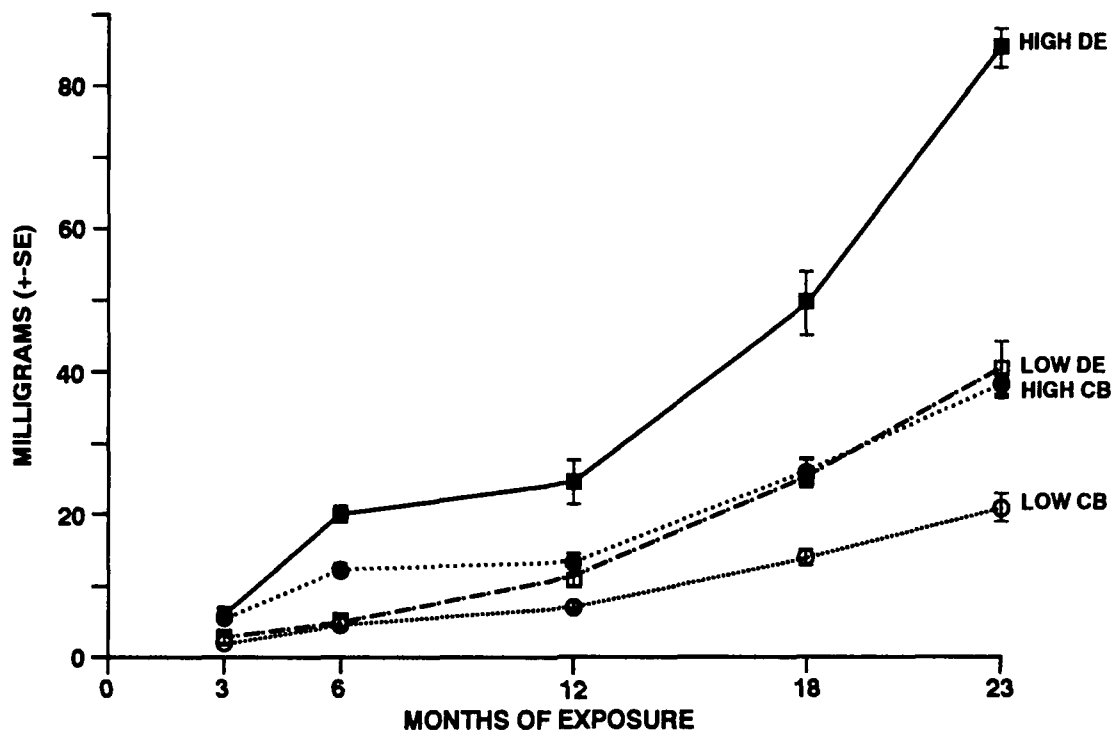


Figure 1. Lung burdens of particles in rats exposed to diesel exhaust (DE) or carbon black (CB). Accumulated lung burdens of particles were statistically higher after 18 and 23 mo in DE-exposed than in CB-exposed rats for each exposure concentration.

Table 2
Median Life Span in Days of Exposure

	Males			Females		
	Median	SE	Difference From Sham	Median	SE	Difference From Sham
Sham	639	0	-	696	11	-
Low CB	605	8	-34	707	9	+11
Low DE	649	10	+10	687	9	-9
High CB	599	6	-40	675	7	-21
High DE	624	9	-15	678	10	-18

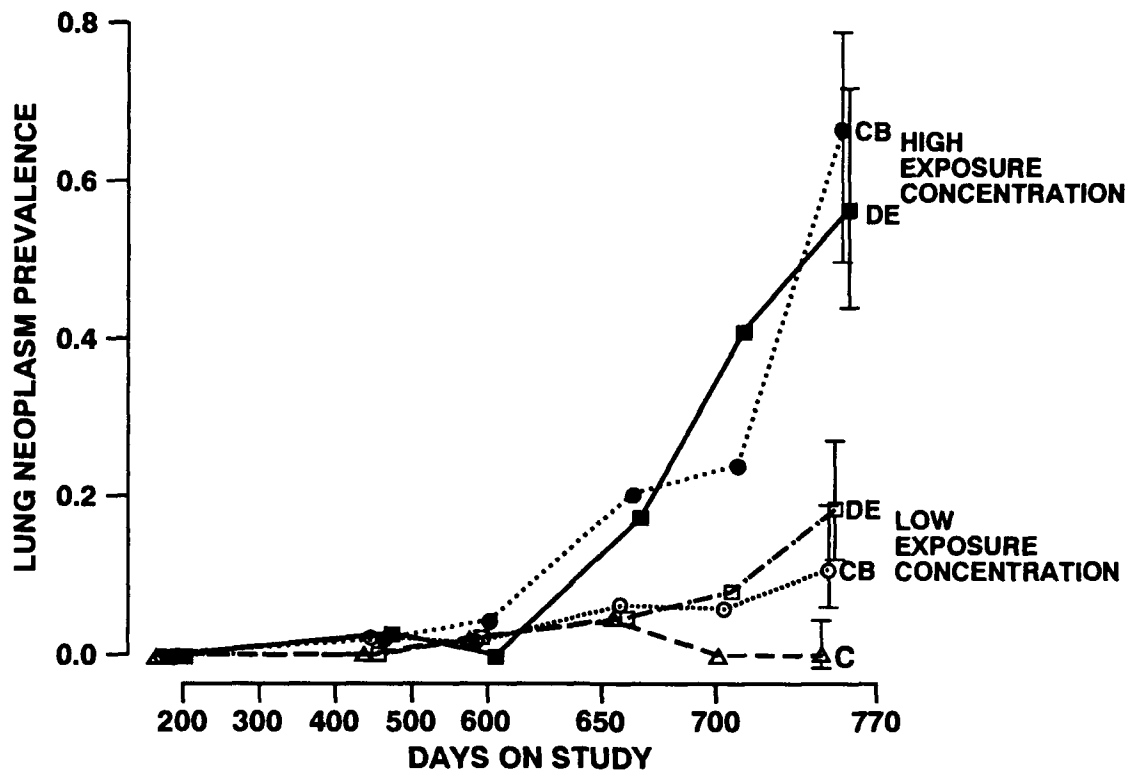


Figure 2. Prevalence of malignant and benign lung neoplasms in rats exposed to diesel exhaust (DE) or carbon black (CB). Most neoplasms occurred late in life. There is no statistical difference in the prevalence of lung neoplasms between DE- vs. CB-exposed rats for both exposure concentrations.

(Research sponsored by the Health Effects Institute under Funds-In-Agreement No. DE-FI04-88AL52257 with the U. S. Department of Energy, and by the Office of Health and Environmental Research, U. S. Department of Energy, under Contract No. DE-AC04-76EV01013.)

TWO-YEAR INHALATION STUDIES OF NICKEL SULFATE HEXAHYDRATE, NICKEL OXIDE, AND NICKEL SUBSULFIDE IN F344 RATS AND B6C3F₁ MICE

J. M. Benson, Y. S. Cheng, F. F. Hahn,
K. R. Maples, K. J. Nikula, C. H. Hobbs, and W. Eastin*

Two-year inhalation studies have been conducted to evaluate the toxic, including carcinogenic, effects of three nickel compounds, nickel oxide (NiO, CAS No. 1313-99-1, calcined at 1200°C), nickel sulfate hexahydrate (NiSO₄·6H₂O, CAS No. 10101-97-0, hereafter referred to as NiSO₄), and nickel subsulfide (Ni₃S₂, CAS No. 1205-72-2, alpha crystalline structure) in both sexes of F344/N rats and B6C3F₁ mice. Inhalation exposure of rats and mice to NiO (1.2-30 mg/m³), NiSO₄ (3.5-60 mg/m³), and Ni₃S₂ (0.6-10 mg/m³) 6 h/day, for 12 days (excluding weekends) resulted in a high incidence of mortality in mice exposed to 7.0 mg NiSO₄/m³ or greater, in rats exposed to 60 mg NiSO₄/m³, and in mice exposed to 10 mg Ni₃S₂/m³. Exposure of rats and mice to NiSO₄ and Ni₃S₂ at all aerosol concentrations and to NiO at the higher concentrations led to development of inflammation in the lung. In addition, rats exposed to the higher concentrations of Ni₃S₂ developed emphysema, while mice developed pulmonary fibrosis. Atrophy of the olfactory epithelium occurred in rats exposed to the three nickel compounds and in mice exposed to NiSO₄ and Ni₃S₂. Nickel sulfate appeared to be the most toxic of the compounds tested. The results of these studies have been summarized elsewhere (Dunnick, J. K. *et al.* *Toxicology* 50: 145, 1988; Benson, J. M. *et al.* *Fundam. Appl. Toxicol.* 9: 251, 1987; Benson, J. M. *et al.* *Fundam. Appl. Toxicol.* 10: 164, 1988).

Inhalation exposure of rats and mice to NiO (0.6-10 mg/m³), NiSO₄ (0.12-2.0 mg/m³), and Ni₃S₂ (0.15-2.5 mg/m³) 6 h/day, 5 days/wk for 13 wk resulted in no exposure-related mortality. Chronic active inflammation and alveolar macrophage hyperplasia in the lungs and lymphoid hyperplasia of the bronchial lymph nodes occurred in animals exposed to the three nickel compounds. Pulmonary fibrosis also developed in mice exposed to Ni₃S₂ and NiSO₄. Atrophy of the olfactory epithelium occurred in rats and mice exposed to NiSO₄ and Ni₃S₂. Equilibrium concentrations of nickel in the lungs of rats and mice were reached by 13 wk of NiSO₄ and Ni₃S₂ exposure. Equilibrium concentrations in lung were not reached by 13 wk in NiO-exposed animals. Nickel sulfate was the most toxic, and nickel oxide was the least toxic of the compounds tested. Results obtained in the 2- and 13-week studies were used to design 2-year inhalation studies on these 3 compounds (Dunnick, J. K. *et al.* *Fundam. Appl. Toxicol.* 12: 584, 1989; Benson, J. M. *et al.* *Inhal. Toxicol.* 2: 1, 1990).

The purpose of the 2-yr studies was to assess the long-term health effects of inhalation exposure to these compounds tested at occupationally relevant exposure concentrations. Results will be useful in determining the carcinogenic potential of inhaled nickel compounds and in assessing the relevance of current workplace exposure standards for these compounds.

Male and female F344/N rats and B6C3F₁ mice were exposed 6 h/day, 5 days/wk in mult tiered, whole-body inhalation exposure chambers. Exposure systems used have been previously described (Benson, J. M., 1987; Benson, J. M., 1988). Exposure concentrations used in these studies are summarized in Table 1. Higher aerosol concentrations were used for mice because they are less sensitive than rats to the inflammatory effects produced in lung by nickel compounds. Interim sacrifices were conducted after 28 and 65 wk of exposure, and all surviving animals were sacrificed following 104 wk of exposure. Endpoints being evaluated include concentrations of nickel in lungs and kidneys (NiSO₄ and Ni₃S₂-exposed animals only), hematological changes (65-wk sacrifice only) and gross and histopathological changes (all sacrifices).

As of August 1992, final reports detailing results from the NiO, Ni₃S₂, and NiSO₄·6H₂O studies were submitted to the National Toxicology Program.

*National Toxicology Program, Research Triangle Park, North Carolina

Table 1
 Aerosol Exposure Concentration Used in the
 Two-Year Nickel Compound Inhalation Studies

Compound	Aerosol Concentration (mg Compounds/m ³)	
	Rats	Mice
NiO	2.5	5.0
	1.25	2.5
	0.62	1.25
	0	0
NiSO ₄	0.5	1.0
	0.25	0.5
	0.12	0.25
	0	0
Ni ₃ S ₂	1.0	1.2
	0.15	0.6
	0	0

(Research sponsored by the National Institute of Environmental Health Sciences/National Toxicology Program under Interagency Agreement No. Y01-ES-30108 with the U.S. Department of Energy under Contract No. DE-AC04-76EV01013.)

EFFECTS OF INHALED $^{239}\text{PuO}_2$ AND CIGARETTE SMOKE IN F344 RATS

G. L. Finch, E. B. Barr, W. E. Bechtold, B. T. Chen, W. C. Griffith,
M. D. Hoover, J. L. Mauderly, C. E. Mitchell, and K. J. Nikula

Workers in the nuclear industries may be exposed to radioactive materials such as $^{239}\text{PuO}_2$, and thus be at risk for the induction of lung cancer. Of additional concern is the possibility that interactions between $^{239}\text{PuO}_2$ and other carcinogens may modify the risks of cancer induction. An important and common lung carcinogen is cigarette smoke; however, the impact cigarette smoking may have on lung cancer risk in individuals who also inhale $^{239}\text{PuO}_2$ is unknown. To better understand this relationship, we are studying the combined effects of inhaled $^{239}\text{PuO}_2$ and cigarette smoke on the induction of lung cancer in rats.

Our study is being conducted in male and female CDF®(F344)/CrIBR (Charles River Laboratories, Raleigh, NC) rats. Three individual blocks of approximately 700 rats each were required to place a total of 2198 rats on study (Table 1). Animals were received at 4 ± 1 wk of age, held in Hazleton H2000 chambers (Hazleton, Aberdeen, SD) for 2 wk, and assigned to one of six experimental groups (Table 1). Beginning at 6 wk of age, groups of rats were exposed by the whole-body mode to either filtered air or to mainstream cigarette smoke (generated from 1R3 research cigarettes, Tobacco Health Research Inst., Lexington, KY; exposed as described by Chen B. T. et al. *J. Aerosol Med.* 5(1): 19, 1992) for 6 h/day, 5 day/wk, for 6 wk. Target cigarette smoke exposure concentrations were either 100 or 250 mg/m³ total particulate matter (TPM), except for the first week when the animals were exposed to 50% of the full target concentration.

Table 1

Experimental Design for the Chronic Study of the Combined Effects of Exposure to Cigarette Smoke and $^{239}\text{PuO}_2$ on Lung Cancer in Rats

		Target $^{239}\text{PuO}_2$ ILB ^a		
		0 Bq	230 Bq	Total
Cigarette Smoke TPM	0 mg/m ³	Life: 232 ^b Sac: 130	Life: 232 Sac: 100	Life: 464 Sac: 230
	100 mg/m ³	Life: 348 Sac: 130	Life: 348 Sac: 100	Life: 696 Sac: 230
	250 mg/m ³	Life: 174 Sac: 130	Life: 174 Sac: 100	Life: 348 Sac: 230
Total:		Life: 754 Sac: 390	Life: 754 Sac: 300	Life: 1508 Sac: 690

^aILB = Initial lung burden.

^bNumber of rats included for either life-span (life) exposure and observation or for assignment to serial sacrifice (sac) groups.

At 12 wk of age, the animals were removed from the chambers and either sham-exposed or exposed nose-only to aerosols of $^{239}\text{PuO}_2$ for 25 min (nominal mean values of 1.0 μm AMAD, 1.6 σ_{g} , 960 Bq/L air concentration) to achieve mean initial lung burdens (ILBs) of approximately 400 Bq. The animals were whole-body counted weekly for 6 wk for the gamma emitter ^{169}Yb which was fused into the $^{239}\text{PuO}_2$ particles. Single-component

negative exponential functions were fitted to the decay-corrected data and evaluated at the time of exposure for each animal to provide an estimate of the ILB and clearance half-time for $^{239}\text{PuO}_2$ over the 6-wk period. At 13 wk of age, the rats were returned to the H2000 chambers for continued cigarette smoke exposures that are scheduled to last for 30 mo, or until survival drops to only 10% of the rats in any one group.

At monthly intervals, animals are being weighed and observed for clinical abnormalities. Moribund animals are euthanized, and a full necropsy is performed for all dead animals. Approximately two-thirds of the animals are being held for chronic exposure (or as controls). The remaining one-third of the rats are sacrificed at various times. Animals from each exposure group from each block are included in the sacrifice schedule. The purposes of the sacrifices include (1) the collection of lung and lesion tissue for histopathological and morphometric analysis, (2) the quantitation of epithelial cell proliferation in selected rats using a 5-bromodeoxyuridine labeling technique, (3) the radiochemical analysis of ^{239}Pu for dosimetric evaluations, (4) the retention of frozen lung and blood samples for future molecular biological and biomarker studies, (5) the measurement of bone mass, and calcium and cadmium concentrations in lumbar vertebrae and femurs (see this report, p. 178), and (6) the assessment of immunocompetence of lymphocytes obtained from spleens (see this report, p. 176).

Additional in-life endpoints are being examined in selected groups of rats. These endpoints include (1) the periodic assessment of respiratory function, (2) the quantitation of clearance of inert radiolabeled ^{85}Sr -FAP tracer particles administered after 3 and 18 mo of smoke exposure (this report, p. 71), and (3) the measurement of nicotine and cotinine in urine at various times after initiation of exposure.

As of September 30, 1992, animals from Blocks A, B, and C have been exposed to cigarette smoke for 12, 8, and 5 mo, respectively. Mean cigarette smoke concentrations are within 5% of the targeted levels for all chambers. The chemical composition of the smoke exposure atmospheres are consistent with our previous observations (Chen, B. T. *et al.* *Inhal. Toxicol.* 1: 331, 1989).

To date, cigarette smoke-exposed animals have gained less weight compared to chamber control rats. After 11 mo of exposing rats in Block A to 100 and 250 mg/m³ TPM of smoke, the male rats weighed 85 and 76% as much as controls, and the female rats weighed 83 and 82% as much as controls, respectively.

No other clinical manifestations or excess mortality have been associated with cigarette smoke and/or $^{239}\text{PuO}_2$ exposure levels to date. The ILBs of $^{239}\text{PuO}_2$ achieved were somewhat greater than expected. Initial $^{239}\text{PuO}_2$ ILBs and clearance rates were significantly lower in the Block A smoke-exposed rats compared with controls, as determined by an analysis of variance.

Gray mottling of the lungs and hypertrophy of bronchial lymph nodes have been observed at necropsy in rats exposed to cigarette smoke. The incidence and severity of these lesions appear to correlate with increasing exposure concentration and duration. Preliminary, qualitative, histopathological examination of a small number of sacrificed rats exposed to cigarette smoke revealed alveolar macrophage pigmentation and hyperplasia, chronic-active inflammation, alveolar epithelial hyperplasia, interstitial fibrosis, and bronchial mucous cell hyperplasia in the lungs. The severity of these lesions appeared to be related to exposure time and concentration. Nasal lesions observed in smoke-exposed rats include inflammation, mucous cell hyperplasia, and squamous metaplasia affecting primarily the respiratory epithelium, and necrosis of the olfactory epithelium with concomitant loss of Bowman's glands. To date, we have not attempted to make correlations between lung or nasal lesions and exposure to $^{239}\text{PuO}_2$.

This study is in progress. At its conclusion, we anticipate that significant new information will be generated regarding (1) the induction of cigarette smoke-induced lung cancer in rats, (2) the potential for interaction between cigarette smoke and $^{239}\text{PuO}_2$ exposure in the induction of lung cancer, and (3) the mechanisms by which these effects occur.

(Research supported by the Assistant Secretary for Defense Programs, U. S. Department of Energy, under Contract No. DE-AC04-76EV01013.)

COMBINED EXPOSURE OF F344 RATS TO BERYLLIUM METAL AND $^{239}\text{PuO}_2$ AEROSOLS

G. L. Finch, F. F. Hahn, W. W. Carlton, A. H. Rebar*,
M. D. Hoover, W. C. Griffith, J. A. Mewhinney**, and R. G. Cuddihy*

Many workers in nuclear weapons industries have the potential for inhalation exposures to plutonium (Pu) and other agents, such as beryllium (Be) metal. Inhaled Pu deposited in the lung delivers high-LET alpha particle radiation and is known to induce pulmonary cancer in experimental animals (BEIR-IV, 1988). Although the epidemiological evidence implicating beryllium in the induction of human lung cancer is weak, various studies in experimental animals have demonstrated the pulmonary carcinogenicity of Be, and it is currently classified as a suspect human carcinogen (U.S. EPA/600/8-84/026F, 1987). To investigate the potential interactions between these agents in the production of lung tumors, we are evaluating the results obtained in a life-span study of rats exposed by inhalation to particles of plutonium dioxide ($^{239}\text{PuO}_2$), Be metal, or these agents in combination.

A total of 2856 rats (F344/N; both male and female; 12 ± 1 wk old at exposure) reared at this Institute were exposed nose-only in eight groups of 354 or 360 animals using a block design, to complete the experimental design shown in Table 1. Rats were exposed in groups of 60. The rats first received $^{239}\text{PuO}_2$ ($0.7 \mu\text{m}$ AMAD, $1.7 \sigma_g$, 5-25 min exposure, 630 Bq/L), followed after 30 min by exposure to Be metal ($1.4 \mu\text{m}$ MMAD, $1.9 \sigma_g$, 8-50 min exposure, 0.2 - 1.2 mg/L). As shown in Table 1, rats were exposed to achieve one of two lung burdens of $^{239}\text{PuO}_2$, and/or one of three lung burdens of Be metal. The $^{239}\text{PuO}_2$ particles were labeled with ^{169}Yb (< 3% by mass) to permit external radioactivity counting and estimation of the lung burden of Pu for each rat.

Table 1

Experimental Design for the Study of the Combined Effects
of $^{239}\text{PuO}_2$ and Be Metal Inhaled by Rats

Desired ILBs ^a of Be Metal	Desired ILBs of $^{239}\text{PuO}_2$		
	0 Bq Pu	56 Bq Pu	170 Bq Pu
0 μg Be	208 ^b	240	240
50 μg Be	240	240	240
150 μg Be	240	240	240
450 μg Be	240	240	240

^aILB = Initial lung burden.

^bNumber of rats per group. Equal numbers of males and females.

Animals were whole-body counted periodically after exposure for determination of $^{239}\text{PuO}_2$ initial lung burden (ILB). For each block of rats entered into the study, we serially sacrificed rats from one exposure group to measure clearance and translocation of the inhaled materials. Additional rats were sacrificed at later times (580 to 860 days after exposure) for quantitation of lung tumor formation rates. Rats not assigned to sacrifice groups were held for their life span. At death, a complete necropsy was performed, and lungs, other selected tissues, and all lesions were fixed in formalin for histological examination. The lungs of all rats in the study are being analyzed for content of Pu and/or Be. Analyses completed thus far indicate that the ILBs of Be metal and $^{239}\text{PuO}_2$ were within 25% of target (data not presented).

*Purdue University, Lafayette, Indiana

**Currently at Waste Isolation Pilot Plant, U. S. Department of Energy, Carlsbad, New Mexico

Exposures were conducted over a 15-mo period from October 1987 to January 1989. All rats involved in the study were dead as of March 1991. Median survival times of rats in all groups were estimated using Kaplan-Meier survival curves. We found that (1) female rats had a lower mortality rate than male rats; (2) for a given $^{239}\text{PuO}_2$ exposure group, increased levels of Be metal increased the mortality rate, and this effect was greater for females than for males; (3) for a given Be metal exposure group, increased levels of $^{239}\text{PuO}_2$ only marginally increased the mortality rate; and (4) a significant interaction between Be metal and $^{239}\text{PuO}_2$ was present, particularly for the 170 Bq ILB group of $^{239}\text{PuO}_2$, as evidenced by a greater mortality rate for the combined exposure groups than for groups exposed to the individual agents alone (data presented in 1990-91 Annual Report, p. 99).

A significant reduction of ^{239}Pu clearance following Be exposure was observed in this study. These data have been previously reported (1989-90 Annual Report, p. 125).

Histological evaluation of the lungs of the rats is in progress. As of September 30, 1992, lung tissues from 623 rats in the study have been examined. The incidence of lung neoplasms is shown in Table 2; substantial numbers of benign lung lesions have also been observed, but are not reported here. The most prevalent neoplasm observed thus far is the adenocarcinoma having alveolar, papillary, or tubular patterns. Other tumor types observed include adenosquamous carcinomas and squamous cell carcinomas (incidence data not presented). Additional findings at this point are that (1) a substantial incidence of lung tumors induced by Be metal is observed in all exposed groups; (2) the incidences of tumors induced by $^{239}\text{PuO}_2$ in the absence of Be metal is approximately as expected; (3) there are no clear trends evident that indicate a difference in response between males and females; and (4) a number of the Be-metal-exposed rats have multiple tumors.

Table 2

Number of Rats in the Study Having One or More
Malignant Lung Tumors/Number Examined^a

Desired ILBs of Be Metal	Desired ILBs of $^{239}\text{PuO}_2$		
	0 Bq Pu	56 Bq Pu	170 Bq Pu
0 μg Be	M: ND ^b F: ND	M: 5/30 F: 0/30	M: 0/14 F: 2/13
50 μg Be	M: 13/30 F: 26/30	M: 6/14 F: 10/14	M: 28/30 F: 26/30
150 μg Be	M: 12/29 F: 21/29	M: 23/30 F: 26/30	M: 27/30 F: 24/29
450 μg Be	M: 6/11 F: 12/17	M: 13/16 F: 18/24	M: 19/24 F: ND

^aIncidence figure listed separately for males and females. Excludes serial sacrifice rats and those dying of acute beryllium toxicity (for the 450 μg ILB group). The incidence of lung tumors in F344/N rats is about $\leq 1\%$. See text for tumor types. These are simply the number of rats having tumors examined to date. They may not affect the incidence when all animals at risk are examined.

^bND = Not yet determined.

The ILBs of Be metal and $^{239}\text{PuO}_2$ used in this study were selected to result in predicted specific lung tumor incidences of 5 and 15% for the 56 and 170 Bq ILBs of $^{239}\text{PuO}_2$, respectively, and of 5, 15, and 45% for the 50, 150, and 450 μg ILBs of Be metal. These estimates for Be metal were based on extrapolations from a limited data base in the literature (Sanders, C. L. *et al. Health Phys.* 35: 193, 1978; Groth, D. H. *Environ.*

Res. 21: 84, 1980; Nolibe, D. et al. Commissariat A L'Energie Atomique 1984 Annual Report, 1984). Our results to date reveal significantly higher tumor incidences than expected. These high tumor incidences are expected to complicate an analysis of the carcinogenic interaction between Be metal and $^{239}\text{PuO}_2$ in rats, because such interactions are best analyzed when lung tumor incidences are relatively low. Although final analyses of these data must await the completion of histologic evaluations of the lungs of exposed rats, preliminary data suggest the need for combined studies of the carcinogenicity of inhaled $^{239}\text{PuO}_2$ and Be metal at lower ILBs of Be.

(Research supported by the Assistant Secretary for Defense Programs, U. S. Department of Energy, under Contract No. DE-AC04-76EV01013.)

EFFECTS OF COMBINED EXPOSURE OF F344 RATS TO $^{239}\text{PuO}_2$ AND WHOLE-BODY X-RADIATION

*D. L. Lundgren, F. F. Hahn, W. C. Griffith,
W. W. Carlton*, M. D. Hoover, and B. B. Boecker*

Many workers in the nuclear weapons industries have a significant potential for exposure to both inhaled plutonium and external whole-body radiation. Inhaled plutonium delivers high-LET (linear energy transfer) alpha radiation, primarily to the pulmonary tissues, where it may add to, or multiply, the risk from low-LET external irradiation. The individual effects of different types of radiation exposures that occur in nuclear weapons industries have been studied in laboratory animals. These have included external exposure to high- and low-LET radiation or internal exposure to a variety of radionuclides irradiating specific organ systems with high- or low-LET radiation.

The purpose of this research is to characterize the effects of combined exposure of rats to both external x-radiation and internally deposited plutonium, as well as to each agent alone. The animals are being observed to determine how specific exposure levels and combinations of radiation may interact to modify cancer risk. As part of the design of these studies, data based upon observations of large populations of laboratory animals are being collected on cancer incidences as a function of age for cancers that occur spontaneously or as a result of exposure to radiation. This information will aid in determining the appropriateness of different mathematical cancer risk models. A model for the development of lung tumors, illustrating the various rates to be taken into account in predicting the occurrence of lung tumors, was published in the 1986-87 Annual Report, p. 318. Our primary interests in this model are the rates at which animals develop lung tumors and whether the combined radiations alter these rates.

The details of the experimental design for this study were presented in the 1986-87 Annual Report, p. 318. Briefly, a total of 3199 (1592 male and 1607 female) 11- to 13-wk old F344/N rats reared at this Institute are being used. A block experimental design was used to enter rats into the study. Rats were randomized by litter for assignment to dose groups within each block so that biological variability would be distributed throughout each dose group. At death, all rats are necropsied, and major organs and all lesions are fixed in 10% neutral buffered formalin for histologic examination.

For this study, radiation doses to the lungs from inhaled $^{239}\text{PuO}_2$ and whole-body x-radiation that would result in 5% and 15% incidences of lung tumors were estimated from results of other studies of $^{239}\text{PuO}_2$ in rats and from previously published studies of the effects of whole-body x-radiation. Details of the methods used for the inhalation exposures of rats to $^{239}\text{PuO}_2$ and their subsequent whole-body x-radiation have been described (1987-88 Annual Report, p. 251). Several interim sacrifices are being conducted during the course of this study. Because the combined radiation may alter both the lung tumor incidence and the death rates, it is necessary to include interim sacrifices to determine the rates at which animals are developing lung tumors (McKnight, B. and J. Crowley. *J. Am. Stat. Assoc.* 79: 639, 1984). Data to determine the clearance patterns of the inhaled ^{239}Pu are being obtained from tissues collected during necropsies of serially sacrificed animals and animals that die spontaneously.

All exposures have been completed. The mean initial lung burdens achieved in each experimental group and the corresponding potential average alpha doses to lung have been summarized (1990-91 Annual Report, p. 94). The initial lung burdens and radiation doses to the lungs were relatively consistent within each ^{239}Pu exposure level, and were within the desired ranges.

The current status of the survival of these rats is summarized in Table 1. No significant life shortening has occurred among the rats exposed only to $^{239}\text{PuO}_2$ compared with the control rats. Also, within each X-ray exposure group, there was no life shortening related to the $^{239}\text{PuO}_2$ exposures. However, a dose-response relationship for life shortening has been observed among the rats exposed to whole-body x-radiation. Among the rats that received a dose of 3.84 Gy of X rays, the median survival times were decreased by 9 to 21% compared

*Purdue University, Lafayette, Indiana

with the respective sham-X-ray- and $^{239}\text{PuO}_2$ -exposed groups. Among those exposed to 11.5 Gy of X rays, the median survival times were decreased by 26 to 37% compared with the respective sham-X-ray- and $^{239}\text{PuO}_2$ -exposed groups. The survival times of the female rats were decreased more than that of the males exposed to X rays.

Table 1

Survival of Rats in the Study of Combined Exposure to Inhaled $^{239}\text{PuO}_2$ and Whole-Body X-Radiation
(as of September 30, 1992)

Experimental Group Numbers	Exposure		Number Exposed		Percentage Alive		Median Survival Time (MST) (days \pm SE)	
	^{239}Pu ILB ^a	X Ray ^b	Males	Females	Males	Females	Males	Females
I	Sham	Sham	160	160	0.6	4.4	617 \pm 12	719 \pm 13
II	56 Bq	Sham	192	191	1.6	5.8	620 \pm 10	752 \pm 13
III	170 Bq	Sham	182	183	0.6	4.4	607 \pm 11	749 \pm 14
IV	Sham	3.84 Gy ^c	158	156	0.6	1.3	557 \pm 10	584 \pm 10
V	56 Bq	3.84 Gy	192	192	0	2.1	565 \pm 10	620 \pm 7
VI	170 Bq	3.84 Gy	188	191	0	1.0	549 \pm 7	593 \pm 13
VII	Sham	11.5 Gy	160	160	0	0	431 \pm 11	485 \pm 13
VIII	56 Bq	11.5 Gy	191	191	0	0	451 \pm 9	473 \pm 14
IX	170 Bq	11.5 Gy	169	183	0	0	449 \pm 10	492 \pm 12
Totals			1592	1607	0.4	2.1	_d	_d

^aILB = Initial lung burden.

^bX-ray exposure divided into two split doses at 30 and 60 days after exposure to $^{239}\text{PuO}_2$.

^cGy = 0.0096 x R.

^dThis quantity was not determined because it is not meaningful.

During the past year, radiochemical analyses of lung samples were completed for 1739 rats exposed to $^{239}\text{PuO}_2$ that have died. These data were used in determining the retention of the initial lung burdens of ^{239}Pu in the rats (Table 2). A preliminary evaluation of these data indicates that there was a dose-response relationship between the clearance of ^{239}Pu from the lungs and the whole-body X-ray dose. The percentage of the initial lung burden in the long-term component of retention increased with increasing X-ray dose as did the clearance half-time of the long-term component. The survival times of the rats analyzed for ^{239}Pu retention did not appear to be a factor in the increased retention (Table 2). When the retention data were truncated at 659 days (time equal to the shortest long-term data) for all groups of rats, the effects of X-ray exposure remained significant (generalized F test; $p < 0.05$). These apparent differences and their significance will be evaluated further as additional data become available.

Histological evaluations have been completed on 2125 (66%) of the 3199 rats entered into this study. The crude incidence of primary lung tumors in the rats that died spontaneously is summarized in Table 3. Fourteen lung tumors (not included in this preliminary tabulation) were also found in 331 of the rats that were serially sacrificed late-in-life to determine tumor prevalence. From these data, it appears that there has been an antagonistic response between the whole-body exposure to X rays and the exposure by inhalation to $^{239}\text{PuO}_2$. Because of the effects of the X-ray exposures on the survival of the rats in this study, care must be used in analyzing the combined effects of inhaled $^{239}\text{PuO}_2$ and subsequent whole-body x-radiation. Additional histopathological evaluations of tissues from rats in this study that have died and analyses of the data are in progress. The final analyses of these data must await the completion of the histopathological evaluations of all rats this study.

Table 2

Pulmonary Retention of ^{239}Pu in Rats Exposed to Whole-Body X-Radiation After Exposure by Inhalation to Aerosols of $^{239}\text{PuO}_2$

Experimental Group ^b	Retention Parameters ^a				Maximum Survival Times (days) of Rats Analyzed for ^{239}Pu Retention
	100-A (%)	T ₁ (days)	A (%)	T ₂ (days)	
II	88	60	12	630	828
III	88	37	12	680	829
V	82	50	18	480	828
VI	84	40	16	450	827
VIII	80	45	20	410	659
IX	81	42	19	410	660

^aRetention described by

$$Y(t) = (100-A)e^{-0.693t/T_2} + Ae^{-0.693t/T_2},$$

where Y(t) is the pulmonary retention of ^{239}Pu expressed as a percentage of the initial lung burden.

^bSee Table 1 for definitions of groups.

Table 3

Crude Incidences of Lung Tumors (Adenomas and Carcinomas) in Rats Exposed by Inhalation to $^{239}\text{PuO}_2$ and Whole-Body X-Radiation and Held for Their Life Span

X-Ray Dose ^b	Desired ^{239}Pu ILB ^a Group and Dose (Gy) to Lungs		
	Sham	ILB = 56 Bq Dose = <0.75 Gy	ILB = 170 Bq Dose = ≥ 0.75 Gy
Sham	1/232 ^c (0.43%) ^d	9/237 (3.8%)	25/272 (9.2%)
3.84 Gy	16/221 (7.2%)	15/224 (6.7%)	29/229 (12.7%)
11.5 Gy	24/238 (10.8%)	26/240 (10.8%)	27/231 (11.7%)

^aILB = Initial lung burden.

^bGy = 0.0096 x R.

^cNumber of rats with lung tumors per number examined.

^d() = Percentage of rats examined having lung tumors.

(Research sponsored by the Assistant Secretary for Defense Programs, U. S. Department of Energy, under Contract No. DE-AC04-76EV01013.)

EFFECTS OF COMBINED EXPOSURE OF F344 RATS TO INHALED $^{239}\text{PuO}_2$ AND A CHEMICAL CARCINOGEN (NNK)

D. L. Lundgren, S. A. Belinsky, K. J. Nikula, W. C. Griffith, and M. D. Hoover

Workers in the nuclear weapons facilities have a significant potential to be exposed to radiation from external sources or from internally deposited radionuclides such as ^{239}Pu and chemical carcinogens. Although the carcinogenic effects of inhaled ^{239}Pu and many chemicals have been studied individually, very little information is available on their combined effects (Fry, R. J. M. and R. L. Ullrich. In *Radiation Carcinogenesis*, Elsevier, New York, p. 437, 1986). One chemical carcinogen that workers could be exposed to is the tobacco-specific nitrosamine 4-(N-methyl-N-nitrosamino)-1-(3-pyridyl)-1-butanone (NNK), a product of the curing and pyrolysis of nicotine in tobacco smoke (Hoffman, D. and S. S. Hecht. *Cancer Res.* 45: 935, 1985). NNK is rather organ-specific in that, regardless of the route of administration, tumors occur in the lungs of rats treated with the carcinogen (Rivenson, D. *et al.* *Cancer Res.* 48: 6912, 1988). Tumors occur to a lesser extent in the liver, nasal passages, and pancreas.

The purpose of this study is to characterize the lifetime effects of combined exposure of rats to NNK and internally deposited plutonium, as well as to these agents alone. The rats are being observed to determine how specific doses of NNK and internally deposited $^{239}\text{PuO}_2$ may interact to increase cancer risk. Data are being collected on cancer incidences as a function of age for cancers that occur spontaneously and as a result of exposure to alpha radiation of the lung with or without exposure to NNK. This information will aid in determining the appropriateness of different mathematical cancer risk models based upon observations of large populations of laboratory animals. A model for the development of lung tumors, illustrating the various rates to be taken into account in predicting the occurrence of lung tumors, has been previously presented (1986-87 Annual Report, p. 318). Our primary interest in this model is the rate at which the rats develop lung tumors and whether the combined exposure to radiation and a chemical carcinogen alters these rates.

The experimental design for this study is summarized in Table 1. Briefly, a total of 740 male 4 ± 1 -wk-old CDF®(F344)/CrIBR rats (Charles River Laboratories, Kingston, NY) are being used in the study. A block experimental design (Table 1) is being used to enter one-half of the rats at a time into the study in each of two blocks. Rats are being randomized by weight for assignment to dose groups within each block. At death, all rats are necropsied, and major organs and all lesions for histological examination are fixed in 4% buffered paraformaldehyde for histologic examination.

For this study, the alpha radiation dose to the lungs from inhaled $^{239}\text{PuO}_2$ expected to result in a 15% incidence of lung tumors was estimated from results of other studies of $^{239}\text{PuO}_2$ in rats completed at this Institute. The methods used for the inhalation exposures of rats to ^{169}Yb -labeled $^{239}\text{PuO}_2$ have been described (1987-88 Annual Report, p. 245). Doses of NNK, dissolved in physiological saline, sufficient to result in a 15%, 50%, or 90% incidence of lung tumors when given by subcutaneous injection three times per week for 20 wk were derived from published data (Belinsky, S. A. *et al.* *Cancer Res.* 50: 3772, 1990). The NNK injections began when the rats were 6 wk of age, and $^{239}\text{PuO}_2$ exposures occurred when the rats were 12 wk of age. NNK injections were suspended during the week of exposures to $^{239}\text{PuO}_2$.

Several interim sacrifices are being conducted during the course of this study. Because the exposure to the combination of $^{239}\text{PuO}_2$ and NNK may alter the lung tumor incidences and/or death rates, it is necessary to include interim sacrifices to determine the rates at which animals develop lung tumors (1986-87 Annual Report, p. 318; McKnight, B. and J. Crowley. *Am. Stat. Assoc.* 79: 639, 1984). Rats are also being sacrificed to determine the clearance patterns of the inhaled ^{239}Pu . Additional data on ^{239}Pu clearance are obtained from necropsies of animals that die spontaneously.

As of September 30, 1992, the first block of rats had received 50 of the scheduled 60 subcutaneous injections of NNK. These rats had also been exposed by inhalation to aerosols of $^{239}\text{PuO}_2$ 6 wk after the initiation of the NNK injections. The initial lung burdens of ^{239}Pu are summarized in Table 2. The early clearance half-times of the inhaled ^{239}Pu , as determined from the whole-body counting of the ^{169}Yb label for the ^{239}Pu , was

Table 1

**Experimental Design to Determine the Combined Effects of Exposure
to a Chemical Carcinogen (NNK^a) and Exposure by Inhalation
to Aerosols of ²³⁹PuO₂ in Male F344 Rats**

NNK Dose per Treatment ^b	Desired ²³⁹ Pu ILB and Expected Doses to the Lungs		
	Sham Exposed 0 Gy	300 Bq 1.0 Gy	Numbers of Rats
Sham Exposed ^c	100 ^d	140 ^e	240
0.3 mg/kg	110	150 ^e	260
1.0 mg/kg	80	120 ^e	200
50 mg/kg ^f	<u>40</u>	<u>0</u>	<u>40</u>
Numbers of Rats	330	410	Total = 740

^aNNK = 4-(N-methyl-N-nitrosamino)-1-(3-pyridyl)-1-butanone.

^bDose of NNK in saline to be given by subcutaneous injection 3 times/wk for 20 wk.

^cSham NNK-exposed rats to be injected with saline only.

^dNumber of rats in each cell of the matrix.

^eFour rats from each group exposed to ²³⁹PuO₂ will be serially sacrificed at eight time points between days 8 and 450 after exposure to determine ²³⁹Pu retention.

^fRats in the 50 mg/kg group are dedicated to molecular biological studies of lung, nasal, and other tumors for comparison with the findings in rats at lower doses of NNK with and without exposure to ²³⁹Pu.

Table 2

Initial Lung Burdens (ILB) of ²³⁹Pu in Rats Exposed by Inhalation to Aerosols of ²³⁹PuO₂ With and Without Exposure to NNK

NNK Treatment	²³⁹ Pu ILB and Early Clearance Half-times	
	ILB (Bq ± SD)	Clearance Half-times in Days (± SD) ^a
Sham	510 ± 70	33 ± 4
0.3 mg/kg	500 ± 71	38 ± 9 ^b
1.0 mg/kg	480 ± 77	33 ± 7

^aBased on the whole-body counting of the ¹⁶⁹Yb label for the ²³⁹Pu corrected for the physical decay of the ¹⁶⁹Yb.

^bClearance half-times significantly different (Student's *t* test; *p* < 0.05) from that in the sham NNK-exposed rats and those exposed to 1.0 mg/kg of NNK.

significantly slower (Student's *t* test; $p < 0.05$) in the group treated with 0.3 mg kg^{-1} of NNK than in the controls or the group treated with 1.0 mg kg^{-1} of NNK (Table 2). Because this difference was not dose-related, there is no obvious explanation for this observation. Once the radiochemical analyses of lung tissue for ^{239}Pu has been completed, we will have a clearer understanding of the effects of NNK treatment on ^{239}Pu clearance. Four rats per group exposed to ^{239}Pu have been sacrificed on days 8, 16, 32, and 64 after exposure to obtain more detailed information on the clearance of ^{239}Pu for dosimetry purposes. Other rats are scheduled to be sacrificed for dosimetry purposes on days 128, 256, 360, and 450 after exposure to ^{239}Pu . The only effect of the NNK injections observed to date has been the slower weight gains in the rats injected with 50 mg/kg NNK (Fig. 1). The injections of the lower doses of NNK and exposure to $^{239}\text{PuO}_2$ have not affected body weight gain.

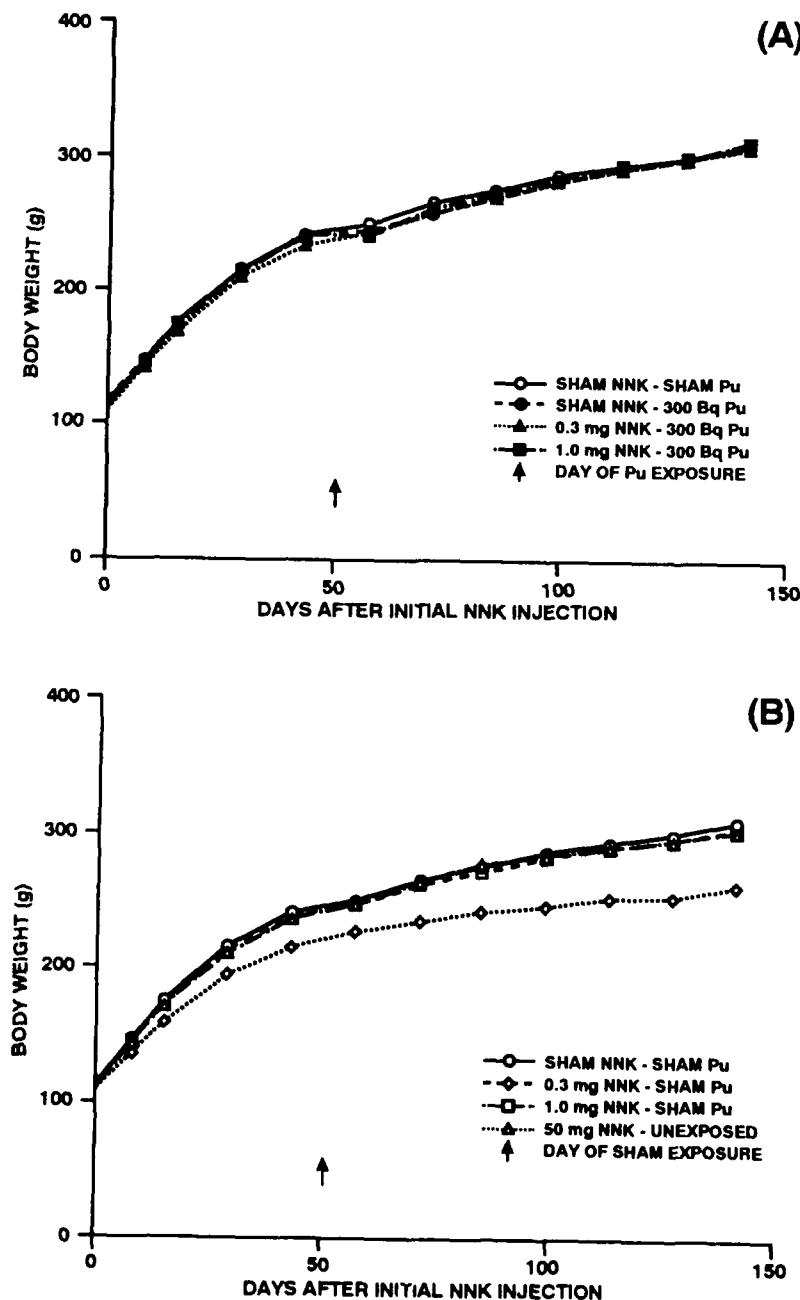


Figure 1. Body weights of male rats treated with NNK by subcutaneous injection beginning at 6 wk of age with (A) and without (B) exposure by inhalation to aerosols of $^{239}\text{PuO}_2$ when 12 wk of age.

(Research sponsored by the Assistant Secretary for Defense Programs, U. S. Department of Energy, under Contract No. DE-AC04-76EV01013.)

EFFECTS OF THORACIC AND WHOLE-BODY EXPOSURE OF F344 RATS TO X RAYS

D. L. Lundgren, F. F. Hahn, W. C. Griffith, and B. B. Boecker

The risk of radiation-induced lung cancer has been determined based on data from groups of people exposed to external X rays, radiation from atomic weapons explosions, or radon and its progeny. The studies described there will provide data that, with the results from other studies, can be used to develop an array of information for evaluating lung cancer risks for people exposed by inhalation to beta- or alpha-emitting particles (1982-83 Annual Report, p. 363). Data from numerous studies of laboratory animals have been reviewed for use in estimating lung cancer risk factors for people (Cuddihy, R. G. In *Proceedings of the 17th Annual Meeting of the National Council on Radiation Protection and Measurements*, Washington, DC, p. 133, 1982). However, some of the studies may have resulted in an underestimate of risk, because the relatively high radiation doses used resulted in life shortening and, theoretically, a reduction in tumor yield. It has been concluded that only studies which include larger groups of animals than previously used can address some of the questions on the dose-response relationships of inhaled radionuclides at relatively low doses (McClellan, R. O. *Health Phys.* 55: 279, 1988).

Based on previous results (1983-84 Annual Report, p. 251), we proposed to expose laboratory rats to relatively low, non-life-shortening doses of X rays or inhaled beta-emitting radionuclides as an experimental approach to estimating the risk of lung cancer in people. Two types of studies to determine the upper and lower limits of lung cancer risk in rats were outlined. One study involved fractionated x-irradiation of the thorax in one group and the single or fractionated exposure of the whole-body of two other groups of rats. The second study involved exposing the lung to relatively low levels of beta irradiation from inhaled, relatively insoluble $^{144}\text{CeO}_2$ (1989-90 Annual Report, p. 119). This report summarizes the status of the X-ray studies. When completed, these results will be compared with those from a study conducted at Battelle Pacific Northwest Laboratory (Sanders, C. L. et al. *Health Phys.* 55: 455, 1988), of the effects of relatively low, alpha-radiation doses to the lungs of rats exposed by inhalation to aerosols of $^{239}\text{PuO}_2$. These data will, in-turn, be compared with other studies on the effects of radionuclides inhaled in relatively insoluble forms, especially those involving relatively low doses to the lungs and with data on the effects of partial or whole-body X- or gamma-radiation.

The experimental design for this work was reported previously (1986-87 Annual Report, p. 313). A total of 3871 (1933 male and 1938 female) 12-wk old, laboratory-reared, specific pathogen-free F344/N rats have been used. Briefly, groups of rats were exposed either to fractionated doses of X rays to the thorax or to the whole body, on 10 successive workdays (M-F), or as a single, whole-body exposure (Table 1). The rats were entered into this study in 12 blocks and randomly assigned to experimental groups by litter to randomize characteristics of a litter. At death, all rats were necropsied; major organs and all other tissues with lesions were fixed in 10% neutral buffered formalin for histologic examination.

A Picker Vanguard X-ray therapy machine (Picker X-Ray Corp., Cleveland, OH) was used to irradiate the rats. This unit was operated at 280 kVp at 18 mA, with 1 mm Al and 0.5 mm Cu filters, resulting in an equivalent energy of 135 keV. The exposure rate was about 0.221 Gy (23 R) min^{-1} at 1 meter. The rats were placed on a turntable that rotates at two revolutions per minute during the exposures. Exposures from the X-ray machine were monitored with a Victoreen R-meter and LiF thermoluminescent dosimeters (Eberline, Albuquerque, NM). Plastic boxes covered with 6.4 mm Pb were constructed so that the bodies of the rats, restrained in standard plastic exposure tubes, were shielded, while the thorax was exposed through an opening in the Pb shield. The exposure times ranged from approximately 1.5 to 26 min per exposure, depending on the exposure required.

All rats in this study were exposed prior to 1992. Their status as of September 30, 1992, is summarized in Table 1. To date, 3332 (86%) of the 3871 rats entered into this study have died. Survival of the male rats continued to be significantly less than that of the female rats (Table 1). The cumulative survival rates in each group is similar to that previously presented (1990-91 Annual Report, p. 89). Briefly, significant life-shortening (Mantel-Cox statistic; $p < 0.05$) occurred among the male rats exposed to the highest level of fractionated thoracic irradiation and among those receiving single and fractionated whole-body x-irradiation. Likewise, female rats

exposed to the two highest levels of fractionated thoracic irradiation and those receiving single and fractionated whole-body x-irradiation had their survival times decreased significantly (Mantel-Cox statistic; $p < 0.05$) (Table 1). The well-established fact that fractionation of the exposure to low-LET will result in a sparing effect is illustrated by the survival of the rats that received fractionated whole-body exposures to X rays compared with those exposed once (Table 1). The sparing effect on survival appeared to be more pronounced among the female rats than among the males. Histological evaluations of the tissues of the rats that have died and the analyses of the results of these observations are continuing.

Table 1

Survival of Rats in the Study to Determine the Lung Tumor Risk from Fractionated Thoracic, Fractionated Whole-Body or Single Whole-Body Exposure to X Rays (as of September 30, 1992)

X-Ray Dose ^a	Number Exposed		Percentage Alive		Median Survival Time (days \pm SE)	
	Males	Females	Males	Females	Males	Females
Fractionated Thoracic						
Sham	504	504	13	27	621 \pm 5	735 \pm 6
3.46 Gy	502	503	11	23	606 \pm 6	719 \pm 9
5.76 Gy	249	251	8	23	594 \pm 5	738 \pm 11
11.5 Gy	118	120	10	19	604 \pm 10	668 \pm 13 ^b
38.4 Gy	60	60	10	12	523 \pm 11 ^b	622 \pm 31 ^b
Fractionated Whole-Body						
5.76 Gy	250	253	6	12	532 \pm 12 ^b	557 \pm 11 ^b
Single Whole-Body						
5.76 Gy	250	250	0	0	501 \pm 6 ^b	514 \pm 10 ^b
Totals	1933	1938	9	19	— ^c	— ^c

^aGy = 0.0096 \times R.

^bLife span significantly decreased ($p < 0.05$) relative to the sham-exposed rats of the same sex.

^cThis quantity was not determined because it is not meaningful.

(Research sponsored by the Office of Health and Environmental Research, U. S. Department of Energy, under Contract No. DE-AC04-76EV01013.)

CARCINOGENIC EFFECTS OF INHALED $^{244}\text{Cm}_2\text{O}_3$ IN F344 RATS

D. L. Lundgren, R. A. Guilmette, F. F. Hahn, and W. W. Carlton*

Radioisotopes of curium constitute a significant portion of the alpha activity in the spent fuel of conventional power reactors. These radionuclides present hazards to people by various routes of exposure, including inhalation. Compared with plutonium, relatively few studies of the toxicity of inhaled curium compounds have been conducted in laboratory animals. Although the oxides of curium are more soluble than those of plutonium, it appears that the incidences of lung tumors in rats exposed to either curium or plutonium are similar in the dose range of 0.20 to 2.0 Gy to the lungs (Sanders, C. L. and J. A. Mahaffey. *Radiat. Res.* 76: 384, 1978). However, in previous studies of the toxic effects of inhaled radiocurium, a direct measurements of the initial lung burdens (ILBs) for each animal were not determined.

The purpose of the study reported here was to obtain information on the dose-response relationships of ^{244}Cm in rats exposed by inhalation to well-characterized aerosols of $^{244}\text{Cm}_2\text{O}_3$ in which the ILB of each animal was determined, thus permitting more accurate dosimetry calculations for each rat than previously available. Included in this study were several hundred rats with relatively low levels of alpha dose to the lung.

Details of the inhalation exposures to monodisperse $^{244}\text{Cm}_2\text{O}_3$ aerosols, dosimetry calculations, and analyses of the survival data have been presented (1985-86 Annual Report, p. 263). Briefly, a total of 1283 (637 males and 646 females) F344/Crl 84-day-old (\pm 7 days) rats reared at this Institute were briefly exposed once to ^{244}Cm . Control rats were sham exposed. Observations were made twice daily for moribund and dead animals. Moribund animals were euthanized. After death, each rat was necropsied, and all major organs were examined grossly, including the brain. Lungs, heart, liver, kidneys, adrenals, spleen, and organs with lesions were removed and fixed in 10% neutral-buffered formalin. Fixed tissues were trimmed, embedded in paraffin, sectioned at 5 μm , stained with hematoxylin and eosin, and examined microscopically.

The crude incidences of non-neoplastic pulmonary lesions in the rats held for life span are summarized in Table 1. Dose-related increases in the incidence of pneumonia (except in the two highest exposure groups), pulmonary fibrosis, and epithelial hyperplasia were noted. Rats in the highest two exposure levels had increased incidences of radiation pneumonitis and squamous metaplasia. The crude incidences of pulmonary neoplasms are summarized in Table 2. Dose-related increases occurred in both the benign and malignant lung tumors, except for the rats in the highest two exposure levels in which survival was markedly decreased. Both a benign and a malignant tumor were found in the lungs of six rats (Table 2). In addition, two or more malignant lung tumors were found in 14 rats in the higher dose groups. For combining the lung tumor incidence data (Table 2) and for calculating the excess number of rats with lung tumors per unit of dose to the lungs (Table 3), a rat that died with two or more lung tumors was considered as having died with a single lung tumor.

In addition to the lung, significant alpha doses were absorbed by both the liver and skeleton of the rats. Primary liver tumors occurred in several of the rats; however, the incidence of these lesions was not dose related (Table 2). Increased incidences of bone neoplasms occurred only in the rats receiving relatively high doses to the skeleton (Table 2). The crude incidences of lung tumors are illustrated in Figure 1. Because of the marked life-span shortening in the rats in the highest exposure group (Table 1), they were not included in this illustration. The decreased incidence of lung tumors in the rats in the 100 kBq group could also be related to the decreased survival of the rats in the group.

The excess numbers of rats that died with lung tumors per unit of dose to the lung are summarized in Table 3 and ranged from 9.2 to 1600 per 10^4 Gy. However, the risk factors in the lower and higher exposure levels should not be considered to be reliable because of the relatively large errors associated with the calculated values. The results of this study with ^{244}Cm are being compared with those from rats exposed to relatively low-level x-irradiation of the thorax (this report, p. 121), relatively low-level beta irradiation of the lung from inhaled ^{144}Ce (1990-91 Annual Report, p. 119), and from relatively low-level alpha irradiation of the lung from inhaled ^{239}Pu (Sanders, C. L. et al. *Health Phys.* 55: 455, 1988).

*Purdue University, Lafayette, Indiana

Table 1

Incidence of Non-Neoplastic Lesions Observed in the Lungs of Rats Held for their Life Span after Exposure by Inhalation to Aerosols of $^{244}\text{Cm}_2\text{O}_3$

Mean ILB ^a kg ⁻¹ Body Weight	Number Examined ^b	Median Survival Time (days \pm SE) ^c	Pneumonia (%)	Radiation Pneumonitis (%)	Pulmonary Fibrosis (%)	Epithelial Hyperplasia (%)	Squamous Metaplasia (%)
Sham	157	805 \pm 12	0.64	0	0.64	3.2	0
0.44	169	819 \pm 13	1.8	0	4.7	8.3	0
1.2	210	802 \pm 12	2.9	0	3.3	17	0.95
2.7	130	798 \pm 17	2.3	0	6.2	22	1.5
8.9	113	762 \pm 12	3.5	0	6.2	22	0
24	115	707 \pm 17	6.1	0	20	53	0.87
100	67	534 \pm 14	0	15	66	58	7.5
220	122	63 \pm 2	0	80	96	9.8	3.3

^aILB = Initial lung burden in kBq.

^bOnly rats held for life-span observation.

^cSurvival data from male and female rats combined here for illustrative purposes only (the median survival times of the two sexes were different).

Table 2

Incidence of Primary Lung, Liver, and Bone Neoplasms in Rats
Exposed Once by Inhalation to Aerosols of $^{244}\text{Cm}_2\text{O}_3$

Mean ILB ^a kg ⁻¹ Body Weight	Number Examined ^b	Lung Tumors			Liver Tumors (%)	Bone Tumors (%)
		Benign (%)	Malignant (%)	Both (%)		
Sham	157	0.64	1.9	2.5	0	1.3
0.44	169	1.2	4.1	5.3	1.8	1.2
1.2	210	2.4	3.8	6.2	4.3	0.5
2.7	130	1.5	6.9	8.5	1.5	1.5
8.9	113	4.4	18	22	0	1.8
24	115	1.7	44	46	1.7	14
100	67	4.5	36	40	1.5	25
220	122	0	4.9	4.9	0	3.3

^aILB = Initial lung burden in kBq.

^bOnly rats held for life-span observation.

Table 3

Excess Number of Rats with Benign and Malignant Lung Tumors per Unit of
Alpha Dose to the Lungs of Rats Exposed by Inhalation to $^{244}\text{Cm}_2\text{O}_3$

Mean ILB ^a kg ⁻¹ Body Weight	Mean Lifetime Dose (Gy) to Lungs (\pm SD)	Excess Numbers of Rats With Lung Tumors per 10 ⁴ Gy \pm SE		
		Benign	Malignant	Both Combined
0.44	0.18 \pm 0.062	300 \pm 590	1300 \pm 1100	1600 \pm 1200
1.2	0.42 \pm 0.12	410 \pm 290	450 \pm 400	860 \pm 490
2.7	0.92 \pm 0.29	98 \pm 140	550 \pm 270	640 \pm 300
8.9	3.2 \pm 0.91	120 \pm 63	490 \pm 120	600 \pm 130
24	9.0 \pm 2.0	12 \pm 15	470 \pm 53	480 \pm 53
100	34 \pm 6.5	11 \pm 8	100 \pm 18	110 \pm 18
220	26 \pm 6.9	-2.5 \pm 2.5 ^b	12 \pm 8.7	9.2 \pm 9.0

^aILB = Initial lung burden in kBq.

^bNegative excess lung tumors occurred when the percentage of rats with tumors in exposed groups was less than that in the respective control group. These should be taken as zero values; however, actual computed values were retained to facilitate the comparisons among exposed rats.

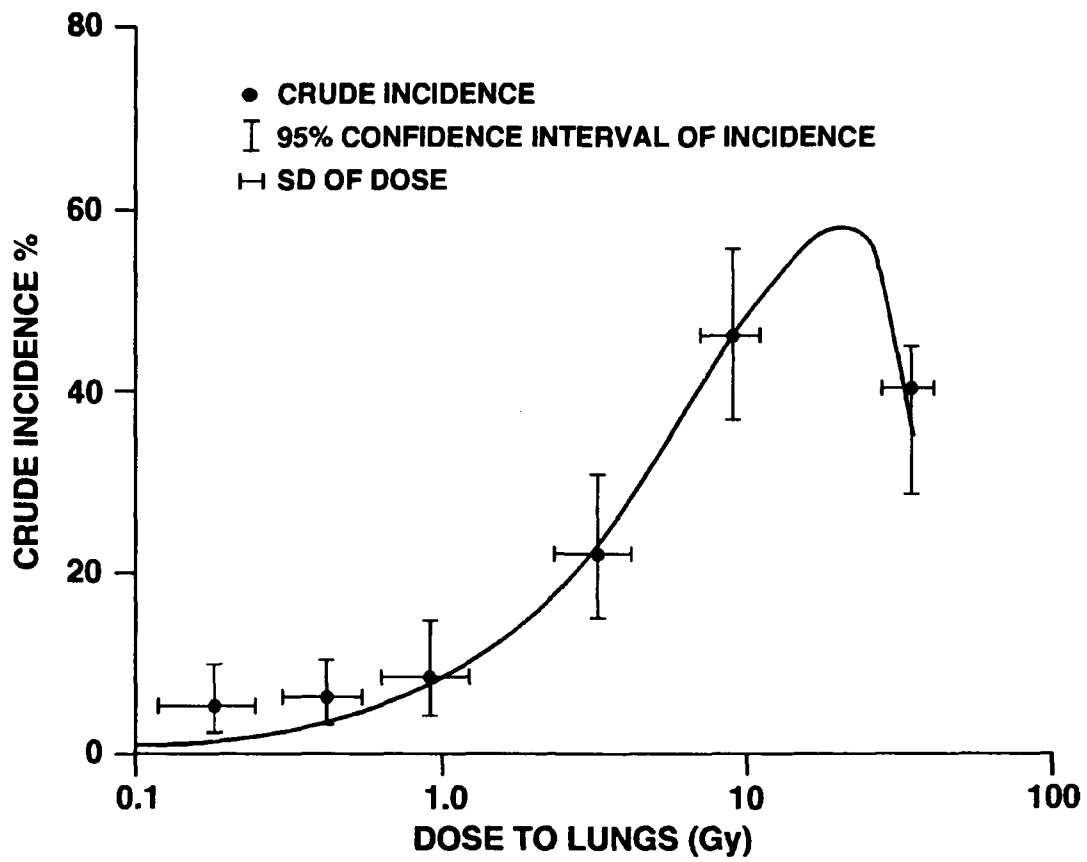


Figure 1. Exponential linear-quadratic curve (—●—) fitted to the crude incidence of primary lung tumors (benign and malignant) in rats exposed by inhalation to $^{244}\text{Cm}_2\text{O}_3$ to achieve desired initial lung burdens (ILBs).

(Research sponsored by the Office of Health and Environmental Research, U. S. Department of Energy under Contract No. DE-AC04-76EV01013).

BIOLOGICAL EFFECTS OF $^{91}\text{YCl}_3$ INHALED BY BEAGLE DOGS

A. F. Hubbs*, B. A. Muggenburg, F. F. Hahn, W. C. Griffith, and B. B. Boecker

This study was conducted to determine the life-span radiotoxicity of $^{91}\text{YCl}_3$ in Beagle dogs. Yttrium-91 is of interest as a beta-emitting radionuclide with a relatively short half-life that occurs in abundance in operating light-water nuclear reactors. After ^{91}Y is inhaled in relatively soluble chemical forms, it translocates from the pulmonary region primarily to liver and skeleton. It is, however, retained in the lung long enough to deliver a large portion of its dose to that organ. ^{91}Y was selected for study as a representative radionuclide because of its potential for human inhalation exposure in the event of a nuclear reactor accident.

Forty-two dogs, equal numbers of both sexes, inhaled aerosols of $^{91}\text{YCl}_3$. The dogs were 12 to 14 mo of age (399 ± 14 day) when exposed to ^{91}Y . In addition, 12 dogs inhaled the aerosol vector (controls). After inhalation, the dogs were whole-body counted for ^{91}Y activity to determine the initial body burden (IBB) and the long-term retention of this radionuclide (LTRB was 0.5 to 20 MBq/kg). Health effects were determined by daily observation of the dogs and by annual medical evaluations that included a physical examination, complete blood cell counts, selected serum chemistry determinations, radiographs, and a medical history review. Sick dogs were examined and appropriate tests conducted to establish a diagnosis. Diseases that appeared to be unrelated to the inhalation of ^{91}Y were treated by standard veterinary procedures. As the dogs died or were euthanized, complete necropsy and histopathology examinations were done. When all the animals in this study were dead, a final review of the pathology and clinical findings was conducted by a pathologist (A.H.) and clinician (B.M.) to establish and use uniform terminology and diagnostic criteria.

Early deaths, which occurred in 11 dogs from 12 to 33 days after inhalation exposure, were primarily due to damage to the blood-forming cells in the bone marrow. Severe thrombocytopenia and leukocytopenia resulted in fatal hemorrhage or acute septicemia. In addition to the animals that died acutely, 21 dogs had moderate-to-severe changes in peripheral blood cell counts that indicated serious damage to the bone marrow. These changes included thrombocytopenia, neutropenia, lymphopenia, monocytopenia, and erythrocytopenia. A few of these dogs also had clinical signs of illness such as ecchymotic hemorrhages on mucous membranes.

The distributions of neoplastic and non-neoplastic diseases in different organ systems in the exposed and control dogs are given in Table 1. These diseases were classified as either the cause of death or major contributing diseases. A major contributing disease was defined as causing moderate-to-severe morphologic changes in tissues with detected clinical signs, a malignant tumor that metastasized, or a benign tumor that was life-threatening. In some dogs significant disease was present in more than one organ system, and, therefore, dogs may have been counted more than once. Of the 31 dogs that survived the acute hematologic crisis, 16 (52%) died from neoplasia, and 6 (14%) had tumors that were classified as major contributing diseases. In the control population, six (50%) died from neoplasia, and one (8%) dog had a tumor that was a major contributing disease. In the dogs that inhaled ^{91}Y , tumor incidence in the respiratory tract appeared to be higher than expected. The apparent increase in tumors in the digestive system is probably not significant because the tumors were found in different digestive organs, and only one tumor that might be related to radiation, an hepatocellular carcinoma, was found in the liver.

Beta dose resulting from the inhaled ^{91}Y was delivered mainly to the respiratory tract, liver, and skeleton. As indicated above, tumors of the respiratory tract were apparently increased in incidence, only one tumor was found in the liver, and no tumors were found in the skeleton. Effects that were observed in the skeleton occurred soon after the inhalation exposure and were associated with the bone marrow. Information on the tumors in the respiratory tract is given in Table 2. In three dogs, tumors were found in the nose. Two dogs died from lung tumors, and lung tumors were found incidentally in two other dogs.

Two control dogs and three dogs that inhaled $^{91}\text{YCl}_3$ had tumors of the mammary glands (not shown in Table 1). One exposed dog had two adrenocortical carcinomas, and three exposed dogs had thyroid carcinomas. One control dog had a thyroid carcinoma.

*Currently at National Industrial and Occupational Safety and Health (NIOSH), Morgantown, West Virginia

Table 1

**Primary Causes of Death and Major Contributing Diseases of
Dogs Injected with $^{91}\text{YCl}_3$ and of Control Dogs**

System	Neoplastic Disease ^a		Non-Neoplastic Disease ^b	
	$^{91}\text{YCl}_3$ Exposed	Control	$^{91}\text{YCl}_3$ Exposed	Control
Respiratory	5 ^c	0	8 ^c	0
Hematopoietic	0	0	12 ^c	0
Digestive	6 ^c	1	8 ^c	3 ^c
Urogenital	2 ^c	1 ^c	9 ^c	5 ^c
Nervous	0	0	5 ^c	0
Cardiovascular	1 ^c	1	12 ^c	3 ^c
Integument	5 ^c	2 ^c	0	0
Endocrine	6 ^c	1	2 ^c	1 ^c
Skeletal	0	0	1 ^c	1 ^c
Other	0	0	4 ^c	1

^aNumber represents the dogs that died with a neoplasm which was considered the primary cause of death or a major contributing disease. There were 46 dogs exposed to $^{91}\text{YCl}_3$ and 12 control dogs.

^bNumber represents the dogs that died with a non-neoplastic disease which was considered the primary cause of death or a major contributing disease.

^cDogs included in this total also appear in other categories.

Table 2

**Occurrence of Cancers of the Respiratory Tracts in Dogs that
Inhaled $^{91}\text{YCl}_3$ and Were Followed for Life-Span Observation**

Tattoo	Relationship to Death	Site	Morphology
118A	PCOD	Nose, Epithelium	Carcinoma, Squamous Cell
134C	PCOD	Nose, Epithelium	Carcinoma, Squamous Cell
171F	PCOD	Nose, Epithelium	Carcinoma, Squamous Cell
173F	PCOD	Lung	Adenocarcinoma, Bronchioloalveolar w/Squamous Metaplasia
174A	PCOD	Lung, Left Diaphragmatic Lobe	Adenocarcinoma, Papillary
171B	INCD ₀₃	Lung, Right Cardiac Lobe	Adenocarcinoma, Papillary
171B	INCD ₀₂	Lung, Right Diaphragmatic Lobe	Adenocarcinoma, Papillary
119A	INCD ₀₄	Lung, Left Diaphragmatic Lobe	Adenocarcinoma, Papillary
173G	INCD ₀₂	Lung, Left Diaphragmatic Lobe	Adenoma, Bronchioloalveolar

PCOD = Primary Cause of Death

INCD = Incidental Findings

In summary, $^{91}\text{YCl}_3$ inhaled by dogs resulted in an increase in the incidence of tumors of the respiratory tract, both in the nasal epithelium and in the pulmonary region of the lung. The incidence of tumors of other organs did not appear to be increased. The effects on the skeleton were confined to the early effects on the bone marrow causing hematologic dyscrasia. Despite the wide gradation of dose to the skeleton in the 31 dogs that survived the early deaths, none of the dogs developed bone marrow or bone tumors. Although a wide range of doses to the liver occurred (0.65 to 10 Gy), only one liver tumor was found. This is too low an incidence to confidently ascribe this tumor to radiation effects. A much higher incidence of liver tumors and liver degeneration was observed in the studies of inhaled $^{144}\text{CeCl}_3$ (1989-90 Annual Report, p. 107) and injected $^{137}\text{CsCl}$ (1989-90 Annual Report, p. 112) in dogs that received similar cumulative beta doses to the liver (6.1 to 35 Gy).

(Research sponsored by the Office of Health and Environmental Research, U. S. Department of Energy, under Contract No. DE-AC04-76EV01013.)

LIFE-SPAN HEALTH EFFECTS OF RELATIVELY SOLUBLE FORMS OF INTERNALLY DEPOSITED BETA-EMITTING RADIONUCLIDES

B. B. Boecker, B. A. Muggenburg, F. F. Hahn, K. J. Nikula, and W. C. Griffith

In life-span studies on the effects of inhaled radionuclides currently in progress, both fission product and transuranic radionuclides are being studied. The primary goals of these studies are to determine the life-span health risks of inhaled radionuclides and the influence of various dose-and effect-modifying factors, and to extrapolate these results to possible human exposures, particularly those for which no direct human data currently exist. One important area addressed in the fission-product studies is the influence of *in vivo* solubility of the inhaled material on the doses received by, and the effects seen in, different organs and tissues. This report presents and compares results from three studies in which young-adult Beagle dogs inhaled $^{90}\text{SrCl}_2$ or $^{144}\text{CeCl}_3$, or were injected with $^{137}\text{CsCl}$. This comparison was chosen because of known differences in the pattern of metabolism and dosimetry among these three radionuclides, ranging from concentration mainly in one organ (^{90}Sr), several organs (^{144}Ce), and the whole body (^{137}Cs). Of particular interest are the relative distributions of radiation dose and long-term biological effects among organs exposed by these three regimens.

Young-adult Beagle dogs (12-14 mo, equal number of both sexes) inhaled, on a single occasion, different activity levels of either $^{90}\text{SrCl}_2$, or $^{144}\text{CeCl}_3$, or were injected once, intravenously, with $^{137}\text{CsCl}$. The exposure aerosols, consisting of the radionuclide plus a CsCl or CeCl₃ vector, had polydisperse size distributions with activity median aerodynamic diameters ranging from 1.5 to 2.4 μm ($\sigma_g = 1.6$ to 2.1). Exposures were completed in less than 1 h. Each dog was whole-body counted immediately after radionuclide exposure and at selected intervals thereafter to determine the initial body burden and its retention as a function of time after exposure. Each dog's health status was evaluated periodically, and illnesses considered not to be associated with the radiation exposure were treated using standard veterinary practices. All dogs were maintained in the ITRI kennel facility until they died or were euthanized when moribund. Complete necropsies and histopathological examinations were performed. When all dogs in a study were dead, all clinical and histopathological results and materials were reviewed to ensure accuracy and consistency of the diagnoses. All diseases were coded for a FOCUS database using the SNOMED system modified for dogs. Absorbed beta doses were computed for individual organs or the whole body as appropriate for the radionuclides and forms used. These dose calculations were based on the whole-body retention data from each radionuclide-exposed dog in the longevity study and tissue distribution and retention data obtained from serially sacrificed dogs in separate, but similar, dosimetry studies. The small photon contribution was ignored, except for the whole-body dose from ^{137}Cs where the photon portion contributed about one-third of the total dose.

Table 1 presents the experimental design features for the three studies compared in this report. In each study, a range of long-term retained burdens was studied, the highest of which led to early deaths within the first 2 yr after exposure. Most of these early deaths were from hematologic dyscrasias resulting from irradiation of the

Table 1

Experimental Design Features for Life-Span Studies of Dogs Exposed to Relatively Soluble Beta-Emitting Radionuclides

Study	LTRB ^a (MBq/kg)	Number of Dogs			
		Exposed Total	>2 yr ^b	Controls Total	>2 yr ^b
^{90}Sr	0.10 - 4.8	66	58	22	22
^{144}Ce	0.096 - 13	55	41	15	15
^{137}Cs	28 - 130	54	42	12	11

^a LTRB = long-term retained burdens for exposed dogs.

^b Survived more than 2 yr after exposure.

bone marrow. Several others were due to radiation pneumonitis, pulmonary fibrosis, or hepatic degeneration. The focus of this report is on the remaining ~80% of the dogs that survived more than 2 yr after exposure and, therefore, were at risk for the development of cancer and other later-occurring diseases.

Cumulative absorbed dose factors (Gy per MBq/kg Long Term Retained Burden) for organs in animals exposed to these three different patterns of radionuclide distribution are given in Table 2. The organs and tissues listed for ^{144}Ce are the four that received the highest total beta doses. Of these four, only two, bone and nasal mucosa, received significant doses from ^{90}Sr . In contrast, the relatively uniform whole-body distribution of ^{137}Cs produced about the same total dose (beta plus gamma) in all four organs.

Table 2

Cumulative Absorbed Beta Doses to 5000 Days after Exposure of Beagle Dogs to Radionuclides in a Relatively Soluble Form

Organ/Tissue	Gy per MBq/kg LTRB ^a		
	$^{90}\text{SrCl}_2$	$^{144}\text{CeCl}_3$	$^{137}\text{CsCl}^b$
Lung	---	24	0.15
Liver	---	60	0.21
Bone	220	18	0.13
Nasal Mucosa	270	92	0.18
Whole Body	N/A ^d	N/A	0.21

^aLTRB = long-term retained burden.

^bDoses for ^{137}Cs include gamma contribution.

---- = Dose <0.1% of skeletal dose.

^dNot applicable.

Neoplasia was a prominent, long-term finding in both the exposed and control dogs (Gillett, N. A. *et al.* JNCI 79: 35, 1987; 1989-90 Annual Report on Long-Term Dose-Response Studies of Inhaled or Injected Radionuclides, p. 66, p. 70). Table 3 gives the number of dogs in which primary malignant or benign tumors were found. All tumors, whether they were the primary cause of death, a major contributing disease, or an incidental finding, are included. For this report, the controls for the three individual studies have been combined. One can roughly compare the number of tumors across the three exposed groups and the combined controls because the number of 2-yr survivors was about the same in each group.

The number of lung tumors was similar in all three exposed groups and the control group. These tumors were mainly bronchioloalveolar carcinomas and adenocarcinomas in dogs that died from 10 to 16.5 yr after exposure. The exceptions were two ^{144}Ce -exposed dogs that died at 4.5 and 7.6 yr after exposure in which a bronchioloalveolar adenoma and adenocarcinoma, respectively, were found. In the liver, bone, and nasal mucosa, pronounced differences were found between the exposed dogs and the controls. No tumors were found in these organs in the control dogs except for two bile duct adenomas in the liver. A large number of liver tumors, both malignant (hemangiosarcoma, hepatocellular carcinoma, cholangiocarcinoma, and neurofibrosarcoma) and benign (biliary cystadenoma and bile duct adenoma) were found in dogs exposed to ^{144}Ce or ^{137}Cs , but not to ^{90}Sr . In contrast, the tumorigenic response in the ^{90}Sr -exposed dogs was primarily the occurrence of bone tumors (osteosarcoma, hemangiosarcoma, and fibrosarcoma). No bone tumors were seen in the other groups, except one osteosarcoma that occurred in a ^{144}Ce -exposed dog at 2.2 yr after exposure. Tumors in the nasal mucosa, mostly carcinomas, occurred in all three studies, but not in the controls. The relative distribution of tumors between the $^{144}\text{CeCl}_3$ and $^{90}\text{SrCl}_2$ studies is consistent with the dosimetry information in Table 2. The occurrence of tumors in the livers and nasal mucosa of $^{137}\text{CsCl}$ -exposed dogs indicates that these tissues are relatively responsive to this radiation insult.

Table 3

Occurrence of Primary Tumors in Selected Organs of Dogs that were Exposed to $^{90}\text{SrCl}_2$, $^{144}\text{CeCl}_3$ or $^{137}\text{CsCl}$ and Lived > 2 yr after Exposure or in Control Dogs

Organ/Tissue	Number of Tumors ^a			
	^{90}Sr	^{144}Ce	^{137}Cs	Controls
Lung	2,1 ^b	3,1	3,0	5,0
Liver	0,1	10,11	5,5	0,2
Bone	45,1	1,0	0,0	0,0
Nasal Mucosa	3,0	5,0	4,0	0,0
Number of Dogs	58	41	42	48

^aSome dogs had more than one tumor. In addition to the tumors listed, a number of tumors were found in other organs of dogs in each of these groups; many were incidental findings at necropsy.

^bNumber malignant, number benign.

These initial analyses have been directed to organs and tissues that have been clearly identified as targets of radiation from these and other internally deposited radionuclides. Investigations are continuing on the question of whether additional organs or tissues may also be at risk from these different patterns of chronic beta irradiation. These results are providing valuable *in vivo* information on the appropriateness of current radiation-protection practices for internally deposited radionuclides.

(Research sponsored by the Office of Health and Environmental Research, U.S. Department of Energy, under Contract No. DE-AC04-76EV01013.)

PRIMARY LUNG CANCER IN THE LONGEVITY STUDY/ CONTROL POPULATION OF THE ITRI BEAGLE DOG COLONY

F. F. Hahn, B. A. Muggenburg, and W. C. Griffith

The incidence and types of primary lung neoplasms found in unexposed dogs are critical in determining the long-term biological effects of inhaled radionuclides. The frequency of lung neoplasms in dogs is generally considered to be low, but incidence rate is difficult to document in pet populations. In North America and Europe, reports of lung carcinoma occurrence range from 0.1% (Nielsen, S. E. In *The Lung* [A. A. Liebow and D. E. Smith, eds.], Williams and Wilkins, Baltimore, p. 226, 1968) to 1% (Stünzi, H. *Pathol. Microbiol.* 39: 358, 1973) for dogs that die and are necropsied. In a survey of all types of neoplasms in the pet dog population of two counties in Northern California, the incidence rate for lung cancer, as diagnosed in dogs admitted to veterinary clinics, was 4.2 per 10,000 dogs per year (Dorn, C. R. *et al. J. Natl. Cancer Inst.* 40: 295, 1968). Here, we report the incidence of primary lung neoplasms in a group of 225 Beagle dogs observed for their normal life span.

The dog colony at ITRI, composed of purebred Beagle dogs, was initiated in 1962. The colony has been closed to the entry of new dogs since 1965. In 1968, a generation breeding program was initiated to establish and maintain a stable gene pool (Bielfeldt, S. W. *et al. Am. J. Vet. Res.* 30: 2221, 1969). The initial generation consisted of 40 female and 20 male dogs.

The longevity study control population consists of all control dogs included in life-span studies of inhaled radionuclides conducted at ITRI and allowed to live out their normal life spans. These control dogs are listed in the appendix tables of the *ITRI Annual Report on Long-Term Dose-Response Studies of Inhaled or Injected Radionuclides*. One control group is not included: the life-span studies of aged dogs, since the animals were selected for study at 8-10.5 yr of age.

The characteristics of the control population are noted in Table 1. The selection criteria and frequency of clinical examinations were the same as for the exposed dogs and similar among longevity studies, although the studies were initiated over a period of 12 yr.

Table 1
Characteristics of Longevity Control Dog Population

Number of Dogs	Age of Selection	Selection Criteria	Frequency of Clinical Examination
225 total (116 females 109 males)	13 ± 1 mo (except 18 were 12 ± 1 wk)	- Normal size ^a - Normal facial configuration - Normal hematologies - Normal blood chemistry - Normal radiographs - Normal EEG & EKG	- Once per year on birthday - As needed for illness - Yearly radiographs

^aDogs too large to fit into standard whole-body counting box and abnormally small dogs were not used.

All dogs were given a complete necropsy at death or euthanasia that included all organ systems. All major organs, as well as lesions, were routinely sampled for histopathologic examination.

The survival and age distribution of the population at risk and the age-specific incidence of tumors were determined using a life-table method of analysis (Rosenblatt, L. S. *et al. Health Phys.* 21: 869, 1971). The

cumulative incidence of tumors is the sum of the age-specific incidence times the probability of survival to that age (Elandt-Johnson, R. C. and N. L. Johnson. *Survival Models and Data Analysis*, John Wiley and Sons, NY, 1980). The BMDP1L Life Tables and Survival Functions statistical software package was used for data analysis.

As of September 30, 1992, 204 dogs (109 males and 95 females) had died or been euthanized. The cumulative survival is shown in Figure 1. The median survival time of the males is greater than the females (14.1 yr vs. 13.7 yr); however, the survival curves are not significantly different as demonstrated by the generalized Savage, Tarone-Ware, and generalized Wilcoxon statistical tests.

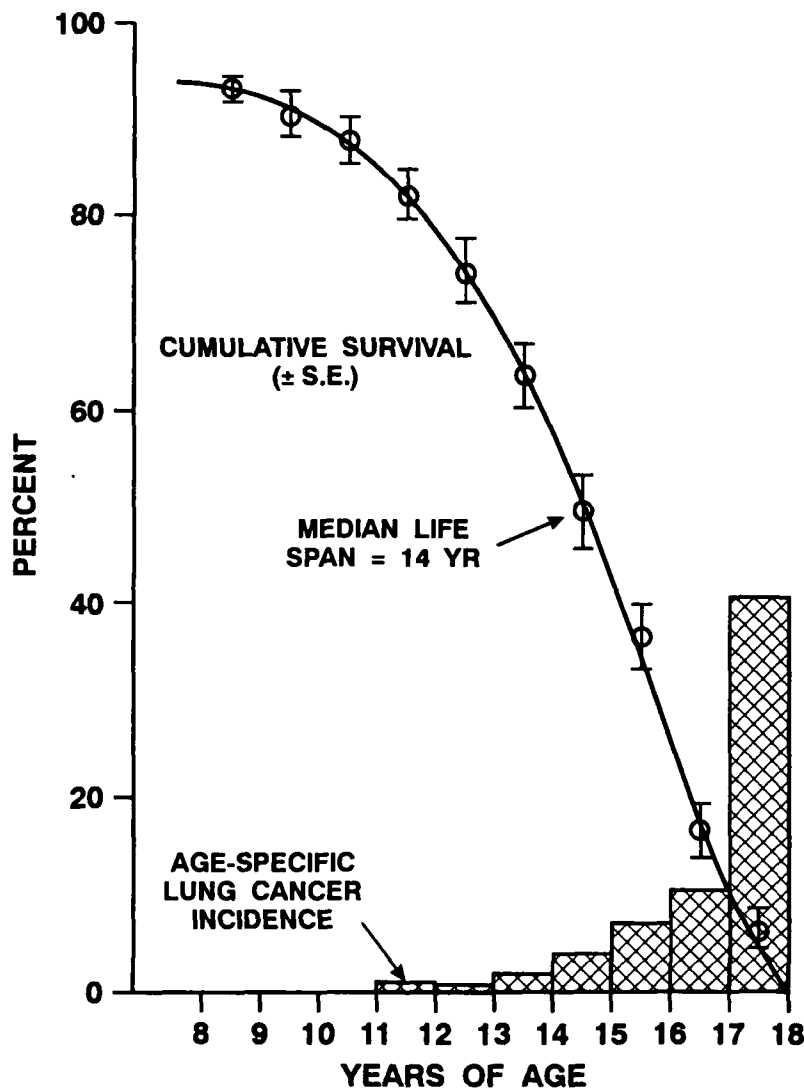


Figure 1. Longevity of control dogs and incidence of primary lung neoplasms (status as of 9/30/92).

The crude incidence of lung neoplasms was greater in females (10%) than in the males (6.4%) based on the number of dogs that had lung tumors and the number dead as of September 30, 1992. However, statistical comparison of these cumulative incidence curves shows no significant difference in the tumor incidence in males and females. This lack of sex predilection is consistent with previous reports of lung tumor incidence in pet populations (Moulton, J. E. et al. *Vet. Pathol.* 18: 513, 1981).

The age-specific incidence of tumors is also shown in Figure 1. The incidence markedly increases after 14 yr of age and is nearly 10% after 16 yr in both males and females. The age-dependence of lung neoplasms

has been noted anecdotally but has been quantified in only one previous publication. A report of the lung tumor incidence in the Beagle dog colony at the University of Utah shows an increased incidence with increased age; however, the absolute incidence is considerably lower than that reported here (Taylor, G. N. *et al.* *Am. J. Vet. Res.* 40: 1316, 1979). For example, the age-specific incidence at 13 to 16 yr is reported to be 0.7% compared to 4.2% for the similar interval in the ITRI longevity control colony.

This study indicates that the primary lung tumor incidence is higher in Beagle dogs than in other species used in long-term studies, with the exception of some mouse strains. For example, in three species frequently used in the Institute, F344 rats have a lifetime incidence of about 1%, C₅₇Bl/J mice approximately 2%, and Syrian hamsters essentially 0%.

Seventeen primary lung neoplasms were found in the control dogs (Table 2). The earliest occurring lung tumor resulted in the dog's death at 11.1 yr of age. The latest occurring was found in a 17.6-yr-old dog that died of renal failure.

Table 2

Summary of Primary Lung Neoplasms Detected in Control Dogs for the Longevity Studies

Dog Number	Age at Death (yr)	Type of Death ^a	Primary Cause of Death or Euthanasia	Lung Tumor Type	Metastasis
Males					
859C	12.7	E	Lung tumor	Papillary adenocarcinoma	No
401A	14.0	D	Lung tumor	Papillary adenocarcinoma	No
1122C	14.2	E	Lung tumor	Papillary adenocarcinoma	No
378A	14.4	E	Lung tumor	Bronchioloalveolar carcinoma	Yes
361B	14.6	D	Lung tumor	Bronchioloalveolar carcinoma	Yes
56A	15.1	E	Olfactory neuroblastoma	Papillary adenocarcinoma	No
998A	15.1	E	Lung tumor	Papillary adenocarcinoma	Yes
Females					
10C	11.1	D	Lung tumor	Papillary adenocarcinoma	No
405W	11.2	D	Anesthetic death	Papillary adenocarcinoma	No
348S	13.6	E	Renal failure	Papillary adenocarcinoma	No
689U	14.1	E	Lung tumor	Papillary adenocarcinoma	No
1152T	15.0	E	Lung tumor	Adenosquamous carcinoma	Yes
407T	15.7	E	Renal failure	Papillary adenocarcinoma	No
61C	15.8	D	Lung tumor	Papillary adenocarcinoma	Yes
663S	16.1	D	Lung tumor	Adenosquamous carcinoma	No
762T	17.6	D	Nephritis	Papillary adenocarcinoma	No
283C	17.6	D	Septicemia	Bronchioloalveolar carcinoma	Yes

^aE = Euthanized

D = Died

All of the lung tumors were carcinomas. Most (12/17) were papillary adenocarcinomas, but three were bronchioloalveolar carcinomas, and two were adenosquamous carcinomas. The morphologic appearance of these tumor types overlaps in some cases. However, the difference in morphologic pattern may have biologic significance. For example, epidermal growth factor receptor expression in canine lung tumors, as determined by immunohistochemistry, is phenotype-dependent, being predominantly seen in papillary adenocarcinomas and squamous cell carcinomas and not in bronchioloalveolar carcinomas (Gillett, N. A. *et al.* *Vet. Pathol.* 29: 46, 1992).

Metastasis, usually to thoracic lymph nodes and tissues only, occurred in six cases (35%). Two of three bronchioloalveolar carcinomas had metastases, and 4 of 12 papillary adenocarcinomas had metastases. The lung tumor was the primary cause of death in 11 of the 17 tumor cases.

The lung tumor types reported here are similar to those in pet populations reported by others. One group reported 74% adenocarcinomas and 20% alveolar carcinomas (bronchioloalveolar carcinomas) in 210 cases (Ogilvie, G. K. *et al.* *J. Am. Vet. Med. Assoc.* 195: 106, 1989). Another group reported 77% adenocarcinomas and 15% alveolar carcinomas (bronchioloalveolar carcinomas) in 171 cases from pet populations (Moulton *et al.*, 1981). A review of 11 primary lung neoplasms in the University of Utah Beagle dog colony noted 10 adenocarcinomas (Taylor *et al.*, 1979.)

In summary, this study shows that Beagle dogs do not have a low incidence of primary lung neoplasms, but the incidence is dominated by a high age-specific incidence late in life.

(Research sponsored by the Office of Health and Environmental Research, U. S. Department of Energy, under Contract No. DE-AC04-76EV01013.).

**V. MECHANISMS OF CARCINOGENIC
RESPONSES TO TOXICANTS**

DEVELOPMENT OF TECHNIQUES TO DETECT GENE DYSFUNCTIONS IN α -RADIATION-INDUCED LUNG CANCER

J. F. Lechner, L. A. Tierney*, S. A. Belinsky,
C. E. Mitchell, J. M. Samet**, and G. Saccomanno***

Epidemiological studies have documented that underground uranium miners have an increased risk for lung cancer (Saccomanno, G. C. et al. *Health Phys.* 50: 605, 1986; Samet, J. M. et al. *Health Phys.* 61: 745, 1991). A fundamental cause for these cancers is exposure to high linear-energy-transfer (LET) radiation through the inhalation of radon progeny (Samet, J. M. *J. Natl. Cancer Inst.* 81: 745, 1989). Exposure to high-LET radiation through inhalation of radon progeny is also a concern for non-miners because the soils in several geographic regions of the United States contain high concentrations of these uranium decay progeny. By diffusion of radon gas, the concentration of radon progeny in the atmospheres of poorly ventilated homes and buildings constructed on these soils can rise to levels that approximate the lifetime exposures which the underground miners received. Consequently, it has been estimated that from 10,000 to 20,000 cases of lung cancer/year in the U. S. may be associated with radon inhalation (Samet, J. M. *West. J. Med.* 156: 25, 1992).

Currently in the United States, the median survival of most individuals diagnosed with lung cancer is 9 mo, primarily because few cases are identified while the disease is localized and amenable to surgical ablation (Epstein, D. M. *Radiol. Clin. North Am.* 28: 489, 1990). However, Saccomanno and associates (Prorok, P. C. et al. In *Radiation Hazards in Mining: Control, Measurement, and Medical Aspects* [M. Gomez, ed.], Kingsport Press, Kingsport, TN, p. 178, 1981) have correlated the presence of dysplastic cells in uranium miners' sputa with high-level exposures to radon. Their data further support the following suppositions: (1) the incidence of morphologically abnormal cells in sputum from a radon-exposed miner is greater than what can be ascribed to smoking history or age alone; and (2) there is a strong trend for more severe types of dysplasia, and for shorter duration in each stage of atypia, with increasing amounts of exposure. Saccomanno and associates have also shown that from 4 to 8 yr can transpire between the time dysplastic cells are detected in uranium miners' sputa and when a lung tumor can be detected by radiographic screening. Because of this time lag, they and others have suggested that sputum cytological screenings of individuals considered to be at risk could be an effective means of discovering pre-clinical disease.

The value of sputum cytology would be enhanced by immunostaining the specimens for the expression of tumor-specific antigens, gene dysfunctions, and aberrant expressions that are commonly found in lung cancer cells. Also, from a carcinogenesis mechanism perspective, the data developed from such analyses will ultimately provide a basis for defining genetic alterations that may arise prior to any obvious change in cell morphology. These data should also advance our understanding of the temporal sequence of genetic alterations during the radiation-caused evolution of a normal lung epithelial cell into its malignant counterpart. One potential clinical impact of this research is the promise for removing doubt as to whether a sputum specimen contains cells exhibiting cancer-associated aberrant genes. Such results could be the basis for providing definitive advice regarding lifestyle or working environment to individuals once dysplastic cells with specific genetic dysfunctions have been detected in their sputum. Such advice could prolong (or perhaps extend indefinitely) the time before onset of clinical disease. Finally, knowledge of the gene dysfunctions that are common in the early stages of disease would provide more rational intervention protocols well in advance of clinical cancer; eventually, these may be in the form of gene-specific therapies.

Before beginning the investigations with the exfoliated and bronchial brushing-derived cells, we have been developing methods that can be used to accurately detect the presence of an aberration using small numbers of cells. Thus, human lung cells that exhibit excessive levels of the tumor suppressor gene *p53* were mixed with normal cells such that the abnormal *p53*-expressing cells accounted for 0.1 to 10% of the mixture. Cells (2,000-5,000) were then placed on a glass slide by cytocentrifugation. These cells were fixed using the "Saccomanno"

*UNM/ITRI Inhalation Toxicology Graduate Student

**University of New Mexico Cancer Center, Albuquerque, New Mexico

***St. Mary's Hospital, Grand Junction, Colorado

protocol (2% carbowax in 50% ethanol) and subsequently stained using immunoreagents specific for decorating p53. The results suggest that the percentage of cells exhibiting the mutant p53 phenotype corresponds well within the expected values, and as few as 1 mutant cell per 100 can be detected. Using these methods, mutant forms of p53 have been regularly detected in tumor tissues of uranium miners.

In addition to the p53 effort, preliminary investigations also have been conducted to establish the protocols for detecting aberrations of the TGF- α , Rb, and ErbB-2 genes by immunostaining procedures. With respect to the latter dysfunctional gene, normal human lung epithelium does not express this growth factor receptor. In contrast, of six tumors from uranium miners (of a current collection of 59 patients) analyzed to date, four of four squamous cell carcinomas were positive for ErbB-2, whereas two of two small cell carcinomas were negative. In contrast, less than 10% of 40 tumors obtained from dogs exposed to $^{239}\text{PuO}_2$ exhibited abnormal expression of this oncogene product.

In other experiments, the BstNI restriction fragment length polymorphism assay has now been tested in our laboratory and found to be a sensitive means to detect as few as one mutated form of K-ras oncogene among 1×10^4 wild-type alleles. In preliminary experiments, the use of fluorescent *in situ* hybridization technology has also been used to successively detect alterations in chromosome 3p21 in a human epithelial cell line known from previous cytogenetic studies to have this deletion.

These technique development experiments are now to the stage where we are beginning to analyze sputum from uranium miners and lavage cells from dogs that developed lung cancer after exposure to $^{239}\text{PuO}_2$; the results will be reported in the near future.

(Research sponsored by the Office of Health and Environmental Research, U. S. Department of Energy, under Contract No. DE-AC04-76EV01013.)

ARBITRARILY PRIMED-POLYMERASE CHAIN REACTION AMPLIFICATION AS A MEANS TO DISCERN GENE ALTERATIONS IN LUNG CANCER

C. H. Kennedy, P. Economou*, and J. F. Lechner

Many genes associated with carcinogenesis, especially tumor suppressor genes, were initially detected by restriction fragment length polymorphism (RFLP) analyses of familiarly segregating alleles (Weston, A. et al. *Proc. Natl. Acad. Sci.* 86: 5099, 1989). Another means to identify gene alterations that occur during the stages of carcinogenesis is to use arbitrarily primed-polymerase chain reaction (AP-PCR) amplification technology. In this procedure, an arbitrary primer is used to produce a fingerprint of a genome (Williams, J. G. K. et al. *Nucleic Acids Res.* 18: 6531, 1990; Welsh, J. and M. McClellan. *Nucleic Acids Res.* 18: 7213, 1990). Different primers produce unique fingerprints consisting of amplification products of DNA that are between 0.2 and 2.5 kb in length. DNA sequences are often lost, under-represented, or amplified in tumor cells. Thus, a fingerprint of the tumor (and perhaps pre-malignant lesions) should have a band (or bands) that is missing, less intense, or more intense as compared to the pattern observed using normal tissue.

The purpose of the work described here was to prepare fingerprints of genomic DNA isolated from tumor and normal human lung tissue using several arbitrary primers. Tumor and normal lung tissues were obtained from the New Mexico Tumor Registry at the University of New Mexico Cancer Center. The histopathology indicated that the tumor was a moderately differentiated, non-keratinized squamous cell carcinoma. DNA was isolated from this tissue by phenol extraction.

Four arbitrary primers were used to prepare fingerprints: AP2 (CGGCCCGGC), AP5 (CGGCCACTGT), λ3'gt-10 (CTTATGAGTATTCTTCAGGGTA), and λ5'gt-10 (AGCAAGTTCAGCCTGGTTAAG). Twenty μL reactions were prepared for AP-PCR using 0.5 U AmpliTaq® DNA polymerase (Perkin Elmer Cetus, Norwalk, CT), 2 μL of 10X PCR buffer (Perkin Elmer Cetus, Norwalk, CT), 0.2 mM of each dNTP, 1 μM arbitrary primer, and 100 ng of DNA. The reaction mixtures were overlaid with oil and taken through 35 cycles of the following treatment: 94°C for 1 min (denaturing of DNA), 42°C for 1 min (primer annealing), and 72°C for 1 min (extension of DNA). The amplified products (stage 1 products) were used to prepare ³²P-labeled stage 2 AP-PCR products. The stage 2 reaction was the same as above except that the final concentration of each dNTP was 2.0 μM, 1 μCi of ³²P-ATP was added, and 2 μL of stage 1 product were used as the template. The DNA was amplified 15 times using the same thermal cycle. The ³²P-labeled products were electrophoresed using a 5% polyacrylamide gel and visualized by autoradiography.

The fingerprints of genomic DNA obtained by AP-PCR indicate that this technique can be used to detect polymorphisms between tumor and normal DNA (Fig. 1). The products obtained using this AP-PCR technique (i.e., all DNA sequences amplified in the presence of arbitrary primers) are being used to probe a human lung cDNA library (Clontech, Palo Alto, CA) in order to isolate and subsequently sequence the differentially expressed genes that are recognized by their ability to hybridize with the individual AP-PCR amplification products. The results of this study suggest that AP-PCR is a viable alternative to RFLP analysis for the identification of gene alterations in lung cancer.

*Currently at the Lovelace Medical Center, Albuquerque, New Mexico

AP2 PRIMER
T N

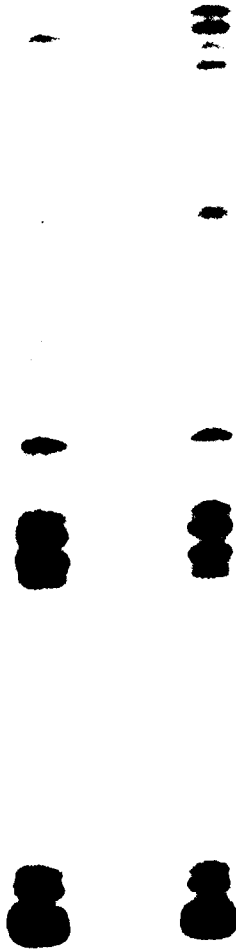


Figure 1. Portion of genomic fingerprints of DNA isolated from tumor (T) and normal (N) lung tissue. Fingerprints were prepared by AP-PCR with the AP2 primer.

(Research sponsored by the Office of Health and Environmental Research, U. S. Department of Energy, under Contract No. DE-AC04-76EV01013.

DEVELOPMENT OF A DNA METHYLTRANSFERASE ASSAY

C. Nickell and S. A. Belinsky

In addition to chromosomal deletions, translocations, amplifications, and mutations, the control of gene transcription is thought to be involved in the development, clonal expansion, and progression of initiated cells (reviewed by Holliday, R. *Science* 238: 163, 1987). Considerable evidence has accumulated demonstrating that 5-methylcytosine modification of mammalian DNA, both in exons and CpG islands located in promoter regions, is important in gene regulation. This evidence indicates an inverse relationship between CpG methylation and gene expression (Cedar, H. *Cell* 53: 3, 1988). For example, a decrease of 5-methylcytosine in the 5' flanking regions or exons of genes has been associated with increased gene transcription (Jones, P. A. and J. D. Buckley. *Adv. Cancer Res.* 54: 1, 1990; Wilson, V. L. et al. *Proc. Natl. Acad. Sci. USA* 84: 3298, 1987). In contrast, substantial hypermethylation has been detected within chromosomal regions thought to contain putative tumor suppressor genes (Baylin, S. B. et al. *Cancer Res.* 46: 2917, 1986; Bustros, A. D. et al. *Proc. Natl. Acad. Sci. USA* 85: 5693, 1988).

Somatically heritable DNA methylation patterns, which are tissue- and species-specific, are maintained by the activity of a CpG dinucleotide-specific DNA methyltransferase (Bird, A. et al. *Cell* 40: 91, 1985; Holliday, 1987). Changes in DNA methylation patterns occur primarily during gametogenesis and cellular differentiation (Holliday, 1987). However, alterations in DNA methylation patterns have been reported in spontaneous and chemical-induced tumors, as well as in immortalized cell lines. In addition, the exposure of cell lines to many carcinogens can alter their 5-methylcytosine pattern, which in turn could result in aberrant gene expression contributing to the establishment of a transformed phenotype (Jones, 1990). These alterations may involve, in part, an increase in the activity of the DNA methyltransferase enzyme (Baylin, S. B. et al. *Cancer Cells* 3: 383, 1991).

A microassay has been developed recently to determine the activity of DNA methyltransferase in cell lysates (Adams, R. L. P. et al. *J. Biochem. Biophys. Methods* 22: 19, 1991). Briefly, cells (200-20,000) are incubated for 2 h at 37°C with 3 µCi of ³H-S-adenosyl methionine and 0.5 µg poly[d(I-C) - d(I-C)]. The incubation is stopped by protease digestion, and the product DNA is isolated by phenol extraction and ethanol precipitation. The DNA solution is transferred to a paper filter where it is immobilized by trichloroacetic acid and ethanol washes. The dried filter is transferred to a counting vial with 1 mL 0.5 M perchloric acid and heated at 60°C for 1 h to solubilize the DNA prior to the addition of scintillation fluid and counting. Enzyme activity is then expressed as dpm/10⁶ cells or dpm/µg total cellular protein.

Studies in our laboratory will determine whether heterogeneity exists within the mouse and rat lung for constitutive DNA methyltransferase activity. Enzyme activity will be determined in alveolar macrophages, type II cells, and Clara cells isolated from the F344 rat and A/J and C3H mice. After determining the constitutive activity of this enzyme in pulmonary cells, the effect of exposure to carcinogens on enzyme activity will be assessed. Our initial studies have focused on optimizing this assay to determine enzyme activity in NIH 3T3 cells and alveolar macrophages isolated by pulmonary lavage from the F344 rat and A/J and C3H mice. The total cellular protein present in these cell lysate samples was first quantitated using the Bradford protein assay (Bradford, M. M. *Anal. Biochem.* 72: 248, 1976). Cell lysate samples ranging in total protein concentration from 0-5 µg were then assayed for methyltransferase activity to establish the linear assay range for each cell type. As shown in Figure 1, enzyme activity in the rat macrophages was linear in the range of 0.25 to 1 µg of protein which corresponds to 1,000 to 10,000 cells per assay. Enzyme activities of 3,500 dpm/µg and 420 dpm/µg protein were observed for rat macrophages and NIH 3T3 cells, respectively. As shown in Table 1, our preliminary data suggest similar respective endogenous methyltransferase activities in macrophages, Clara cells, and type II cells isolated from A/J and C3H mice.

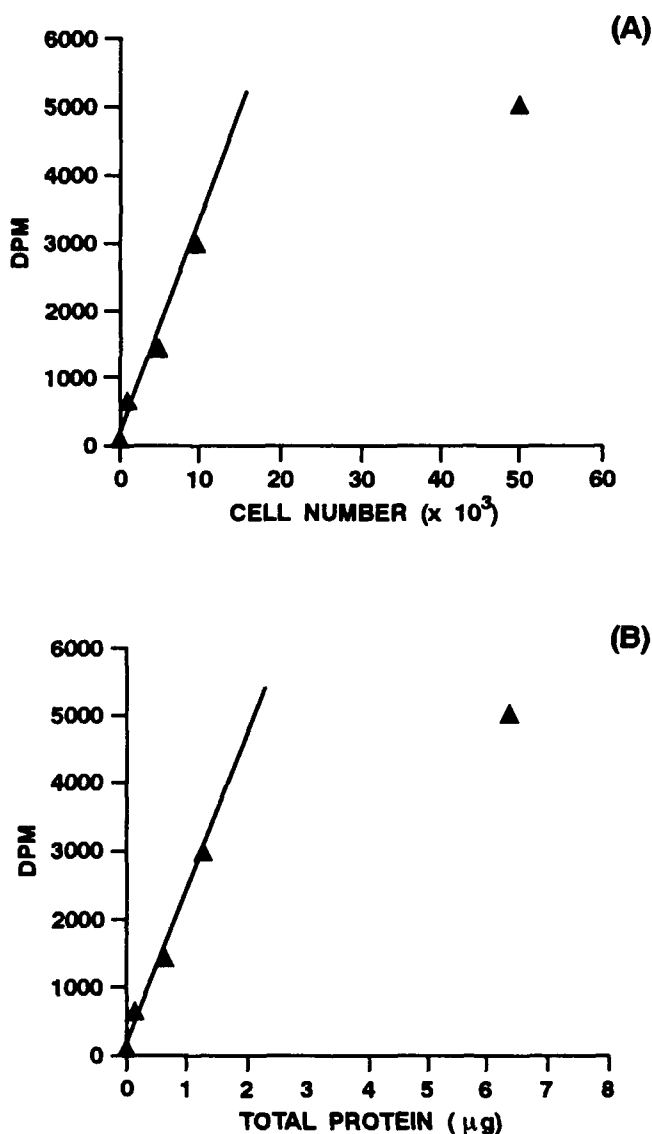


Figure 1. DNA methyltransferase activity in alveolar macrophages from the F344 rat. Methyltransferase activity is depicted in cell lysates as a function of cell number (A). Enzyme activity is also expressed as a function of total cellular protein present over the range from 0 to 6.5 μg (B).

Table 1

Methyltransferase Activity in
A/J and C3H Mouse Lung Cells

	DPM/ μg Total Cellular Protein	
	A/J	C3H
Macrophages	470	485
Clara cells	19	10
Type II cells	45	70

(Research sponsored by the Office of Health and Environmental Research, U. S. Department of Energy, under Contract No. DE-AC04-76EV01013.)

FLOW CYTOMETRIC ANALYSIS OF MICRONUCLEUS INDUCTION FOLLOWING X IRRADIATION

A. W. Hickman and N. F. Johnson*

Exposure of cells to ionizing radiation or chemicals can result in the formation of micronuclei. Quantitation of micronucleus formation can be used to assess genetic damage. However, scoring micronuclei by traditional light microscopy is a time-consuming process. Because of this, the number of cells scored for micronuclei (typically 100-500 cells) may not be sufficient to detect small numbers of cells with micronuclei. In addition, small micronuclei may be indistinguishable from nonspecific debris in the cell. This study was undertaken to implement a flow-cytometric technique for quantifying micronucleus formation (adapted from Schreiber, G. A. *et al.* *Cytometry* 13: 90, 1992).

A lung epithelial cell strain previously isolated from male F344 rats and characterized by Li *et al.* (*Toxicology* 27: 257, 1983) was plated at a density of 2×10^6 per 225-cm² tissue culture flask. After 24 h, plated cells were exposed to graded doses of X rays (0, 0.1, 0.25, 0.5, 1.0, 2.5, 5.0, or 7.5 Gy) delivered by a Picker Vanguard Console Therapy Unit (Picker X-Ray Corp., Cleveland, OH). Brooks *et al.* (*Int. J. Radiat. Biol.* 58: 799, 1990) have shown that X-ray doses of 0.75 Gy will induce micronucleus formation. Cells were allowed to grow an additional 24 h following exposure and were then treated with 3 µg cytochalasin B/mL medium to block cytokinesis.

After a further 24 h of incubation, cells were harvested. A portion of the cells was fixed in a solution of 3:1 methanol:acetic acid, and a portion was stained with equal amounts of ethidium bromide (10 µg/mL) and ethidium bromide (10 µg/mL)-Hoechst 33342 (1.5 µg/mL) dye solutions for flow cytometric analysis.

Fixed cells were air-dried on glass slides, stained with Diff-Quik (Baxter Healthcare Corp., Miami, FL), and scored for micronuclei by light microscopy; at least 1000 main nuclei, with associated micronuclei, were counted per slide. Cells stained for flow cytometric analysis were analyzed using a FACSTAR⁺ (Becton Dickinson, San Jose, CA), with dual lasers adjusted to the 488 nm line and the 351-363 nm UV multilines. Micronuclei were distinguished from debris of similar size by comparing the relative fluorescence intensity from the ethidium bromide to that from the Hoechst 33342 and to emissions excited by energy transfer from the Hoechst to the ethidium bromide. Only particles having fluorescence ratios similar to those for main nuclei, identified by their characteristic small-angle scatter, were counted as micronuclei.

Scorings of micronuclei (as percentage of all DNA-containing particles) by light microscopy and flow cytometry are compared in Figure 1. A linear relationship ($r^2 = 0.996$) between the two was observed, although there was not a one-to-one correspondence between values obtained by the two methods. The discrepancy may result from the inability to distinguish between small micronuclei and debris using light microscopy. In addition, a linear dose-response relationship was observed between radiation dose to the cells and micronucleus induction scored by flow cytometry (Fig. 2).

The results of this study indicate that this assay is useful for quantitating micronucleus induction following exposure to X rays. The assay allows rapid counting of nuclei and micronuclei, facilitates counting large numbers of cells, and allows discrimination of micronuclei from debris. The assay has the potential for use in a variety of studies of genotoxicity involving exposure to both ionizing radiations and chemicals.

*UNM/ITRI Inhalation Toxicology Graduate Student

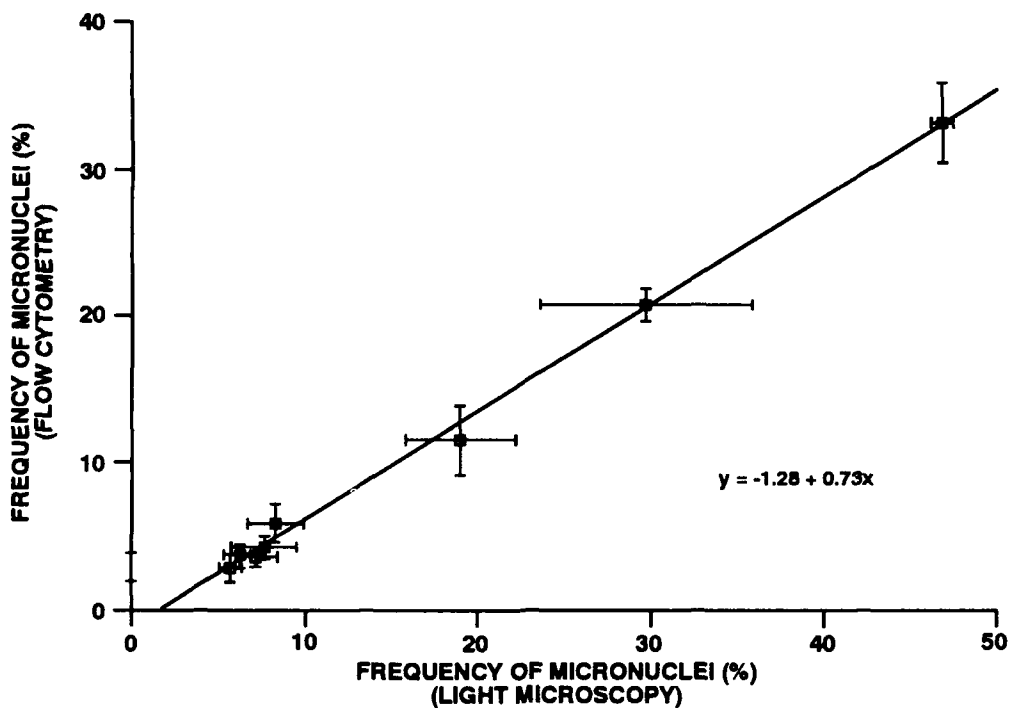


Figure 1. Comparison of micronucleus scoring by light microscopy and flow cytometry. Results are expressed as micronuclei as a percentage of all DNA-containing particles. Results are means \pm standard errors of the means for three scorings by each method; $r^2 = 0.996$.

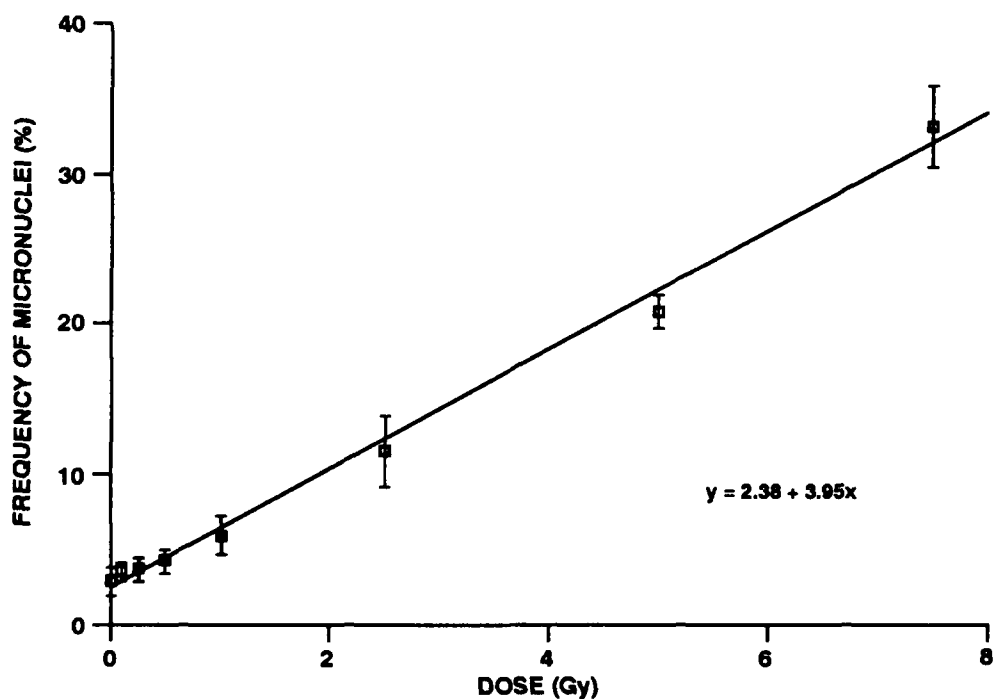


Figure 2. Micronucleus formation following X irradiation, as determined by flow cytometric analysis. Results are expressed as micronuclei as a percentage of all DNA-containing particles. Results are mean \pm standard error of the mean for three scorings; $r^2 = 0.994$.

(Research sponsored by the Office of Health and Environmental Research, U. S. Department of Energy, under Contract No. DE-AC04-76EV01013.)

CHARACTERIZATION OF INTRON SEQUENCES FLANKING THE CONSERVED REGIONS OF THE p53 TUMOR SUPPRESSOR GENE IN THE F344 RAT LUNG

S. A. Belinsky and S. Wachocki

Over the past decade, considerable progress has been made in the identification of genetic dysfunctions present in human lung cancers. The activation of proto-oncogenes, inactivation of tumor suppressor genes, chromosomal deletions, and alterations in growth factor pathways have been detected in varying degrees in small cell and nonsmall cell lung cancers (Bergh, J. C. S. *Am. Rev. Respir. Dis.* 142: S20, 1990). One frequent alteration identified in human lung cancers is the inactivation of the p53 tumor suppressor gene. Inactivation of the p53 gene often occurs via a single-point mutation within the conserved regions of this gene (exons 5-8) (Chiba, I. and J. D. Minna. *Oncogene* 5: 1603, 1990). Mutations within the p53 gene have been detected in approximately 40% of human adenocarcinomas (Chiba and Minna, 1990; Rodenhuis, S. *et al.* *Cancer Res.* 48: 5738, 1988; Kishimoto, V. *et al.* *Cancer Res.* 52: 4799, 1992) and in 65% of tumors of squamous cell phenotype. At present, the mechanisms resulting in the mutation of this gene have not been well defined. The majority of mutations detected in exons 5-8 of the p53 gene are G to T transversions (Chiba and Minna, 1990). In a recent study of 19 lung tumors from uranium miners exposed to radon and tobacco smoke (Vahakangas, K. H. *et al.* *The Lancet* 339: 576, 1992), mutations within p53 were detected in 9 of 19 tumors. However, none of the mutations were G to T transversions, and none occurred at the hotspot codons described previously for lung cancers. These results suggest that the mutational spectrum associated with inactivation of this tumor suppressor gene in lung tumors from uranium miners may be related to the genotoxic effects of radon. Moreover, it is apparent that the mechanisms underlying the inactivation of the p53 gene may be influenced by exposure to different carcinogens in the environment. At present, studies have not examined the prevalence for mutations within p53 in rodent lung tumors. However, recent reports have demonstrated the inactivation of this gene in kidney, and esophageal, nasal, and Zymbal gland tumors induced in the rat (Ohgaki, H. *et al.* *Cancer Res.* 52: 2995, 1992; Makino, H. *et al.* *Proc. Natl. Acad. Sci. USA* 89: 4850, 1992; Recio, L. *et al.* *Cancer Res.* 52: 1, 1992).

Mutations within p53 have been found at many different nucleotides within exons 5-8 and recently at the splice donor site for introns 4 and 7 (Soudon, J. *et al.* *Leukemia* 5: 917, 1991; Sameshima, Y. *et al.* *Biochem. Biophys. Res. Comm.* 173: 697, 1990). The methods of single strand conformation polymorphism (Orita M. *et al.* *Proc. Natl. Acad. Sci. USA* 86: 2766, 1989) and direct sequencing (Tindall, K. and L. Stankowski. *Mutat. Res.* 220: 241, 1988) are routinely used to screen and identify mutations within this gene. Both of these methods rely on the amplification of specific gene fragments by the polymerase chain reaction (PCR) (Saiki, R. K. *et al.* *Science* 239: 487, 1988). Thus, in order to create PCR primers flanking key exons and their splice sites, it was necessary to characterize the intron sequences bordering these conserved regions of the rat p53 gene. Intronic sequences were obtained by PCR amplification of p53 exons 4-6 or 6-9 from rat genomic DNA using primers located within these exons. Sequencing primers were then constructed within each exon to sequence in either the 5' or 3' direction. The PCR and sequencing primers used for this study are shown in Table 1. Complete sequences were obtained for introns 5 and 8, while 91 base pairs beginning at the 3' end of intron 4 were identified. Intron 7 was sequenced from the 5' and 3' ends. Approximately 90 bases within the middle of this intron were not sequenced. Intron 6 was not found in the rat as shown from the sequence of a PCR product produced by amplification using primers localized within introns 5 and 7. Primers based within these introns will now be used to amplify DNA from lung tumors previously induced in the F344 rat by beryllium, diesel exhaust, carbon black, and X rays. These PCR products will be used to determine the prevalence and specificity for mutations within exons 5-8 of the p53 gene. These studies could help in determining more accurate risk factors for exposure to fuel emissions, ionizing radiation, and occupational carcinogens.

Table 1

Exon Amplification and Sequencing Primers of Exons 5-8 of the p53 Gene

DNA Sequence	Exon	Application	DNA Strand
5'-TTACCAAGGCAACTATGGCTTCCAC-3'	4	Amplification	Sense
5'-ATGCGAATTCTACTCAATTCCCTCAATAAGCTG-3'	5	Amplification	Sense
5'-CTCAGGTGGCTCATACGGTACCAC-3'	6	Amplification	Antisense
5'-ATGCGAATTCCCTTAAGGGTGAATATTCTCCATC-3'	9	Amplification	Antisense
5'-CTGGGCTTCCTGCAG-3'	4	Sequencing	Sense
5'-TGTCTTCGCCAGCTG-3'	5	Sequencing	Antisense
5'-GTCGTGAGACGCTGC-3'	5	Sequencing	Sense
5'-CTGGAGTCTTCCAGC-3'	7	Sequencing	Antisense
5'-TCCGACTATACCACT-3'	7	Sequencing	Sense
5'-ACAAACACGAACCTC-3'	8	Sequencing	Antisense
5'-AAGAAGAGCATTGCC-3'	8	Sequencing	Sense

(Research sponsored by the Office of Health and Environmental Research, U. S. Department of Energy, under Contract No. DE-AC04-76EV01013.)

EXAMINATION OF THE K-ras PROTO-ONCOGENE IN LUNG TUMORS INDUCED IN THE F344 RAT BY X RAYS

S. A. Belinsky, C. E. Mitchell, and F. F. Hahn

The activation of proto-oncogenes has been implicated in part for the development of many human cancers (Bishop, *J. M. Science* 235: 305, 1987). Several proto-oncogenes and their products have been found either to be mutated, amplified, rearranged, or overexpressed in human lung cancer (Gazdar, A. F. *Curr. Opin. Cell Biol.* 2: 321, 1990). The activation of one proto-oncogene, the K-ras gene, is detected as a point mutation generally localized to codon 12, 13, or 61 (Barbacid, M. *Ann. Rev. Biochem.* 56: 780, 1987). Mutation of this gene has been observed in approximately 30% of human adenocarcinomas of the lung (Rodenhuis, S. *et al. Cancer Res.* 48: 5738, 1988). In addition, activation of this gene is detected in 100% of lung tumors induced in the A/J mouse lung by a variety of carcinogens (Belinsky, S. A. *et al. Cancer Res.* 49: 5305, 1989; You, M. *et al. Proc. Natl. Acad. Sci.* 86: 3070, 1989). The mutational specificity observed in these mouse lung tumors was compound-specific, and in general, reflected the predicted base mispairing properties of the individual DNA adducts generated during carcinogen activation. In the rat, the prevalence for activation of the K-ras gene appears to be compound dependent. Activation of this gene was detected in 100% of lung tumors induced by tetranitromethane (Stowers, J. *et al. Cancer Res.* 47: 3212, 1987), an oxidant used in rocket fuel, while none of the lung tumors induced by NNK contained an activated ras gene (Belinsky, S. A. and M. W. Anderson. *Proc. Am. Assoc. Cancer Res.* 31: 778, 1990). Finally, activation of the K-ras gene is observed in approximately 40% of 239 plutonium-induced rat lung tumors (Stegelmeier, B. L. *et al. Mol. Carcinog.* 4: 43, 1991). Mutational specificity within codon 12 of the K-ras gene was observed with both tetranitromethane (GGT to GAT) and plutonium (GGT to AGT). Thus, these studies indicate that (1) activation of the K-ras gene is involved in the development of some lung tumors in the rat and (2) that the activating mutational profile could provide mechanistic information about the individual compound.

Studies underway here are examining the carcinogenicity in rats from X rays delivered by either whole-body or thoracic exposure. Lung tumors have been induced following exposure to either single or fractionated doses of X rays. The purpose of this study was to determine whether activation of the K-ras gene is involved in the development of X-ray-induced lung tumors in the F344 rat. Initially, nine lung tumors, collected from moribund sacrifices were selected for analysis. Details of the tumor type, dose regime, and exposure are shown in Table 1. DNA was isolated by digestion with Pronase in 1% sodium dodecyl sulfate, followed by phenol-chloroform extraction and ethanol precipitation. Samples were incubated with RNase T1 (100 units) and RNase A (300 units) for 3 h at 37°C, and DNA was recovered by ethanol precipitation. These tumors were screened by a restriction fragment length polymorphism (RFLP) assay, which uses the polymerase chain reaction (PCR) and digestion of amplified DNA by a restriction enzyme to select for mutations present in the first or second position of codon 12 (Kahn, S. M. *et al. Oncogene* 6: 1079, 1991). This analysis can detect one mutant allele in the presence of 1×10^4 wild-type alleles compared to direct sequencing which detects mutant alleles at a frequency of one in five normal alleles. The key to this technique lies in the construction of the 5' sense first exon primer. This primer is constructed to include a C residue instead of the normal G at the first position of codon 11. Amplification of the normal K-ras allele using this primer creates a BstN1 restriction enzyme cleavage site (CCTGG) overlapping the first two nucleotides of codon 12. The amplification of a K-ras mutant at either the first or second position of codon 12 does not create this BstN1 site. To further enhance the sensitivity of this assay, a second PCR is performed to selectively reamplify the mutant species which is left uncut by BstN1. This second PCR is useful for the detection of mutant alleles and also enables identification of the specific K-ras mutation by direct sequencing. Following digestion again with BstN1, DNA fragments are resolved by separation on a 4% agarose gel or an 8% acrylamide gel. Wild-type K-ras first exon is detected as a cleaved fragment of 87 base pairs, while a single, 116 base-pair fragment is observed for the mutant allele (Fig. 1).

The nine lung tumors induced by X rays were examined for mutations within codon 12 of the K-ras gene by the BstN1 RFLP assay. DNA from a lung tumor containing a K-ras codon 12 GGT to GAT mutation was used as a positive control (Fig. 1, lane 10). None of the tumors induced by X-ray exposure appeared to contain a mutation within codon 12 (Fig. 1). In addition, preliminary results from direct sequencing of exon 1 from these tumors have not detected mutations in codon 13. Studies are in progress to examine codon 61 in exon 2 and to increase the sample number to include a total of 14 adenocarcinomas and 20 squamous cell carcinomas.

Table 1
Lung Tumors Induced in the F344 Rat by X rays

Animal No.	Tumor Type Diagnosis	Dose Regime ^a	Total Dose (cGy)	Exposure
S156-3898	Adenocarcinoma	10 x 35	350	Thoracic
S620-4611	Adneocarcinoma	10 x 60	600	Whole body
U635-4613	Adenocarcinoma	10 x 60	600	Whole body
T133-3902 ^b	Adenocarcinoma	10 x 35	350	Thoracic
X404-3920 ^b	Adenocarcinoma	10 x 400	400	Thoracic
T242-4324	Adenosquamous carcinoma	10 x 60	600	Thoracic
I007-4674	Squamous cell carcinoma	1 x 600	600	Whole body
I149-4508	Squamous cell carcinoma	2 x 200	400	Whole body
U166-3906	Squamous cell carcinoma	10 x 35	350	Thoracic

^aDose regimens were conducted as either a single dose or as 2 or 10 fractionated doses.

^bThese two adenocarcinomas were observed to invade the pleural surface of the lung.

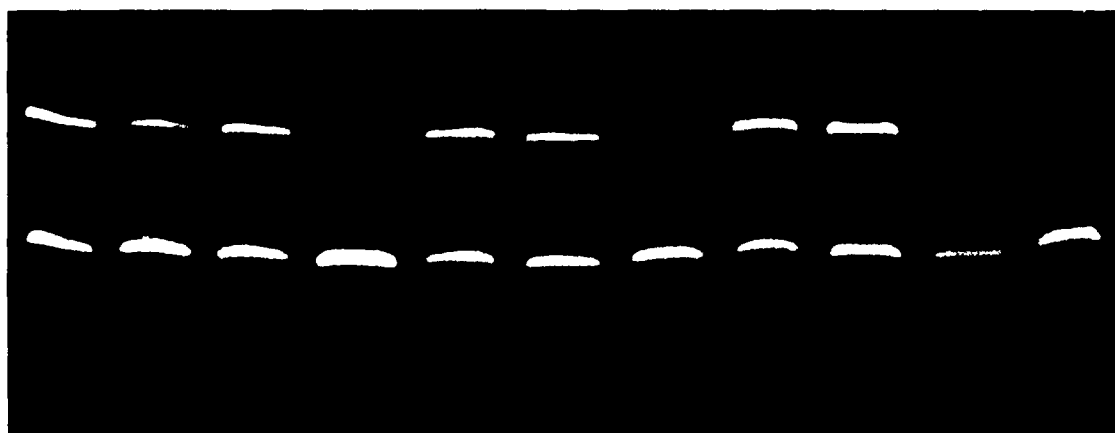


Figure 1. Evaluation of X-ray-induced lung tumors for mutations in codon 12 of the K-ras gene by the BstNI restriction polymorphism assay. Detection of codon 12 mutations is indicated by the band corresponding to 116 base pairs. Bands visible at 87 and 50 base pairs represent wild-type K-ras allele and primer dimers, respectively. Lanes 1-9 are DNA samples from nine X-ray-induced lung tumors. Lane 10 represents a DNA sample (rat lung tumor) containing a GGT to TGT mutation, and lane 11 is a negative control containing wild-type (W) rat lung DNA.

(Research sponsored by the Office of Health and Environmental Research, U. S. Department of Energy, under Contract No. DE-AC04-76EV01013.)

COMPARATIVE PULMONARY TUMORIGENICITY OF NNK AND BERYLLIUM IN STRAIN A AND C3H MICE

S. A. Belinsky, K. J. Nikula, and G. L. Finch

The overall objective of this study is to use inbred strains of mice sensitive (A/J) and resistant (C3H) to lung tumor formation (Malkinson, A. M. *Toxicology* 54: 241, 1989) in order to generate preneoplastic, benign, and malignant lesions. To identify the phenotypic differences and progressive alterations. The lesions will be involved in susceptibility for the development of cancer. Two model compounds are being used to induce lung tumors in A/J and C3H mice. 4-(methyl-N-nitrosamino)-1-(3-pyridyl)-1-butanone (NNK), a potent genotoxic carcinogen in rats and mice (Belinsky, S. A. et al. *Cancer Res.* 50: 3772, 1990; Belinsky, S. A. et al. *Cancer Res.* 49: 5305, 1991) and a major constituent of tobacco (Hoffmann, D. et al. *Cancer Res.* 39: 81, 1979), and beryllium, an inorganic compound classified as a nongenotoxic carcinogen because it is generally negative in short-term genotoxicity assays (e.g., Ames test) (Asby, J. et al. *Mut. Res.* 240: 217, 1990). Although the epidemiological evidence implicating beryllium in the induction of lung tumors is weak, various studies in experimental animals have demonstrated the pulmonary carcinogenicity of beryllium, which is currently classified as a suspect human carcinogen (U.S. EPA/600/8-84/026F, 1987). In addition, people who inhale beryllium can contract a lung disease characterized by granulomatous lung lesions and beryllium-specific, cell-mediated immune responses (Kriebel, D. et al. *Am. Rev. Respir. Dis.* 137: 464, 1988). Recent studies at ITRI are finding that exposure of F344/N rats by inhalation to a single dose of beryllium metal (50 µg initial lung burden) results in pulmonary inflammation and up to an 80% incidence of tumors over the rats life span (this report, p. 112). At present, the tumorigenic potency of beryllium metal in the mouse is unknown. The mechanism of neoplastic induction by beryllium remains to be elucidated, but could involve disrupting the fidelity of DNA synthesis by inhibiting DNA polymerase α . Affecting the fidelity of DNA transcription could lead to a marked increase in spontaneous damage to DNA and the activation or inactivation of critical genes leading to cell transformation.

Although repeated administration of NNK induces tumors in the C3H mouse, the size, multiplicity, and latency of the tumors differ considerably from those observed in the more sensitive A/J mouse (Devereux, T. R. et al. *Carcinogenesis* 12: 299, 1991). One hypothesis being addressed in these studies is that affecting genomic stability by decreasing the fidelity of DNA synthesis will increase the susceptibility for lung tumor development. This hypothesis is being evaluated by comparing lung tumor incidence and multiplicity in A/J and C3H mice following exposure to NNK, to tumor incidence in mice exposed to beryllium. If the mechanism of neoplasia by beryllium involves marked changes in genomic stability through effects on the fidelity of DNA polymerase α (Sirover, M. A. et al. *Proc. Natl. Acad. Sci. [USA]* 73: 21332, 1976), this effect should enhance tumor susceptibility in the resistant C3H strain as assessed by a greater tumor multiplicity and increased tumor size, compared with tumors induced by NNK.

A total of 928 mice are being used in this study (Table 1). A total of 184 A/J and 184 C3H/HeJ mice (6-8 wk old, female) were exposed in December 1991 to a single dose of beryllium metal by inhalation. Animals were exposed nose-only to beryllium at a concentration of 1 gm/m³ for approximately 60 min. Eight mice per exposure run (three runs were required to expose all the mice) were sacrificed 7 days after exposure to quantitate group mean initial lung burdens of beryllium. Initial lung burdens resulting from these exposures were approximately 60 µg for the A/J and 70 µg for the C3H mice, lung burdens which resulted in an 80% tumor incidence in the F344/N rat. A/J and C3H mice received NNK (50 mg/kg, i.p.) three times a week for 7 wk, a protocol known to induce tumors in these strains. Interim sacrifices of 10 mice per group at 20, 28, 36, 44, and 52 wk following exposure to beryllium or initiation of NNK treatment are in progress. In addition, 70 mice per exposure are being held for moribund sacrifices anticipated to occur at 14 to 24 mo after initiation of the study (Table 1). To date, no excess mortality over controls has been observed in any of the exposure groups.

Lung sections have been examined histologically from A/J and C3H mice sacrificed 20, 28, and 36 wk following beryllium exposure. A moderate to marked, multifocal, granulomatous pneumonia was observed in all mice of both strains. The pneumonia was characterized by accumulation of macrophages, neutrophils in alveoli, proteinaceous debris, and interstitial inflammatory cell infiltrates. Alveolar epithelial hyperplasia was associated with the inflammatory lesions. The severity of the lesions progressed from 20 to 28 wk post-exposure but appeared to have reached a plateau in most mice by the 36-wk time point. Pulmonary adenocarcinomas were observed

in histologic sections from two of the A/J mice sacrificed 36 wk after beryllium exposure. In mice sacrificed 20 wk after the initiation of NNK treatment, multiple tan nodules (1-2 mm, 9-48/lung), most likely representing hyperplastic lesions and adenomas, were detected on the surface of lungs from A/J mice. No lesions were grossly observed on the surface of lungs from C3H mice.

Table 1
Experimental Design

Study	A/J Mouse			C3H Mouse		
	Control ^a	NNK	Beryllium	Control ^a	NNK	Beryllium
Interim Sac. ^b	50	90	90	50	90	90
Terminal Sacrifice ^c	50	70	70	50	70	70
Beryllium Analysis ^d	0	0	24	0	0	24
Total Animals	100	160	184	100	160	184

^aFifty A/J and 50 C3H mice will be exposed to filtered air (sham controls for beryllium exposure). Fifty A/J and 50 C3H mice will be treated for 7 wk (3 times per wk) with saline (vehicle for the NNK injections).

^bTen treated animals from each group will be sacrificed 20, 28, 36, 44, and 52 wk after initiation of the study.

^cAnimals will be subjected to a moribund sacrifice with the study terminating approximately 24 mo after the initiation of treatment. An additional 8 animals per compound and timepoint are included for cell proliferation endpoints.

^dSacrifice to determine internal lung burdens of beryllium.

In previous work, the K-ras gene was activated in lung tumors induced by NNK in both the A/J and C3H mouse. The activating mutation detected was a GC to AT transition in codon 12 (Belinsky, S. A., 1989; Devereux, T. R., 1991). This mutation is consistent with the formation of the O⁶-methylguanine adduct generated by the metabolism of NNK. Mutational specificity for activation of the K-ras gene has also been observed with a variety of carcinogens such as benzo(a)pyrene, ethylnitrosourea, and urethane (You, M. *et al. Proc. Natl. Acad. Sci. [USA]* 86: 3070, 1989). Thus, identifying the specific activating mutation present within the K-ras gene provides some information concerning the mechanisms for tumor initiation by specific carcinogens. Therefore, the mechanism by which beryllium activates the K-ras gene will be examined in lung tumors from A/J mice and from C3H mice if tumors are generated.

The rapid development of tumors in the A/J mouse compared to the C3H mouse suggests that factors controlling the proliferation of preneoplastic cells must be involved in tumor development. This issue will be addressed by determining and comparing cell turnover in hyperplastic, benign, and malignant tumors from the sensitive A/J and resistant C3H mouse strains. Cell proliferation is being assessed in a separate group of animals at each interim sacrifice. Multiple injections of 5'-bromodeoxyuridine are being used to label cells in the S phase of eight mice from each treatment group and five control mice. Lungs from these mice are subsequently fixed; and immunohistochemistry and morphometry are used to quantitate cell proliferation. In addition, heterogeneity for cell proliferation among lesions at a specific stage of development (e.g., adenoma) will be compared within a given lung and a specific group of animals.

Tissues from this study will provide the foundation for numerous studies initiated over the next 2 yr. These studies will focus on the role of tumor suppressor genes (e.g., p53, Rb) in determining susceptibility for development of murine lung cancer, in regulating transcription of the K-ras gene, and in evaluating the role of endogenous DNA methylation in the control of gene transcription and suppressor gene function with regard to tumor progression.

(Research sponsored by the Office of Health and Environmental Research and the Assistant Secretary for Defense Programs, U. S. Department of Energy, under Contract No. DE-AC04-76EV01013.)

ROLE OF *MCM3* IN REGULATING THE CELL CYCLE

G. Kelly and T. R. Carpenter*

Alterations in the tumor-suppressor gene p53 are the most common genetic alterations observed in human tumors. Genes controlling the cell cycle and the tumor-suppressor gene p53 are interrelated (Cowell, J. K. *Semin. Cancer Biol.* 1: 437, 1990). Over-expression of wild-type p53 protein arrests the growth of osteosarcoma cells in G₁ (Diller, L. *et al. Mol. Cell. Biol.* 10: 5772, 1990), and the p53 gene product is phosphorylated by the enzyme p34^{cdc2} kinase *in vitro*. p34^{cdc2} is a serine-threonine kinase which must be active before DNA synthesis (G1/S boundary) or mitosis (G2/M boundary) (Nurse P. and Y. Bisset. *Nature* 292: 558, 1981). Therefore, the phosphorylated p53 protein may play a role in regulating the cell cycle (Bishoff, J. R. *et al. Proc. Natl. Acad. Sci. USA* 87: 4766, 1990).

Recently, Richardson *et al.* (*Genes Dev.* 4: 1332, 1990) used sequence information from homologous regions of the *S. cerevisiae* and *S. pombe* p34^{cdc28/cdc2} genes to amplify the corresponding human homologue of this gene with degenerative Polymerase Chain Reaction (PCR) primers that span the conserved sequences of the gene. We are adopting a similar approach using sequence information from several vertebrate organisms (Hollstein, M. D. *et al. Science* 253: 49, 1991; Soussi, T. *et al. Oncogene* 5: 945, 1990) to design degenerative PCR primers that should allow us to amplify a yeast analogue of the p53 tumor-suppressor gene. Initial efforts will use the primers specific for these regions of conserved amino acid sequence to amplify areas of the yeast genome with a sequence similar to p53.

In our laboratory, a battery of six degenerate PCR primers that span the conserved regions of vertebrate p53 proteins was designed and synthesized. These primers were then used to amplify genomic DNA fragments from *S. cerevisiae* and *S. pombe* genomes. The primer sets that spanned homology domains III-IV and IV-V amplified fragments of approximately 200 and 140 base pairs, respectively, from both *S. cerevisiae* and *S. pombe* DNA. The size of the PCR product corresponded to the expected distance between these homology domains.

The *S. cerevisiae* degenerate PCR product spanning homology domains IV-V was cloned into Bluescript plasmids using standard techniques (Ausubel, F. M. *et al.* [eds.]. *Current Protocols in Molecular Biology*, John Wiley and Sons, New York, NY, 1987). This PCR product, designated clone9, was used to identify a 4.5 kb clone (designated as 16F6) from an *S. cerevisiae* genomic library. Transfection of the 16F6 clone, which is on a high copy number episomal yeast plasmid, into *S. cerevisiae* (strain DH10) resulted in small colonies consisting of large cells with small buds. This phenotype is morphologically similar to the phenotype observed when the human p53 cDNA is over-expressed in *S. cerevisiae* (Nigro, J. M. *et al. Mol. Cell. Biol.* 12: 1357, 1992). DNA sequence analysis of both clone9 and the genomic clone 16F6 showed that the degenerate primers designed to span the p53-conserved boxes IV-V also amplified similarly sized fragment from the yeast gene *MCM3* (minichromosome maintenance 3). *MCM3* encodes a protein of 971 amino acids and is located on the left arm of chromosome 5 between the *cyc7* and *rad23* genes (Mang, G. T. *et al. Genetics* 106: 365, 1984). Temperature-sensitive mutants of *MCM3* exhibit a cell-cycle arrest phenotype consistent with incomplete replication of the yeast genome (Gibson, S. *et al. Mol. Cell. Biol.* 10: 5707, 1990). A comparison of the rat p53 amino acid sequence in region IV-V with the corresponding region of *MCM3* using the Bestfit® sequence homology comparison software (GCG Sequence Analysis Software Package, Madison, WI) showed that the two areas share a 49% amino acid sequence similarity and a 28% amino acid sequence identity. By comparison, the same regions in the rat p53 and salmon p53 proteins shared 88% similarity and 86% identity. This comparison of the p53 and the *MCM3* amino acid sequences indicates that although the two genes share sufficient nucleotide sequence homology to account for the degenerative PCR amplification of the *MCM3* gene with p53 specific primers, the conserved amino acid domains of mammalian p53 proteins are not readily apparent in *MCM3*.

The *MCM3* protein is about three times the size of p53 and lacks a central proline rich domain that is a hallmark of p53. However, *MCM3* and p53 do share a number of significant characteristics. *MCM3* and p53 are both active in late G₁ and appear to regulate entry into the S phase of the cell cycle (Zakut-Houri, R. *et*

*UNM/ITRI Inhalation Toxicology Graduate Student

al. EMBO J. 4: 1251, 1985). *MCM3* is phosphorylated by p34^{cdc2} kinase as is p53 (Johnson, L. H. and N. F. Lowndes. *Nucleic Acids Res.* 20: 2403, 1992). *MCM3* appears to regulate the initiation of replicative DNA synthesis as does p53, and finally both proteins have acidic amino termini, basic carboxy ends, and contain putative nuclear localization signals. These properties suggest *MCM3* may be a functional analogue of the mammalian p53 protein.

We are subcloning the *MCM3* gene into a mammalian expression vector to test our hypothesis that the *MCM3* gene can function as an analogue of p53. Specifically, we will ask the question, "Will *MCM3* mimic the action of p53 in human cells?" The yeast genomic clone 16F6 we isolated contains a 4.6 kb insert of yeast DNA. Restriction mapping of the 16F6 clone will be used to identify a smaller portion of the insert containing the entire *MCM3* open reading frame for subcloning into a mammalian cell expression vector such as λpCEV27-lacZ' (Miki, T. *et al. Proc. Natl. Acad. Sci. USA* 88: 5167, 1991). This vector is designed for high level stable expression in eukaryotic cells and has been kindly provided by Dr. S. A. Aaronson, Laboratory of Cellular and Molecular Biology, National Cancer Institute. The ability of wild-type p53 to suppress transformation has been shown in several cell model systems (Berger, M. S. *et al.* In *Oncogenes and Cancer* [S. A. Aaronson *et al.*, eds.], Japan Sci. Soc. Press/UNU Sci. Press, Utrecht, Netherlands, p. 183, 1987; Tolmach, L. J. *et al. Radiat. Res.* 71: 653, 1977; Smerdon, M. J. *et al. Biochemistry* 18: 3732, 1979), including the osteogenic sarcoma derived Saos-2 cell line, which is null for endogenous p53 (Chen, P. H. *et al. Science* 250: 1576, 1990). Transfection of wild-type p53 into Saos-2 cells suppresses their neoplastic phenotype as measured by the formation of soft agar colonies and tumorigenicity in nude mice (Chen *et al.*, 1990). We will transfet the yeast gene *MCM3* into Saos-2 cells (ATCC® HTB-85) and determine the tumorigenicity of the resulting clones in a nude mouse assay. These activities will characterize the extent to which *MCM3* is functionally analogous to human p53.

(Research sponsored by the Office of Health and Environmental Research, U. S. Department of Energy, under Contract No. DE-AC04-76EV01013.)

IDENTIFICATION OF YEAST ANALOGUES OF p53 BY ASSOCIATION WITH THE SV40 LARGE T ANTIGEN

G. Kelly, T. R. Carpenter*, and N. F. Johnson

DNA is the target for radiogenic transformation, and cell division shortly after exposure to radiation is essential for fixation of DNA damage (Borek, C. *Adv. Cancer Res.* 37: 159, 1982). The irradiated cells normally arrest DNA replication to allow time for DNA repair (Tolmach, L. J. *et al. Radiat. Res.* 71: 653, 1977; Smerdon, M. J. *et al. Biochemistry* 18: 3732, 1979; Painter, R. B. and B. R. Young. *Proc. Natl. Acad. Sci. USA* 77: 7315, 1980). This replication arrest appears to be mediated by the p53 tumor suppressor gene product. Cells lacking a normal p53 are deficient in DNA repair and are more likely to accumulate mutations and chromosomal rearrangements (Lane, D. P. *Nature* 358: 15, 1992). This latter supposition suggests that in radiation-induced tumors, the inactivation of genes regulating DNA replication and repair (i.e., p53 and associated cell-cycle controlling genes) may be an early event which results in genetic instability and an increased risk of alterations in dominant oncogenes.

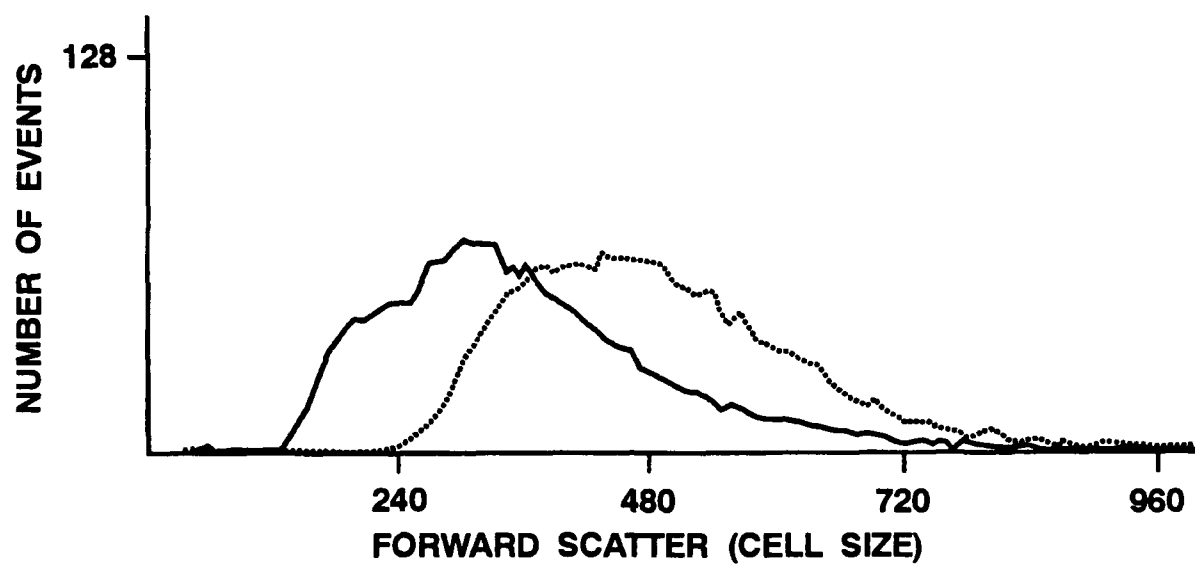
Because of the links between p53, radiation-caused DNA damage and carcinogenesis, the biochemical functions of the p53 tumor-suppressor gene are being examined. These efforts are concentrated on a yeast model because yeast cells are readily amenable to genetic manipulations. In addition, much of our current knowledge of genes controlling the cell cycle has been obtained by studying strains of yeast that exhibit aberrant cell-cycling phenotypes. However, none of these investigations to date have identified a yeast equivalent to the mammalian p53 gene. On the other hand, the product of the human p53 gene suppresses the growth of two species of yeast, *S. pombe* and *S. cerevisiae* (Bischoff, J. R. *et al. Mol. Cell. Biol.* 12: 1405, 1992; Nigro, J. M. *et al. Mol. Cell. Biol.* 12: 1357, 1992). In addition, the growth suppression activity in *S. pombe* is dependent on the *in vivo* phosphorylation of the human gene product by the endogenous yeast cell-cycle regulatory protein p34^{cdc2} kinase (Bischoff *et al.*, 1992). These observations strongly suggest that one or more proteins with a significant degree of structure-function similarity must exist in the two species.

p53 was originally discovered as a protein that bound to the SV40 large T antigen (SV40 LT) (Schmleg, F. I. and D. Simmons. *Virology* 164: 132, 1988). This approach has been adopted as a route to identifying a yeast analogue of the p53 tumor suppressor gene. A construct containing the SV40 LT antigen under control of the inducible *gall* promoter has been cloned and transfected into *S. cerevisiae*. Expression of the SV40 LT antigen in these cells has been confirmed by Western blot analysis using anti-SV40 LT antigen antibody. Flow cytometric analyses indicate that yeast cells expressing the SV40 LT have a shortened G₁ portion of the cell-cycle (Fig. 1) and a reduced mode cell size, which can be reversed when the transcription from the *gall* promoter is inhibited (Fig. 2). These observations suggest that expression of the SV40 LT antigen in *S. cerevisiae* causes a premature commitment to cell cycling (Hartwell, L. H. *et al. Science* 183: 46, 1974; Sorsburg, S. L. and P. Nurse. *Ann. Rev. Cell Biol.* 7: 227, 1991). A premature commitment would be expected if the SV40 LT bound negative regulators of the yeast cell-cycle like a p53 analogue. Complexes between the SV40 LT antigen and endogenous yeast proteins will be identified by immunoprecipitation and polyacrylamide gel electrophoresis. We anticipate that a number of yeast proteins will complex with the SV40 LT antigen and co-precipitate with antibodies to that antigen, because the mammalian equivalents of these proteins behave in this manner. These proteins may include the yeast equivalents of the catalytic subunit of DNA polymerase- α (Dornreiter, I. *et al. EMBO J.* 9: 3329, 1990), the product of the retinoblastoma susceptibility gene (RB-1) (Cowell, J. K. *Sem. Cancer Biol.* 1: 437, 1990), p53 (Schmleg and Simmons, 1988), and p120 (Ewen, M. E. *et al. Cell* 58: 257, 1989).

Sequence analysis of the yeast proteins that complex with the SV40 LT antigen will identify endogenous proteins that may serve as models of tumor suppressor gene products. Functional evidence for a tumor suppressive phenotype will be obtained by introducing yeast genes that encode these proteins into tumorigenic mammalian cells lacking an endogenous p53 gene and measuring reversion of tumorigenicity. These data will enable us to examine the role of these genes in the regulation of the cell-cycle. Furthermore, this information will allow us to predict how dysfunctions in these genes lead to uncontrolled cellular replication which is a hallmark of the neoplastic phenotype.

*UNM/ITRI Inhalation Toxicology Graduate Student

(A)



(B)

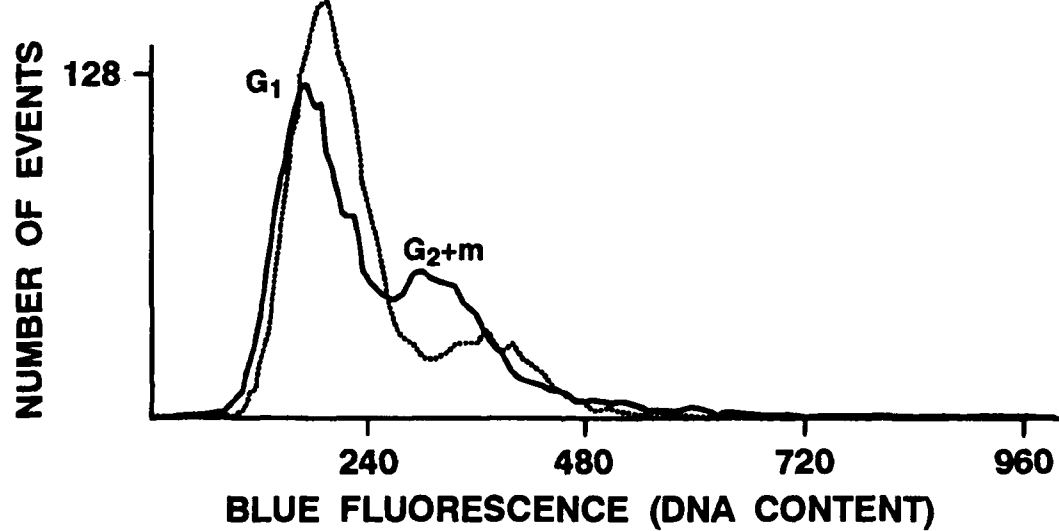


Figure 1. Flow cytometric analysis of SV40 LT antigen activity in *S. cerevisiae*. Panel A, forward light scatter measuring cell size. Panel B, propidium iodide fluorescence measuring DNA content. Solid line cells, expressing the SV40 LT antigen. Dashed line, cells not expressing the SV40 LT antigen.

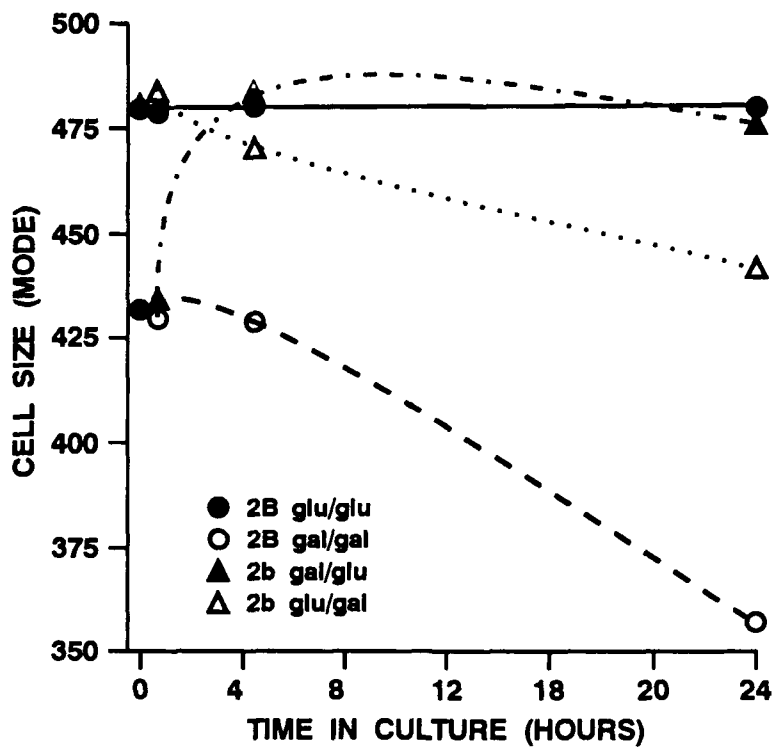


Figure 2. Effect of SV40 LT antigen on *S. cerevisiae* cell size. Mode cell size of yeast cells containing the SV40 LT antigen gene under control of the *gal1* promoter. Glu/Glu yeast cells grown overnight in glucose and resuspended in normal glucose media (●); Glu/Gal yeast cells grown overnight in glucose and resuspended in galactose-containing media (△); Gal/Glu yeast cells grown overnight in galactose-containing media and resuspended in glucose (▲); Gal/Gal yeast cells grown overnight in galactose and resuspended in galactose (○).

(Research sponsored by the Office of Health and Environmental Research, U. S. Department of Energy, under Contract No. DE-AC04-76EV01013.)

VI. NONCARCINOGENIC RESPONSES TO INHALED TOXICANTS

RESPONSE OF THE LUNG TO INSTILLED VERSUS INHALED PARTICLES

R. F. Henderson, K. E. Driscoll*, R. C. Lindenschmidt*,
J. R. Harkema, E. B. Barr, and I. Y. Chang

There is a need to evaluate the potential pulmonary toxicity of relatively insoluble airborne dusts generated in industrial or environmental settings. Such dust, if it is of a size that will deposit in the deep lung, will clear slowly and if inhaled chronically, can accumulate in the lung. The logical route of exposure for the study of the toxicity of such particles in animal models is by inhalation. However, because of the expense of setting up an inhalation exposure system for particles, many investigators choose to evaluate the pulmonary toxicity of particles by instillation of the particles via the trachea. The purpose of this study was to compare the response of rat lungs to instilled versus inhaled particles in order to evaluate the practice of using the instillation technique in particle toxicity studies.

The particles chosen for the study were α -quartz (Min-U-Sil, U. S. Silica, Berkeley Springs, WV), a known toxic particle, and TiO_2 (anhydrous powder, Fisher Scientific, Pittsburgh, PA), a particle of relatively low toxicity. Both particles are relatively insoluble in the lung. In the first study, female F344/N rats (11-15 wk of age) were exposed for 4 wk by inhalation to 0, 0.1, 1.0, or 10 mg/m^3 of one of the particles; lung burdens were determined by atomic absorption analyses in rats sacrificed 1 wk after the end of the exposures. Bronchoalveolar lavage fluid (BALF) analyses were performed at 1 wk, 8 wk, and 24 wk and histopathology evaluations at 24 wk after the end of the exposures. In the second study, the amounts of particles retained in the lungs of the inhalation-exposed rats at 1 wk after the end of the inhalation exposures were instilled as a saline suspension through the trachea into the lungs of another set of rats. Responses were measured by BALF analyses and histopathology at the same times after instillation as for the inhalation study.

Parameters measured in BALF included total and differential cell counts (to characterize the cellular inflammatory response), protein (as a marker of transudation of serum protein), lactate dehydrogenase (LDH) activity (as a marker of cell damage or lysis) and β -glucuronidase (β -glu) activity (as a measure of macrophage phagocytic activity or lysis).

The lung burdens of particles retained in the rats at the end of the inhalation exposures and the amount of instilled particles are shown in Table 1. Because there was no response to the inhaled TiO_2 , we matched the instilled lung burdens to those found in the quartz-exposed rats to aid in comparing the responses to the two types of particles by instillation.

Table 1

Lung Burdens of Particles in Rats Exposed by Inhalation or Instillation

Lung Burdens 1 Week After Inhalation Exposure ^a (μ g particle/g lung; $\bar{X} \pm SE$, n = 4)			Lung Burdens Instilled (μ g/lung)	
Exposure Conc. (mg/m^3)	TiO_2	SiO_2	TiO_2	SiO_2
0.1	4.4 \pm 1.5	52.7 \pm 16.7	50	50
1.0	72 \pm 32	203 \pm 28	200	200
10	440 \pm 100	760 \pm 100	750	750

^aExposures were 6 h/day, 5 days/wk for 4 wk.

*The Procter & Gamble Co., Cincinnati, Ohio

At lung burdens up to 750 µg TiO₂/lung by instillation or after inhalation of up to 10 mg/m³, 6 h/day, 5 days/wk for 4 wk, there were no significant changes in the BALF parameters at any time studied after the exposures. Thus, based on analysis of BALF, TiO₂ did not appear to be toxic as assessed by either method of exposure. Comparison of the histopathological response is in progress.

The comparison of the response of the lung to the α-quartz particles delivered by the two methods as measured by BALF parameters is shown in Table 2. The values are reported as total amounts of each parameter removed by lavage. The values from the instillation study, in which only the right lung was lavaged, were normalized for the whole lung based on historical data for the ratio of the weight of the right lung to the weight of the total lung in rats. The time course of the response to the quartz was similar whether the particles were instilled or inhaled, with an increase in most of the BALF parameters with time after exposure.

At the lowest lung burdens of α-quartz, there were no statistically significant responses for any of the parameters by either method of exposure. At the medium dose, statistically significant increases in polymorphonuclear leukocytes (PMN) were noted at 1 wk after the inhalation exposures ended and at 8 and 24 wk after the instillation. At the 1 wk observation time, the values for PMN were approximately the same by the two exposure methods, but the high values in the control rats that had been instilled with saline alone may have obscured any response that might have been due to quartz. Three BALF parameters (LDH, β-glu, and acid protease) were elevated at 24 wk after the inhalation exposure but not after the instillation exposure. Again, for one of these parameters, β-glu, the values in the BALF were almost the same for the two routes of exposure, but the baseline values were higher in the saline-instilled animals, causing the values in the quartz-instilled animals to be statistically indistinguishable from the control values. At the highest lung burdens, a few differences in the values that were statistically different by the two routes of exposure were observed, but in general, the changes in BALF were similar after instillation or inhalation exposure.

Comparing the response at equal lung burdens is difficult. One issue is the choice of the amount of particles to instill to mimic the inhalation exposure. We chose to instill the amount remaining in the lung at 1 wk after the end of the exposure as representative of the lung burden to which the lung would be responding after the exposure. It was recognized, however, that the amount of particles remaining in the pulmonary region at the end of the inhalation exposure was less than the total amount of particles deposited in that region, because a fraction would be cleared from this region during the 4-wk exposure. Nevertheless, an examination of the lavage fluid parameters indicates that an approximately equivalent response was obtained for most parameters for instilled lung burdens that simulated the lung burdens at the end of a 4-wk inhalation exposure. An exception was the neutrophil count. In most instances the neutrophil count was higher in the instilled animals. As noted above, the higher baseline for neutrophil counts in the control, saline-instilled rats potentially obscured a response at 1 wk after instillation.

The results of this study indicate, based on the BALF analyses, that a particle of low toxicity (TiO₂) in the lung was appropriately evaluated by either the inhalation or instillation study. The toxic particle (α-quartz) was clearly shown to induce an inflammatory response by either route of exposure, and the time course of the response was similar in both sets of animals. Despite some differences in significant responses to the medium dose, it is evident that one can estimate the approximate lung burden that will induce an inflammatory response by instillation techniques.

This study indicates that intratracheal instillation of particles is a useful approach to compare the relative pulmonary toxicity of relatively insoluble particles in terms of the acute inflammatory response and the potential for causing chronic pulmonary disease. Inhalation exposures are still essential for the study of the deposition patterns of inhaled particles and the rates of clearance of deposited particles. Studies designed to determine the lung burdens achieved by inhalation of airborne particles require the use of inhalation exposures as well. However, for comparing the relative inflammatory response of the lung to different types of insoluble particles or different industrial preparations of such particles and for certain mechanistic studies such as those reported earlier (Henderson, R. F. *et al. Toxicol. Appl. Pharmacol.* 109: 127, 1991), intratracheal instillation of particles can be a valuable tool.

Table 2
Response of Lung to Inhaled vs. Instilled α -Quartz, \bar{X} (SEM)^a

BALF Parameter	Weeks After Exposure	Control		Low		Medium		High	
		Inhaled		Inhaled		Inhaled		Inhaled	
		Inhaled	50 μg	0.1 mg/m ³	200 μg	1.0 mg/m ³	750 μg	10 mg/m ³	750 μg
PAM, 10 ⁶ cells	1	2.07 (0.36)	0.98 (0.08)	1.80 (0.34)	1.29 (0.18)	2.33 (0.65)	0.88 (0.12)	1.66 (0.18)	1.34 (0.15)
	8	1.68 (0.21)	1.16 (0.12)	1.44 (0.32)	0.75 (0.07)	1.44 (0.23)	NA ^b	1.53 (0.30)	2.09 (0.36)
	24	1.57 (0.23)	1.00 (0.09)	0.93 (0.16)	1.29 (0.21)	1.28 (0.06)	1.12 (0.11)	1.45 (0.17)	2.43* (0.40)
PMN, 10 ³ cells	1	46 (22)	2.6 (1.1)	80 (76)	3.7 (3.7)	41 (35)	43* (16)	39 (23)	190* (40)
	8	5.0 (3.0)	6.6 (3.1)	48 (25)	13.4 (7.3)	401* (73)	NA	877* (132)	180* (30)
	24	26 (19)	14.5 (5.1)	224 (111)	7.1 (3.2)	1190* (223)	28 (15)	2320* (450)	1680* (200)
LDH, IU	1	0.50 (0.05)	0.49 (0.02)	0.57 (0.11)	0.43 (0.01)	0.62 (0.05)	0.60 (0.17)	0.66 (0.06)	0.73 (0.03)
	8	0.26 (0.06)	0.57 (0.03)	0.30 (0.05)	0.41 (0.01)	0.50 (0.06)	0.82 (0.07)	0.79* (0.10)	1.03 (0.19)
	24	0.34 (0.04)	0.50 (0.05)	0.40 (0.03)	0.58 (0.03)	0.63 (0.02)	1.02* (0.04)	1.30* (0.12)	2.00* (0.10)
β -Glu, mIU	1	1.54 (0.64)	1.70 (0.20)	2.53 (0.67)	1.60 (0.20)	2.00 (0.41)	1.30 (0.10)	3.44 (0.52)	1.40 (0.10)
	8	0.82 (0.21)	1.60 (0.20)	1.44 (0.29)	1.50 (0.10)	1.93 (0.44)	2.00 (0.30)	3.88 (1.47)	1.50 (0.30)
	24	0.95 (0.31)	0.80 (0.10)	1.69 (0.49)	0.8 (0.10)	3.88 (0.87)	4.20* (0.20)	18.2* (2.8)	17.2* (2.5)
Protein, mg	1	2.19 (0.28)	2.10 (0.10)	2.27 (0.32)	2.50 (0.10)	2.45 (0.23)	2.20 (0.10)	2.29 (0.25)	2.40 (0.10)
	8	1.98 (0.26)	1.80 (0.10)	2.29 (0.15)	1.90 (0)	2.60 (0.22)	2.00 (0.10)	2.99* (0.09)	2.10 (0.20)
	24	1.58 (0.17)	2.20 (0.10)	1.98 (0.25)	2.00 (0.20)	2.55 (0.20)	2.50 (0.20)	4.06* (0.43)	4.00* (0.20)
Acid protease, μg Hb/4 h	1	323 (45)	380 (21)	330 (58)	260 (10)	348 (42)	340 (20)	367 (46)	380 (10)
	8	279 (25)	320 (17)	304 (13)	180 (1.0)	340 (22)	420 (20)	384* (27)	370 (20)
	24	294 (18)	340 (13)	287 (32)	360 (20)	315 (29)	460 (20)	498* (38)	670* (30)

*Values are total removed by lavage. The values for the instilled animals have been normalized to the whole lung.

^bNA - sample not available.

*Statistically different from control values by ANOVA using the Bonferroni correction for multiple comparisons, p < 0.05.

(Research sponsored by the Office of Health and Environmental Research, U. S. Department of Energy, under Contract DE-AC04-76EV01013 and the P & G Co. under FIA DE-FI04-87AL44004.)

INFLAMMATORY AND PROLIFERATIVE RESPONSES OF PULMONARY AIRWAY EPITHELIUM IN F344 RATS AFTER EXPOSURE TO BACTERIAL ENDOTOXIN

J. A. Hotchkiss, N. F. Johnson, S. A. Belinsky,
D. G. Thomassen*, J. F. Lechner, and J. R. Harkema

Endotoxins are lipopolysaccharide-protein molecules released from the walls of gram-negative bacteria. They are believed to be the principal agents responsible for the acute inflammatory response in gram-negative, bacteria-induced pneumonias. Airway infections induced by endotoxin-producing bacteria are often characterized by an influx of neutrophils and excessive production and secretion of mucus from airway mucosa.

We have previously shown that repeated airway instillations of endotoxin results in an increase in the amount of intraepithelial mucosubstances, secretory cell hyperplasia, and excess luminal mucus in pulmonary airways of rats (Harkema, J. R. and J. A. Hotchkiss. *Am. J. Pathol.* 141(2): 307, 1992). The structural alterations observed in the airways of rats instilled with endotoxin are similar to the increased number of mucous (goblet) cells and hypersecretion of airway mucus that are important characteristics of human respiratory disorders, especially chronic bronchitis and cystic fibrosis.

The purpose of this study was to examine the early inflammatory and proliferative events that precede the development of endotoxin-induced, secretory cell hyperplasia/metaplasia in rat pulmonary airways. A total of 92 male F344/NTac rats (14 wk old) were briefly anesthetized with 5% halothane in O₂ and intratracheally instilled with 1.0 mg endotoxin (*E. coli* serotype 0111:B; Sigma Chemical Co., St. Louis, MO) in 500 µL sterile pyrogen-free saline (n = 50) or 500 µL of saline alone (n = 42). Rats were sacrificed 3, 6, 12, 24, 48, 96, or 168 h after intratracheal instillation. Two hours prior to sacrifice, all rats were intraperitoneally injected with bromodeoxyuridine (BrdU; 50 mg/kg body wt) to label nuclei of cells in the S-phase of the cell cycle. Rats were deeply anesthetized with 5% halothane in O₂ and killed by exsanguination. The lungs were removed and the left extrapulmonary bronchus temporarily clamped off, while the right lung lobes were lavaged with saline. The lavage fluid was recovered and analyzed for total and differential cell counts. The right extrapulmonary bronchus was tied off, and the right lung lobes were removed. The clamp on the left lung lobe was removed; and the left lung lobe was fixed with 10% neutral buffered formalin by intratracheal perfusion at a constant pressure of 30 cm of fixative. The right apical, cardiac, and intermediate lung lobes were rapidly frozen in liquid nitrogen then stored at -80°C for future RNA analyses. The right diaphragmatic lobe was inflated with a cryopreservative (1:1 saline:OCT tissue cryoprotectant), frozen in liquid nitrogen, and stored at -80°C. The left lobe was cut into 5-6 transverse slices approximately 5 mm thick taken perpendicular to the main (axial) intrapulmonary airway and processed for light microscopy.

We examined the main intrapulmonary airway at a level corresponding approximately to airway generation 5. Sections from the proximal face of the lung tissue block were stained with hematoxylin/eosin and Alcian Blue (pH 2.5) for light microscopic quantitation of intraepithelial neutrophils (expressed as neutrophils/mm basal lamina), with Alcian Blue (pH 2.5)/Periodic Acid Schiff's sequence for determination of the volume density (Vs; nL mucosubstances/mm² basal lamina) of acidic and neutral intraepithelial mucosubstances, or were immunohistochemically stained to detect BrdU (BrdU-labeled nuclei/mm basal lamina).

Intraepithelial neutrophils in both saline- and endotoxin-instilled rats increased significantly (Fig. 1A). Intratracheal instillation of 500 µL of saline alone or the same volume of saline containing 2 mg/mL endotoxin resulted in an approximately 60-fold increase in intraepithelial neutrophils 3 h after instillation. By 96 h after instillation, the number of neutrophils migrating through the pulmonary airway epithelium had returned to control levels in both groups. Intratracheal instillation of endotoxin, but not saline alone, induced a significant increase in the number of BrdU-labeled airway epithelial cells 24 and 48 h after instillation (Fig. 1B). Compared to rats sacrificed 3 h after instillation, both saline alone and endotoxin induced a significant increase in intraepithelial mucosubstances (Fig. 1C). There was a significant increase in the volume density of stored mucosubstances

*Office of Energy Research, U. S. Department of Energy, Washington, District of Columbia

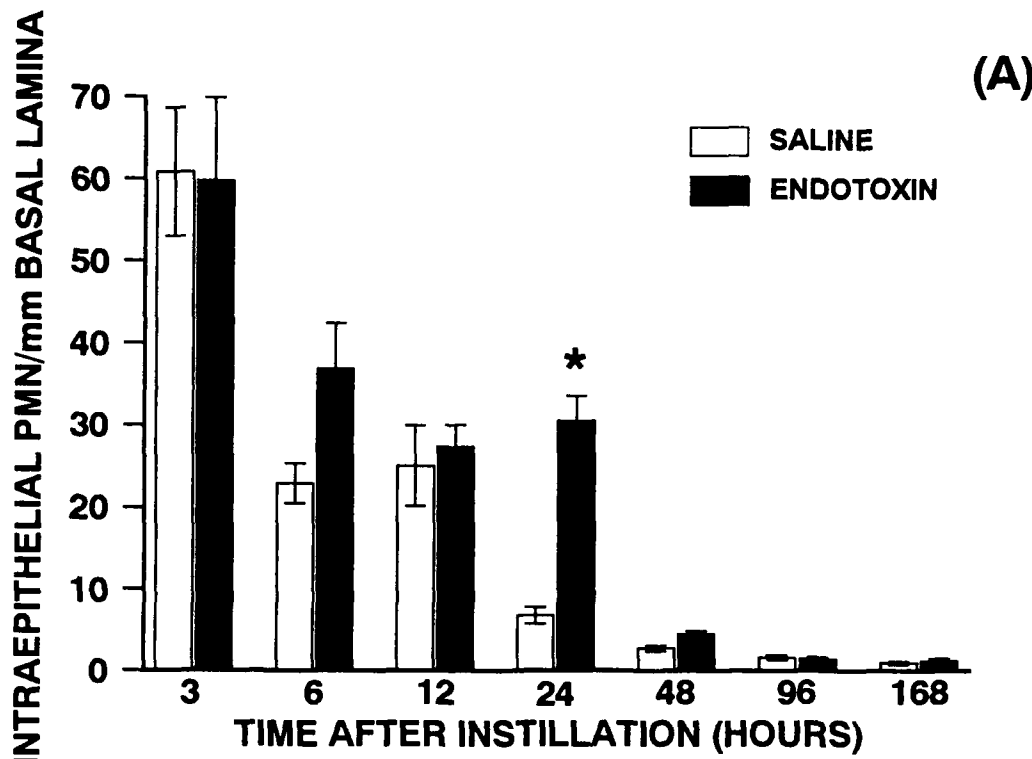


Figure 1A. Number of neutrophils within pulmonary airway epithelium per mm basal lamina in rats intratracheally instilled with saline or endotoxin in saline and sacrificed 3, 6, 12, 24, 48, 96, or 168 h after instillation. Bars indicate mean \pm SEM. * = significantly different than saline control ($p \leq 0.05$).

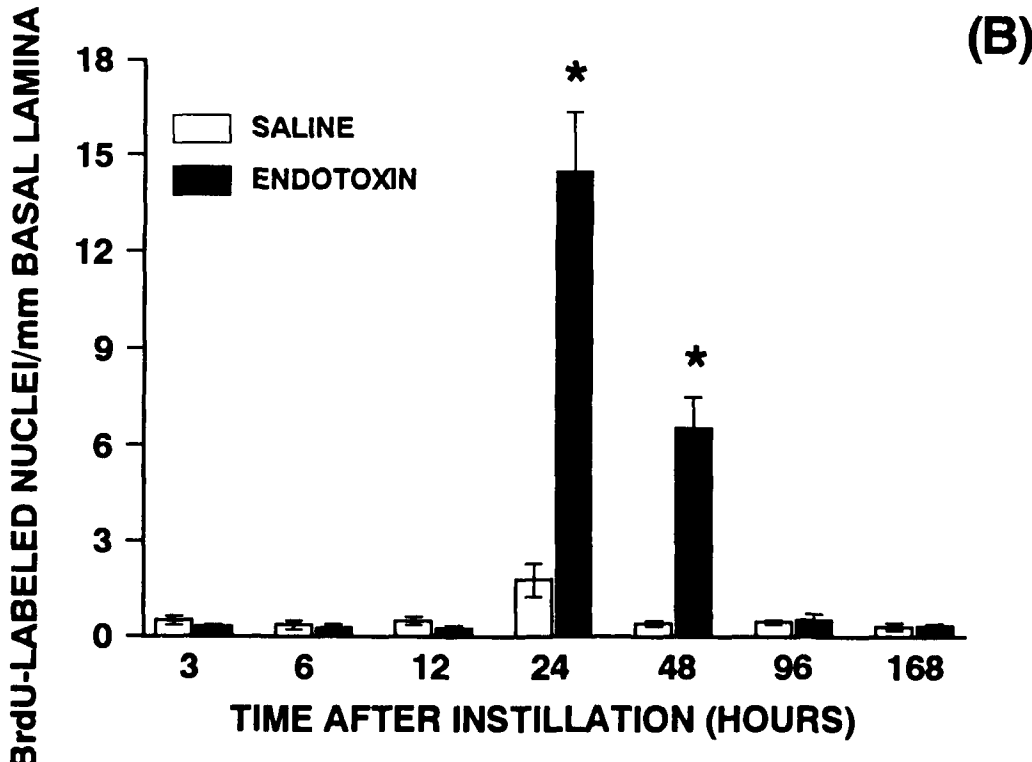


Figure 1B. Number of BrdU-labeled pulmonary airway epithelial cells per mm basal lamina in rats intratracheally instilled with saline or endotoxin in saline and sacrificed 3, 6, 12, 24, 48, 96, or 168 h after instillation. Bars indicate mean \pm SEM. * = significantly different than saline control ($p \leq 0.05$).

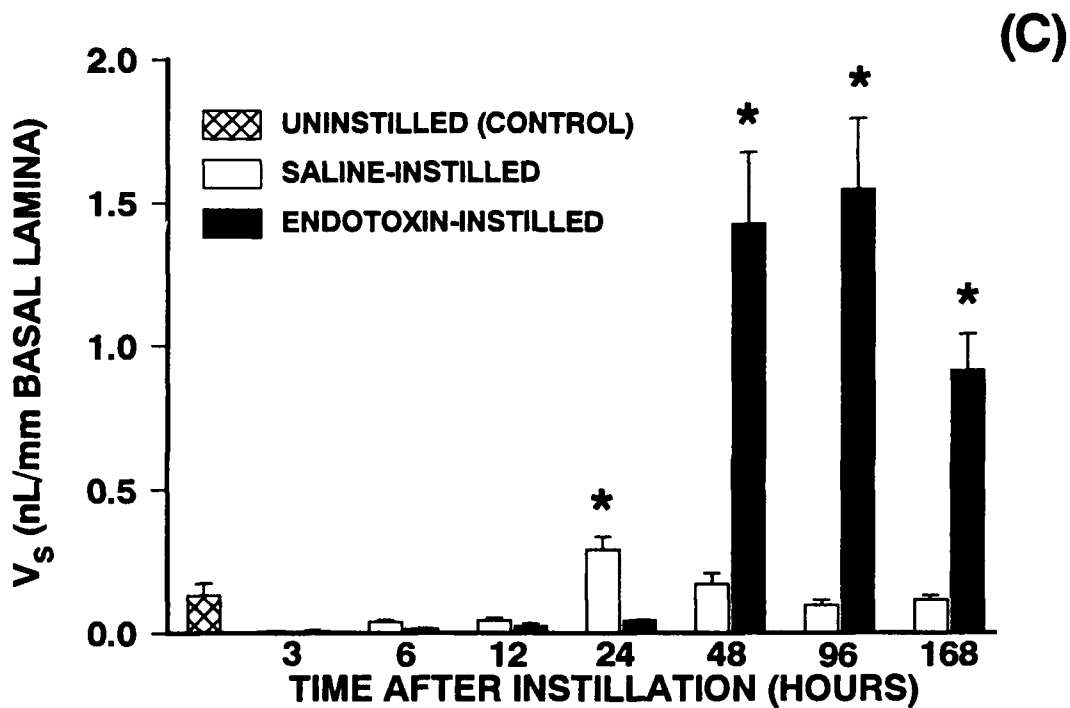


Figure 1C. Amount of stored mucosubstances in the surface epithelium of pulmonary airways of rats intratracheally instilled with saline or endotoxin in saline and sacrificed 3, 6, 12, 24, 48, 96, or 168 h after instillation. Bars indicate mean \pm SEM. * = significantly different than saline control ($p \leq 0.05$).

in saline-instilled rats at all sacrifice times after 12 h. Endotoxin instillation also induced a significant increase in stored mucosubstances, but the increase was observed later (48 h vs. 24 h), and it was approximately 10-fold greater than in saline-instilled rats.

In this study, we have examined the early inflammatory and proliferative responses of rat pulmonary airways during the development of endotoxin-induced, secretory cell metaplasia/hyperplasia. A single intratracheal instillation of 1.0 mg of endotoxin resulted in a rapid but transient influx of neutrophils, a burst of airway epithelial cell proliferation, and a dramatic increase in intraepithelial mucosubstances. Although we did not enumerate the specific cell types present, we have previously shown that the increase in intraepithelial mucosubstances in pulmonary airways following repeated instillations of endotoxin was associated with an increase in the total number of mucous goblet cells as well as a decrease in the numbers of serous secretory cells (Harkema and Hotchkiss, 1992). Further studies are needed to determine if the serous cells which normally populate rat pulmonary airways can differentiate directly into mucous goblet cells and if the epithelial cells which proliferate in response to endotoxin instillation eventually differentiate into mucous goblet cells.

In the future, we will analyze the frozen tissues from this study to determine when and in which cells the airway mucin gene is expressed in response to endotoxin. These cellular and molecular analyses are being conducted to better characterize the toxicant-induced changes involved in the metaplastic process. Results from these studies will help us to understand the pathogenesis of mucous goblet cell metaplasia and may provide insight into methods of treatment of these common airway lesions.

(Research sponsored by the Office of Health and Environmental Research, U. S. Department of Energy, under Contract No. DE-AC04-76EV01013.)

RAT STRAIN AND SUBSTRAIN DIFFERENCES IN RESPONSE TO OZONE

R. F. Henderson, J. A. Hotchkiss, D. G. Burt, C. H. Hobbs, and J. R. Harkema

Animal models are used to determine dose-response relationships for inhaled toxicants, including ozone. Responses of the animals are used to predict potential responses in humans. If different animal models vary widely in their responses, it is difficult to use the animal data to predict toxicity for humans unless the mechanism for the differences in animal responses is known. Recently, strain differences have been reported in the response of mice to ozone (Kleeberger, S. R. *et al.* *Am. J. Physiol.* 258: L313, 1990). M. V. Pino *et al.* (*Am. Rev. Respir. Dis.* 143: A698, 1991) also reported that Wistar rats are more sensitive to ozone than Sprague-Dawley rats. The purpose of this study was to determine the sensitivity of F344/N rats to ozone for comparison with the earlier results reported for Wistar and Sprague-Dawley rats. In this study we compared the response of three different stock/strains of rats (Sprague-Dawley, Wistar, and F344/N) and F344/N rats from two sources (F344/N ITRI and F344/NTac) to ozone.

The rodents were exposed to ozone, and the pulmonary response was evaluated by histopathology and by analysis of bronchoalveolar lavage from the animals. The rats (6/group) were exposed in the Hazleton 2000 chambers to 0, 0.16 or 0.8 ppm ozone, 6 h/day for 1 or 7 days. The ozone concentration was monitored by a Dasibi monitor using probes in the breathing zone of the rats. Ozone was generated by an Erwin Sander Model IV Ozonizer.

Animals were killed 1 day after the last exposure by exsanguination via the renal arteries or abdominal aorta while the rats were under 5% halothane anesthesia. The heart/lung block was removed, the left lung was clamped off, and the right lung was lavaged twice with physiological saline. The volume of each wash fluid was adjusted for the size of the animal with 6 mL used for the F344/NTac, 7 mL for the F344/N ITRI, 8 mL for the Wistar, and 9 mL for the Sprague-Dawley rats. For each rat, the washes were combined and analyzed for total and differential cell counts as measures of the inflammatory response. The acellular supernatant from the lavage was analyzed for lactate dehydrogenase (LDH) activity as a measure of cytotoxicity and total protein as a measure of increased permeability of the alveolar/capillary barrier. The total amount of each analyte removed by the lavage was normalized per gram of lung for comparisons among the stocks/strains. The BALF data were analyzed by ANOVA with the Bonferroni correction factor for multiple corrections. A $p \leq 0.05$ was considered significant. The left lung was fixed at 30 cm water pressure with 10% neutral buffered formalin and processed for light microscopy.

In general, the control values (0 ppm ozone) for the lavage parameters were similar for all four stocks/strains/substrains studied (Table 1). The lavage fluid from control animals suggested that the F344/NTac rats had higher LDH activity in their lavage fluid than did the other animals, but the differences were not statistically significant except for the control LDH values at 7 days. Those LDH values were statistically higher in the F344/NTac rats than in any other group of control rats.

As has been observed in earlier studies, lavage fluid protein and neutrophil counts were sensitive indicators of the response to ozone. BALF parameters did not change significantly in response to 1 day of exposure to the low level of ozone in any of the animals, but the high level exposure induced an influx of neutrophils (PMN) and protein into the bronchoalveolar space (Table 1). The PMN influx was highest in the Wistar, F344/N ITRI, and Sprague-Dawley rats and much less in the F344/NTac rats. Protein influx was highest in the Wistar and F344/N ITRI rats and lowest in the F344/NTac rats with an intermediate influx in the Sprague-Dawley rats.

By 7 days of exposure, all of the animals had apparently adapted to some extent to the ozone exposure, and the lavage fluid values had returned to control levels for the high level-exposed rats. At the low level of exposure to ozone, apparently the adaptation was not complete, and protein values in BALF were slightly elevated in all stocks/strains/substrains. A time course study would have to be done in order to determine the time of the peak response to ozone at the different concentrations and to delineate the time course of the adaptive process. Histopathologic evaluations are still in progress.

Table 1

Changes in BALF in Response to Ozone^a
 $(\bar{X} \pm SE; n = 7)$

	One Day of Exposure			Seven Days of Exposure		
	Ozone, ppm	0	0.16	0.8	0	0.16
PAM, 10⁶ cells/g lung						
Wistar	1.77 ± 0.19	2.44 ± 0.26	2.91 ± 0.19 ^b	2.06 ± 0.42	2.54 ± 0.38	3.85 ± 0.44 ^b
F344/N ITRI	2.90 ± 0.25	2.77 ± 0.30	3.22 ± 0.22	1.86 ± 0.14	3.08 ± 0.48	3.56 ± 0.41 ^b
F344/NTac	1.91 ± 0.20	2.73 ± 0.21	3.73 ± 0.37 ^b	3.25 ± 0.44	3.03 ± 0.30	3.25 ± 0.29 ^b
Sprague-Dawley	1.48 ± 0.27	2.68 ± 0.32	3.03 ± 0.40	2.01 ± 0.27	2.69 ± 0.26	3.67 ± 0.62
PMN, 10³ cells/g lung						
Wistar	8 ± 5	37 ± 14	2180 ± 230 ^b	4 ± 3	4 ± 4	36 ± 14
F344/N ITRI	10 ± 5	216 ± 81	1750 ± 370 ^b	16 ± 6	19 ± 10	167 ± 30
F344/NTac	8 ± 8	8 ± 5	239 ± 57 ^b	21 ± 11	47 ± 26	57 ± 26
Sprague-Dawley	9 ± 4	32 ± 11	1950 ± 460 ^b	15 ± 9	9 ± 6	220 ± 207
LDH, mIU/g lung						
Wistar	190 ± 13	225 ± 17	322 ± 49	186 ± 27	186 ± 47	369 ± 41 ^b
F344/N ITRI	180 ± 27	190 ± 25	185 ± 43	209 ± 15	244 ± 26	305 ± 59
F344/NTac	263 ± 44	248 ± 24	153 ± 34	361 ± 35	242 ± 39	313 ± 23
Sprague-Dawley	169 ± 19	177 ± 31	278 ± 49	235 ± 25	146 ± 28	260 ± 30
Protein, mg/g lung						
Wistar	1.92 ± 0.06	2.01 ± 0.23	8.63 ± 1.14 ^b	2.02 ± 0.13	3.05 ± 0.17 ^b	1.98 ± 0.13
F344/N ITRI	1.48 ± 0.10	1.96 ± 0.20	8.20 ± 1.22 ^b	1.99 ± 0.14	3.82 ± 0.31 ^b	2.75 ± 0.32
F344/NTac	1.47 ± 0.20	1.63 ± 0.10	3.41 ± 0.22 ^b	2.39 ± 0.17	3.23 ± 0.18 ^b	2.04 ± 0.18
Sprague-Dawley	2.19 ± 0.13	2.08 ± 0.22	5.71 ± 1.04 ^b	1.69 ± 0.17	3.04 ± 0.23 ^b	2.16 ± 0.23

^aBALF = bronchoalveolar lavage fluid; LDH = lactate dehydrogenase activity; PAM = pulmonary alveolar macrophages;
 PMN = neutrophils. BALF values are the total amount of each parameter removed from the right lung divided by the net weight of the right lung (before lavage) in g.

^bValue differs from control, $p \leq 0.05$.

The distinct difference between the F344/N rats from two sources in their responses to ozone was unexpected and indicates that relatively subtle genetic and/or environmental factors may influence the response to ozone. Studies are planned to determine the mechanistic basis for the different sensitivities of the rats to ozone. Additional studies on the factors involved in animal susceptibility to ozone should help to clarify the mechanisms of ozone toxicity and to provide insight into how to identify ozone-susceptible persons in the human population.

(Research sponsored by the Office of Health and Environmental Research, U. S. Department of Energy, under Contract No. DE-AC04-76EV01013.)

STRAIN-RELATED DIFFERENCES IN OZONE-INDUCED SECRETORY METAPLASIA IN THE NASAL EPITHELIUM OF F344 RATS

J. R. Harkema, C. M. Wierenga*, L. K. Herrera, J. A. Hotchkiss,
W. A. Evans**, D. G. Burt, and C. H. Hobbs

Ozone is a common oxidant pollutant in urban centers. Approximately 25% of the United States population resides in areas that currently exceed the National Ambient Air Quality Standard (NAAQS) for ozone. Ozone exposure has been shown to induce increased DNA synthesis of the rat nasal epithelium within 24 h after exposure (Hotchkiss, J. A. and J. R. Harkema. *Toxicol. Appl. Pharmacol.* 114: 182, 1992). This is a response to oxidant injury within the nose that is restricted to the nasal transitional epithelium (NTE) lining the lateral wall and nasal and maxilloturbines in the proximal aspect of the rat nasal airway. With repeated exposures to ozone, the proliferative response attenuates as this epithelium differentiates into a secretory epithelium with numerous mucous cells containing acidic and neutral glycoproteins (Harkema, J. R. et al. *Toxicol. Pathol.* 17: 525, 1989). Because mucus is known to be an efficient anti-oxidant (Cross, C. E. et al. *Lancet* 1: 1328, 1984), the secretory metaplasia of the NTE induced by ozone (a potent oxidant) is believed to be an adaptive response of the tissue to protect itself from further ozone-induced injury (Harkema, J. R. et al. *Toxicologist* 11: A183, 1991).

Recently it has been reported that ozone-induced inflammatory and epithelial responses in the pulmonary airways of rats and mice vary among different strains (Kleeberger, S. R. et al. *Am. J. Physiol.* 258: L313, 1990; Pino, M. V. et al. *Am. Rev. Respir. Dis.* 143: A698, 1991). In the rat, ozone exposure causes more severe lung airway injury in Wistar rats than Sprague-Dawley rats (Pino et al., 1991). The effect of strain on the susceptibility of nasal epithelium to ozone-induced injury has not been examined. The purpose of the present experiment was to determine if ozone-induced secretory metaplasia is different among inbred strains/outbred stocks of rats. We hypothesize that there are significant differences in the response of NTE to repeated ozone exposures among various inbred strains/outbred stocks of rats.

Fifty-six male rats, 8-12 mo of age, were used in this study. The rats came from two different outbred stocks (Sprague-Dawley rats from Taconic, Germantown, NY, and Wistar rats from Charles River Laboratories, Wilmington, MA) and two inbred substrains of F344 rats (F344/N rats from the ITRI breeding colony and F344/NTac rats from Taconic, Germantown, NY). The rats were divided into two groups ($n = 7$) per strain/stock and were exposed to 0 or 0.8 ppm ozone in whole body chambers for 6 h/day for 7 days. The rats were anesthetized using 5% halothane and killed by exsanguination via the abdominal aorta or renal arteries, 24 h after the end of exposure. Immediately after death, the head of each rat was removed from the carcass and the nasal airways flushed retrograde with 10% neutral buffered formalin. The eyes, lower jaw, skin, and facial muscles were removed, and the head was immersed in a large volume of the same fixative for at least 24 h.

After fixation, the heads were decalcified using a 13% aqueous formic acid solution. After decalcification, the nasal cavity was transversely sectioned immediately posterior to the upper incisor teeth and through the incisive papilla of the hard palate (Fig. 1), as previously described by Young et al. (*Fundam. Appl. Toxicol.* 1: 309, 1981). The selected tissue block from the proximal aspect of the nose was embedded in paraffin, sectioned at 6 μ m, and stained with Alcian Blue (pH 2.4)/Periodic Acid Schiff (AB/PAS) for identification of acidic and neutral intraepithelial mucosubstances (IM). The volume density of AB/PAS-stained mucosubstance in the surface epithelium was determined by image analysis, as previously described (Harkema, J. R. and J. A. Hotchkiss. *Exp. Lung Res.* 17: 743, 1991). The method we used to estimate the volume of stored mucosubstance per unit surface area of epithelial basal lamina has been described by Harkema et al. (*Am. J. Pathol.* 128: 29, 1987). The data were expressed as the mean volume density/surface area (V_s ; nL/mm² basal lamina) of AB/PAS-positive mucosubstances within the NTE \pm the standard error of the mean (Fig. 2).

*Department of Energy/Associated Western Universities Summer Student Research Participant

**Postdoctoral Fellow

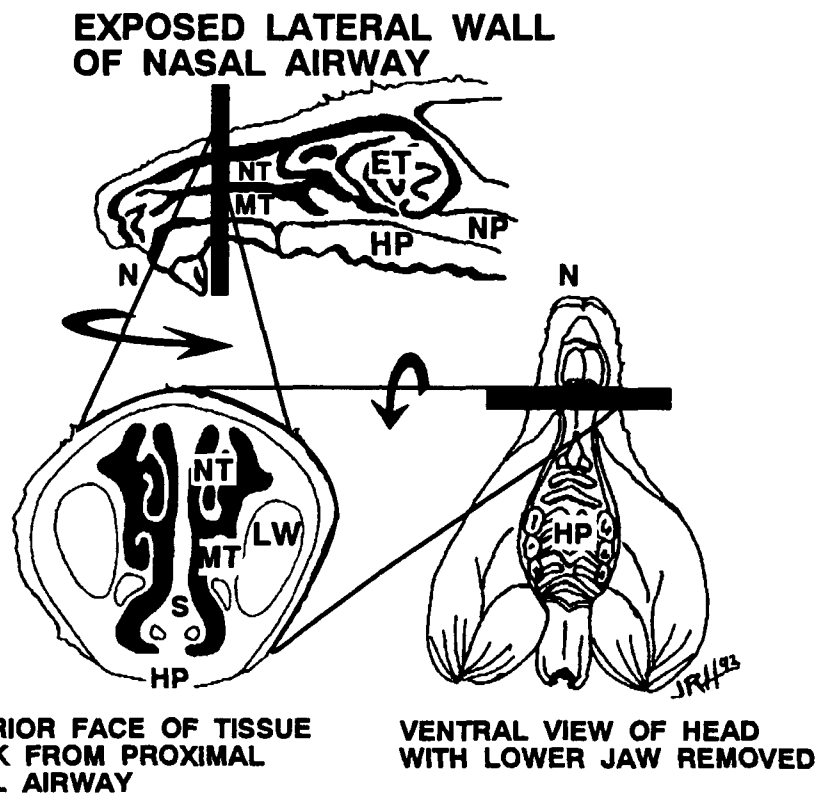


Figure 1. Diagrammatic representation of the location of the nasal tissue selected for morphometric analyses. The surface epithelium lining the maxilloturbinates (MT) was analyzed by image analysis for the amounts of histochemically stained mucus substances. NT = nasal turbinate; ET = ethmoid turbinates; HP = hard palate; N = naris; NP = nasopharynx; LW = lateral wall; S = septum; Bar = intranasal location of tissue block that was taken for quantitative analyses.

Amounts of IM in control rats were scant and not significantly different among the various strains/stocks of rats. Ozone-induced secretory metaplasia was present in all the strains/stocks of rats. All ozone-exposed animals had significantly more IM than air controls. The severity of the secretory metaplasia, however, varied among the ozone-exposed rat strains/stocks. Ozone-exposed F344/NTac rats and ozone-exposed Wistar rats had significantly more IM than the ozone-exposed F344/N rats from the ITRI colony and the ozone-exposed Sprague-Dawley rats (Fig. 2). The amounts of IM after exposure to 0.8 ppm ozone ranged from 0.87 ± 0.20 nL/mm² (mean \pm SEM) in Sprague-Dawley rats to 2.49 ± 0.38 nL/mm² in Wistar rats.

The reason for the strain/stock-related variability in the severity of ozone-induced secretory metaplasia in the NTE is unknown. The results of this study indicate that the Wistar rats and the F344/NTac rats are more sensitive to ozone exposure compared to the F344/N rats from the ITRI colony and the Sprague-Dawley rats. It is interesting that Pino *et al.* (1991) also found that Wistar rats were more sensitive to ozone-induced injury compared to Sprague-Dawley rats, when they examined the epithelium lining the lung centriacinarus. In addition, the results of the present study demonstrated that there can be substrain-related differences in response to ozone between F344/N rats from two different colonies. Ozone-induced secretory metaplasia was more pronounced (i.e., twice as much IM in the NTE) in F344/NTac rats than in F344/N rats from the ITRI breeding colony. These results raise questions about the most appropriate strain (or substrain) or stock of rat to be used in future animal toxicology studies designed to help establish a new NAAQS for ozone.

Individual variability in airway response to ozone is not limited to rats. Variability in pulmonary function responses to acute ozone exposures have been reported among human subjects (McDonnell, B. A. *Pharmacogenetics* 1: 110, 1991). By further investigating the genetic, cellular, and biochemical differences among the various rat strains/stocks in their response to ozone, we may better understand the underlying factors responsible for individual variability in ozone toxicity observed in humans.

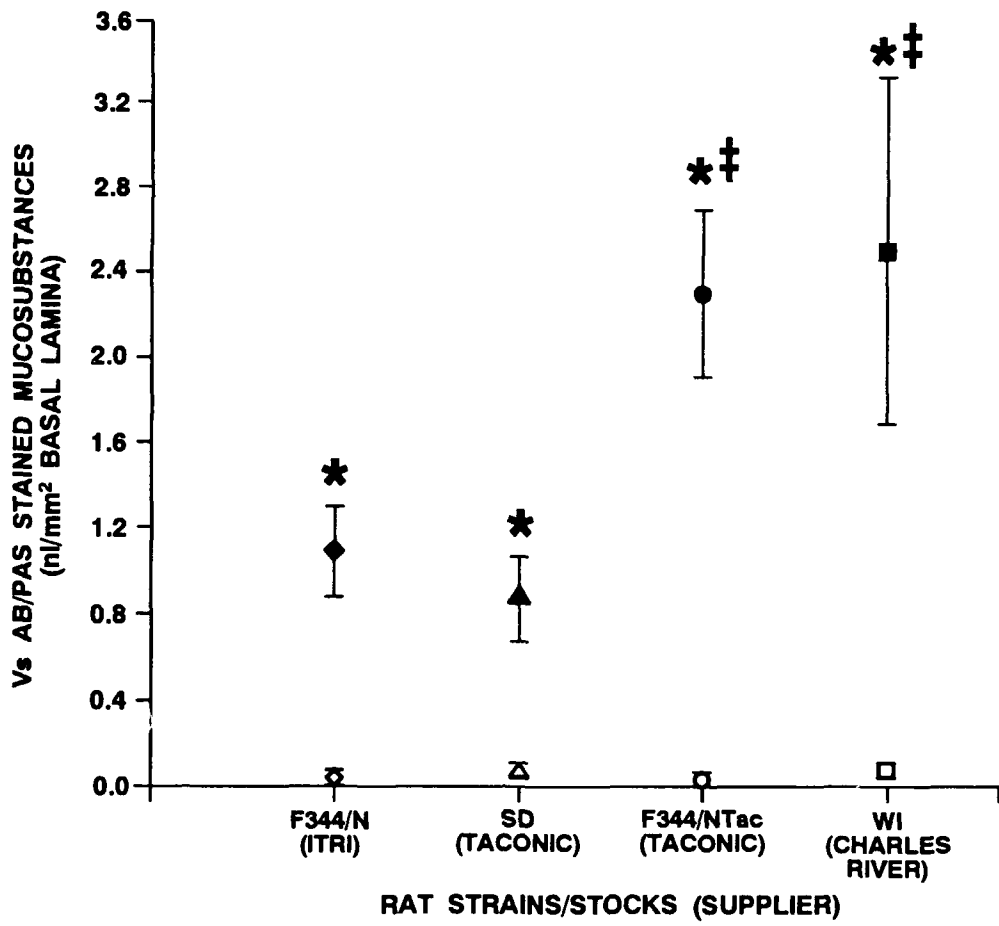


Figure 2. The amounts of intraepithelial mucosubstances in the maxilloturbinates of four different strains/stocks of rats after exposure to 0.8 ppm ozone (closed data points and bars = group means \pm standard error of the means) or 0 ppm ozone (open data points and bars = group means \pm standard error of the means). Vs = volume density of intraepithelial mucosubstances/surface area; * = significantly different from air-exposed (0 ppm) controls, $p < 0.05$; ‡ = significantly different from group means of ozone-exposed F344/N rats from ITRI colony and Sprague-Dawley rats exposed to ozone (SD), $p < 0.05$; WI = Wistar rats.

(Research sponsored by the Office of Health and Environmental Research, U. S. Department of Energy, under Contract No. DE-AC04-76EV01013.)

EFFECTS OF INHALED BERYLLIUM METAL ON C3H MOUSE LUNG CLEARANCE AND TOXICITY

G. L. Finch, M. D. Hoover, and K. J. Nikula

Beryllium (Be) metal is used in the nuclear power, aerospace, and electronics industries. The inhalation of Be may result in chronic beryllium disease, a progressive granulomatous lung disease. Furthermore, Be is a suspected human carcinogen, and our studies are demonstrating that Be is a lung carcinogen in rats (this report, p. 112). In addition, we are examining the acute and chronic inflammatory responses of rat lung tissue to Be, and we have described the amounts of Be metal in the lungs of rats required to retard the clearance of co-administered particles (1990-91 Annual Report, p. 167). To permit comparisons with data describing the effects of Be in rats, the study reported here evaluates the toxic effects of inhaled Be metal in mice.

We exposed groups of 34 female mice (C3H/HeJ; 11 ± 2 wk at exposure) to aerosolized Be metal in order to achieve target initial lung burdens (ILBs) of 0, 1, 4, 15, or 60 µg. On a lung weight-normalized basis, these levels represent the range of ILBs of Be metal previously examined in rats. To determine the effects of Be on lung clearance, we also exposed the mice to aerosolized ⁸⁵Sr-labeled fused aluminosilicate particles (⁸⁵Sr-FAP) immediately before the Be exposure. The Be metal was generated using a jet-o-mizer system (1986-87 Annual Report, p. 45), and the ⁸⁵Sr-FAP particles were generated using a Lovelace nebulizer (Newton, G. J. et al. In *Generation of Aerosols*, [K. Willeke, ed.], Ann Arbor Press, p. 399, 1980). Each exposure was conducted in a 96-port, nose-only exposure box. Beryllium exposure periods ranged from 20-90 min at a mass concentration of 6-1000 mg/m³. Exposure times and mass concentrations were varied to deliver the targeted range of ILBs. Based on our previous experience with this aerosol, we estimated the MMAD to be 1.4 µm, with a σ_g of 1.8. ⁸⁵Sr-FAP exposure periods ranged from 60-66 min at an exposure concentration of 55-67 kBq/L. The measured ⁸⁵Sr-FAP AMAD and σ_g were 1.2 µm and 1.7, respectively. All mice were exposed on one of two consecutive days to the ⁸⁵Sr-FAP followed by the Be metal exposure. Control groups of mice received only ⁸⁵Sr-FAP.

At various times after exposure, mice were whole-body counted in well-type, liquid scintillation detectors to determine their body burden of the ⁸⁵Sr-FAP tracer particles. Counting will be continued up to 210 days post exposure (dpe). For each mouse, the decay-corrected, whole-body counting data for ⁸⁵Sr collected through 28 dpe were modeled using a single-component, negative exponential function, then evaluated at t=0 days to estimate the ILB for each mouse.

Mice were sacrificed at 8, 15, and 40 dpe as of September 30, 1992. Additional sacrifices are scheduled for 90 and 210 dpe. At necropsy, the lungs were removed, and the left lung lobes were inflation-fixed in formalin for histopathological evaluation. Right lung lobes were lavaged three times with 1 mL of isotonic saline, and lavage fluids were analyzed for total cells numbers, cell types present, total protein (a general indicator of lung damage), and the enzymes lactate dehydrogenase (LDH; a cytoplasmic enzyme) and β-glucuronidase (a phagolysosomal enzyme), both indicative of phagocyte activity and damage (Henderson, R. F. In *Concepts in Inhalation Toxicology*, Hemisphere Publishing Corp., New York, p. 415, 1989). Analysis of the lavaged right lung lobes and residual lavage fluids for Be will be performed to measure the lung burden for each animal and to confirm the delivery of the target lung burdens of 1, 4, 15, and 60 µg.

The whole-body counting data obtained through 28 dpe indicate that (1) the target ⁸⁵Sr-FAP ILBs were achieved (approximately 11 kBq), and (2) a relationship between Be ILB and clearance of ⁸⁵Sr-FAP exists. Clearance half-times for ⁸⁵Sr for the groups were 31, 27, 30, 55, and 55 for the control, 1 µg, 4 µg, 15 µg, and 60 µg ILBs, respectively. An unbalanced repeated measures analysis of variance (BMDP 5V, Los Angeles, CA) indicated a significant (p < 0.01) impairment of clearance with increasing Be metal ILB.

Gross observation of the lungs at necropsy indicated the presence of enlarged bronchial lymph nodes and multifocal lung lesions at higher doses of Be metal, as compared to the lower doses and controls. Preliminary histopathologic evaluation of mice sacrificed at 8 or 15 dpe indicated an animal-to-animal variation in the severity of the lung lesions within individual exposure groups. The presence of free particles, heavily particle-laden macrophages, and particles within the interstitium was observed at the two highest Be ILBs. Hyperplasia of

alveolar macrophages, neutrophilic alveolitis, and interstitial mononuclear infiltrates also appeared to occur in a dose-dependent manner.

The pattern of inflammatory response observed histologically was reflective of lung damage as revealed by lavage. The numbers and types of cells observed through the 40 dpe sacrifice are shown in Table 1. At each timepoint, the four exposure groups were compared to controls using unpaired *t*-tests with a Bonferroni correction for multiple comparisons and a level of statistical significance set at $p < 0.05$ (BMDP 7D, Los Angeles, CA). Although the numbers of macrophages appeared to increase slightly in the higher dose groups, the trend was not statistically significant. The numbers of lymphocytes and neutrophils, however, did significantly increase with ILB. Similarly, levels of the enzymes β -glucuronidase and LDH, total protein, and the ratio of wet-lung-to-whole-body weight increased with increasing dose, reaching maximum levels in the 60 μg ILB group (data not shown).

Table 1

Cell Types Present in Lavage Fluids Obtained from Mice Exposed to Beryllium Metal^a

Estimated Be ILB ^b	Days After Exposure	Number of Cells per mL of Lavage Fluid		
		Macrophages ($\times 10^5$)	Lymphocytes ($\times 10^3$)	Neutrophils ($\times 10^3$)
Control	8	2.5 (0.5)	2.6 (1.2)	1.7 (0.7)
	15	3.4 (0.3)	7.7 (2.9)	1.8 (1.2)
	40	3.4 (0.4)	23 (6.1)	2.4 (1.2)
1 μg	8	2.8 (0.2)	4.3 (2.8)	3.6 (2.7)
	15	3.0 (0.4)	7.3 (2.4)	3.6 (1.6)
	40	2.9 (0.4)	18 (3.0)	1.6 (1.1)
4 μg	8	3.1 (0.8)	2.4 (1.5)	5.6 (3.8)
	15	3.3 (0.5)	18 (4.4)	16 (5.2)*
	40	2.5 (0.6)	32 (5.8)	2.4 (1.9)
15 μg	8	3.1 (0.9)	7.8 (3.6)	30 (6.6)*
	15	3.5 (0.2)	18 (3.6)	33 (4.4)*
	40	4.1 (0.6)	41 (4.7)	25 (5.4)*
60 μg	8	5.5 (1.3)	28 (7.0)	220 (53)*
	15	3.2 (0.2)	34 (3.7)*	68 (19)*
	40	3.1 (0.4)	50 (9.9)*	36 (4.5)*

^aMean values are given with standard error of the mean in parentheses; $n = 4$ to 6 per group.

For each timepoint, values significantly different from controls at the $p < 0.05$ level are denoted with an asterisk.

^bILB = Initial lung burden.

In summary, our data indicate that at sufficiently high lung burdens, inhaled Be metal inhibits particle clearance and induces persistent lung damage in mice. Qualitatively, it appears that these effects are similar to those observed in rats (1990-91 Annual Report, p. 167), although the mice may be more resistant when lung burdens are expressed on a weight-normalized basis.

This study is still in progress. Upon completion of all sacrifices and final analysis of the data, we expect this study to provide a basis for understanding the similarities and/or differences between the responses of rats and mice to inhaled beryllium, thus improving our ability to extrapolate rat and mouse beryllium-induced lung cancer models to humans.

(Research Supported by the Assistant Secretary for Defense Programs, U.S. Department of Energy, under Contract No. DE-AC04-76EV01013.)

CHARACTERIZATION OF BERYLLIUM-INDUCED GRANULOMATOUS LUNG DISEASE IN STRAIN A AND C3H MICE

K. J. Nikula, M. D. Tohulka*, D. S. Swafford**, M. D. Hoover, and G. L. Finch

Exposure to beryllium (Be) can induce both acute and chronic disease in people. Approximately 3% of people who inhale Be develop chronic beryllium disease (CBD), characterized by Be-specific, cell-mediated immune responses and microgranulomas within the lung (Haley, P. J. *Toxicol. Pathol.* 19: 514, 1991). The latency period of the disease may extend to 25 yr. The number of subclinical cases in the exposed population is unknown (Kriebel, D. et al. *Am. Rev. Respir. Dis.* 137: 464, 1988). Dogs and nonhuman primates, but not rats, that inhale Be develop cell-mediated immune responses and lung lesions (Haley, 1991).

We wished to determine if mice that inhale Be develop cell-mediated immune responses which are manifested as a granulomatous lung disease that mimics human CBD. The advantages to studying the mechanisms of Be-induced lung disease in mice include the existence of several syngeneic strains, the availability of cell markers and molecular probes, and practical reasons. In the present study, female A/J and C3H/HeJ mice of 7 ± 2 wk of age were exposed to Be metal particles ($1.4 \mu\text{m}$ estimated MMAD) via acute (90 min), nose-only inhalation to yield an initial lung burden of $60 \mu\text{g}$. The mice were sacrificed 28 wk after exposure. Cells were harvested from peripheral blood, spleen, and bronchial lymph nodes from 10 exposed mice and 4 control mice of each strain for *in vitro* lymphocyte proliferation assays. These cells were exposed to Be sulfate ($100 \mu\text{M}$), cultured for 3 days, pulsed with tritiated thymidine, and assayed 18 h later for thymidine uptake to indicate DNA synthesis. This assay is similar to one used to demonstrate Be-specific immune responses in people.

The right cardiac lung lobes of the mice were removed, inflated with a solution of Tissue Tek cryopreservative and sucrose, quickly frozen in isopentane followed by liquid nitrogen, and stored at -90°C until they were sectioned at $8 \mu\text{m}$ on a cryostat. Preliminary trials showed that optimum immunoreactivity of lymphocyte membrane markers was preserved by fixing the tissue sections in 4°C acetone for 10 sec, without air drying. Rat IgG primary antibodies (PharMinigen, Sorrento Valley, CA) to detect mouse B (CD45R/B220), helper-T (CD4), and cytotoxic/suppressor-T (CD8a) lymphocytes were visualized in serial sections with goat anti-rat (mouse adsorbed) IgG Vectastain ABC reagents (Vector Laboratories, Burlingame, CA). Diaminobenzidine was used as the chromagen. Isotype-specific rat immunoglobulins were used as negative controls.

Following cardiac lobe removal, the remaining lung lobes were inflated with 4% paraformaldehyde, fixed for 24 h, embedded in paraffin, sectioned at $5 \mu\text{m}$, and stained with hematoxylin and eosin (H & E). Morphology was examined using light microscopy.

Ten exposed mice and five control mice of each strain were injected intraperitoneally with 0.2 mg/g body weight of a 5-bromo-2-deoxyuridine solution (BrdU, 20 mg/mL) three times daily for 2 days prior to sacrifice, and on the morning of sacrifice (7 total injections) to label the nuclei of replicating cells. The lungs were removed, constant-pressure ($25 \text{ cm H}_2\text{O}$) perfused with formalin, paraffin embedded, and sectioned at $5 \mu\text{m}$. Anti-BrdU antibody was used to immunohistochemically identify replicating cells by light microscopy.

The *in vitro* assay did not show lymphocyte proliferation in response to Be in any of the blood, spleen, or lymph node samples, but there was proliferation in response to a mitogen (phytohemagglutinin, $10 \mu\text{g/mL}$), which was used as a positive control for detecting cell replication. Histological examination of lung sections from Be-exposed mice revealed marked, multifocal, granulomatous pneumonia, perivasculär mononuclear cell infiltrates, and multifocal interstitial mononuclear cell aggregates. The mononuclear cell aggregates were of two types: microgranulomas composed of macrophages and lymphocytes, and round, dense cellular aggregates composed mostly of lymphocytes. Accumulation of macrophages, many of which were binucleate or multinucleate giant cells, and neutrophils in alveoli, proteinaceous debris, alveolar epithelial cell hyperplasia, and interstitial

*Department of Energy/Associated Western Universities Teacher Research Associate Program Participant

**UNM/ITRI Inhalation Toxicology Graduate Student

inflammatory cell infiltrates characterized the granulomatous pneumonia. Most macrophages within these areas and within the microgranulomas contained dense, black, irregular particles that were presumed to be Be metal.

The majority of lymphocytes in the lungs of Be-exposed mice were helper-T lymphocytes. They were located in the interstitium within foci of granulomatous inflammation, in perivascular cuffs, in microgranulomas, and at the margins of discrete, focal aggregates of B lymphocytes. The B-cell aggregates, which seemed to correspond to the center of the round lymphocytic aggregates in the H & E stained sections, sometimes contained small numbers of helper-T lymphocytes along with B lymphocytes. Scant numbers of suppressor/cytotoxic-T lymphocytes were scattered within the lesions. BrdU labeling showed lymphocyte proliferation *in situ* within microgranulomas, perivascular cuffs, and round lymphocytic aggregates; however, the technique used did not allow classification of proliferating lymphocyte subsets. In control mice, small numbers of widely scattered helper-T, B, and suppressor/cytotoxic-T lymphocytes were present in the interstitium.

There were no major differences, based on the qualitative light microscopic examinations, between the Be-exposed A/J and C3H/HeJ mice in the characteristics of the morphologic response, the lung lymphocyte subsets, or the intrapulmonary location and degree of lymphocyte replication *in situ*.

In summary, A/J and C3H/HeJ mice that inhale Be metal develop chronic lung lesions characterized by granulomatous pneumonia and interstitial mononuclear infiltrates. The accumulations of macrophages and neutrophils in alveoli, proteinaceous debris, and alveolar epithelial cell hyperplasia in areas of inflammation are responses similar to those elicited by other cytotoxic and irritant metal compounds, for example NiO, Ni₃S₂, and NiSO₄·6H₂O (Dunnick, J. K. *et al.* *Fundam. Appl. Toxicol.* 12: 584, 1989). The interstitial mononuclear infiltrates, in contrast, are remarkable in Be-exposed mice because of their abundance and large lymphocytic component. Furthermore, the replication of lymphocytes *in situ* implies that the presence of lymphocytes in the lesions is not merely due to non-specific recruitment of circulating lymphocytes. However, the techniques used do not permit the identification of the antigen or mitogenic stimulus. The lung lesions in mice that inhale Be metal morphologically parallel CBD in humans. Parallels include the presence of microgranulomas with a significant lymphocytic component, and perivascular and interstitial mononuclear cell infiltrates. Furthermore, in both people with CBD and mice that inhale Be, helper-T cells are the main lymphocytic cell type in the lungs. One exception to the morphologic similarities between the lesions in the two species is the rarity in the mice of Langhans giant cells, which commonly occur in the immune granulomas of people with CBD (Daniele, R. P. *Ann. Int. Med.* 102: 93, 1985). In conclusion, mice that inhale Be metal develop granulomatous pneumonia suggestive of an immune-mediated response, but a Be-specific response has not been demonstrated. Demonstration of a Be-specific immune response is needed before the disease in mice can serve as an animal model of the human disease and thus be used to study the mechanisms of CBD.

(Research sponsored by the Office of Health and Environmental Research, U. S. Department of Energy, under Contract No. DE-AC04-76EV01013.)

IMMUNE MEMORY RESPONSE IN LUNG

D. E. Bice and B. A. Muggenburg

Antibody-forming cells (AFC) are recruited into antigen-exposed lung lobes, where they mature to plasma cells and produce antibody (Bice, D. E. et al. *Am. Rev. Respir. Dis.* 126: 635, 1982). Antibody production by these cells provides an important pulmonary defense. Along with the recruitment of AFC, immune memory cells may also be recruited into exposed lung lobes (Mason, M. J. et al. *Reg. Immunol.* 2: 149, 1989). Our hypothesis is that memory lymphocytes respond in the lung to antigen challenges, providing an important pulmonary defense to help prevent recurrent pulmonary infections. The exposure of these cells to antigen would result in the localized production of high levels of antibody and would increase the number of antigen-specific lymphocytes important in cell-mediated immune responses only in the lung lobes challenged with antigen. The focus of this study was to determine if immune memory cells are recruited into the lung after primary immunization and if they respond to an antigen challenge.

Following anesthesia by inhalation of halothane, the lungs of 12 young Beagle dogs were instilled with two antigens in 1 mL of saline using a fiberoptic bronchoscope (Bice et al., 1982). For the primary immunization, 10 mg of Keyhole Limpet Hemocyanin (KLH), a soluble antigen, were instilled into the left cardiac lung lobe (LCL), and 10^{10} sheep red blood cells (SRBC), a particulate antigen, were instilled into the right cardiac lung lobe (RCL). As a control, 1 mL of saline was instilled into the left diaphragmatic lung lobe (LDL). At 21 days after primary instillation, the same airways in the LCL and RCL lobes were challenged by instillation of 1 mg of KLH (LCL) and 10^9 SRBC (RCL). One mL of saline was instilled into the LDL as a control.

Lavage samples, five washes with 10 mL of saline for each wash, of all three exposed lobes were collected on days 3, 5, 7, 10, 12, and 14 after both primary and challenge instillations. Cytology slides were prepared. Total and differential cell counts were used to determine the number of polymorphonuclear leukocytes (PMN), alveolar macrophages, and lymphocytes recovered at the time of each lavage. The production of anti-KLH and anti-SRBC IgG antibody was measured by using an enzyme-linked immunosorbant assay (ELISA). The significance of differences in response between the two antigens was evaluated with a paired *t*-test. Differences with *p* values < 0.05 were considered significant.

The evaluation of the number of PMN in lavage fluid was essential for this study because acute inflammation appears to be important in the recruitment of lymphocytes into the lung (Bice, D. E. et al. *Reg. Immunol.* 126: 635, 1982). There were no significant differences in the number of PMN in the LCL and RCL after primary immunization or antigen challenge. However, significantly more PMN were found in the lavage fluid from the lung lobes exposed to antigen than in the lavage fluid from the control lobe (*p* < 0.05). The number of PMN returned to normal by day 14 after primary immunization or antigen challenge. These results indicate that there was an equal level of inflammation in lung lobes exposed to soluble or particulate antigen after primary and challenge instillations.

Significantly more lymphocytes and macrophages were observed in the lavage fluid from both lung lobes exposed to antigen than in the control lobes after primary immunization and challenge (*p* < 0.05). However, the number of lymphocytes and macrophages remained high longer in the RCL exposed to SRBC than in the LCL exposed to KLH. The number of lymphocytes and alveolar macrophages in lavage fluid from the RCL was also significantly higher than in the LCL after antigen challenge. The elevated number of these cells in the lung lobe exposed to SRBC antigen is possibly due to differences in the SRBC and KLH antigens. Because KLH is a soluble protein, it may have cleared more rapidly than the particulate antigen, SRBC.

AFC are recruited into lung lobes exposed to different antigens at an equal rate, and the recruitment is not antigen-specific (Bice et al., 1982). Confirming this observation, the levels of anti-KLH and anti-SRBC IgG antibodies were the same in both the RCL and LCL lobes after primary immunization (Figs. 1 and 2). In contrast to primary immune responses, the anti-KLH and anti-SRBC IgG responses were elevated after challenge on an antigen-specific basis. The level of anti-KLH IgG antibody was significantly higher in the LCL (challenged with KLH) than in the RCL (challenged with SRBC) (*p* < 0.05) (Fig. 1), and the level of anti-SRBC IgG antibody was significantly higher in the RCL (challenged with SRBC) than in the LCL (*p* < 0.05) (Fig. 2).

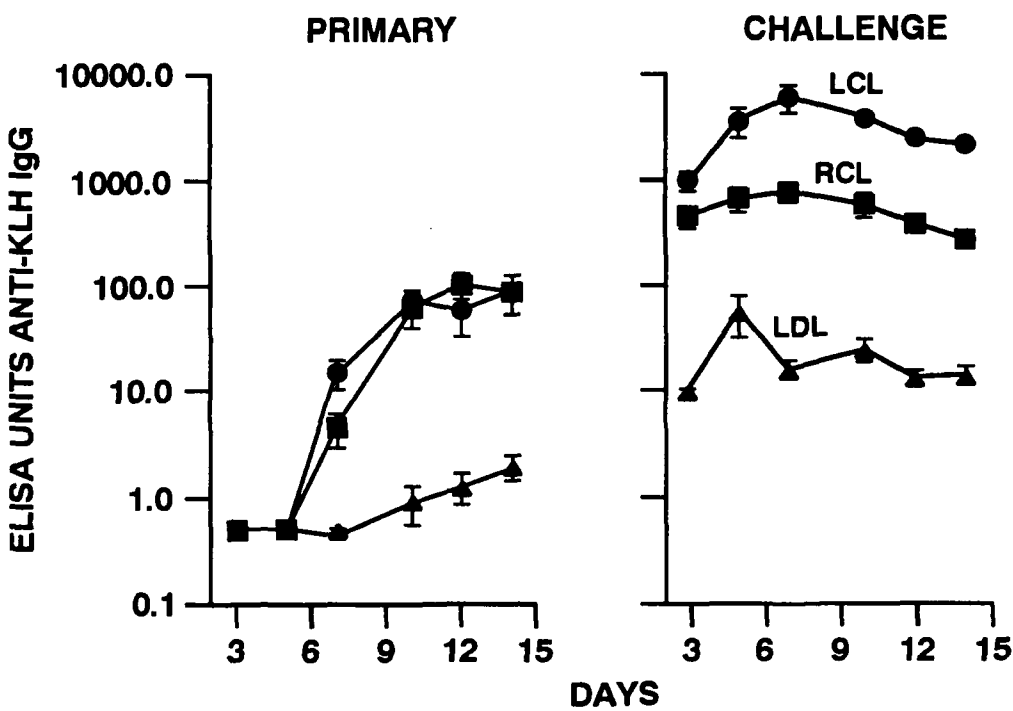


Figure 1. Levels of anti-keyhole limpet hemocyanin (KLH) IgG antibody present in lavage fluid from the left cardiac lung lobe (LCL) exposed to KLH, the right cardiac lung lobe (RCL) exposed to sheep red blood cells (SRBC), and the left diaphragmatic lung lobe (LDL) instilled with 1 mL saline. Labeled symbols apply to both primary and challenge instillations.

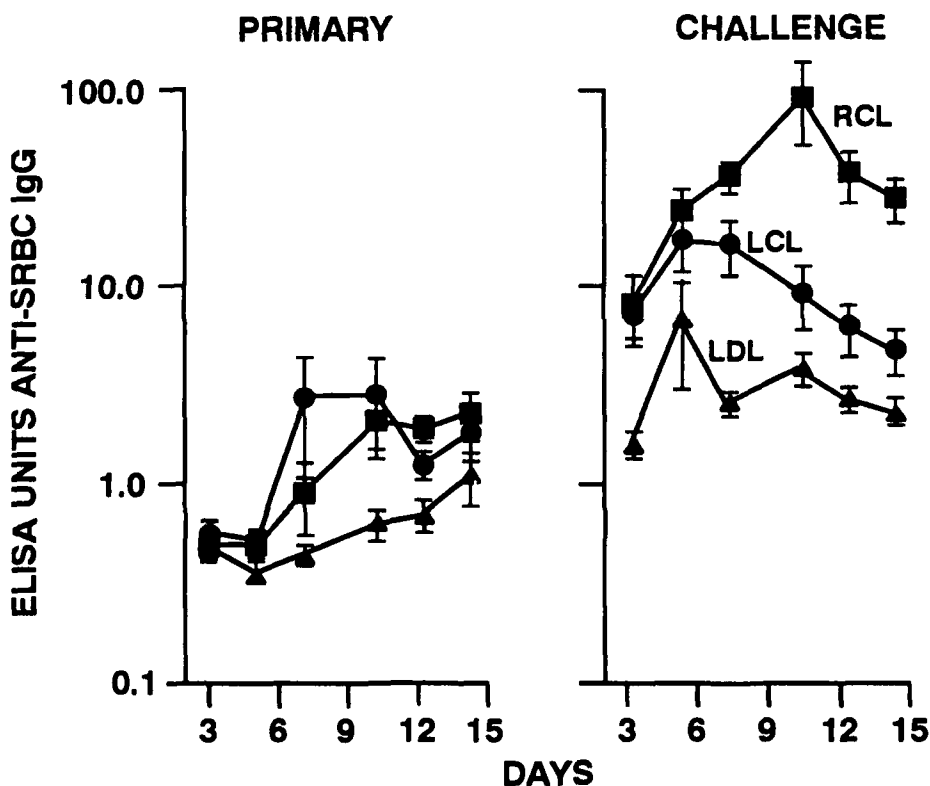


Figure 2. Levels of anti-sheep red blood cells (SRBC) IgG antibody present in lavage fluid from the left cardiac lung lobe (LCL) exposed to keyhole limpet hemocyanin (KLH), the right cardiac lung lobe (RCL) exposed to SRBC, and the left diaphragmatic lung lobe (LDL) instilled with 1 mL saline. Labeled symbols apply to both primary and challenge instillations.

The antigen-specific responses to antigen challenge support the contention that immune memory cells recruited and/or produced after primary immunization responded locally to antigen challenge. The stimulation of immune memory cells specific for KLH or SRBC by challenge of lung lobes exposed to these antigens would result in an antigen-specific clonal expansion of lymphocytes in the lung. The increase of the number of antigen-specific lymphocytes would significantly elevate antibody levels to KLH in the LCL and SRBC in the RCL. It can be assumed that the number of antigen-specific T lymphocytes important in cell-mediated immune responses would also be clonally expanded in the lung by an antigen challenge. Studies are needed to verify that cell-mediated immune responses are also evaluated in the lung after antigen challenges.

(Research sponsored by the Office of Health and Environmental Research, U. S. Department of Energy, under Contract No. DE-AC04-76EV01013.)

EFFECT OF CIGARETTE SMOKE EXPOSURE ON THE IMMUNOLOGIC STATUS OF F344 RATS

S. M. Savage*, G. L. Finch, B. T. Chen, and M. L. Sopori*

Cigarette smoking is known to impair the immune system, and long-term inhalation of cigarette smoke leads to immunosuppression in both humans and animals (Holt, P. G. and D. Keast. *Bacteriol. Rev.* 41: 205, 1977). We have demonstrated that the antibody-forming cell (AFC) responses of spleen cells to both T-dependent and T-independent antigens are significantly inhibited in rats exposed nose-only, twice per day for more than 35 wk, to mainstream cigarette smoke (Sopori, M. L. et al. *Toxicol Appl. Pharmacol.* 97: 489, 1989). Despite the inhibition of the AFC response, mainstream cigarette smoke did not affect the number or ratio of B and T cells or their responses to mitogens. Moreover, the frequency of antigen-binding cells was comparable between normal and smoke-exposed rats. However, following cross-linking of antigen receptors (B cell surface immunoglobulins) with anti-IgM antibody, the ability of spleen cells to proliferate in response to antigens and mitogens was significantly reduced in smoke-exposed rats (Savage, S. M. et al. *Toxicol. Appl. Pharmacol.* 111: 523, 1991). This defect appears to stem primarily from the inability of B cells from smoke-exposed animals to elevate intracellular calcium levels in response to cross-linking of the antigen receptor. Therefore, in rats, chronic exposure to cigarette smoke affects the antigen-induced membrane signal transduction pathway regulating intracellular calcium (Ca) levels. To examine the potential effect of exposure route and regime on immunologic responses, we describe here studies of these same endpoints in rats chronically exposed to cigarette smoke using a whole-body exposure route.

For the following immunologic analyses, we selected groups of strain CDF®(F344)/CrIBR (Charles River Laboratories, Raleigh, NC) rats scheduled for serial sacrifice from all three blocks of a chronic study designed to examine cancer risks in animals exposed to cigarette smoke and/or $^{239}\text{PuO}_2$ (this report, p. 110). Rats were selected from each of three groups receiving either filtered air or mainstream cigarette smoke administered at levels of 100 or 250 mg/m³ total particulate matter (TPM). This study does not include rats that received $^{239}\text{PuO}_2$ during the chronic study. The animals were obtained, housed, and exposed to cigarette smoke as described elsewhere in this report (p. 110).

Groups of three males and three females were sacrificed after 7, 10, 16, or 32 wk of exposure to cigarette smoke. At necropsy, spleens were aseptically removed, and a fraction of the spleen was placed into sterile RPMI-1640 (GIBCO, Grand Island, NY). Samples were held over ice and transported from the Institute to the LMF laboratory. Techniques used for the isolation of the spleen cell suspensions have been described (Sopori, M. L. et al. *Cell. Immunol.* 87: 177, 1984). Total nucleated cell numbers per unit weight of spleen were measured by cell counting. The relative percentages of T and B lymphocytes were determined using fluorescently conjugated specific monoclonal antibody (W3/13) for T cells and anti-rat IgM for B cells. The distribution of T-cell subsets was measured by flow cytometry using CD4⁺ (helper)-specific W3/25 and CD8⁺ (suppressor)-specific OX-8 monoclonal antibodies (Sopori et al., 1989).

The functional responses of T and B cells were assessed as follows. T cells were evaluated for their ability to proliferate in response to either alloantigens, in a mixed lymphocyte assay (as described by Sopori et al., 1984), or the T-cell-specific mitogens Concanavalin-A (ConA) and phytohemagglutinin (PHA; assays described by Sopori, M. L. et al. *Cell. Immunol.* 105: 174, 1987). The functional competency of B cells was measured by their response to the B-cell-specific mitogen lipopolysaccharide (LPS) and by increases in the cytosolic-free calcium after cross-linking of antigen receptors with anti-IgM antibody. Groups were compared using a Student's *t*-test with a *p* < 0.05 level of significance.

Exposure to cigarette smoke at either concentration for a period of 7 to 16 wk did not influence either the number or subset distribution of T or B cells. In addition, T-cell responses to the T-specific mitogens ConA or PHA, or to alloantigens, were comparable between control and the treated groups. Data from animals sacrificed after 32 wk of smoke exposure are currently being analyzed.

*Lovelace Medical Foundation, Albuquerque, New Mexico

The function of the B cells, as reflected by the proliferative response to LPS, also was not altered by cigarette smoke exposure. However, B-cell, antigen-mediated responses, as measured by increases in cytosolic-free calcium, were significantly reduced compared to controls in rats exposed for 16 wk to the 250 mg/m³ of smoke. This reduction was not observed compared to controls at the 7- and 10-wk timepoints.

In summary, the only cigarette smoke-exposure related effect we have observed was that the ability of B cells to mobilize cytosolic Ca in response to cross-linking of antigen receptors was reduced in the 16-wk smoke-exposed group. This finding was consistent with our earlier results using a different exposure mode and regime (Savage *et al.*, 1991), thus suggesting that the whole-body route of exposure is appropriate for examining the influences of cigarette smoking on immunologic status. Although efforts continue to examine groups of rats exposed for longer periods of time, it appears that there is no significant influence of exposure route on immunologic responses to cigarette smoke in the rat through 16 wk of exposure. We will continue to examine the influences of cigarette smoke exposure on immune function using both whole-body and nose-only exposure modes.

(Research sponsored by the Assistant Secretary for Defense Programs, U. S. Department of Energy, under Contract No. DE-AC04-76EV01013, and by National Institutes of Health Grants No. A131386 and DA04208.)

BONE AND BLOOD MEASUREMENT FROM F344 RATS EXPOSED TO CIGARETTE SMOKE

M. Bhattacharyya*, C. Wang*, S. Abrikosova*, S. Brown*, B. T. Chen, and G. L. Finch

It has been suggested that in people, cigarette smoking might be a factor that contributes to bone loss leading to osteoporosis (*Osteoporosis*, U.S. D.H.H.S., Public Health Service, National Institutes of Health, Government Printing Office Document No. 507-A-6, 1984). We are conducting a chronic study in rats to determine how smoking and the inhalation of $^{239}\text{PuO}_2$ might interact in producing lung cancer (this report, p. 110). The purpose of the portion of the chronic study reported here is to determine whether rats exposed to cigarette smoke experience bone loss as a result of their exposure, and whether any loss that might occur could be associated with cadmium (Cd) from the cigarette smoke being present in the blood.

We selected a group of strain CDF®(F344)/CrIBR (Charles River Laboratories, Raleigh, NC) rats from Block A of our chronic study (this report, p. 110) for bone and blood analysis. Rats were selected from each of three groups receiving either filtered air, or mainstream cigarette smoke administered at levels of 100 or 250 mg/m³ total particulate matter (TPM), for a total of either 4 or 16 wk of exposure. This study does not include any rats from the chronic study that received $^{239}\text{PuO}_2$. The animals were obtained, housed, and exposed to cigarette smoke as described elsewhere in this report (p. 110).

Groups of rats were sacrificed after being on study for either 4 or 16 wk. We sacrificed a total of 18 rats after 4 wk of exposure, consisting of three males and three females from each exposure group (controls, 100 mg/m³, or 250 mg/m³ of smoke TPM). At 16 wk of exposure, four male rats from each exposure group were sacrificed. For both groups, bone and blood samples were taken at necropsy. To collect blood, heparin was injected into the heart, then the axial artery was nicked with a teflon-coated blade and blood collected using a plastic pipette. Right femurs and lumbar vertebrae were removed and cleaned of muscle using teflon-coated blades. The concentrations of Cd in blood were analyzed by furnace atomic absorption spectroscopy and were done only at the 4 wk sacrifice. The bone samples were measured for dry weight (DW), extracted weight (EW, the fat-free dry weight), ash weight (AW), and calcium (Ca) content, to determine bone mass (DW), total mineral content (AW and Ca), bone mineral density (AW/DW, Ca/DW, and Ca/EW), and bone mineral composition (Ca/AW). Values for both sexes within each exposure group were compared by an analysis of variance followed by a least significant difference test (SAS Institute, Cary, NC).

Results of blood Cd analyses showed that concentrations in all rats were very low, less than 0.2 ppb, the detection limit for the assay on that day. Nonsmokers with no occupational exposure to Cd typically have blood Cd concentrations about 0.2 ppb. Thus, we concluded that the 1R3 cigarettes used for this study are low in Cd content, which has been reported for some cigarettes.

After 4 wk of cigarette smoke exposure, bone measurements for right femur and lumbar vertebrae were remarkably similar for all groups (data not presented). Femurs were about three times heavier (DW) than the lumbar vertebrae, and measures of bone density (AW/DW, Ca/DW, and Ca/EW) were lower for the more trabecular vertebrae than the femurs, as expected. Cigarette smoke exposure did not induce changes in any of the bone properties examined.

After 16 wk of exposure (Table 1), femurs and lumbar vertebrae had significantly increased DW, AW, and Ca compared to the 4-wk sacrifice, reflecting the growth of the rats. Measurements of bone density, however, were nearly constant with time. Femurs at 16 wk showed no indication of smoke-induced bone loss. Lumbar vertebrae showed a trend of decreasing DW, AW, and Ca content with increased smoke exposure, although this effect did not reach statistical significance. These decreases may be correlated with decreased body weight, although if this were the case, the same trend should have been observed with femurs as well. An alternate

*Biology and Medicine Research Division, Argonne National Laboratory, Argonne, Illinois

explanation is that the smoke exposure was beginning to induce decreases in the mineral content of the lumbar vertebrae, a trabecular bone, and not the femurs. Indicators of bone density for the lumbar vertebrae were not decreased with increasing exposure.

Table 1
Bone Measurements in Rats Exposed to Cigarette Smoke for 16 Weeks^a

Bone Type and Property	Unit	Cigarette Smoke Exposure Level			Significance
		0 mg/m ³	100 mg/m ³	250 mg/m ³	
RIGHT FEMUR					
Dry Wt. (DW)	mg	537 ± 7	536 ± 18	530 ± 25	ns
Ash Wt. (AW)	mg	326 ± 7	317 ± 10	327 ± 16	ns
Ca Content (Ca)	mg	105 ± 3	106 ± 4	104 ± 4	ns
AW/DW	g/g	0.607 ± 0.007	0.592 ± 0.009	0.617 ± 0.005	ns
Ca/DW	g/g	0.196 ± 0.003	0.199 ± 0.006	0.196 ± 0.002	ns
Ca/EW ^b	g/g	0.206 ± 0.003	0.213 ± 0.005	0.207 ± 0.003	ns
Ca/AW	g/g	0.322 ± 0.001	0.335 ± 0.004	0.318 ± 0.004	p<0.05
LUMBAR VERTEBRAE					
Dry Wt. (DW)	mg	198 ± 12	185 ± 12	159 ± 13	ns
Ash Wt. (AW)	mg	107 ± 6	98 ± 7	88 ± 5	ns
Ca Content (Ca)	mg	34.1 ± 2.0	30.7 ± 2.5	27.4 ± 1.6	ns
AW/DW	g/g	0.540 ± 0.011	0.529 ± 0.005	0.559 ± 0.014	ns
Ca/DW	g/g	0.172 ± 0.005	0.166 ± 0.003	0.173 ± 0.006	ns
Ca/EW	g/g	0.182 ± 0.006	0.178 ± 0.005	0.184 ± 0.005	ns
Ca/AW	g/g	0.319 ± 0.004	0.314 ± 0.007	0.310 ± 0.008	ns

^aValues are mean ± standard error, four male rats per group.

^bEW = extracted weight as defined in text.

In summary, the exposure of rats to cigarette smoke for 4 wk did not produce elevated Cd concentration in the blood. Indications were found of smoking-induced decreases in DW and mineral content of the lumbar vertebrae, but not femurs, after 16 wk of exposure, although the decreases were not statistically significant. We are currently collecting and analyzing bone and blood samples from rats exposed for longer periods of time to determine if the trends observed thus far reach significance.

(Research supported by the Assistant Secretary for Defense Programs, U. S. Department of Energy, under Contract No. DE-AC04-76EV01013, and the Office of Health and Environmental Research, U. S. Department of Energy, under Contract No. W-31-109-ENG-38.)

VII. MECHANISMS OF NONCARCINOGENIC RESPONSES TO INHALED TOXICANTS

ULTRASTRUCTURAL EVALUATION OF A LUNG EPITHELIAL CELL STRAIN AS AN ALVEOLAR TYPE II CELL MODEL

N. F. Johnson, A. W. Goldrath*, and E. K. Perryman**

This study was designed to determine if a strain of lung epithelial cells (LEC), a proposed immortalized type II cell line, was appropriate as an *in vitro* model for toxicological studies. Type II cells in animals are potential critical cells at risk resulting from neoplastic transformation for radiation and chemical exposures. Type II cells comprise approximately 10% of the total lung population and are, therefore, difficult to study *in vivo*. When type II cells are isolated and cultured, they rapidly lose their characteristic morphology, functions, and growth potential (1990-91 Annual Report, p. 145). Thus, a model that involves type II cells is needed for toxicological studies.

A. P. Li *et al.* (*Toxicology* 27: 257, 1983) reported an immortalized cell line that possessed normal type II cell characteristics and might be an appropriate *in vitro* model of type II cells. This conclusion was based on a series of experiments which showed that these cells were not tumorigenic, displayed contact inhibition of growth, were unable to grow in soft agar, could incorporate [¹⁴C]choline, possessed lamellar-like inclusions, and could activate procarcinogens. The goal of this study was to re-examine the ultrastructure of the LEC line in culture and in the re-established epithelium of a tracheal implant and to assess the value of LEC as a suitable type II cell model.

Tracheas, denuded of their epithelial lining by repeated freeze/thaw cycles, were repopulated with LEC that had been cultured and trypsinized. Control tracheas were cultured with media. The tracheas were transplanted subcutaneously on the backs of F344/N rats and harvested after 3 wk. Tracheas and samples from the cell pellets used for the re-populations were fixed with glutaraldehyde in Sorensen's buffer. The tissue and cell samples were then processed in Spurr's resin for electron microscopy.

One-micron-thick sections of embedded cell pellets and tracheal implants were stained with toluidine blue. Thin sections (70-80 nm) were obtained by ultramicrotome sectioning of both cell pellets and implants from each group (control and LEC), and stained with uranyl acetate and lead acetate. Grids were viewed with a Hitachi 7000 STEM electron microscope.

Thick sections of the LEC cell pellets revealed a heterogeneous population with great variation in cell size. Electron micrographs of the LEC pellet showed differences in ultrastructure (Fig. 1). Many of the cells possessed distended rough endoplasmic reticulum and scroll-like, electron-dense inclusions. Characteristics observed in other cells were occasional binucleation, numerous mitochondria, little rough endoplasmic reticulum, and numerous long microvilli, a few of which were forked. The thick sections of the tracheal implants showed a well-established epithelial lining. The controls showed only a loose fibrous matrix containing fibroblasts, macrophages, leukocytes, and capillaries. The lamellar or scroll-like inclusions did not resemble lamellar bodies of normal type II cells. The tracheal grafts repopulated with LEC revealed an epithelium that consisted of flattened squamous cells and slightly higher, almost cuboidal cells (Fig. 2). These cells possessed long, and occasionally forked microvilli, lipid droplets, active, rough endoplasmic reticulum, bundles of cytofilaments, and pinocytotic vesicles. The cytoplasm of these cells did not show any of the lamellar or scroll-like inclusions observed in the cell pellets.

From our ultrastructural data, it appears that the LEC line did not represent normal type II cells. Type II cells exhibit short, stubby microvilli, distinct lamellar bodies, and multi-vesicular bodies *in situ* and rapidly lose these characteristics in culture but maintain them in the re-established epithelium of tracheal grafts (this report, p. 184). The LEC cell line did not possess ultrastructural characteristics indicative of normal type II cells in culture or from the re-established epithelium of tracheal grafts. Although our study did not repeat the investigations completed by Li *et al.* (1983), we believe that an ultrastructural evaluation of the LEC in culture (cell pellets)

*Department of Energy/Associated Western Universities Summer Student Research Participant

**Department of Energy/Associated Western Universities Faculty Participant

and in the tracheal grafts suggests that these cell are not of type II origin. It was shown that these cells incorporate [¹⁴C]choline; however, negative and positive controls were not included, and only low levels (10%) of incorporation were shown (Li *et al.*, 1983). Other aspects of the previous study showed that the LEC line was not tumorigenic and could metabolize procarcinogens. This information is relevant; however, it does not necessarily imply that these cells are of type II origin. Thus, we conclude that the established LEC cell line may not be a suitable model for *in vitro* study of the type II cell of the lung.

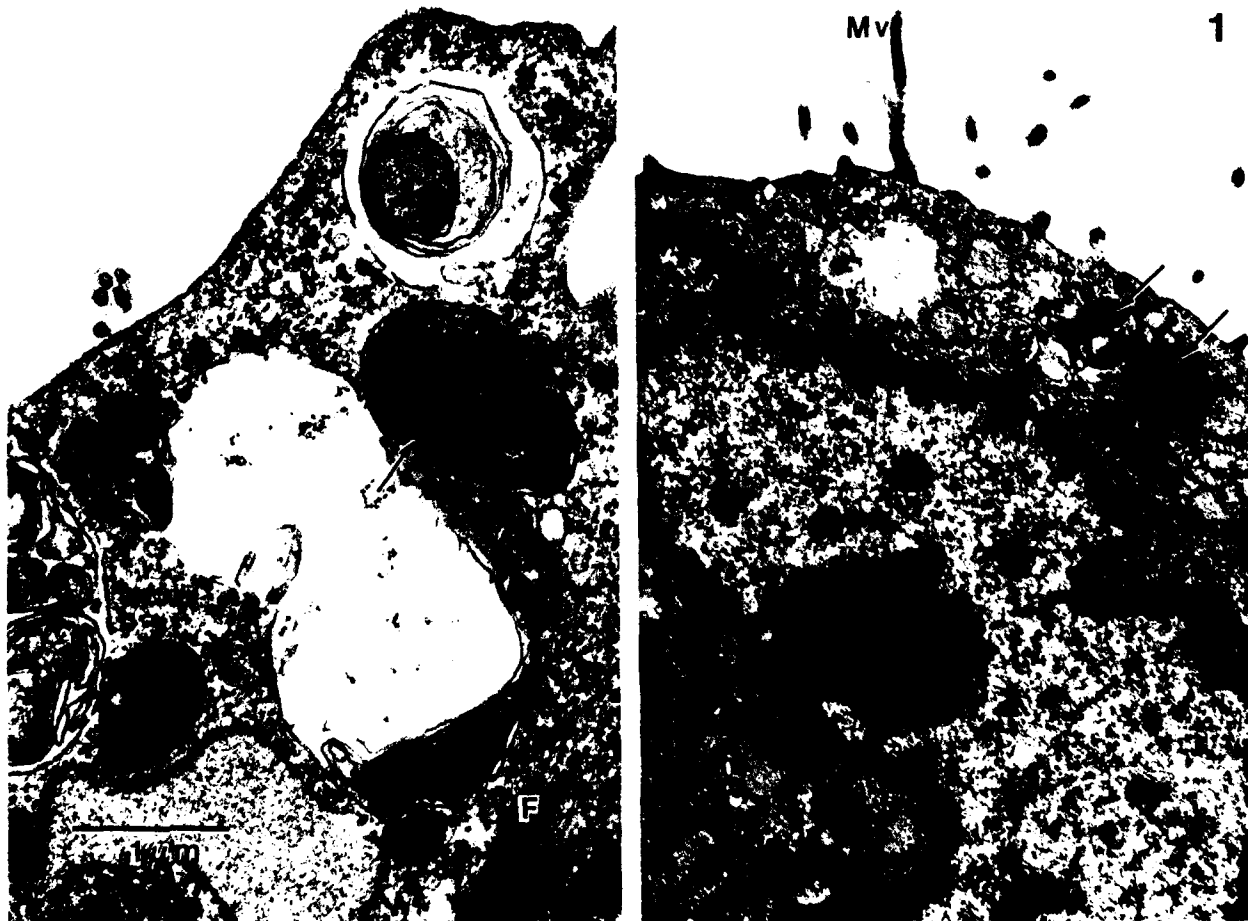


Figure 1. TEM section of a cell pellet of LEC line showing scroll-like bodies (arrows), bundles of cytofilaments (F) and long, forked microvilli (Mv).

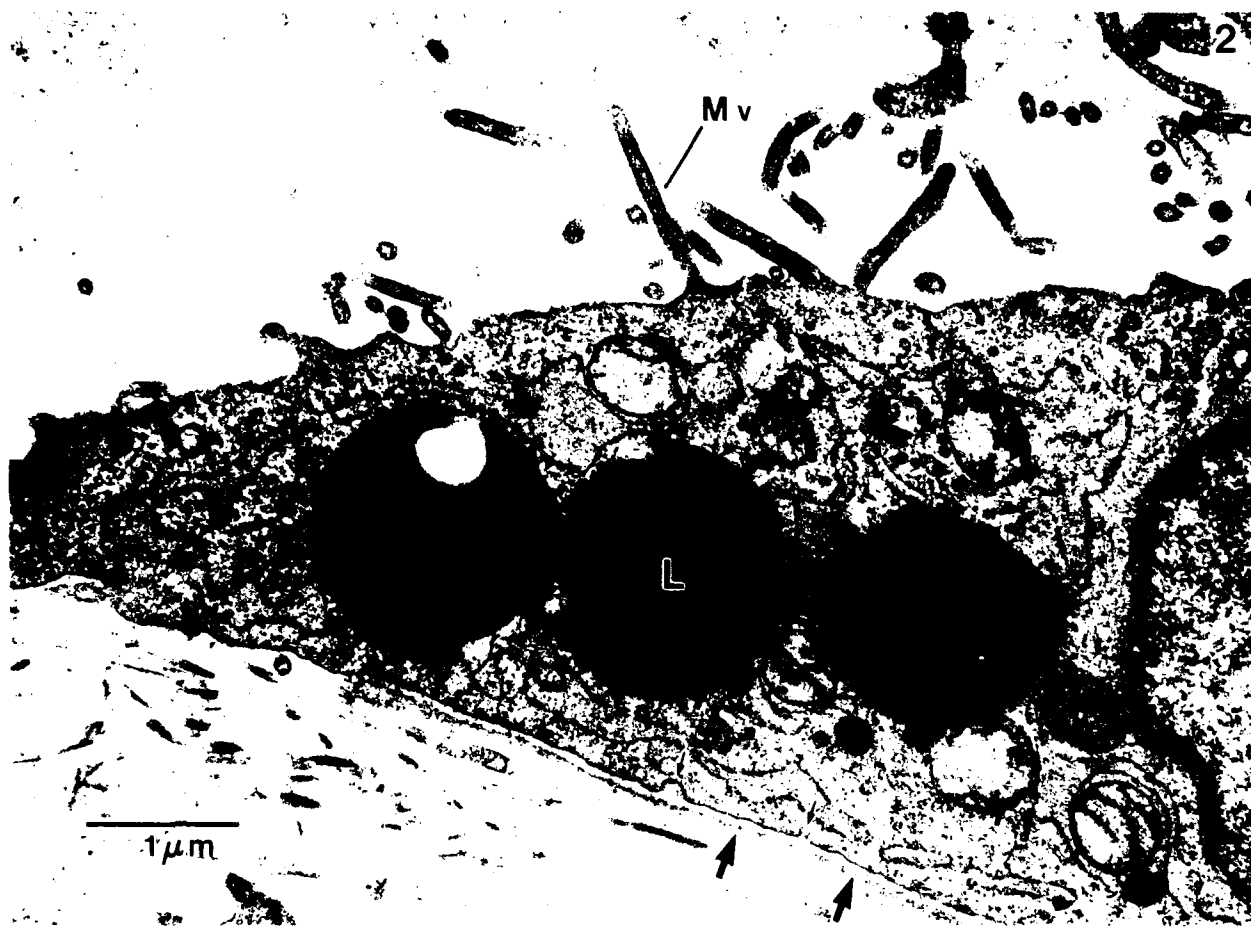


Figure 2. Transmission electron micrograph of tracheal implant repopulated with LEC. Notice the long, numerous microvilli (Mv), prominent lipid droplets (L), pinocytotic vesicles (small arrows), and a well established basal lamina (large arrows).

(Research sponsored by the Office of Health and Environmental Research, U. S. Department of Energy, under Contract No. DE-AC04-76EV01013.)

DIFFERENTIATION PATTERN OF F344 RAT ALVEOLAR TYPE II CELLS

N. F. Johnson, E. K. Perryman*, and A. W. Goldrath**

The purpose of this study was to determine the differentiation pattern of F344 rat alveolar type II cells. Type II cells are progenitor cells involved in the repair and maintenance of the alveolar lining epithelium and are thought to give rise to some forms of peripheral lung tumors. Enriched (75%) and sorted (96%) populations of type II cells were produced using a discontinuous Percoll density gradient (enriched) or flow cytometry combined with the Percoll gradient (sorted). Cytospins of the original sorted population stained by a modified Papanicolaou method confirmed the high percentage (96%) of type II cells. The contaminants were lymphocytes and macrophages. In addition, ultrastructural examination and differential counting of a cell pellet of the enriched population confirmed the 75% purity of type II cells, while the contaminating cells were macrophages (2.5%), lymphocytes (9.6%), ciliated cells (7.5%), and unidentifiable cells (5.4%).

A tracheal transplant model allows the differentiation capacity of lower airway cells to be determined. The system uses rat tracheas denuded of epithelial cells by repetitive freezing and thawing. For our first experiment, sorted populations of type II cells (5×10^5 /trachea) were placed into the denuded tracheal grafts, which were implanted subcutaneously on the back of male F344/N rats for 5 wk. Secondly, the enriched populations (2×10^5 /trachea) were allowed to repopulate within denuded tracheal grafts for 3 wk. The controls for both of these were transplanted denuded tracheal grafts filled only with culture medium appropriate for the type II cells. After the stated time periods, the grafts were removed and fixed in formalin for the sorted populations, and with glutaraldehyde in Sorensen's phosphate buffer for the enriched populations. After the grafts were embedded in resin, 1-nm thick sections were cut and stained with toluidine blue; these light microscopy preparations indicated that epithelial linings were reestablished in both groups of repopulated grafts. In addition, histological sections stained with hematoxylin and eosin with Alcian Blue confirmed that the inoculated cells had reestablished a complete lining in the graft. The control trachea revealed no reepithelialization; the lumen contained macrophages, fibroblasts, and capillaries.

Ultrastructural examination of 70- to 80-nm thin sections of the epithelium established from the sorted type II cells indicated that these cells self-replicated and acted as progenitor cells, giving rise to cells with morphological features of type I cells (Fig. 1). The replication of type II cells was inferred because the cell number inoculated into the graft was insufficient to repopulate the luminal surface. The cells exhibited a flattened, elongated shape, but they still contained lamellar bodies (though reduced in number) and short stubby microvilli characteristic of type II cells. The tracheal implants repopulated with enriched populations showed that many epithelial cells coexpressed ultrastructural characteristics of both type II and Clara cells. Type II and ciliated cells were also present. Figure 2 illustrates one of these coexpressive epithelial cells with its lamellar bodies and the Clara-like granules near the apex of the cell. In addition, smooth endoplasmic reticulum, as well as polyribosomes indicative of immature cells, were present in the coexpressive cells. Many of the ultrastructural features of the coexpressive cells clearly matched those described for rat Clara cells (Plopper, C. A. et al. *Exp. Lung Res. 1*: 139, 1980), including short irregular microvilli and the unusual rod-shaped granules filled with fibrillar-like material. The presence of ciliated cells within the reestablished epithelium was also not surprising because Clara cells can self-replicate and give rise to the terminally differentiated ciliated cells (Evans, M. J. et al. *Lab. Invest. 38*: 648, 1978).

These results substantiate and extend a previously proposed differentiation pathway for epithelial cells for the peripheral lung as summarized by Johnson et al. (In *Biolog., Toxicology and Carcinogenesis of Respiratory Epithelium*, Hemisphere Publishing, p. 88, 1990). Our data (1) confirm that the alveolar type II cell is a progenitor cell for alveolar type I cells, and (2) suggest that the alveolar type II cells and Clara cells share a common differentiation pathway. The first conclusion is already well documented in the scientific literature, while the second is supported by the observation that both Clara and alveolar type II cells synthesize surfactant-associated

*Department of Energy/Associated Western Universities Faculty Participant

**Department of Energy/Associated Western Universities Summer Student Research Participant

proteins A and B (Kalina, M. et al. *Am. J. Respir. Cell Mol. Biol.* 6: 594, 1992). The occurrence of coexpressive cells in the tracheal grafts with enriched populations, but not the sorted, suggests that the types and amounts of the cellular contaminants within the inoculum may play a role in the differentiation of type II cells. As recently reviewed (Jetton, A. M. *Am. J. Physiol.* 260: L361, 1991), numerous cytokines, for example, transforming growth factor from macrophages, could act by way of a paracrine mechanism to induce differentiation. Also, lung fibroblasts have been reported to synthesize and secrete such cytokines. In summary, we propose, based on our electron microscopy data, that type II cells can differentiate toward Clara cells.



Figure 1. Transmission electron micrograph of graft with repopulated epithelial lining from sorted type II cells. Note that the flattened cells possess lamellar bodies (arrowheads) and short stubby microvilli (arrows) characteristic of type I cells. Basal lamina (BL).



Figure 2. Transmission electron micrograph of epithelial lining from enriched populations of type II cells. Note cocompressive cell containing both lamellar bodies (asterisks) and Clara-like granules (arrowheads). Ciliated cells (C) are adjacent and also encircle the lumen (L).

(Research sponsored by the Office of Health and Environmental Research, U. S. Department of Energy, under Contract No. DE-AC04-76EV01013.)

IN VITRO EXPRESSION OF F344 RAT OLFACCTORY-SPECIFIC CYTOCHROME P4502G1

J. A. Hotchkiss, J. L. Francis, L. K. Brookins, and A. R. Dahl*

The cytochromes P450 are a superfamily of proteins that catalyze monooxygenation of xenobiotics and endogenous substrates. Isozymes of cytochrome P450 exhibit organ, tissue, and cell-type specificity which correlates with observed organ- and tissue-specific injury resulting from exposure to toxicants. An olfactory-specific cytochrome P450, P4502G1, has been identified in rats (Nef, P. et al. *J. Biol. Chem.* 264: 6780, 1989) and rabbits (Ding, X. and M. Coon. *Biochem.* 27: 8330, 1988). Purified and reconstituted rabbit P4502G1 (P450NMB) catalyzes the N-deethylation, O-deethylation, and N-demethylation of several nasal procarcinogens and the hydroxylation of testosterone (Ding and Coon, 1988); however, the substrates for the rat form of the isozyme are not known. To investigate the metabolic profile of the rat form of P4502G1, we have cloned and expressed the cDNA in COS 1 cells. A major purpose of this study was to develop efficient transfection procedures to produce COS 1 cells expressing high transient levels of rat cytochrome P4502G1. We will use this *in vitro* expression system to produce sufficient quantities of rat P4502G1 in order to determine the metabolic capacities and substrate specificities of this isozyme. Electroporation was chosen to introduce plasmid DNA (pSVL2G1) into COS 1 cells. RNA slot blot and Northern analyses were used to determine optimal transfection conditions and time-dependent transient expression of rat P4502G1.

The rat form of cytochrome P4502G1 was synthesized by reverse transcription and polymerase chain reaction amplification using isozyme-specific primers and mRNA isolated from the olfactory mucosa of F344 rats. The cDNA was inserted into a eukaryotic expression vector containing an SV40 promoter. The COS 1 cells were transfected using the Cell-Porator Electroporation System (Life Technologies, Gaithersburg, MD). The process of electroporation causes the cell membrane to become permeable to macromolecules by exposing it to an electrical pulse. The pressure exerted causes the membrane to become thin, and a "pore" formation is created. The optimum conditions for electroporation of COS 1 cells were determined empirically. The pulse length was varied to ensure closure of the membrane for cell survival following electrical stimulation. Other parameters which affect the efficiency of transfection were held constant (Field strength: 1000 V/cm, cell concentration: 5×10^6 , carrier DNA: 500 μ g, plasmid DNA: 10 μ g, and temperature: 4°C).

The effect of the pulse length on COS 1 cell viability was evaluated over a pulse length range of 0-45.9 ms coupled with the above constant parameters. Cell viability was determined by trypan blue dye exclusion. Immediately after electroporation, the cell viability ranged from 20-80% (Fig. 1). However, 18-24 h after electroporation, cell death was virtually 100% at all pulse lengths except the shortest (1.4 ms). A series of plasmid clones with rat P4502G1 cDNA inserted into the pSVL vector were tested for their abilities to direct the expression of P4502G1 when transfected into COS 1 cells. Cells were electroporated at pulse lengths of 1.4 and 1.2 ms (other parameters held constant). These electroporated cells were plated into 100-mm dishes at a concentration of 1×10^6 per dish and harvested at 48 h. Total RNA was isolated according to the method of P. Chomczynski and N. Sacchi (*Anal. Biochem.* 162: 156, 1987) and used in a Northern analysis to determine if P4502G1 mRNA was being transcribed. The membrane was probed with the 5' and 3' sections of rat P4502G1 cDNA (acquired from Dr. D. Lancet, Weizmann Institute, Israel). The radiolabeled probe hybridized with a single band of the appropriate size (i.e., 1.5 kb) in RNA samples isolated from cells electroporated using a pulse length of 1.2 ms.

We examined the temporal expression of P4502G1 in COS 1 cells transfected using the empirically determined optimum conditions. The electroporated cells were plated and harvested every 24 h for 5 days. At each time-point we (1) determined the number of cells per dish, (2) prepared cell smears with a cyt centrifuge, and (3) isolated total RNA. An RNA slot blot was used to evaluate the relative amount of P4502G1 mRNA present in the transfected COS 1 cells. Scanning densitometry was used to quantitate the relative amounts of P4502G1 present at each time-point. The greatest amount of P4502G1 mRNA per μ g total RNA was observed 24 h after transfection (Fig. 2). There was an 11.9-fold decrease in P4502G1 during the following 4 days, while there was an approximately 2.5-fold increase in the number of COS 1 cells per dish. The cytopins were

*UNM/ITRI Inhalation Toxicology Graduate Student

immunohistochemically stained to detect P4502G1 protein using sheep anti-rabbit NMb and a horseradish-peroxidase-conjugated secondary antibody. The results of the immunohistochemical analyses of P4502G1 expression by transfected COS 1 cells paralleled those obtained by RNA slot blot analysis.

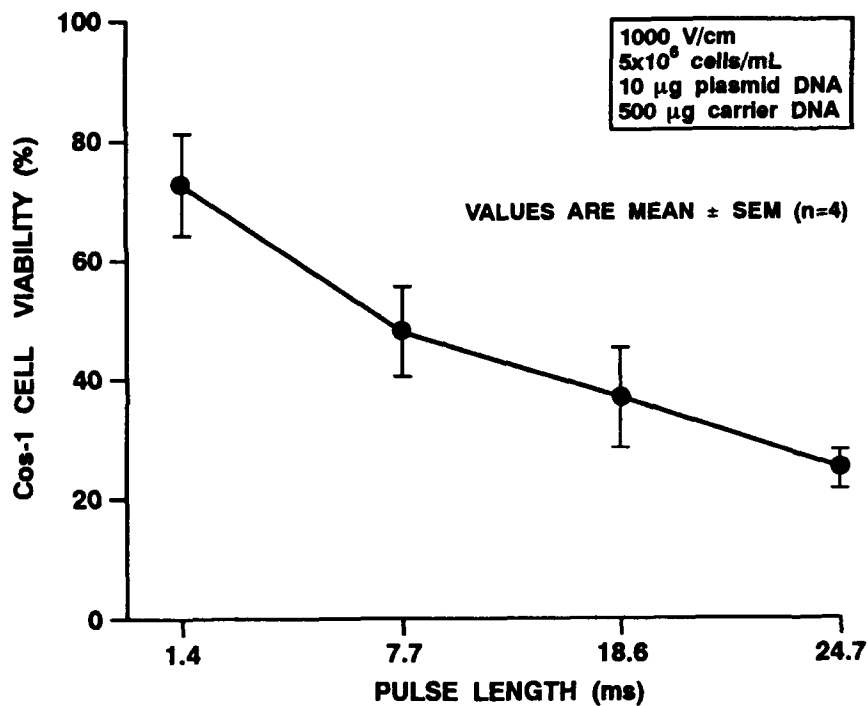


Figure 1. The effect of pulse length on the viability of electroporated COS 1 cells.

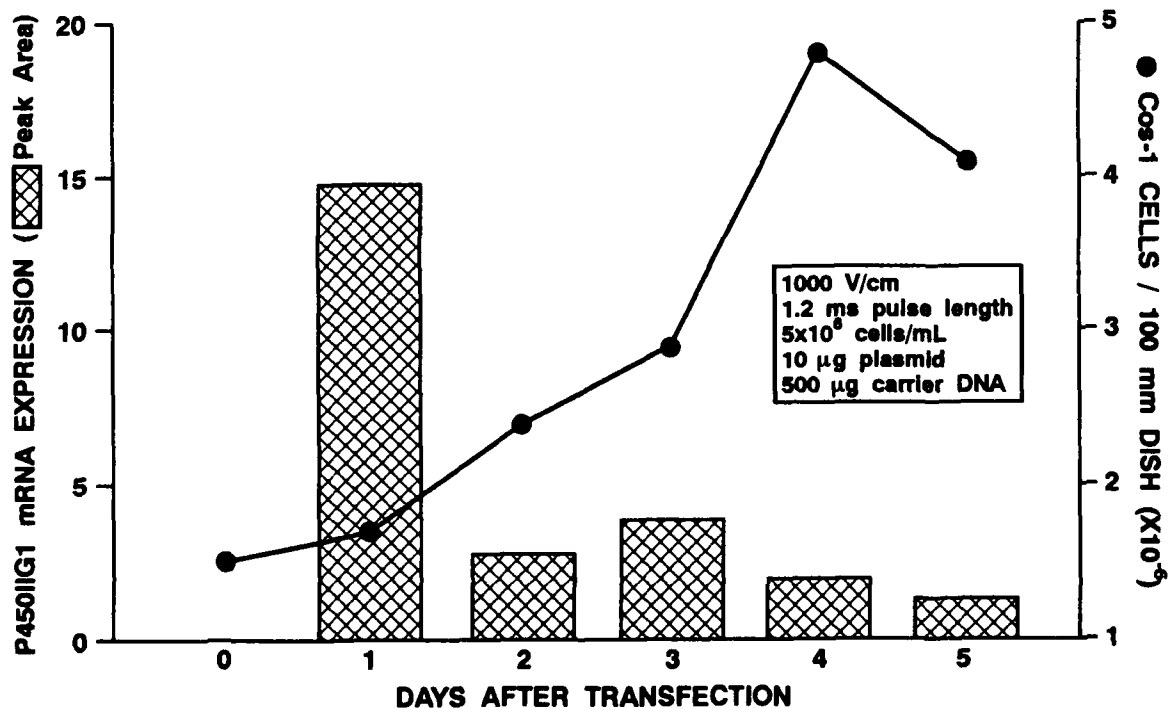


Figure 2. Quantitation of total cell number and rat P4502G1 mRNA following transfection of COS 1 cells with plasmid pSVL2G1.

We have not determined the cause of the rapid decrease in P4502G1 expression. Further experiments are needed to determine whether the decrease in P4502G1 protein synthesis was due to inhibition of P4502G1 transcription or whether, perhaps due to toxicity of P4502G1 protein to the COS 1 cells, the majority of cells initially transfected were rapidly killed. Southern analysis of transfected COS 1 cells for the presence of pSVL2G1 plasmid DNA will determine if there was a transcriptional block (i.e., plasmid present in the cells) or an elimination of plasmid containing cells (i.e., a decrease in plasmid over time).

In summary, we have demonstrated the *in vitro* expression of rat olfactory P4502G1 in COS 1 cells. This system will be used to study the substrate specificities and the catalytic properties of rat P4502G1.

(Research sponsored by the Office of Health and Environmental Research, U. S. Department of Energy, under Contract No. DE-AC04-76EV01013.)

COMPARATIVE LOCALIZATION OF CARBOXYLESTERASE IN F344 RAT, BEAGLE DOG, AND HUMAN NASAL TISSUE

K. J. Nikula, J. L. Lewis, R. Novak*, and A. R. Dahl

Nasal carboxylesterases hydrolyze inhaled organic esters, including acetates and acrylate esters, to their constituent carboxylic acids and alcohols. Lesions of the olfactory epithelium are a common result of exposure to acetates and acrylates in rodents, and the lesions are ascribed to the action of the acids (Miller, R. R. *et al.* *Fundam. Appl. Toxicol.* 1: 271, 1981). Localization of carboxylesterases within the nose is important for the prediction of sites of toxicity for inhaled substrates as well as for the prediction of residual metabolic capacity after mucosal damage has occurred (Lewis, J. L. *et al.* *Anat. Rec.* 232: 620, 1992). The use of acrylates and acetates in industrial processes may result in significant exposure to workers. Localization of other nasal enzymes indicates that important interspecies differences exist that reduce confidence in extrapolating from results in laboratory animals to the prediction of risk in people. To assess the validity of interspecies extrapolations, we compared the immunohistochemical localization of nasal carboxylesterase in the F344 rat, Beagle dog, and human tissue.

Antibody to purified rabbit hepatic carboxylesterase was elicited in goats in Bethyl Laboratories (TX). The antibody in goat serum was characterized by Western blot analysis of tissue homogenates from the species and tissues used in this study as previously described (Lewis *et. al.*, 1992). The purified antigen was shown to metabolize p-nitrophenyl butyrate and to be inhibited by malathion, indicating it was a Form B carboxylesterase.

Nasal tissue was obtained from four F344/N rats, three Beagle dogs, and eight people (medical histories known). The rats and dogs were healthy animals from the ITRI colonies. The tissues from the rats and dogs were obtained immediately after the animals were sacrificed. The people, all residents of New Mexico, were patients undergoing rhinoplasty for cosmetic purposes or for correction of upper respiratory tract obstruction resulting from conditions such as chronic rhinitis or trauma. The rat skulls, including the nasal tissues, were fixed in B-5 fixative (6 g ZnCl and 1.2 g Na-acetate in 100 mL distilled water mixed with 10 mL of acetic acid) and decalcified in 13% formic acid. Tissues were rinsed in tap water and sectioned transversely into four blocks (Young, J. T. *et al.* *Fundam. Appl. Toxicol.* 1: 309, 1981). The dog skulls were opened on the midsagittal plane; sections were taken from the ethmoturbinates and maxilloturbinates. These tissues were fixed in B-5 fixative and blocked into 3-mm sections. The human nasal tissue samples were taken from the lower portion of the middle turbinate, a region normally lined by respiratory mucosa. Because the B-5 fixative required mixing immediately prior to use and was not routinely available in the surgery room, Lana's fixative (1% glutaraldehyde:4% formaldehyde in 1% picric acid) was used for the human tissue to simplify the procedure. In comparative analyses with formalin or glutaraldehyde, we have found that Lana's produces the best tissue preservation and the lowest background for immunostaining in these tissues under these conditions. Samples were placed in Lana's fixative immediately following removal. After fixation, tissues were blocked into 3-mm sections. The tissue blocks from all three species were dehydrated in a graded series of alcohols and paraffin embedded. The blocks were sectioned at 5 μ m. Rat nasal tissue was used to verify that the quality and localization of immunostaining for nasal carboxylesterase were not altered by fixation with B-5 versus Lana's or by subsequent treatment with formic acid.

Immunohistochemistry was performed using Vector ABC immunoperoxidase reagents, DAB chromogen, and primary antibody concentrations of 1:2000 and 1:3000 immunized goat sera. Control sections were treated with a 1:2000 concentration of normal goat sera substituted for immunized goat sera in the primary incubation. Following immunohistochemistry, sections were counterstained with periodic acid-Shiff stain and Alcian blue (pH 2.5) to demonstrate the presence of neutral and acidic mucosubstances, respectively.

Immunoreactivity to the anti-carboxylesterase sera was observed in all species. Preincubation of sections with bis-p-nitrophenyl phosphate, an irreversible carboxylesterase inhibitor, eliminated staining in all tissue sections, indicating the observed immunoreactivity was specific to carboxylesterase. In the olfactory mucosa throughout

*Institute of Chemical Toxicology, Wayne State University, Detroit, Michigan

the nasal passages of the rat, immunoreactivity was present in acinar and duct cells of all Bowman's glands, as well as in the apical portion of sustentacular cells. The respiratory epithelium showed immunoreactivity in ciliated cells and to a lesser extent in secretory cells. Immunoreactivity in the dog olfactory mucosa was nearly identical to the rat with staining of the apical portion of the sustentacular cells and the acinar and duct cells of all Bowman's glands. The dog respiratory mucosa, in contrast to the rat, showed staining not only in the ciliated and secretory cells, but also in acinar cells of all subepithelial glands.

Immunohistochemical staining of the human nasal tissue varied depending on the histopathological status of the samples. In the samples with normal epithelium, diffuse immunostaining of ciliated and secretory cells of the luminal respiratory epithelium was similar to the staining in the rat and dog respiratory epithelium. There was also staining in some, but not all, subepithelial glands. Staining was greatly reduced in hyperplastic epithelia, with only scattered, multifocal patches of epithelial cells staining. Immunoreactivity of glands beneath the hyperplastic portion of the epithelium was also greatly reduced or absent. Epithelial immunostaining was completely eliminated in nasal epithelia exhibiting squamous metaplasia. Staining of glands beneath the metaplastic epithelium was lost or greatly reduced.

The results of our work indicate that nasal carboxylesterase is similarly present and distributed in normal nasal mucosa across species; therefore, the results support interspecies generalization with respect to this enzyme. However, our results also point out some striking differences in CE levels that are related to nasal lesions. The presence of various pathological states in human nasal mucosa may represent a common situation in many subpopulations. Exposure to multiple toxicants or irritants in industrial settings may produce the histopathological conditions for which metabolic data from clean laboratory animals are least applicable. Recent analyses of human nasal biopsies from Mexico City indicate that even without occupational exposures, urban populations may be exposed to enough air pollutants that nasal pathology is the norm (Calderon-Garciduenas, L. *et al. Am. J. Pathol.* 140: 225, 1992). The lesion-related differences shown in our study may mean that enzyme activity will be overestimated for the human population when the estimates are based on data obtained from disease-free laboratory animals maintained in clean environments.

(Research sponsored by the Office of Health and Environmental Research, U. S. Department of Energy, under Contract No. DE-AC04-76EV01013.)

ROLE OF NEUTROPHILS IN THE DEVELOPMENT AND RESOLUTION OF CIGARETTE SMOKE-INDUCED LESIONS IN F344 RAT NASAL EPITHELIUM

J. A. Hotchkiss, G. L. Finch, and J. R. Harkema

Neutrophils (PMN) are phagocytic cells associated with acute inflammation induced by tissue injury or infection. PMN are known to release both reactive oxygen metabolites such as the hydroxyl radical and hydrogen peroxide and proteases such as neutrophil elastase. Although PMN play a positive role by phagocytizing and removing bacteria, cellular debris, and foreign particles, recent *in vitro* studies suggest that PMN can also injure endothelial and pulmonary epithelial cells by causing cell detachment, inhibition of protein and DNA synthesis, and possible inhibition of cell proliferation (Ayars, G. H. *et al.* *Am. Rev. Respir. Dis.* 130: 964, 1984; Simon, R. H. *et al.* *J. Clin. Invest.* 78: 1375, 1986).

The purpose of this study was to determine the role of PMN in the development and resolution of cigarette smoke (CS)-induced nasal epithelial injury. Twenty-four male CDF® (F344)/Crl BR rats, 11-12 wk old, were exposed to either filtered air ($n = 12$) or 250 mg/m^3 of CS ($n = 12$) for 6 h/day for 5 days in whole-body exposure chambers as described elsewhere in this report (p. 110). Six rats from each group were depleted of circulating PMN (PMN-depleted) during the exposure period with three intraperitoneal (i.p.) injections of rabbit anti-rat PMN antisera (ANA), given at 48-h intervals beginning 24 h prior to the first exposure. The remaining six rats (controls) from each group were injected i.p. on a similar schedule with normal rabbit serum (NRS), leaving the PMN intact (PMN-sufficient). These animals were sacrificed 18 h after the fifth day of exposure.

An additional 24 male CDF (F344)/Crl BR rats, 11-12 wk old, were similarly exposed; however, all of these rats were PMN-sufficient during exposure. Immediately after the last day of exposure, they were injected i.p. with either ANA ($n = 6$ in each group) or NRS ($n = 6$ in each group) and at 48 h intervals thereafter. During this recovery period, the animals were exposed only to filtered air. These rats were sacrificed 5 days after the fifth day of exposure.

On the day of sacrifice, the rats were anesthetized and killed by exsanguination. Prior to exsanguination, a blood sample was drawn from each rat for total and differential white blood cell analysis. Immediately after death, the head of each rat was removed from the carcass and the nasal airways flushed with 10% neutral-buffered formalin. After fixation, the heads were decalcified using 13% formic acid, the nasal cavity was transversely sectioned immediately posterior to the upper incisor teeth and through the incisive papilla of the hard palate, and this tissue block was embedded in paraffin. Six-micron sections were cut from the anterior face of the paraffin-embedded tissue blocks and stained with Alcian Blue (pH 2.5)/Periodic Acid Schiff sequence (AB/PAS) for identification of acidic and neutral intraepithelial mucosubstances (IM) or hematoxylin and eosin (H&E) for histologic examination.

Two regions within the anterior nasal cavity were selected for morphometric quantitation of IM and determination of the epithelial cell numeric density and mitotic index; (1) the maxilloturbinates which are lined by nasal transitional epithelium and (2) the mid-septum (using the ventral tips of the nasal turbinates and the point of attachment of the maxilloturbinate with the lateral wall as landmarks) which is lined with respiratory epithelium. The methods used to determine the volume density (V_s) of IM, the epithelial cell numeric density, and mitotic index have been described previously (Harkema, J. R. *et al.* *Am. J. Pathol.* 130: 605, 1988; Hotchkiss, J. A. *et al.* *Exp. Lung Res.* 15: 589, 1991). The data were tested for differences between group means using an unpaired Student's *t*-test with Bonferroni correction for multiple comparisons. The criterion for statistical significance was set at $p \leq 0.05$.

Rats injected with ANA had no detectable circulating PMN at the time of sacrifice, while the animals that received NRS still had normal levels of circulating neutrophils. Five of six CS-exposed, PMN-depleted rats died during the fifth day of exposure, while none of the CS-exposed, PMN-sufficient or air-exposed, PMN-deficient rats died. Histopathological examination of the major organs suggested that the rats died of severe multifocal coagulative necrosis with secondary sepsis.

After 5 days of exposure, there was a significant increase in mitotic index in the septum and maxilloturbines in CS-exposed, PMN-sufficient rats, compared to air-exposed control rats (Table 1). However, after a 5-day recovery period, the mitotic indices in the septum and maxilloturbines of both PMN-sufficient and PMN-depleted rats had decreased to levels that were not significantly different than air-exposed control rats.

Table 1

Mitotic Indexes of Surface Epithelia Lining the Nasal Septum and Maxilloturbines of Air- or Cigarette Smoke-Exposed Rats

	Experimental Group	Septum	Maxilloturbinate
End of Exposure	<u>Air-Exposed</u> (PMN-Depleted + PMN-Sufficient)	0.02 ± 0.02	0.0 ± 0.0
	<u>CS-Exposed</u> (PMN-Sufficient)	0.51 ± 0.2*	1.72 ± 0.40*
5 Day Recovery	<u>Air-Exposed</u> (PMN-Depleted + PMN-Sufficient)	0.05 ± 0.05	0.04 ± 0.04
	<u>CS-Exposed</u> (PMN-Sufficient)	0.22 ± 0.09	0.16 ± 0.11
	<u>CS-Exposed</u> (PMN-Depleted)	0.16 ± 0.06	0.19 ± 0.06

* = Significantly different than air-exposed controls ($p \leq 0.05$).

At the end of exposure, the numeric density of epithelial cells lining the septum (Fig. 1) but not the maxilloturbines was significantly greater in PMN-sufficient, CS-exposed rats than in air-exposed control rats. The epithelium overlying both regions had focal regions of squamous metaplasia. After 5 days of recovery, the numeric density of epithelial cells overlying the maxilloturbines of CS-exposed, PMN-sufficient, but not CS-exposed, PMN-depleted rats had returned to control levels. In the septum, the CS-exposed, PMN-depleted rats had a significantly more epithelial cells after 5 days of recovery than did the CS-exposed PMN-sufficient animals. However, both CS-exposed recovery groups had significantly higher numeric densities than their air-exposed controls (Fig. 1).

The volume density of IM in the septum of PMN-sufficient rats decreased ~10-fold (Fig. 2), while the amount of IM in the maxilloturbines increased ~10-fold after 5 days of exposure to CS. After 5 days of recovery, compared to air-exposed, PMN-sufficient rats, the quantity of IM in the maxilloturbines of CS-exposed, PMN-depleted rats, but not CS-exposed, PMN-sufficient rats, was still significantly elevated. After 5 days of recovery, the quantity of IM in the septa of both CS-exposed, PMN-depleted and PMN-sufficient rats was not significantly different than air-exposed, PMN-sufficient rats. However, the volume density of IM in the septa of air-exposed, PMN-depleted rats was approximately three times greater than PMN-sufficient air controls.

This study suggests that PMN play an integral role in the repair of CS-induced nasal epithelial injury, and protecting airway epithelia, damaged by toxicant exposure, against opportunistic bacterial infections. CS-exposure resulted in significant nasal epithelial hyperplasia, squamous metaplasia, and secretory cell metaplasia. During the recovery period, epithelial hyperplasia was significantly reduced in PMN-sufficient rats, compared to PMN-depleted rats. The data suggest that PMN which infiltrate a site of injury may kill epithelial cells or increase epithelial cell exfoliation. In summary, PMN appear to play an essential role in the rat's ability to resist opportunistic bacterial infections during CS-induced epithelial injury and may help to return CS-induced hyperplastic nasal epithelium to its normal cell density after cessation of exposure.

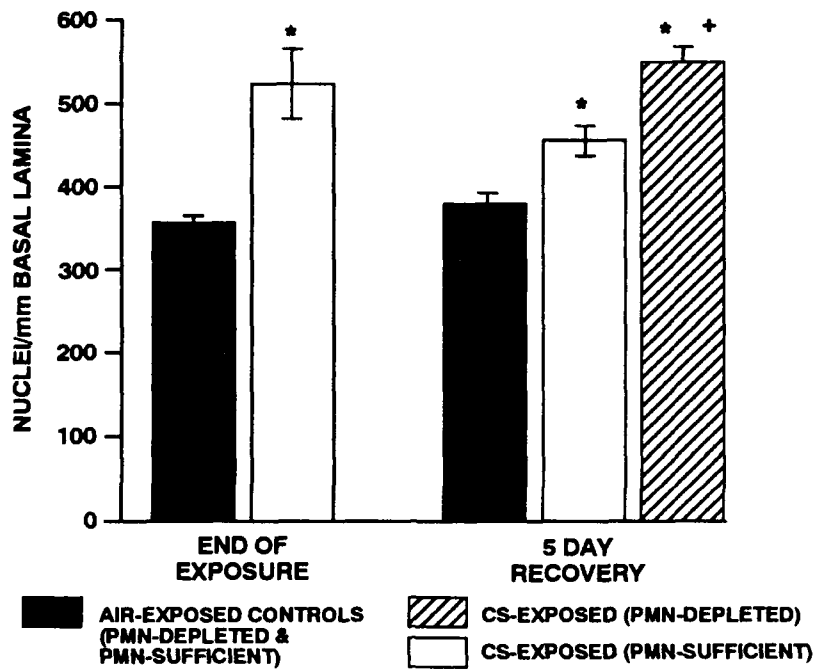


Figure 1. Epithelial cell numeric density in nasal mid-septum epithelium from PMN-depleted and PMN-sufficient rats exposed to air or 250 mg/m^3 cigarette smoke (CS) at the end of exposure or after 5 days recovery in air. Values are the mean \pm SEM. * = significantly different than air-exposed controls; + = significantly different than CS-exposed PMN-sufficient rats.

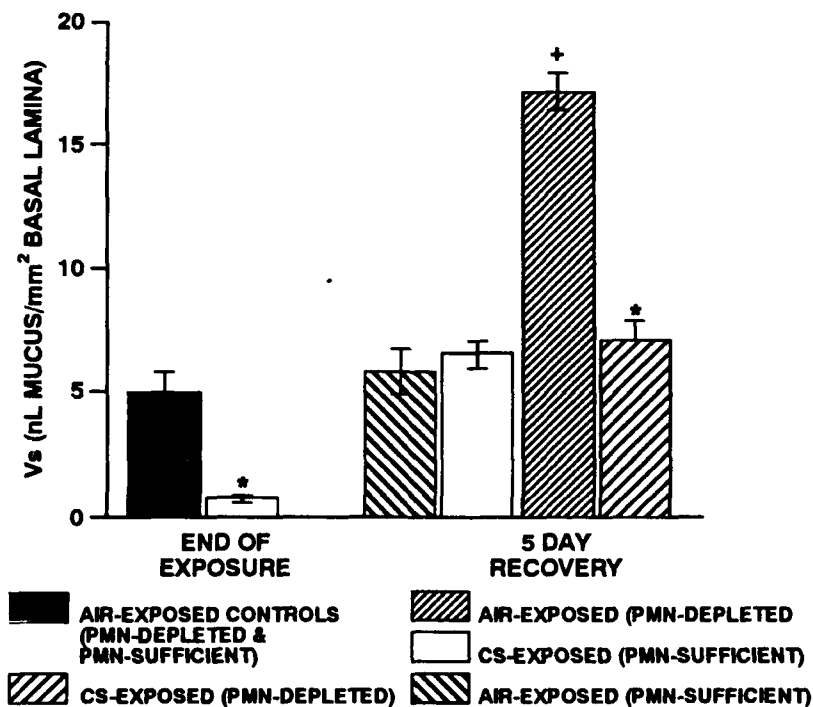


Figure 2. Volume density of intraepithelial mucus substances in nasal mid-septum epithelium from PMN-depleted and PMN-sufficient rats exposed to air or 250 mg/m^3 cigarette smoke (CS) at the end of exposure or after 5 days recovery in air. Values are the mean \pm SEM. * = significantly different than air-exposed controls; + = significantly different than PMN-sufficient air-exposed control rats.

(Research sponsored by the Office of Health and Environmental Research and the Assistant Secretary for Defense Programs, U. S. Department of Energy, under Contract No. DE-AC04-76EV01013.)

CONTINUED ANTIBODY PRODUCTION IN PULMONARY ALLOGRAFTS IN NONIMMUNE RECIPIENTS

D. E. Bice, A. J. Williams, and B. A. Muggenburg

After pulmonary immunization and antigen challenge, antibody continues to be produced in the lung for at least 5 yr (Bice, D. E. *et al.* *Immunology* 74: 215, 1991). Repeated antigen exposures are not necessary, suggesting that specific mechanisms must allow immune cells to maintain long-term antibody production in the lung. Data presented in this report help to elucidate these mechanisms. Our results show that cells responsible for long-term antibody production remain in the lung, rather than entering the recirculating pool of lymphocytes, and that antibody produced by cells in the lung contributes significantly to systemic antibody levels. In addition to understanding basic pulmonary immunity, the observation that significant amounts of antibody continue to be produced in a lung allograft transplanted into a donor treated with drugs to prevent allograft rejection is also important in understanding pulmonary immune defenses in humans who have received lung transplants. These individuals frequently have pulmonary infections that can lead to death, and any data concerning immunity in transplanted lungs are beneficial.

For primary immunization, 10 mg keyhole limpet hemocyanin (KLH) in 1 mL saline were instilled into the left cardiac lung lobe (LCL) of three anesthetized donor Beagle dogs using a fiberoptic bronchoscope (Bice, D. E. and B. A. Muggenburg. *Am. Rev. Respir. Dis.* 138: 565, 1988a). The LCL lobe was challenged with 1 mg KLH in 1 mL saline at 21 and 40 or 42 days after primary immunization. Using the same schedule as for KLH, the right cardiac lung lobe (RCL) of the donor dogs was instilled with a primary immunization of 10^{10} sheep red blood cells (SRBC) in 1 mL saline and challenges of 10^9 SRBC in 1 mL saline. Two control lobes, the left (LDL) and right diaphragmatic lobes (RDL), each received 1 mL saline at the time of each immunization and challenge.

To quantitate the level of immunity produced by instillation of antigen, blood and lavage fluid from exposed and control lung lobes were obtained on days 3, 5, 7, 10, 12 and 14 after immunization and the first challenge (Bice, D. E. and B. A. Muggenburg. *Am. Rev. Respir. Dis.* 138: 661, 1988b). On day 5 after the second challenge, lavage fluid and blood samples were taken again.

Donor dogs were anesthetized, the left lung was perfused with 1 liter of cold Collin's solution, and the dogs were then sacrificed by exsanguination. The lung-associated lymph nodes were removed from the donor lung (day 6 after the second challenge) which was then transplanted into a recipient dog that had not been immunized with KLH or SRBC. The cold ischemia time for the donor lung was 4 to 6 h. The lymph nodes associated with the recipient's left lung were left intact. Perpetual daily cyclosporin and 14 days of azothioprine were used to prevent rejection.

To evaluate antibody production in recipient dogs, blood and lavage fluid from the LCL (transplanted), the RCL (recipient) and LDL and RDL control lobes were obtained starting 3 days after transplantation. Samples continued to be taken through 240 days after transplantation. The lavage fluids, sera, and *in vitro* culture media were assayed for specific IgG, IgA, and IgM antibody to KLH and SRBC using an enzyme-linked immunosorbent assay (ELISA) (Bice and Muggenburg, 1988b). Data are complete for anti-KLH and anti-SRBC IgG and IgA, and the data are expressed as ELISA units calculated by multiplication of O.D. values times the dilution that gave an O.D. of approximately 1.0.

To evaluate the level of anti-KLH or anti-SRBC IgG, IgA, and IgM antibody being produced by blood lymphocytes or lymphocytes lavaged from the lung, cells from lavage fluid or blood were cultured for 7 days at 10^6 /mL in RPMI-1640 (Grand Island Biologicals) complete media at 37°C (Bice *et al.*, 1991). Cycloheximide, an inhibitor of protein synthesis, was added to half of the *in vitro* cultures to verify that the antibody was produced by the cells rather than released from their membranes (Bice *et al.*, 1991). At this time, data are complete only for anti-KLH IgG produced by blood cells and cells lavaged from the lung.

The donor dogs showed typical responses in the serum and lung lavage fluid after primary immunization and challenge of the LCL lobe with KLH. After transplantation, anti-KLH IgG and IgA antibody continued to be produced at high levels in the LCL lobe through 50 days (Fig. 1A). After this time, there was a marked decrease of anti-KLH antibody in lavage fluid from the LCL lobe. However, low levels of anti-KLH IgG and IgA were present in lavage fluid from the LCL (donor) lobe through 240 days after transplantation (Fig. 1B). In addition, cells producing anti-KLH antibody were lavaged from the allograft lungs of two of the dogs for around 50 days and from one of the dogs from more than 100 days after transplantation (data not shown).

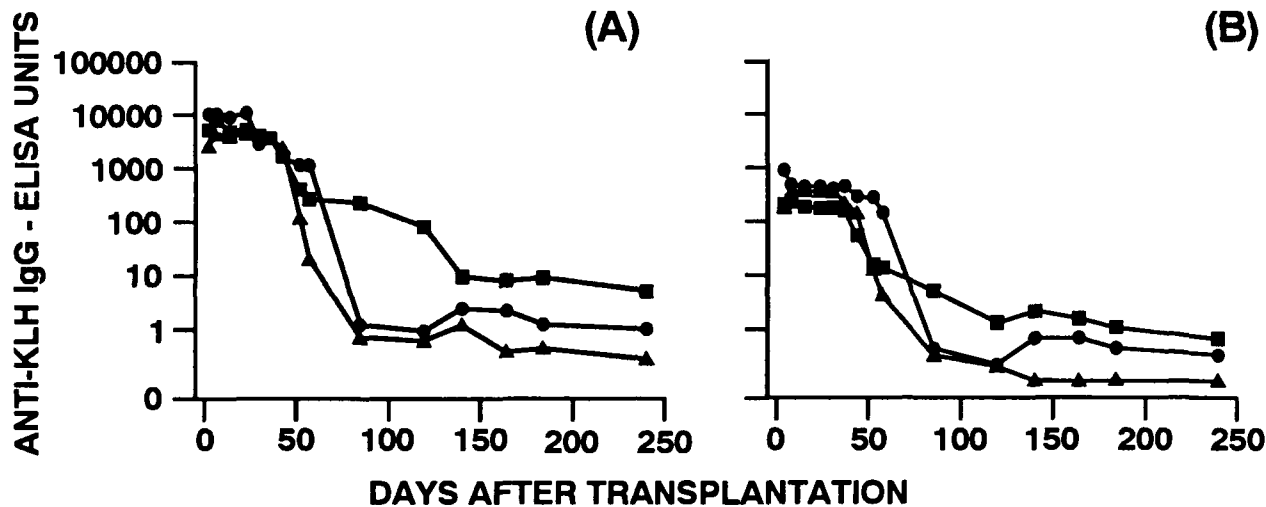


Figure 1. Levels of anti-keyhole limpet hemocyanin (KLH) IgG (A) and IgA (B) antibody present in lavage fluid from the left cardiac lung lobe (LCL) exposed to KLH through 240 days after transplantation of an immune donor lung into nonimmune recipients. Each curve represents data from a single dog.

In contrast to immunity in the LCL lobe, anti-KLH IgG and IgA antibody was not detectable in lavage fluid from the recipient's RCL or RDL lobes. In addition, no detectable anti-KLH antibody was produced by cells lavaged from the RCL lobe.

High levels of anti-KLH IgG and IgA antibody were also present in serum starting at 3 days after transplantation (Fig. 2A). The levels of anti-KLH antibody fell gradually in serum, although serum contained detectable antibody 240 days after transplantation (Fig. 2B). No detectable anti-KLH IgG antibody was produced by blood lymphocytes.

Low levels of anti-SRBC IgG and IgA were observed in lavage fluid from the LCL and in serum. No detectable anti-SRBC antibody was observed from the RCL or RDL lobes.

These observations show that immune cells present in the lung interstitial tissues and/or alveoli at the time of transplantation continue to make antibody for extended times after transplantation and treatment with immunosuppressive therapy necessary to prevent allograft rejection. This observation suggests that immune cells responsible for long-term antibody production are likely not part of the recirculating pool of lymphocytes. In addition, the relatively high level of anti-KLH antibody in blood from the lung allograft recipient indicates that antibody produced in the transplanted lung makes a significant contribution to systemic antibody levels.

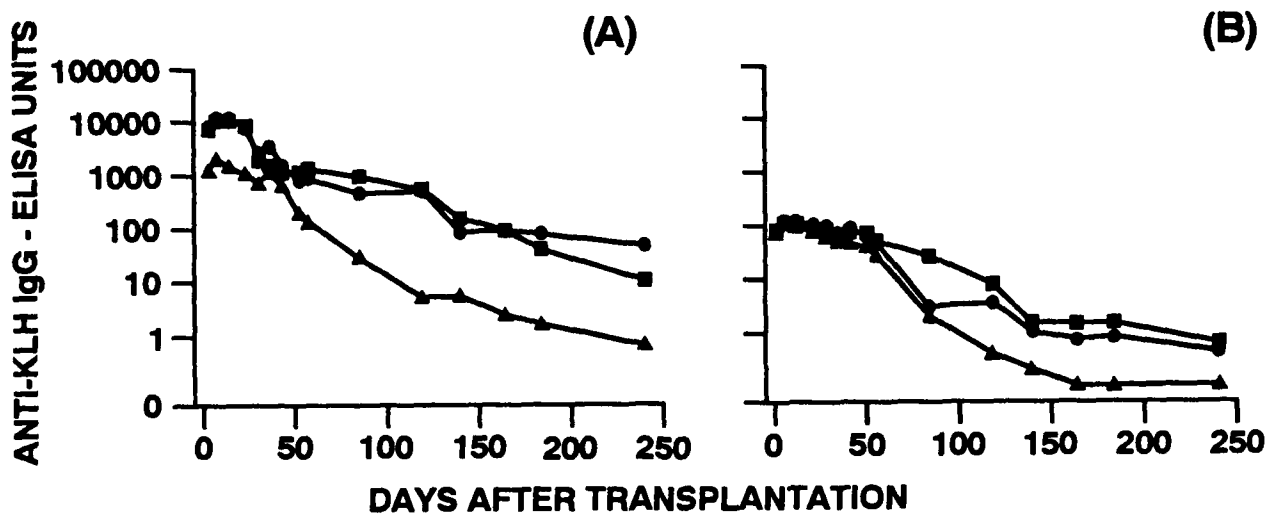


Figure 2. Levels of anti-keyhole limpet hemocyanin (KLH) IgG (A) and IgA (B) antibody in serum through 240 days after transplantation of an immune donor lung into nonimmune recipients. Each curve represents data from a single dog.

(Research sponsored by the Office of Health and Environmental Research, U. S. Department of Energy, under Contract No. DE-AC04-76EV01013).

LYMPHOCYTE CHARACTERISTICS AND MITOGEN-SPECIFIC *IN VITRO* PROLIFERATION IN UNEXPOSED RHESUS MONKEYS

G. L. Finch, D. E. Bice, K. F. Pavia*, and P. J. Haley**

Chronic beryllium disease (CBD) in humans is characterized by cell-mediated, beryllium (Be)-specific immune responses against Be in the lung that culminate in clonal expansion of pulmonary lymphocytes and eventually granulomatous lung disease. The preferential proliferation of T-helper lymphocytes ($CD4^+$) has been reported (Newman, L. S. *et al.* *Am. Rev. Respir. Dis.* 139: 1479, 1989). Recently, an *in vitro* lymphocyte proliferation assay (LPA) has been used to confirm the presence of Be-specific responses in symptomatic CBD patients, and to screen asymptomatic individuals who have been exposed to Be and therefore may be at risk for development of CBD (Newman *et al.*, 1989).

To examine the cellular mechanisms involved in human CBD induction and progression, we have conducted investigations in Be-exposed animal models, including dogs (Haley, P. J. *et al.* *Lab. Invest.* 61: 219, 1989), mice (1990-91 Annual Report, p. 193, and this report, p. 171), and nonhuman primates (1990-91 Annual Report, p. 159). The use of the LPA on lymphocytes obtained from the blood and lungs of exposed animals has been central to these studies. However, one troubling aspect of the assay has been the variability in the proliferative responses of lymphocytes to administered Be in exposed and control individuals. To further understand the population and antigen-sensitivity of lymphocytes in the absence of exposure to Be, this study was conducted on a group of unexposed rhesus monkeys.

Eight male rhesus monkeys (*Macaca mulatta*; approximately 8 yr old, White Sands Research Center, Alamogordo, NM) were used in this study. The monkeys were provided food (Purina Monkey Chow supplemented with fresh fruit) and water *ad libitum*, except that food was withheld overnight before the lavage procedures. The monkeys were studied in groups of four on any given experiment day. Each animal was studied two times with a minimum of 30 days between samplings. For lavage, the monkeys were sedated using an intramuscular injection of 10 mg/kg ketamine, then maintained in a deep plane of anesthesia using 1.5% halothane in oxygen. A fiberoptic bronchoscope was guided into the left and right diaphragmatic lung lobes, and the lavage was performed using a total of 35 mL sterile saline. While the animal was under anesthesia, approximately 8 mL of blood were obtained from the femoral vein. Lung cells recovered in lavage fluids were pelleted by centrifugation and resuspended in RPMI-1640 (Grand Island Biological Co., Grand Island, NY) supplemented with 10% heat-inactivated human serum (blood type AB). White blood cells were isolated by centrifugation over isolymp. Cells were counted using an automated cell counter (Coulter Electronics, Hialeah, FL), and cell types present were determined from cytocentrifuge preparations. T-lymphocyte subtypes in blood were quantified using flow cytometry (Becton-Dickinson FACStar-plus) after staining with CD4 (helper/inducer-type; anti-leu-3a-CD4-PE) and CD8 (cytotoxic/suppressor-type; anti-leu-2a-CD8-FITC; both Becton-Dickinson, San Jose, CA) specific anti-human mouse monoclonal antibodies (Rappocciolo, G. *et al.* *Vet. Pathol.* 29: 53, 1992).

Techniques used for the LPA were generally as described by Haley *et al.* (1989). Briefly, white blood cells were studied at a concentration of $2 \times 10^5/0.1$ mL in flat-bottomed, 96-well microtiter plates, and lung lavage cells were studied at a concentration of $1 \times 10^5/0.1$ mL in round-bottomed, 96-well plates. Cell cultures were exposed to phytohemagglutinin (PHA, a known T-lymphocyte mitogen; 2 μ g/mL; cultured with cells for 3 days) and $BeSO_4$ (1, 10, and 100 μ M; cultured with cells for 5 days). $BeSO_4$ was used on blood and lung lavage cells; PHA was used only on blood cells, because insufficient lung lavage cells were available. Control wells received no PHA or $BeSO_4$, and blank wells contained PHA or $BeSO_4$ without cells. All wells were pulsed 18 h before harvesting with 3H -thymidine to label dividing cells. Cells were automatically harvested (Skatron, Lier, Norway) and counted (Packard 2500-TR, Meriden, CT) using a water rinse; data were expressed as disintegrations per min (DPM) for each well after subtraction of background counts. All samples were run in triplicate or quadruplicate depending on the number of cells available. Stimulation indices (SI) were calculated

*Sterling-Winthrop, Inc., Rensselaer, New York

**Sterling-Winthrop, Inc., Malvern, Pennsylvania

as the mean DPM of PHA- or BeSO₄-stimulated cultures divided by the mean DPM of unstimulated (control) cultures.

The numbers and types of cells obtained from the animals after processing as described above were similar for the two replicate samplings (Table 1). The relatively minor differences observed in either cell number or type were not statistically significant using a Student's *t*-test. In general, animals had consistent values over the two samplings; e.g., if a monkey had a relatively high cell yield by lavage in the first experiment, then it also did in the second experiment. There were, however, exceptions to this trend.

Table 1

Cell Numbers and Types Obtained From the Lungs and Blood of Rhesus Monkeys^a

	First Sampling	Second Sampling
Lavage Cells^b		
Total number of cells	(6.6 ± 2.0) × 10 ⁶	(6.0 ± 2.9) × 10 ⁶
Macrophages (%)	81.5 ± 8.6	88.2 ± 4.4
Lymphocytes (%)	17.4 ± 9.3	10.2 ± 4.7
Blood Cells^c		
Number of cells/mL	(2.0 ± 0.8) × 10 ⁶	(2.2 ± 1.1) × 10 ⁶
Monocyte (%)	15.5 ± 4.4	8.8 ± 5.2
Lymphocytes (%)	84.2 ± 4.2	90.4 ± 6.1

^aValues given are mean ± standard deviation; n = 8 per group.

^bSegmented neutrophils and eosinophils were occasionally observed in lung lavage cytocentrifuge preparations, but were never greater than 3% of the cells present.

^cBlood cell counts and differentials were after separation over isolymp, so that nearly all of the neutrophils were removed.

The types of lymphocytes present in blood were determined only in the second experiment. A total of 28% (S.D. = 10, range 16 to 49) of the lymphocytes were labeled by the CD4⁺ antibody, and 29% (S.D. = 13, range 17 to 54) of the lymphocytes were labeled by the CD8⁺ antibody. The mean ratio of CD4⁺ to CD8⁺ phenotypes in individual monkeys was 1.12 (S.D. = 0.48, range 0.29 to 1.73). These values are consistent with data reported for 24 rhesus monkeys by Rappocciolo *et al.* (1992), who found values of 26%, 37%, and 0.70 for the incidences of CD4⁺, CD8⁺, and ratio of CD4⁺/CD8⁺, respectively. In addition, we observed that 3% (S.D. = 2, range 1 to 8) of the lymphocytes were stained by both antibodies, and 41% (S.D. = 14, range 16 to 59) of the lymphocytes were not labeled by either antibody.

Results of the LPA are given in Table 2. For the lung lavage cells, increasing BeSO₄ concentration significantly ($p < 0.05$) decreased the SI. The animals were relatively consistent between the two samplings, with the exception of one monkey (M150) that had unexpectedly high (greater than the mean + 2 standard deviations) incorporation of ³H in the control wells in the second sampling. For blood, the PHA was highly mitogenic as expected. The extent of proliferation in response to PHA was similar to that observed by G. Rappocciolo *et al.* (1992). The relatively high degree of variability in response to PHA among the animals was due to a high level (greater than the mean + 2 standard deviations) of ³H incorporation in control wells for one monkey. This was observed in both samplings. Unlike the lung lavage cells, there were no significant influences of BeSO₄ concentration on SI for the blood lymphocytes. We hypothesize that the primary difference is caused by Be toxicity to the relatively high numbers of macrophages in the lung cell cultures, compared to the blood. These macrophages might be taking up a considerable percentage of the ³H in control and low concentration BeSO₄ cultures by pinocytosis, whereas at higher BeSO₄ concentrations, cells might be either killed or functionally less active.

Table 2

Stimulation Indices for Blood and Lung Lymphocytes Obtained From Rhesus Monkeys^a

	First Sampling	Second Sampling
Lavage Cells^b		
dpm of control cultures ^c	(2.6 ± 0.9) × 10 ³	(4.1 ± 4.4) × 10 ³
BeSO ₄ - 1 μM	1.2 ± 0.1	1.2 ± 0.3
BeSO ₄ - 10 μM	0.5 ± 0.4*	0.3 ± 0.1*
BeSO ₄ - 100 μM	0.4 ± 0.4*	0.2 ± 0.2*
Blood Cells		
dpm of control cultures	(13 ± 23) × 10 ³	(10 ± 17) × 10 ³
PHA ^d	64 ± 59	84 ± 145
BeSO ₄ - 1 μM	ND ^e	1.0 ± 0.6
BeSO ₄ - 10 μM	0.9 ± 0.4	0.8 ± 0.2
BeSO ₄ - 100 μM	0.9 ± 0.7	0.8 ± 0.5

^aStimulation index (SI) is defined as the mean dpm of mitogen-stimulated cultures (PHA or BeSO₄) divided by the mean dpm of unstimulated (control) cultures.

^bValues given for SI are mean ± standard deviation; n = 8 per group. An asterisk (*) denotes statistical significance at a p < 0.01 level compared to the 1 μM BeSO₄ concentration.

^cFor lung lavage cells, stimulation indices were measured only for BeSO₄ and not for PHA, due to the relatively low cell numbers available.

^ddpm = disintegrations per minute of ³H in cultures receiving no mitogen; n = 8 per group.

^ePHA = phytohemagglutinin.

^fND = not determined because of insufficient numbers of cells.

Of considerable interest is the extent and sources of variability in the LPA data. We are examining contributions to the total variance from the replicate samples, mitogens, and individual animals, using an analysis of variance.

In conclusion, we have described lung lavage and blood cell number, differential type, and lymphocyte populations and function, for a group of eight unexposed rhesus monkeys from the Institute's colony. These data are of interest because of the potential use of this group of animals in immunologic studies, and because the data will hopefully provide an insight into the factors that influence the LPA.

(Research sponsored by the Office of Health and Environmental Research, U. S. Department of Energy, under Contract No. DE-AC04-76EV01013.)

**VIII. UNIVERSITY OF UTAH STUDIES
OF INJECTED ACTINIDES**

STATIC AND DYNAMIC BONE HISTOMORPHOMETRY OF ^{239}Pu -TREATED DOGS

W. S. S. Jee*, R. B. Setterberg*, Y. F. Ma*, M. Li*, X. G. Liang*, F. Johnson*, and H. Z. Ke*

The first quantitative investigation of local radiation doses and the biological activity at corresponding specific sites of high and low tumor incidence in Beagle dogs was made by T. J. Wronski *et al.* (*Radiat. Res.* 83: 74, 1980), who determined the micro (i.e., local) distribution of Pu on trabecular surfaces and related the observed changes to the turnover activity at those sites. It was shown that the initial, high concentration of Pu on trabecular surfaces of some high-tumor-incidence sites remained nearly constant for the first month after injection, but declined rapidly between the first and second month, followed by a long period during which the concentration of Pu declined only gradually. Changes in rates of biological activity and Pu concentrations were thought to be caused by an early radiation damage. While this is possible, a more recent view is that the confinement period at the time of injection and subsequent increase in physical activity might be responsible for those changes. In view of this and other possible inconsistencies, it is advisable to compare the early metabolism of low levels of Pu under conditions of confinement and nonconfinement. At the same time, data should be collected on the translocation kinetics of Pu at the local level, and the observed local Pu concentrations should be related to their concentrations in plasma and to the respective biological activities at those sites. This information is necessary for the construction of metabolic-dosimetric models, which, together with data on the chronic toxicity, will form the basis for future risk estimates.

The purpose of this experiment was to provide early detailed dosimetric and biological data on young adult dogs injected with ^{239}Pu under conditions of "Confinement" (in a metabolism cage) and "Nonconfinement" (housed in the kennel facility). Initial gross and local deposition of Pu, its retention and local translocation, and the corresponding biological elements that determine these parameters are being determined to construct appropriate metabolic/dosimetric models for dogs injected with ^{239}Pu . This report deals with our progress in providing data on the turnover of cancellous bone measured as a function of time after exposure.

Fourteen dogs were injected without prior confinement with 0.6 kBq ^{239}Pu per kg and sacrificed sequentially at times ranging from 1 to 64 wk after injection. For comparison, 15 additional dogs were confined for the usual 4-wk period at injection and were sacrificed sequentially in groups of three between 4 wk and 64 wk after injection. All dogs received up to three treatment regimens with fluorescent bone growth markers for the evaluation of bone turnover rates as a function of temporary confinement and nonconfinement.

Forty-micron-thick, undecalcified, plastic-embedded ground sections of the proximal, mid-shaft, and distal humerus, proximal ulna, and second lumbar vertebral body were processed and analyzed (Wronski *et al.*, 1980). The static and dynamic histomorphometry analyses included the percentage of trabecular bone area, trabecular width, number and separation, and bone-volume-based bone formation rate (Frost, H. M. *et al.* *Metab. Bone Dis. Relat. Res.* 2: 285, 1981; Kimmel, B. A. and W. S. S. Jee. *Anat. Rec.* 203: 31, 1982; Parfitt, A. M. *et al.* *J. Clin. Invest.* 72: 1396, 1983; Table 1). The current report deals only with data derived from the lumbar vertebral body, distal humerus, and proximal ulna from confined dogs sacrificed at 4, 8, 16, 32, and 64 wk after injection of ^{239}Pu (Table 1). We assume that during the bone labeling period, there was no net gain or loss of bone mass (i.e., bone formation = bone resorption); thus, we used the bone-volume-based bone formation rate as an index of bone turnover.

The data are too limited to draw any definite conclusions, but there are some interesting trends worth mentioning. There are differences in bone mass and architecture (thickness, number, separation, and turnover) among the three bones. The lumbar vertebral body is constructed of less and thinner trabecular bone. Furthermore, it possesses a higher bone formation rate (turnover rate) than the other two bones. Also, in all three bones, the turnover rates are much lower at 4 wk and sometimes at 8 wk than at other times. Again, these data are too preliminary to discuss their significance; that will have to await collection of data from a known site of high cancellous bone turnover (i.e., proximal humerus; Kimmel and Jee, 1982) and from the comparison of the same bones between confined and nonconfined dogs.

*Radiobiology Division, University of Utah School of Medicine, Salt Lake City, Utah

Table 1

Bone Histomorphometry of Confined Beagle Dogs

Group	n ^a	Trabecular Bone Area (%)	Trabecular Thickness (μm)	Trabecular Number (#/mm)	Trabecular Separation (μm)	Bone Formation Rate/BV ^b (%/yr)
2nd Lumbar Vertebral Body						
4 wk	3	27.3 ± 2.8 ^c	100 ± 12.6	2.78 ± 0.23	278 ± 27	118.0 ± 25.3
8 wk	3	29.9 ± 3.8	98 ± 9.0	3.05 ± 0.26	239 ± 29	126.2 ± 25.7
16 wk	3	29.9 ± 1.1	108 ± 8.7	2.78 ± 0.29	265 ± 33	149.5 ± 56.2
32 wk	3	30.7 ± 2.9	109 ± 15.9	2.86 ± 0.16	248 ± 13	190.1 ± 54.8
64 wk	2	28.9 ± 0.1	107 ± 0.7	2.71 ± 0.03	273 ± 13	84.8 ± 2.4
Distal Humerus (DHE2)^d						
4 wk	3	35.1 ± 4.7	139 ± 20.8	2.54 ± 0.14	256 ± 21	18.9 ± 11.8
8 wk	3	40.6 ± 4.4	184 ± 38.5	2.24 ± 0.30	268 ± 31	102 ± 83.3
16 wk	3	37.9 ± 5.2	154 ± 10.0	2.45 ± 0.26	257 ± 45	93.7 ± 16.1 ^e
32 wk	3	41.8 ± 1.7	163 ± 11.0	2.58 ± 0.16	226 ± 17	27.7 ± 21 ^f
64 wk	2	45.0 ± 1.1 ^e	155 ± 19.0	2.93 ± 0.29 ^g	189 ± 15 ^{e,g,h}	55.17 ± 1.0 ^{e,f}
Proximal Ulna (PUA2)^d						
4 wk	3	46.7 ± 6.7	168 ± 31.8	2.81 ± 0.21	190 ± 20	31.5 ± 13.8
8 wk	3	54.8 ± 8.6	198 ± 30.5	2.78 ± 0.27	164 ± 39	49.8 ± 15.2
16 wk	3	55.0 ± 6.4	212 ± 22.6	2.60 ± 0.23	175 ± 34	66.7 ± 22.0
32 wk	3	51.1 ± 8.4	129 ± 15.8 ^f	3.95 ± 0.38 ^{e,f,g}	126 ± 30	44.6 ± 14.4
64 wk	2	46.0 ± 4.1	221 ± 37.7	2.13 ± 0.55 ^h	265 ± 88	119.6 ± 85.7

^an = number of dogs.^bBV = bone volume.^cMean ± SD.^dDHE2 = last 2 cm of distal humerus; PUA2 = 2 cm distal to proximal end of ulna.^ep < 0.05 vs. 4 wk value.^fp < 0.05 vs. 16 wk value.^gp < 0.05 vs. 8 wk value.^hp < 0.05 vs. 32 wk value.

(Research sponsored by the Office of Health and Environmental Research, U. S. Department of Energy, under Contract Nos. DE-AC02-76EV00119 and DE-AC04-76EV01013.)

STATISTICS OF HITS TO BONE CELL NUCLEI

I. L. Kruglikov***, E. Polig*, and W. S. S. Jee***

In this study, the statistics of hits to nuclei of bone-lining cells is being developed. The bone-lining cell is present only during the period of quiescence of the given bone structural unit (BSU). This period of quiescence is the time interval between two remodeling cycles of a BSU, when no cell-mediated resorption occurs in the formation of bone. The stochastic nature of the lifetime of the BSU has been discussed previously (Polig, E. and W. S. S. Jee. *Calcif. Tissue Int.* 41: 130, 1987). For the following, it is assumed that the lifetime of the bone-lining cells, ρ , is identical to the period of quiescence of its associated BSU. The law of remodeling, which was defined for the replacement of BSUs, also governs the fate of the bone-lining cells:

$$g(\delta) = \lambda\delta^\beta , \quad \lambda, \beta \geq 0 , \quad (1)$$

where $g(\delta)$ is the conditional probability that a bone-lining cell of age δ disappears within the infinitesimal interval $(\delta, \delta + d\delta)$; λ is a scaling factor dependent on the respective bone turnover rate; and β depends on the time sequence of bone remodeling. Only the stationary situation is considered here, when both the bone turnover rate and the above law of remodeling do not change in time. In general, one can describe the hits to the nuclei of the bone-lining cells as a Poisson process during the random period of quiescence, the distribution of which depends on the law of remodeling.

Let the conditional probability that the number of hits to a bone cell nucleus equals v , provided the duration of the irradiation interval is ρ , be $\phi(v|\rho)$:

$$\phi(v|\rho) = \frac{(\alpha\rho)^v}{v!} e^{-\alpha\rho} , \quad (2)$$

where α is the mean hit rate for the given target (Polig, E. et al. *Radiat. Res.* 131: 133, 1992). The conditional expectation $E\{v|\rho\}$ is $\alpha\rho$. The unconditional probability P_v of v hits is obtained by integration over all possible values of ρ . The unconditional mean number of hits \bar{v} to a bone cell nucleus is $\bar{v} = \alpha\bar{\rho}$, where $\bar{\rho}$ is the mean quiescence period. Constant irradiation conditions are characterized by a constant parameter α . It is seen that the expectation value \bar{v} is independent of the form of the distribution of the quiescence periods. The variance of the number of hits is $Var\{v\} = E\{v^2\} - E^2\{v\} = \alpha^2 Var\{\rho\} + \alpha\bar{\rho}$. The deviation from the Poisson statistics is characterized by the relative variance,

$$R_v(v) = \frac{Var\{v\}}{\bar{v}} = 1 + \alpha R_v(\rho) ,$$

where ($R_v(\rho) = Var\{\rho\}/\bar{\rho}$) is the relative variance of the quiescence periods. In the low dose regime ($\alpha\bar{\rho} \ll 1$), the variation of the number of hits is essentially determined by the Poisson statistics, and in the high dose regime ($\alpha\bar{\rho} \gg 1$), it is determined by the variation of the period of quiescence.

In the particular case of random remodeling ($\beta = 0$), there is an exponential distribution of quiescence periods ρ , and the above relationships yield $Var\{v\} = \alpha\bar{\rho}[1 + \alpha\bar{\rho}]$, and $R_v(v) = 1 + \alpha\bar{\rho}$. In the limiting case of deterministic remodeling ($\beta \rightarrow \infty$), the lifetime of all cells is constant ($\bar{\rho}$). Thus $Var\{v\} = \bar{v} = \alpha\bar{\rho}$, and the relative variance is one. In the general case, the density of the quiescence period ρ follows a Weibull distribution (Polig and Jee, 1987):

$$f(\rho) = \frac{1}{\mu\rho} \left[\frac{\mu\Gamma(\mu)\rho}{\bar{\rho}} \right]^{1/\mu} \exp\left\{-\left(\frac{\mu\Gamma(\mu)\rho}{\bar{\rho}}\right)^{1/\mu}\right\} , \quad (3)$$

*Kernforschungszentrum Karlsruhe, Institut für Genetik und für Toxikologie von Spaltstoffen, Karlsruhe, Germany

**Physical-Mathematical Laboratory, Institute of Medical Radiology, Ministry of Health of the Ukraine, Kharkov, Ukraine

***Radiobiology Division, University of Utah School of Medicine, Salt Lake City, Utah

where $\mu = 1/(\beta + 1)$, and $\Gamma(\mu)$ is the Gamma function. One can show that in the general case, the inequalities $\alpha\bar{\rho} \leq \text{Var}\{v\} \leq \alpha\bar{\rho}[1 + \alpha\bar{\rho}]$, and $1 \leq R_v(v) \leq 1 + \alpha\bar{\rho}$ hold.

Up to this point, the cells irradiated over the whole quiescence period were considered. The situation for pre-existing cells that experience an instantaneous uptake of an alpha emitter is different. These cells represent the first generation of cells irradiated by a constant hit rate α , with irradiation starting at time t with no previous irradiation. To describe the irradiation of these cells, the residual lifetime γ , which is the interval from t up to the end of the lifetime, is used. Let us consider the general case of age-dependent remodeling when the quiescence periods have the Weibull distribution. In this case, the density distribution of γ is

$$q(z) = \text{Prob}\{z \leq \gamma < z+dz\} = \frac{1}{\bar{\rho}} \exp\left\{-\left(\frac{z}{\bar{\rho}}\right)^{\mu}\right\} \Gamma(1/\mu). \quad (4)$$

The mean and variance of hits to the nuclei of first generation bone-lining cells are, respectively,

$$\mathbf{E}^{(1)}\{v\} = \frac{\alpha\bar{\rho}}{\mu} \Gamma(2\mu)\Gamma^{-2}(\mu), \quad (5)$$

$$\text{Var}^{(1)}\{v\} = [\Gamma(3\mu)\Gamma^{-2}(2\mu)\Gamma(\mu) - 1] [\mathbf{E}^{(1)}\{v\}]^2 + \mathbf{E}^{(1)}\{v\}, \quad (6)$$

which yields

$$\frac{1}{2}\alpha\bar{\rho} \leq \mathbf{E}^{(1)}\{v\} \leq \alpha\bar{\rho},$$

and

$$\frac{1}{2}\alpha\bar{\rho}(1 + \frac{1}{2}\alpha\bar{\rho}) \leq \text{Var}^{(1)}\{v\} \leq \alpha\bar{\rho}(1 + \alpha\bar{\rho}).$$

Thus, even for specific values of the mean hit rate α and mean quiescence period $\bar{\rho}$, the law of remodeling significantly affects the values of the mean and variance of hits to the bone-lining cells. For constant turnover rate ($\bar{\rho} = \text{constant}$), the mean number of hits to bone-lining cells of the first generation is two times larger for random remodeling than for deterministic remodeling.

The probabilities of no hits, $P_0(\beta)$, to these cells for random and deterministic remodeling are

$$P_0^{(1)}(\beta=0) = P_0(\beta=0) = \frac{1}{1 + \alpha\bar{\rho}},$$

and

$$P_0^{(1)}(\beta=\infty) = \frac{1}{\alpha\bar{\rho}} \{1 - e^{-\alpha\bar{\rho}}\}, \quad P_0(\beta=\infty) = e^{-\alpha\bar{\rho}},$$

respectively. The ranges of possible values of $P_0^{(1)}(\beta)$ and $P_0(\beta)$ for different $\alpha\bar{\rho}$ are shown in Figure 1. For the first generation of the bone cells, age-dependent remodeling gives a higher probability of no hits than does random remodeling. However, for the same $\alpha\bar{\rho}$, the difference is not more than 13.3% of the total number of cells. The highest probability of no hits is attained in the case of deterministic remodeling. For subsequent generations, age-dependent remodeling gives a lower probability of no hits than does the random one. For the same $\alpha\bar{\rho}$, the difference is not more than 20.4% of the total number of cells. The highest probability of no hits is attained in the case of random remodeling.

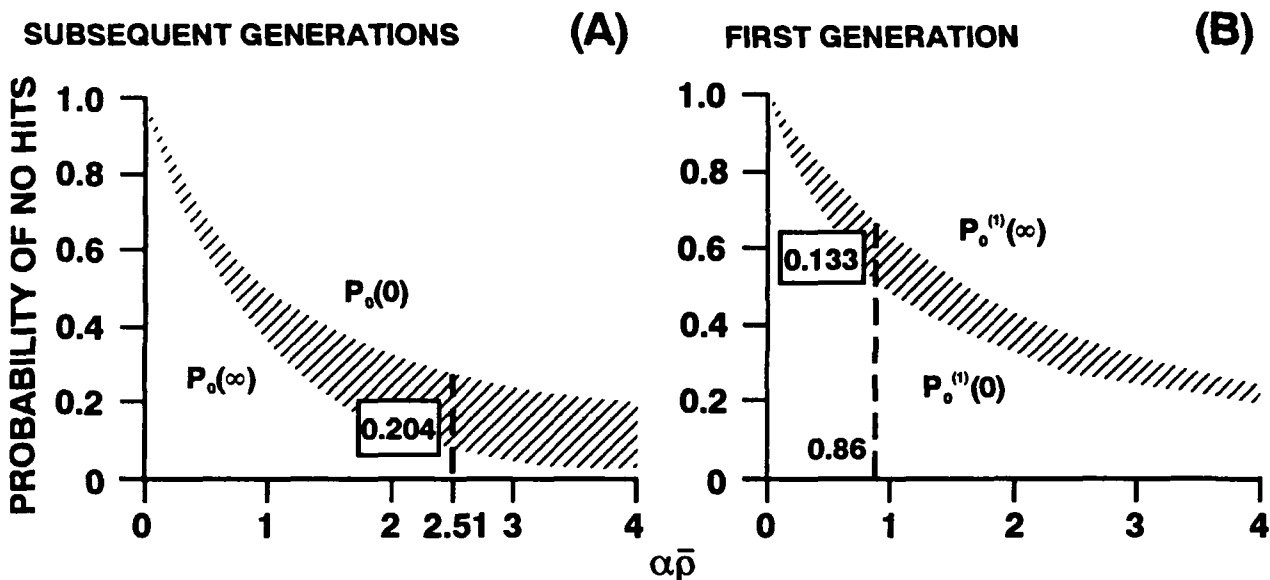


Figure 1. Probability of no hits to the nuclei of bone-lining cells as a function of $\bar{\alpha}p$ for subsequent (A) and first (B) generations of bone cells in the cases of random ($P(0)$) and deterministic ($P(\infty)$) remodeling.

(Research sponsored by the Office of Health and Environmental Research, U. S. Department of Energy, under Contract Nos. DE-AC02-76EV00119 and DE-AC04-76EV01013.)

SKELETAL MALIGNANCIES AMONG BEAGLE DOGS INJECTED WITH ^{241}Am

R. D. Lloyd*, G. N. Taylor*, W. Angus*, S. C. Miller*, and B. B. Boecker

Seventy skeletal malignancies were identified in 44 dogs among 117 Beagle dogs injected as young adults with graded dosages ranging from about 0.07 to 104 kBq ^{241}Am kg $^{-1}$ and maintained for lifetime observation. Sixty-two of these tumors were osteosarcomas; four were fibrosarcomas of bone, and four were chondrosarcomas of bone (Table 1). Of these 117 dogs, 114 survived beyond the minimum age for radiation-induced bone cancer of 2.79 yr, but all are now dead. To describe the dependence of percent occurrence of bone sarcoma on skeletal radiation dose, the expression $A = 0.76 + 30D$ was derived where A = percent of dogs with skeletal malignancy within any dosage group, D = average skeletal dose (Gy) at 1 yr before death (for doses < 3 Gy), and 0.76

Table 1

Dosimetry and Bone Cancer Occurrence Data in Beagle Dogs Injected with ^{241}Am Citrate

Dose Level	Injected kBq kg $^{-1}$	No. of Dogs in Study ^a	Dogs with Bone Cancer ^b	Percent \pm Uncertainty ^c	Skeletal Dose \pm SD 1 yr Before Death, Gy	Age, yr, at Death with Bone Cancer \pm SD
<u>Control Dogs</u>						
0.0	0	132 ^d	1	0.76 \pm 0.8	—	16.1
<u>Am Dogs</u>						
0.2	0.066 \pm 0.002	14	0	0 \pm 7.1 ^e	0.06 \pm 0.02	
0.5	0.197 \pm 0.004	14	1 ^f	7.1 \pm 7.6	0.22 \pm 0.05	13.8
1.0	0.58 \pm 0.015	25 ^g	3 ^h	12.0 \pm 7.3	0.57 \pm 0.13	13.7 \pm 1.4
1.7	1.75 \pm 0.04	24	10 ⁱ	41.7 \pm 13.8	1.49 \pm 0.39	11.5 \pm 1.4
2.0	3.55 \pm 0.06	12	10 ^j	83.3 \pm 27.5	2.52 \pm 0.59	9.1 \pm 1.3
3.0	11.3 \pm 0.19	13	12	92.3 \pm 29.0	4.57 \pm 0.87	6.1 \pm 0.6
4.0	33.6 \pm 4.44	12	8	66.7 \pm 22.0	11.2 \pm 3.3	5.3 \pm 0.5
5.0	104 \pm 15	(2) ^k	0		1.84 \pm 1.01	
Total (Am dogs)		114 ^l	44 ^m			

^aNumber that survived at least to 2.79 yr of age, the minimum latent period for death with radiation-induced bone tumor in our dog colony.

^bAll observed tumors were osteosarcomas except as noted.

^cWith one exception, stated uncertainties are geometric means of roughly half of the 95% confidence intervals for the individual groups taken from Table A-5, page 125, of Lilienfeld *et al.* (eds.) (*Cancer Epidemiology: Methods of Study*, The Johns Hopkins Press, Baltimore, MD, 1967).

^dPlus one additional dog that only lived to 1.81 yr age.

^eThe uncertainty for a group of dogs with zero tumors was taken to be a standard deviation of ± 1 (Marshall, J. H., ANL-7760, Part II, p. 18, 1970).

^fOne fibrosarcoma of bone plus two separate primary chondrosarcomas of bone, all in the same dog.

^gPlus one additional dog that lived to only 2.04 yr of age and 232 days after injection (no bone tumor).

^hIncluding one chondrosarcoma of bone plus two fibrosarcomas of bone.

ⁱIncluding one chondrosarcoma of bone.

^jIncluding one fibrosarcoma of bone.

^kNeither dog survived to 2.79 yr of age. Both died without bone tumors.

^lPlus three dogs that died before 2.79 yr of age without tumors.

^mForty-four Am-injected dogs with 70 total bone tumors, eight of which were other than osteosarcomas.

*Radiobiology Division, University of Utah School of Medicine, Salt Lake City, Utah

represents the lifetime percent malignant bone tumor response among 132 suitable control dogs in our colony not given any radioactivity. All dosage groups with skeletal doses of > 3 Gy at a year before death were excluded from the derivation of this expression because they exhibited close to 100% occurrence and appeared to be beyond the region of linearity with dose. Similar analysis of corresponding data for dogs given ^{226}Ra as young adults, excluding the two highest dosage groups in which the bone tumor response was about 100%, yielded the expression, $A = 0.76 + 4.7D$ ($D < 20$ Gy). The ratio of the coefficients in these two expressions, 6 ± 0.8 , indicates the effectiveness for bone cancer induction of ^{241}Am relative to ^{226}Ra (Fig. 1). This compares to the relative effectiveness obtained earlier for a ^{239}Pu to ^{226}Ra ratio of about 16 ± 5 (R. D. Lloyd *et al.* In *Annual Report on Long-Term Dose-Response Studies of Inhaled or Injected Radionuclides*, LMF-130, p. 144, 1991).

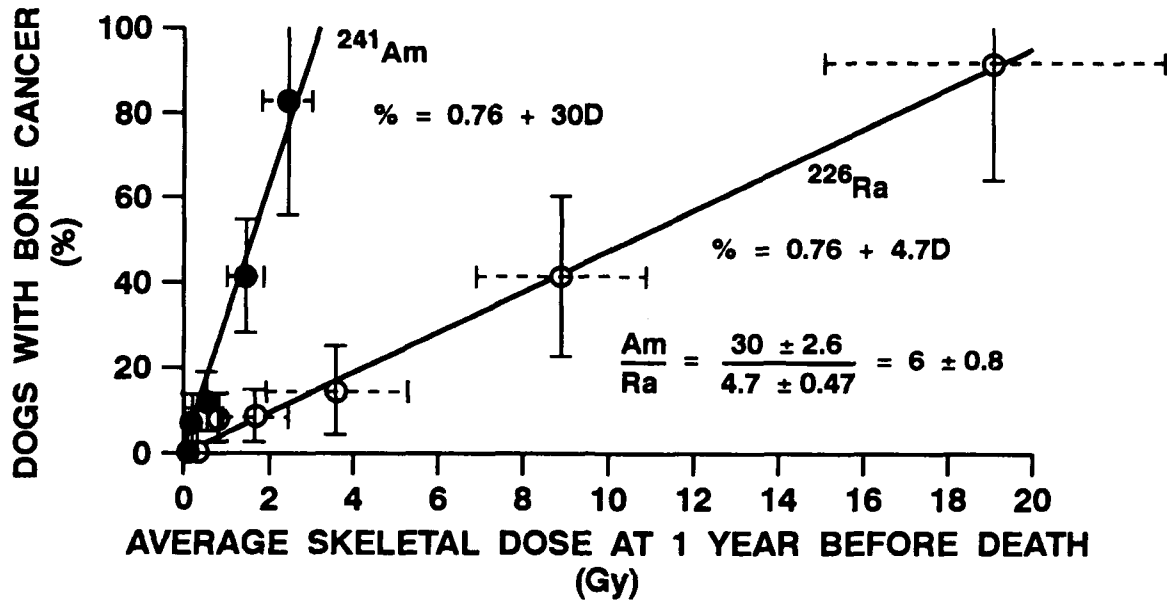


Figure 1. Relative effectiveness for induction of bone malignancies in young adult dogs given either ^{241}Am or ^{226}Ra .

(Research sponsored by the Office of Health and Environmental Research, U. S. Department of Energy, under Contract Nos. DE-AC02-76EV00119 and DE-AC04-76EV01013.)

OCCURRENCE OF METASTASES IN BEAGLE DOGS WITH SKELETAL MALIGNANCIES INDUCED BY INTERNAL IRRADIATION

R. D. Lloyd*, W. Angus*, G. N. Taylor*, G. B. Thurman**, and S. C. Miller*

Metastases from malignant bone tumors often are responsible for the fatal effects of these cancers. Various characteristics of primary skeletal malignancies in a group of Beagle dogs injected with bone-seeking radionuclides were reported in detail by G. B. Thurman (University of Utah Report COO, p. 119, 1971) and summarized by G. B. Thurman *et al.* (*Growth* 35: 119, 1971). Recent completion of the histopathology reports for nearly all life-span dogs studied during the period 1952 to 1987 at the Radiobiology Laboratory, University of Utah, made it possible for us to compare the occurrence of grossly apparent metastases from skeletal malignancies induced by skeletal irradiation from internal emitters (^{226}Ra , ^{239}Pu , ^{228}Ra , ^{228}Th , ^{90}Sr) with a number of other factors unique to each animal.

There were 212 malignant bone tumors in 186 of these dogs for which we subsequently received information on their metastatic occurrence. These data have enabled us to correlate the parameters reported previously with the appearance of bone tumor metastases. Data available for the animals included growth-rate of the primary tumor, volume of the primary tumor at death, sex of the animal, growth period of the primary tumor ("age"), degree of calcification of the primary tumor, skeletal location of the primary tumor (identity of the bone, side of the body, location along the length of a long bone), cumulative radiation dose to the skeleton at the estimated beginning of primary tumor growth, dose equivalent to the skeleton at the same point in time, and year of death.

Growth period (length of time between tumor initiation and the death of the dog) and tumor volume at death were arranged separately in order of increasing values, and each list was marked off into quartiles (fourths). Growth periods ranged from 193 to 1990 days; the minimum tumor volume at death was 0.3 cm^3 , and the maximum was 1167 cm^3 . Division into quartiles also was used for analysis of cumulative radiation dose to the skeleton vs. frequency of metastasis and for a corresponding analysis of dose equivalent (dose multiplied by a quality factor that allows for the differing relative sensitivity of the Beagle dog to the induction of bone sarcoma by various radionuclides at the same average skeletal dose). The quality factors in Beagle dogs, expressed as the effectiveness relative to ^{226}Ra , for the various radionuclides were taken from published reports: R. D. Lloyd *et al.* (*Strahlentherapie* 80: 65, 1986) for $^{226}\text{Ra} = 1.0$, $^{228}\text{Ra} = 2.0$, and $^{228}\text{Th} = 8.5$; NCRP Report No. 110 (1991) for $^{90}\text{Sr} = 0.1$; and R. D. Lloyd *et al.* (*Health Phys.* 64: 45, 1993) for $^{239}\text{Pu} = 16$.

For any data set marked into quartiles and for which a significant difference in proportion of metastases was found by the "*t*" test between subgroups, the non-parametric Kendall rank correlation test (Siegel, S. *Non-parametric Statistics*, McGraw-Hill, New York, 1956) was used to determine the significance of any trend that could be identified within the entire data set. Data sets divided into quartiles were analyzed (Sokal, R. R. and F. J. Rohlf. In *Biometry*, W. H. Freeman, San Francisco, p. 70, 1969) by Odds-Ratio Chi Square methods with Yates' correction for continuity, supplemented by Fisher's Exact Test for comparisons having zeros in any category. Proportions of tumors that metastasized from the various bones of the skeleton were compared by means of their relative uncertainties.

Each value of number of tumors yielding metastases and total number of tumors in the same bone were assigned an uncertainty based upon the standard deviation for the binomial distribution (Sokal and Rohlf, 1969). For a pair of data with values within ± 1 S. D., the "p" value was taken to be >0.10 ; for those outside 1.0 but within ± 1.96 S. D., the "p" value was taken to be >0.05 ; and for those outside of ± 1.96 S. D., the "p" value was taken to be <0.05 , all compared with respect to the corresponding data for the entire skeleton. The growth rates (mean doubling times) for various categories of primary skeletal malignancies (with or without metastases) were compared by means of the Group Comparison ("*t*") Test.

*Radiobiology Division, University of Utah School of Medicine, Salt Lake City, Utah

**Department of Biochemistry, Vanderbilt University School of Medicine, Nashville, Tennessee

Some of the animals had more than one skeletal malignancy. If these were of different cell types, the identity of the tumor that was the origin of the metastases found in other tissues was not in doubt. Because most of the primary tumors were classified as osteosarcomas, including multiples in the same animal, we could not be sure which primary tumor was the origin of the metastases in dogs with more than one primary bone tumor. Therefore, we analyzed the data such that we counted the growth rate of (1) only the most rapidly growing tumor in each dog with multiple tumors, (2) only the most slowly growing tumor in animals with multiple tumors, (3) only the most rapidly growing tumor in the dogs with metastases and only the most slowly growing tumor in the dogs without metastases, or (4) only the most rapidly growing tumor in the dogs without metastases and only the most slowly growing tumor in the dogs with metastases. In addition, only those dogs with just a single primary tumor were included in another analysis to ensure that the correct malignancy could be identified as the source of a given metastasis. If there was a substantial difference in the probability of metastatic development between tumors with different growth rates as reported by S. M. LaRue *et al.* (In *Book of Abstracts for the 40th Annual Meeting of the Radiation Research Society*, p. 112, 1992), our study would show that either slowly growing or rapidly growing tumors could be more prone to metastasis.

For most of the comparisons, no significant differences could be established between dogs with and without metastases. However, larger tumor volumes at death appeared to be associated with the probability of metastasis. Only for the comparison of the quartile of the smallest tumor volumes at death with the largest was there a significant difference in the proportion of metastasis ("p" < 0.05). There was no difference identified between adjacent categories of tumor volume. However, the fraction of dogs with metastasis increased monotonically with increasing tumor volume at death for all four quartiles: 1st quartile = 15 metastases in dogs with 53 tumors = 0.208 (mean volume = 2.2 cm³); 2nd = 0.283 (19.2 cm³); 3rd = 0.340 (72 cm³); and 4th = 0.472 (395 cm³). According to the non-parametric Kendall rank correlation test, the "p" value for this outcome is 0.042. Therefore, it appears that there is an effect of tumor volume at death on the likelihood of metastasis, with the larger tumors having a greater probability of metastasis than smaller tumors.

Various comparisons of dogs with and without metastases as a function of tumor growth rate did not, for the most part, yield significantly different results between these two groups. The exceptions were when only one tumor per dog was considered for animals having multiple primary tumors (longest doubling time for dogs with metastases and shortest doubling time for dogs without; "p" < 0.001) and when only the tumor with the longest doubling time was included for all dogs with multiple primary tumors ("p" < 0.02). We found that this effect was a result of only two tumors with doubling times of >45 days. Both had been characterized by Thurman (1971) as among the tumors with the least uncertainty in calculated doubling time. Rates of metastasis in dogs with primary tumors in paired bones, especially the left side, were significantly higher than corresponding values of dogs with primary tumors in unpaired bones. The occurrence of metastases in dogs with primary tumors in the ribs appeared to be more pronounced than those in animals with primary tumors in other bones as compared with the average for the whole skeleton.

We conclude that analysis of the association between a variety of parameters and the occurrence of metastases from radiation-induced bone tumors serves to improve our understanding of the metastatic process. The foregoing analyses also yielded some information about the relative importance of various factors that were expected to influence metastasis.

(Research sponsored by the Office of Health and Environmental Research, U. S. Department of Energy, under Contract Nos. DE-AC02-76EV00119 and DE-AC04-76EV01013.)

THYROID LESIONS INDUCED BY ^{241}Am IN THE BEAGLE DOG

G. N. Taylor*, R. D. Lloyd*, F. W. Bruenger*, and S. C. Miller*

The concentration of ^{241}Am in the thyroid gland of Beagle dogs, after a single intravenous injection of Am in a citric acid-sodium citrate buffer solution at pH 3.5, is slightly less than the concentration in the liver and moderately greater than in the skeleton (Lloyd, R. D. et al. *Health Phys.* 18: 149, 1970). However, since the mass of the combined thyroid tissue in these dogs is only about 600 mg, the percentage of injected Am retained at this site is relatively low. Part of the impact of this unusually high concentration of ^{241}Am in the thyroid glands of the Beagle dog, with respect to clinical, morphological, and neoplastic changes, is presented in this summary.

All of the dogs observed were purebred Beagles, born and raised at the Radiobiology Laboratory, University of Utah. The ^{241}Am was administered in graded dosages via a single injection in the cephalic vein at about 17 to 18 mo of age (Dougherty, T. F. et al. *Radiat. Res.* 17: 625, 1962). The volume of the injection solution was approximately 8 to 10 mL. Serum thyroxine levels (T4) were determined by radioimmune assay methods, using reagents supplied by PANTEX (Malibu, CA). Autoradiographs were prepared from acetone-fixed, paraffin-embedded tissues. Weighted cumulative tumor rates were determined by the method of Kaplan and Meier (*J. Am. Stat. Assoc.* 53: 457, 1958). Evaluation of statistical significance was by the group comparison ("t") test for thyroid weights, analysis of variance for T4 evaluations, and Cox Regression Analysis for thyroid tumor rates.

The percentage of injected activity retained in the thyroid gland following a single intravenous injection was 0.055 ± 0.00066 (mean \pm SD), and the percentage remained constant for the range of injected dosages shown in Table 1. Autoradiography indicated that most of the activity was in the basement membranes of the follicles and in the vascular walls of the smaller arterioles. Only small amounts were present in the follicular epithelium or the colloid. The resulting radiation doses (mean \pm SD) were 1.4 ± 0.9 and 0.76 ± 0.38 times those delivered to the skeleton and the liver, respectively.

Table 1
Incidence of Thyroid Tumors in Beagle Dogs
Given a Single Intravenous Injection of ^{241}Am

^{241}Am Injected (kBq kg $^{-1}$)	Number of Dogs	Average Age ^a at Death (days)	Average Dose to Thyroid (Gy)	Thyroid Tumors ^b (%)	Bone and/or Liver Tumors (%)
101.75	2	941 ± 33	29.8 ± 1.5	0	0
33.58	12	1874 ± 285	28.4 ± 9.2	0	83
11.27	13	2239 ± 220	8.67 ± 4.8	0	92
3.55	12	3327 ± 420	4.04 ± 2.1	0	92
1.74	24	4633 ± 804	2.14 ± 1.2	13	58
0.58	22	4634 ± 804	0.61 ± 0.13	12	45
0.20	14	4906 ± 860	0.25 ± 0.06	0	21
0.07	14	4488 ± 953	0.08 ± 0.02	7	0
(Control)					
0	132	4749 ± 1062	0	11	4

^aThe average age at injection was approximately 505 days.

^bIncludes both benign and malignant tumors.

*Radiobiology Division, University of Utah School of Medicine, Salt Lake City, Utah

Characteristic symptoms related to Am-induced thyroid changes, such as lethargy, obesity, epilation, or myxedema were not observed. This was true even in those instances where marked ablation of the gland had produced subnormal levels of serum T4. However, ablation of the thyroids was never absolute, and small islands of follicular cells could be found even in the dogs with the most severe radiation-induced involution.

Evaluation of the average thyroxine (T4) levels in the peripheral blood at various post-injection times indicated functional impairment of the thyroid gland at several Am dosage levels. However, the relatively wide day-to-day variation of the T4 values in both the controls and the irradiated animals made the results of single tests a relatively imprecise index of radiation-induced thyroid injury. The radiation-induced depression of the serum T4 was most clearly evident in the two highest dosage levels studied: 100 and 34 kBq kg⁻¹, which differed significantly from each other and also from the controls ($p < 0.01$; Fig. 1). The T4 values for the 11 kBq kg⁻¹ group were similar to those in the controls ($p > 0.20$), even though the radiation-induced histological alterations were usually appreciable. The T4 values of the 3.6, 1.7, and 0.58 kBq kg⁻¹ groups were not significantly different from each other ($p > 0.20$) and were grouped together for statistical purposes. Dogs in this combined group had significantly higher T4 levels than either the controls or the 11 kBq kg⁻¹ group ($p < 0.01$). This result is consistent with the observed hypertrophy of the follicular epithelium that occurred in a moderate number of these lower dosage animals.

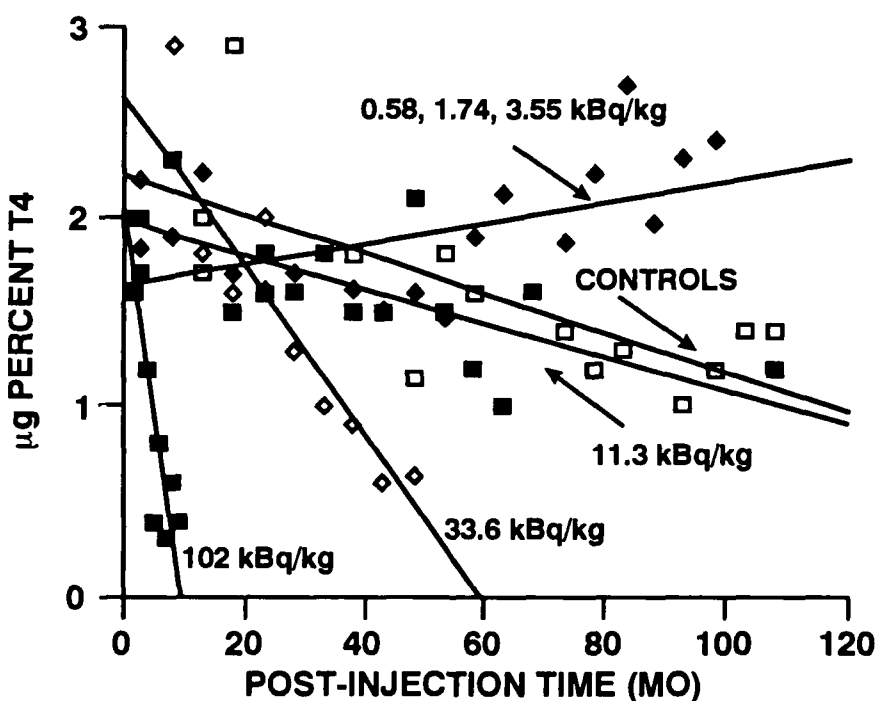


Figure 1. Comparison of T4 values in Beagle dogs injected with various dosage levels of ^{241}Am . The curves are least-squares fits to the plotted points.

Statistically significant ($p < 0.001$) reductions in the thyroid weights occurred in most of the dogs injected at the three highest levels. The most extreme atrophy occurred in the animals given 34 kBq kg⁻¹. Although some variation occurred, the thyroid weights measured in the five lowest dosage levels were within normal limits.

Histologically, in the two dogs injected at the highest dosage level studied, 100 kBq kg⁻¹, and at about 425 days post-injection, the follicular epithelium was mostly low cuboidal and became almost squamous in some areas. Atrophy, degeneration, and necrosis of the epithelium occurred focally. Scattered foci of follicular hyperplasia composed of small clusters of cells and some microfollicles were distributed among the follicles that were present at time of injection. These older follicles were anatomically normal except for the very low cuboidal epithelium. The epithelium of these such abnormal foci usually exhibited some degree of hypertrophy, indicating that TSH

or other stimulation was extant even though much of the older epithelium was nonresponsive. Nearly normal amounts of colloid were present, but based on the low serum T4, metabolic functions in much of the follicular epithelium and colloid compartment were probably impaired to an even greater degree than was suggested by the microscopic appearance. Vascular lesions, interstitial fibrosis, and leukocytic infiltrates were not seen. The absence of extreme anatomical changes at this high dosage level was possibly related to the relatively short survival times. The causes of death at this highest dosage level were combinations of kidney, liver, and bone marrow failure, all sites of high radiation exposure.

Histological changes in the thyroid were most marked in the dogs given 34 kBq kg⁻¹, probably because of the relatively high thyroid dose and the moderately long survival times after injection, averaging 1380 ± 290 days. Follicular atrophy and interstitial fibrosis were invariably present, and loss of follicles and colloid was marked. The glands were frequently reduced to a small fibrotic mass that was sometimes difficult to find at necropsy. Some of the few residual follicles contained hyperplastic foci that were, in some instances, suggestive of an early adenomatous change. These clones of follicular cell hyperplasia occasionally contained microfollicles, generally without colloid. Most of the follicular epithelium in such foci was markedly hypertrophic, suggesting elevated levels of TSH; however, levels of this hormone were not measured in any of the dogs in this study. Cytoplasmic PAS-positive, colloid-like inclusions were present in many of the cells in the hyperplastic foci. Reduced vascularity and hyalinization of some of the arterioles were seen in the most atrophic glands. Focal lymphocytic infiltrates occurred in a few of the animals in this high dosage group but were seldom seen in the other dosage levels.

Marked Am-induced changes also developed in the dogs injected with 11 kBq kg⁻¹. However, compared to the 34 kBq kg⁻¹ level, fibrosis was less extreme, the extent of the hyperplasia was greater, and a larger number of colloid-bearing follicles was present. The number of follicles and the amount of colloid appeared adequate for normal function. Follicular hyperplasia and the presence of PAS-positive, colloid-like cytoplasmic inclusions were the most marked of any of the levels. The lesions observed at even lower dosages were principally hypertrophy of the follicular cells and a minor degree of interstitial fibrosis. However, such changes were observed in only some of the animals, and hyperplasia was seldom seen.

A comparison of the incidence of thyroid tumors in the controls with those of the Am-treated dogs is presented in Table 1. Statistical evaluation indicated that the incidence in the control and irradiated dogs was not significantly different ($p > 0.3$). Based on the control population, 6.4 thyroid tumors were expected in the irradiated animals, and seven were observed. The thyroid neoplasms developed mostly in the dogs with long survival times, averaging 11.1 ± 1.8 yr post-injection in the controls and 12.8 ± 2.2 yr in the irradiated groups. The incidence of thyroid tumors in the males was approximately two times that of the females, which contrasts with the higher incidence observed in women (NCRP, *Induction of Thyroid Cancer by Ionizing Radiation*, NCRP, Bethesda Maryland, p. 56, 1985).

In summary, selective deposition of Am that occurred in the thyroid glands of Beagle dogs after a single intravenous injection produced obvious functional and anatomical changes. However, statistically significant increases in the incidence of thyroid neoplasia did not occur.

(Research sponsored by the Office of Health and Environmental Research, U. S. Department of Energy, under Contract Nos. DE-AC02-76EV00119 and DE-AC04-76EV01013.)

IX. THE APPLICATION OF MATHEMATICAL MODELING TO HEALTH ISSUES

AGE-SPECIFIC LUNG CANCER RISK ESTIMATES FOR EXPONENTIALLY DECAYING PATTERNS OF IRRADIATION

B. R. Scott and B. B. Boecker

When radioactive particles are deposited in the respiratory tract via inhalation, exponentially decaying patterns of irradiation of the lung can arise. When long-lived radionuclides reside in inhaled insoluble particles that deposit in the lung, different amounts of radiation dose will be delivered in different age intervals. Epidemiological studies have demonstrated that radiosensitivity of the lung can vary significantly with age (National Academy of Sciences/National Research Council, BEIR V Report, Washington DC, 1990). Therefore, to facilitate radiation risk evaluation, it is desirable to have average risk coefficients that account for variation in radiosensitivity which occurs during chronic irradiation of the lung from deposited radioactive particles. Such coefficients can be developed if one has quantitative information on the variation in radiosensitivity with age and on the pattern of irradiation of the lung. This report discusses results obtained using an empirical model for evaluating lung cancer mortality risk for chronic exposure of the lung to exponentially decaying patterns (single exponential) of irradiation. The results provided apply to low-LET radiation doses less than 50 Gy to the lung (or high-LET alpha radiation dose equivalents less than 50 Sv).

Age- and gender-specific risk coefficients for lung cancer mortality that were developed in BEIR V (NAS/NRC, 1990) for brief exposure at high dose rates to low-LET radiation were used to obtain empirical age- and gender-specific mortality models for brief exposure at high dose rates. High dose rates refer to low-LET radiation dose rates greater than or equal to 0.1 Gy/h (International Commission on Radiological Protection, ICRP Publication 60, Pergamon Press, Oxford, 1991). The brief exposure, high-dose-rate, gender-specific models were then used with the preferred dose rate effectiveness factor of two recommended in ICRP 60 (ICRP, 1991) to convert model-based risk coefficients to corresponding estimates appropriate for brief exposure at low dose rates from radionuclides deposited in the lung. Low dose rates of low-LET radiation imply dose rates less than 0.1 Gy/h.

Results obtained for brief exposures at low dose rates were used to generate risk coefficients for the average risk of lung cancer mortality associated with the long-term exposure of the lung to exponentially decaying patterns (single exponential). To obtain the average risk, which is averaged over the different ages at which the radiation dose is delivered, risk at a given age during exposure was weighted by the instantaneous dose rate to the lung at that age. An analytical solution was developed for the average risk of lung cancer mortality as a function of age T_0 at the start and age T_1 at the end of the exposure period considered, and the effective lung retention half-time ($T_{1/2}$). Because the data base used is limited to $T_0 \geq 5$ yr and $T_1 \leq 85$ yr, T_1 was fixed at 85 yr for the analysis carried out.

The analytical solution obtained for the average risk was rather complicated, and a discussion of the complexities of the analytical solution is beyond the scope of this report. We have used the analytical solution to generate estimates for the average risk of lung cancer mortality by lung retention half-time, age at initial exposure, and gender. Results obtained for chronic low-LET irradiation of the lung can be converted to corresponding estimates for chronic irradiation by high-LET alpha particles by multiplying the coefficients for low-LET irradiation by a radiation weighting factor of 20 (ICRP, 1991). However, results for alpha irradiation of the lung are not presented in this report.

Figure 1 shows estimates of the average risk for lung cancer mortality in males caused by exponentially decaying patterns of low-LET beta and/or gamma irradiation of the lung for three retention half-times (500 days, 700 days, and 7000 days). Similar results were obtained for females (not shown), although risk estimates for females were generally lower than for males. The half-times of 700 and 7000 days correspond to two sub-compartments of the alveolar interstitial region of the proposed ICRP dosimetry model (Bailey, M. R. *et al.* *Radiat. Prot. Dosim.* 38: 153, 1991) which govern long-term retention in the lung.

The 7000-day half-time is being considered as a default value to be used for slowly clearing material deposited in the alveolar interstitium of the lung (Bailey, 1991). The 500-day half-time is based on the earlier ICRP 30 system (International Commission on Radiological Protection, ICRP Publication 30, Pergamon Press, Oxford,

1979) and represents the assigned clearance half-time for highly insoluble materials that are deposited in the pulmonary region of the lung. Results presented in Figure 1 indicate that going from a retention half-time of 500 days to one of 700 days has little impact on average risk. Note also that when a given dose is protracted over many tens of years (e.g., $T_{1/2} = 7,000$ days), a large part of the absorbed dose can be delivered at sensitive ages if initially exposed at ages less than about 40 yr. This leads to higher average risks than would occur if the same dose had been delivered over a few years (e.g., $T_{1/2} = 500$ to 700 days), for the same age at initial exposure. However, if people are initially exposed at ages 40 to 60 yr, greater risks should occur when they are exposed for relatively shorter times than would occur if the exposure lasts for tens of years, when the total dose is fixed. Because risk estimates in Figure 1 were derived indirectly based on data for A-bomb survivors whose total lungs were irradiated, the data apply to exposure scenarios whereby the total lung is irradiated.

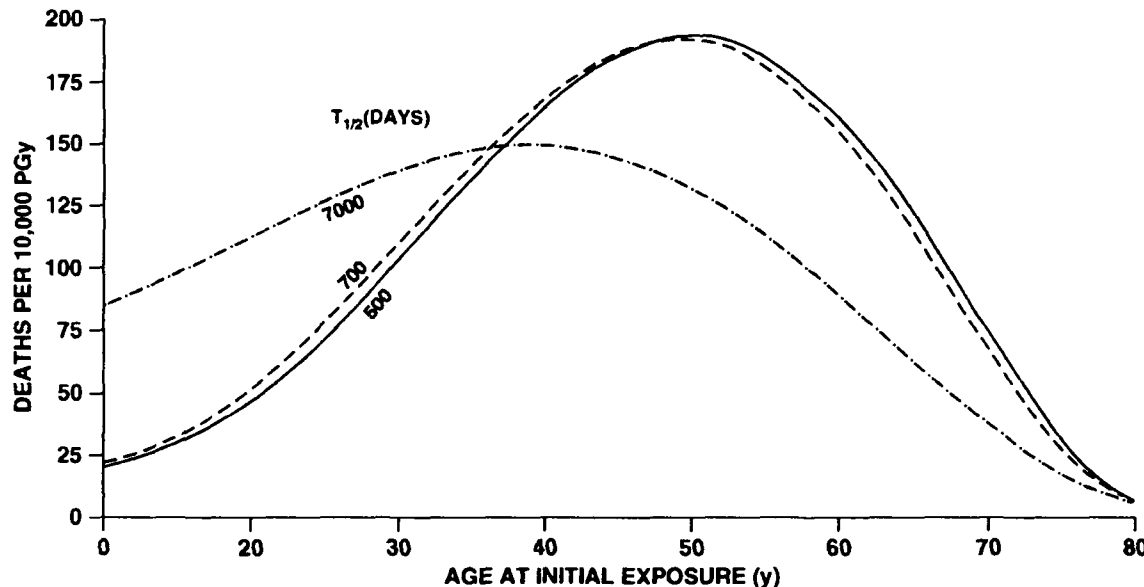


Figure 1. Estimates of average risk for lung cancer mortality in males for exponentially decaying patterns of internal low-LET irradiation (beta and/or gamma radiation) of the lung. Risk estimates were averaged over ages during exposure; results are provided for three retention half times: 500, 700, and 7,000 days.

Results presented indicate that, for radioactive particles deposited in the lung via a single inhalation exposure, age-related changes in radiosensitivity during radiation dose accumulation are not likely to be important for effective retention half-times less than about 700 days. For effective retention half-times in this range, age at initial exposure is likely to be much more important than the age interval over which significant radiation dose is delivered. However, for effective retention half-times exceeding 700 days (or for repeated exposure over many years), the age interval over which significant radiation dose is delivered could also strongly influence lung cancer risk.

(Research sponsored by the Office of Health and Environmental Research, U. S. Department of Energy, under Contract No. DE-AC04-76EV01013.)

**PREDICTION OF SURVIVAL TIMES AFTER REPEATED EXPOSURES
BASED ON SURVIVAL TIMES FOLLOWING A SINGLE EXPOSURE
OF BEAGLE DOGS BY INHALATION TO $^{239}\text{PuO}_2$**

J. H. Diel

Knowledge of the effects of inhalation exposure to radionuclides is highly variable depending on the type of radiation, the species, the time sequence of exposure, and many other factors. Consequently, we must find a means of using our knowledge in the areas that are reasonably well known to predict what might happen in other situations. This paper describes an approach to predict the survival time after repeated inhalation exposures based on a single exposure to the same material. The method is used in the context of exposures of relatively long-lived animals where only a few animals are exposed and makes maximal use of the information from each individual animal to obtain the best prediction.

The study that was used to evaluate this method of prediction is one in which Beagle dogs were exposed by inhalation to aerosols of $^{239}\text{PuO}_2$, either once or repeatedly at 6-mo intervals until clinical signs of radiation pneumonitis or pulmonary fibrosis appeared (Diel, J. H. *et al. Radiat. Res.* 129: 53, 1992). Survival time was measured as the time from first or only exposure until the dogs died a natural death or were euthanized for humane reasons.

The assumption used for the determination of the relative effectiveness of single and repeated exposures was that the same effect is produced independent of the time sequence of radiation dose accumulation if the same cumulative radiation dose is achieved at the same time after exposure. This assumes that the energy deposited and the time required for the biological system to respond to that energy deposition are both important. This is equivalent to equal effects being produced for animals having the same average dose rate at death.

Retention of Pu in the lung of a dog exposed once by inhalation to $^{239}\text{PuO}_2$ was characterized by a two-component, negative exponential function. Retention of Pu from repeated exposures was obtained by adding the retention of Pu from each exposure. Half-times of retention were assumed to be the same for repeated exposures as for single exposures, but the fraction retained depended on the number of previous exposures. Dose rate was obtained by calculating the energy deposited per unit mass of the lung. Dose is the integral over time of the dose rate, and average dose rate is the total dose to a given time divided by the time.

The average dose rate versus effect equation used assumes that the time to death from radiation pneumonitis and pulmonary fibrosis was proportional to some power of the average dose rate. The variability of the individual values about this predicted relationship was assumed to be log-normal and of equal variance for all values of the average dose rate on a log scale.

For this model, the average dose rate and survival time of each dog exposed once and dying of radiation pneumonitis and pulmonary fibrosis were used as individual points in fitting the data to the average dose rate versus effect equation. The resulting measure of variability was used to predict the probability of a repeatedly exposed dog with a given average dose rate dying of radiation pneumonitis and pulmonary fibrosis at a given time.

Because some of the repeatedly exposed dogs died from causes other than radiation pneumonitis and pulmonary fibrosis, comparison of the predicted survival with the measured survival required that the measured survival time data be corrected for competing causes. Standard methods (Kaplan, E. L. and P. Meier. *J. Am. Stat. Soc.* 53: 457, 1958) were used for this correction.

Retention of Pu in the lungs of dogs exposed once was characterized by a two-component exponential equation with 28% retained with a half-time of 63 days and the remaining 72% retained with a half-time of 1333 days. For the repeated exposures, the fraction retained at the shorter half-time depended on the number of previous exposures; it varied from 28% for the first exposure to 3% for the tenth exposure.

Dogs dying of radiation pneumonitis after a single inhalation exposure survived from 891 to 2741 days after exposure and died with average dose rates ranging from 1.0 to 9.2 Gy/day. The average dose rate (ADR --Gy/day) versus survival time (T --days) was found to be:

$$T = 219 ADR^{-0.474} \quad (1)$$

The variability around this fit was relatively small with a geometric standard deviation of 1.052. To check the consistency of the results with the assumptions of the model, the values of the differences between the logs of the predictions and the logs of the measured survival times for the dogs dying of radiation pneumonitis were computed. For each average dose rate, the values were found to be consistent with the assumption that the variability was the same for all values of the independent variable and had a normal distribution with mean 0 (Wilk-Shapiro test, $p > 0.1$).

Figure 1 compares the survival prediction of the model with the Kaplan-Meier corrected survival data. The differences between the data and predictions were not statistically significant (Kolmogorov-Smirnov test, $p > 0.2$).

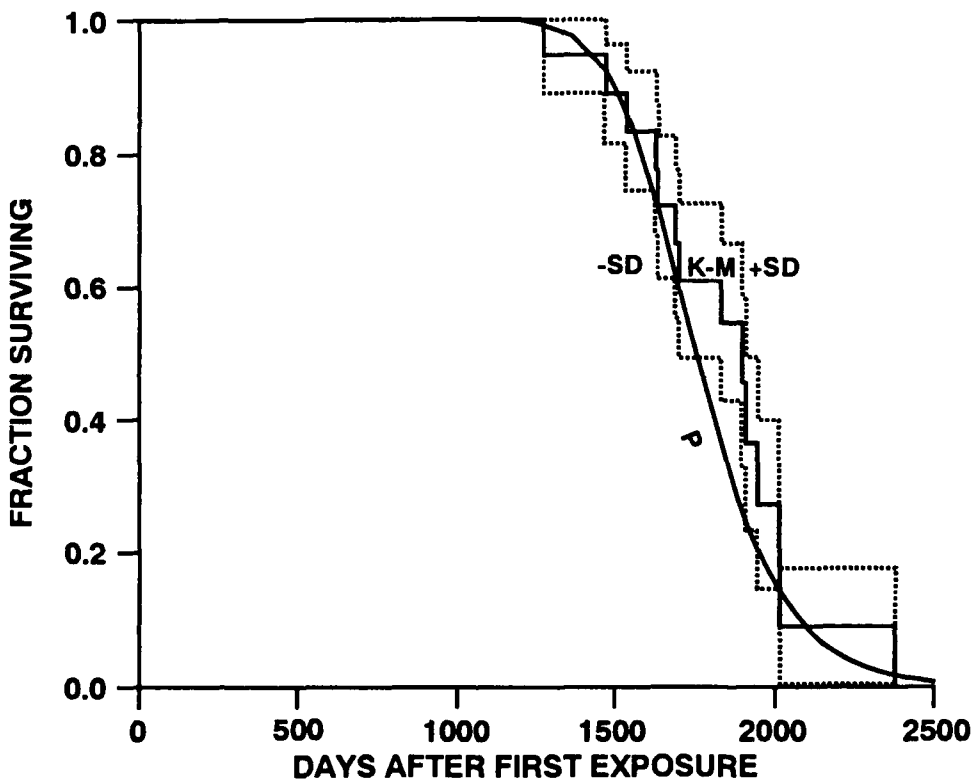


Figure 1. Survival predictions for dogs exposed repeatedly and dying of radiation pneumonitis (P) based on measured survival after a single exposure compared to Kaplan-Meier (K-M) estimates of survival of repeatedly exposed dogs dying with the effect. Standard deviation of survival ($\pm SD$) is also based on Kaplan-Meier.

The method presented is useful for predicting average response to a different time sequence of exposure. Average dose rate takes into account both total energy deposited and the time over which this energy is deposited. The average dose rate is appropriate for this prediction as would be expected for this early occurring effect that results from accumulated damage to the lung.

(Research sponsored by the Office of Health and Environmental Research, U. S. Department of Energy, under Contract No. DE-AC04-76EV01013.)

ANALYSIS OF SOFTWARE OF THE PROPOSED NCRP RESPIRATORY TRACT DOSIMETRY MODEL

I. Y. Chang, R. H. Mooty, W. C. Griffith, and H. C. Yeh*

The Respiratory Tract Dosimetry Modeling Committee of the National Council on Radiation Protection and Measurements (NCRP) has developed a respiratory tract dosimetry model for estimating respiratory tract deposition, clearance, and dosimetry of inhaled radioactive particles. The draft report for the model is under review by the NCRP. Here, we present some results of the analysis of the model in predicting deposition fractions and respiratory tract doses.

With the model, doses are evaluated by first calculating the fractions of the inhaled particles that are deposited in various regions of the respiratory tract. Secondly, physical movement and dissolution/translocation of deposited particles are described by a series of mathematical differential equations. Thirdly, at any given time after exposure, the radiation dose is calculated. The dose calculations require users to input certain parameters that describe, in the deposition calculation phase; (1) aerosol properties of the substances, such as particle diameter, particle density, and atmospheric pressure; (2) physiological parameters of the individual, such as breathing frequency, tidal volume, functional residual capacity, pauses between breaths and nasal/oral breathing percentages; and (3) the body height of the individual to account for age- and height-related differences in the size of the TB region airways. In the clearance and dosimetry calculation phase, parameters are required to define (1) the chemical form of the inhaled radionuclide, (2) the lung weight of the individual, and (3) the total inhaled radioactivity. For details of the calculations, refer to the draft NCRP report, and publications by R. F. Phalen *et al.* (*Radiat. Prot. Dosim.* 38: 179, 1991), O. R. Moss and K. F. Eckerman (*Radiat. Prot. Dosim.* 38: 185, 1991), and I. Y. Chang *et al.* (*Radiat. Prot. Dosim.* 38: 193, 1991).

Reasonable ranges of the parameters given above were defined and calculated to determine the sensitivity of deposition and dose to changes in the parameters. Examples of the values of the parameters tested are listed in Table 1.

Table 1
Examples of the Values of the Parameters Tested for Adult Males

Parameter	Values and Description
Particle Real Diameter	0.001 - 100 μm
Particle Density	1, 2, 8 g/cm^3
Breathing Frequency	13, 15, 25 breaths/min (for light, low and heavy exertion)
Tidal Volume	770, 1300, 2500 mL (for light, low and heavy exertion)
Atmospheric Pressure	1 atm
Pause	0, 0.5 sec
Nasal/Oral Breathing	100%/0%, 50%/50%
Functional Residual Capacity	2225.6 cc
Chemical Form	$^{239}\text{PuO}_2$
Lung Weight	1000 g
Total Inhaled Radioactivity	100 Bq

*New Mexico Teacher Research Associate Program Participant

In comparing the deposition curves for an adult male with light and heavy activity levels (Fig. 1), lower deposition is observed for heavy exertion in the naso-oro-pharyngolaryngeal (NOPL) region for smaller particles due to the higher air flow in the airways. Higher air flow decreases the residence time for particles to diffuse. Accordingly, more particles are available to deposit in the tracheobronchial (TB) and pulmonary (P) regions. With higher air flow, larger particles have a harder time negotiating the curves in the airways, and are more likely to impact on the airway walls. Therefore, a larger fraction is deposited in the NOPL region. When translated into radiation doses, the dosimetry curves for $^{239}\text{PuO}_2$ are presented in Figure 2. The dosimetry curves are shifted left for larger particles (see discussion below) with a larger particle density set for $^{239}\text{PuO}_2$.

For people who breathe through their mouths and noses at the same time, the model predicts an increase in particle deposition in the NOPL region for smaller particles and a decrease for larger particles (Fig. 3). Breathing simultaneously through the nose and the mouth decreases the air flow rate, thus giving more residence time for smaller particles to diffuse. For the same reason, larger particles can negotiate the airway curves better, resulting in fewer particles being deposited in the NOPL region. Lower (or higher) deposition in the NOPL regions means more (or less) availability of particles to deposit in the TB and P regions.

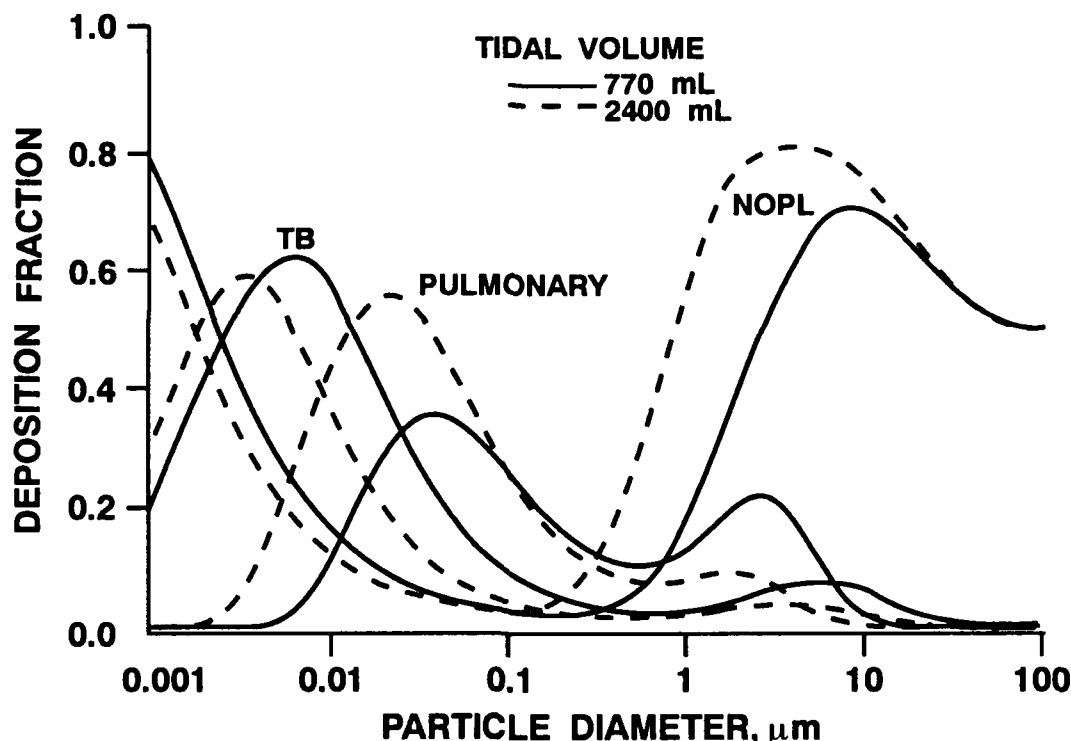


Figure 1. Deposition of inhaled radioactive substances for a male adult with light (tidal volume = 770 mL, breathing frequency = 13) and heavy (tidal volume = 2400 mL, breathing frequency = 25) activity levels. Particle density was set at 1 g/cm³.

According to the model, particle density only affects the deposition fraction for larger particles, due to sedimentation and inertial impaction of the particles. For smaller particles, particle density does not affect the deposition fraction significantly (Fig. 4).

The software is being revised as the NCRP model undergoes review and revision. We expect it to be available after the NCRP report has been approved and published.

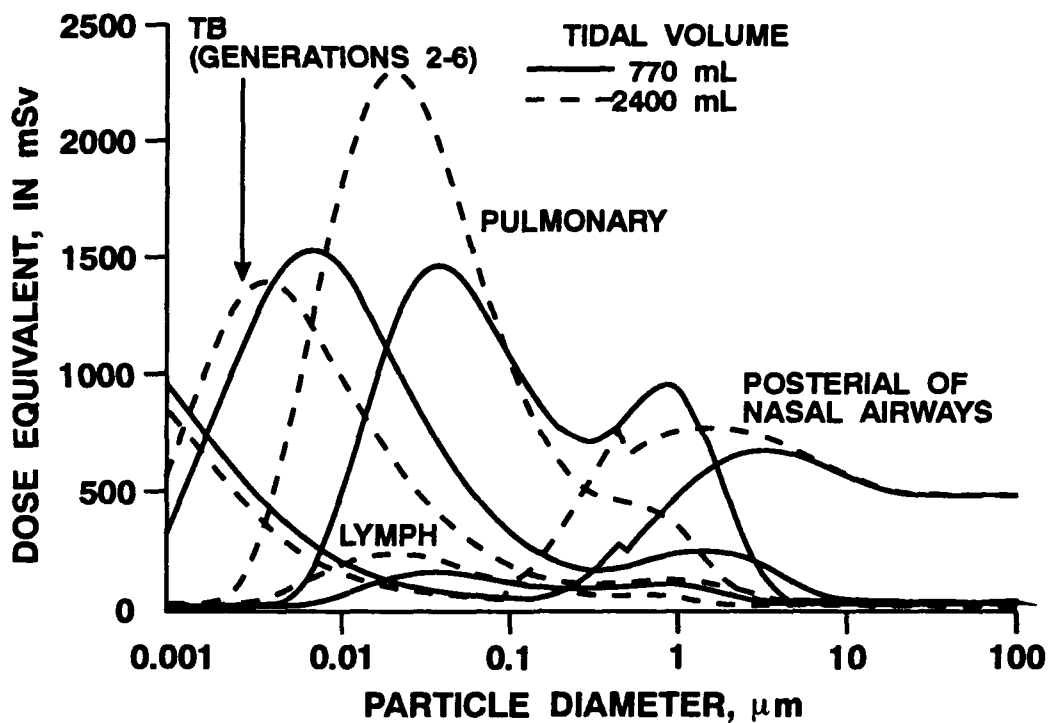


Figure 2. Dosimetry of $^{239}\text{PuO}_2$ for a male adult with light (tidal volume = 770 mL, breathing frequency = 13) and heavy (tidal volume - 2400 mL, breathing frequency = 24) activity levels at 30 days after receiving a total radiation dose of 100 Bq. Particle density was set at 7.64 g/cm³. The discontinuity in the curves are due to a difference in a distribution factor defined as 50%/50% distribution for anterior/posterior of the nose for particle size < 0.5 μm and 60%/40% distribution for particle size $\geq 0.5 \mu\text{m}$.

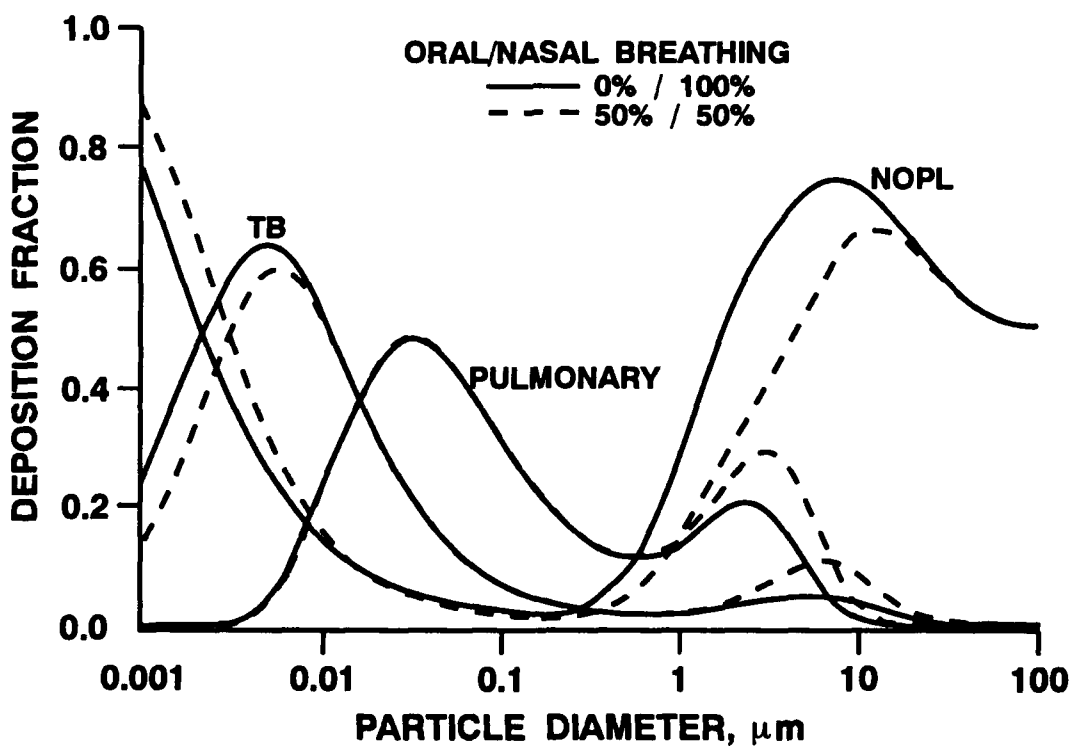


Figure 3. Deposition of inhaled radioactive substances for a male adult with two oral/nasal breathing modes (0% / 100% and 50% / 50%), tidal volume 770 mL, breathing frequency 13/min and particle density 1 g/cm³.

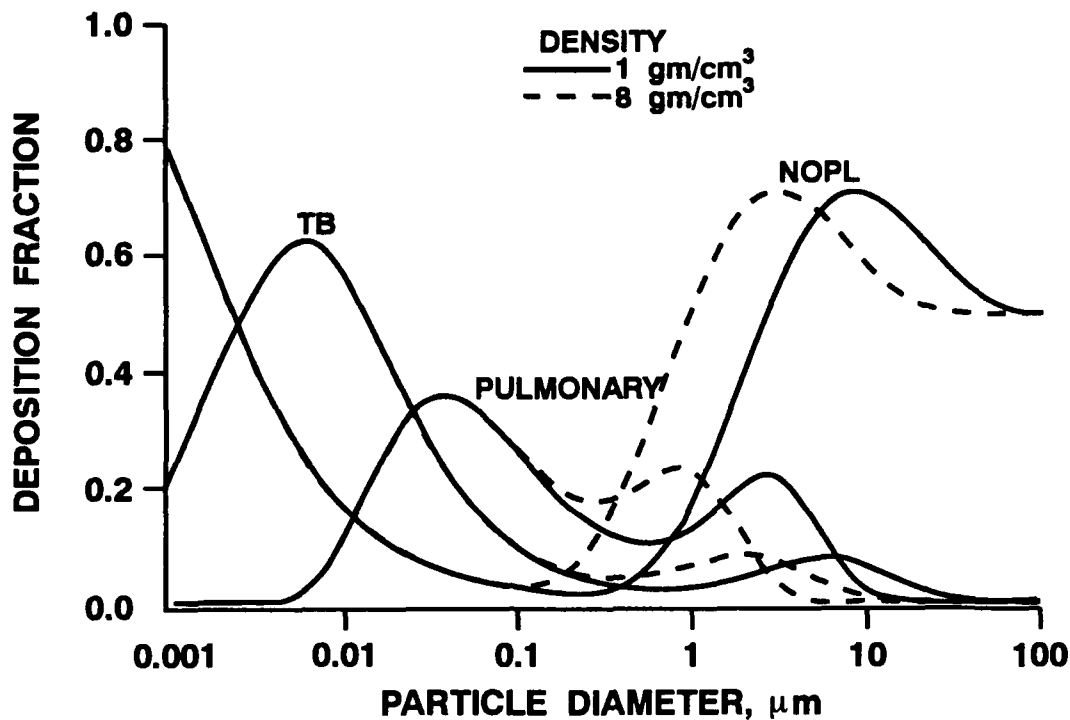


Figure 4. Deposition of inhaled radioactive substances for a male adult with two particle densities (1 and $8 \text{ g}/\text{cm}^3$), tidal volume 770 mL and breathing frequency 13 min^{-1} .

(Research sponsored by the Office of Health and Environmental Research, U. S. Department of Energy, under Contract No. DE-AC04-76EV01013.)

RECOMMENDATIONS FOR LIMITING RISK OF STOCHASTIC EFFECTS OF EXPOSURE OF THE RESPIRATORY TRACT TO β/γ -EMITTING HOT PARTICLES

B. R. Scott, Y. S. Cheng, and B. B. Boecker

Airborne particles emitting β and γ radiations have been detected in indoor work areas of nuclear power plants during normal operations (Karasawa, H. and M. Funabashi. In *Proceedings of the International Radiation Protection Association Congress, IRPA8*, 1: 706, 1992) and may be infrequently and randomly inhaled by workers. The particles most commonly contain ^{60}Co or fission products. Current radiation protection practices for limiting exposure of workers do not apply directly to infrequent and random inhalation of radioactive particles.

A radiation protection concern is how the risk of stochastic effects (e.g., lung or nasal cancer) arising from infrequent and random inhalation of these hot particles can be limited. Here, *hot particles* refer to particles emitting β/γ radiations with an activity greater than or equal to 3.7 kBq (0.1 μCi). Particles with activities greater than or equal to 0.037 kBq (1 nCi), but less than 3.7 kBq (0.1 μCi), are called *warm particles*. Particles with activity less than 0.037 kBq, but greater than zero, are called *cool particles*.

The purpose of this study was three-fold: (1) to evaluate the potential aerodynamic sizes of hot ^{60}Co particles at U.S. nuclear power plants; (2) to determine the probabilities of hot ^{60}Co particles depositing in regions of the respiratory tract; and (3) to recommend an approach for limiting the risk of stochastic effects of hot β/γ particle exposure of the respiratory tract when the inhalation of a hot particle is a rare and random event.

Whether a radioactive particle in the workplace will be airborne and inspired will usually be governed by stochastic considerations. For an airborne particle to be inspired, it must be contained in a tidal volume of air presented for inspiration. It must also enter the respiratory tract with an inspired tidal volume of air. During inspiration, not all particles contained in a tidal volume of air presented for inspiration enter the respiratory tract. The joint probability $P_A(T)$ that a free radioactive particle in the workplace, within the activity range of interest, is airborne and is contained in a tidal volume presented to a worker for inspiration during a monitoring period $T = (T_1, T_2)$ (i.e., from time T_1 to time T_2) is called the *availability*. The availability can be evaluated by assuming a Poisson distribution of activity-range specific radioactive particles in tidal volumes of air presented for inspiration. If $f(T)$ is the average fraction of free radioactive particles (e.g., β/γ -emitting hot particles) that are airborne during T , and $N_A(T)$ is the average number of these particles contained in a tidal volume of air presented for inspiration during T , then an estimate of $P_A(T)$ is $f(T)N_A(T)$ which will be very much less than one for work sites at U.S. nuclear power plants because $N_A(T) \ll 1$.

Formally, *inspirability* represents the average fraction (indicated here as $P_I(d_{ae})$) of the variable number of airborne aerodynamic-size-specific particles presented for inspiration, in a tidal volume of air, that are inspired. The variable d_{ae} is the aerodynamic diameter. For a single airborne hot particle contained in a tidal volume of air presented for inspiration, $P_I(d_{ae})$ should be viewed as an estimate of the conditional probability that the particle would be inspired if presented for inspiration.

Figure 1A provides estimates of regional deposition probabilities (corrected for inspirability but not for availability) for unit density spherical particles, as a function of their aerodynamic diameter, based on the proposed new NCRP model for respiratory tract dosimetry (Phalen, R. F. et al. *Radiat. Prot. Dosim.* 38: 179, 1991) with inspirability corrections included (Chang, I. Y. et al. *Radiat. Prot. Dosim.* 38: 193, 1991). The results obtained apply to a young adult male who breathes through his nose. A tidal volume of 1300 mL and breathing frequency of 13 breaths per min were selected as typical values (Phalen et al., 1991; Chang et al., 1991).

Figure 1B shows calculated aerodynamic equivalent diameters for spherical hot ^{60}Co particles as a function of the total activity of the particle and its specific activity, expressed as a percentage of the specific activity of pure ^{60}Co (i.e., relative specific activity). A 1% relative specific activity corresponds to 418 GBq per g (11.3 Ci per g). An upper bound of 6% relative specific activity was used in the calculations because the relative specific activity for the ^{60}Co particle usually does not exceed 5% of its equilibrium value. As indicated in

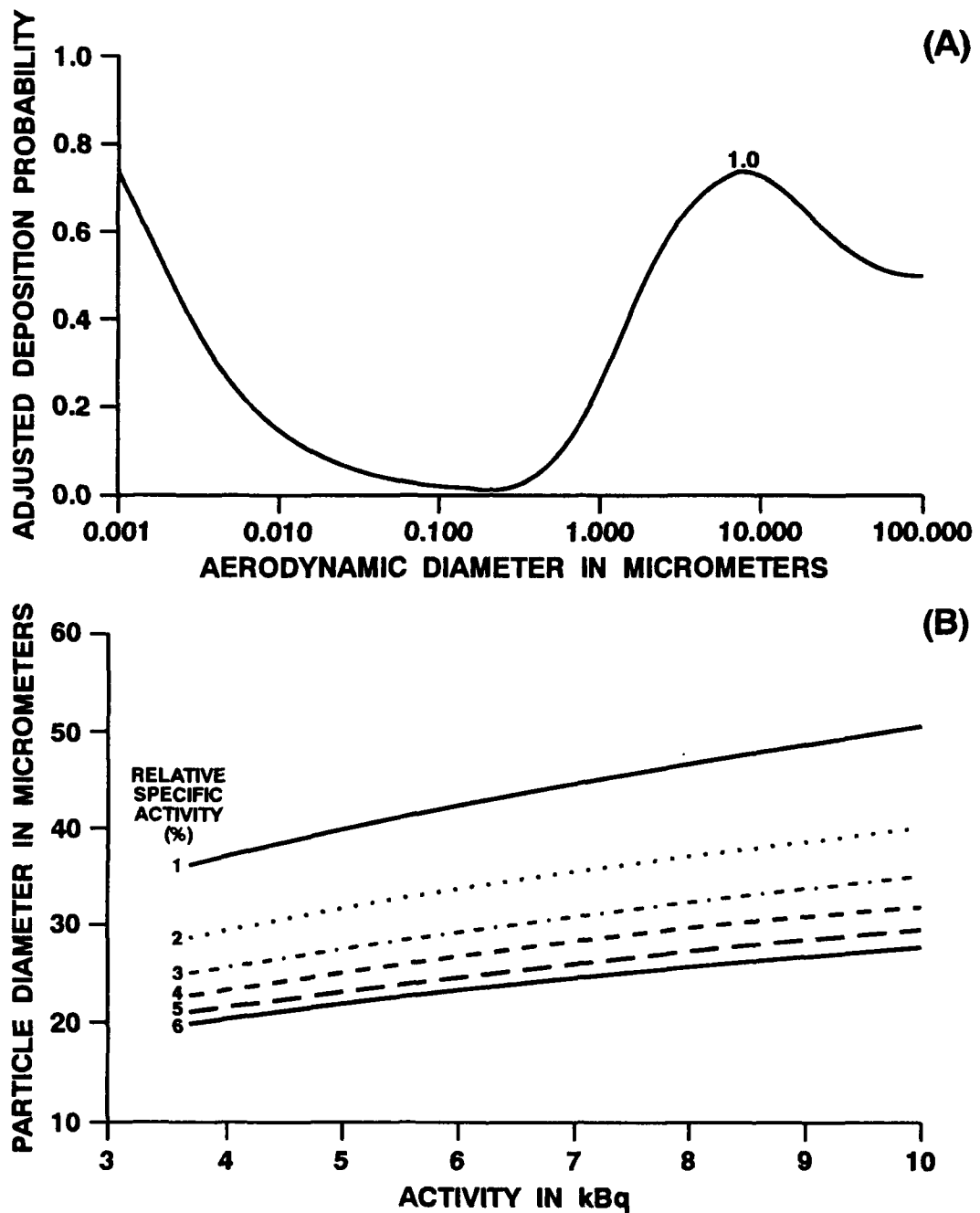


Figure 1. (A) Particle regional deposition probability estimates (corrected for inspirability but not for availability) for the nasopharyngeal region of an adult male as a function of aerodynamic equivalent diameter (in micrometers). (B) Aerodynamic equivalent diameter (in micrometers) for hot spherical ^{60}Co particles, as a function of their activity (in kBq) and relative specific activity (expressed as a percentage of the specific activity of pure ^{60}Co and ranging from 1% to 6%). A density of 8 g/cm^3 was used (Lantz and Steward, 1988).

Figure 1B, all hot ^{60}Co particles are expected to have aerodynamic diameters exceeding about $20 \mu\text{m}$, and based on results presented in Figure 1A, would deposit with high probability in the nasopharyngeal region, if inhaled.

Based on the results in Figure 1B, exposure of the respiratory tract to ^{60}Co hot particles could be limited using an assigned aerodynamic diameter of $20 \mu\text{m}$, regardless of the actual hot particle aerodynamic size. Formally, we called this diameter the *assigned aerodynamic diameter* (d_{as}) for airborne β/γ -emitting hot particles. The

assigned aerodynamic diameter based on hot ^{60}Co particles can also be used for all airborne β/γ -emitting hot particles with densities less than those for ^{60}Co particles (i.e., less than 8 g/cm^3 [Lantz, M. W. and J. B. Steward. *Radiat. Prot. Manage.* 5: 25, 1988]). Measured airborne radioactive particles at a nuclear power plant in Japan were reported to have densities in the range of 1.8 to 2.6 g/cm^3 (Karasawa and Funabashi, 1992). The aerodynamic diameters for spherical β/γ -emitting hot particles with such densities exceeds $20 \mu\text{m}$; thus, use of $d_{as} = 20 \mu\text{m}$ for such particles will facilitate limiting hot particle exposure of the respiratory tract.

For a given airborne β/γ -emitting hot particle in the work area of interest, it is not likely that we would know whether the hot particle is inspired by a worker and deposits in the respiratory tract. Using a *formal approach*, limiting hot particle exposure of the respiratory tract can be facilitated by constructing the distribution of the possible effective doses (possibility distribution) that could arise in the respiratory tract from a hot particle of a given activity and radionuclide content released in the workplace. The 90th percentile of this distribution is used as the *assigned effective dose* $E_{as}(T)$ to the respiratory tract associated with the hot particle. The assigned effective doses for different airborne hot particles can be added and the results obtained used in limiting the risk of stochastic effects. The effective dose $E_{as}(T)$ will be treated like other effective doses arising from other parts of the body and added to those effective doses to obtain the effective dose to the total body.

The distribution of possible effective doses to the respiratory tract should be based on deposition probability corrected for availability and inspirability, evaluated at the assigned aerodynamic diameter, for the type of particle considered (hot, warm, and cool particles will have different assigned aerodynamic diameters). Using the formal approach, this distribution would be generated by the Monte Carlo method (Monte Carlo dosimetry model required). For inhalation of hot particles, only effective doses to the nasopharyngeal region need to be evaluated. For warm or cool β/γ particles, the entire respiratory tract has to be considered.

Using a *practical approach*, the proposed ICRP dosimetry model could be used to compute the deposition, in a subregion of the nasopharyngeal region, of a large number N of radionuclide-specific β/γ -emitting hot particles that contained radionuclide i . (See James, A. C. *et al. Radiat. Res. Dosim.* 37: 221, 1991, for general description of the proposed ICRP model.) Each particle would have activity $\langle\alpha\rangle$ and aerodynamic diameter d_{as} , where $\langle\alpha\rangle$ is the average activity of radionuclide i associated with the airborne hot particles of interest. The ICRP proposed model would have to be adapted to allow deposition of the particles only in a given subregion of the nasopharyngeal region. An effective dose to the entire respiratory tract could be calculated for each site of deposition using ICRP tissue weighting factors. The frequency to attribute to that effective dose, for a given site of deposition, would be the availability and inspirability corrected local deposition probability (for the specific subregion) evaluated at the assigned aerodynamic diameter. The frequency of attribution to an effective dose of zero is approximately $1 - P_A(T)P_i(d_{as})$.

With the practical approach, a distribution of possible effective doses to the respiratory tract from the N hot particles could be generated for each radionuclide i of interest and the radionuclide-specific maximum estimated. If the 90th percentile of the distribution exceeds zero, and if $N_i(T)$ particles that contain radionuclide i are calculated to deposit in the nasopharyngeal region during the monitoring period, then the radionuclide-specific maximum effective dose when multiplied by $N_i(T)/N$ would represent the radionuclide-specific assigned effective dose $E_{as,i}(T)$. If the 90th percentile of the distribution does not exceed zero, then the radionuclide-specific assigned effective dose is set to zero. Calculation of $N_i(T)$ could be based on ICRP reference anatomical and physiological parameters. Protection provided by respirators should be included when calculating $N_i(T)$. Assigned effective doses for each radionuclide considered should be added. The total assigned effective dose for the respiratory tract can then be added to the effective doses arising from exposures of other parts of the body, and one can limit the total body effective dose.

A limiting scheme based on constructing the distribution of the possible effective doses to the respiratory tract arising from β/γ -emitting hot particles has been proposed here. While the limiting scheme recommended was developed for workers in the nuclear power industry, it could be used for other exposure scenarios involving infrequent and random deposition of β/γ -emitting hot particles in the respiratory tract.

(Research sponsored by the Assistant Secretary for Defense Programs, U. S. Department of Energy, under Contract No. DE-AC04-76EV01013.)

EVIDENCE OF ERRORS IN DS86 NEUTRON KERMA BASED ON BIOLOGICAL DOSIMETRY

B. R. Scott

Results of neutron-activation measurements in Hiroshima indicate that calculated neutron doses based on the DS86 dosimetry system (Radiation Effects Research Foundation, Final Report, Volumes 1 and 2, Hiroshima, 1987) may be too low (Straume, T. et al. *Health Phys.* 63: 421, 1992). Because current estimates of attributable risk for radiation-induced cancer are mainly based on an epidemiological study of atomic bomb survivors (National Research Council, National Academy of Sciences, BEIR V Report, 1990), the BEIR V risk estimates could be significantly inflated if the neutron doses used are too low.

In this study, a model for death from early effects following total-body exposure to mixed neutron-gamma fields was used to estimate effective radiation doses (neutron dose multiplied by neutron relative biological effectiveness [RBE], plus gamma ray dose), based on data for deaths occurring from 2 days to 2 mo after irradiation, for people exposed inside Japanese-style wooden houses in Hiroshima. Effective radiation dose is expressed as equivalent gamma ray dose in cGy or Gy. The mortality data were taken from Ohkita and Rotblat (*In Effects of Nuclear War on Health and Health Services*, World Health Organization, Annex 3, Geneva, p. 83, 1987).

The approach taken was to use the Weibull hazard function mortality model for mixed radiation fields (Scott, B. R. *Radiat. Res.* 98: 182, 1984; Scott, B. R. et al. *Health Phys.* 58: 791, 1990), to input the observed lethality hazard (i.e., negative logarithm of the proportion of survivors at a given distance), and to calculate effective radiation dose to bone marrow as a function of the distance from the hypocenter. The hypocenter is the point on the earth's surface directly below a nuclear explosion. Because statistical errors for model parameters could not be evaluated, published subjective bounds (U. S. Nuclear Regulatory Commission [NRC], Report NUREG/CR-4214, Washington, DC, 1989) were used to obtain upper and lower bounds on the effective radiation dose.

The effective radiation doses at various distances from the hypocenter were also estimated using DS86 neutron and gamma ray kerma (energy per unit mass transferred to charged particles by neutrons and photons) and plausible estimates (central, upper bound, and lower bound estimates) of the neutron RBE for lethal injury to bone marrow for the Hiroshima weapon. DS86 neutron and gamma ray kerma to bone marrow were used as estimates of respective absorbed doses to bone marrow. The central estimate of the neutron RBE was based on two studies: (1) a 30-day lethality study in which mice were exposed to fission neutrons plus gamma rays from a reactor (Ledney, G. D. et al. In *Treatment of Radiation Injuries* [Browne, D. et al. eds.], Plenum Press, p. 153, 1990), and (2) on a replica study of the Hiroshima weapon where the dose-response curve for dicentrics and rings among lymphocytes (*in vitro* irradiated) from humans was found to be steeper for the weapon replica study by a factor of 1.37 than had been found for fission neutrons from a reactor (Dobson, R. L. et al. *Radiat. Res.* 128: 143, 1991). The factor of 1.37 was used to adjust the neutron RBE for lethal injury to bone marrow that was based on reactor fission neutrons to a value more appropriate for the Hiroshima weapon. Based on the mixed-field Weibull model used, effective radiation dose D_{eff} in Gy (or cGy) was calculated using the equation

$$D_{\text{eff}} = LD_{50g}[1.4427H]^{1/v} = D_g + (RBE_n)D_n , \quad (1)$$

where D_g and D_n are neutron and gamma ray absorbed doses to bone marrow; LD_{50g} is the median lethal gamma ray dose for brief exposure; v is the shape parameter in the Weibull dose-response model; RBE_n is the neutron RBE; and H is the lethality hazard. Central, upper bound, and lower bound estimates of v (6, 8, and 4, respectively) and LD_{50g} (3.0, 3.5, and 2.5 Gy, respectively) were taken from a previous publication (NRC, 1989) and used to obtain central, upper bound, and lower bound estimates of D_{eff} as a function of distance from the hypocenter in Hiroshima. The parameter RBE_n was estimated to be 2.5 based on published data (Ledney et al., 1990) and modified ($RBE_n = 1.37 \times 2.5 = 3.4$) as previously discussed. To account for the uncertainty in RBE_n , subjective lower and upper bounds of 1 and 5, respectively, have been used. The value of 5 corresponds to the highest value reported for neutrons for deterministic effects of irradiation of bone marrow or the gastrointestinal tract (International Commission on Radiological Protection, Publication 58, Ann. ICRP 20/4, 1990). Thus, unlike the neutron RBE for stochastic effects in bone marrow, which can exceed 20 at low doses, the neutron RBE for deterministic effects is usually less than 5.

Figure 1 shows values of D_{eff} in equivalent gamma ray cGy for death from early effects of irradiation vs. distance from the hypocenter in Hiroshima, based on mortality among people exposed inside wooden houses. Only data for distances between 0.7 and 1.1 km from the hypocenter center were considered here. For greater distances, deaths from effects not related to radiation were a complicating factor. For closer distances, under-reporting of deaths was a complicating factor.

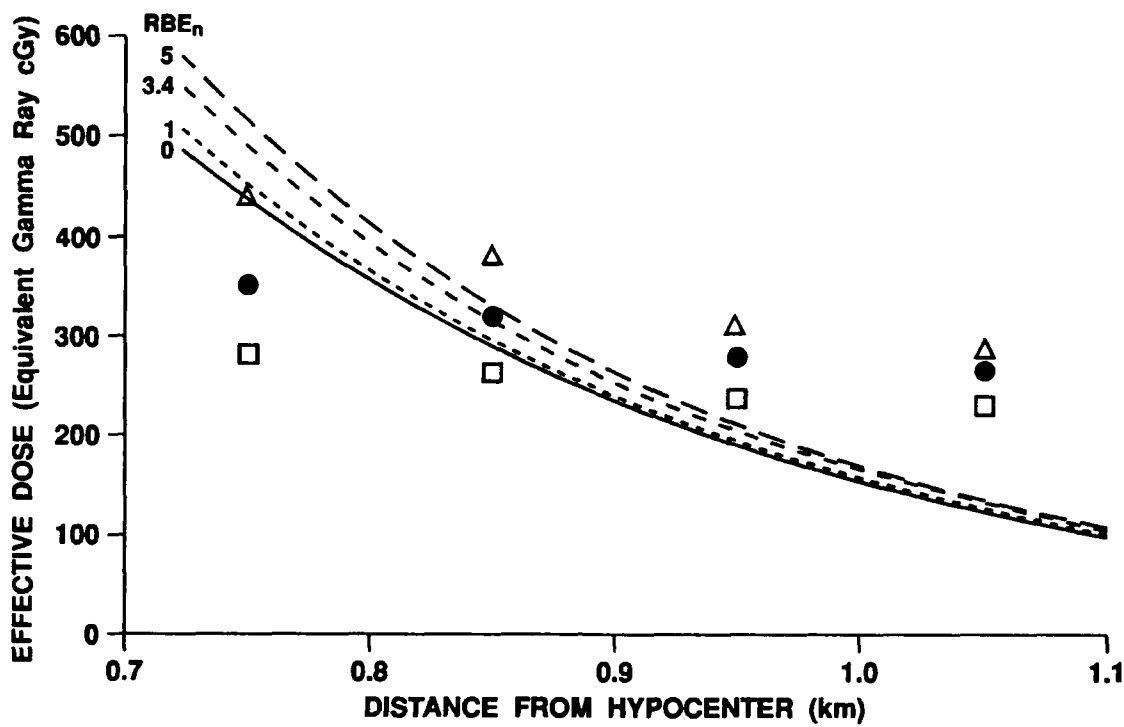


Figure 1. Effective radiation dose to bone marrow for lethal injury vs. distance from the hypocenter in Hiroshima. Data points are based on mortality data for people inside wooden houses. Lower bound, central, and upper bound estimates are represented by squares, filled circles, and triangles, respectively. Smooth curves are based on DS86 dosimetry with four different values used for RBE_n (0, 1, 3.4, and 5).

The four smooth curves shown in Figure 1 are based on DS86 neutron and gamma doses with four different values used for RBE_n (0, 1, 3.4, and 5) to calculate D_{eff} . D_{eff} was calculated using the right-hand side of Eq. (1). A value of 0 was used for RBE_n to see if the effective radiation dose would still be overestimated if no neutron dose was counted. If so, then this would indicate overestimation of gamma kerma.

Note that the results in Figure 1 suggest possible significant systematic error in the DS86 neutron dose estimates, gamma ray dose estimates, or both. For distances beyond 0.9 km, effective radiation doses are underestimated using DS86 dosimetry which is consistent with the hypothesis that neutron doses are too low. For distances less than 0.8 km, effective radiation doses are overestimated. Because effective radiation doses were overestimated for this distance range even when no neutron dose was counted ($\text{RBE}_n = 0$), one can conclude that for distances less than 0.8 km from the hypocenter, DS86 gamma kerma may be overestimated. Because gamma ray kerma estimates depend on neutron kerma estimates, neutron kerma may also be overestimated for this dose range.

These results imply that BEIR V risk estimates for cancer induction by irradiation derived from data for atomic bomb survivors are likely to be inflated and, therefore, may provide a safety factor for radiation protection applications. However, for evaluating attributable radiation risk, it is suggested that BEIR V estimates of cancer risks that are based on data for atomic bomb survivors be used to obtain upper bounds on attributable radiation risk, rather than to obtain central estimates.

(Research sponsored by the Office of Health and Environmental Research, U. S. Department of Energy, under Contract No. DE-AC04-76EV01013.)

X. APPENDICES

APPENDIX A

STATUS OF LONGEVITY AND SACRIFICE EXPERIMENTS IN BEAGLE DOGS

Each annual report of the Inhalation Toxicology Research Institute from LF-38, 1967, through LMF-121, 1987-1988 included an appendix containing detailed tabular information on all dogs in the life-span studies of inhaled radionuclides and many sacrifices series associated with these studies. In LMF-121, similar kinds of summary tables were also included for dogs in long-term and life-span studies of injected actinides that were conducted at the University of Utah. All dogs remaining alive in the Utah studies were transferred to ITRI on September 15, 1987, where they are being maintained and studied for the remainder of their life spans. Responsibility for managing the completion of the Utah life-span studies has been assigned to ITRI. A small team of investigators at the University of Utah and investigators at ITRI are working together to complete the observations and summaries.

Along with other changes made in the regular ITRI Annual Report beginning with Report LMF-126, *Inhalation Toxicology Research Institute Annual Report, 1988-1989*, it was decided that the growing body of detailed information on these studies in dogs would no longer be included. Instead, separate yearly reports are being prepared that contain specific updated information on all ITRI and University of Utah long-term and life-span studies in Beagle dogs. The first three of these reports, entitled *Annual Report on Long-Term Dose-Response Studies of Inhaled or Injected Radionuclides* have been published for 1988-1989 as Report LMF-128, for 1989-1990 as Report LMF-130, and for 1990-91 as Report LMF-135. They describe the studies, updated experimental design charts, survival plots, pathology summaries and detailed tabular information on all dogs in a manner consistent with past practices. A similar report for the 1991-1992 period is now in preparation.

Recognizing that these data are of interest to a limited number of individuals, these reports are provided without charge to individuals requesting them. To obtain these reports, please send a request to:

Director
Inhalation Toxicology Research Institute
P. O. Box 5890
Albuquerque, NM 87185

APPENDIX B

ORGANIZATION OF PERSONNEL AS OF DECEMBER 31, 1992

LOVELACE BIOMEDICAL AND ENVIRONMENTAL RESEARCH INSTITUTE

Directors and Officers

R. O. McClellan, DVM, Chairman	J. P. Bundrant
D. J. Ottensmeyer, MD, Vice Chairman	N. Corzine
J. L. Mauderly, DVM, President	J. J. Doull, MD
R. K. Jones, MD, Vice President	B. D. Goldstein, MD
B. B. Boecker, PhD, Asst. Secretary/Treasurer (non-director)	M. B. Grizzard, MD
C. H. Hobbs, DVM, Asst. Secretary/Treasurer (non-director)	W. A. Gross, PhD
J. J. Lechner, PhD, Asst. Secretary/Treasurer (non-director)	D. E. Kilgore, MD
	J. Lovelace-Johnson
	D. P. Pasternak, MD
	M. W. Twiest, MD
	A. C. Upton, MD

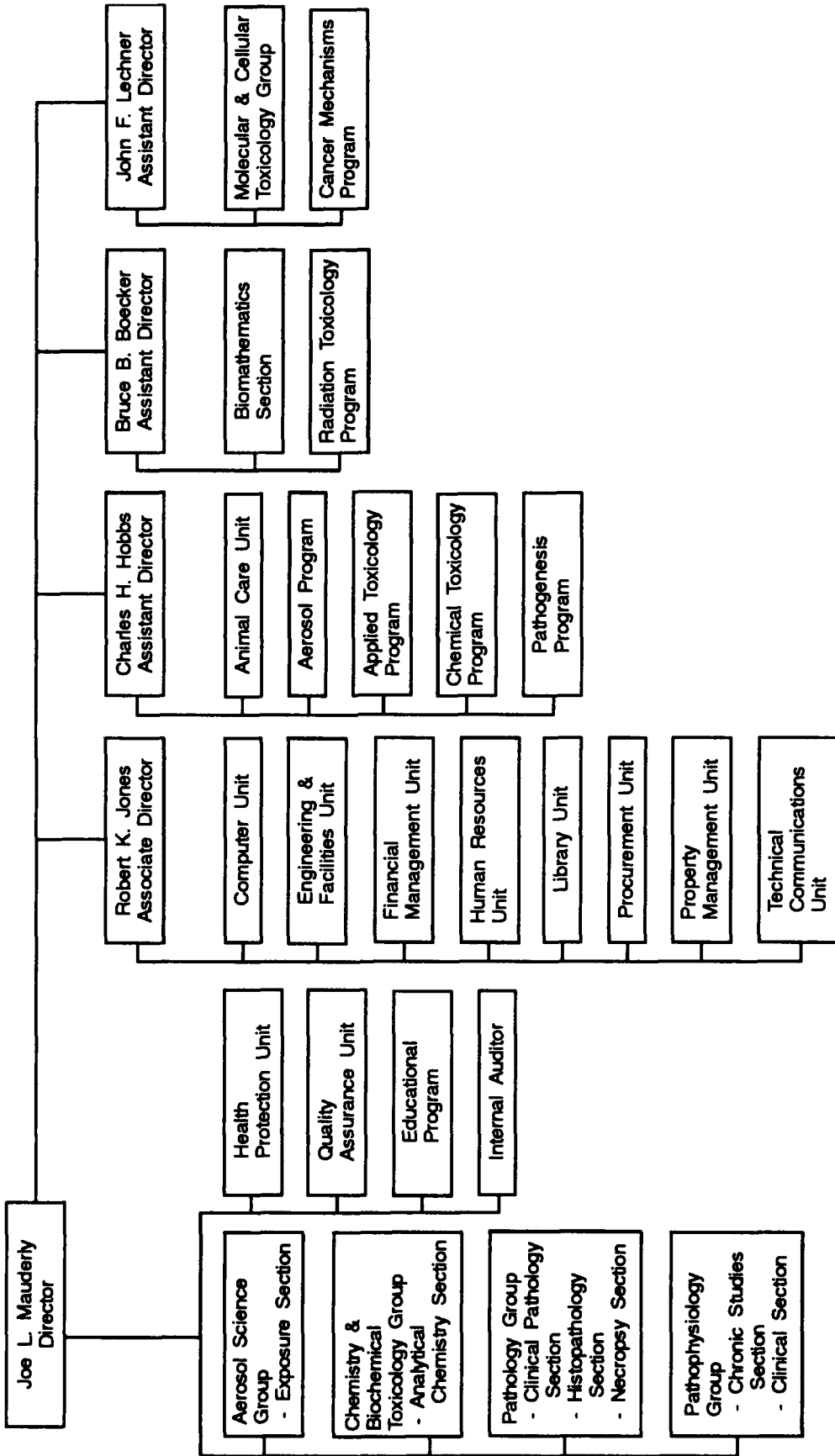
INHALATION TOXICOLOGY RESEARCH INSTITUTE

J. L. Mauderly, DVM, Director
R. K. Jones, MD, Associate Director
B. B. Boecker, PhD, Assistant Director
C. H. Hobbs, DVM, Assistant Director
J. F. Lechner, PhD, Assistant Director
D. E. Bice, PhD, Educational Coordinator

Scientific Groups	Scientific Programs	Research Support Sections and Units	Administrative Support Units
<ul style="list-style-type: none"> • Aerosol Science H. C. Yeh, PhD • Chemistry and Biochemical Toxicology R. F. Henderson, PhD • Molecular and Cellular Toxicology N. F. Johnson, PhD • Pathology F. F. Hahn, DVM, PhD • Pathophysiology J. M. Benson, PhD 	<ul style="list-style-type: none"> • Aerosols Y. S. Cheng, PhD • Applied Toxicology C. H. Hobbs, DVM • Cancer Mechanisms J. F. Lechner, PhD • Chemical Toxicology A. R. Dahl, PhD • Pathogenesis J. R. Harkema, DVM, PhD • Radiation Toxicology R. A. Guilmette, PhD 	<ul style="list-style-type: none"> • Analytical Chemistry K. R. Ahlert • Animal Care D. G. Burt, DVM • Biochemical Toxicology R. F. Henderson, PhD • Biomathematics B. B. Boecker, PhD • Chemistry A. R. Dahl, PhD • Chronic Studies J. M. Benson, PhD • Clinic B. A. Muggenburg, DVM, PhD • Clinical Pathology F. F. Hahn, DVM, PhD • Exposure E. B. Barr, MSE • Histopathology R. A. Smith • Necropsy J. Hogan, BA 	<ul style="list-style-type: none"> • Computer J. H. Diel, PhD • Engineering and Facilities J. A. Lopez, BSChE • Financial Management K. M. Aragon, MBA • Health Protection J. J. Thompson, PhD • Human Resources B. K. Solari, BA • Library S. E. Spurlock, MLS • Procurement G. A. Allen • Property Management P. F. Kaplan • Quality Assurance D. L. Harris, MS • Technical Communications P. L. Bradley, MA

INHALATION TOXICOLOGY RESEARCH INSTITUTE

Organizational Structure



ADMINISTRATIVE SUPPORT

E. C. Bankey, MBA
L. L. Burton
M. G. Campos
M. B. Morgan

CHEMISTRY AND BIOCHEMICAL TOXICOLOGY GROUP

Internal Auditor
Executive Secretary
Clerical Specialist
Administrative Associate

AEROSOL SCIENCE GROUP

H. C. Yeh, PhD
B. T. Chen, PhD
Y. S. Cheng, PhD
G. A. Feather, BS
A. F. Fencl, BS
T. D. Holmes, BS
M. D. Hoover, PhD
M. Marinkovich
M. M. Murphy, BS
G. J. Newton, BS
S. M. Smith, BS*
J. A. Stephens
D. Yazzie

Supervisor/Aerosol Scientist
Aerosol Scientist
Aerosol Scientist
Research Technologist
Research Technologist
Sr. Research Technologist
Aerosol Scientist
Research Technologist
Research Technologist
Aerosol Scientist
Research Technologist
Aerosol Scientist
Graduate Participant
Sr. Research Technologist
Research Technologist

Analytical Chemistry Section

K. R. Ahlert
L. I. Archuleta
D. M. Sugino
A. M. Tafoya

Exposure Section

E. B. Barr, MSE*
R. D. Brodbeck
S. N. Lucas
H. A. Sanchez
R. K. White, BS
K. L. Williamson
T. L. Zimmerman

MOLECULAR AND CELLULAR TOXICOLOGY GROUP

N. F. Johnson, PhD
S. A. Belinsky, PhD
T. R. Carpenter, DVM*
X. P. Galarza, BS
A. W. Hickman, Jr., MS*
R. J. Jaramillo, BS
G. Kelly, PhD
D. M. Klinge, BS
F. T. Lauer
A. D. Magallanez, BS
C. E. Mitchell, PhD
C. Nickell, PhD
M. M. Padilla
N. D. Stephens, BS*
L. A. Tierney, DVM*

BIOMATHEMATICS SECTION

B. B. Boecker, PhD
I. Y. Chang, MS
W. C. Griffith, Jr., BS
B. R. Scott, PhD

*Part-time Employee

PATHOLOGY GROUP

F. F. Hahn, DVM, PhD	Supervisor/Exptl. Pathologist
D. E. Bice, PhD	Immunologist
C. J. Candelaria	Clerical Specialist
L. M. Funk, MD*	Visiting Scientist
K. M. Garcia, BA	Sr. Research Technologist
D. M. Goddu, BS	Research Technologist
J. R. Harkema, DVM, PhD	Experimental Pathologist
L. K. Herrera, BS	Research Technologist
J. A. Hochkiss, PhD	Cell Biologist
P. C. Lawson, BS	Sr. Research Technologist
J. L. Lewis, PhD*	Toxicologist
K. J. Nikula, DVM, PhD	Experimental Pathologist
S. Q. Simpson, MD*	Visiting Scientist
R. Singh	Visiting Technician
A. J. Williams, II, BS	Research Technologist

PATHOPHYSIOLOGY GROUP

F. F. Hahn, DVM, PhD	Supervisor/Exptl. Pathologist	J. M. Benson, PhD	Supervisor/Toxicologist
D. E. Bice, PhD	Immunologist	M. L. Allen	Research Technologist
C. J. Candelaria	Clerical Specialist	L. F. Blair	Research Technologist
L. M. Funk, MD*	Visiting Scientist	D. C. Esparza, BS	Sr. Research Technologist
K. M. Garcia, BA	Sr. Research Technologist	G. L. Finch, PhD	Toxicologist
D. M. Goddu, BS	Research Technologist	K. G. Gillett, BS	Research Technologist
J. R. Harkema, DVM, PhD	Experimental Pathologist	R. A. Guilmette, PhD	Radiobiologist
L. K. Herrera, BS	Research Technologist	S. A. Likens, MS	Sr. Research Technologist
J. A. Hochkiss, PhD	Cell Biologist	D. L. Lundgren, PhD	Radiobiologist
P. C. Lawson, BS	Sr. Research Technologist	E. J. Salas	Research Technologist
J. L. Lewis, PhD*	Toxicologist	M. B. Snipes, PhD	Radiobiologist
K. J. Nikula, DVM, PhD	Experimental Pathologist	B. M. Tibbets, BA	Research Technologist
S. Q. Simpson, MD*	Visiting Scientist	B. S. Winkenweder*	Laboratory Assistant
R. Singh	Visiting Technician		
A. J. Williams, II, BS	Research Technologist		
<hr/>		<hr/>	
<u>Clinical Pathology Section</u>		<u>Chronic Studies Section</u>	
F. F. Hahn, DVM, PhD	Supervisor/Exptl. Pathologist	J. M. Benson, PhD	Supervisor/Toxicologist
D. A. Angerstein, AA	Research Technologist	C. A. Dison	Research Technologist
<hr/>		<hr/>	
<u>Histopathology Section</u>		<u>Clinical Section</u>	
R. A. Smith	Supervisor/Chief Res. Technologist	B. A. Muggenburg, DVM, PhD	Supervisor/Physiologist
S. C. Barnett	Research Technologist	M. A. Berry, DVM*	Clinical Veterinarian
R. B. Garlick	Laboratory Technician	T. R. Carpenter, DVM*	Graduate Participant
Y. N. Knighton	Laboratory Technician	M. A. Weinhold, AS	Research Technologist
		M. E. Thompson	Laboratory Technician
<hr/>		<hr/>	
<u>Necropsy Section</u>		<u>Necropsy Section</u>	
J. Hogan, BA	Supervisor/Chief Res. Technologist	J. Hogan, BA	Part-time Employee
C. M. Maruszak	Laboratory Technician-Trainee	C. M. Maruszak	
J. L. Pitcher	Laboratory Technician	J. L. Pitcher	
P. R. Romero-Stage	Laboratory Technician	P. R. Romero-Stage	

<u>ANIMAL CARE UNIT</u>	D. G. Burt, DVM S. L. Basson, BS D. M. Bolton F. Campbell, Jr. D. M. Chavez D. T. Cordaro M. O. Crenner*	Supervisor/Attending Veterinarian Chief Animal Technologist Animal Technician Animal Technician Animal Technician Sr. Animal Technician Animal Caretaker Animal Technician Sr. Animal Technician Animal Caretaker Animal Caretaker Animal Caretaker Animal Caretaker Animal Caretaker Clerical Specialist Sr. Animal Technician Animal Technician Animal Technician Animal Technician Animal Technician L. M. Martinez*	E. Anzures D. Aragon L. G. Archuleta W. F. Beierman, BSEE R. T. Cossey, ASEE J. A. Detmer A. R. Espanin J. V. Gallegos*	Supervisor/Facilities Engineer Electrical Maintenance Worker Lead Janitor Sr. Research Technologist Assistant Facilities Engineer Instrum. & Controls Maint. Worker/Tech. Specialist Technical Secretary General Maintenance Worker Janitor Laboratory Assistant Heating & Refrig. Maintenance Worker Laborer Technical Specialist Laboratory Assistant Laboratory Assistant Technical Specialist Mechanical Equip. Maintenance Worker Janitor
<u>COMPUTER UNIT</u>	J. H. Dietl, PhD	Supervisor/Computer Scientist		
M. F. Conrad, AS J. L. Holmes, BS R. L. Lucero E. Taplin, BBA	Research Technologist Software Specialist Laboratory Technician Software Specialist	K. M. Aragon, MBA M. M. Gurule A. I. Medrano P. S. Oh, BS	Supervisor/Budget Officer Clerical Specialist Clerical Specialist Accountant	
<u>HEALTH PROTECTION UNIT</u>				
J. H. Thompson, PhD A. C. Grace, MS L. C. Haling M. S. Hall, MS J. R. Lackey C. W. Pohl B. D. Ritchey, BS P. E. Sanchez W. C. Schleyer, III, MS	Supervisor/Health Protection Mgr. Environmental Restoration Coordinator Executive Secretary Sr. Research Technologist Research Technologist Sr. Research Technologist Clerical Specialist Health Physicist			

*Part-time employee.

HUMAN RESOURCES UNIT

B. K. Solari, BA
A. F. Baca
Surveillance Worker-Trainee
J. A. Davis, BS
Assistant Human Resources Manager
M. L. Grooms
Clerical Specialist
T. J. Hostkins
Clerical Specialist
J. T. Nunez
Surveillance Worker
P. Padilla
Surveillance Worker-Trainee
G. J. Quintana
Clerical Specialist
R. L. Ripple
Surveillance Worker-Trainee
I. J. Salinas

LIBRARY UNIT

S. E. Spurlock, MLS
C. S. Snidow
Supervisor/Technical Librarian
Clerical Specialist

PROCUREMENT UNIT

G. A. Allen
V. K. Aragon
L. Vigil
Supervisor
Clerical Specialist
Clerical Specialist

PROPERTY MANAGEMENT UNIT

P. F. Kaplan
A. J. Garcia
K. Perales
Supervisor
Clerical Specialist
Clerical Specialist

QUALITY ASSURANCE UNIT

D. L. Harris, MS
T. A. Ahlert, BA
Supervisor/Quality Assurance Officer
Administrative Specialist

TECHNICAL COMMUNICATIONS UNIT

P. L. Bradley, MA
C. M. Herrera
S. L. Perez
W. L. Piper, BA
S. F. Randock, BA
Supervisor/Technical Editor
Clerical Specialist
Clerical Specialist
Clerical Specialist
Clerical Specialist

TASK FORCE ON LIFE-SPAN RADIATION TOXICITY STUDIES**

B. B. Boecker, PhD	Assistant Director
M. G. Campos	Clerical Specialist
I. Y. Chang, MS	Software Specialist
M. F. Conrad, AS	Research Technologist
J. H. Dietl, PhD	Computer Scientist
K. M. Garcia, BA	Sr. Research Technologist
K. G. Gillett, BS	Research Technologist
W. C. Griffith, Jr., BS	Biomathematician
R. A. Guilmazte, PhD	Radiobiologist
F. F. Hahn, DVM, PhD	Experimental Pathologist
B. A. Muggenburg, DVM, PhD	Physiologist
K. J. Nikula, DVM, PhD	Experimental Pathologist
M. B. Snipes, PhD	Radiobiologist

**Individuals have primary assignment in Scientific Groups or Units on preceding pages.

EDUCATIONAL PARTICIPANTS

Name	School/University	ITRI Group/Unit/Section
<u>Department of Energy/Associated Western Universities Summer Student Research Participants</u>		
Stacey L. Addams	University of WI-Parkside, WI	Pathophysiology Group
Deborah L. Boger	Pomona College, CA	Pathology Group
Russell M. Goering	NM Institute of Mining/Technology, NM	Aerosol Science Group, Chronic Exposure Section
Ananda W. Goldrath	CA Polytechnic State University, CA	Molecular & Cellular Toxicology Group
Terri G. Houghton	NM Institute of Mining/Technology, NM	Health Protection Unit
Ami A. Hunt	Mary Washington College, VA	Chemistry & Biochemical Toxicology Group
Tho Hong Huynh	Haverford College, PA	Pathology Group
Mark C. Lane	Texas Tech University, TX	Aerosol Science Group
Michelle A. Stevens	Trinity University, TX	Molecular & Cellular Toxicology Group
Carol M. Wierenga	Calvin College, MI	Pathology Group
<u>Department of Energy/Associated Western Universities Environmental Management Career Opportunities for Minority Student Research Participant</u>		
Linda M. Reddick	Xavier University, LA	Pathophysiology Group
<u>Department of Energy/Associated Western Universities Teacher Research Associates Program (TRAC) Participants</u>		
Dana M. Beatty	Oak Harbor High School, WA	Chemistry & Biochemical Toxicology Group
Rodney K. Crabtree	Byng High School, OK	Molecular & Cellular Toxicology Group
Gracie C. Mays	Little Rock Central High School, AK	Molecular & Cellular Toxicology Group
Mark D. Tohulka	Homestead Sr. High School, FL	Pathology Group
<u>New Mexico Summer Teacher Enrichment Program (STEP) Participants</u>		
Anthony B. Jaramillo	Mesa Vista High School, NM	Financial Management Unit
Rajmahn H. Mooty	Santa Fe Technical High School, NM	Biomathematics Section
Kevin D. Rohrbacher	Manzano High School, NM	Aerosol Science Group
Gary G. Scott	Del Norte High School, NM	Chemistry & Biochemical Toxicology Group
<u>Department of Energy/Associated Western Universities Faculty Participant</u>		
Elizabeth K. Perryman	CA Polytechnic State University, CA	Molecular & Cellular Toxicology Group

EDUCATIONAL PARTICIPANTS

Name	School/University	ITRI Group/Unit/Section
<u>Student Employees - Summer 1992</u>		
Mary O. Crenner	University of New Mexico	Animal Care Unit
Jason A. Daniello	University of New Mexico	Animal Care Unit
Kim K. Decatur	New Mexico State University	Animal Care Unit
John V. Gallegos	University of New Mexico	Engineering & Facilities Unit
David Griege	University of New Mexico	Engineering & Facilities Unit
Phillip A. Gutierrez	Rio Grande High School	Chemistry & Biochemical Toxicology Group
David C. Hawkins	New Mexico State University	Engineering & Facilities Unit
Jonathan C. Hawkins	University of New Mexico	Engineering & Facilities Unit
Neil S. Jaramillo	New Mexico State University	Engineering & Facilities Unit
Thomas A. Knowlton	University of New Mexico	Engineering & Facilities Unit
Frankie A. Lucero	University of New Mexico	Engineering & Facilities Unit
Paul A. Melendres	Valley High School	Animal Care Unit
Salomon Moya	University of New Mexico	Molecular & Cellular Toxicology Group
Luis Armando Najera	New Mexico State University	Engineering & Facilities Unit
Douglas J. Podzemny	University of New Mexico	Animal Care Unit
David J. Stichman	University of New Mexico	Engineering & Facilities Unit
Ashley M. Tschida	University of New Mexico	Animal Care Unit
Brian S. Winkenweder	University of New Mexico	Pathophysiology Group
<u>UNM/ITRI Inhalation Toxicology Graduate Students</u>		
Thomas R. Carpenter		
Jennifer L. Francis		
Albert W. Hickman, Jr.		
Carlo M. Padilla		
Shawna M. Smith		
Nicole D. Stephens		
Deborah S. Swafford		
Lauren A. Tierney		
<u>Postdoctoral Fellows</u>		
Donna Davila		
William A. Evans		
Courtney Nickell		

APPENDIX C

ORGANIZATION OF RESEARCH PROGRAMS

OCTOBER 1, 1991 - DECEMBER 31, 1992

PROGRAM AND PROJECT TITLES	SPONSOR*	COORDINATOR
<u>RADIATION TOXICOLOGY - R. A. GUILMETTE, PROGRAM MANAGER</u>		
Effective Dose from Inhaled Nuclear Energy Materials	DOE/OHER	R. A. Guilmette
Dose-Response Relationships for Inhaled Radionuclides	DOE/OHER	B. A. Muggenburg
Radiation Dose and Injury to Critical Cells from Radon	DOE/OHER	N. F. Johnson
Deposition of Radon and Radon Progeny in the Respiratory Tract	DOE/OHER	H. C. Yeh
Toxicity of Injected Radionuclides - ITRI Effort	DOE/OHER	B. B. Boecker
Toxicity of Injected Radionuclides - Utah Effort	DOE/OHER	S. C. Miller
Health Effect Model for Reactor Accidents	NRC	B. B. Boecker
INSRP/BEES Panel	BNL	M. D. Hoover
Internal Dosimetry	WSRC	R. A. Guilmette
<u>BRUCE B. BOECKER, ASSISTANT DIRECTOR</u>		
<u>CHARLES H. HOBBS, ASSISTANT DIRECTOR</u>		
<u>AEROSOLS - Y. S. CHENG, PROGRAM MANAGER</u>		
Biologically Relevant Properties of Energy Related Aerosols	DOE/OHER	H. C. Yeh
Dynamics of Radon Daughter Interactions with Indoor Aerosols	DOE/PHYS	Y. S. Cheng
Underground Aerosol Characterization at the WIPP Site	DOE/AL	G. J. Newton
Y-12 Radiological Protection Program	DOE/Y-12	M. D. Hoover
HQ CAM Study	DOE/HQ	M. D. Hoover
Characterization of Aerosols Produced by Surgical Procedures	NIOSH	H. C. Yeh
Evaluation of Respirators - II for Asbestos Fibers	NIOSH	Y. S. Cheng
Experimental Tests on Continuous Air Monitors	EG&G	M. D. Hoover
Idaho Gas Contamination	INEL	G. J. Newton
Plutonium Dispersal Study	SNL	G. J. Newton
Air Sampling Program at SNL Area V	SNL	Y. S. Cheng
Dissolution of Metal Tritides in Biological Systems	SNL	M. D. Hoover
Russian Topaz-II Study	SNL	

PROGRAM AND PROJECT TITLES	SPONSOR*	COORDINATOR
<u>Chemical Toxicology - A. R. Dahl, Program Manager</u>		
Influence of Respiratory Tract Metabolism on Effective Dose	DOE/OHER	A. R. Dahl
Biological Markers of Human Exposure to Organic Compounds	DOE/OHER	W. E. Bechtold
Disposition of Inhaled Xenobiotics	NIEHS	R. F. Henderson
Nitrogen Heterocycles: Metabolic Effect and Toxicity	WSU	A. R. Dahl
Metabolism of 1,3-Butadiene, Butadiene Monoepoxide and Butadiene Diepoxyde by Human and Mouse Liver and Lung Tissue Homogenates	CMA	R. F. Henderson
Fate of Inhaled Vapors in Rats, Dogs, and Monkeys	NIH/NIEHS	A. R. Dahl
Disposition of Inhaled Toxicants in the Olfactory System	NIH/NIDCD	J. L. Lewis
Toxicity of Nickel Compounds to the Respiratory Tract	NIPERA	J. M. Benson
<u>Applied Toxicology - C. H. Hobbs, Program Manager</u>		
Effects of L-Deprenyl on Physiologic Functions	DAHI	B. A. Muggenburg
Treatment of Chronic Prostatic Hypertrophy	Aria	B. A. Muggenburg
Combined Exposure, Plutonium-Cigarette Smoke	DOE/DP	G. L. Finch
Combined Exposure, Plutonium-Beryllium	DOE/DP	G. L. Finch
Combined Exposure, Plutonium-X Ray	DOE/DP	D. L. Lundgren
Combined Exposure, Plutonium-Chemical Carcinogen	DOE/DP	D. L. Lundgren
Combined Exposure, Radiation, Fiber	DOE/DP	D. L. Lundgren
Precorionic and Chronic Studies of Nickel Compounds	NIEHS	J. M. Benson
Chronic Inhalation of Hygroscopic Material in Rats	P&G	J. M. Benson
90-Day Study of Powdered Detergent Constituents Inhaled by F344 Rats	P&G	M. B. Snipes
<u>Pathogenesis - J. R. Harkema, Program Manager</u>		
Cellular & Biochemical Mediators of Respiratory Tract Disease	DOE/OHER	R. F. Henderson
Airway Epithelial Injury, Adaptation and Repair	DOE/OHER	J. R. Harkema
Role of Immune Responses in Respiratory Disease	DOE/OHER	D. E. Bice
Mechanisms of Granulomatous Disease from Inhaled Beryllium	DOE/OHER	G. L. Finch

PROGRAM AND PROJECT TITLES	SPONSOR*	COORDINATOR
<u>Pathogenesis (Cont.) - J. R. Harkema, Program Manager</u>		
Evaluation of Pulmonary Immune Responses to Viral Agents	UA	D. E. Bice
Rodent Immunity after Immunization of Nasal Airways	3M Company	D. E. Bice
Respiratory Function Alterations Following Chronic Ozone Inhalation in Rats	HEI	J. R. Harkema
Effect of Chronic Ozone Inhalation on Nasal Mucociliary Apparatus in Rats	HEI	J. R. Harkema
<u>JOHN F. LECHNER, ASSISTANT DIRECTOR</u>		
<u>Cancer Mechanisms - J. F. Lechner, Program Manager</u>		
Links Between Radiation-Induced Lung Cancer in Laboratory Animals and People	DOE/OHER	F. F. Hahn
Pu-Malignant Events in Radiation-Induced Lung Cancer	DOE/OHER	J. F. Lechner
Lung Cancer in Uranium Miners - Gene Dysfunction	DOE/OHER	J. F. Lechner
Cellular Models of Radiation-Induced Lung Cancer	DOE/OHER	J. F. Lechner
Molecular Mechanisms of Radiation-Induced Cancer	DOE/OHER	G. Kelly
Gene Dysfunction in Chemical Induced Carcinogenicity	DOE/OHER	S. A. Belinsky
* BNL - Brookhaven National Laboratory CMA - Chemical Manufacturing Association DAHI - Deprenyl Animal Health Inc. DOE/AL - Department of Energy Field Office, Albuquerque DOE/DP - Department of Energy, Office of Defense Programs DOE/HQ - Department of Energy, Headquarters DOE/OHER - Department of Energy, Office of Health and Environmental Research DOE/PHYS - Department of Energy, Physical and Technological Research DOE/Y-12 - Y-12 Plant EG&G - Rocky Flats Plant HEI - Health Effects Institute INEL - Idaho National Engineering Laboratory		
NIDCD - National Institute on Deafness and Communicable Diseases NIEHS - National Institute of Environmental Health Sciences NIH - National Institutes of Health NIOSH - National Institute of Occupational Safety & Health NiPERA - Nickel Producers Environmental Research Association NRC - Nuclear Regulatory Commission P&G - Proctor & Gamble SNL - Sandia National Laboratories UA - University of Arizona WSRC - Westinghouse Savannah River Co. WSU - Wayne State University		

APPENDIX D
PUBLICATION OF TECHNICAL REPORTS
OCTOBER 1, 1991 - SEPTEMBER 30, 1992

LMF-134 - Shyr, L. J., G. L. Finch and P. L. Bradley (eds.): *Inhalation Toxicology Research Institute Annual Report - October 1, 1990 through September 30, 1991*, LMF-134, National Technical Information Service, Springfield, VA 22161.

LMF-135 - Boecker, B. B., B. A. Muggenburg, S. C. Miller and P. L. Bradley (eds.): *Annual Report on Long-Term Dose Response Studies of Inhaled or Injected Radionuclides - October 1, 1990 through September 30, 1991*, U.S. Department of Energy, Office of Health and Environmental Research, LMF-135, National Technical Information Service, U.S. Department of Commerce, Springfield, VA 22161.

LMF-136 - Bennett, W. C., J. J. Thompson and A. S. Shankar: *Site Environmental Report - 1991*.

APPENDIX E-1
ITRI PUBLICATIONS IN THE OPEN LITERATURE
OCTOBER 1, 1991 - SEPTEMBER 30, 1992

- Barr, E. B. and Y. S. Cheng: Evaluation of the API Aerosizer Mach 2 Particle Sizer. In *Proceedings of the Third Symposium on Particles in Gases and Liquids: Detection, Characterization, and Control* held in San Jose, CA, July 29-August 2, 1991 (in press).
- Bechtold, W. E., J. D. Sun, L. S. Birnbaum, S. N. Yin, G. L. Li, S. Kasicki, G. Lucier and R. F. Henderson: S-Phenylcysteine Formation in Hemoglobin as a Biological Exposure Index to Benzene. *Arch. Toxicol.* 66: 303-309, 1992.
- Bechtold, W. E., J. K. Willis, J. D. Sun, W. C. Griffith and T. V. Reddy: Biological Markers of Exposure to Benzene: S-phenylcysteine in Albumin. *Carcinogenesis* 13: 1217-1220, 1992.
- Bechtold, W. E., J. J. Waide, T. Sandstrom, N. Stjernberg, D. McBride, J. Koenig, I. Y. Chang and R. F. Henderson: Biological Markers of Exposure to SO₂: S-Sulfonates in Nasal Lavage. *J. Exposure Anal. Environ. Epidemiol.* (submitted).
- Benson, J. M., A. L. Brooks and R. F. Henderson: Comparative *In Vitro* Cytotoxicity of Nickel Compounds to Pulmonary Alveolar Macrophages and to Rat Lung Epithelial Cells. In *Nickel in Human Health - Current Perspectives* (E. Nieboer and J. O. Nriagu, eds.), pp. 319-330, John Wiley & Sons, 1992.
- Benson, J. M., D. G. Burt, Y. S. Cheng, F. F. Hahn, P. J. Haley, R. F. Henderson, C. H. Hobbs, J. A. Pickrell and J. K. Dunnick: Effects of Inhaled Nickel on Lung Biochemistry. In *Nickel in Human Health - Current Perspectives* (E. Nieboer and J. O. Nriagu, eds.), pp. 451-465, John Wiley & Sons, 1992.
- Bice, D. E., D. N. Weissman and B. A. Muggenburg: Long-Term Maintenance of Localized Antibody Responses in the Lung. *Immunology* 74: 215-222, 1991.
- Bice, D. E.: The Lung as a Target Organ. In *Principles and Practice of Immunotoxicology* (in press).
- Boecker, B. B., B. A. Muggenburg, F. F. Hahn, K. J. Nikula and W. C. Griffith: Life-Span Health Effects of Relatively Soluble Forms of Internally Deposited Beta-Emitting Radionuclides. In *Proceedings of the International Radiation Protection Association 8th Congress*, pp. 864-867, 1992.
- Boehme, D. S., J. A. Hotchkiss and R. F. Henderson: Glutathione and GSH-Dependent Enzymes in Bronchoalveolar Lavage Fluid Cells in Response to Ozone. *Exp. Mol. Pathol.* 56: 37-48, 1992.
- Boehme, D. S., K. R. Maples and R. F. Henderson: Glutathione Release by Pulmonary Alveolar Macrophages in Response to Particles *In Vitro*. *Toxicol. Lett.* 60: 53-60, 1992.
- Bond, J. A., L. A. Wallace, S. Osterman-Golkar, G. W. Lucier, A. Buckpitt and R. F. Henderson: Symposium Overview-Assessment of Exposure to Pulmonary Toxicants: Use of Biological Markers. *Fundam. Appl. Toxicol.* 18: 161-174, 1992.
- Brooks, A. L., R. A. Guilmette, F. F. Hahn, P. J. Haley, B. A. Muggenburg, J. A. Mewhinney and R. O. McClellan: Distribution and Biological Effects of Inhaled ²³⁹Pu(NO₃)₄ in Cynomolgus Monkeys. *Radiat. Res.* 130: 79-87, 1992.
- Brooks, A. L., K. Rithidech, N. F. Johnson, D. G. Thomassen and G. J. Newton: Evaluating Chromosome Damage to Estimate Dose to Tracheal Cells. In *The 29th Hanford Symposium on Health and the Environment. Indoor Radon and Lung Cancer. Myth or Reality?* held in Richland, WA, October 15-19, 1990 (in press).

- Chang, I. Y., W. C. Griffith, L. J. Shyr, H. C. Yeh, R. G. Cuddihy and F. A. Seiler: Software for the Draft NCRP Respiratory Tract Dosimetry Model. *Radiat. Prot. Dosim.* 38: 193-200, 1991.
- Chen, T. B., W. E. Bechtold and J. L. Mauderly: Description and Evaluation of a Cigarette Smoke Generation System for Inhalation Studies. *J. Aerosol Med.* 5: 19-30, 1992.
- Chen, B. T., H. C. Yeh and Y. S. Cheng: Evaluation of an Environmental Reaction Chamber. *Aerosol Sci. Tech.* 17: 9-24, 1992.
- Chen, T. B., W. E. Bechtold and J. L. Mauderly: A Continuous Generator of Cigarette Smoke: Description and Evaluation. *Beitr. Zur Tabakforschung International* (in press).
- Chen, T. B.: Instrument Calibration - Chapter 22. In *Aerosol Measurement* (K. Willeke and P. Barones, eds.), Van Nostrand (in press).
- Chen, B. T., R. Irwin, Y. S. Cheng, M. D. Hoover and H. C. Yeh: Aerodynamic Behavior of Fiber-and Disc-Like Particles in a Millikan Cell Apparatus. *J. Aerosol Med.* (submitted).
- Chen, B. T., H. C. Yeh and C. H. Hobbs: Size Classification of Carbon Fiber Aerosols. *Aerosol Sci. Technol.* (submitted).
- Cheng, Y. S.: Drag Forces on Nonspherical Aerosol Particles. *Chem. Eng. Commun.* 108: 201-223, 1991.
- Cheng, Y. S., H. C. Yeh and D. L. Swift: Aerosol Deposition in Human Nasal Airway for Particles 1 nm to 20 μm . *Radiat. Prot. Dosim.* 38: 41-47, 1991.
- Cheng, Y. S.: Diffusion and Condensation Techniques - Chapter 20. In *Aerosol Measurement* (K. Willeke and P. Barones, eds.), Van Nostrand (in press).
- Cheng, Y. S., B. T. Chen and H. C. Yeh: Performance of an Aerodynamic Particle Sizer. *Appl. Occup. Environ. Health* (in press).
- Cheng, Y. S., Y. F. Su and T. B. Chen: Plate-Out Rates of Radon Progeny and Particles in a Spherical Chamber. In *Proceedings of the 29th Hanford Symposium on Health and Environment, Indoor Radon and Lung Cancer, Myth or Reality?* held in Richland, WA, October 16-19, 1990 (in press).
- Cheng, Y. S. and E. B. Barr: Calibration and Performance of an API Aerosizer. *J. Aerosol Sci.* (submitted).
- Cheng, Y. S., B. T. Chen, H. C. Yeh, I. A. Marshall, J. P. Mitchell and W. D. Griffiths: The Behavior of Compact Non-Spherical Particles in the APS33B: Ultra-Stokesian Drag Forces. *Aerosol Sci. Technol.* (submitted).
- Cheng, Y. S., Y. F. Su, G. J. Newton and H. C. Yeh: Use of a Graded Diffusion Battery in Measuring the Activity Size Distributions of Thoron Progeny. *J. Aerosol Sci.* (submitted).
- Cheng, Y. S., Y. F. Su, H. C. Yeh and D. L. Swift: Deposition of Thoron Progeny in Human Head Airways. *Aerosol Sci. Technol.* (in press).
- Dahl, A. R., J. D. Sun, L. S. Birnbaum, J. A. Bond, W. C. Griffith, J. L. Mauderly, B. A. Muggenburg, P. J. Sabourin and R. F. Henderson: Toxicokinetics of Inhaled 1,3-Butadiene in Monkeys: Comparison to Toxicokinetics in Rats and Mice. *Toxicol. Appl. Pharmacol.* 110: 9-19, 1991.
- Dahl, A. R. and P. Gerde: Uptake and Metabolism of Toxicants in the Respiratory Tract. *Environ. Health Perspect.* (submitted).
- Dahl, A. R. and J. L. Lewis: Respiratory Tract Uptake and Metabolism of Inhalants. *Ann. Rev. Pharmacol. Toxicol.* (in press).

Davila, D. R., R. A. Guilmette, D. E. Bice, B. A. Muggenburg, D. S. Swafford and P. J. Haley: Long-Term Consequences of $^{239}\text{PuO}_2$ Exposure in Dogs: Persistent T Lymphocyte Dysfunction. *Int. J. Radiat. Biol.* 61: 123-133, 1992.

Diel, J. H., R. A. Guilmette, B. A. Muggenburg, F. F. Hahn and I. Y. Chang: Influence of Dose Rate on Survival Time for $^{239}\text{PuO}_2$ Induced Radiation Pneumonitis or Pulmonary Fibrosis in Dogs. *Radiat. Res.* 129: 53-60, 1992.

Dunnick, J. K., M. R. Elwell, J. B. Benson, C. H. Hobbs, Y. S. Cheng, F. F. Hahn, P. J. Haley and A. F. Eidson: Inhalation Toxicity of Nickel Compounds. In *Nickel and Human Health - Current Perspectives* (E. Nieboer and J. O. Nriagu, eds.), pp. 437-450, John Wiley & Sons, 1992.

Economou, P., J. F. Lechner and J. M. Samet: Familial and Genetic Factors in the Pathogenesis of Lung Cancer. In *Epidemiology of Lung Cancer* (J. M. Samet, ed.) (in press).

Eidson, A. F., A. Taya, G. L. Finch, M. D. Hoover and C. Cook: Dosimetry of Beryllium in Cultured Canine Pulmonary Alveolar Macrophages. *J. Toxicol. Environ. Health* 34: 433-448, 1991.

Finch, G. L., P. J. Haley, M. D. Hoover and R. G. Cuddihy: Responses of Rat Lungs Following Inhalation of Beryllium Metal Particles to Achieve Relatively Low Lung Burdens. To be published in *Proceedings of the 7th International Symposium on Inhaled Particles* held in Edinburgh, Scotland, September 16-21, 1991 (in press).

Finch, G. L.: *In Vitro Measurement of Macrophage Phagocytosis Using a Sheep Red Blood Cell Assay*. In *Methods in Toxicology*, Academic Press (submitted).

Gerde, P., B. A. Muggenburg, M. D. Hoover and R. F. Henderson: Clearance of Particles and Lipophilic Solutes from the Central Airways. To be published in *Proceedings of the 7th International Symposium on Inhaled Particles* held in Edinburgh, Scotland, September 16-21, 1991 (in press).

Gillett, N. A., R. R. Pool, G. N. Taylor, B. A. Muggenburg and B. B. Boecker: Strontium-90 Induced Bone Tumours in Beagle Dogs: Effects of Route of Exposure and Dose Rate. *Int. J. Radiat. Biol.* 61: 821-831, 1992.

Gillett, N. A., B. L. Stegelmeier, G. Kelly, P. J. Haley and F. F. Hahn: Expression of Epidermal Growth Factor Receptor in Plutonium-239 Induced Lung Neoplasms in Dogs. *Vet. Pathol.* 29: 425-449, 1992.

Gillett, N. A., B. L. Stegelmeier, I. Y. Chang and G. Kelly: Expression of Transforming Growth Factor Alpha in Plutonium-239 Induced Lung Neoplasms in Dogs: Investigations of Autocrine Mechanisms of Growth. *Radiat. Res.* 126: 289-295, 1991.

Gillett, N. A., R. R. Pool and B. A. Muggenburg: Tumors of Bone. In *DOE/OHER Beagle Pathology Atlas* (in press).

Griffith, W. C. and R. A. Guilmette: Multiparameter Analysis of Fallout Plutonium Burdens in Human Liver. *Radiat. Prot. Dosim.* 38: 113-119, 1991.

Griffith, W. C., B. B. Boecker, F. F. Hahn, B. A. Muggenburg and M. B. Snipes: The Effect of Dose Protraction on the Incidence of Lung Carcinomas in Beagle Dogs with Internally Deposited Beta-Emitting Radionuclides. In *Proceedings of the 8th International Congress of the International Radiation Protection Association*, pp. 896-899, 1992.

Guilmette, R. A. and A. F. Eidson: Using Animal Dosimetry Models to Interpret Human Bioassay Data for Actinide Exposures. *Int. J. Radioanalytical Nucl. Chem. Articles* 1561: 425-449, 1992.

Guilmette, R. A. and W. C. Griffith: The Effect of Isotope on the Dosimetry of Inhaled Plutonium Oxide. In *Proceedings of the 8th International Congress of the International Radiation Protection Association*, pp. 900-903, 1992.

Guilmette, R. A. and B. A. Muggenburg: Effectiveness of Continuously Infused DTPA Therapy in Reducing the Radiation Dose from Inhaled $^{244}\text{Cm}_2\text{O}_3$ Aerosols. *Health Phys.* 62: 311-318, 1992.

Guilmette, R. A. and B. B. Boecker (eds.): *Radiation Protection Dosimetry: Respiratory Tract Dosimetry*, Vol. 38, 1991.

Guilmette, R. A., N. F. Johnson, G. J. Newton, D. G. Thomassen and H. C. Yeh: Risks from Radon Progeny Exposure: What We Know, and What We Need to Know. *Ann. Rev. Pharmacol. Toxicol.* 31: 569-601, 1991.

Guilmette, R. A. and B. A. Muggenburg: Decorporation Therapy for Inhaled Plutonium Nitrate Using Repeatedly and Continuously Administered DTPA. *Int. J. Radiat. Biol.* (in press).

Guilmette, R. A. and T. J. Gagliano: Construction of a Model of Human Nasal Airways Using *In Vivo* Morphometric Data. To be published in *Proceedings of the 7th International Symposium on Inhaled Particles* held in Edinburgh, Scotland, September 16-21, 1991 (in press).

Hahn, F. F., W. C. Griffith, B. B. Boecker, B. A. Muggenburg and D. L. Lundgren: Comparison of the Effects of Inhaled $^{239}\text{PuO}_2$ and β -Emitting Radionuclides on the Incidence of Lung Carcinomas in Laboratory Animals. In *Proceedings of the 8th International Congress of the International Radiation Protection Association*, pp. 916-919, 1992.

Hahn, F. F., P. J. Haley, A. F. Hubbs, M. D. Hoover and D. L. Lundgren: Radiation-Induced Mesotheliomas in Rats. In *Mechanisms in Fibre Carcinogenesis* (R. C. Brown et al., eds.), pp. 91-99, Plenum Press, New York, 1991.

Hahn, F. F.: Toxicology of the Lung. To be published in *Chronic Inhalation Bioassays for Respiratory Tract Carcinogenesis* (D. E. Gardner, J. D. Crapo and R. O. McClellan, eds.), Raven Press, New York, NY (in press).

Hahn, F. F., W. C. Griffith, C. H. Hobbs, B. A. Muggenburg, G. J. Newton and B. B. Boecker: Biological Effects of ^{91}Y in Relatively Insoluble Particles Inhaled by Beagle Dogs. To be published in *Proceedings of the 7th International Symposium on Inhaled Particles* held in Edinburgh, Scotland, September 16-21, 1991 (in press).

Haley, P. J.: Mechanisms of Granulomatous Lung Disease from Inhaled Beryllium: The Role of Antigenicity in Granuloma Formation. *Toxicol. Pathol.* 19: 514-525, 1991.

Haley, P. J.: Pulmonary Toxicity of Stable and Versus Radioactive Lanthanides. *Health Phys.* 61: 809-820, 1991.

Haley, P. J.: Immunological Responses Within the Lung After Inhalation of Airborne Chemicals. In *Toxicology of the Lung* (D. E. Gardner, J. D. Crapo and R. O. McClellan, eds.) (in press).

Haley, P. J., G. L. Finch, M. D. Hoover, J. A. Mewhinney, D. E. Bice and B. A. Muggenburg: Beryllium-Induced Lung Disease in the Dog Following Repeated BeO Exposure. *Environ. Res.* (in press).

Haley, P. J., M. Schuyler, K. Gott and T. B. Casale: Mast Cell Hyperplasia in Experimental Hypersensitivity Pneumonitis. *Int. Arch. Allergy Appl. Immunol.* 96(2): 168-174, 1992.

Harkema, J. R.: Epithelial Cells of the Nasal Passages. In *Comprehensive Treatise on Pulmonary Toxicology: Comparative Biology of the Normal Lung*, Vol. 1 (R. A. Parent, ed.), pp. 27-36, CRC Press, Boca Raton, FL, 1992.

Harkema, J. R. and J. A. Hotchkiss: *In Vivo* Effects of Endotoxin on Intraepithelial Mucosubstances in Rat Pulmonary Airways: Quantitative Histochemistry. *Am. J. Pathol.* 141: 1-11, 1992.

Harkema, J. R., S. E. Jones, D. K. Naydan and D. W. Wilson: An Atypical Neuroendocrine Tumor in the Lung of a Beagle Dog. *Vet. Pathol.* 29: 176-179, 1992.

Harkema, J. R.: Comparative Aspects of Nasal Airway Anatomy: Relevance to Inhalation Toxicology. *Toxicol.*

- Harkema, J. R. and J. A. Hotchkiss: *In Vivo Effects of Endotoxin on Nasal Epithelial Mucosubstances: Quantitative Histochemistry*. *Exp. Lung Res.* 17: 743-761, 1991.
- Harkema, J. R., A. Mariassy, J. A. St. George, D. M. Hyde and C. G. Plopper: *Epithelial Cells of the Conducting Airways: A Species Comparison*. In *The Airway Epithelium* (in press).
- Harkema, J. R. and J. A. Hotchkiss: *In Vivo Effects of Endotoxin on DNA Synthesis in Rat Nasal Epithelium*. *J. Microscopic Res. Tech.* (submitted).
- Harkema, J. R., C. G. Plopper, D. M. Hyde, J. A. St. George, D. W. Wilson and D. L. Dungworth: *Response of Macaque Bronchiolar Epithelium to 0.15 and 0.30 ppm Ozone*. *Am. J. Pathol.* (submitted).
- Helfinstine, S. Y., R. A. Guilmette and G. A. Schlapper: *In Vitro Dissolution of Curium Oxide Using a Phagolysosomal Simulant Solvent System*. *Environ. Health Perspect.* 97: 131-137, 1992.
- Henderson, R. F., E. B. Barr, Y. S. Cheng, W. C. Griffith and F. F. Hahn: *The Effect of Exposure Pattern on the Accumulation of Particles and the Response of the Lung to Inhaled Particles*. *Fundam. Appl. Toxicol.* 19: 367-374, 1992.
- Henderson, R. F. and B. A. Muggenburg: *Bronchoalveolar Lavage in Animals*. In *Bronchoalveolar Lavage* (R. P. Baughman, ed.), pp. 265-287, Mosby Year Book, St. Louis, 1992.
- Henderson, R. F., P. J. Sabourin, M. A. Medinsky, L. S. Birnbaum and G. L. Lucier: *Benzene Dosimetry in Experimental Animals: Relevance for Risk Assessment*. In *Relevance of Animal Studies to the Evaluation of Human Cancer Risk* (R. D. Amato, T. J. Slaga, W. H. Farland and C. Henry, eds.), pp. 93-105, Wiley-Liss, 1992.
- Henderson, R. F.: *Short-Term Exposure Guidelines for Emergency Response - The Approach of the Committee on Toxicology*. In *Proceedings from the Conference on Chemical Risk Assessment in the DOD: Science, Policy, and Practice* (in press).
- Henderson, R. F., W. E. Bechtold and K. R. Maples: *Biological Markers as Measures of Exposure*. *J. Exposure Anal. Environ. Epidemiology* (in press).
- Henderson, R. F. and J. L. Mauderly: *The Toxicity of Particles from Combustion Processes*. In *Proceedings of the International Conference on Toxicology of Combustion Products held in Pavia, Italy, October 28-30, 1991* (in press).
- Henderson, R. F., J. R. Harkema, J. A. Hotchkiss, I. Y. Chang and B. R. Scott: *Effect of Cumulative Exposure on Response to Ozone*. *Toxicol. Appl. Pharmacol.* (submitted).
- Herbert, R. A., N. A. Gillett, A. H. Rebar, D. L. Lundgren, M. D. Hoover, I. Y. Chang, W. W. Carlton and F. F. Hahn: *Sequential Analysis of the Pathogenesis of Plutonium-Induced Pulmonary Neoplasms in the Rat: Morphology, Morphometry, and Cytokinetics*. *Radiat. Res.* (submitted).
- Hoover, M. D. and G. J. Newton: *Radioactive Aerosols*. In *Aerosol Measurement* (K. Willeke and P. Baron, eds.), (in press).
- Hotchkiss, J. A. and J. R. Harkema: *Endotoxin or Cytokines Attenuate Ozone-Induced DNA Synthesis in Rat Nasal Transitional Epithelium*. *Toxicol. Appl. Pharmacol.* 114: 182-187, 1992.
- Hotchkiss, J. A., S. J. Kennel and J. R. Harkema: *A Rat Monoclonal Antibody Specific for Murine Type 1 Pneumocytes*. *Exp. Mol. Pathol.* (in press).
- Hotchkiss, J. A., S. G. Kim, R. F. Novak and A. R. Dahl: *Enhanced Expression of P450IIE1 Following Inhalation Exposure to Pyridine*. *Toxicol. Appl. Pharmacol.* (in press).

Hubbs, A. F., F. F. Hahn and D. L. Lundgren: Invasive Tracheobronchial Aspergillosis in an F344/N Rat. *Lab. Anim. Sci.* 41: 521-524, 1991.

Hubbs, A. F., F. F. Hahn and D. G. Thomassen: Enhanced *In Vivo* and *In Vitro* Proliferative Potential of Carcinogen-Exposed Canine Tracheal Epithelial Cells. *Toxicol. In Vitro* (submitted).

Hubbs, A. F., K. J. Nikula, F. F. Hahn and D. L. Lundgren: Primary Intrathoracic, Extraskeletal, Osteosarcoma in an F344/N Rat. *Vet. Pathol.* (submitted).

Johnson, N. F.: The Utility of Animal Inhalation Studies to Assess the Risk of Mineral Fiber-Induced Pulmonary Cancer. In *Relevance of Animal Studies to Evaluate Human Cancer Risk* (R. D'Amato, T. J. Slaga, W. H. Farland and C. Henry, eds.), pp. 19-36, Wiley-Liss, 1992.

Johnson, N. F., M. D. Hoover, D. G. Thomassen, Y. S. Cheng, A. Dalley and A. L. Brooks: *In Vitro* Activity of Silicon Carbide Whiskers in Comparison to Other Industrial Fibers Using Four Cell Culture Systems. *Am. J. Ind. Med.* 21: 807-823, 1992.

Johnson, N. F.: The Relevance of Animal Bioassays to Assess Human Health Hazards to Inorganic Fibrous Materials. In *Mechanisms in Fibre Carcinogenesis* (R. C. Brown, J. A. Hoskins, N. F. Johnson *et al.*, eds.), pp. 59-69, Plenum Press, New York, 1991.

Johnson, N. F.: The Limitations of Inhalation, Intratracheal, and Intercoelomic Routes of Administration for Identifying Hazardous Fibrous Materials. In *Fiber Toxicology* (D. Warheit, ed.), Pergamon Press (in press).

Johnson, N. F., G. J. Newton and R. A. Guilmette: Effects of Acute Radon Progeny Exposure on Rat Alveolar Macrophage Number and Function. In *Proceedings of the 29th Hanford Hanford Symposium on Health and the Environment, Indoor Radon and Lung Cancer: Reality or Myth?* held in Richland, WA, October 16-19, 1990 (in press).

Jones, S. E., D. R. Davila, P. J. Haley and D. E. Bice: The Effects of Age on Immune Responses in the Antigen-Instilled Dog Lung. I. Antibody Responses in the Lung and Lymphoid Tissues of Dogs Following Primary and Secondary Antigen Instillation. *Mech. Ageing Dev.* (in press).

Kennedy, C. H., K. B. Cohen, W. E. Bechtold, I. Y. Chang, A. R. Dahl and R. F. Henderson: Disposition and Metabolism of 1,1,2,2-Tetrabromoethane in F344 Rats After Gavage Administration. *Toxicol. Appl. Pharmacol.* (submitted).

Kusewitt, D. F., F. F. Hahn and B. A. Muggenburg: Ultrastructure of a Spindle Cell Carcinoma in the Mammary Gland of a Dog. *Vet. Pathol.* 29: 179-181, 1992.

Lewis, J. L., C. E. Rhoades, D. E. Bice, J. R. Harkema, J. A. Hotchkiss, D. M. Sylvester and A. R. Dahl: Interspecies Comparison of Cellular Localization of the Cyanide Metabolizing Enzyme Rhodanese Within Olfactory Mucosa. *Anat. Rec.* 232: 620-627, 1992.

Lundgren, D. L., F. F. Hahn, J. H. Diel and M. B. Snipes: Repeated Inhalation Exposure of Rats to Aerosols of $^{144}\text{CeO}_2$. I. Dosimetry. *Radiat. Res.* (in press).

Lundgren, D. L., F. F. Hahn and J. H. Diel: Repeated Inhalation Exposure of Rats to Aerosols of $^{144}\text{CeO}_2$. II. Biological Effects. *Radiat. Res.* (in press).

Lundgren, D. L., P. J. Haley, F. F. Hahn, J. H. Diel, W. C. Griffith, and B. R. Scott: Pulmonary Carcinogenicity of Repeated Inhalation Exposure of Rats to Aerosols of $^{239}\text{PuO}_2$. *Int. J. Radiat. Biol.* (submitted).

Maples, K. R., J. L. Lane and A. R. Dahl: An Effective Method for Synthesizing [d6]-Butadiene Monoepoxide. *J. Labelled Compounds and Radiopharmaceuticals* 31: 469-475, 1992.

Maples, K. R. and N. F. Johnson: Fiber-Induced Hydroxyl Radical Formation: Correlation with Mesothelioma Induction in Rats and Humans. *Carcinogenesis* (submitted).

Maples, K. R. and A. R. Dahl: Levels of Epoxides in Blood During Inhalation of Alkenes and Alkene Oxides. *Inhal. Toxicol.* (submitted).

Mauderly, J. L.: Diesel Exhaust - Chapter 5. In *Environmental Toxicants - Human Exposures and Their Health Effects* (M. Lippman, ed.), pp. 119-162, Van Nostrand Reinhold Publishers, New York, NY, 1992.

Mauderly, J. L. and J. M. Samet: General Environment - Chapter 6.1. In *The Lung: Scientific Foundations* (R. G. Crystal and J. B. West, eds.), pp. 187-200, Raven Press, Ltd., New York, 1991.

Mauderly, J. L. and N. A. Gillett: Changes in Respiratory Function of the Aging Rat. In *ILSI Monograph on the Pathology of Aging Animals, Vol. 1, Rat* (U. Mohr, C. C. Capen and D. L. Dungworth, eds.), Springer Verlag, Berlin, FRG (in press).

Mauderly, J. L., E. B. Barr, A. F. Eidson, J. R. Harkema, R. F. Henderson, J. A. Pickrell and R. K. Wolff: Pneumonconiosis in Rats Exposed Chronically to Oil Shale Dust and Diesel Exhaust, Alone and in Combination. To be published in *Proceedings of the 7th International Symposium on Inhaled Particles* held in Edinburgh, Scotland, September 16-21, 1991 (in press).

Mauderly, J. L.: Toxicological and Epidemiological Evidence for Health Risks from Inhaled Engine Emissions. *Environ. Health Perspect.* (submitted).

Mauderly, J. L.: Toxicological Approaches to Complex Mixtures. *Environ. Health Perspect.* (in press).

Medinsky, M. A., D. M. Chico and F. F. Hahn: Correlation of Urinary Enzyme Activity and Renal Lesions After Injection of Nickel Chloride. In *Nickel in Human Health - Current Perspectives* (E. Nieboer and J. O. Nriagu, eds.), pp. 183-192, John Wiley and Sons, 1992.

Mitchell, C. E., R. W. West and D. G. Thomassen: Transformation Responses of Rat Tracheal Epithelial Cells Exposed to 1,6-Dinitropyrene and 4-Nitropyrene in Culture. *Carcinogenesis* (submitted).

Muggenburg, B. A., R. A. Guilmette, L. M. Romero and J. A. Mewhinney: Improvements in Lung Lavage to Increase its Effectiveness in Removing Inhaled Radionuclides. In *Proceedings of the 8th International Congress of the International Radiation Protection Association*, pp. 920-923, 1992.

Muggenburg, B. A., R. A. Guilmette, W. C. Griffith, F. F. Hahn, N. A. Gillett and B. B. Boecker: The Toxicity of Inhaled Particles of $^{238}\text{PuO}_2$ in Dogs. To be published in *Proceedings of the 7th International Symposium on Inhaled Particles* held in Edinburgh, Scotland, September 16-21, 1991 (in press).

Newton, G. J., R. G. Cuddihy, H. C. Yeh and B. B. Boecker: Design and Performance of a Recirculating Radon Progeny Aerosol Generation and Animal Inhalation Exposure System. In *Proceedings of the 29th Hanford Symposium on Health and the Environment, Indoor Radon Progeny and Lung Cancer: Fact or Reality?* held in Richland, CA, October 16-19, 1990 (in press).

Nikula, K. J., P. J. Sabourin, B. C. Frietag, A. J. Birdwhistell, J. A. Hotchkiss and J. R. Harkema: Biochemical and Morphologic Responses of Rat Nasal Epithelia to Hyperoxia. *Fundam. Appl. Toxicol.* 17: 675-683, 1991.

Phalen, R. F., R. G. Cuddihy, G. L. Fisher, O. R. Moss, R. B. Schlesinger, D. L. Swift and H. C. Yeh: Main Features of the Proposed NCRP Respiratory Tract Model. *Radiat. Prot. Dosim.* 38: 179-184, 1991.

Sabourin, P. J., L. T. Burka, W. E. Bechtold, A. R. Dahl, M. D. Hoover, I. Y. Chang and R. F. Henderson: Species Differences in Urinary Butadiene Metabolites: Identification of 1,2-Dihydroxy-4-(N-acetylcysteinyl) butane, a Novel Metabolite of Butadiene. *Carcinogenesis* 13: 1633-1638, 1992.

- Sabourin, P. J., M. A. Medinsky, F. Thurmond, L. S. Birnbaum and R. F. Henderson: Effect of Dose on the Disposition of Methoxyethanol, Ethoxyethanol, and Butoxyethanol Administered Dermally to Male F344/N Rats. *Fundam. Appl. Toxicol.* 19: 124-132, 1992.
- Sabourin, P. J., M. A. Medinsky, L. S. Birnbaum, W. C. Griffith and R. F. Henderson: Effect of Exposure Concentration on the Disposition of Inhaled Butoxyethanol by F344 Rats. *Toxicol. Appl. Pharmacol.* 114: 232-238, 1992.
- Sabourin, P. J., B. A. Muggenburg, R. C. Couch, D. Lefler, G. Lucier, L. S. Birnbaum and R. F. Henderson: Metabolism of (¹⁴C) Benzene by Cynomolgus Monkeys and Chimpanzees. *Toxicol. Appl. Pharmacol.* 114: 277-284, 1992.
- Scott, B. R.: Biophysical and Biomathematical Adventures in Radiobiology. In *Proceedings of Southern University's Fifth Annual College of Sciences Symposium, Versatility and Wonders of Physics* held in Baton Rouge, LA, February 6-8, 1991 (submitted).
- Shyr, L. J. and B. A. Muggenburg: A Comparison of the Predicted Risks of Developing Osteosarcoma for Dogs Exposed to ²³⁸PuO₂ Based on Average Bone Dose or Endosteal Cell Dose. *Radiat. Res.* 132: 13-18, 1992.
- Shyr, L. J., J. H. Diel, I. Y. Chang and R. A. Guilmette: A Method for Studying the Effect of the Distribution of Inhaled ²³⁹PuO₂ Particles on Dose-Rate Distribution in the Beagle Dog Lung. *Radiat. Prot. Dosim.* 38: 229-235, 1991.
- Shyr, L. J., J. H. Diel, I. Y. Chang and R. A. Guilmette: The Use of Autoradiographic Data for Estimating Tumor Cell Dose in Alpha Immunotherapy. In *Proceedings of the 5th International Radiopharmaceutical Dosimetry Symposium* held in Oak Ridge, TN, May 7-10, 1991 (in press).
- Shyr, L. J., P. J. Sabourin, M. A. Medinsky, L. S. Birnbaum and R. F. Henderson: Physiologically Based Modeling of 2-Butoxyethanol Disposition in Rats Following Different Routes of Exposure. *Environ. Res.* (submitted).
- Su, Y. F. and Y. S. Cheng: Generation of Monodisperse Polystyrene Latex Spheres by Nebulization and Electrical Classification. *Aerosol Sci. Technol.* (in press).
- Swift, D. L., N. Montassier, P. K. Hopke, K. Karpen-Hayes, Y. S. Cheng, Y. F. Su, H. C. Yeh and J. C. Strong: Inspiratory Deposition of Ultrafine Particles in Human Nasal Replicate Cast. *J. Aerosol Sci.* 23: 65-72, 1992.
- Swift, D. L., Y. S. Cheng, Y. F. Su and H. C. Yeh: Radon Progeny Aerosol Deposition in the Human Nasal and Oral Passages. *Ann. Occup. Hyg.* (in press).
- Taya, A., D. B. Carmack, B. A. Muggenburg and J. A. Mewhinney: An Interspecies Comparison of the Phagocytosis and Dissolution of ²⁴¹AmO₂ Particles by Rat, Dog and Monkey Alveolar Macrophages *In Vitro*. *Int. J. Radiat. Biol.* 62: 89-95, 1992.
- Taya, A. and J. A. Mewhinney: Cytotoxicity, Uptake and Dissolution of ²⁴¹AmO₂ Particles in Dog Alveolar Macrophages *In Vitro*. *Int. J. Radiat. Biol.* 62: 81-88, 1992.
- Taya, A., J. A. Mewhinney and R. A. Guilmette: Subcellular Distribution of ²⁴¹Am in Beagle Lungs Following Inhalation of ²⁴¹Am(NO₃)₃ Aerosols. In *Proceedings of the 7th International Symposium on Inhaled Particles* held in Edinburgh, Scotland, September 16-20, 1991, (in press).
- Thomassen, D. G., G. J. Newton, R. A. Guilmette and N. F. Johnson: A Biodosimetric Approach for Estimating Radiation Dose to the Respiratory Epithelium from Inhaled Radon Progeny. *Radiat. Prot. Dosim.* 38: 65-71, 1991.

Thomassen, D. G.: Understanding Mechanisms of Carcinogenesis Using Rat Tracheal Epithelial Cells *In Vitro*. In *Proceedings of the Symposium on Current Concepts and Approaches on Animal Test Alternatives* held in Aberdeen Proving Ground, MD, February 4-6, 1992 (in press).

Thomassen, D. G.: Characterization and Comparison of Mitogenic Activity in Bovine Pituitary Extract for Normal and Transformed Rat Tracheal Epithelial Cells. *In Vitro Cell. Dev. Biol.* (submitted).

Thomassen, D. G.: Neoplastic Progression of Rat Tracheal Epithelial Cells is Associated with a Reduction in the Number of Growth Factors Required for Clonal Proliferation in Culture. *In Vitro Cell. Dev. Biol.* (submitted).

Thomassen, D. G., G. J. Newton, S. M. Maio and W. C. Griffith: Inhaled Radon Progeny Induce Preneoplastic Changes in Rat Tracheal Epithelial Cells. *Radiat. Res.* (submitted).

Ward, J. B., M. M. Ammenheuser, W. E. Bechtold, E. B. Whorton, Jr. and M. S. Legator: hprt Mutant Lymphocyte Frequencies in Workers at a 1,3-Butadiene Production Plant. *Environ. Health Perspect.* (submitted).

Weissman, D. N., D. E. Bice, B. A. Muggenburg, P. J. Haley, G. M. Shopp and M. R. Schuyler: Primary Immunization in the Canine Lung. *Am. Rev. Respir. Dis.* 145(1):6-12, 1992.

Yamada, Y., Y. S. Cheng, H. C. Yeh and D. L. Swift: Deposition of Ultrafine Monodisperse Particles in a Human Tracheobronchial Cast. To be published in *Proceedings of the 7th International Symposium on Inhaled Particles* held in Edinburgh, Scotland, September 16-21, 1991 (in press).

Yeh, H. C. and J. R. Harkema: Gross Morphometry of Airways. In *Toxicology of the Lung* (D. E. Gardner, J. D. Crapo and R. O. McClellan, eds.), Raven Press (in press).

Yeh, H. C.: Electrical Techniques - Chapter 19. In *Aerosol Measurement* (K. Willeke and P. Barones, eds.), Van Nostrand (submitted).

APPENDIX E-2

UNIVERSITY OF UTAH PUBLICATIONS IN THE OPEN LITERATURE

OCTOBER 1, 1991 - SEPTEMBER 30, 1992

- Bagi, C. M. and S. C. Miller: Ultrastructure, Tartrate Resistant Acid Phosphatase Activity and Calcitonin Responsiveness of Osteoclasts at Sites of Demineralized Bone Matrix Implant-Induced Osteogenesis. *Clin. Orthop. Rel. Res.* 269: 257-265, 1991.
- Bagi, C. M. and S. C. Miller: Dose-Related Effects of 1,25-Dihydroxyvitamin D₃ on Growth, Modeling and Morphology of Fetal Mouse Metatarsals Cultured in Serum-Free Medium. *J. Bone Min. Res.* 7: 29-40, 1992.
- Bagi, C. M., S. C. Miller, B. M. Bowman, G. L. Blomstrom and E. P. France: Differences in Cortical Bone in Overloaded and Underloaded Femurs from Ovariectomized Rats: Comparison of Bone Morphometry with Torsional Testing. *Bone* 13: 35-40, 1992.
- Bruenger, F. W., G. Kuswik-Rabiega and S. C. Miller: Decorporation of Aged Actinide Deposits by Oral Administration of Lipophilic Polyaminocarboxylic Acids. *J. Medicinal Chemistry* 35: 112-118, 1992.
- Bruenger, F. W., R. D. Lloyd and S. C. Miller: The Influence of Age at Time of Exposure to ²²⁶Ra or ²³⁹Pu on Distribution, Retention, Postinjection Survival and Tumor Induction in Beagle Dogs. *Radiat. Res.* 125: 248-256, 1991.
- Bruenger, F. W., S. C. Miller and R. D. Lloyd: A Comparison of the Natural Survival of Beagle Dogs Injected Intravenously with Low Levels of ²³⁹Pu, ²²⁸Th, ²²⁶Ra, ²²⁸Ra and ⁹⁰Sr. *Radiat. Res.* 126: 328-337, 1991.
- de Saint-Georges, L. and S. C. Miller: The Microvascular Bed of Bone and Marrow in the Diaphysis of the Rat Hematopoietic Long Bones. *Anat. Rec.* 233: 169-177, 1992.
- Iizuka, T., S. C. Miller and S. C. Marks, Jr.: Studies on Alveolar Bone Remodeling After Tooth Extraction in Normal and Osteopetrosic (ia) rats. *J. Oral Pathol. Med.* 21: 150-155, 1992.
- Jee, W. S. S., J. Inuoe, K. W. Jee, T. Haba, H. Z. Ke, X. J. Li and R. B. Setterberg: Histomorphometry Assay of Growth Bones. To be published in *The Handbook of Bone Morphometry, Second Edition* (H. Takahashi, ed.), Nashimura Col. Ltd., Niigata City, Japan (in press).
- Kuswik-Rabiega, G., F. W. Bruenger and S. C. Miller: Regiospecific Synthesis of Mono- or Diacetylated Polyethylenopolyamine Derivatives. *Synthetic Communications* 22: 1307-1318, 1992.
- Lloyd, R. D., W. Angus, G. N. Taylor, G. B. Thurman and S. C. Miller: Occurrence of Metastases in Beagles with Skeletal Malignancies Induced by Internal Irradiation. *Health Phys.* (submitted).
- Lloyd, R. D., F. W. Bruenger, S. C. Miller, W. Angus, G. N. Taylor, W. S. S. Jee and E. Polig: Distribution of Radium-Induced Bone Malignancies in Beagles and Comparison with Humans. *Health Phys.* 60: 435-438, 1991.
- Lloyd, R. D., G. N. Taylor, W. Angus, F. W. Bruenger and S. C. Miller: Bone Cancer Occurrence Among Young Adult Beagles Given ²³⁹Pu. *Health Phys.* (in press).
- Lloyd, R. D., G. N. Taylor, W. Angus, F. W. Bruenger and S. C. Miller: Soft Tissue Tumors Among Beagles Injected with ²²⁶Ra. *Health Phys.* (submitted).
- Marks, S. C., Jr., E. K. Larson, B. M. Bowman and S. C. Miller: Local Induction of Alveolar Bone in Adult Dogs by Infusion of Prostaglandin E₁. In *Biological Mechanisms of Tooth Eruption and Craniofacial Adaptation* (Z. Davidovitch, ed.), Ohio State University Press, pp. 137-143, 1992.

- Marks, S. C., Jr., L. K. Osier and S. C. Miller: Prostaglandins and New Bone Formation. In *Bone Grafts: From Basic Science to Clinical Application* (M. B. Habal and A. H. Reddi, eds.), W. B. Saunders, Philadelphia, pp. 226-234, 1992.
- Marks, S. C., Jr. and S. C. Miller: Site-Directed Formation of New Lamellar Bone in Adult Dogs by Infusion of Prostaglandin E₁. In *Fundamentals of Bone Growth: Methodology and Applications* (A. D. Dixon, B. G. Samat and D. A. N. Hoyte, eds.), CRC Press, Boca Raton, Chapter 37, pp. 375-381, 1991.
- Miller, S. C. and S. C. Marks, Jr.: Local Stimulation of New Bone Formation by Prostaglandin E₁: Quantitative Histomorphometry and Comparison of Delivery by Minipumps and Controlled-Release Pellets. *Bone* (in press).
- Miller, S. C. and S. C. Marks, Jr.: Alveolar Bone Augmentation Following the Local Administration of Prostaglandin E₁ by Controlled-Release Pellets. *Bone* (in press).
- Miller, S. C. and W. S. S. Jee: Bone Lining Cells. In *Bone, Vol. 4: Bone Metabolism and Mineralization* (B. K. Hall, ed.), CRC Press, Boca Raton, pp. 1-19, 1992.
- Miller, S. C. and T. J. Wronski: Long-Term Osteopenic Changes in Cancellous Bone Structure in Ovariectomized Rats. *Anat. Rec.* (in press).
- Miller, S. C.: Calcium Homeostasis and Mineral Turnover in the Laying Hen. In *Bone Biology and Skeletal Disorders in Poultry* (C. C. Whitehead, ed.), Butterworth and Heinemann, Oxford (in press).
- Miller, S. C., B. M. Bowman, M. A. Miller and C. M. Bagi: Calcium Absorption and Osseous Organ-, Tissue-, and Envelope-Specific Changes Following Ovariectomy in Rats. *Bone* 12: 439-446, 1991.
- Miller, S. C., F. W. Bruenger, G. K. Kuswik-Rabiega and R. D. Lloyd: The Decoration of Plutonium by the Oral Administration of a Partially Lipophilic Polyaminocarboxylic Acid. *Health Phys.* 63: 195-197, 1992.
- Polig, E. and W. S. S. Jee: Hit Rates and Radiation Doses to Nuclei of Bone Lining Cells from Alpha-Emitting Radionuclides. *Radiat. Res.* 131: 133-142, 1992.
- Polig, E., W. S. S. Jee, R. B. Setterberg and F. Johnson: Local Distribution and Dosimetry of ²²⁶Ra in the Trabecular Skeleton of the Beagle. *Radiat. Res.* 131: 24-34, 1992.
- Rosen, D., S. C. Miller, R. Armstrong, E. DeLeon, A. Thompson, H. Bentz, M. Matthews and S. Adams: Systemic Administration of Transforming Growth Factor Beta 2 (TGF- β 2) Increases Cancellous Bone Formation in Juvenile and Adult Rats. *J. Bone Miner. Res.* (submitted).
- Taylor, G. N., R. D. Lloyd, C. W. Mays, W. Angus, S. C. Miller, L. Shabestari and F. F. Hahn: Plutonium or Americium-Induced Liver Tumors in Beagles. *Health Phys.* 61: 337-347, 1991.
- Taylor, G. N., R. D. Lloyd, F. W. Bruenger and S. C. Miller: ²⁴¹Am-Induced Thyroid Lesions in the Beagle. *Health Phys.* (submitted).
- Taylor, G. N., R. D. Lloyd, C. W. Mays, L. Shabestari and S. C. Miller: Promotion of Radiation-Induced Liver Neoplasia by Ethanol. *Health Phys.* 62: 178-182, 1992.
- Woodard, J. C. and W. S. S. Jee: Skeletal System. To be published in *Fundamentals of Toxicologic Pathology* (W. M. Haschek-Holik and C. Rorisseau, eds.), Academic Press (in press).

APPENDIX F

PRESENTATIONS BEFORE REGIONAL OR NATIONAL SCIENTIFIC MEETINGS AND EDUCATIONAL AND SCIENTIFIC SEMINARS

OCTOBER 1, 1991 - SEPTEMBER 30, 1992

Bechtold, W. E., R. F. Henderson, L. J. Shyr and A. R. Dahl: Strategies for the Use of Biological Markers of Exposure. American Petroleum Workshop on Research Strategies for the Use of Biological Monitoring, Washington, DC, January 28-29, 1992.

Bechtold, W. E. and M. R. Strunk: Biological Exposure Indices for Butadiene: The Analysis of 1,2-Dihydroxy-4-(N-Acetylcysteinyl-S)-Butane and (1 or 2)-Hydroxy-(N-acetylcysteinyl-S)-3-butene in the Urine of Workers Exposed to Butadiene. American Industrial Hygiene Conference, Boston, MA, May 30-June 5, 1992.

Belinsky, S. A.: DNA Induction and Oncogene Expression in Chemically Induced Lung Cancer. Johns Hopkins University, Baltimore, MD, July 6, 1992.

Belinsky, S. A.: Oncogene Activation in Mouse Liver and Lung Tumors. Pharmaceutical Manufacturers Association Joint Drug Metabolism and Drug Safety Annual Meeting, New Orleans, LA, October 13-16, 1991.

Benson, J. M., Y. S. Cheng, R. F. Henderson and F. F. Hahn: The Time Course of Lesion Development in the Respiratory Tract of Rats Exposed by Inhalation to Nickel Subsulfide. Society of Toxicology Annual Meeting, Seattle, WA, February 23-27, 1992.

Benson, J. M., F. F. Hahn, Y. S. Cheng, M. B. Snipes, B. A. Muggenburg, I. Y. Chang and M. A. Medinsky: Nickel Toxicokinetic and Clearance Inhalation Studies. The Fifth International Conference on Nickel Biochemistry, Toxicology, and Ecology Issues. Sudbury, Ontario, Canada, September 7-11, 1992.

Bice, D. E.: Pulmonary Immune Memory. Department of Microbiology, University of New Mexico, Albuquerque, NM, November 26, 1991.

Bice, D. E.: Effects of Inhaled Toxicants on Immunological Response of the Respiratory Tract. Inhalation Toxicology Pharmacy 589 Course, University of New Mexico, Albuquerque, NM, April 22, 1992.

Bice, D. E., A. J. Williams and B. A. Muggenburg: Persistence of Localized Antibody Production in Pulmonary Allografts in Nonimmune Recipients. 1992 American Lung Association/American Thoracic Society International Conference, Miami Beach, FL, May 17-22, 1992.

Bice, D. E., B. A. Muggenburg, D. E. Weissman, S. E. Jones, A. G. Harmsen and A. J. Williams: Pulmonary Responses to Antigens. Aspen Lung Conference, Aspen, CO, June 2-4, 1992.

Bice, D. E.: Localized Response to Antigen Deposited in the Lung. Eli Lilly and Company, Indianapolis, IN, July 29, 1992.

Bice, D. E. and B. A. Muggenburg: Responses of Immune Memory Cells in the Lung. 7th International Congress of Mucosal Immunology, Prague, Czechoslovakia, August 15-22, 1992.

Bice, D. E., A. J. Williams and B. A. Muggenburg: Continued Antibody Production in Pulmonary Allografts in Nonimmune Recipients. 8th International Congress of Immunology, Budapest, Hungary, August 22-28, 1992.

Bice, D. E.: The Development of Long-Term Antibody Production in the Lung. Department of Veterinary Pathology, University of California at Davis, Davis, CA, September 18, 1992.

Boecker, B. B.: Health Risk of Inhaled Radioactive Materials: A Case Study. Inhalation Toxicology Pharmacy 589 Course, University of New Mexico, Albuquerque, NM, April 29, 1992.

Boecker, B. B., B. A. Muggenburg, F. F. Hahn, K. J. Nikula, N. A. Gillett and W. C. Griffith: Life-Span Health Effects of Relatively Soluble Forms of Internally Deposited Beta-Emitting Radionuclides. Eighth International Congress of the International Radiation Protection Association, Montreal, Quebec, Canada, May 17-22, 1992.

Carpenter, T. R.: Biochemical Basis of Tumor Suppression Yeast Models in Carcinogenesis. UNM Pharmacy 593 Course, University of New Mexico, Albuquerque, NM, March 11, 1992.

Chen, B. T., J. V. Benz, H. C. Yeh, G. L. Finch and J. L. Mauderly: Internal and External Deposition in Rats by Nose and Whole-Body Smoke Exposures. American Association for Aerosol Research Meeting, Traverse City, MI, October 7, 1991.

Chen, B. T.: Generation and Characterization of Gases and Vapors. Inhalation Toxicology Pharmacy 589 Course, University of New Mexico, Albuquerque, NM, February 12, 1992.

Chen, B. T., H. C. Yeh and C. H. Hobbs: Size Classification of Carbon Fiber Aerosols. American Industrial Hygiene Conference, Boston, MA, May 30-June 5, 1992.

Cheng, Y. S. and H. C. Yeh: Deposition of Particles and Radon Progeny in the Human Head Airway. American Association for Aerosol Research Meeting, Traverse City, MI, October 7, 1991.

Cheng, Y. S., H. C. Yeh and R. A. Guilmette: Nasal Airway Geometry and Aerosol Deposition in Humans and Laboratory Animals. Chemical Industrial Institute of Toxicology, Research Triangle Park, NC, October 28, 1991.

Cheng, Y. S., B. T. Chen and H. C. Yeh: Performance of an Aerodynamic Particle Size. International Symposium on Air Sampling Instrument Performance, Research Triangle Park, NC, October 29-November 1, 1991.

Cheng, Y. S., H. C. Yeh and R. A. Guilmette: Nasal Airway Geometry and Aerosol Deposition in Human and Laboratory Animals. U.S. Environmental Protection Agency, Chapel Hill, NC, October 30, 1991.

Cheng, Y. S.: Exposure Systems. Inhalation Toxicology Pharmacy 589 Course, University of New Mexico, Albuquerque, NM, January 29, 1992.

Cheng, Y. S.: Health Effects of Indoor Radon. Association of Chinese-American Engineers and Scientists - New Mexico, Albuquerque, NM, March 20, 1992.

Cheng, Y. S., B. T. Chen and Y. F. Su: Plate Out Rates of Radon Progeny and Aerosols in a Spherical Chamber. American Industrial Hygiene Conference, Boston, MA, May 30-June 5, 1992.

Cheng, Y. S., B. T. Chen and Y. F. Su: Aerosols in Occupational Environments. Professional Development Course. American Industrial Hygiene Conference, Boston, MA, May 30-June 5, 1992.

Dahl, A. R.: The Contribution of Respiratory Tract Metabolism to the Uptake and Toxicity of Inhalants. DOE/AWU Lecture Program, California Polytechnic State University, Department of Chemistry, San Luis Obispo, CA, December 5, 1991.

Dahl, A. R.: Deposition and Clearance of Gases and Vapors. Inhalation Toxicology Pharmacy 589 Course, University of New Mexico, Albuquerque, NM, February 19, 1992.

Dahl, A. R., P. J. Sabourin, W. E. Bechtold, T. E. Burka and R. F. Henderson: Comparative Toxicokinetics of Butadiene in Rodents and Monkeys. Society of Toxicology Annual Meeting, Seattle, WA, February 23-27, 1992.

Dahl, A. R.: Uptake and Metabolism of Toxicants in the Respiratory Tract. National Academy of Science Workshop, Pharmacokinetics: Defining Dosimetry for Risk Assessment, Washington, DC, March 4-5, 1992.

Dahl, A. R.: New Explanations for Gas and Vapor Uptake Anomalies-After 50 Years of Research. DOE/AWU Lecture Program, Brigham Young University, Salt Lake City, UT, March 24, 1992.

Dahl, A. R.: Vapors and Metabolic Capacity of the Respiratory Tract. Inhalation Toxicology Pharmacy 589 Course, University of New Mexico, Albuquerque, NM, March 25, 1992.

Dahl, A. R.: Contributions of Respiratory Tract Metabolism to the Uptakes of Inhalants. DOE/AWU Lecture Program, New Mexico Tech, Socorro, NM, April 15, 1992.

Dahl, A. R.: Contribution of Respiratory Tract Metabolism to the Uptake and Toxicity of Xenobiotics. U.S. FDA Center for Drug Evaluation and Research, Rockville, MD, April 22, 1992.

Dahl, A. R.: Factors Affecting Uptake and Fate of Inhaled Vapors and Gases. Toxicology in Michigan Today - A Symposium on Inhalation Toxicology, Novi, MI, May 15, 1992.

Davila, D. R., S. E. Jones, D. E. Bice and P. J. Haley: Age Effects on Local and Systemic T Cell Responses to Lectins after Antigen Instillation in the Lung. Federation of the American Societies for Experimental Biology Meeting, Anaheim, CA, April 5-9, 1992.

Economou, P., G. Kelly, J. Samet and J. F. Lechner: DNA Polymorphic Differences Between Normal and Tumor Samples Can Be Detected with Arbitrary Primers. Keystone Symposium on Negative Growth Control, Keystone, CO, January 26-February 2, 1992.

Evans, W. A., J. R. Harkema, K. R. Maples, J. A. Hotchkiss, B. T. Chen and G. L. Finch: Effects of Cigarette Smoke on Mucosubstances in Rat Nasal Epithelium. American Lung Association/American Thoracic Society International Conference, Miami Beach, FL, May 17-22, 1992.

Finch, G. L., B. T. Chen, W. E. Bechtold, K. J. Nikula, L. Kolar, K. R. Maples and J. R. Harkema: Responses of Rats to a Two-Week Exposure to Cigarette Smoke. Society of Toxicology Annual Meeting, Seattle, WA, February 23-27, 1992.

Finch, G. L. and M. D. Hoover: Environmental Monitoring Work Task Proposals of the Beryllium Monitoring Subcommittee. Beryllium Industry Scientific Advisory Committee, Tucson, AZ, June 30, 1992.

Francis, J. L., L. K. Brookins, J. A. Hotchkiss and A. R. Dahl: *In Vitro* Expression of Rat Olfactory-Specific Cytochrome P-450. 10th Annual Meeting of the Mountain West Chapter of the Society of Toxicology, Logan, UT, September 18, 1992.

Gerde, P., B. A. Muggenburg, M. D. Hoover and R. F. Henderson: Clearance of Polycyclic Aromatic Hydrocarbons from the Alveolar Region of the Respiratory Tract. Society of Toxicology Annual Meeting, Seattle, WA, February 23-27, 1992.

Griffith, W. C., B. B. Boecker, N. A. Gillett, R. A. Guilmette, F. F. Hahn and B. A. Muggenburg: Comparison of Risk Factors for Bone Cancer Induced by Inhaled $^{90}\text{SrCl}_2$ and $^{238}\text{PuO}_2$. Radiation Research Society 40th Annual Meeting, Salt Lake City, UT, March 14-18, 1992.

Griffith, W. C., B. B. Boecker, F. F. Hahn, B. A. Muggenburg and M. B. Snipes: The Effect of Dose Protraction on the Incidence of Lung Carcinomas in Beagle Dogs with Internally Deposited Beta-Emitting Radionuclides. Eighth International Congress of the International Radiation Protection Association, Montreal, Quebec, Canada, May 17-22, 1992.

Griffith, W. C.: Comparison of Lung Cancer Risk Models for Inhalation of Radon Decay Products. Health Physics Society Annual Meeting, Columbus, OH, June 20-25, 1992.

Guilmette, R. A.: Radon Research in the DOE and ITRI. Indoor Air Pollution Course, University of New Mexico, Albuquerque, NM, March 31, 1992.

- Guilmette, R. A. and W. C. Griffith: The Effect of Isotope on the Dosimetry of Inhaled Plutonium Oxide. Eighth International Congress of the International Radiation Protection Association, Montreal, Quebec, Canada, May 17-22, 1992.
- Guilmette, R. A.: Inhaled Radionuclides. Biokinetics, Dosimetry, and Therapy. Health Physics Society Annual Meeting, Columbus, OH, June 20-25, 1992.
- Guilmette, R. A., P. S. Lindhorst, and L. L. Hanlon: Interaction of Pu and Am with Bone Mineral *In Vitro*. Health Physics Society Annual Meeting, Columbus, OH, June 20-25, 1992.
- Hahn, F. F.: Pathology in Toxicology. General Toxicology I Pharmacy 480/580 Course, University of New Mexico, Albuquerque, NM, October 9, 1991.
- Hahn, F. F.: Pathologic Responses of the Respiratory Tract. General Toxicology I Pharmacy 480/580 Course, University of New Mexico, Albuquerque, NM, October 14, 1991.
- Hahn, F. F., W. C. Griffith, C. H. Hobbs, B. A. Muggenburg, G. J. Newton and B. B. Boecker: Hot Beta Particles in the Lung: Results from Dogs Exposed to Fission Product Radionuclides. Radiation Research Society 40th Annual Meeting, Salt Lake City, UT, March 14-18, 1992.
- Hahn, F. F.: Lung Cancer. Inhalation Toxicology Pharmacy 589 Course, University of New Mexico, Albuquerque, NM, April 8, 1992.
- Hahn F. F., W. C. Griffith, B. B. Boecker, B. A. Muggenburg and D. L. Lundgren: Comparison of Inhaled $^{239}\text{PuO}_2$ and β -Emitting Radionuclides on the Incidence of Lung Carcinomas in Laboratory Animals. Eighth International Congress of the International Radiation Protection Association, Montreal, Quebec, Canada, May 17-22, 1992.
- Haley, P. J., G. L. Finch, D. R. Davila and M. D. Hoover: The Immunotoxicity of Beryllium Metal and Beryllium Oxide in Cynomolgus Monkeys. Society of Toxicology Annual Meeting, Seattle, WA, February 23-27, 1992.
- Harkema, J. R. and J. A. Hotchkiss: Experimental Models to Study Secretory Cell Metaplasia/Hyperplasia in Rat Airways. Cystic Fibrosis Seminar Series, San Francisco, CA, November 11, 1991.
- Harkema, J. R.: The Effects of Ozone on Nasal Epithelium. Interdisciplinary Toxicology Seminar Series, University of Illinois, Chicago, IL, November 21, 1991.
- Harkema, J. R., K. R. Maples, J. A. Hotchkiss, B. T. Chen and G. L. Finch: Effects of Cigarette Smoke on Tissue Glutathione Levels and Epithelial Morphology in Rat Nasal Airways. American College of Veterinary Medicine Meeting, Orlando, FL, December 10-13, 1991.
- Harkema, J. R., K. R. Maples and J. A. Hotchkiss: Cell Proliferation and Glutathione Levels in Nasal Airways of Rats Exposed to Ozone. Society of Toxicology Annual Meeting, Seattle, WA, February 23-27, 1992.
- Harkema, J. R.: Noncarcinogenic Responses in the Respiratory Tract. Inhalation Toxicology Pharmacy 589 Course, University of New Mexico, Albuquerque, NM, April 1, 1992.
- Harkema, J. R., E. Bermudez, K. T. Morgan, and P. Mellick: Effects of Chronic Ozone Exposure on the Nasal Mucociliary Apparatus in the Rat. American Lung Association/American Thoracic Society International Conference, Miami Beach, FL, May 17-22, 1992.
- Harkema, J. R.: Microscopic and Molecular Techniques to Study Mucous Cell Metaplasia/Hyperplasia in Respiratory Airways. Conference on Applications of Advances in Toxicology to Risk Assessment, Dayton, OH, May 19-21, 1992.
- Henderson, R. F.: Response of the Lung to Inhaled Particles from Combustion Processes. International Conference on Toxicology of Combustion Products, Pavia, Italy, October 28, 1991.

Henderson, R. F., W. E. Bechtold, K. R. Maples and L. J. Shyr: Biological Markers or Measures of Exposure. Conference on Measuring, Understanding and Predicting Exposures in the 21st Century, Atlanta, GA, November 20, 1991.

Henderson, R. F.: Introduction to Inhalation Toxicology. Inhalation Toxicology Pharmacy 589 Course, University of New Mexico, Albuquerque, NM, January 22, 1992.

Henderson, R. F., P. J. Sabourin, B. A. Muggenburg, R. Couch, L. S. Birnbaum and G. L. Lucier: Metabolism of Benzene by Nonhuman Primates. Society of Toxicology Annual Meeting, Seattle, WA, February 23-27, 1992.

Henderson, R. F., J. R. Harkema, J. A. Hotchkiss and I. Y. Chang: Relation of Cumulative Exposure to Ozone Toxicity in the Nose. American Lung Association/American Thoracic Society International Conference, Miami Beach, FL, May 17-22, 1992.

Henderson, R. F.: Progress on Butadiene Studies. Chemical Manufacturers Association Annual Research Meeting, Research Triangle Park, NC, June 10, 1992.

Hickman, A. W.: Application of a Canine ²³⁸Pu Dosimetry Model to Human Bioassay Data. UNM Pharmacy 593 Course, University of New Mexico, Albuquerque, NM, January 29, 1992.

Hickman, A. W., R. J. Jaramillo and N. F. Johnson: Flow Cytometric Analysis of Micronucleus Formation Following X Irradiation. 10th Annual Meeting of the Mountain West Chapter of the Society of Toxicology, Logan, UT, September 18, 1992.

Hobbs, C. H.: Toxicology for Chemists. Introduction to Inhalation Toxicology, American Chemical Society Meeting, Newport Beach, CA, April 8, 1992.

Hoover, M. D.: Generation and Characterization of Particles. Inhalation Toxicology Pharmacy 589 Course, University of New Mexico, Albuquerque, NM, February 5, 1992.

Hoover, M. D. and G. J. Newton: Requirements for Filter Selection and Handling for Use in Alpha CAMs. The Second Annual Alpha Continuous Air Monitoring Symposium, Santa Fe, NM, May 6, 1992.

Hoover, M. D.: Interference from Dusts in Continuous Air Monitors. Health Physics Society Annual Meeting, Columbus, OH, June 20-25, 1992.

Hotchkiss, J. A., S. Reddy, R. Novak and A. R. Dahl: cDNA Cloning and *In Vitro* Expression of Rat Cytochrome P-450IIG1. Federation of the American Societies for Experimental Biology Meeting, Anaheim, CA, April 5-9, 1992.

Johnson, N. F. and R. J. Jaramillo: Flow Cytometric Analysis of Phagolysosomal pH in Rat Alveolar Macrophages and Respiratory Epithelial Cells. Rocky Mountain Cytometry Meeting, Vail, CO, October 4-5, 1991.

Johnson, N. F.: Radon Dose and Injury to Critical Cells of the Lung. UNM Pharmacy 593 Course, University of New Mexico, Albuquerque, NM, February 19, 1992.

Johnson, N. F.: Glass Fiber Dissolution in Cultured Rat Alveolar Macrophages and Respiratory Tract Epithelial Cells. Society of Toxicology Annual Meeting, Seattle, WA, February 23-27, 1992.

Johnson, N. F. and G. J. Newton: Estimation of Dose to the Peripheral Lung of Rats Exposed to Radon Progeny. Radiation Research Society 40th Annual Meeting, Salt Lake City, UT, March 14-18, 1992.

Johnson, N. F.: Biological Effects of Radon Progeny Exposure. Health Physics Society Annual Meeting, Columbus, OH, June 20-25, 1992.

Johnson, N. F.: Glass Fiber Dissolution in Rat Respiratory Tract Cells and Alveolar Macrophages. Biopersistence of Respiratory Synthetic Fibers and Minerals Conference, Lyon, France, September 7-9, 1992.

Johnson, N. F., R. A. Guilmette and G. J. Newton: Alveolar Type II Cell, a Cell at Risk from Inhaled Radon Progeny? 10th Annual Meeting of the Mountain West Chapter of the Society of Toxicology, Logan, UT, September 18, 1992.

Kennedy, C. H., K. B. Cohen, A. R. Dahl and R. F. Henderson: Disposition and Metabolism of 1,1,2,2-Tetrabromoethane in F344/N Rats after Gavage Administration. Society of Toxicology Annual Meeting, Seattle, WA, February 23-27, 1992.

Kennedy, C. H., W. E. Bechtold and R. F. Henderson: Disposition and Metabolism of 2-Ethoxyethanol After Inhalation by F344/N Rats. 10th Annual Meeting of the Mountain West Chapter of the Society of Toxicology, Logan, UT, September 18, 1992.

Lechner, J. F.: Carcinogenesis Investigation with Human Lung Epithelial Cells. Pulmonary Research Group, University of California, Davis, CA, December 3, 1991.

Lechner, J. F., K. Elliget, V. Wilson, R. Modali, B. Gerwin and C. C. Harris: An Epigenetic Mechanism May Coordinate Regulate Expression of Several Human Bronchial Epithelial Cell Genes. Keystone Symposium on Negative Growth Control, Keystone, CO, January 26-February 2, 1992.

Lechner, J. F.: Transformation Studies with Human Lung Epithelial Cells. Lovelace Medical Foundation, Albuquerque, NM, February 12, 1992.

Lechner, J. F.: Evidence for a Master Switch that Controls Initiation of Squamous Differentiation of Human Airway Epithelial Cells. Oncology Center, Johns Hopkins University, Baltimore, MD, February 26, 1992.

Lechner, J. F.: Overview of Cellular and Molecular Biology Research at ITRI. Los Alamos National Laboratory, Los Alamos, NM, March 10, 1992.

Lechner, J. F.: Analysis of Gene Dysfunctions in Lung Cancers. Medicine Grand Rounds Conference, University of New Mexico, Albuquerque, NM, March 25, 1992.

Lechner, J. F., V. Wilson, R. Modali, B. Gerwin, T. Lehman and C. Harris: Transforming Growth Factor Regulation of Bronchial Epithelium. American Association for Cancer Research Meeting, San Diego, CA, May 20-23, 1992.

Lewis, J. L., K. J. Nikula and A. R. Dahl: Comparative Analysis of Activity and Distribution of Nasal Carboxylesterases. Society of Toxicology Annual Meeting, Seattle, WA, February 23-27, 1992.

Lundgren, D. L., R. G. Cuddihy, W. C. Griffith, F. F. Hahn, W. W. Carlton, M. D. Hoover and B. B. Boecker: Effects of Combined Exposure of Rats to $^{239}\text{PuO}_2$ and Whole-Body X-Irradiation. Radiation Research Society 40th Annual Meeting, Salt Lake City, UT, March 14-18, 1992.

Lundgren, D. L., D. R. Melo, B. A. Muggenburg and R. A. Guilmette: Effects of Age on the Deposition of ^{137}Cs with Prussian Blue in Beagle Dogs. Health Physics Society Annual Meeting, Columbus, OH, June 21-25, 1992.

Maples, K. R., J. R. Harkema, J. A. Hotchkiss, B. T. Chen, K. R. Nikula and G. L. Finch: Effects of Cigarette Smoke on the Glutathione Status of the Upper and Lower Respiratory Tracts of Rats. Society of Toxicology Annual Meeting, Seattle, WA, February 23-27, 1992.

Maples, K. R. and N. F. Johnson: Fiber-Induced Hydroxyl Radical Formation. 10th Annual Meeting of the Mountain West Chapter of the Society of Toxicology, Logan, UT, September 18, 1992.

Mauderly, J. L.: Effective Presentations. Inhalation Toxicology Pharmacy 589 Course, University of New Mexico, Albuquerque, NM, October 2, 1991.

Mauderly, J. L.: Current Research at the Inhalation Toxicology Research Institute. Lovelace Medical Foundation, Albuquerque, NM, October 16, 1991.

Mauderly, J. L.: Toxicological and Epidemiological Evidence for a Lung Cancer Risk from Diesel Exhaust. Colorado State University, College of Veterinary Medicine and Biomedical Sciences, Fort Collins, CO, October 28, 1991.

Mauderly, J. L.: Effective Presentations. Technical Writing English 219 Course, University of New Mexico, Albuquerque, NM, October 30, 1991.

Mauderly, J. L.: Toxicological and Epidemiological Evidence for a Lung Cancer Risk from Diesel Exhaust. National Center for Toxicological Research, Jefferson, AR, January 13, 1992.

Mauderly, J. L.: Effective Presentations. Annual Meeting of the Society of Toxicology, Seattle, WA, February 23-27, 1992.

Mauderly, J. L., E. B. Barr, A. F. Eidson, J. R. Harkema, R. F. Henderson, J. A. Pickrell and R. K. Wolff: Contributions of Diesel Exhaust and Oil Shale Dust to Effects of Mixed Chronic Inhalation Exposures. Society of Toxicology Annual Meeting, Seattle, WA, February 23-27, 1992.

Mauderly, J. L., E. B. Barr, W. C. Griffith, R. F. Henderson, K. J. Nikula and M. B. Snipes: Influence of Particle-Associated Organic Compounds on the Carcinogenicity of Diesel Exhaust. American Mining Industry Group Meeting, Albuquerque, NM, March 24, 1992.

Mauderly, J. L.: Effects of Inhaled Toxicants on Pulmonary Function. Inhalation Toxicology Pharmacy 589 Course, University of New Mexico, Albuquerque, NM, April 15, 1992.

Mauderly, J. L.: Toxicological and Epidemiological Evidence for Health Risks from Inhaled Engine Emissions. Risk Assessment of Urban Air; Emissions, Experiments, Risk Identification, and Risk Quantification Conference, Stockholm, Sweden, May 31-June 5, 1992.

Mauderly, J. L., E. B. Barr, A. F. Eidson, J. R. Harkema, R. F. Henderson, J. A. Pickrell and R. K. Wolff: Contributions of Diesel Exhaust and Mineral Dust to Effects of Chronic Inhalation Exposures. Risk Assessment of Urban Air; Emissions, Experiments, Risk Identification, and Risk Quantification Conference, Stockholm, Sweden, May 31-June 5, 1992.

Mauderly, J. L.: Toxicological and Epidemiological Evidence for Health Risks from Inhaled Engine Emissions. American Mining Congress Joint Meeting of Occupational Health, Coal Mine Safety, and Metal/Nonmetal Mine Safety Committees and of the Diesel Group, Denver, CO, June 17, 1992.

Mitchell, C. E., W. E. Bechtold and S. A. Belinsky: Metabolism of Nitrofluoranthenes by Rat Subcellular Fractions. American Association for Cancer Research Meeting, San Diego, CA, May 20-23, 1992.

Muggenburg, B. A., R. A. Guilmette, L. M. Romero and J. A. Mewhinney: Improvements in Lung Lavage to Increase its Effectiveness in the Removal of Inhaled Radionuclides. Eighth International Congress of the International Radiation Protection Association, Montreal, Quebec, Canada, May 17-22, 1992.

Newton, G. J., M. D. Hoover, H. C. Yeh and B. B. Boecker: The Challenge in Meeting New Health Protection Standards for Airborne Plutonium in the Workplace at the Nuclear Weapons Production Facilities. American Association for Aerosol Research Meeting, Traverse City, MI, October 7, 1991.

Newton, G. J. and M. D. Hoover: The Potential for Release of Radioactive Aerosols During Decontamination and Decommissioning of Radioactively Contaminated Sites. Technology Focus Group of the Office of Technology Development, US DOE, Dallas, TX, April 29, 1992.

Newton, G. J. and M. D. Hoover: Measuring, Monitoring, and Mitigating Plutonium-Contaminated Aerosols Formed During Buried Waste Retrieval. Idaho National Engineering Laboratory, Idaho Falls, ID, May 4, 1992.

Newton, G. J. and M. D. Hoover: Requirements for Homogeneity of Particle Collection in Alpha CAMs. The Second Annual Alpha Continuous Air Monitoring Symposium, Santa Fe, NM, May 6, 1992.

Newton, G. J.: Representative Aerosol Sampling. Health Physics Society Annual Meeting, Columbus, OH, June 20-25, 1992.

Nickell, C., G. L. Finch, P. J. Haley and S. A. Belinsky: Activation of the *Ki-ras* Gene in Lung Tumors Induced in the Fischer Rat by the Nongenotoxic Carcinogen Beryllium. Keystone Symposium on Negative Growth Control, Keystone, CO, January 26-February 2, 1992.

Nikula, K. J., E. B. Barr, W. C. Griffith, R. F. Henderson and J. L. Mauderly: Influence of Particle-Associated Organic Compounds on the Carcinogenicity of Inhaled Diesel Exhaust. American College of Veterinary Medicine Meeting, Orlando, FL, December 10-13, 1991.

Nikula, K. J.: Morphology of the Respiratory Tract. Inhalation Toxicology Pharmacy 589 Course, University of New Mexico, Albuquerque, NM, February 19, 1992.

Nikula, K. J., M. B. Snipes, E. B. Barr, W. C. Griffith, R. F. Henderson and J. L. Mauderly: Influence of Soot-Associated Organic Compounds on the Carcinogenicity of Inhalants. Risk Assessment of Urban Air; Emissions, Experiments, Risk Identification, and Risk Quantification Conference, Stockholm, Sweden, May 31-June 5, 1992.

Royce, F., T. Tsuda, J. R. Harkema, J. A. Hotchkiss and C. Basbaum: Mucin Gene Expression in Rat Airways Exposed to Endotoxin. American Lung Association/American Thoracic Society International Conference, Miami Beach, FL, May 17-22, 1992.

Sabourin, P. J., W. E. Bechtold, M. D. Hoover and R. F. Henderson: Effect of Vapor Concentration on the Disposition of Isobutene. Society of Toxicology Annual Meeting, Seattle, WA, February 23-27, 1992.

Scott, B. R.: Predictive Models for Stochastic and Nonstochastic Radiobiological Effects of Mixed Radiation Fields. Armed Forces Radiobiology Research Institute, Bethesda, MD, December 3, 1991.

Scott, B. R.: Models for Radiobiological Effects of Combined Exposure to Neutrons and Photons. Radiation Research Society 40th Annual Meeting, Salt Lake City, UT, March 14-18, 1992.

Shankar, A. S.: Air Pollution Issues Facing Albuquerque and New Mexico. UNM Pharmacy 593, University of New Mexico, Albuquerque, NM, November 13, 1991.

Shyr, L. J., T. Gilbert, A. R. Dahl and R. F. Henderson: Investigation of 1,3-Butadiene Metabolism in Monkeys Using Physiologically Based Models. Society of Toxicology Annual Meeting, Seattle, WA, February 23-27, 1992.

Smith, S. M.: Deposition of Ultrafine Aerosols in Human Tracheobronchial Tree Casts. UNM Pharmacy 593 Course, University of New Mexico, Albuquerque, NM, February 12, 1992.

Snipes, M. B.: Deposition and Clearance of Particles. Inhalation Toxicology Pharmacy 589 Course, University of New Mexico, Albuquerque, NM, February 26, 1992.

Snipes, M. B., L. J. Reddick, J. R. Harkema and A. H. Rebar: Specific Biological Effects of an Anti-Rat PNM Antiserum Interperitoneally Injected into F344/N Rats. American Lung Association/American Thoracic Society International Conference, Miami Beach, FL, May 17-22, 1992.

Snipes, M. B., J. W. Spoo, W. C. Griffith, K. J. Nikula and R. A. Guilmette: Retention and Clearance of Particles Deposited in the Conducting Airways of Beagle Dogs. American Industrial Hygiene Conference, Boston, MA, May 30-June 5, 1992.

Swafford, D. S., G. L. Finch and P. J. Haley: The Effects of Subcutaneous Injection of Beryllium on the Immunopathology of Inhaled Beryllium in C3H/HeJ and A/J Mice. Federation of the American Societies for Experimental Biology Meeting, Anaheim, CA, April 5-9, 1992.

Thomassen, D. G. and G. Kelly: Activation of *Ki-ras* in Radiation-Induced Preneoplastic Variants of Rat Tracheal Epithelial Cells. Keystone Symposium on Negative Growth Control, Keystone, CO, January 26-February 2, 1992.

Thomassen, D. G.: Understanding Mechanisms of Carcinogenesis Using Rat Tracheal Cells *In Vitro*. Symposium on Current Concepts and Approaches on Animal Test Alternatives, Aberdeen Proving Ground, MD, February 4-6, 1992.

Thomassen, D. G., G. Kelly, G. J. Newton and W. C. Griffith: Radiation-Induced Preneoplastic Transformation and *Ki-ras* Activation in Rat Tracheal Epithelial Cells. Radiation Research Society 40th Annual Meeting, Salt Lake City, UT, March 14-18, 1992.

Yeh, H. C., B. A. Muggenburg and J. R. Harkema: Deposition of ^{220}Rn Progeny in Rhesus Monkeys. American Association for Aerosol Research Meeting, Traverse City, MI, October 7, 1991.

APPENDIX G

SEMINARS PRESENTED BY VISITING SCIENTISTS

OCTOBER 1, 1991 - SEPTEMBER 30, 1992

- Dr. John Strong, Biomedical Research Department, AEA Environment & Energy, Harwell Laboratory, Didcot, United Kingdom: *Description of the Radon Exposure System at Harwell*, October 4, 1991.
- Dr. Peter Shields, Laboratory Human Carcinogenesis, National Cancer Institute-National Institutes of Health, Bethesda, MD: *Molecular Epidemiology of Lung Cancer in Chinese Women*, October 7, 1991.
- Dr. Garold S. Yost, Department of Pharmacology and Toxicology, The University of Utah, Salt Lake City, UT: *Mechanisms of 3-Methylindole Bioactivation in Human and Animal Pulmonary and Hepatic Tissues*, October 9, 1991.
- Mr. Stephen Bjarnason, Bureau of Chemical Hazards, Environmental Health Directorate, Health & Welfare, Ottawa, Canada: *In Vitro Techniques, Risk Assessment and Air Pollution*, November 5, 1991.
- Dr. Albert J. Fornace, Jr., Laboratory of Molecular Pharmacology, National Cancer Institute, National Institutes of Health, Bethesda, MD: *Mammalian Genes Induced by Radiation and Other Growth-Arrest Conditions*, December 5, 1991.
- Dr. Stephen B. Baylin, Johns Hopkins Oncology Center, Baltimore, MD: *Abnormalities of DNA Methylation in Human Cancer*, December 12, 1991.
- Dr. Albert P. Li, Monsanto Corporate Research, Monsanto Company, St. Louis, MO: *Application of Cultured Human Hepatocytes in the Evaluation of Xenobiotic Metabolism and Toxicity*, January 7, 1992.
- Dr. David M. Prescott, Department of Molecular, Cellular and Developmental Biology, University of Colorado, Boulder, CO: *Rearrangements of Gene Sequences in Ciliates*, January 13, 1992.
- Dr. Robert Mason, Pulmonary Division, National Jewish Hospital, Denver, CO: *Role of Surfactant in Adult Lung Disease*, January 23, 1992.
- Dr. Dan Pennington, Pulmonary Division, University of California, VA Medical Center, San Francisco, CA: *Mast Cells Product Growth Factors Active in Fibrosis*, February 28, 1992.
- Dr. Roland C. Grafstrom, Karolinska Institute, Stockholm, Sweden: *Cultured Human Oral Epithelium: Growth, Transformation and Tobacco-Related Pathology*, February 3, 1992.
- Dr. Carol Basbaum, UCSF Medical School, University of California, San Francisco, CA: *The Use of Mucin and Lysozyme cDNAs to Study Airway Secretory Cell Differentiation*, February 13, 1992.
- Dr. Per Gerde, National Institute of Occupational Health, Stockholm, Sweden: *Regional Retention of Polycyclic Aromatic Hydrocarbons in the Respiratory Tract of the Beagle Dog*, March 2, 1992.
- Dr. Joseph D. Brain, Respiratory Biology Program, Harvard School of Public Health, Boston, MA: *Non-Alveolar Lung Phagocytes: Assessing Their Form and Function in Environmental Lung Disease*, March 23, 1992.
- Dr. Richard J. Lemen, University of Arizona, Health Sciences Center, Tucson, AZ: *Mechanisms of Viral Induced Airway Injury in Beagles - An Update*, April 2, 1992.
- Dr. John W. Stather, National Radiological Protection Board, Didcot, United Kingdom: *The UK National Registry for Radiation Workers*, April 9, 1992.

- Dr. Paul Kraemer, Los Alamos National Laboratory, Life Sciences Division, Los Alamos, NM: *Changes in Growth Control in a Multi-Step Cell Culture Model of Cancer*, May 7, 1992.
- Dr. James K. Briant, Pacific Northwest Laboratory, Richland, WA: *Getting to the Heart of the Matter: Aerosol Particle Transport by Cardiogenic Air Motion*, May 14, 1992.
- Dr. Werner Stöber, Chemical Industry Institute of Toxicology, Research Triangle Park, NC: *Advances in Lung Clearance Models*, May 15, 1992.
- Dr. Mohan Sopori, Lovelace Medical Foundation, Albuquerque, NM: *Effects of Cigarette Smoke/Nicotine on the Immune System*, May 27, 1992.
- Dr. David G. Hoel, Division of Biometry and Risk Assessment, National Institute of Environmental Health Sciences, Research Triangle Park, NC: *Cancer Trends*, June 9, 1992.
- Dr. David Weissman, Albuquerque Veterans Administration Hospital and Department of Medicine, University of New Mexico School of Medicine, Albuquerque, NM: *Function Immunity of the Human Lung*, June 10, 1992.
- Dr. Yasushi Ohnuki, Huntington Medical Research Institute, Pasadena, CA: *Chromosomal Changes and Progressive Tumorigenesis of Human Bronchial Epithelial Cell Lines*, July 7, 1992.
- Dr. Keith C. Meyer, Department of Medicine, University of Wisconsin-Madison Medical School, Madison, WI: *An Immune Model of Beryllium-Induced Pulmonary Granulomata in Mice*, July 13, 1992.
- Dr. Robert Devlin, Health Effects Research Laboratory, U.S. Environmental Protection Agency, Research Triangle Park, NC: *The Use of a Cell Line as a Model System to Study the Interactions of Ozone with Human Airway Epithelial Cells*, August 24, 1992.
- Dr. Donna F. Kusewitt, Lovelace Medical Foundation, Albuquerque, NM: *UVR-Induced Corneal Disease in the Marsupial Monodelphis Domestica*, August 25, 1992.

APPENDIX H

ADJUNCT SCIENTISTS AS OF DECEMBER 31, 1992

Dr. Carol Basbaum
Department of Anatomy
University of California School of Medicine
San Francisco, CA 94143

Dr. William W. Carlton
Department of Veterinary Microbiology,
Pathology and Public Health
School of Veterinary Medicine
Purdue University
West Lafayette, IN 47907

Dr. Linda Funk
Pulmonary Division
Department of Medicine
University of New Mexico
Albuquerque, NM 87131

Dr. William M. Hadley
Dean, College of Pharmacy
University of New Mexico
Albuquerque, NM 87131

Dr. Donna Kusewitt
Lovelace Medical Foundation
Albuquerque, NM 87108

Dr. Raymond F. Novak
Wayne State University
Institute of Chemical Toxicology
Detroit, MI 48201

Dr. Judy Raucy
College of Pharmacy
University of New Mexico
Albuquerque, NM 87131

Dr. Alan H. Rebar
School of Veterinary Medicine
Purdue University
West Lafayette, IN 47907

Dr. Jonathan M. Samet
Pulmonary Division
Department of Medicine
The University of New Mexico
Albuquerque, NM 87131

Dr. Steven Simpson
Pulmonary Division
Department of Medicine
University of New Mexico
Albuquerque, NM 87131

Dr. David L. Swift
Johns Hopkins University
School of Hygiene and Public Health
Baltimore, MD 211205

Dr. Ross Zumwalt
Office of Medical Investigation
Assistant Chief Medical Investigator
University of New Mexico
School of Medicine
Albuquerque, NM 87131

APPENDIX I

EDUCATION ACTIVITIES AT THE INHALATION TOXICOLOGY RESEARCH INSTITUTE

There is an increasing concern that a sufficient number of scientists will not be available to meet the future needs of the Department of Energy, especially in the areas of waste management and environmental restoration. The reasons why fewer students are selecting careers in science are reviewed in a supplement to *Science: "Science: The End of the Frontier?"* published in January 1991. ITRI has always had educational programs that encourage students to select careers in science, and these programs should help provide scientists to fill positions needed by the Department of Energy. Our programs provide research opportunities in inhalation toxicology and pulmonary biology for undergraduate and graduate students, postdoctoral fellows, and visiting scientists. Our Institute has provided training for hundreds of researchers.

Precollege Students

To stimulate an interest in science in precollege students, we provide tours and demonstrations at ITRI and support students who participate in science fairs. Approximately 100 middle and high school students visited ITRI in FY-1992. We also provided the opportunity for high school students to work in our research laboratories. This program has worked well during the last two summers, and we will have high school students working in our laboratories in FY-1993.

Additional support for precollege students is provided through research opportunities at ITRI for middle school and high school science teachers. Two programs provide such experience: the Summer Teacher Enrichment Program (STEP), specifically for New Mexico teachers; and the Teacher Research Associates Program (TRAC), for teachers throughout the United States. These programs involve science teachers in all steps of a scientific study. Teachers design experiments, conduct experimental assays, evaluate data, and present their results. The direct involvement of teachers provides them with information valuable to students interested in careers in science. The STEP and TRAC participants are very enthusiastic about their work at ITRI and have found ways to incorporate their experiences into the classroom. We will have eight high school teachers at ITRI during the summer of FY-1993.

Since the beginning of STEP in 1984, 29 New Mexico middle school and high school science teachers have participated in research at ITRI through that program. TRAC started in 1989, and 12 high school teachers have been supported here by this program. There were four teachers in each program at ITRI during the summer of FY-1992.

We continue to encourage ITRI staff members to initiate long-term interactions with individual science teachers at middle and high schools to interest students in science. For example, one staff member lectured at a high school and his presentations were followed by a visit of this chemistry class to ITRI. We hope these interactions will support more active involvement of our staff members in the class room, will provide a contact for science teachers to encourage visits by students, and provide opportunities for the teacher and their students to use some of our facilities. Our staff members continue their involvement in precollege education as science fair judges and as tutors and mentors.

Undergraduate Students

The goal of our Summer Student Research Participant Program is to encourage college students who have selected careers in science to enter graduate school. Students in our summer programs are provided the opportunity to initiate and complete a scientific investigation under the direction of an ITRI staff member. By being involved in the study design, the conduct of the experiments, analysis of data, and the presentation of results, the students understand the research and experience the excitement of new discovery. Since 1966, 529 students have participated in this program: 11 students participated during FY-1991. Although most students participate in research at ITRI during the summer, this program is available to students year-round.

Only a few students from the New Mexico universities apply for our summer research programs, but we will continue to encourage more students from New Mexico to participate. At present, most applications come from students who reside in other states. We will continue to notify professors at New Mexico universities of our educational programs and encourage them to provide applications to students who have the capability of going on

to graduate school. We hope that this approach will make more students in New Mexico aware of our programs, and attract a higher number of minority applicants. Three of the eight students in our graduate program in Inhalation Toxicology are from New Mexico. One student became interested in our graduate program from her experiences in our summer research program.

Graduate Students

Our Inhalation Toxicology Research Institute/University of New Mexico (UNM) Graduate Program in Inhalation Toxicology continued to grow in FY-1992. To obtain a Ph.D. degree, course work is completed at UNM, and the research portion of the doctoral degree is carried out at ITRI, with an ITRI staff member serving as the research advisor. Two new students were accepted into this program in FY-1992. We have obtained support from industry for our graduate program. Lilly Laboratories have contributed funds for several years to pay for travel expenses incurred when our students present papers at scientific meetings. E. I. duPont de Nemours & Company provides stipend support for one student. Our graduate students also continue to apply for additional fellowship support.

In addition to the ITRI-UNM program, graduate students attending other universities can also carry out the research necessary for their graduate degrees at the Institute. All course work for the advanced degree is completed at the university before the student starts research at ITRI. The advanced degree is awarded by the participating university upon completion of all degree requirements. Since 1968, 33 graduate students have conducted all or part of their research at ITRI.

Our graduate programs take advantage of the complementary academic resources available at universities and the research resources available at ITRI. For example, we established joint graduate programs in pathology with the Schools of Veterinary Medicine at Colorado State and Purdue Universities. Graduate veterinary students complete the research portion of a Ph.D. degree at ITRI as part of their residency program in pathology. A program in health physics has recently been established with Texas A&M University, with funding from the Department of Energy.

Postgraduate Students

Finding qualified postdoctoral participants continues to be difficult; during FY-1992 we had three postdoctoral fellows participating in research at ITRI. We provide research appointments to recent doctoral graduates to continue in their research training. Students in life science, chemistry, veterinary medicine, or engineering carry out research under the direction of ITRI staff members. This program is designed to develop research capabilities in inhalation toxicology and one or more of the areas of basic pulmonary biology. A continuing goal is to increase the number of postdoctoral participants at ITRI.

University Faculty and Industrial Scientists

Opportunities are available for scientists from universities or industry to visit ITRI or collaborate in research. These visits range from a few days, to obtain information or learn techniques, to a full year, to conduct research. During FY-1992, participants included scientists from UNM, the Albuquerque Veterans Medical Center, Purdue University, and the California Polytechnic State University.

Other Educational Activities

Several staff members hold academic appointments and present lectures to university students. ITRI also holds periodic workshops in inhalation toxicology, and these have received international recognition. The book, "Concepts in Inhalation Toxicology," published in 1989 from the workshop held in 1987, has become a key text in the field. The last workshop was held in October 1992, and approximately 90 attendees benefitted from the lectures and laboratory demonstrations.

David E. Bice, Ph.D.
Education Coordinator

APPENDIX J
AUTHOR INDEX

<u>FIRST AUTHOR</u>	<u>PAGE NUMBERS</u>
Barr, E. B.	18
Bechtold, W. E.	92, 99
Belinsky, S. A.	145, 147, 149
Benson, J. M.	74, 83, 108
Bhattacharyya, M.	178
Bice, D. E.	173, 195
Boecker, B. B.	130
Chang, I. Y.	217
Chen, B. T.	45, 51
Cheng, Y. S.	21, 28, 31, 43, 57
Dahl, A. R.	69
Diel, J. H.	215
Finch, G. L.	71, 110, 112, 169, 198
Guilmette, R. A.	66, 79
Hahn, F. F.	133
Harkema, J. R.	166
Henderson, R. F.	97, 157, 163
Hickman, A. W.	143
Hoover, M. D.	1, 5, 11, 37
Hotchkiss, J. A.	86, 160, 187, 192
Hubbs, A. F.	127
Jee, W. S. S.	201
Johnson, N. F.	181, 184
Kelly, G.	151, 153
Kennedy, C. H.	89, 101, 139
Kruglikov, I. L.	203
Lechner, J. F.	137
Lloyd, R. D.	206, 208
Lundgren, D. L.	63, 115, 118, 121, 123
Maples, K. R.	54
Mitchell, C. E.	94
Newton, G. J.	8, 14, 34, 40
Nickell, C.	141
Nikula, K. J.	105, 171, 190
Savage, S. M.	176
Scott, B. R.	213, 221, 224
Snipes, M. B.	24, 77
Taylor, G. N.	210
Yeh, H. C.	48, 60